ISSN 1343-2230
CNS-REP-64
November, 2004

CNS-REP-64

CNS Report

FERMILAB
FEB 3 2005
LIBRARY

CNS/RIKEN Joint Symposium on Frontier of gamma-ray spectroscopy and its application (Gamma04)

RIKEN Campus, Wako, Japan

March 18 – 19, 2004

Center for Nuclear Study (CNS)

Graduate School of Science, the University of Tokyo
Wako Branch at RIKEN, 2-1 Hirosawa, Saitama 351-0198, Japan
Correspondence: cnsoffice@cns.s.u-tokyo.ac.jp

CNS/RIKEN Joint Symposium on

Frontier of gamma-ray spectroscopy and its application (Gamma04)

Nishina Hall, RIKEN Wako Campus

March 18(Thursday) – 19(Friday), 2004

Organizing Committee
E. Ideguchi, T. Motobayashi, S. Shimoura, H. Tamura
T. Ishii, T. Otsuka, K. Asahi, H. Watanabe, N. Aoi

Preface

The CNS/RIKEN Joint Symposium on Frontier of gamma-ray spectroscopy and its application has been held during March 18-19, 2004 at Nishina hall of RIKEN Wako campus.

The purpose of the symposium was to discuss recent progress in the field of gamma-ray spectroscopy in both high spin and high isospin as well as recent development of advanced gamma-ray detectors.

Main topics discussed were

- Latest frontier of gamma-ray spectroscopy on high-spin, high-isospin nuclei and hypernuclei
- Development of gamma-ray detectors
- Application of gamma-ray detection techniques
- Perspectives for nuclear physics with gamma-ray detectors
- Other related topics

In the symposium, more than 60 people, including 7 from abroad, participated. Good presentations and valuable discussions were made. We hope this symposium to be held every two or three years to continue and develop international cooperation and to stimulate physicists in the fields of high-spin and exotic-nuclei studies.

This symposium was supported in part by Grant-in-Aid for Scientific Research of the Ministry of Education, Culture, Sports, Science and Technology of Japan, Grant number 15204018.

Contents

List of participants		i
Effect of loosely-bound single-particle levels on pair-correlation and deformation : its consequence in neutron-drip-line nuclei	I. Hamamoto (Lund)	1
Gamma-ray spectroscopy with radioactive beams: a tool to study reaction mechanisms at the Coulomb barrier	G. de France (GANIL)	13
Nano-second isomer spectroscopy of the 48Ca region through deep-inelastic collisions	T. Ishii (JAERI)	27
Spectroscopy of Lead and Trans-Lead Nuclei using an Evaporation Residue Detector	W. Reviol (Wash.U.)	35
Instability of nuclear wobbling motion and phase transition to tilted axis rotation	M. Matsuzaki (Fukuoka)	47
Three- and four-body structure of light hypernuclei	E. Hiyama (KEK)	53
Gamma spectroscopy of hypernuclei -- present status and future plans	H. Tamura (Tohoku)	75
Lambda-N interaction studied from hypernuclear gamma spectroscopy	M. Ukai (Tohoku)	85
Pairing effect on the giant dipole resonance width at low temperature	N.D. Dang (RIKEN)	99
High-Spin Isomer in ^{93}Mo	T. Fukuchi (CNS)	109
Shell Model Description of High Spin Isomers in Ba Isotopes	N. Yoshinaga (Saitama)	117
The RISING project at GSI and its first results	T.R. Saitoh (GSI)	131
Study of high-spin states by using secondary fusion reaction	E. Ideguchi (CNS)	153
Gamma-ray spectroscopy on unstable nuclei at RIBF	H. Sakurai (Tokyo)	167

Characterisation of highly segmented Germanium detectors	A. Boston (Liverpool)	177
Perspectives of AGATA and lifetime measurements for dipole bands in the ^{142}Gd region with EUROBALL	R. M. Lieder (Juelich)	193
Gamma-ray Compton imaging by strip germanium telescope	S. Motomura (RIKEN)	207
Detector array for low intensity radiation	S. Takeuchi (RIKEN)	215
Structure of ^{11}Be studied in beta-delayed neutron- and gamma-decay from polarized ^{11}Li	Y. Hirayama (Osaka)	225
Gamow-Teller beta decay of ^{46}Cr	T. Onishi (Tokyo)	235
g-Factor measurements of high-spin isomers and condensed matter studies with gamma-TDPAD method	H. Watanabe (RIKEN)	243
Gamma-ray spectroscopy with 6 Clover detectors at Tohoku ISOL	M. Fujita (Tohoku)	253
A new experimental technique for B(E2) measurement of ^{16}C	N. Imai (RIKEN)	261
In-Beam Gamma-ray Spectroscopy of Neutron-rich Nucleus ^{23}F	S. Michimasa (CNS)	269
New effective interaction for pf-shell nuclei and its implications for the stability of the N=Z=28 closed core	M. Honma (Aizu)	277
Gamma-ray spectroscopy by secondary fusion reactions using CRIB	A. Odahara (Nishinihon)	289
High-spin shape isomer and Ge-telescope	Y. Gono (Kyushu)	301

List of Participants

Nori Aoi	RIKEN, Japan	aoi@riken.jp
Koichiro Asahi	RIKEN/TIT, Japan	asahi@phys.titech.ac.jp
Hidetada Baba	Rikkyo University, Japan	baba@daq.rikkyo.ac.jp
Andrew Boston	University of Liverpool, UK	ajb@ns.ph.liv.ac.uk
Nguyen Dinh Dang	RIKEN, Japan	dang@postman.riken.go.jp
Gilles de France	GANIL, France	defrance@ganil.fr
Masahiro Fujita	Tohoku University, Japan	mafujita@cyric.tohoku.ac.jp
Tomonori Fukuchi	CNS, University of Tokyo, Japan	fukuchi@cns.s.u-tokyo.ac.jp
Yasuyuki Gono	Kyushu University, Japan	gono@kutl.kyushu-u.ac.jp
Ikuko Hamamoto	University of Lund, Sweden	ikuko@matfys.lth.se
Yoshikazu Hirayama	Osaka University, Japan	kazu@adam.phys.wani.osaka-u.ac.jp
Emiko Hiyama	KEK, Japan	Hiyama@post.kek.jp
Michio Honma	University of Aizu, Japan	m-honma@u-aizu.ac.jp
Eiji Ideguchi	CNS, University of Tokyo, Japan	ideguchi@cns.s.u-tokyo.ac.jp
Nobuaki Imai	RIKEN, Japan	imai@rarfaxp.riken.go.jp
Tetsuro Ishii	JAERI, Japan	ishii@popsvr.tokai.jaeri.go.jp
Tomoko Iwanami	RIKEN, Japan	iwanami@postman.riken.go.jp
Hironori Iwasaki	University of Tokyo	hiwasaki@phys.s.u-tokyo.ac.jp
Ong Hooi Jin	University of Tokyo	onghjin@nucl.phys.s.u-tokyo.ac.jp
Gibelin Julien	RIKEN, Japan	gibelin@rarfaxp.riken.go.jp
Shouko Kanno	Rikkyo University, Japan	komacha@ne.rikkyo.ac.jp
Takashi Kishida	RIKEN, Japan	kishida@rarfaxp.riken.go.jp
Rainer M. Lieder	Juelich, Germany	r.lieder@fz-juelich.de
Masayki Matsuzaki	Fukuoka University of Education, Japan	matsuza@fukuoka-edu.ac.jp
Shinichiro Michimasa	CNS, University of Tokyo, Japan	mitimasa@cns.s.u-tokyo.ac.jp
Yuji Miyashita	Tohoku University, Japan	miyashita@cyric.tohoku.ac.jp
Tohru Motobayashi	RIKEN, Japan	motobaya@riken.jp
Shinji Motomura	RIKEN, Japan	motomura@riken.jp
Megumi Niikura	CNS, University of Tokyo, Japan	niikura@cns.s.u-tokyo.ac.jp
Atsuko Odahara	Nishinippon Institute of Technology, Japan	odahara@nishitech.ac.jp
Takeo Onishi	University of Tokyo, Japan	takeo@nucl.phys.s.u-tokyo.ac.jp
Shinsuke Ota	Kyoto University / CNS	ota@cns.s.u-tokyo.ac.jp
Takaharu Otsuka	University of Tokyo, Japan	otsuka@phys.s.u-tokyo.ac.jp
Walter Reviol	Wahington University, USA	reviol@wustl.edu

Akito Saito	RIKEN, Japan	akito@ne.rikkyo.ac.jp
Takehiko R. Saitoh	GSI, Germany	take2602@hotmail.com
Hideyuki Sakai	University of Tokyo/CNS, Japan	sakai@phys.s.u-tokyo.ac.jp
Hiroyoshi Sakurai	University of Tokyo, Japan	sakurai@phys.s.u-tokyo.ac.jp
Helen Scraggs	University of Liverpool, UK	
Michiko Sekimoto	KEK-IPNS, Japan	sekimoto@post.kek.jp
Susumu Shimoura	CNS, University of Tokyo, Japan	Shimoura@cns.s.u-tokyo.ac.jp
Saeko Sumita	RIKEN, Japan	s-sumita@postman.riken.go.jp
Masaru Suzuki	University of Tokyo, Japan	masaru@nucl.phys.s.u-tokyo.ac.jp
Tomokazu Suzuki	Tohoku University, Japan	tomokazu@cyric.tohoku.ac.jp
Eri Takeshita	Rikkyo University, Japan	eri@ne.rikkyo.ac.jp
Satoshi Takeuchi	RIKEN, Japan	takesato@rarfaxp.riken.go.jp
Kazuko Takeuchi	CNS, University of Tokyo, Japan	takeuti@cns.s.u-tokyo.ac.jp
Mitsuru Tamaki	CNS, University of Tokyo, Japan	tamaki@cns.s.u-tokyo.ac.jp
Hirokazu Tamura	Tohoku University, Japan	tamura@lambda@phys.tohoku.ac.jp
Hoang T.K. Trang	JAERI, Japan	
Mifuyu Ukai	Tohoku University, Japan	m-ukai@lambda.phys.tohoku.ac.jp
Yasuo Wakabayashi	CNS, University of Tokyo, Japan	bayashi@cns.s.u-tokyo.ac.jp
Hiroshi Watanabe	RIKEN, Japan	hiroshi@rarfaxp.riken.go.jp
Naotaka Yoshinaga	Saitama University, Japan	yoshinaga@phys.saitama-u.ac.jp
Yu-Min Zhao	RIKEN, Japan	ymzhao@riken.jp
Shigeru Kubono		
Koji Higashiyama		
Kiyoshi Tanida		
Takashi Ichihara		
Masayasu Ishihara		
Naoyuki Itagaki		
Yoshiyuki Yanagisawa		
Kosuke Morita		
Yosuke Kondo		
Kazunari Yamada		
Mitsuo Sakai		
Yasuhiro Togano		
Jun Saito		
Shinichiro Fujii		
Akinori Yamaguchi		

Effect of weakly-bound neutron levels on pair-correlation and deformation : its implication in neutron-drip-line nuclei

Ikuko Hamamoto[a,b]

[a] Division of Mathematical Physics, LTH, University of Lund, Lund, Sweden.
[b] The Niels Bohr Institute, University of Copenhagen, Blegdamsvej 17, DK-2100 Copenhagen Ø, Denmark

A characteristic feature unique to the weakly-bound neutron systems is the importance of the coupling to the nearby continuum of unbound states, as well as the impressive role played by weakly-bound neutrons with low orbital angular-momenta ℓ. Weakly-bound small-ℓ neutrons have an appreciable probability to be outside of the core nucleus and are thereby insensitive to the strength of the potential provided by the well-bound nucleons in the system, while the wave-functions of weakly-bound large-ℓ neutrons stay mostly inside the nuclear potential.

In a given spherical nucleus the occupation probability of low-ℓ orbits in the presence of pair-correlation decreases considerably already when the one-particle energy approaches continuum. When one-particle levels enter into the continuum, the low-ℓ orbit soon becomes almost unavailable for the many-body pair-correlation. In contrast, the contribution to the pair-correlation by high-ℓ orbits which have one-particle resonant levels with narrow width in the one-body potential may be formally estimated in the BCS approximation using the resonant energies, though the associated wave-functions are indeed bound-state wave-functions. One also finds that the effective pair-gap of weakly-bound low-ℓ neutrons is much reduced compared with that of neutrons with larger ℓ values.

Though in medium-size spherical nuclei the number of neutrons that occupy the levels with, say ℓ=0 and 1 may not be a significant fraction of the total, in deformed nuclei the components of the low-ℓ orbits spread in essence over all Nilsson orbitals with small Ω values. The structure of one-particle levels in deformed β-stable nuclei is known to be approximately expressed in terms of asymptotic quantum numbers $[Nn_z\Lambda\Omega]$. Weakly-bound neutron levels in deformed Woods-Saxon potentials are studied in the absence of pair-correlation. It is found that for weakly-bound neutron levels with $\Omega^\pi = 1/2^+$ the $s_{1/2}$ component becomes overwhelmingly dominant as the binding energy of the levels approaches zero, irrespective of the size of deformation and the kind of one-particle orbits. This also means that the major component of any weakly-bound $\Omega^\pi = 1/2^+$ neutrons in deformed nuclei must be $s_{1/2}$ and thereby would exhibit halo phenomena. Consequently, all $\Omega^\pi = 1/2^+$ levels, which lie close to or in the continuum, become practically unavailable for both deformation and many-body pair-correlation.

I plan to talk about what is outlined above, showing some concrete numerical examples. If I list our own publications on the subject, then : I.Hamamoto and B.R.Mottelson, C.R.Acad.Sci., Ser.IV, **4**, 433 (2003) ; Phys.Rev. **C68**, 034312 (2003) and to be published in Phys.Rev.**C** ;
the part related to deformation : I.Hamamoto, submitted to Phys.Rev.**C**.

Effect of weakly-bound neutrons on pair-correlation and deformation

Features in neutron-drip-line nuclei :

- Importance of the coupling to the nearby continuum of unbound states.
- Role played by weakly-bound low-l neutrons.

Many-body correlations in drip line nuclei.

deformation vs. pairing

1) Many-body pair correlation in spherical nuclei,

(solving HFB eqs. in coordinate space with correct asymptotic boundary conditions.

2) One-particle orbits in deformed finite-well potential,

(solving coupled eqs. in coordinate space with correct asymptotic boundary conditions.

β-stable nuclei

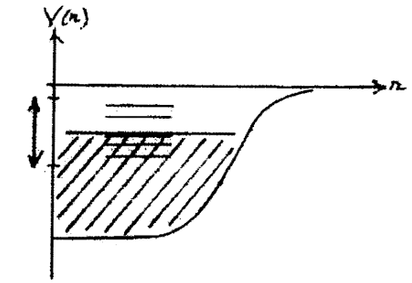

---

neutron drip line nuclei

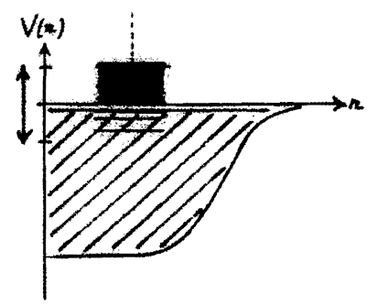

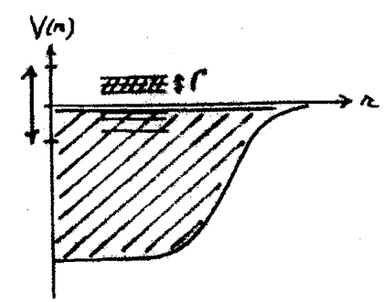

Importance of one-particle resonant states with small width Γ in the many-body correlations.

ex. No one-particle resonant levels for $s_{1/2}$ orbits.

Neutron radial wave functions in Woods-Saxon potentials.

$r \cdot R_{nlj}(r)$

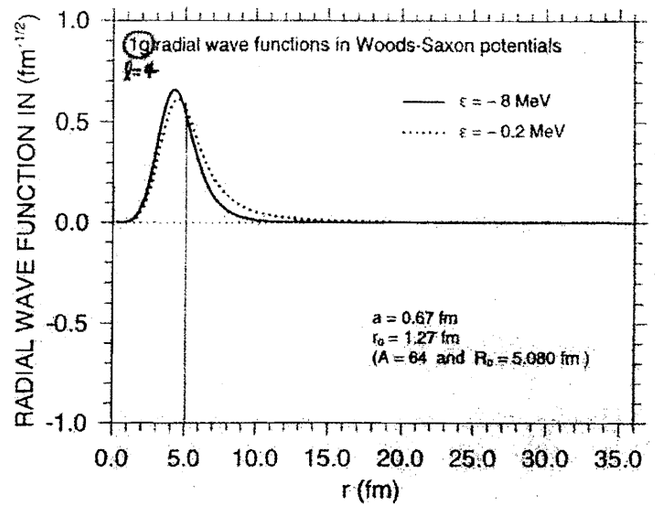

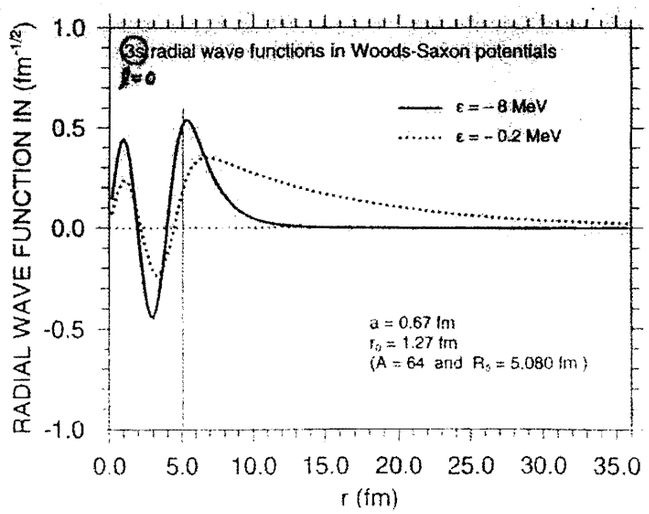

Energies of neutron orbits in Woods-Saxon potentials.

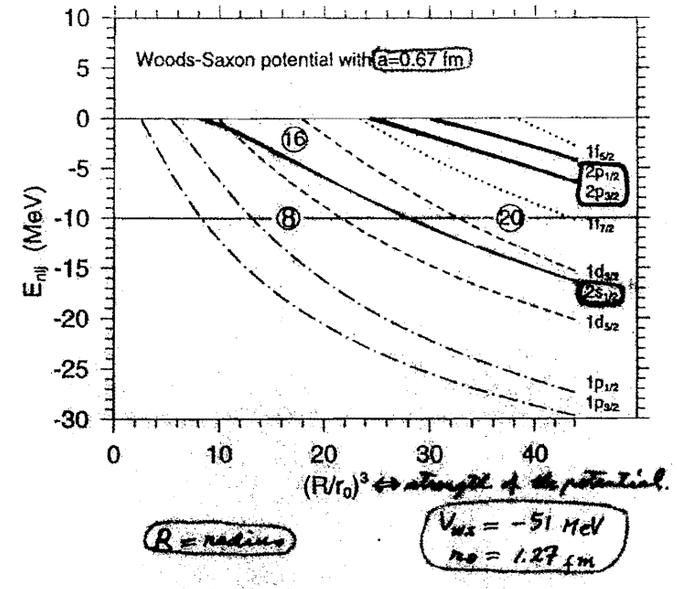

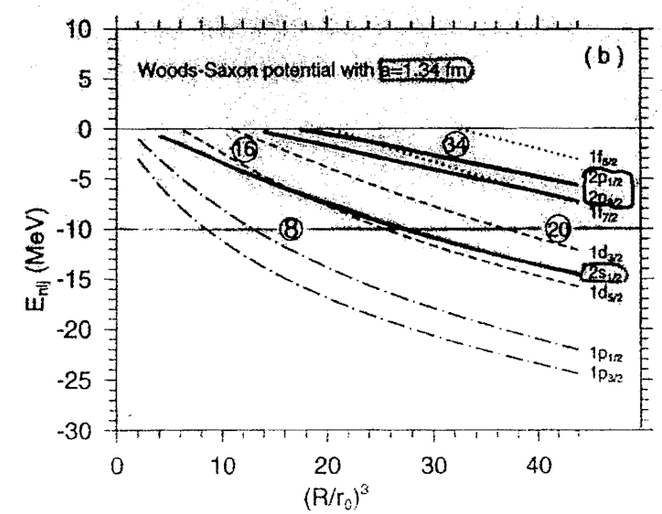

HFB eq. in a simplified model

[spherical symmetry and monopole pairing]

$$\Psi_i(E_{qp}, \vec{r}\sigma) = R_i^{\ell j}(E_{qp}, r)\, Y_{\ell j}^{m_j}(\hat{r}, \sigma) \qquad i = 1, 2$$

$$r\, R_i^{\ell j}(E_{qp}, r) = u_{\ell j}(E_{qp}, r) \quad \text{and} \quad v_{\ell j}(E_{qp}, r)$$

HFB eq.

$$\left(\frac{d^2}{dr^2} - \frac{\ell(\ell+1)}{r^2} + \frac{2m}{\hbar^2}\left(\boxed{\lambda + E_{qp}} - V(r) - V_{so}(r)\right)\right) u_{\ell j} - \frac{2m}{\hbar^2}\Delta(r) v_{\ell j} = 0$$

$$\left(\frac{d^2}{dr^2} - \frac{\ell(\ell+1)}{r^2} + \frac{2m}{\hbar^2}\left(\boxed{\lambda - E_{qp}} - V(r) - V_{so}(r)\right)\right) v_{\ell j} + \frac{2m}{\hbar^2}\Delta(r) u_{\ell j} = 0$$

We take $E_{qp} > 0$ and $\lambda < 0$ (bound system)

Then, $\boxed{(\lambda - E_{qp})} < 0$ $\quad v_{\ell j}$: bound-state wave function

$\boxed{\lambda + E_{qp}} \gtrless 0$ $\quad u_{\ell j}$

$$V(r) + V_{so}(r) \Rightarrow V_{WS} f(r) - V_{WS}\, v \left(\frac{\Lambda}{2}\right)^2 \frac{1}{r}\frac{df(r)}{dr}(\vec{\sigma}\cdot\vec{\ell})$$

potential strength

where

$$f(r) = \frac{1}{1 + exp\left(\frac{r-R}{a}\right)}$$

$$R = r_0 A^{1/3} \quad \text{with} \quad r_0 = 1.27\,\text{fm}$$

$$a = 0.67\,\text{fm} \qquad v = 32$$

Pairing field

$$\Delta(r) \propto f(r) \qquad \text{or} \qquad \Delta(r) \propto r\frac{df(r)}{dr}$$

The strength

$$\bar{\Delta} \equiv \frac{\int_0^\infty r^2 dr\, \Delta(r) f(r)}{\int_0^\infty r^2 dr\, f(r)}$$: input of numerical calculations.

For $\boxed{(\lambda + E_{qp}) < 0}$, HFB eq. is an eigenvalue (E_{qp}^{disc}) problem.

for $r \to \infty$

$$u_{\ell j}(E_{qp}, r) \propto r\, h_\ell(\alpha_1 r) \quad \text{where} \quad \alpha_1^2 \equiv -\frac{2m}{\hbar^2}(\lambda + E_{qp})$$

$$v_{\ell j}(E_{qp}, r) \propto r\, h_\ell(\beta r) \quad \text{where} \quad \beta^2 \equiv -\frac{2m}{\hbar^2}(\lambda - E_{qp})$$

Normalization : $\int_0^\infty \left(|\, u_{\ell j}(E_{qp}^{disc}, r)\,|^2 + |\, v_{\ell j}(E_{qp}^{disc}, r)\,|^2\right) dr = 1$

$\boxed{\int_0^\infty |\, v_{\ell j}(E_{qp}^{disc}, r)\,|^2\, dr}$: occupation prob. of the discrete level.

For $\boxed{(\lambda + E_{qp}) > 0}$, HFB solution exists for $^\forall E_{qp}$.

for $r \to \infty$

$$u_{\ell j}(E_{qp}, r) = C\left(\cos(\delta_{\ell j}) r j_\ell(\alpha_2 r) - \sin(\delta_{\ell j}) r n_\ell(\alpha_2 r)\right)$$

$$v_{\ell j}(E_{qp}, r) \propto r\, h_\ell(\beta r)$$

$$\alpha_2^2 \equiv \frac{2m}{\hbar^2}(\lambda + E_{qp}) \qquad C = \sqrt{\frac{1}{\pi}\frac{2m}{\hbar^2}\alpha_2}$$

$$\int dr\, u_{\ell j}(E, r)\, u_{\ell j}(E', r) = \delta(E - E')$$

$\boxed{\int_0^\infty |\, v_{\ell j}(E_{qp}, r)\,|^2\, dr}$: occupation prob. per unit energy interval.

$\boxed{\int_{\Delta E_{qp}} dE_{qp} \int_0^\infty |\, v_{\ell j}(E_{qp}, r)\,|^2\, dr}$: occupation prob.

HFB solved in coordinate space with correct asymptotic boundary conditions.

A. Bulgac, preprint No. FT-194-1980, Institute of Atomic Physics, Bucharest, 1980, nucl-th/9907088.

M. Grasso, N. Sandulescu, N. Van Giai and R. J. Liotta, Phys. Rev. C64, 064321 (2001).

from HFB bound-state wave-functions, $v_{\ell j}(E_{qp}, r)$

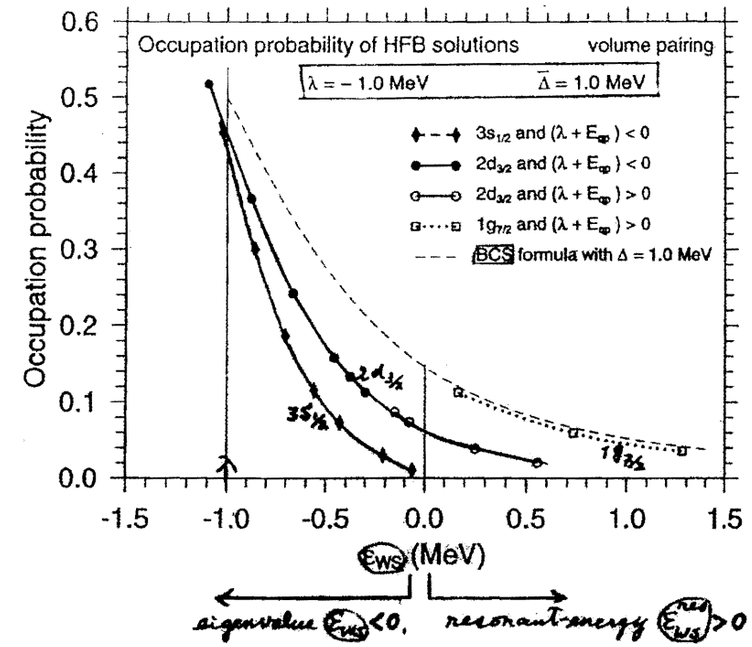

eigenvalue $\varepsilon_{WS} < 0$, resonant-energy $\varepsilon_{WS}^{res} > 0$

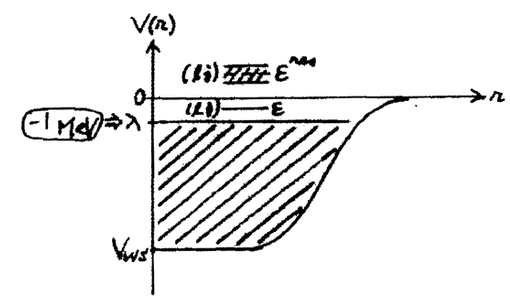

BCS formula: $v^2 = \frac{1}{2}\left(1 - \frac{\varepsilon_{WS} - \lambda}{\sqrt{(\varepsilon_{WS} - \lambda)^2 + \Delta^2}}\right)$ with $\Delta = 1$ MeV

Δ_{eff} in finite-well (Woods-Saxon) potential

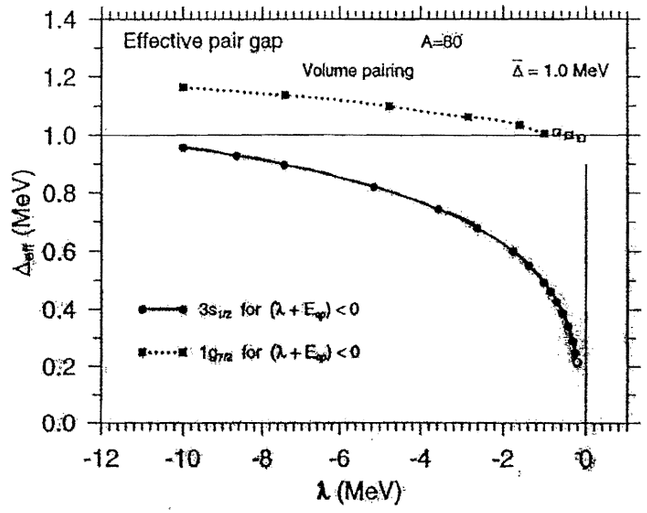

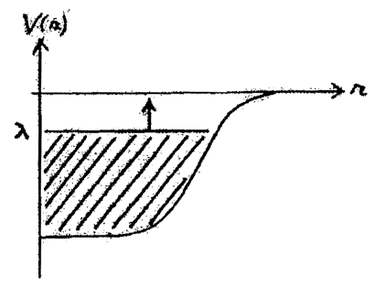

∴ ~~Pairing anti halo effect~~

Halo may exist in the presence of many-body pair correlation.

$$\left[\rho_{HFB} \sim \frac{\exp(-2\kappa r)}{r^2}, \quad \kappa \equiv \sqrt{\frac{2mE_{qp}}{\hbar^2}} \quad \kappa_{min} \simeq \sqrt{\frac{2m\Delta}{\hbar^2}} \text{ for } \lambda \to 0\right]$$

$3s_{1/2}$ orbit — solutions for $(\lambda+E_{qp}^{disc})<0$ vs. $(\lambda+E_{qp})>0$.

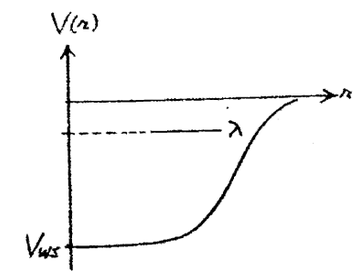

$\boxed{\bar{\Delta} = 1\ \text{MeV}}$ fixed

Vary $\lambda(<0)$, keeping $\boxed{E_{WS}(V_{WS}) = \lambda}$.

expect [occ. prob. ≈ 0.5] !

(a) As $[E_{WS} = \lambda] \to 0$, occ. prob. moves smoothly from discrete solution to continuum solutions. In general, one has to sum up the occ. prob. in ~~both~~ kinds of solutions.

(b) Pairing anti-halo effect ?

Halo phenomena may exist in the presence of pair field, though r_{rms} may not approach ∞.

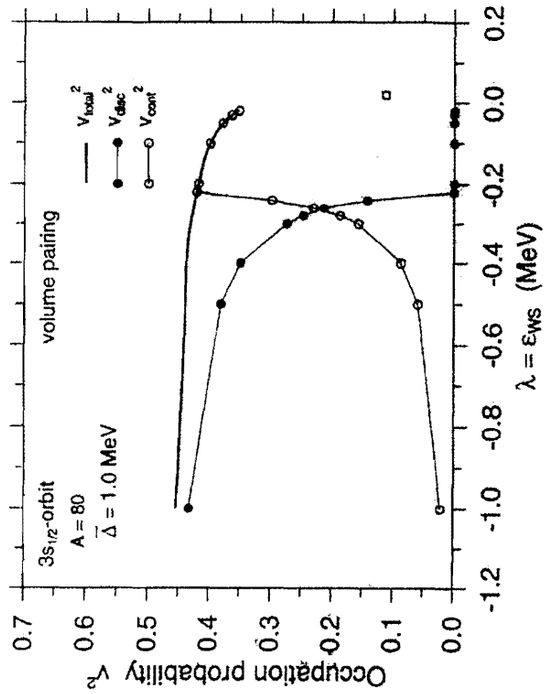

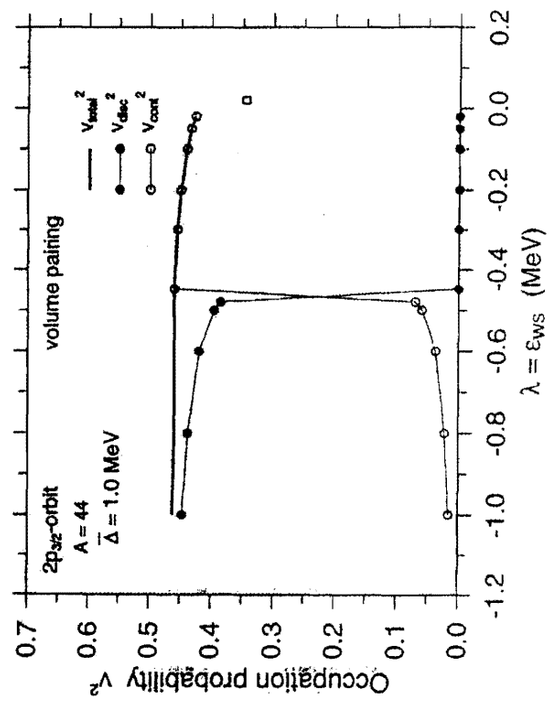

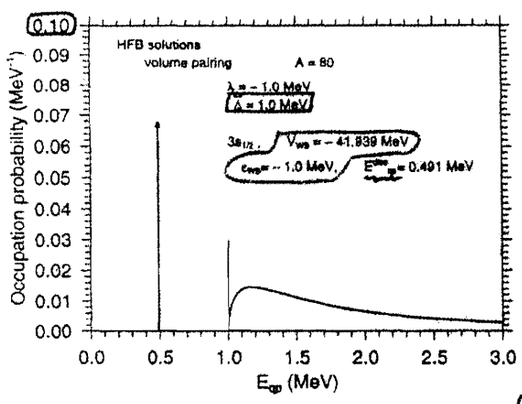

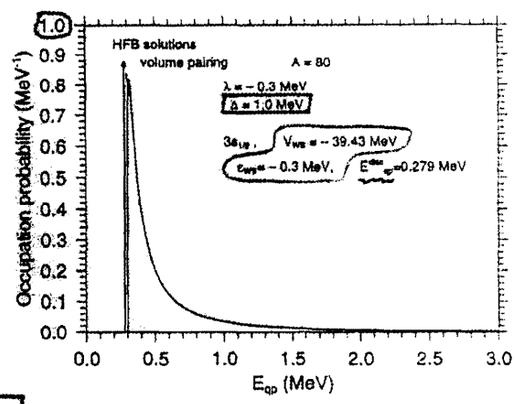

$\boxed{\lambda = \varepsilon_{WS}}$

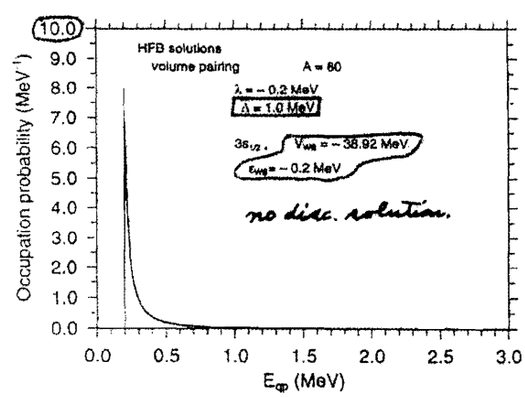

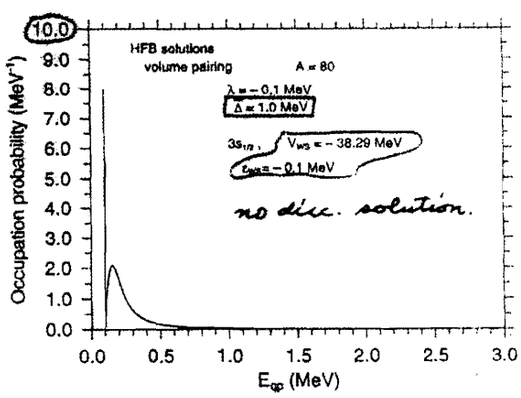

2) One-particle orbits in deformed finite-well potential.

[Coupled eqs. in coordinate space with correct asymptotic boundary conditions are solved.]

Single-particle wave-function in Y_{20}-deformed Woods-Saxon potential,

$$\Psi_m(\vec{r}) = \frac{1}{r}\sum_{\ell j} R_{\ell jm}(r)\, Y_{\ell jm}(\hat{r}),$$

which satisfies

$$H\,\Psi_m = \varepsilon_m\,\Psi_m.$$

The coupled equation for the radial wave-function is written as

$$\left(\frac{d^2}{dr^2} - \frac{\ell(\ell+1)}{r^2} + \frac{2m}{\hbar^2}(\varepsilon_m - V(r) - V_{so}(r))\right) R_{\ell jm}(r) = \frac{2m}{\hbar^2}\sum_{\ell' j'}(Y_{\ell jm} \mid V_{coupl} \mid Y_{\ell' j' m})R_{\ell' j' m}(r)$$

where

$$\begin{aligned} V(r) &= V_{WS}\, f(r) \\ V_{coupl}(\vec{r}) &= -\beta k(r) Y_{20}(\hat{r}) \\ V_{so}(r) &= -V_{WS}\, v \left(\frac{A}{2}\right)^2 \frac{1}{r}\frac{df(r)}{dr}(\vec{\sigma}\cdot\vec{\ell}) \end{aligned}$$

$$f(r) = \frac{1}{1 + exp\left(\frac{r-R}{a}\right)},$$

$$k(r) = RV_{WS}\frac{df(r)}{dr}.$$

asymptotic behavior of $R_{\ell jm}(r)$ for $r \to \infty$

$$R_{\ell jm} \propto r\, h_\ell(\beta r)$$

where $h_\ell(-iz) \equiv j_\ell(z) + in_\ell(z)$

and

$$\beta^2 \equiv -\frac{2m\,\varepsilon_m}{\hbar^2}$$

The normalization condition is written as

$$\sum_{\ell j}\int_0^\infty |\, R_{\ell jm}(r)\,|^2\, dr = 1$$

One-particle levels in deformed (Y_{20}) h.o. potentials.

$[N\, n_z\, \Lambda\, \Omega]$ asymptotic quantum numbers

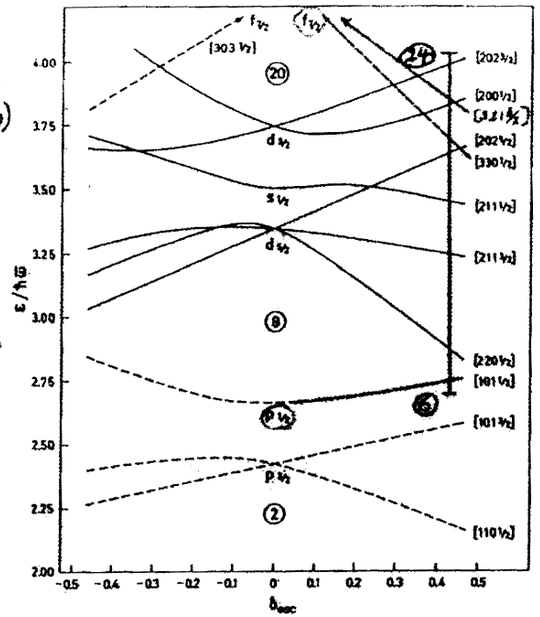

Figure 5-1 Spectrum of single-particle orbits in spheroidal potential (N and $Z<20$). The

Y_{20} deformed Woods-Saxon potential

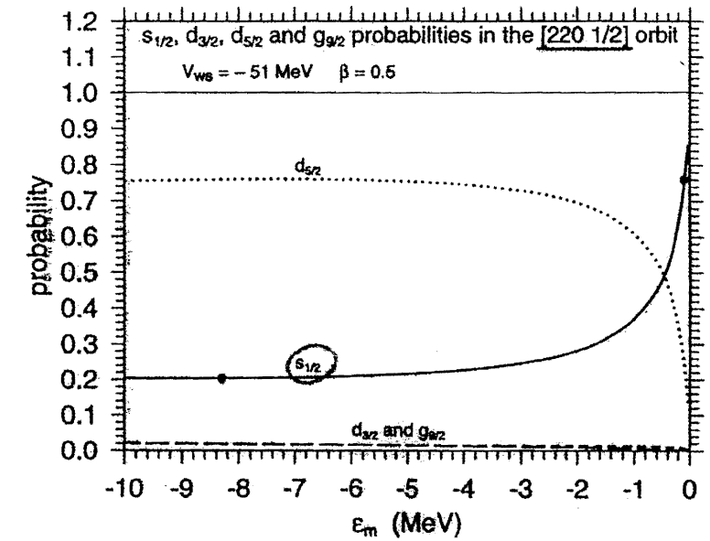

In Y_{20} deformed Woods-Saxon potentials.

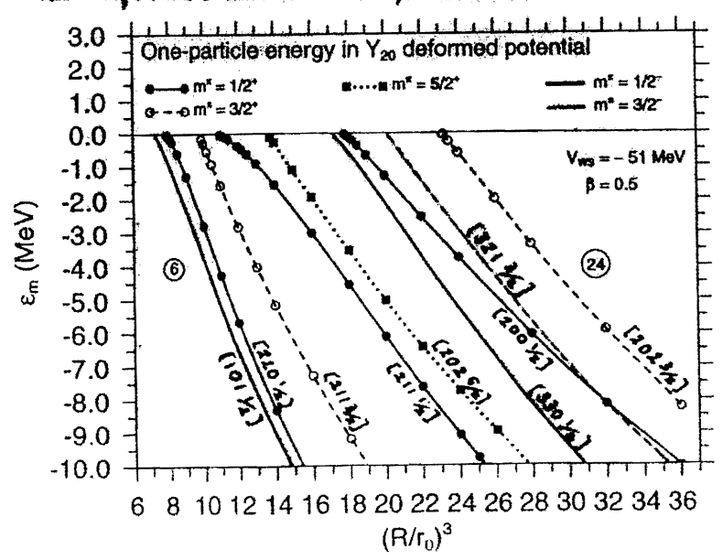

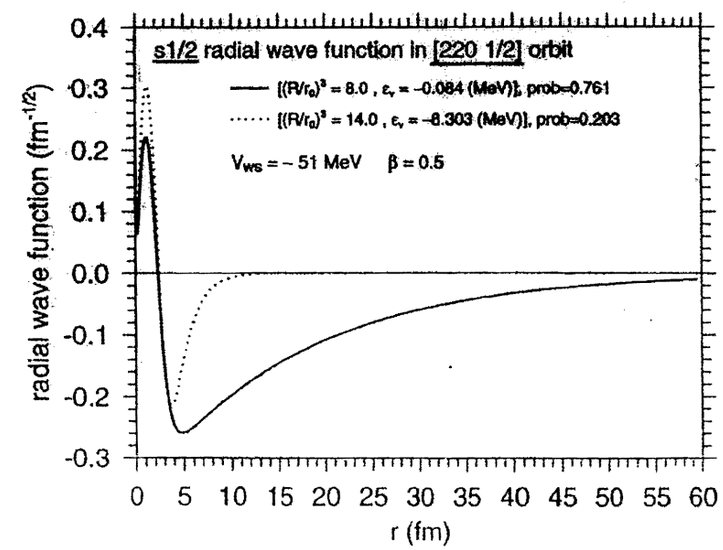

▼ The odd-parity excitations in Table 5-8 have this symmetry, but very small matrix elements of **P**, since this operator obeys the selection rules $\Delta n_3 = 1$, $\Delta\Lambda = 0$ or $\Delta n_3 = 0$, $\Delta\Lambda = 1$. Hence, the properties of these excitations are not expected to be significantly affected by the removal of the spurious degree of freedom associated with the center-of-mass motion.

Decoupling parameters

The classification in Table 5-8 is further supported by measurements of various properties of the intrinsic states. Thus, the experimentally determined decoupling parameters for the $K = 1/2$ bands are given in Table 5-8 and can be compared with the theoretical values listed together with the configuration. The theoretical estimates are obtained from Eq. (5-46) together with the wave functions in Table 5-9, and are seen to provide an interpretation of the characteristic differences observed for the decoupling parameters of the different bands. For the orbits [220 1/2] and [330 1/2], which have especially large moments of inertia, higher-order rotational coupling effects can be important. Such effects may be responsible for the theoretical underestimate ▲ of a for these bands; see the discussion on p. 308.

One-particle w.f. in Y_{20} deformed $\boxed{\text{h.o.}}$ potentials.

$[Nn_3\Lambda\Omega]$	$j=1/2$	$j=3/2$	$j=5/2$	$j=7/2$
[101 1/2]	0.920	0.392		
[220 1/2]	−0.523	−0.285	0.803	
[211 3/2]		−0.236	0.972	
[202 5/2]			1.000	
[211 1/2]	0.419	0.735	0.533	
[200 1/2]	0.743	−0.615	0.265	
[202 3/2]		0.972	0.236	
[330 1/2]	0.279	−0.646	−0.188	0.685

$s_{1/2}$-prob

$(0.523)^2 = 0.274$

$(0.419)^2 = 0.175$

$(0.743)^2 = 0.552$

Table 5-9 Single-particle wave functions for nuclei with $19 \leq A \leq 25$. The table gives the expansion coefficients $\langle Nl\Omega|\nu\rangle$ of the one-particle orbits ν labeled by the asymptotic quantum numbers $[Nn_3\Lambda\Omega]$. The wave functions are obtained from the Hamiltonian (5-10) employing the parameters of Table 5-1 and the deformation $\delta = 0.4$. The phases are as in Table 5-2b and Eq. (5-17).

▼ *M1- and GT-matrix elements for $A = 25$*

The empirical evidence on $M1$ moments in the [202 5/2] and [211 1/2] bands in ^{25}Mg and ^{25}Al is collected in Table 5-10 and is analyzed on the basis of expressions (4-87) and (4-88). For the $K = 5/2$ bands, the constancy of the quantity $(g_K - g_R)$ derived from the different matrix elements provides ▲ tests of the rotational coupling scheme.

Y_{20} deformed Woods-Saxon potential

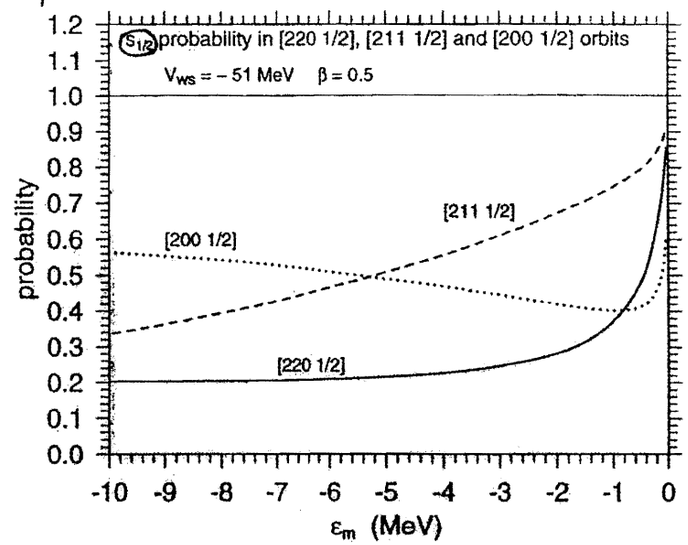

One-particle levels in Y_{20} deformed h.o. potentials.

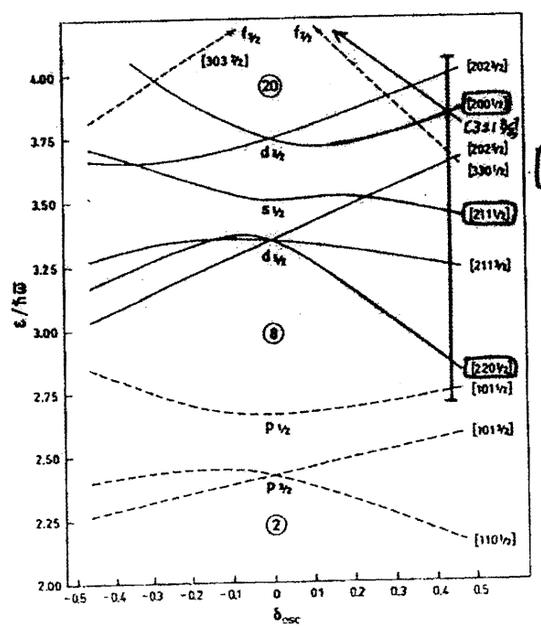

$\boxed{\Omega^\pi = 1/2^+}$

Y_{20} deformed Woods-Saxon potential

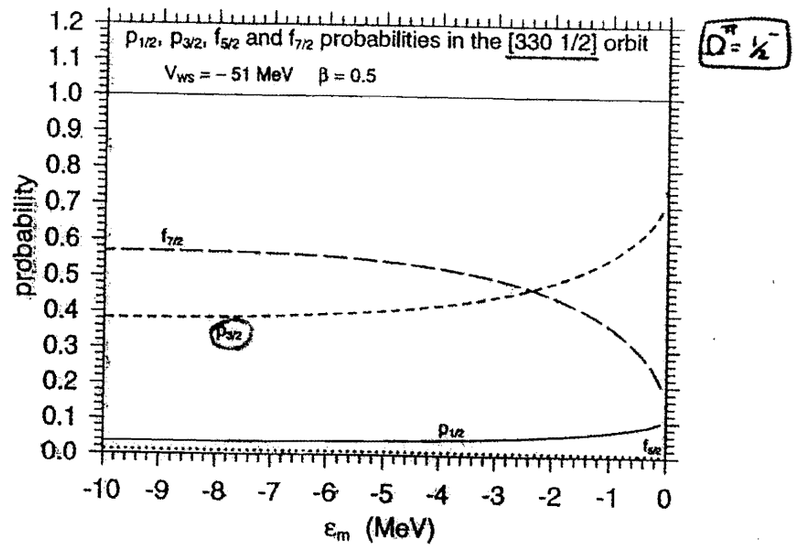

Some conclusions.

In neutron drip line nuclei, where $|\lambda| \ll$ 7-10 MeV
⇑
β-stable nuclei.

(pair-correlation in spherical nuclei):

1) low-l n. orbits with $\lambda \lesssim \varepsilon_{WS} < 0$ have much smaller occ. prob. than higher-l n. orbits.

2) For $\varepsilon_{HF} > 0$, only higher-l orbits with very small Γ in the HF potential may significantly contribute to pair correlation. The occ. prob. of those higher-l one-particle resonant levels may be approximately estimated using the BCS formula.

3) $\Delta_{\nu\nu}$ of weakly-bound lower-l neutrons is much smaller than that of higher-l neutrons. ⟹ halo for [$\bar{\Delta} \neq 0$.]

4) If n. pick-up reactions on those nuclei can be performed, the strength of the $s_{1/2}$ neutron may appear both at a discrete state and in the continuum.

(deformed nuclei with $\Delta = 0$):

5) In weakly-bound neutron levels with $\Omega^{\pi} = 1/2^{+}$, the $s_{1/2}$ component becomes dominant as $|\varepsilon_{\Omega}| \to 0$, irrespective of the size of deformation and the kind of one-particle orbits. The rotational spectra of deformed halo nuclei must come from the deformed core.

6) Wave-functions of weakly-bound deformed n. orbits with small Ω can be very different from those described by $[N n_z \Lambda \Omega]$.

Nuclear dynamics at the barrier with gamma rays

G. de France, GANIL

The EXOGAM gamma ray array has been designed to optimize the use of radioactive beams from the SPIRAL facility, which delivers beams since fall 2001. The solid angle coverage, hence the efficiency, has been maximized to run low to medium gamma ray multiplicity spectroscopic studies. Furthermore background rejection (e.g. from the radioactive nature of the beam) and anti-Compton shielding is performed with BGO and CsI scintillators surrounding high resolution Germanium detectors to preserve good peak to background ratio. This efficient setup has also been used to study nuclear dynamics at the Coulomb barrier.

A long standing question in nuclear physics is related to wether the fusion cross section is enhanced around (or below) the barrier or not when loosely bound projectiles are used. To adress this question, we have performed a serie of experiments using stable, tighly bound (4He), and radioactive, loosely bound (6,8He) projectiles leading to the same compound nucleus. The alpha particle experiment has been performed at the Pelletron laboratory in TIFR, Mumbai while the radioactive beam runs were made at the SPIRAL facility, Caen.

In addition to fusion, transfer, breakup and inelastic processes occur at energies around the Coulomb barrier. Charged particle detection was ensured by an annular Silicon strip detector mounted at forward angles. The cross sections for the various reaction mechanisms have been measured by analyzing single gamma ray spectra as well as charged particles-gamma ray coincidences.

Results from these runs will be discussed and the setup will be descibred in some details.

Nuclear dynamics at the barrier

or

γ-ray spectroscopy with radioactive beams: a tool to study reaction mechanisms at the Coulomb barrier.

G. de France, GANIL

gamma04 symposium, CNS, 2004

GANIL

Outline

- GANIL facility
- Fusion reactions involving ^{6,8}He
  - –Motivations for these experiments
  - –The runs
  - –Results and interpretation
  - –Conclusions

- *Shape coexistence (some prelim. results)*
- *EXOGAM*

GANIL

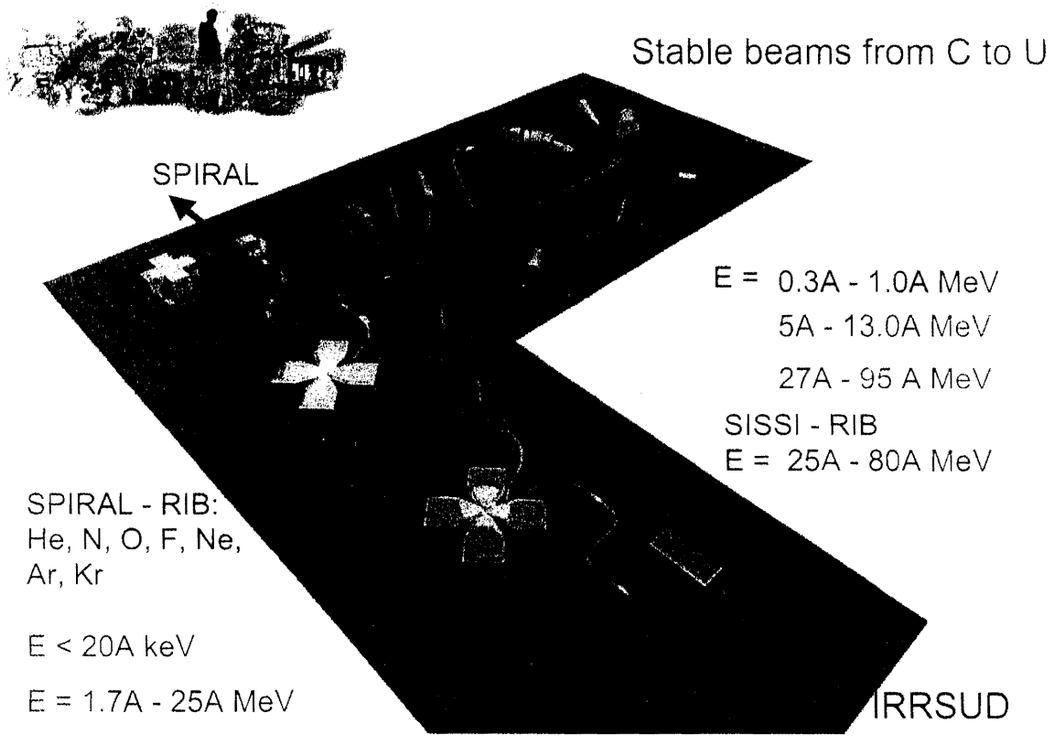

Fusion involving ^{6,8}He : Motivations (1)

A. Navin, Y. Blumenfeld et al

Sub-barrier fusion: 1D barrier penetration model too simplistic *(keep it for comparison)* : $\sigma_f(E) = \pi \lambda\!\!\!^{-2} \sum_l (2l+1)\, T_l(E)$

$T_l(E) = [1 + \exp\{2\pi/\hbar\omega\,(V_{Bl} - E)\}]^{-1}$; $V_{Bl} = V_B + \hbar^2 l(l+1)/2\mu r^2$

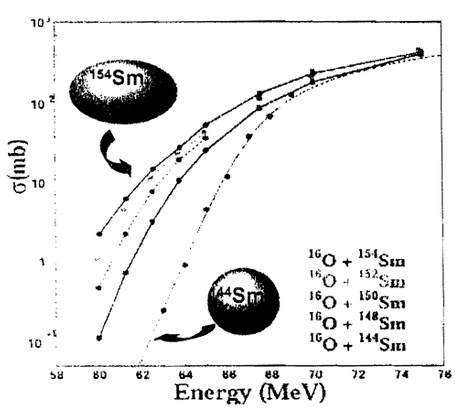

σ_f very much affected by:

- the ***intrinsic structure*** of the colliding nuclei
- the ***coupling of elastic channel to other direct reaction channels*** = modification of the barriers seen by the interacting nuclei:

Barrier distribution measurements crucial:

- *to recognize inelastic, transfer and breakup channels*
- *to include them in the calculations*

Motivations (2)

- ***What is the effect of weak binding and g.s. structure of unstable isotopes of He on reaction processes at energies near the Coulomb barrier?***
  - -Fusion
  - -Transfer, Breakup, Elastic scattering
  - *and with respect to the stable counterpart* **^{4}He**
  - ➔ model independent

- ***Search for experimental signature for:***
  - Transfer involving weakly bound nuclei (^{6,8}He)
  - Relative importance of transfer *vs.* breakup

Fusion with RIB/stable beams

- ➢ What is the effect of break-up on σ_{fus}?
- ➢ Any difference with fusion of (tightly bound) stable beams ?

... Or is it just a matter of detail?

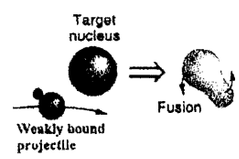

Expectations:

Enhancement due to the large radius 'halo structure' -lower barrier,coupling to pygmy resonance- *(Takigawa & Sagawa, PLB 265 (1991) 23)*

Enhancement below the 1D barrier; reduction at the barrier (loss of flux due to breakup) *(Hussein et al., PRC 46 (1992) 377)*

Enhancement due to channel coupling (breakup) at energies below the barrier *(Dasso & Vitturi PRC 50 (1994) R12)*

Enhancement below the barrier and reduction above due to coupling to continuum (breakup) *(Hagino et al., PRC 61 037602 (2000))*

Reduction below and above *(Nakatsukasa et al., fusion03 conf.)*

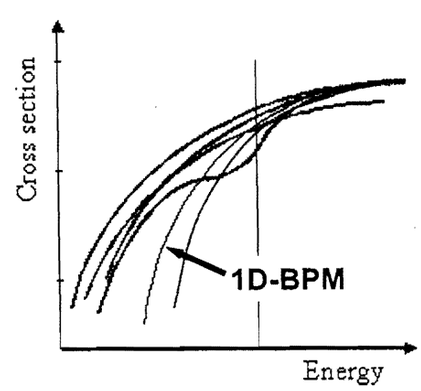

Experiments till now... 1) α-decay

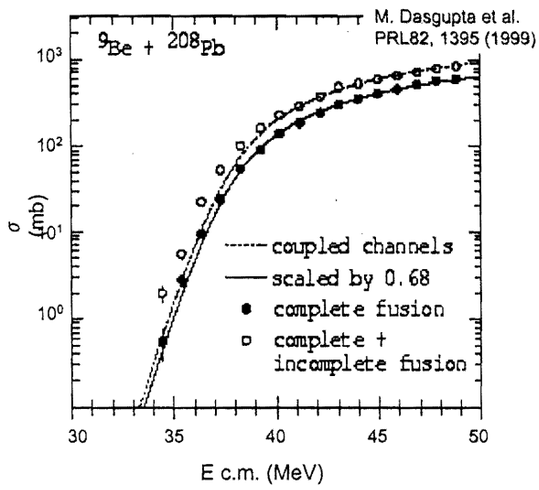

- Loosely bound Be isotopes usually compared to the stable ^{9}Be => Need to have a very clear and comprehensive knowledge of ^{9}Be
- Very precise measurements of fusion cross section via α decay of the compound nucleus (^{217}Rn)
- Strong contamination with Po observed (> expected from Rn decay) => another source
- Due to ^{9}Be break up => incomplete fusion

Break up of ^{9}Be induces fusion suppression ...

Experiments till now... 2) γ-decay

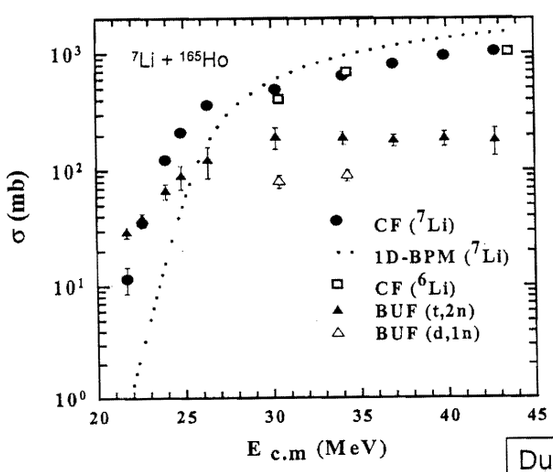

V. Tripathi et al.,
PRL 88, 172701 (2002)

- Measurement of ^{7}Li and comparison with ^{6}Li
- Measurements of fusion cross section via γ decay of the evaporation residues (2n to 5n channels)
- Measurement of breakup-fusion (t,2n) and (d,1n) channels

Due to ^{7}Li break up:
suppression above Vb
enhancement below

Experiments till now... 3) fission

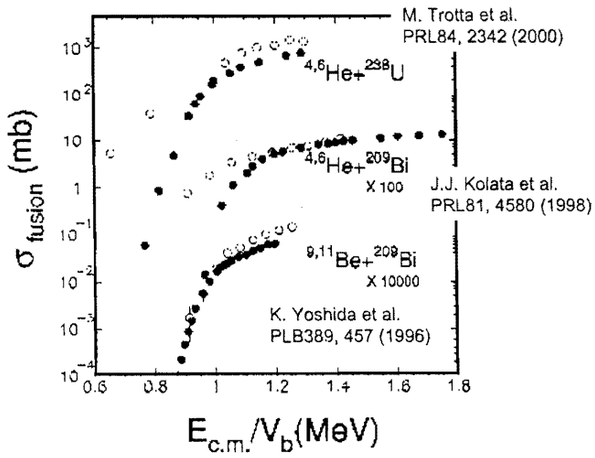

Fig from N. Alamanos et al. PRC65, 054606 (2003)

- Measurements and comparison tightly/loosely bound nuclei
- Measurements of fusion cross section via fission fragments
- Huge enhancement below the barrier. Correction from neutron transfer induced fission

...Suppression or enhancement ?

Experimental approach

16.5<E_{lab}<34 MeV α
19.5, 30 MeV ^{6}He
27 MeV ^{8}He

Projectile
^{4,6,8}He

Target
^{63,65}Cu &
^{188,190,192}Os

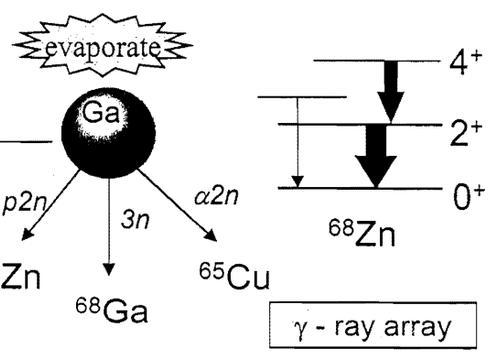

γ - ray array

Pelletron, Spiral
Intensity (pps):
2×10^{10} α
$1\text{-}3.5\times10^{7}$ ^{6}He
7×10^{4} ^{8}He

^{6,8}He: Annular Si **CD** detector for charged particle detection (elastic,transfer & breakup)

Intensity of low lying γ transitions → σ_{ER}
$\Sigma\,\sigma_{E.R} = \sigma_{FUSION}$

Particle gamma coincidence for transfer angular distributions

Setups

Mumbai

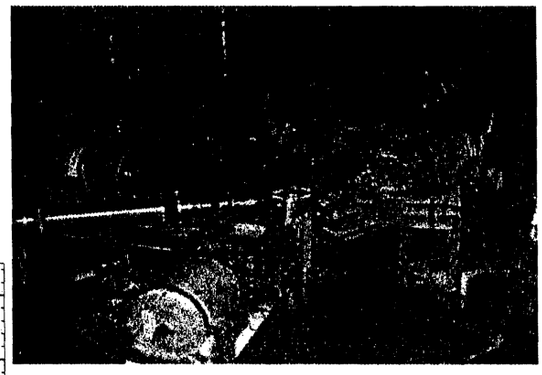

- 4 Compton suppressed Clovers
- 14 BGO Multiplicity setup

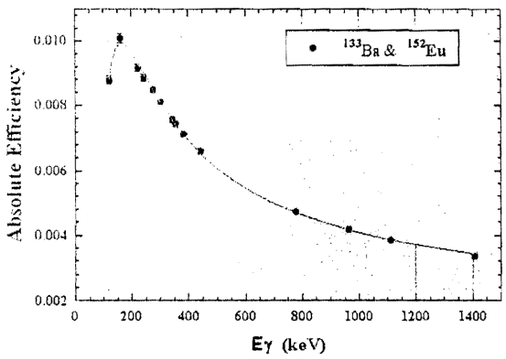

Setups

Caen

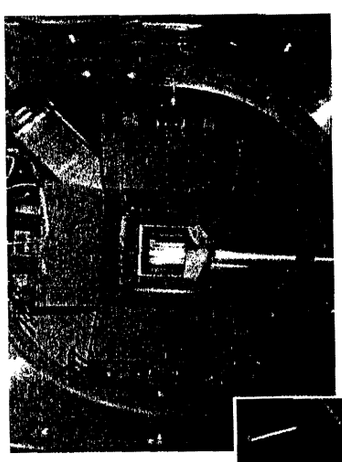

- 8 Clovers (5 big)
- Annular Si strip det. (16x16)
- Plastic det.
- Faraday cup

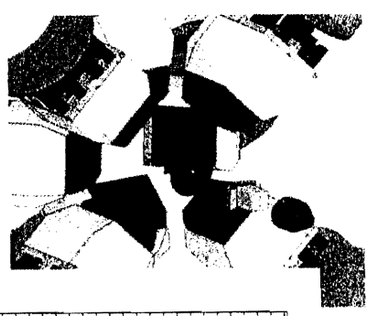

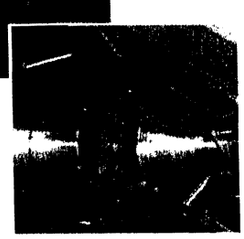

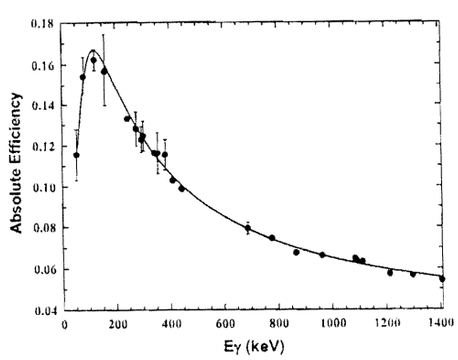

Target thicknesses

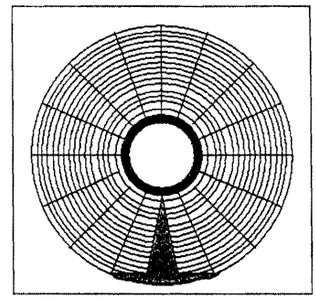

- Annular Si strip detector : 16*16

- Osmium thickness measurement:

  - ^{184}W target; known thickness 530μg/cm^2

  - Rutherford scattering peak + simulation ⇒ efficiency

  - $^{63}Cu+^{190}Os$
    0.78 +/- 0.16 mg/cm^2

  - $^{65}Cu+^{190}Os$
    1.04 +/- 0.21 mg/cm^2

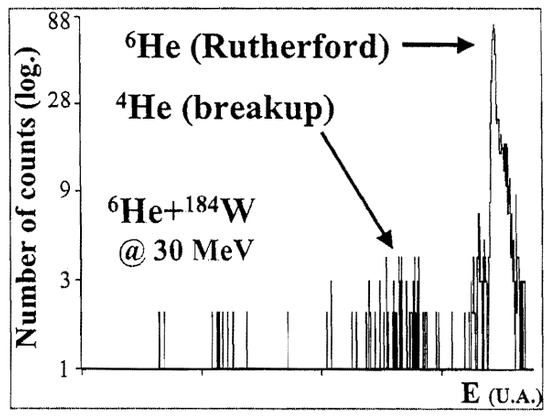

Results

- "First"? Singles γ -ray measurements with RIB to obtain fusion and transfer cross sections

- γ-rays observed in coincidence with charged particles → transfer, incomplete fusion...
- Dominance of $^{65,66}Cu$ for ^6He
  $^{63,64}Cu$ for ^8He

Cross sections obtained from the above γ-rays

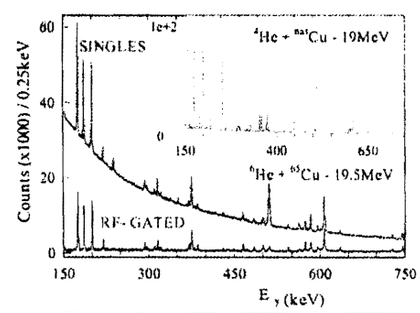

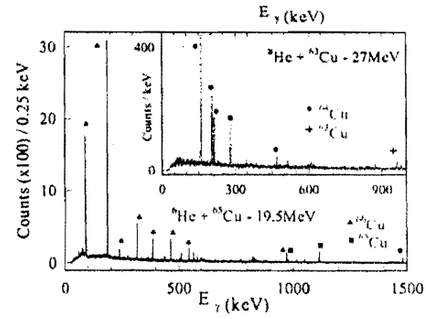

Results

- Comparison of evaporation residues with statistical model calculations (CASCADE with Ignatyuk level density formalism; a=A/9) for $^{4,6}He + ^{65}Cu$

- Good agreement for ***all*** channels in the case of $\alpha + ^{65}Cu$ but Large discrepancy in cross section for ^{66}Cu in $^{6}He+^{65}Cu$

Evidence for non compound nuclear process → transfer or other direct reaction channel contribution?

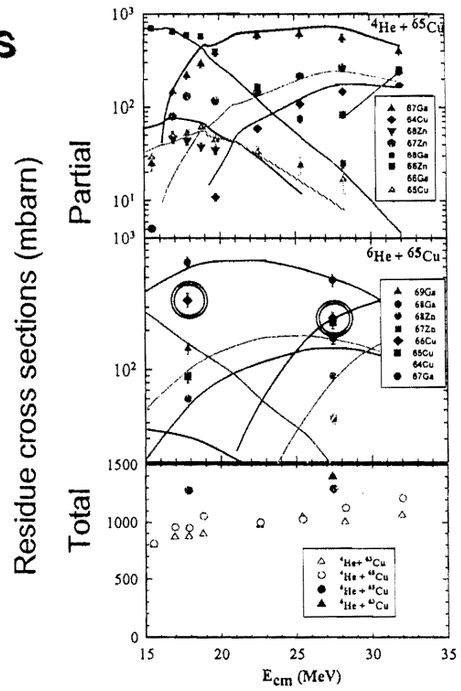

Results

Similarly for ^{4,6} He + ^{63}Cu

Larger cross-section for ^{64}Cu as compared to CASCADE: transfer to continuum, incomplete fusion ?...

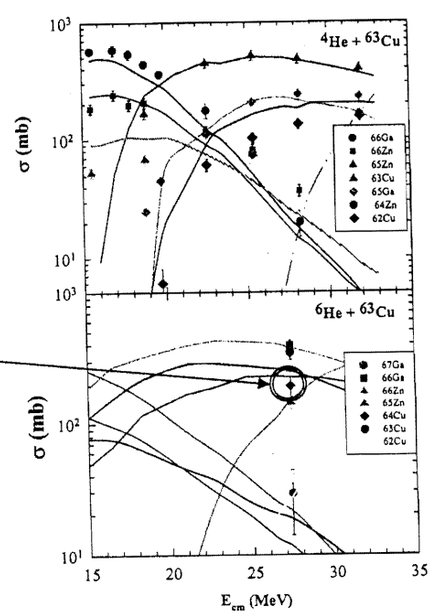

Particle – γ coincidence: ^{6}He

Transfer Q-value spectra; charged particle spectra gated by ^{65,66}Cu for ^{6}He

- Large spectroscopic factor of α+2n configuration for the g.s. of ^{6}He
- Observed Q-value spectra consistent with transfer, peaking at Q_{opt} ~0 as expected (^{6}He+^{65}Cu → α +^{67}Cu)
- Transfer (2n) to the continuum
  - → transfer followed by evaporation
  - → measured ratio of residues consistent with expectation:
    - $E^* >> S_{1n}$ → non-observation of ^{67}Cu
    - $E^* \sim S_{2n}$ → observation of ^{66}Cu
- Similarities of 2n transfer in ^{6}He and ^{8}He (except peak at low energy: α evaporation? 4n transfer ?...)

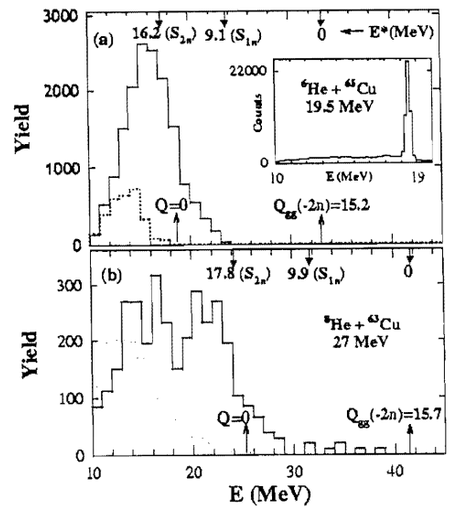

Cross sections

To obtain reaction cross section & relative contribution of transfer/BUF and breakup:

- Reaction cross sections obtained from elastic scattering angular distribution
- Larger reaction cross section for ^{6,8}He compared to α
- $\sigma_R - (\sigma_{fus} + \sigma_{trans}) = \sigma_{breakup}$

  $\sigma_{trans} \sim 1.5\ \sigma_{breakup}$

Direct evidence of relative large transfer cross-section with RIB near V_c *(335±50 mb at 19.5 MeV; 355±50 mb at 30 MeV)*

~ 30% compared to complete fusion (projectile + target)

→implications on issue of adding transfer/BUF to fusion for comparing with models.

→additional constraint on CC calculation?

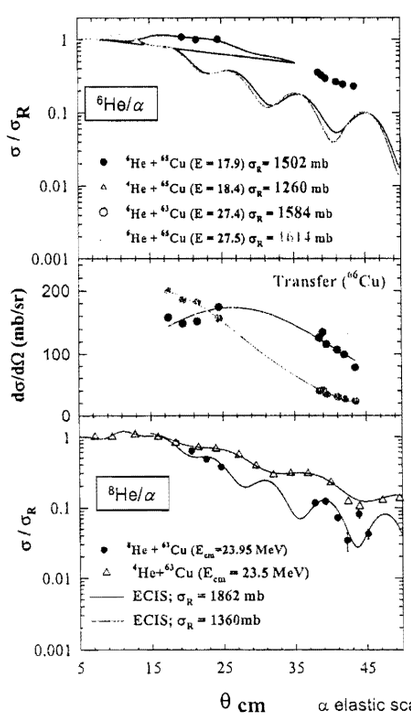

α elastic scattering NPA 147, 107 *(1970)*; NPA 388, 573 *(1982)*

What about Os ?

- Coulomb excitation of ^{190}Os
- spectra from charged particle-γ coincidences
- σ_{exp} = 300 +/- 28 +/- 60 mb
- σ_{COULEX} = 320 +/-30 mb
- further confirmation of target thickness

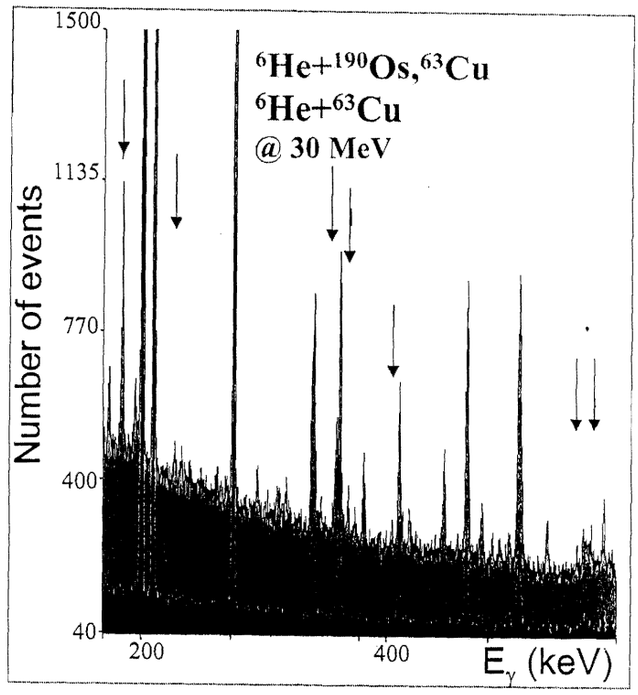

Extracting cross sections

- Single γ-ray spectrum at 30 MeV (Cu background subtracted)
- measurement of 3n and 4n channels
- correction for branching ratios, feeding, isomers (^{193}Pt), etc.

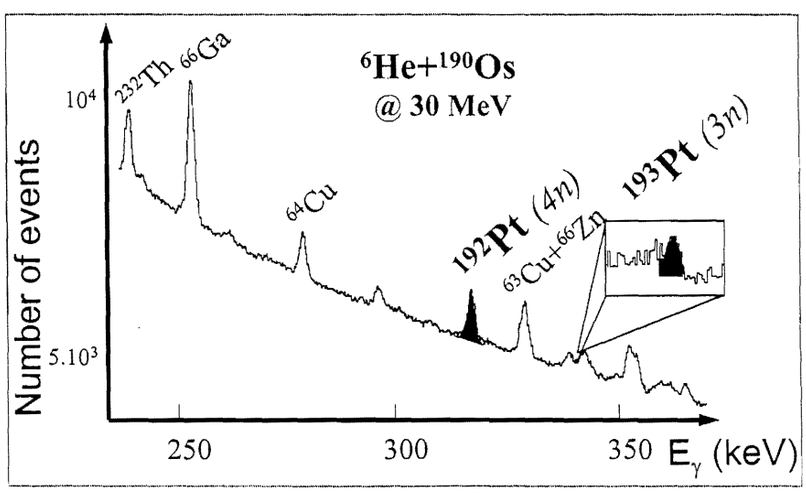

Extracting cross sections...

- 30 MeV results:

  - σ_{4n} ~ 345 +/-13 +/-69 mb
  - σ_{3n} ~ 62 +/-14 +/-12 mb

- systematical error obtained from the FWHM of the target thickness distribution obtained from each ring/sector pair ⇒ 20%

- 19.5 MeV results
  - voie 3n ultra dominant
  - σ_{3n} < 11 mb

Comparing cross sections...

- comparison ^{6}He / ^{4}He

- significant reduction of fusion cross section attributed to breakup of ^{6}He but large error bars especially at the barrier

- interpretation in terms of loss of flux

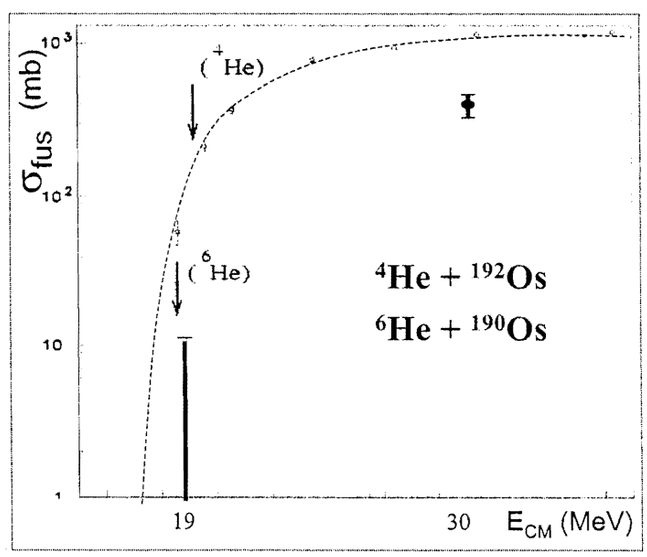

Summary on fusion involving ^{6,8}He

- Using fusion with RIBs is not obvious (background, intensities,etc.) Even more delicate for building an excitation function with a cyclotron
- ... but it works when triggering conditions, background,etc. are properly handled
- Fusion and transfer cross sections measured with γ -rays and Si strip with RIBs down to 10^7pps (^{6}He); 10^5pps is the lower limit (^{8}He)
- σ_{fus} strongly reduced below and above the barrier for ^{6}He as compared to ^{4}He. Large error bars...
- Interpreted in term of flux reduction due to ^{6}He breakup
- Separation of transfer and breakup thanks to γ-particle coincidences
- Large transfer cross section measured (larger than breakup)

Collaborators

A.Navin, V.Tripathi, C.Simenel, Y. Blumenfeld, J.M. Casandjian, G. de France,
D.Tai[illegible], A.Chatterjee, M Dasgupta, S. Kailas, [illegible] K. Mahata, ,
, K. Ramachandran, M. Rejmund, A. Shrivastava, , E.Tryggestad

BHABHA ATOMIC RESEARCH CENTER

Tata Institute of Fundamental Research | IPN, IN2P3-CNRS

CEA/ SACLAY | NSCL, MSU | Daresbury Lab

Many thanks !

Nano-second isomer spectroscopy of the ^{48}Ca region through deep-inelastic collisions

T. Ishii,[1,*] M. Asai,[1] A. Makishima,[2] M. Matsuda,[1] S. Ichikawa,[1] T. Kohno,[3] and M. Ogawa[3]

[1] *Japan Atomic Energy Research Institute, Tokai, Ibaraki 319-1195, Japan*
[2] *National Defense Medical College, Tokorozawa, Saitama 359-8513, Japan*
[3] *Tokyo Institute of Technology, Meguro, Tokyo 152-8550, Japan*

**Electronic address: ishii@popsvr.tokai.jaeri.go.jp*

We have measured γ rays from nano-second isomers produced in deep-inelastic collisions of 8.5 MeV/nucleon ^{48}Ca beams with a ^{198}Pt target at the JAERI tandem-booster facility. The γ rays from isomers were measured using an isomer-scope [1, 2], which detects projectile-like fragments by Si $\Delta E - E$ detectors and absorbs prompt γ rays emitting at the target by a tungsten γ-ray shield. Figure 1 shows a γ-ray spectrum setting the window for K isotopes on the $\Delta E - E$ plot. This instrument also allows us to identify the mass number as well as the atomic number of an isomer by ΔE distributions derived from γ-ray intensities.

In one-proton-hole nucleus of $^{47}_{19}$K$_{28}$, the $\pi f_{7/2} \rightarrow d^{-1}_{3/2} \rightarrow s^{-1}_{1/2}$ cascade transitions were observed from the decay of the $7/2^-$ isomer at 2020 keV with $T_{1/2} = 6.3(4)$ ns. The first excited $3/2^+$ state in ^{47}K was also found to be isomeric with $T_{1/2} = 1.1(3)$ ns. This transition is a very hindered l-forbidden $M1$ transition of $B(M1; 3/2^+ \rightarrow 1/2^+) < 5 \times 10^{-4}$ W.u. The isomer with $T_{1/2} = 13(2)$ ns was also found in ^{48}K and its level scheme was proposed.

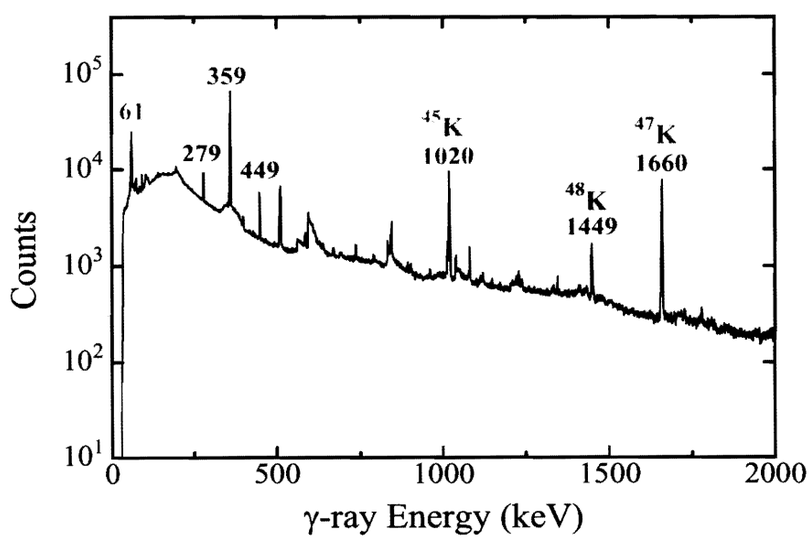

Figure 1: A γ-ray spectrum of K isotopes measured with the isomer-scope.

References

[1] T. Ishii *et al.*, Nucl. Instrum. Methods **A382**, (1997) 153.
[2] T. Ishii *et al.*, Phys. Rev. Lett. **83**, (2000) 39.

Nano-second isomer spectroscopy of the ^{48}Ca region through deep-inelastic collisions

T. Ishii, M. Asai, M. Matsuda, S. Ichikawa
Japan Atomic Energy Research Institut
A. Makishima
National Defense Medical College
T. Kohno, and M.Ogawa
Tokyo Institute of Technology

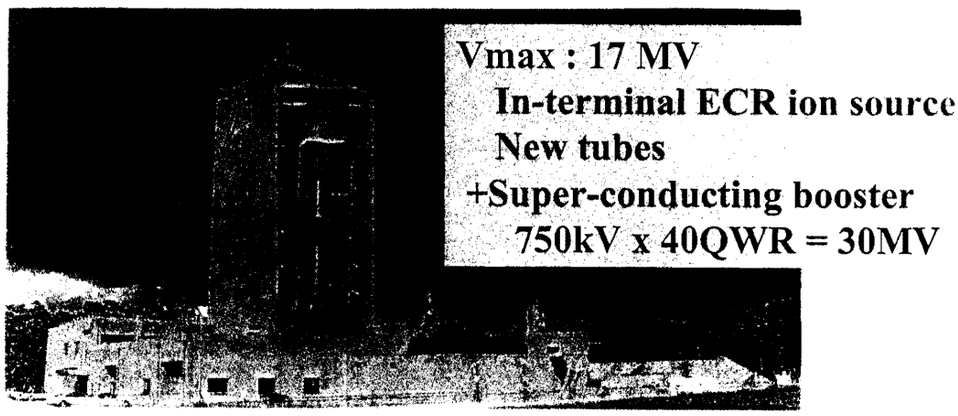

Experiments

1. Deep-Inelastic Collisions
   $^{48}Ca(8.5MeV/A)+^{198}Pt(4mg/cm^2)$

2. Isomer-scope : γ-shield + Si(ΔE-E) + Ge
   γ-rays from isomers with $T_{1/2}$>1ns
   identification of mass numbers
   in-plane/out-of-plane γ-ray anisotropies

Results

1. $^{47}_{19}K_{28}$ isomers
   $f_{7/2} \rightarrow d_{3/2}^{-1}$ *M2 transition*
   $d_{3/2}^{-1} \rightarrow s_{1/2}^{-1}$ *very hindered L-forbidden M1 transition*
   $< 2\times10^{-4}$ W.u.
2. $^{48}_{19}K_{29}$ level scheme

Isomer-scope

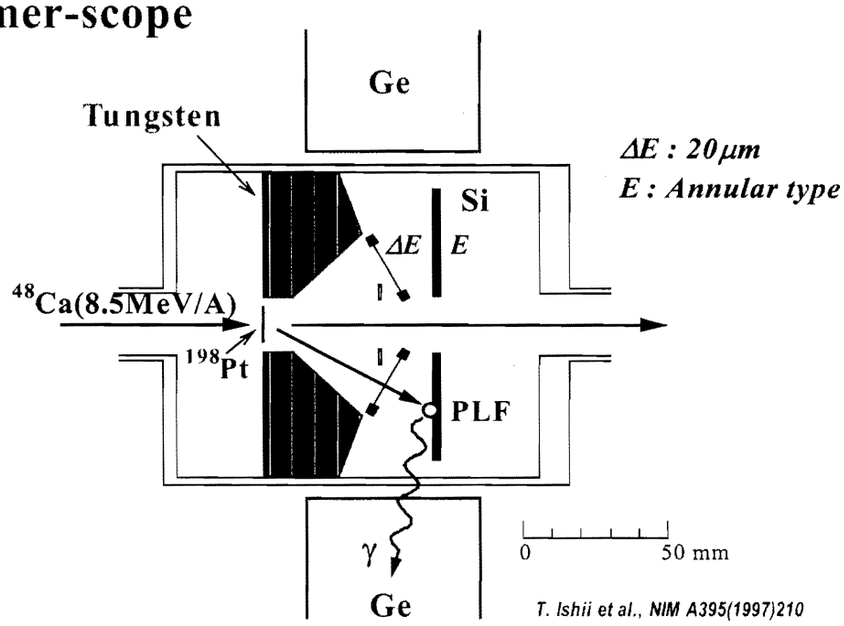

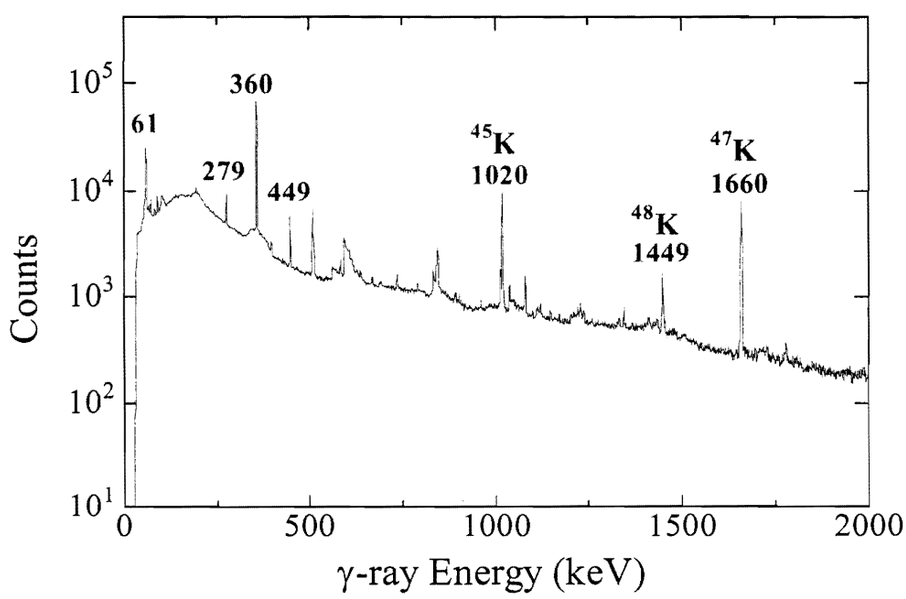

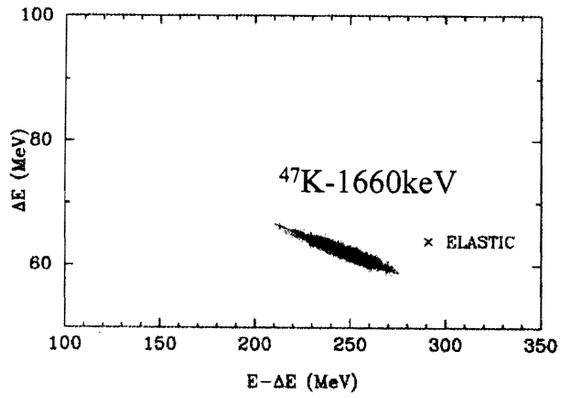
100
80
60
ΔE (MeV)
47K-1660keV
× ELASTIC
100
150
200
250
300
350
E−ΔE (MeV)

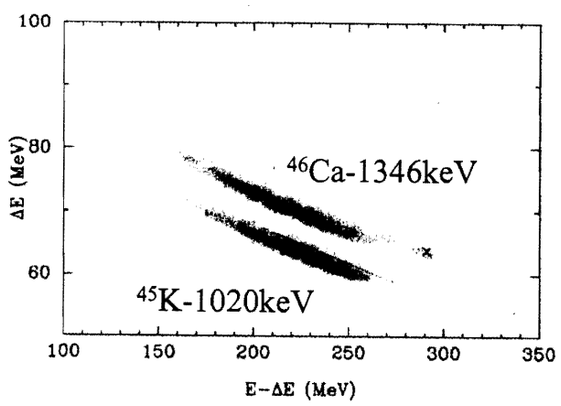
100
80
60
ΔE (MeV)
46Ca-1346keV
45K-1020keV
100
150
200
250
300
350
E−ΔE (MeV)

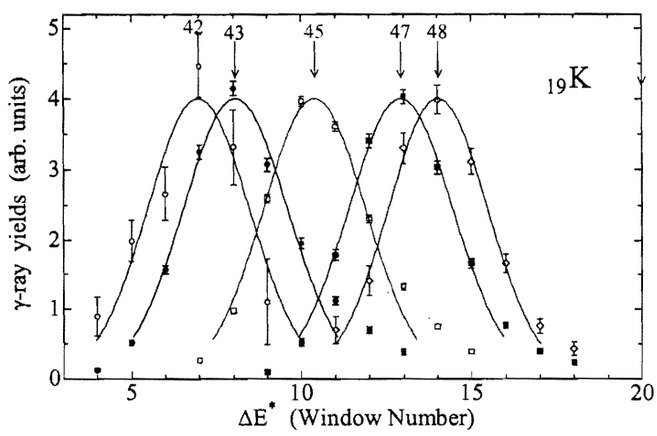
42
43
45
47
48
19K
γ-ray yields (arb. units)
0
1
2
3
4
5
5
10
15
20
ΔE* (Window Number)

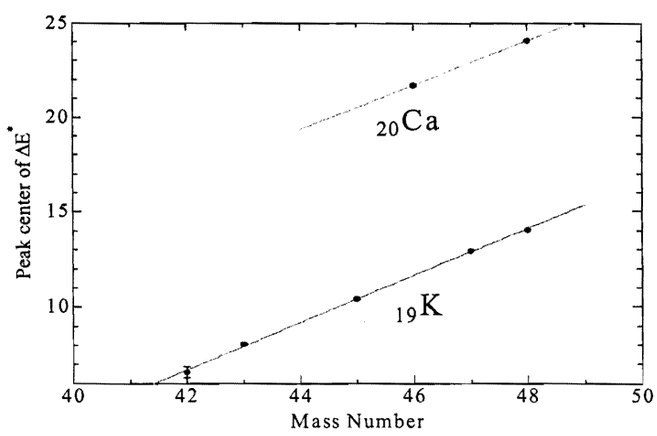
25
20
15
10
Peak center of ΔE*
20Ca
19K
40
42
44
46
48
50
Mass Number

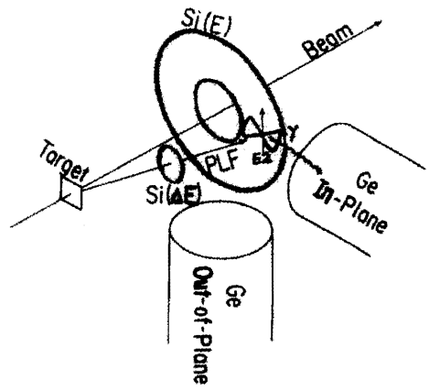
Si(E)
Beam
Target
PLF
Si(ΔE)
Ge
In-Plane
Ge
Out-of-Plane

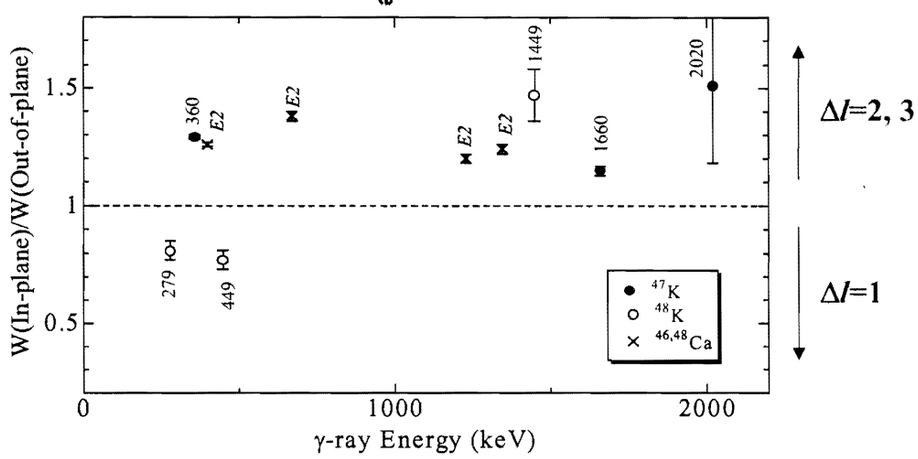
W(In-plane)/W(Out-of-plane)
1.5
1
0.5
0
1000
2000
γ-ray Energy (keV)
360
E2
E2
E2
E2
1449
1660
2020
279
449
47K
48K
46,48Ca
ΔI=2, 3
ΔI=1

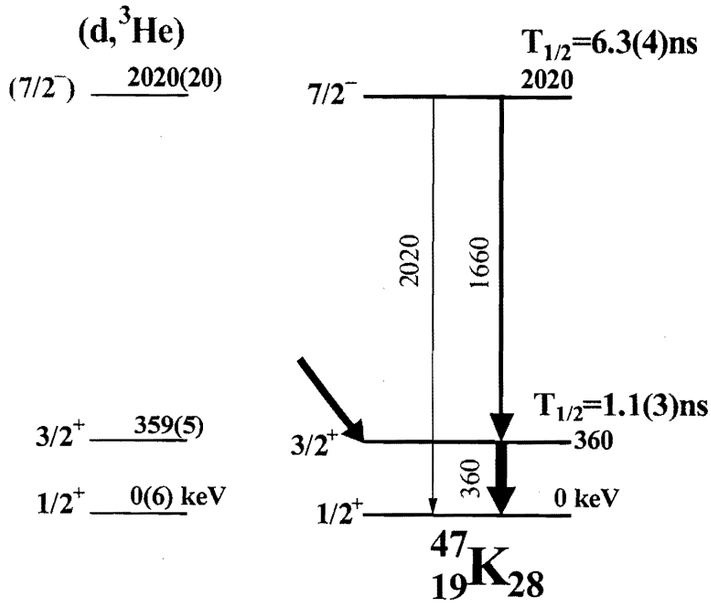
(d,3He)
(7/2−) 2020(20)
3/2+ 359(5)
1/2+ 0(6) keV
7/2− 2020
T1/2=6.3(4)ns
2020
1660
3/2+ 360
T1/2=1.1(3)ns
360
1/2+ 0 keV
47 19K28

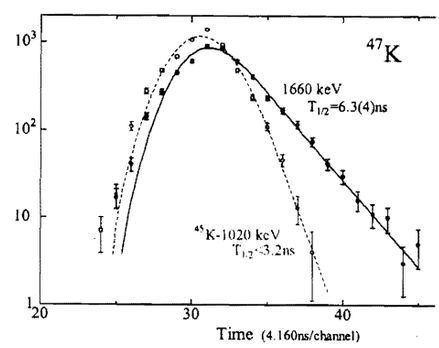
47K
1660 keV
T1/2=6.3(4)ns
45K-1020 keV
T1/2<3.2ns
Time (4.160ns/channel)

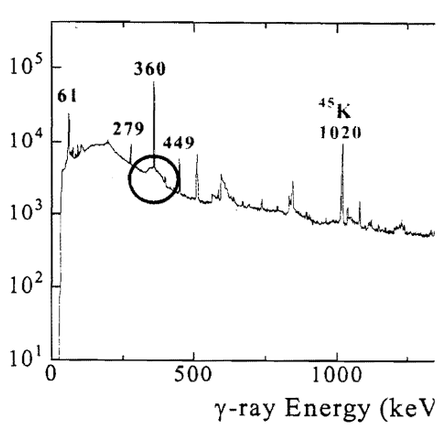
61
360
279
449
45K
1020
0
500
1000
γ-ray Energy (keV

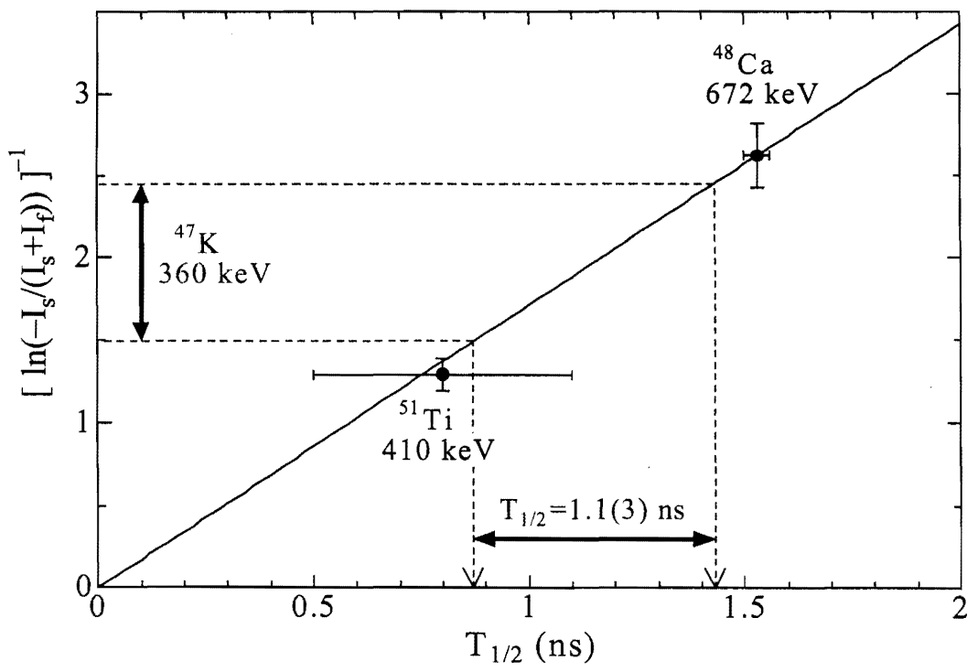

L-forbidden M1 transitions near doubly magic nuclei

		B(M1) μ_N^2
$^{47}_{19}K_{28}$	$d_{3/2}^{-1} \rightarrow s_{1/2}^{-1}$	$< 9 \times 10^{-4}$
$^{49}_{21}Sc_{28}$	$d_{3/2}^{-1} \rightarrow s_{1/2}^{-1}$	$7(2) \times 10^{-4}$
$^{39}_{19}K_{20}$	$s_{1/2}^{-1} \rightarrow d_{3/2}^{-1}$	0.025(3)
$^{207}_{81}Tl_{126}$	$d_{3/2}^{-1} \rightarrow s_{1/2}^{-1}$	0.022(5)
$^{209}_{83}Bi_{126}$	$f_{7/2} \rightarrow h_{9/2}$	$3.8(4) \times 10^{-3}$

A. Arima and L.J. Huang-Lin, PL 41B(1972)429

$Y^{(2)} \times s$ core polarization

meson exchange

cancellation

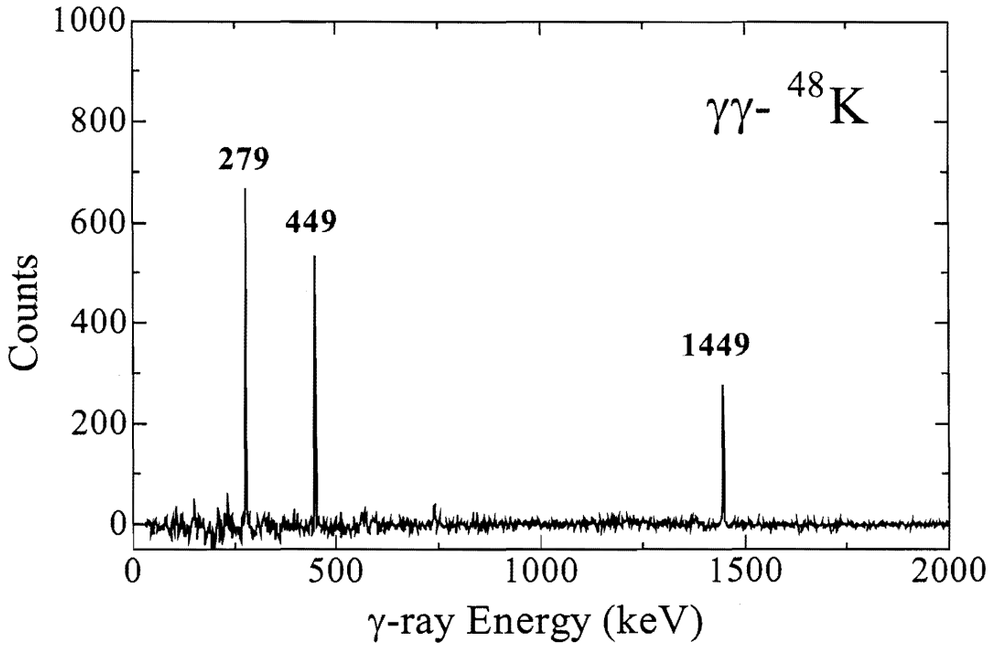
γγ- 48K
279
449
1449
Counts
γ-ray Energy (keV)

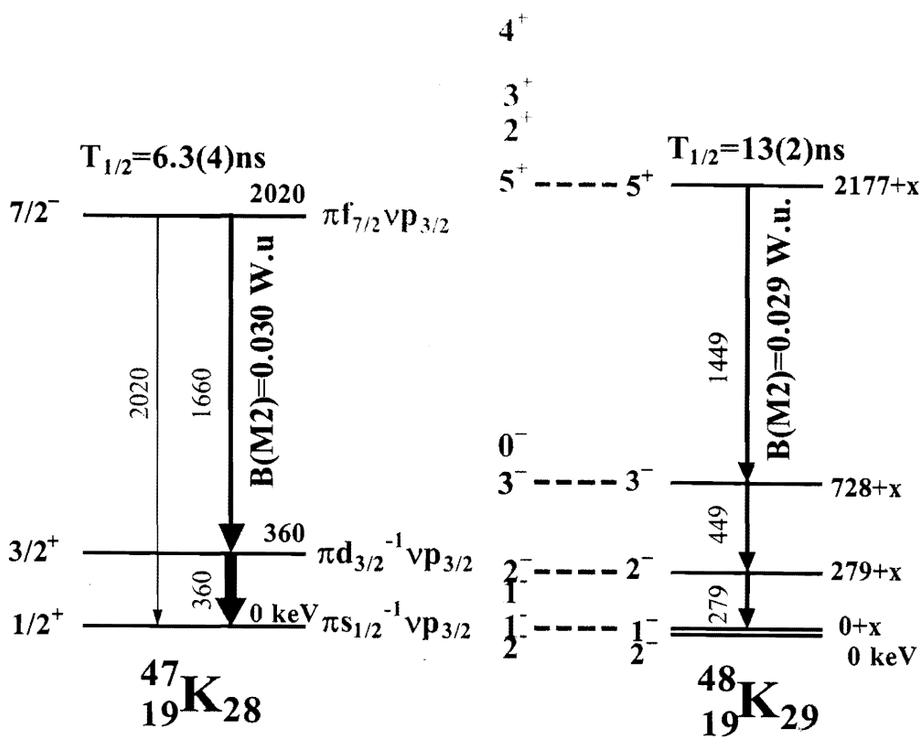
T1/2=6.3(4)ns
7/2−
2020
πf7/2νp3/2
2020
1660
B(M2)=0.030 W.u
3/2+
360
πd3/2-1νp3/2
360
1/2+
0 keV
πs1/2-1νp3/2
47 19K28
4+
3+
2+
5+
5+
T1/2=13(2)ns
2177+x
1449
B(M2)=0.029 W.u.
0−
3−
3−
728+x
449
2−
2−
279+x
279
1−
1−
2−
2−
0+x
0 keV
48 19K29

Summary

- Using ^{48}Ca beams and the isomer-scope, ns-isomers in ^{47}K and ^{48}K were found.

- The L forbidden $\pi d_{3/2} \rightarrow s_{1/2}$ M1 transition in ^{47}K is very hindered (< 1/2000 W.u.).

- A level scheme of ^{48}K is proposed.

SPECTROSCOPY OF LEAD AND TRANS-LEAD NUCLEI USING AN EVAPORATION RESIDUE DETECTOR [+#]

W. Reviol

Chemistry Department, Washington University, St. Louis, MO 63130, USA

The spectroscopy of light lead nuclei and of Z > 82 nuclei produced in fusion evaporation reactions is hampered by the presence of a large fission background. In particular the in-beam spectroscopy of these species requires a "filter" or "tag" to separate the gamma rays of the evaporation residues from those of the fission products and other sources of background. There are several solutions to this problem, among them the direct detection of the evaporation residues by time-of-flight and pulse height with a dedicated detection system.

The Washington University group has built a detection system for evaporation residues consisting of 64 fast plastic scintillator detectors arranged in four angular rings. Its main characteristics are a large solid angle coverage, a high granularity, and a fast timing. The detection system is called HERCULES, an acronym that stands for "High Efficiency Residue Counter Under Lots of Elastic Scattering", and it is optimized for experiments in conjunction with the Gammasphere array.

For the commissioning run of the Gammasphere plus HERCULES combination, the ^{48}Ti + ^{142}Nd reaction at two different beam energies near the Coulomb barrier has been used. In this experiment, new spectroscopic information on yrast and near-yrast states in the very neutron deficient nuclei ^{186}Pb and ^{186}Tl has been obtained which were populated in the 4n and 3pn fusion-evaporation exit channels, respectively [1].

The talk will cover (i) a description of the HERCULES system and its performance, (ii) a presentation of the physics results from the commissioning run, and (ii) a very brief outlook for spectroscopic studies in the actinide region.

[+] In collaboration with D.G. Sarantites, C.J. Chiara, O. Pechenaya, and L.G. Sobotka.

[#] Work supported by US DOE.

[1] W. Reviol, et al., Phys. Rev. C **68**, 054317 (2003).

Spectroscopy of Lead and Trans-Lead Nuclei using an Evaporation Residue Detector

W. Reviol, D.G. Sarantites, C.J. Chiara, O. Pechenaya, J. Elson, and L.G. Sobotka
Washington University, St. Louis, Missouri, USA

"Frontier of gamma-ray spectroscopy and its application"
RIKEN, Wako, Saitama, Japan, March 18-19, 2004

03/18/04 1

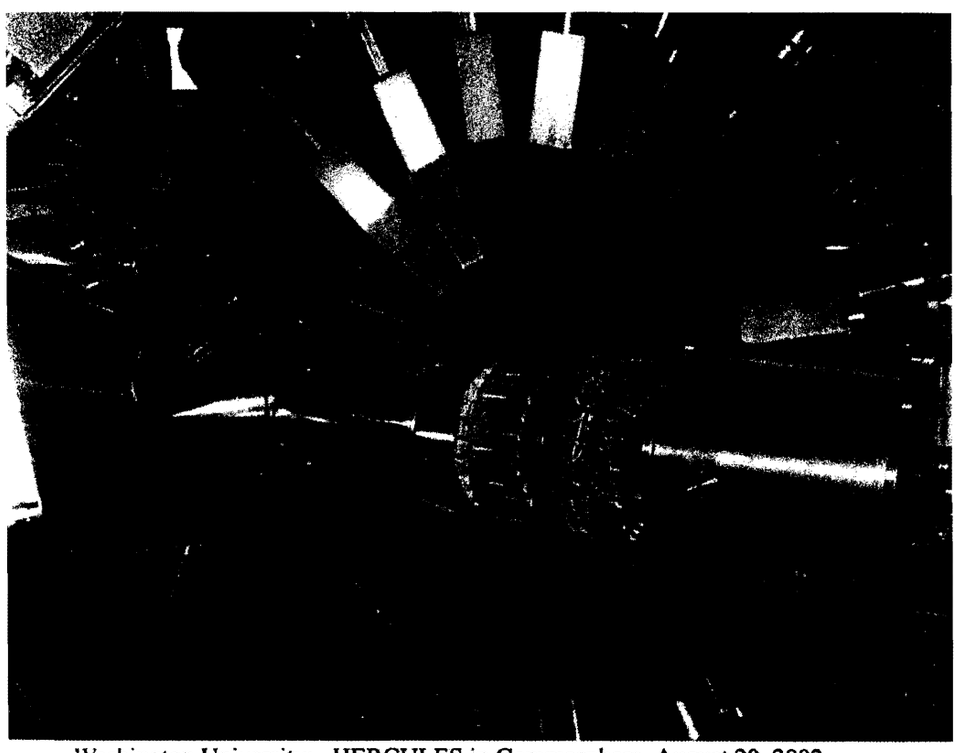

Washington University: HERCULES in Gammasphere, August 20, 2002

03/18/04 2

Detailed spectroscopy in actinides and light lead nuclei...

Problems:

- ~ A 100 mb fusion cross section but > 95 % of it lost in the fission channel;
  + ~ 500mb Coulex and transfer.
- Inner ball gating on multiplicity of evaporated protons, α's or neutrons is not selective (too many channels are open).
- Z-identification of residues by ΔExE (ion. chamber) does not work either.

*A **"tag"** is needed!*

Solutions (plural!):

- **Recoil mass separation and Recoil Decay Tagging.**
  - Clean spectra – low cross sections – good identification capabilities!
    Limitations due to spectrograph angular acceptance:
    Low efficiency and choice of beam-target combination.
  - Limited applicability of RDT (500 ns ≤ $t_{1/2}(\alpha)$ ≤ 500 μs).
- **Direct residue detection by ToF and Pulse Height. (HERCULES)**
  - Limitation due to presence of elastic scattering: "somewhat dirty".
  - Almost no identification capability.
- **Isomer Tagging near the target.**
  - Applicability limited and no identification capability..

Design Considerations for HERCULES

- Fabrication of thin (1.0 mg/cm^2) and uniform plastic foils: *(Stop only the ER's)*
  - *(2.5 mg/cm^2 to stop Fission Fragments)*
- Response of scintillators to heavy evaporation residues: *(Ensure high trigger efficiency a low E_{kin} and high Z)*
- Radiation damage from elastics: *(Control loss in pulse height, compensate for it)*
- Fast electronics recovery: *(Achieve full recovery in 10 ns)*
- High segmentation in the array: *(Reduce rate in each detector)*
- Geometry: *(Must have ERs reach the detector before next beam burst)*

Parameters →

Ring	# Dets	Angular Range	Msr/Ring
1	8	3.2° – 7.1°	41.3
2	14	7.1° – 11.2°	73.8
3	18	11.2° – 15.2°	102.6
4	24	15.2° – 19.1°	128.4

Scintillator - Photomultiplier System (Front View)

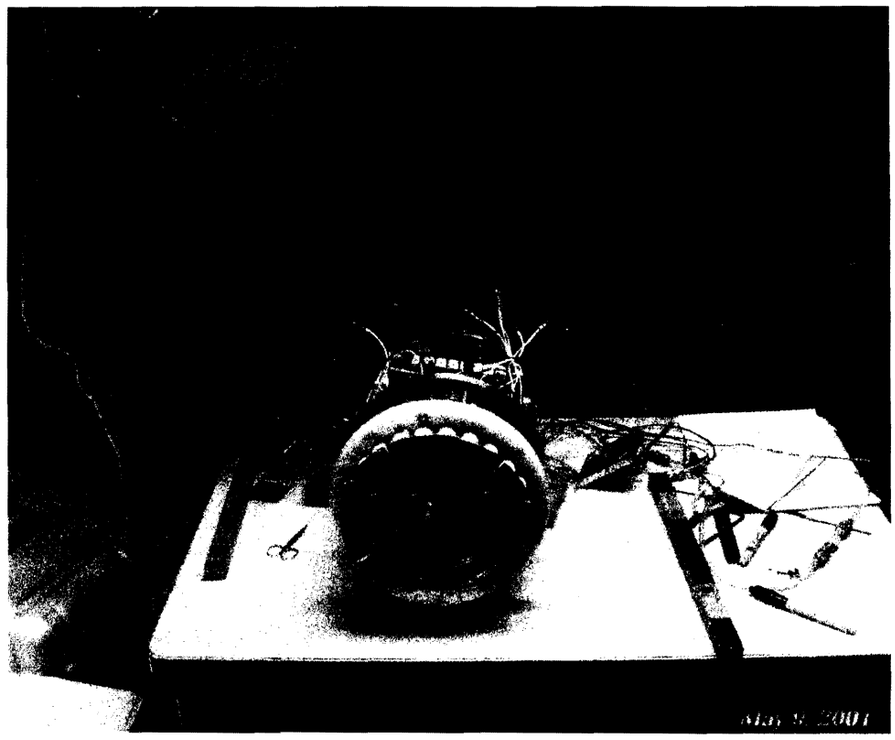

64 det's in four rings

03/18/04

Source Measurements

- **^{252}Cf: H.F. = Ba-like (Z=56), L.F. = Mo-like (Z=42)**
- **Detector thickness 0.97 to 2.5 mg/cm^2.**
  - Spin coating, uniformity ~1% !
- **Light output as a function of Z and E**
  - Source plain and with Al degrader foils from 0.25 → 2.92 mg/cm^2 : $E_{incident}$ = 82 – 6 MeV.
- **Identification of HF and LF for whole E range.**
  - Measured Pulse height and ToF at 20 cm source-detector distance
  - Use CsF γ-detector as trigger.

Light Output Measurements with ^{252}Cf Source

HF: like ^{146}Ba, LF: like ^{106}Mo,
(Detector to Source dist.=20 cm)

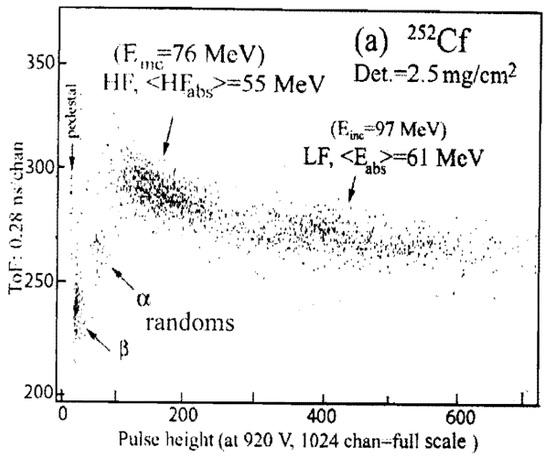

No degrader

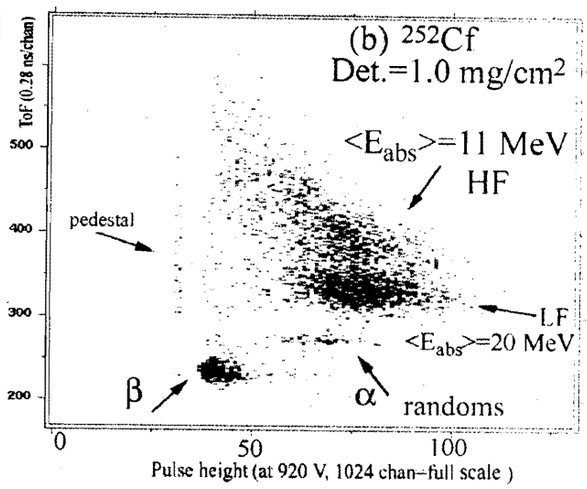

Al degrader
(2.36 mg/cm^2)

03/18/04

7

Light Output as a Function of E and Z

Energy of Fragments -- Al degraders 0.15 - 2.88 mg/cm^2

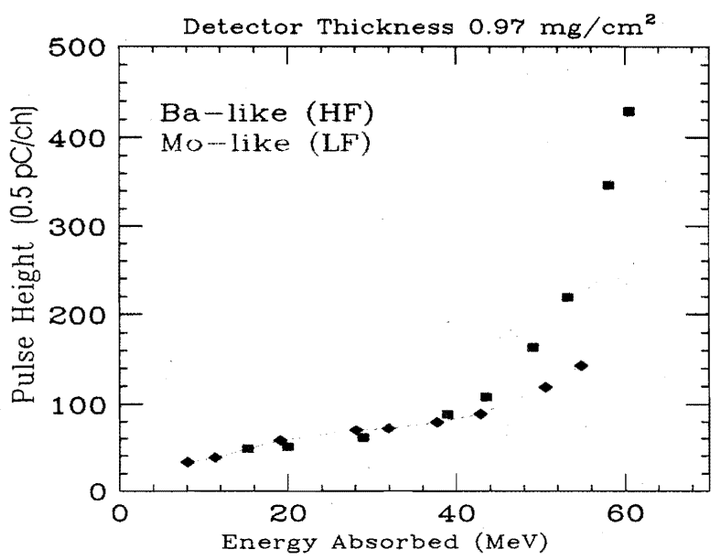

Overlap for E < 40 associated with dE/dx versus E behavior below the Bragg-peak.
dE/dx decreases with decreasing E but quenching of light output decreases also (Z-dependence of quenching disappears).

03/18/04

8

Accelerator Experiments

- **Response to Heavy Evapor. Residues (6 hrs).**
  - Elastic Scattering of 160 MeV ^{197}Au on ^{197}Au (ATLAS). Prototype HERCULES detectors at angles $5^o < \Theta_{lab} < 120^o$, Si detectors at symmetric angles. See also ^{252}Cf source measurements!

- **Radiation Damage by Scattered Beam (2 d).**
  - $^{40}Ar + ^{170}Er$ at 210 MeV and 5 pnA (ATLAS). Prototype HERCULES detectors at 5° and 9°.

- **Test Run at Gammasphere (1 d).**
  - $^{48}Ca + ^{126}Te$ at 210 MeV (88-Inch). Full HERCULES device and 100 Compton-suppressed Ge detectors.

- **Commissioning Run at Gammasphere (6 d).**
  - For set up: $^{48}Ti + ^{126}Te$ at 230 and 238 MeV (6 hrs).
  - $^{48}Ti + ^{142}Nd$ at 230 and 238 MeV (88-Inch). Targets with various thicknesses. Blocked the first ring for $\theta \leq 6^o$. Trigger: γ [4].

Radiation Damage of the Scintillators

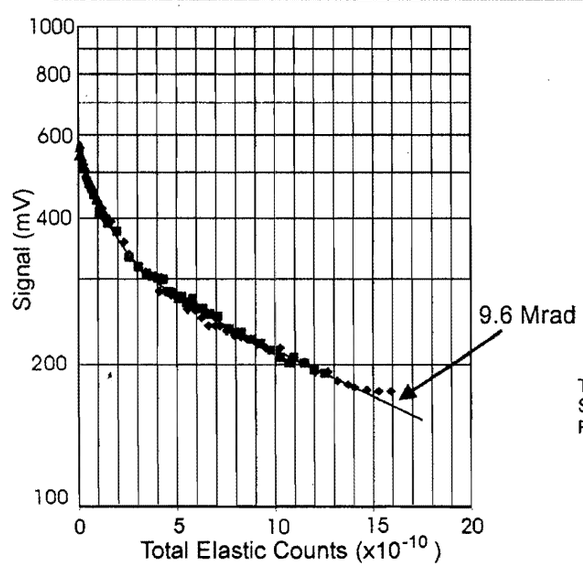

Elastic Scattering
210 MeV $^{40}Ar + ^{170}Er$
3 Detectors, 1 mg/cm^2

Triangles: Detector Position Ring 2
Squares, Diamonds: Position Ring 1
Fit: Sum of two Exponentials

Loss in Pulse Height depends on Integrated Dose
Ring 1 Detectors "last" for several days

The Commissioning Run for HERCULES at Gammasphere

A series of experiments were carried out at the 88-Inch Cyclotron at LBNL in a 6 day run:

(1) 215-MeV $^{48}Ti+^{126}Te$ (0.74 mg/cm^2 on 0.3 mg/cm^2 Au).
(2) 238-MeV $^{48}Ti+^{126}Te$ (same target).
(3) 230-MeV $^{48}Ti+^{142}Nd$ (1.1 mg/cm^2 ; 0.16, 0.48 mg/cm^2 Au).
(4) 230-MeV $^{48}Ti+^{142}Nd$ (0.46 mg/cm^2 ; 0.1, 0.37 mg/cm^2 Au).
(5) 238-MeV $^{48}Ti+^{142}Nd$ (same target).
(6) 238-MeV $^{48}Ti+^{142}Nd$ (1.0 mg/cm^2 ; 0.84 mg/cm^2 Au **target stack).**

The Setup:

HERCULES at 31 cm from the target; 5.6° - 19.1° coverage. **Gammasphere** with 102 detectors. Trigger: γ^4.

The nuclei of interest: $^{186}Pb+4n$ and $^{186}Tl+p3n$.

The Bass fusion cross section is ~ 180 mb and the evaporation residue (ER) cross section is ~ 1 mb. The ER's are selected by Time of Flight and Pulse Height.

$^{48}Ti+^{126}Te$ at 238 MeV
(0.74 mg/cm^2 Au backing)

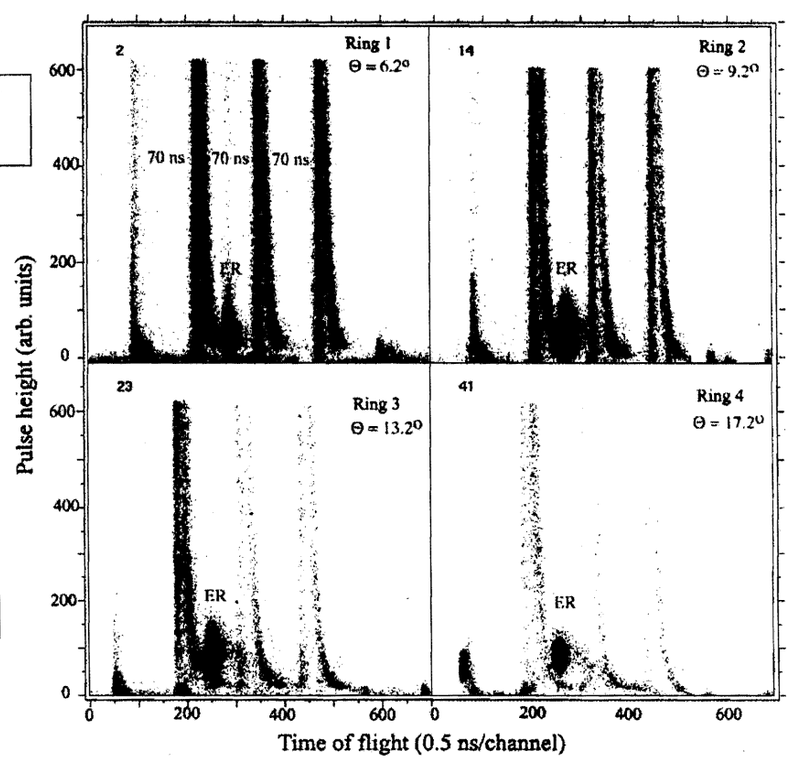

ER cross section ~100 mb

$^{48}Ti+^{142}Nd$ at 230 MeV
(0.46 mg/cm^2 Au backing)

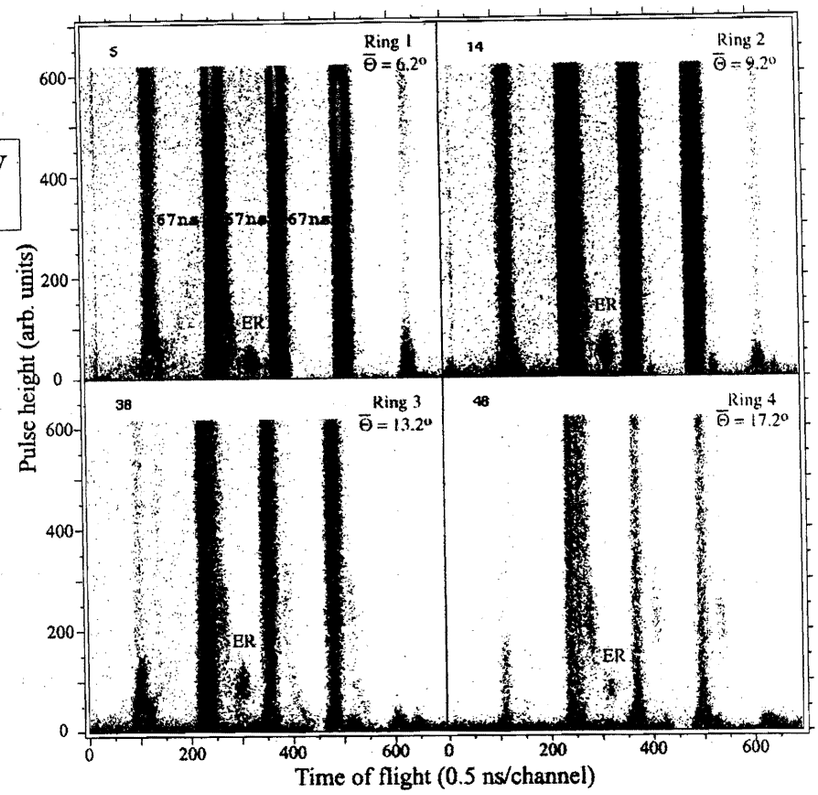

ER cross section ~1 mb

03/18/04

13

Angular Distributions
of Evap. Residues
(Diff. Reaction Channels)

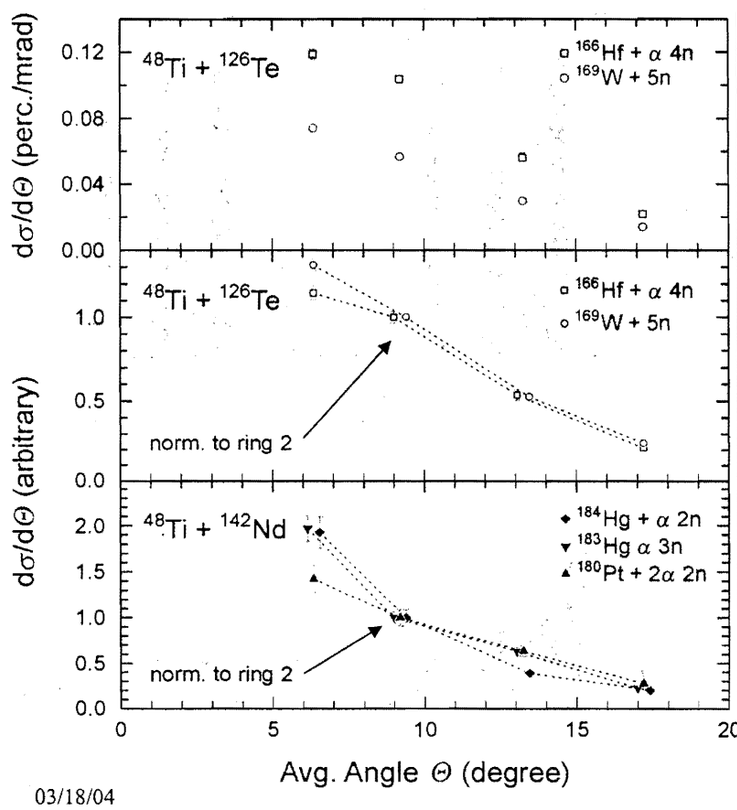

E_{lab}=238 MeV
0.74 mg/cm^{2}126Te
+ 0.3 mg/cm^2 Au

Elab=238 MeV
0.46 mg/cm^2 ^{142}Nd
+0.37 mg/cm^2 Au

03/18/04

14

$^{48}Ti + ^{142}Nd$
@ 230, 238 MeV

The Power of HERCULES

The Power of Gammasphere

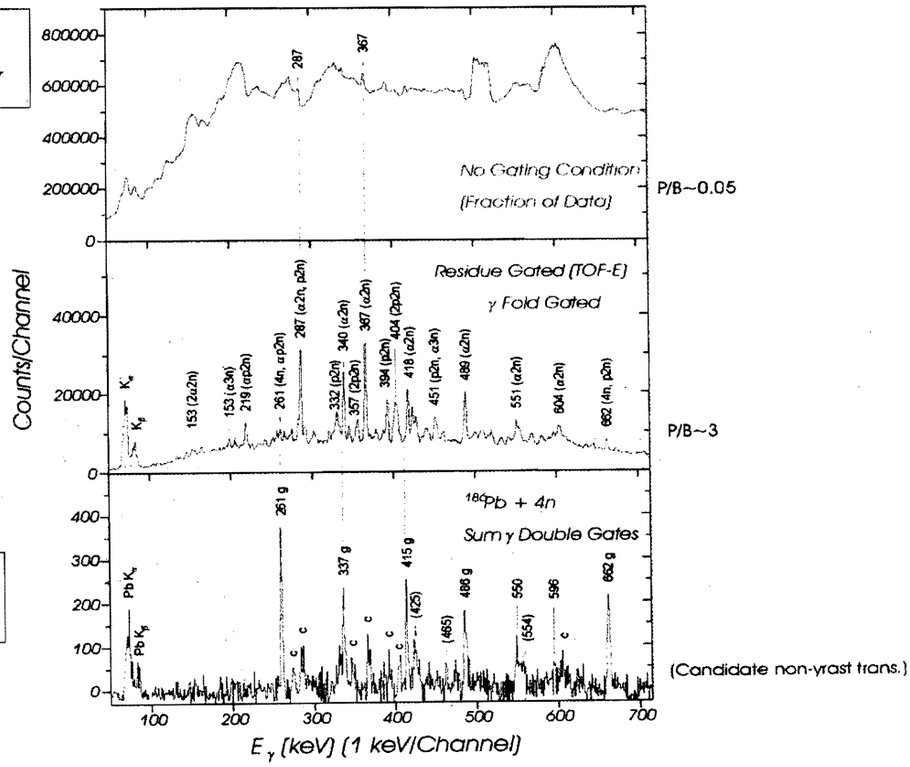

03/18/04

15

Coincidence Spectra
$^{186}Tl + p3n$

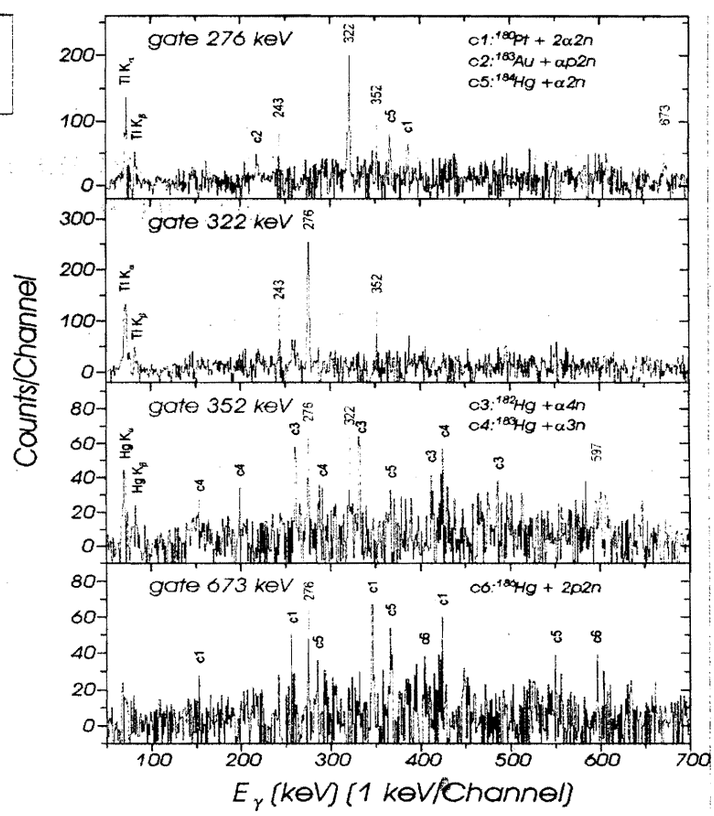

Only the **276** and **322** keV trans. were previously known (Kreiner et al. PRL 47 (1981).

03/18/04

16

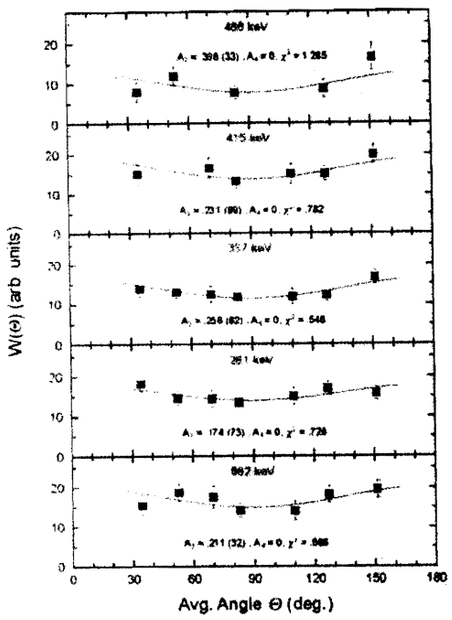

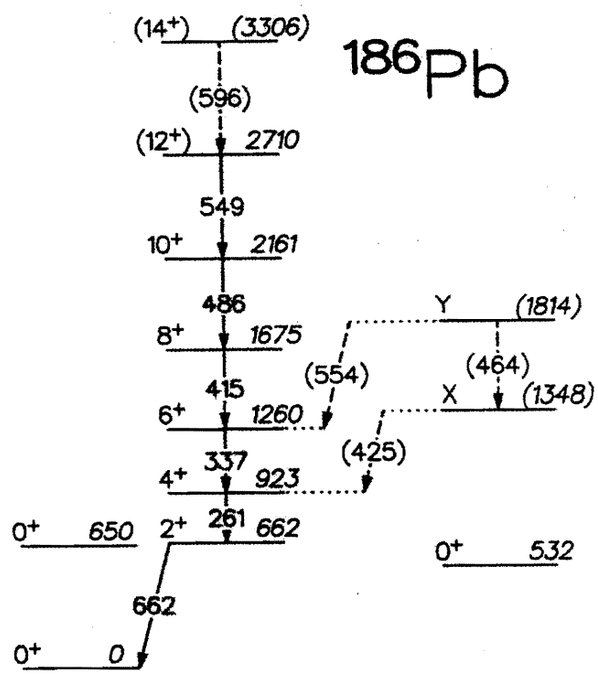

^{186}Pb candidate non-yrast transitions: "minimum" conclusion

- The 425- and 554-keV transitions carry at most 10% relative intensity each.
- Any non-yrast structure in ^{186}Pb is by at least one order of magnitude weaker populated than the yrast band.

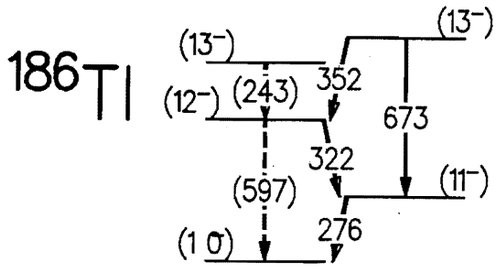

E_γ(keV)	A_2/A_0
243	-0.07 (17)
352	-0.25 (18)
322	0.02 (16)
276	-.038 (40)

Certain: multipolarities
Uncertain: bottom spin

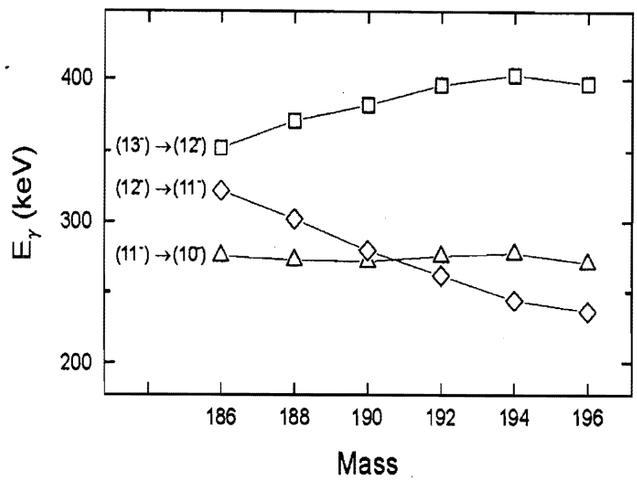

$\pi\, h_{9/2} \otimes \nu\, i_{13/2}$ (oblate)

A brief outlook.....

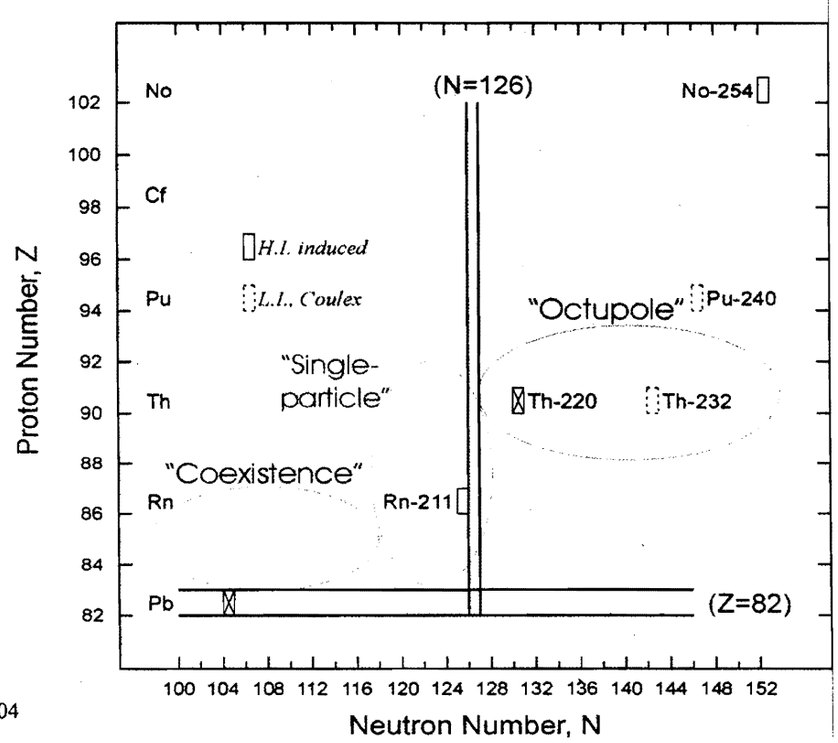

Compound Nucleus: 226Th	Typical Product of Interest
22Ne + 204Hg	222Th + 4n
18O + 208Pb	

Compound Nucleus: 224Th	
48Ca + 176Yb	220Th + 4n
26Mg + 198Pt	
22Ne + 202Hg	
20Ne + 204Hg	
19F + 205Tl	
18O + 206Pb	
16O + 208Pb	

Compound Nucleus: 222Th	
86Kr + 136Xe	218Th + 4n
48Ca + 174Yb	
36S + 186W	
30Si + 192Os	
26Mg + 196Pt	
24Mg + 198Pt	
22Ne + 200Hg	
21Ne + 201Hg	
20Ne + 202Hg	
19F + 203Tl	
18Ne + 204Hg	
17F + 205Tl	
16O + 206Pb	
14O + 208Pb	

Summary and Conclusion

- Presented a detailed description of the **HERCULES** detector system.
- Showed that **HERCULES** performs in experiments at **Gammasphere** as expected and presented first results from its commissioning run (^{186}Pb, ^{186}Tl).
- **^{186}Pb**: Established E2 character of prolate yrast band and saw candidate non-yrast states.
- **^{186}Tl**: Observed low-lying weakly-deformed (oblate) structure.
- For **detailed spectroscopy** in the presence of a large fission background, various, complimentary methods and setups are needed!

Instability of nuclear wobbling motion and phase transition to tilted axis rotation

Masayuki Matsuzaki and Shin-Ichi Ohtsubo

Department of Physics, Fukuoka University of Education, Munakata, Fukuoka 811-4192, Japan

We study a possible correspondence between the softening of the wobbling mode and the "phase transition" of the one-dimensionally rotating mean field to a three-dimensionally rotating one by comparing the properties of the wobbling mode obtained by the one-dimensional cranking model + random phase approximation with the total routhian surface obtained by the three-dimensional tilted-axis cranking model.

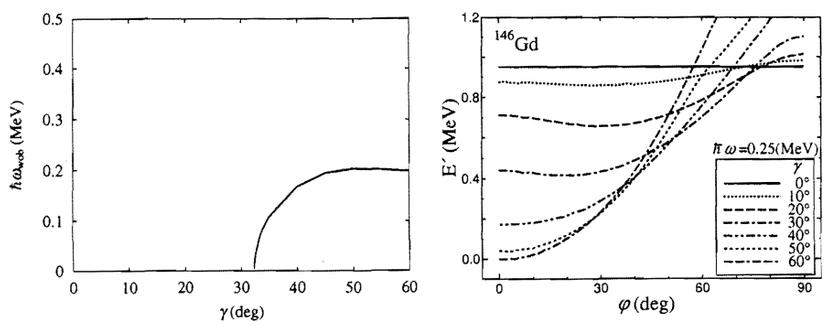

Figure 1: Left: triaxiality dependence of excitation energy of the wobbling motion, right: cross sections at the x-y plane of the energy surfaces of the $[(\nu h_{9/2}, f_{7/2})^2(\pi h_{11/2})^2]_{16^+}$ four quasiparticle configuration in ^{146}Gd, calculated at $\hbar\omega_{\rm rot} = 0.25$ MeV with $\epsilon_2 = 0.19$, $\Delta_n = 0.8$ MeV, and $\Delta_p = 0.6$ MeV.

The anharmonicity in the observed wobbling mode in ^{163}Lu is also analyzed.

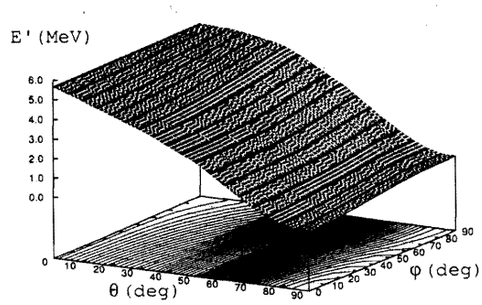

Figure 2: Energy surface of the triaxial superdeformed configuration in ^{163}Lu as a function of the tilting angle (θ, φ) calculated at $\hbar\omega_{\rm rot} = 0.5$ MeV with $\epsilon_2 = 0.43$, $\gamma = 20°$, and $\Delta_n = \Delta_p = 0.3$ MeV. The interval of contours is 100 keV.

Instability of nuclear wobbling motion and phase transition to tilted axis rotation

Masayuki Matsuzaki, Shi-Ichi Ohtsubo

Introduction

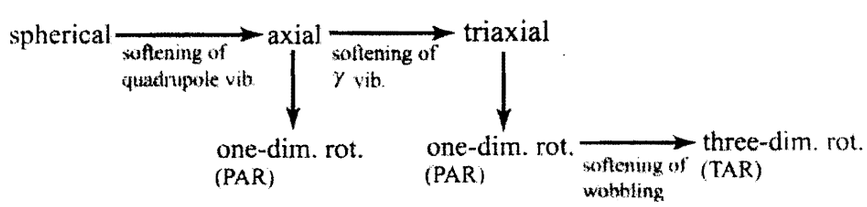

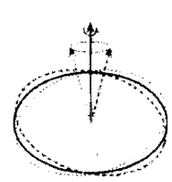

Wobbling motion in terms of RPA

- RPA based on cranking model (à la Marshalek) gives wobbling motion:
  - excitation energy (in rotating frame)

$$\hbar\omega_{\rm wob} = \hbar\omega_{\rm rot}\sqrt{\frac{(\mathcal{J}_x - \mathcal{J}_y^{(\rm eff)}(\omega_{\rm wob}))(\mathcal{J}_x - \mathcal{J}_z^{(\rm eff)}(\omega_{\rm wob}))}{\mathcal{J}_y^{(\rm eff)}(\omega_{\rm wob})\mathcal{J}_z^{(\rm eff)}(\omega_{\rm wob})}}$$

  - dynamical inertia $\mathcal{J}_y^{(\rm eff)}(\omega_{\rm wob})$, $\mathcal{J}_z^{(\rm eff)}(\omega_{\rm wob})$

Instability of wobbling (^{146}Gd)

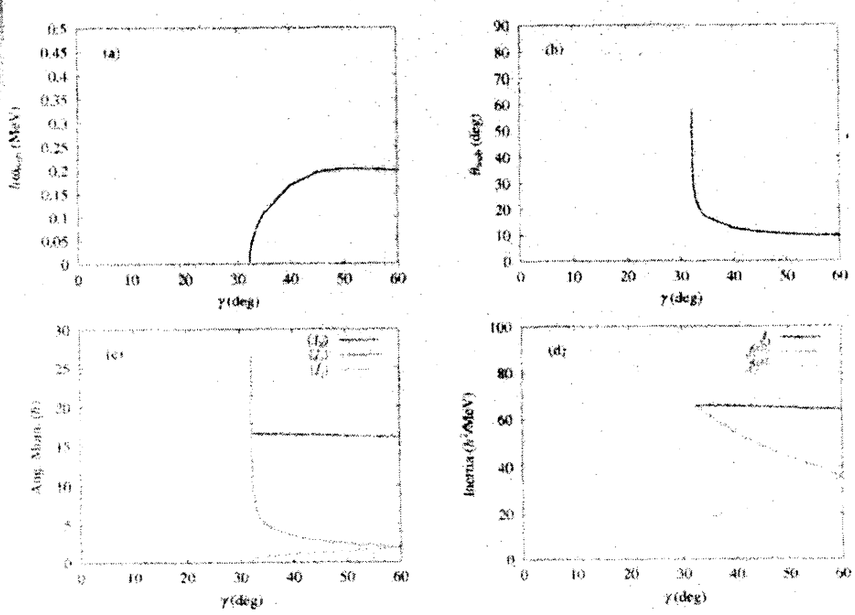

Energy surfaces (^{146}Gd)

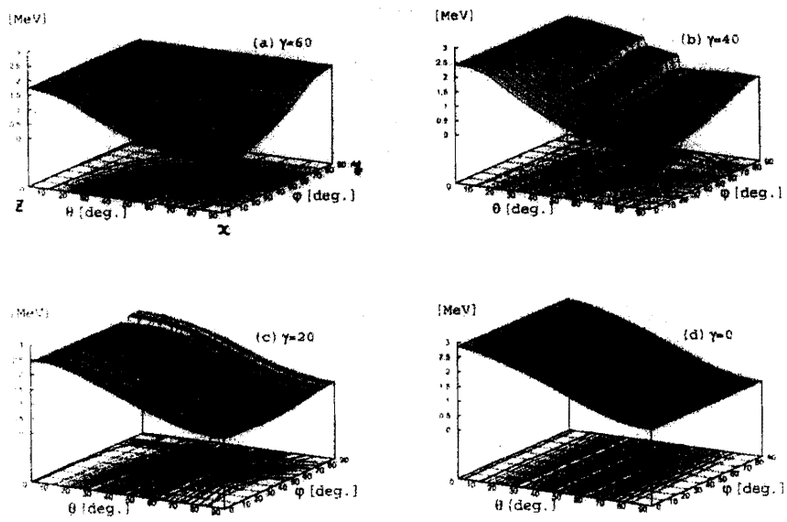

^{146}Gd Tilted Axis Cranking

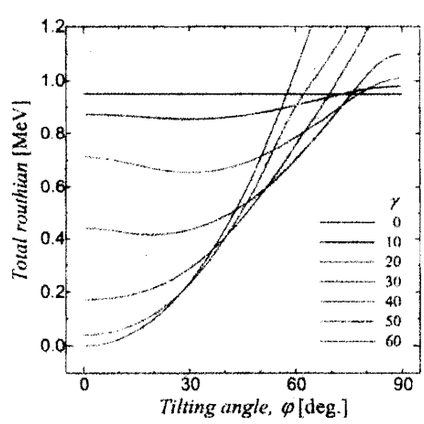

$$\left(\begin{array}{l} \hbar\omega_{\rm rot} = 0.25{\rm MeV}, \epsilon_2 = 0.19 \\ \Delta_n = 0.8{\rm MeV}, \Delta_p = 0.6{\rm MeV} \end{array} \right)$$

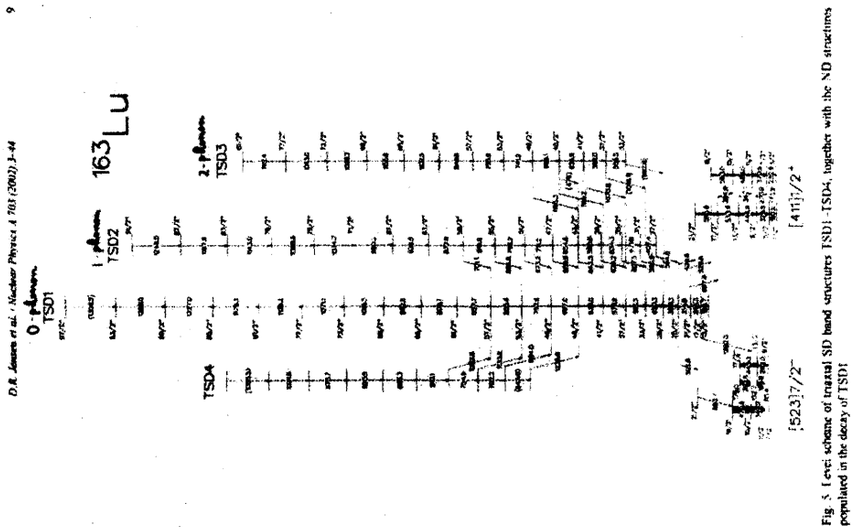

Fig. 5. Level scheme of triaxial SD band structures TSD1–TSD4, together with the ND structures populated in the decay of TSD1

Anharmonicity in 2 phonon states (^{163}Lu)

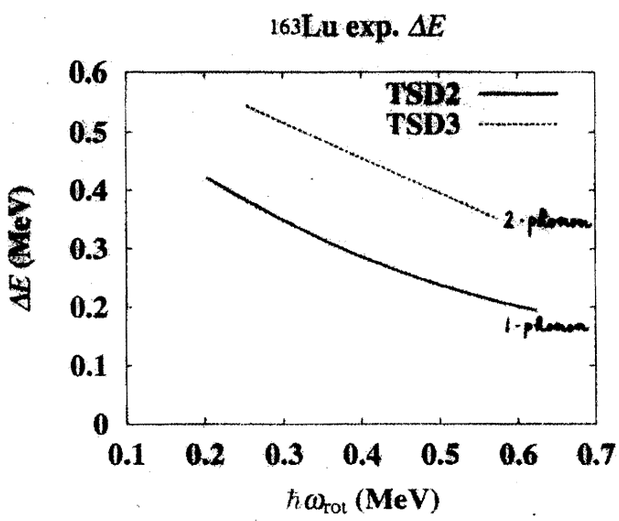

Energy surface

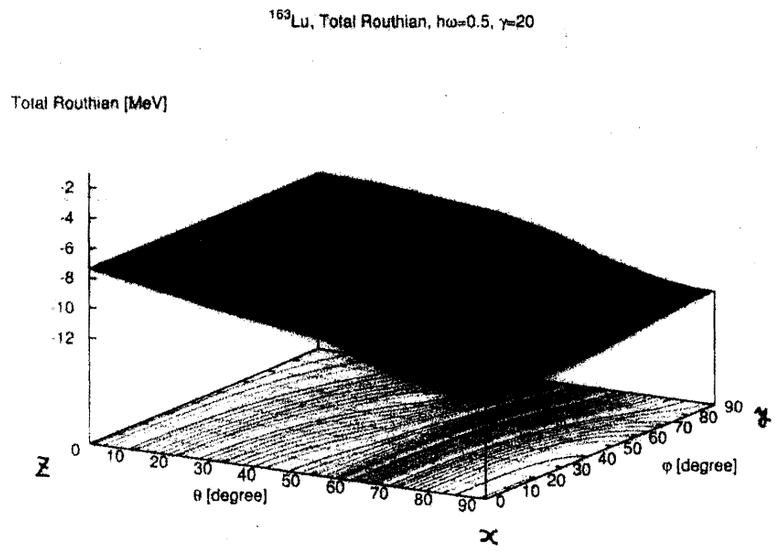

Summary

- Correspondence between RPA and TAC is good
- Theoretically, instability of wobbling leads to tilted axis rotation — **"Phase transition"**
- Anharmonicity in 2 phonon wobbling

Three- and four-body structure of light hypernuclei

E. Hiyama[1]
High Energy Accelerator Research Organization(KEK), Tsukuba, 305-0801, Japan

One of the main goals of hypernuclear physics is to investigate the hyperon-nucleon (YN) and hyperon-hyperon (YY) interactions. Interesting and important hypernuclear few-body problems contribute. To solve the three- and four-body problem precisely, we employ Gaussian-expansion method (GEM) [1,2] which has been successfully applied to calculate properties of various bound three- and four-body systems. The basis functions describe well both short-range correlations and the long-range tail. Here we emphasize what is interesting and important from the view point of hypernuclear physics. Along this line, the recent epock-making experimental data and the related our theoretical calculations are reported. Then, the following three subjects will be presented: 1)In order to obtain useful information on the spin-orbit force of the YN interactions, The discussion on the energy splittings of the $5/2^+ - 3/2^+$ doublet in ${}^{9}_{\Lambda}$Be and $3/2^- - 1/2^-$ doublet in ${}^{13}_{\Lambda}$C will be performed on the basis of three- and four-body model in connection with the recent high-resolution γ-ray experiments done at BNL-E930 and -E929. 2)Energy level of double-Λ hypernuclei, ${}^{7}_{\Lambda\Lambda}$He, ${}^{7}_{\Lambda\Lambda}$Li, ${}^{8}_{\Lambda\Lambda}$Li, ${}^{9}_{\Lambda\Lambda}$Li, ${}^{9}_{\Lambda\Lambda}$Be and ${}^{10}_{\Lambda\Lambda}$Be are predicted on the basis of the $\alpha+x+\Lambda+\Lambda$ four-body model with $x = n, p, d, t,{}^3$He and α, respectively Here, an effective $\Lambda\Lambda$ interaction is constructed so as to reproduce, within the framework of the $\alpha + \Lambda + \Lambda$ model, B_Λ of ${}^{6}_{\Lambda\Lambda}$He which was observed recently in NAGARA event of the emulsion experiment . The *Demachi-Yanagi* event, identified recently as ${}^{10}_{\Lambda\Lambda}$Be, is interpreted as an observation of its 2^+ excited state on the basis of the present calculation. 3)The four-body calculations of ${}^{4}_{\Lambda\Lambda}$H taking both $NN\Lambda\Lambda$ and $NNN\Xi$ channels are performed. And importance of the role of $\Lambda\Lambda - \Xi N$ coupling in this system in order to make this system bound will be discussed.

References

1. E. Hiyama, Y. Kino and M. Kamimura, Prog. Par. Nucl. Phys. **51**, 233 (2003).
2. M. Kamimura, Phys. Rev. A **38**, 621 (1988).

[1] work corabollation with M. Kamimura, T. Motoba, T. Yamada and Y. Yamamoto

Three- and four-body structure of light hypernuclei

E. Hiyama (KEK)
M. Kamimura (Kyushu Univ.)
T. Motoba(Osaka E.C. Univ.)
T. Yamada(Kanto Gakuin Univ.)
Y. Yamamoto(Tsuru Univ.)

Recently, hypernuclear physics has been excited by obtaining some epoch-making experimental data.

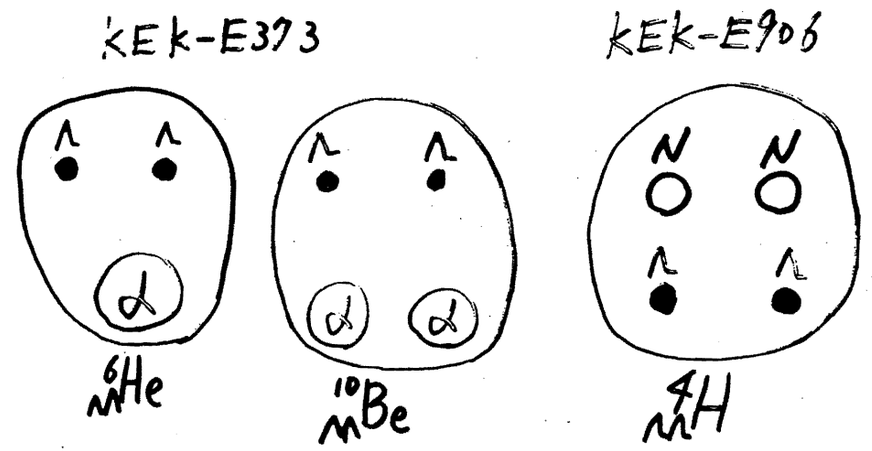

The purpose of my talk:

To introduce those data reported and to discuss our theoretical 3- and 4-body structure studies related those data.

In near future, at TJLAB, BNL, DAΦNE and A new facility, J-PARC at KEK-JAERI and PANDA project at GSI using $\bar{p}$ beam, they are Planning to produce many single Λ hypernuclei and double Λ hypernuclei.

- Why is it interesting and important to study structure of light hypernuclei?
- Why do the facilities intend to produce so many hypernuclei?

Answer

[1]

One of the major purpose of strangeness nuclear physics:

To understand the baryon-baryon interaction.

However, since there are very limited YN scattering data and no YY data, YN and YY interactions so far proposed have a large degree of ambiguity.

In near future, J-PARC facility, as for the YN scattering data, they are planning to do this experiments.

However, even at J-PARC facility, it is very difficult to perform YY scattering experiment.

Therefore, it is very important to obtain information about YY interaction from spectroscopy experiments of many double Λ hypernuclei.

For this purpose, it is planned to produce many double Λ hypernuclei at J-PARC and GSI.

My contribution

To understand the hypernuclear structure by performing our 3- and 4-body calculations and to Use this structure information to understand the YN and YY interactions.

How to constrain YN spin-orbit force

Successful example: ${}^{9}_{\Lambda}$Be , ${}^{13}_{\Lambda}$C

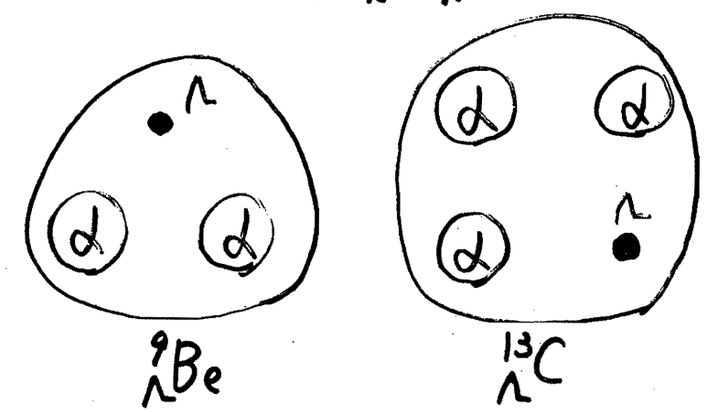

BNL-E930

- Meson theory
- quark model

BNL-E929

What types of spin-orbit interaction is favor for explanation of the experimental data?

Level structure of A=7 to 10 double Λ hypernuclei

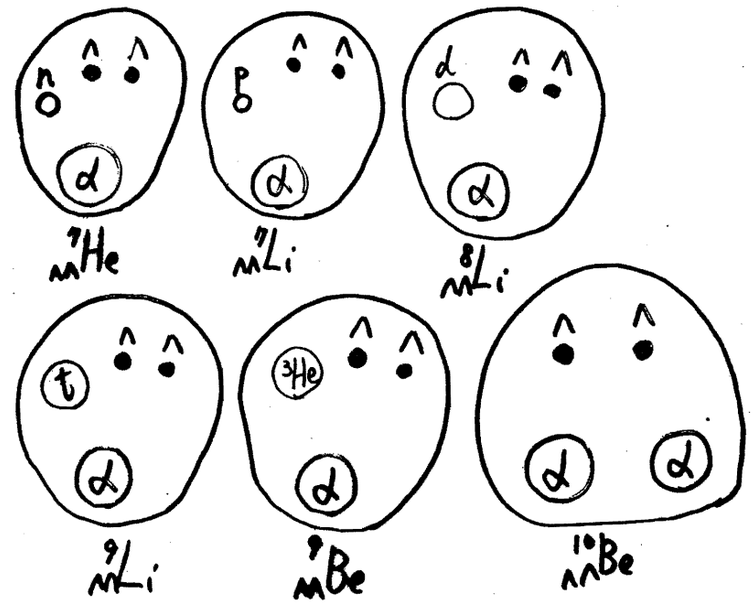

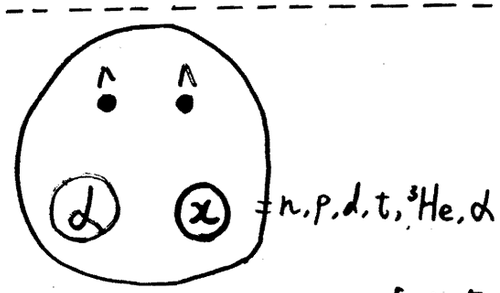

What is interesting in study of A=7 to 10 double Λ hypernuclei?

Why it is interesting and important to study of light hypernuclei?

[2]

How largely is the nuclear structure changed when Λ particle is injected into a nucleus or unstable nucleus?

We can predict novel dynamical change using few-body calculational method.

Example: $^{6}_{\Lambda}$He , $^{7}_{\Lambda}$He

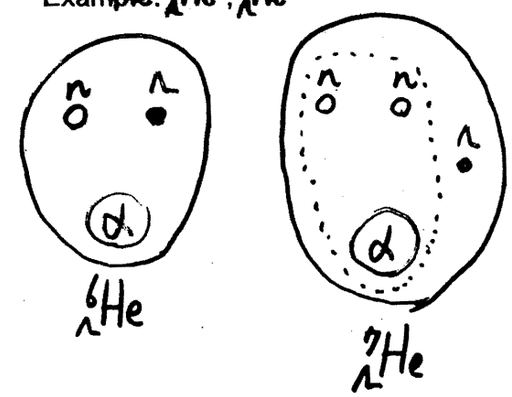

Outline of my talk

[1] YN spin-orbit force and ${}^{9}_{\Lambda}$Be and ${}^{13}_{\Lambda}$C

[2] Energy spectra of A=7 to 9 double Λ hypernuclei

[3] Neutron-rich hypernuclei, ${}^{6}_{\Lambda}$He and ${}^{7}_{\Lambda}$He

Gaussian Expansion Method

developed by Kyushu Univ.
Kamimura

(1) 3-cluster structure of light nuclei

(2) Coulomb 3-body muonic molecular ions appearing in the muon-catalyzed fusion cycles (1987～)

(3) 3-nucleon bound states with realistic NN and 3N force (1988)

(4) Meta-stable anti-protonic helium atom (He^{++}+p+e)(1995～)

Gaussian Expansion Method (GEM)

3-body case

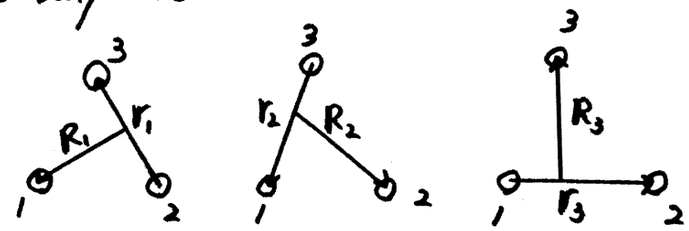

$c=1$ $\qquad$ $c=2$ $\qquad$ $c=3$

$$\Phi_{JM} = \Phi^{(1)}_{JM}(r_1,R_1) + \Phi^{(2)}_{JM}(r_2,R_2) + \Phi^{(3)}_{JM}(r_3,R_3)$$

$$\Phi^{(c)}_{JM}(r_c,R_c) = \sum_{nlNL} A^{(c)}_{nlNL}\left[\phi_{nl}(r_c)\otimes\chi_{NL}(R_c)\right]_{JM}$$

$$\phi_{nlm}(r) = r^l e^{-\left(\frac{r}{r_n}\right)^2} Y_{lm}(\hat{r})$$

$$\chi_{NLM}(R) = R^L e^{-\left(\frac{R}{R_N}\right)^2} Y_{LM}(\hat{R})$$

$$\left.\begin{aligned} r_n &= r_1 a^{n-1} \quad (n=1\sim n_{max}) \\ R_N &= R_1 A^{N-1} \quad (N=1\sim N_{max}) \end{aligned}\right\} \text{geometrical progression}$$

$$(H-E)\Phi_{JM} = 0$$

is solved by Rayleigh-Ritz variational meth

PHYSICAL REVIEW C, VOLUME 64, 044001

Benchmark test calculation of a four-nucleon bound state

(1) H. Kamada,* A. Nogga, and W. Glöckle
Institut für Theoretische Physik II, Ruhr-Universität Bochum, D-44780 Bochum, Germany

(2) E. Hiyama
High Energy Accelerator Research Organization, Institute of Particle and Nuclear Studies, Tsukuba 305-0801, Japan

M. Kamimura
Department of Physics, Kyushu University, Fukuoka 812-8581, Japan

(3) K. Varga
Solid State Division, Oak Ridge National Laboratory, Oak Ridge, Tennessee 37380
and Institute of Nuclear Research of the Hungarian Academy of Sciences (ATOMKI), Debrecen 4000, PO Box 51, Hungary

(4) Y. Suzuki
Department of Physics, Niigata University, Niigata 950-2181, Japan

M. Viviani and A. Kievsky
INFN, Sezione di Pisa, I-56100 Pisa, Italy

S. Rosati
INFN, Sezione di Pisa, I-56100 Pisa, Italy
and Department of Physics, University of Pisa, I-56100 Pisa, Italy

(5) J. Carlson
Theoretical Division, Los Alamos National Laboratory, Los Alamos, New Mexico 87545

Steven C. Pieper and R. B. Wiringa
Physics Division, Argonne National Laboratory, Argonne, Illinois 60439

(6) P. Navrátil
Lawrence Livermore National Laboratory, P. O. Box 808, Livermore, California 94551
and Nuclear Physics Institute, Academy of Sciences of the Czech Republic, 250 68 Řež near Prague, Czech Republic

B. R. Barrett
Department of Physics, P.O. Box 210081, University of Arizona, Tucson, Arizona 85721

(7) M. Barnea
The Racah Institute of Physics, The Hebrew University, 91904 Jerusalem, Israel

W. Leidemann and G. Orlandini
Dipartimento di Fisica and INFN (Gruppo Collegato di Trento), Università di Trento, I-38050 Povo, Italy
(Received 20 April 2001; published 27 August 2001)

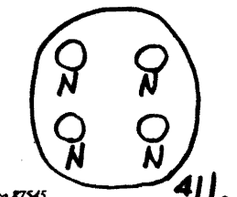

^{4}He

Benchmark calculation of ^{4}He $\qquad$ NN: AV8′

Binding energ., $\langle r^2\rangle^{1/2}$, two-body correlation function

Gaussian Expansion Method -> Hypernuclear structure

↓

Study of the YN and YY interaction

E. Hiyama, Y. Kino and M. Kamimura
Progress in Particle and Nuclear Physics.
Vol 51 (2003) 223-307.

Outline of my talk

[1] YN spin-orbit force and ${}^{9}_{\Lambda}$Be and ${}^{13}_{\Lambda}$C

[2] Energy spectra of A=7 to 9 double Λ hypernuclei

[3] Neutron-rich hypernuclei, ^{6}He and ^{7}He

Since there are very limited YN scattering data and no YY data, then it is absolutely to extract useful information on YN and YY interactions from Structure studies of many kinds of light hypernuclei systematically.

How to constrain the YN and YY interactions?

Successful example in the case of YN spin-orbit force and single Λ hypernuclei.

Two types of YN spin-orbit forces proposed so far.

(i) based on Meson theory

(ii) based on constituent quark model

To compare these two-types of potentials and discuss their validity is one of the most fashionable subjects in strangeness nuclear physics.

If we use these two types of spin-orbit forces in hypernuclear structure calculation, then how is the spin-orbit energy splitting in the level structure?

Tamura et al.

BNL-E930

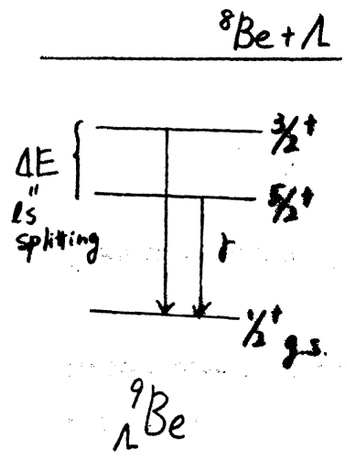

Kishimoto et al.

BNL-E929

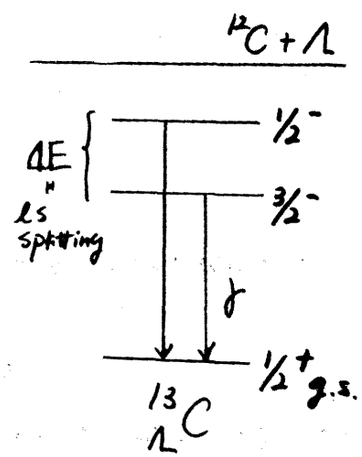

$^9_\Lambda Be = {}^8Be + \Lambda$

$^{13}_\Lambda C = {}^{12}C + \Lambda$

$^8Be =$ (α) + (α)

$^{12}C =$ (α) + (α) + (α)

$^9_\Lambda Be \Rightarrow$

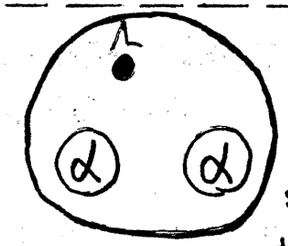

$^{13}_\Lambda C =$

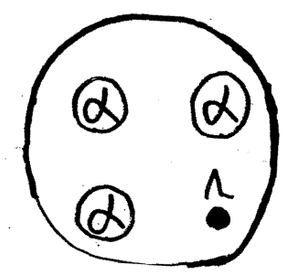

Contributions of spin-spin and tensor terms of YN interaction are very small.

ΛN spin-orbit force and $^{9}_{\Lambda}Be$ and $^{13}_{\Lambda}C$

CAL: E. Hiyama et al.
Phys. Rev. Lett. 85 (2000) 270

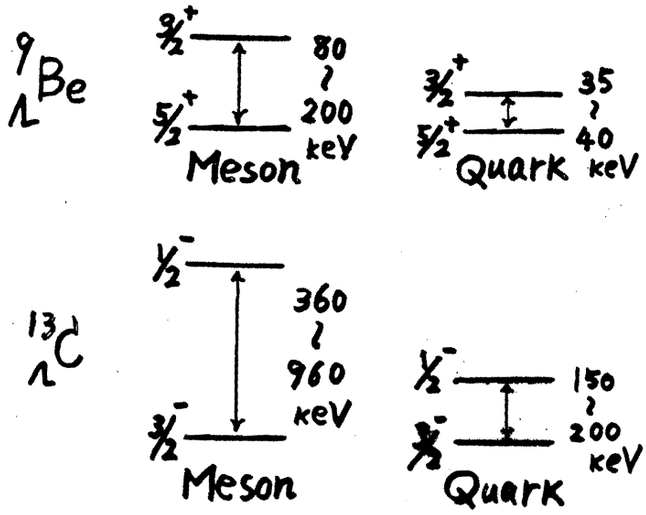

i) ΛN LS: NN $\frac{1}{20} \sim \frac{1}{30}$ (quark)

ii) Quark model < Meson-exch model

BNL-E930

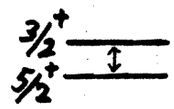

$31.4^{+2.5}_{-3.6}$ keV

EXP H. Akikawa et al. Phys. Rev. Lett. 88 (2002) 82501

BNL-E929

152 ± 54 ± 36 keV

EXP S. Ajimura et al. Phys. Rev. Lett. 86 (2001) 4255

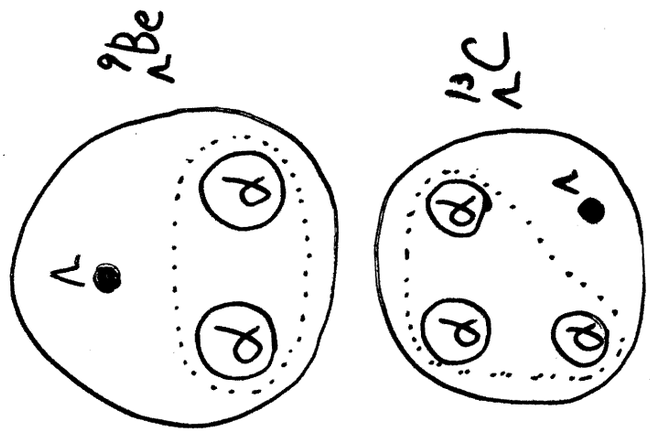

· Meson-theory-based YN interaction
Nijmegen model '97(a) to (f).

· Quark-model-based YN interaction
proposed by Kyoto-Niigata Group

By comparing our theoretical calculation and the Experiments of γ-ray spectroscopy, we can understand that the desirable strength of YN spin-orbit strength should be closed to the strength which quark-model proposed.

In this way, it is so important to obtain information about YN interaction from the study of hypernuclear structure.

Similary, it is also important to study structure of double Λ hypernuclei to understand the YY interaction.

Outline of my talk

[1] YN spin-orbit force and ${}^{9}_{\Lambda}$Be and ${}^{13}_{\Lambda}$C

[2] Energy spectra of A=7 to 9 double Λ hypernuclei

[3] Neutron-rich hypernuclei, ${}^{6}_{\Lambda}$He and ${}^{7}_{\Lambda}$He

What kinds of double Λ hypernuclei were observed, recently?

Recently, 2 epoch-making experimental data have been reported by the KEK-E373.

(1) Observation of ${}^{6}_{\Lambda\Lambda}$He

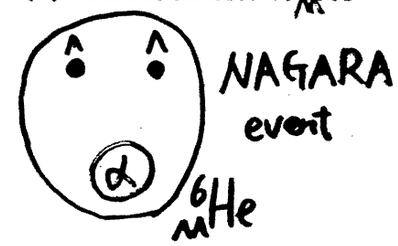

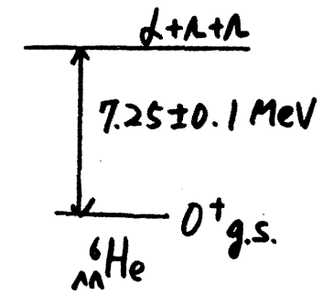

(2) Observation of ${}^{10}_{\Lambda\Lambda}$Be

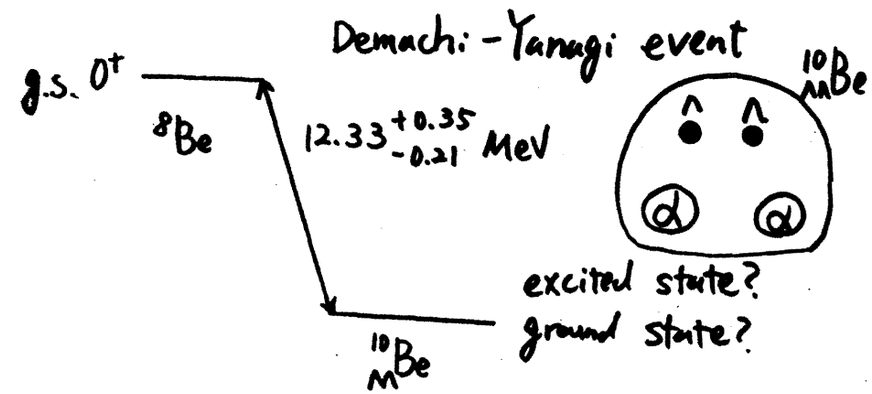

Analysis of KEK-E373 experiments is still in progress. Furthermore, it is planned to produce many double Λ hypernuclei, J-PARC and BNL.

Important issues:

(i) Does the Λ Λ interaction which is designed to reproduce the binding energy of $^{6}_{\Lambda\Lambda}$He reproduce the *Demachi-Yanagi* event consistently?

(ii) Using this Λ Λ interaction, how is the theoretical prediction of level structure of other double Λ hypernuclei?

(i) Does the $\Lambda\Lambda$ interaction which is designed to reproduce the binding energy of ${}^{6}_{\Lambda\Lambda}$He reproduce the *Demachi-Yanagi* event consistently?

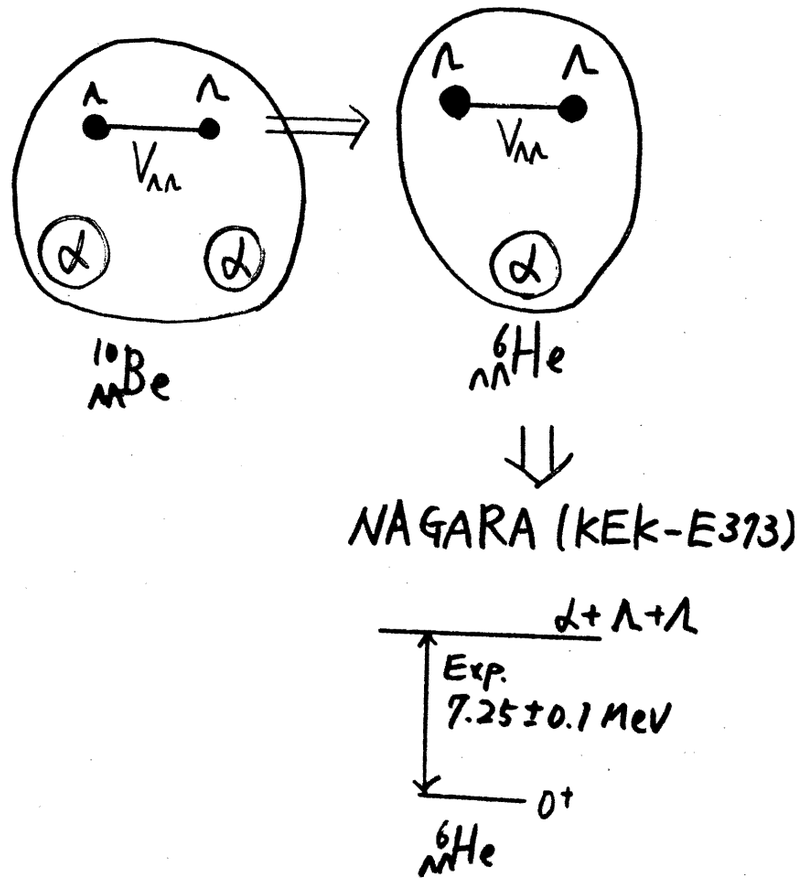

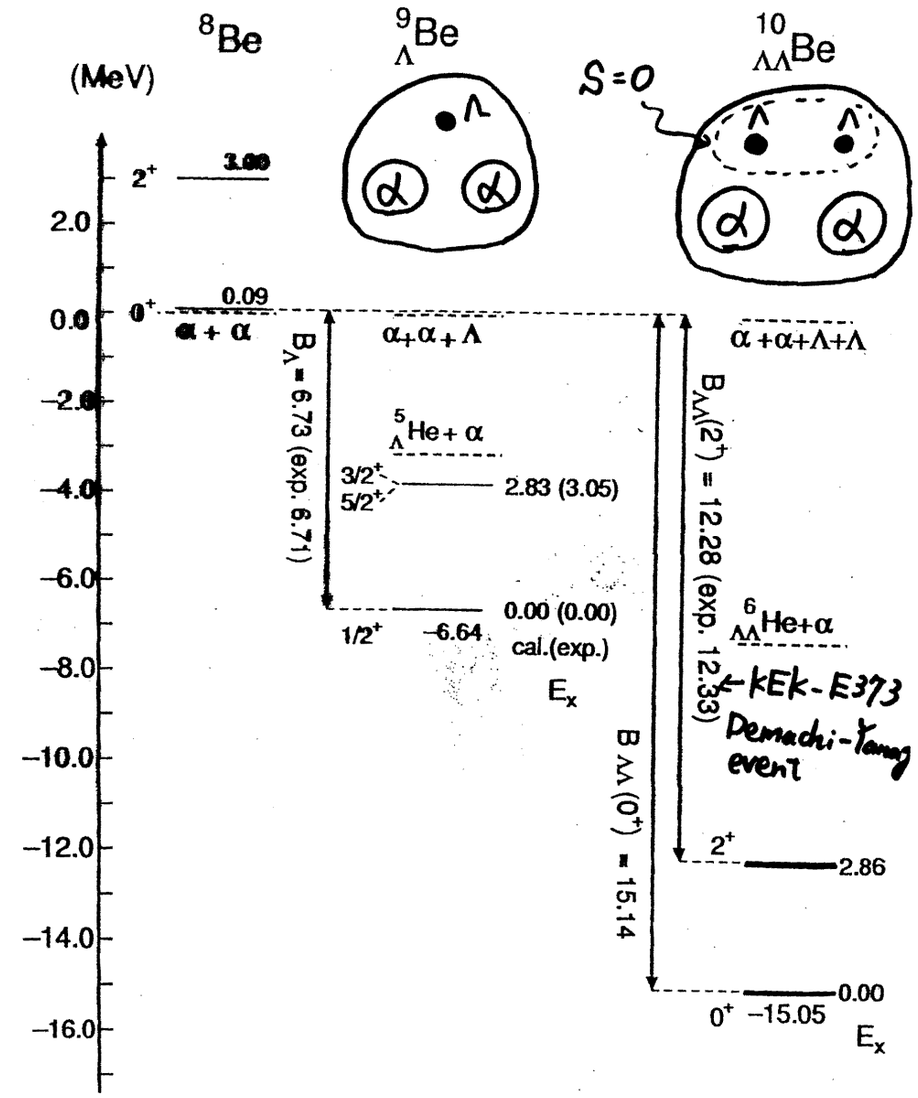

Our 4-body calculation is predictive.

Hoping to have the data of many double Λ hypernuclei in the future experiments, we have predicted level structure of double Λ hypernuclei with A=7 ~ 10 within the framework of the α+x+Λ+Λ 4-body model, where x=n, p, d, t, ^{3}He and α.

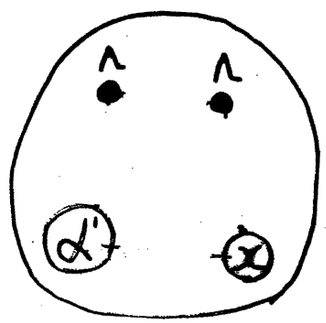

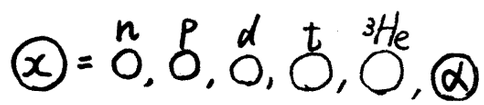

(ii)Using this Λ Λ interaction, how is the theoretical prediction of level structure of other double Λ hypernuclei?

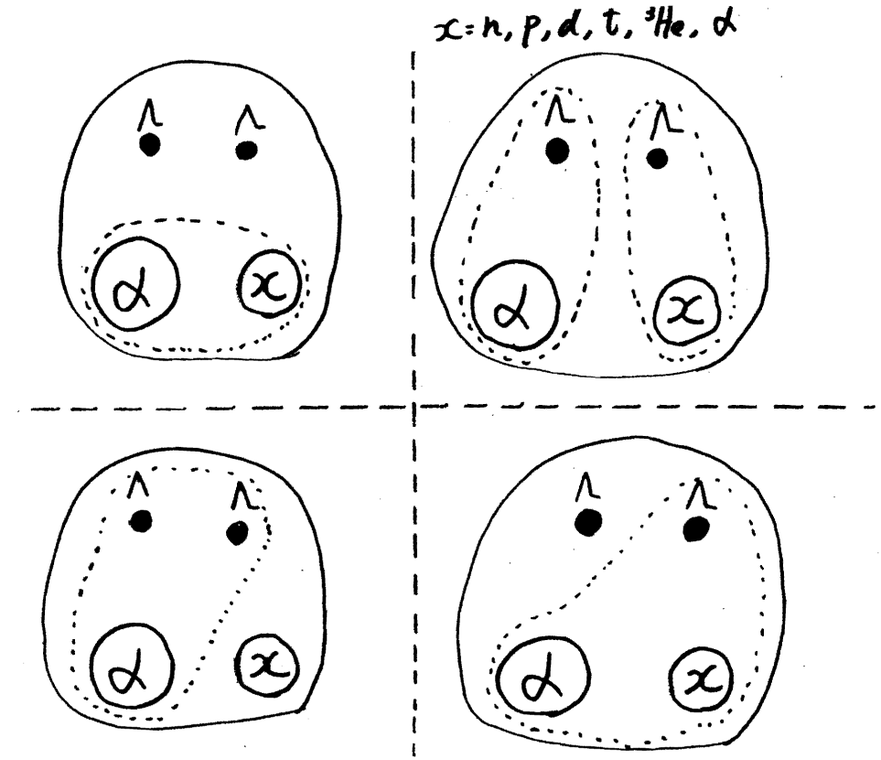

It is important that all the 2-body interactions should be chosen so as to reproduce both the binding energy of any subsystems composed of 2- and 3-consistuent particles, and 2-body low-energy scattering phase shifts.

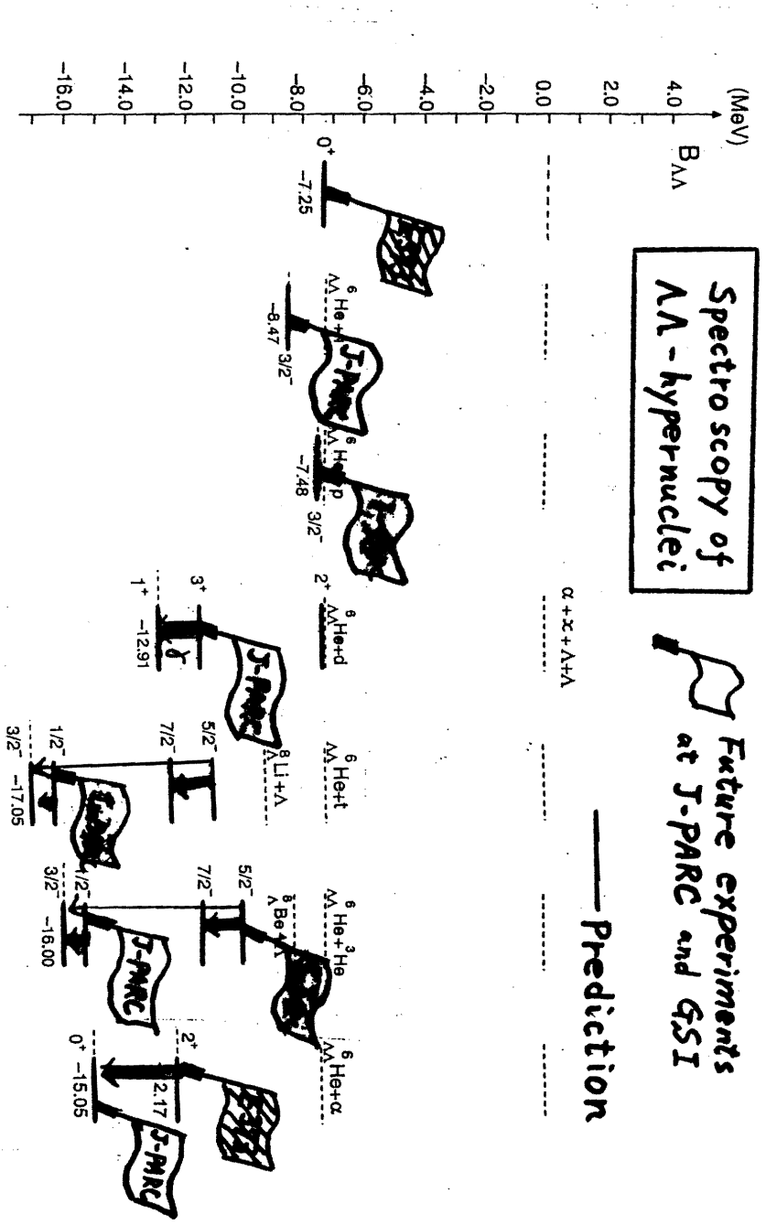

Outline of my talk

[1] YN spin-orbit force and $^{9}_{\Lambda}$Be and $^{13}_{\Lambda}$C

[2] Energy spectra of A=7 to 9 double Λ hypernuclei

[3] Neutron-rich hypernuclei, $^{6}_{\Lambda}$He and $^{7}_{\Lambda}$He

How largly is structure-change when Λ particle is injected into a nucleus or an unstable nucleus?
We can predict novel dynamical change using few-body calculational methods.

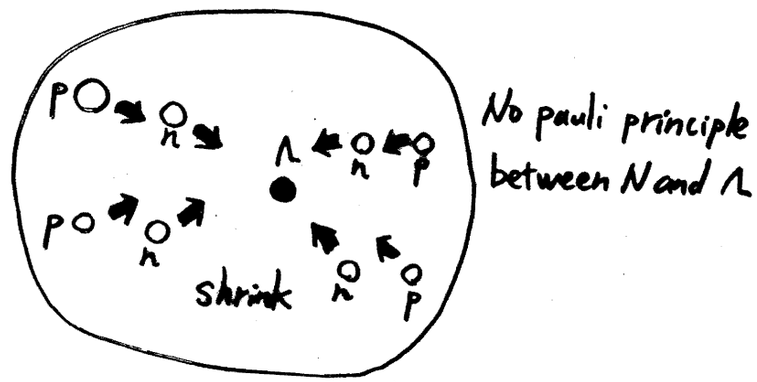

Λ hypernuclei

Λ particle plays a "glue-like" role and produce a dynamical shrinkage of the core nucleus.

Shrinkage of nucleus by the addition of Λ
E. Hiyama, M. Kamimura, K. Miyazaki and T. Motoba
Phys. Rev. C59 (1999), 2351

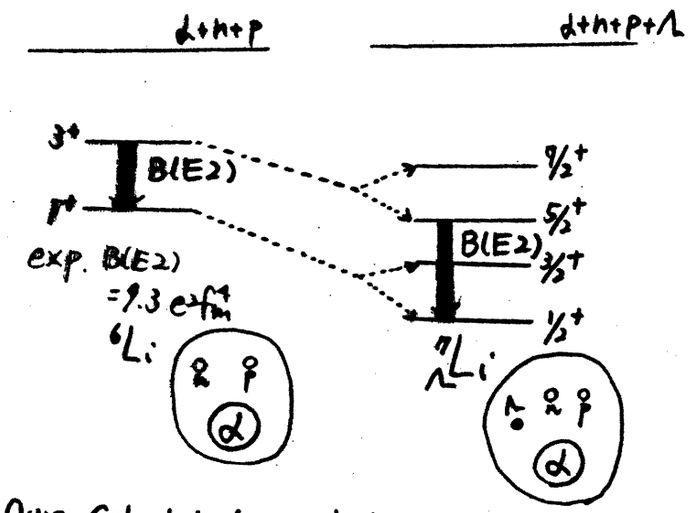

Our Calculated result:
$B(E2; 5/2^+ \to 1/2^+) = 2.85\ e^2 fm^4$ ⇐ Prediction
Nuclear size: Reduced by 22%
$B(E2) \propto r^4$

KEK-E419
K. Tanida et al. Phys. Rev. Lett. 86, 1982 (2001)
$B(E2: 5/2^+ \to 1/2^+) = 3.6 \pm 0.5^{+0.5}_{-0.9}\ e^2 fm^4$
Reduced by 19%

"Glue-like" role of Λ particle provide us with another interesting subject.

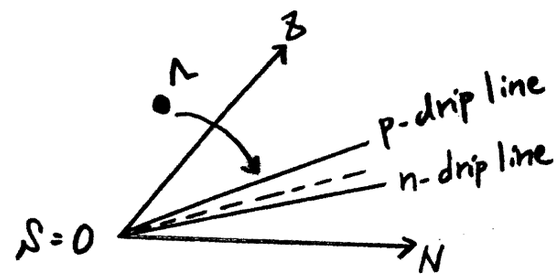

Interesting phenomena concerning the neutron halo have been observed near the neutron drip line of light nuclei.

How does the halo structure change when a Λ particle is injected into neutron-rich nucleus?

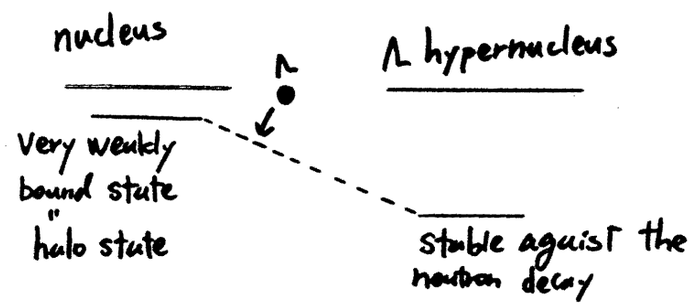

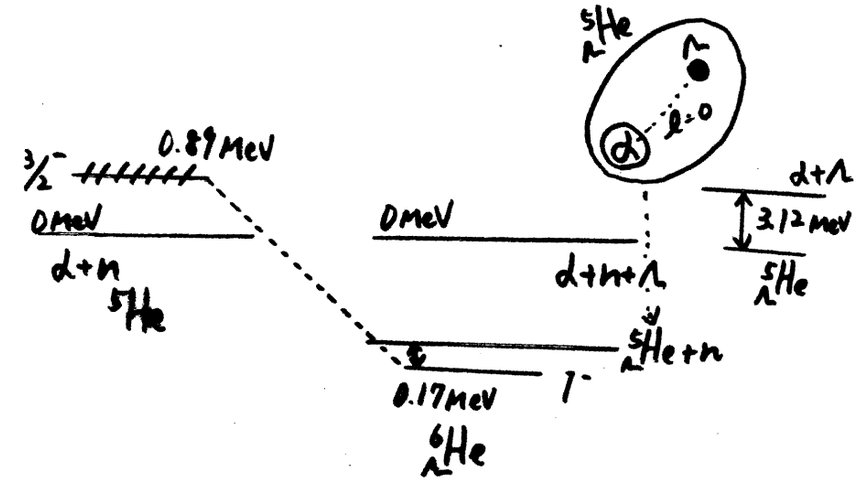

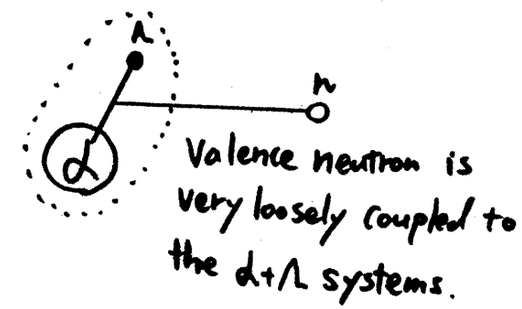

How do the 3 particle locate to each other?

Is there neutron halo in $^6_\Lambda$He hypernucleus?

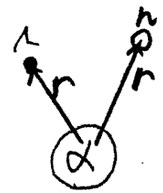

density distribution

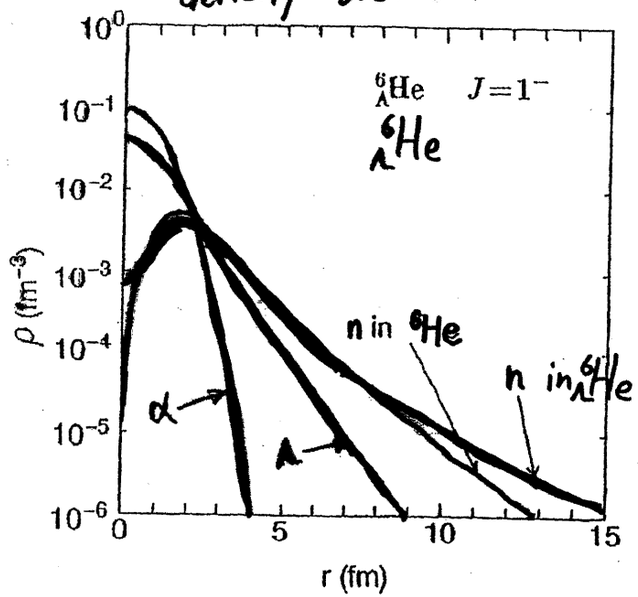

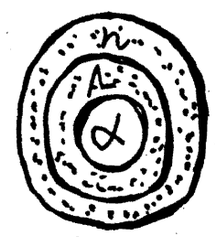

$^6_\Lambda$He

three-layer structure

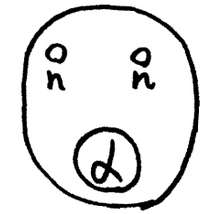

^{6}He : one of the lightest n-rich halo nuclei

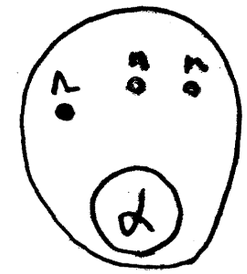

$^7_\Lambda$He : one of the lightest n-rich hypernuclei

^{7}Li(e, e′k$^+$)$^7_\Lambda$Li : TJLAB

No experimental data

E. Hiyama et al. Phys. Rev. C53, 2075 (1996)

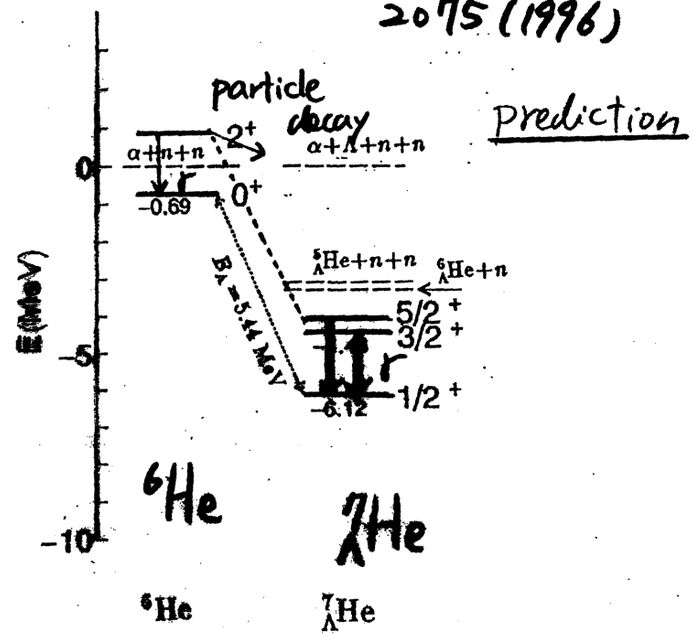

$^7_\Lambda$He

$5/2^+ \to 1/2^+$, $3/2^+ \to 1/2^+$ } · useful for the study of the excitati mechanism in n-rich hypernuclei as well as n-rich nuclei

In n-rich nuclei and n-rich hypo-nuclei, there will be many examples such as combinatio of ^{6}He and $^7_\Lambda$He.

BNL, J-PARC

Conclusion

[1] YN spin-orbit force and ^{9}Be and ^{13}C

[2] Energy spectra of A=7 to 9 double Λ hypernuclei

[3] Neutron-rich hypernuclei, ^{6}He and ^{7}He

There are a lot of interesting and important few-body problems in hypernuclear physics.

In near future, at TJLAB, BNL, DAΦNE, J-PARC And GSI facilities, they are planning to produce many single Λ and double Λ hypernuclei.

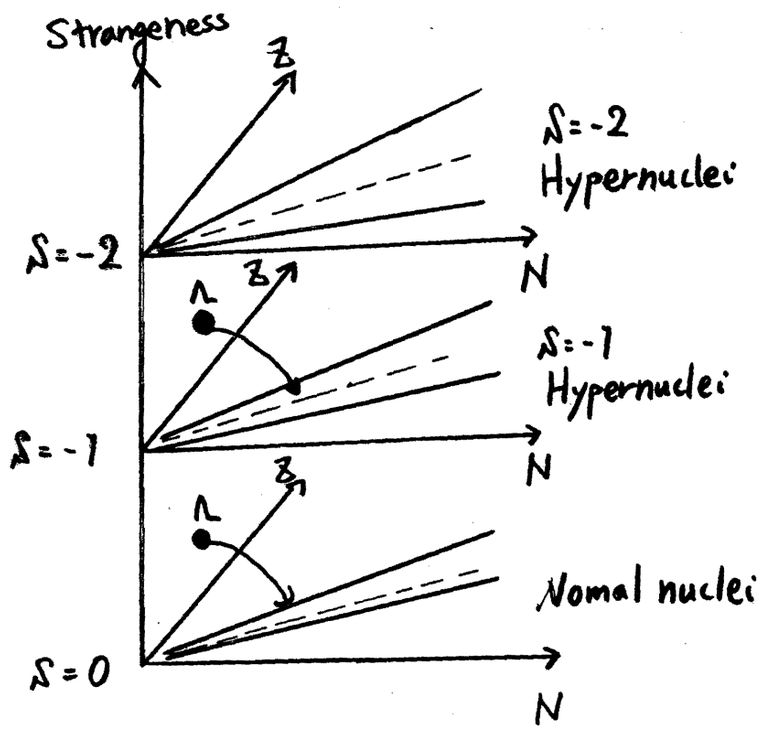

At TJLAB, BNL, DAΦNE, J-PARC and GSI facilities, they will discover numerous single Λ hypernuclei and double Λ hypernuclei in near future.

This would provide nuclear physics community with encouraging subjects continuously.

Gamma spectroscopy of hypernuclei – present status and future plans

H. Tamura
Department of Physics, Tohoku University, Aoba-ku, Sendai 980-0861, Japan

I will summarize our Hyperball project of high-precision γ spectroscopy of Λ hypernuclei, talking about motivations and techniques, physics results, and future plans. Details of recent results on the ΛN spin-dependent interactions will be covered by Dr. Ukai in the next talk.

Hyperball is a large-acceptance germanium detector array featured by high-rate electronics and BGO background suppression counters. It first enabled γ spectroscopy of hypernuclei under severe background from high energy meson beams. With Hyperball, we have investigated structure of several p-shell hypernuclei, ${}^{7}_{\Lambda}$Li [1,2,3], ${}^{9}_{\Lambda}$Be [4], ${}^{10}_{\Lambda}$B, ${}^{11}_{\Lambda}$B, ${}^{15}_{\Lambda}$N, and ${}^{16}_{\Lambda}$O. In these experiments, we use direct reactions of (K^-,π^-) and (π^+, K^+) to populate specific states of hypernuclei, but in addition we also tried a pioneering experiment of in-beam γ spectroscopy with stopped K^- beams [5].

Structure of hypernuclei is featured by "hypernuclear fine structure", a spin doublet with a small energy spacing caused by Λ-spin direction. We have revealed hypernuclear fine structure in ${}^{7}_{\Lambda}$Li, ${}^{9}_{\Lambda}$Be, and ${}^{16}_{\Lambda}$O, from which we have derived strengths of all the ΛN spin-dependent interactions (spin-spin force, two spin-orbit forces, and tensor force). These strengths allow us to discuss validity of various baryon-baryon interaction models. Another interesting subject in hypernuclear structure is "impurity effect" of Λ particle in a nucleus, such as the shrinkage of hypernuclei which we confirmed from the $B(E2)$ measurement in ${}^{7}_{\Lambda}$Li [2].

I will also present our future plans and necessary experimental techniques, particularly our proposing experiments with intense K^- beams available at the 50 GeV proton synchrotron at J-PARC [6].

1. H. Tamura *et al.*, Phys. Rev. Lett. **84** (2000) 5963.
2. K. Tanida *et al.*, Phys. Rev. Lett. **86** (2001) 1982.
3. J. Sasao *et al.*, Phys. Lett. **B 579** (2004) 258.
4. H. Akikawa *et al*, Phys. Rev. Lett. **88** (2002) 082501.
5. K. Tanida *et al*, Nucl. Phys. **A 721** (2003) 999c.
6. K. Imai *et al.*, Letter of Intent for Nuclear and Particle Physics Experiments at the J-PARC, KEK, L06 (2003), `http://www-ps.kek.jp/jhf-np/LOIlist/LOIlist.html`.

CNS-RIKEN Symposium
March 18, 2004

Gamma-Ray Spectroscopy of Hypernuclei
-- Present Status and Future Plans--

Dept. of Physics, Tohoku University
H. Tamura

Contents

1. Introduction

keywords.. **"Hyperball"**

2. Present Status of γ spectroscopy

   "Hypernuclear fine structure"

3. Future Plans

   "J-PARC"

4. Summary

Hyperball (Tohoku/ Kyoto/ KEK, 1998)

- Large acceptance for small hypernuclear γ yields
  - Ge (r.e. 60%) x 14
  - $\Omega \sim 15\%$
  - $\varepsilon_{peak} \sim 3\%$ at 1 MeV
- High-rate electronics for huge background
- BGO counters for π^0 and Compton suppression

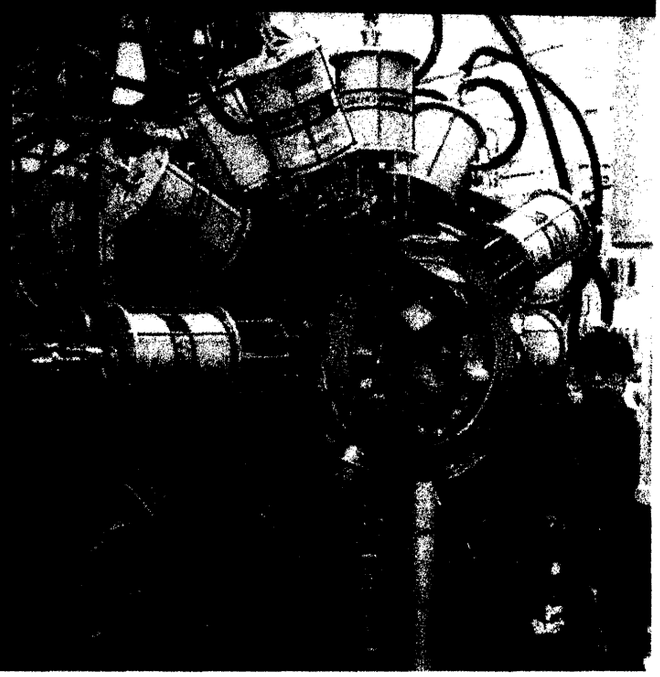

Resolution of hypernuclear spectroscopy
1 MeV -> 2 keV FWHM

2. Present status

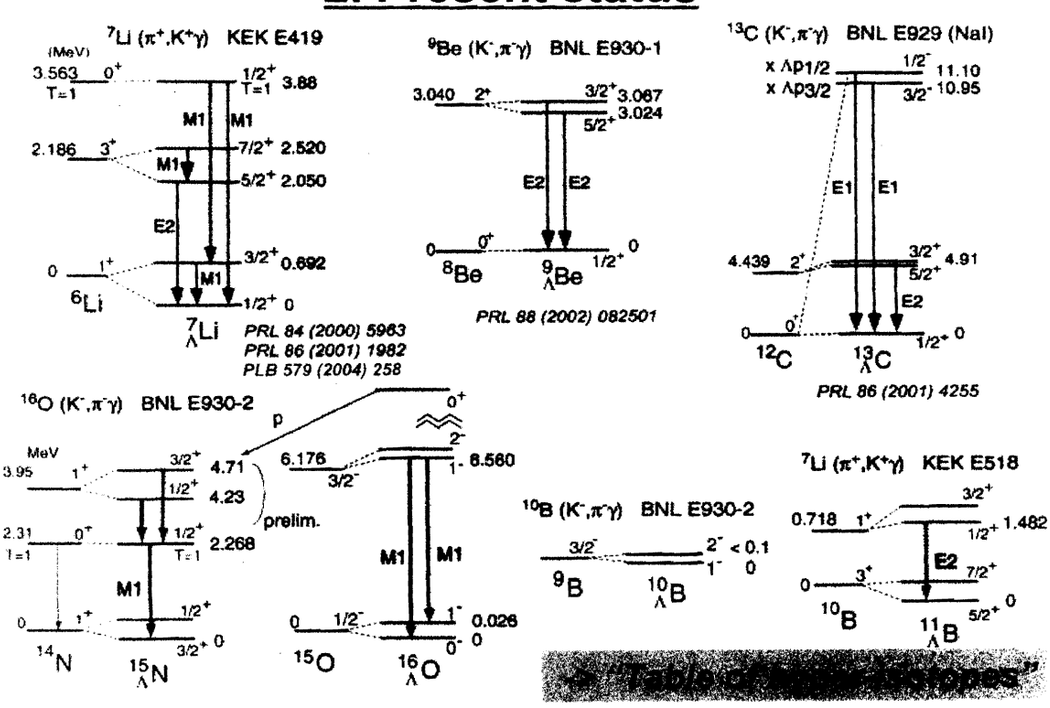

γ spectroscopy and ΛN spin-dependent interactions

· Low-lying levels of Λ hypernucleus

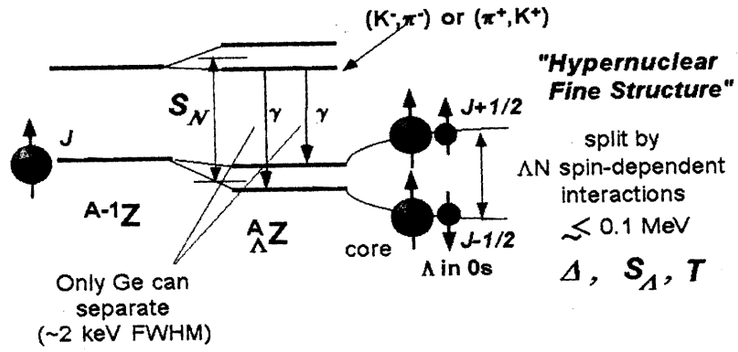

· 2-body ΛN effective interaction

Dalitz and Gal, Ann. Phys. 116 (1978) 167
Millener et al., Phys. Rev. C31 (1985) 499

$$V_{\Lambda N}^{eff} = V_0(r) + \underset{\Delta}{V_\sigma(r)\,\vec{s}_\Lambda \vec{s}_N} + \underset{S_\Lambda}{V_\Lambda(r)\,\vec{l}_{\Lambda N}\vec{s}_\Lambda} + \underset{S_N}{V_N(r)\,\vec{l}_{\Lambda N}\vec{s}_N} + \underset{T}{V_T(r)\,S_{12}}$$

p-shell : 4 radial integrals for $p_N\, s_\Lambda$ w.f.

$^7_\Lambda$Li Best-studied Hypernucleus

Tanida et al., PRL 86(2001) 1982

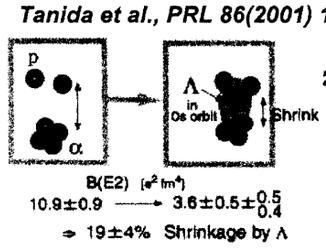

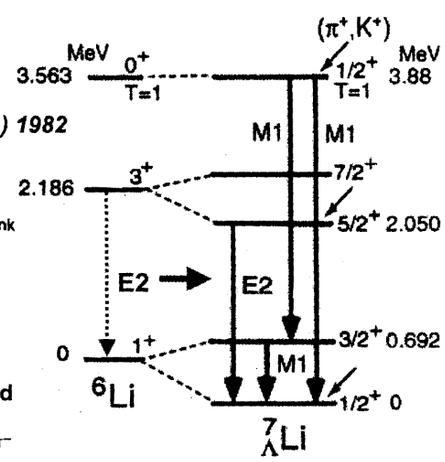

KEK E419

^{7}Li $(\pi^+,K^+\gamma)$ $^7_\Lambda$Li

Tamura et al., PRL 94(2000) 5963

Doppler shift attenuation method

$\tau = 5.8 \pm^{0.9}_{0.7} \pm 0.7$ ps

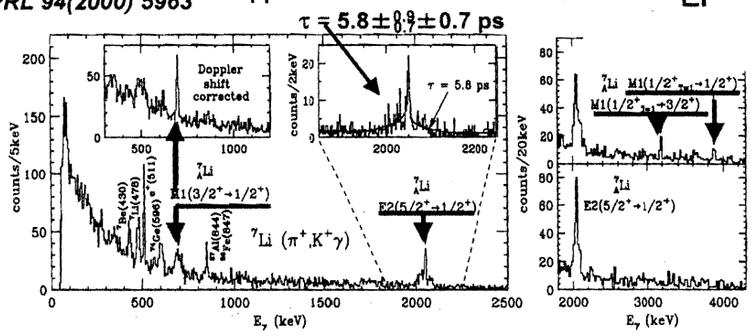

$^{7}_{\Lambda}$Li
Best-studied Hypernucleus

BNL E930('01)

^{10}B (K$^-$,$\pi^-\gamma$) $^{10}_{\Lambda}$B*(3$^+$) -> $^{7}_{\Lambda}$Li +^{3}He

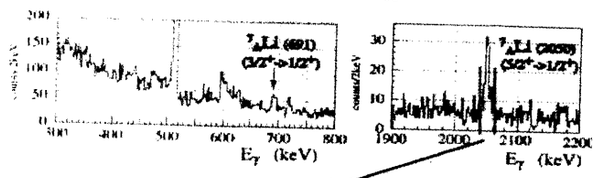

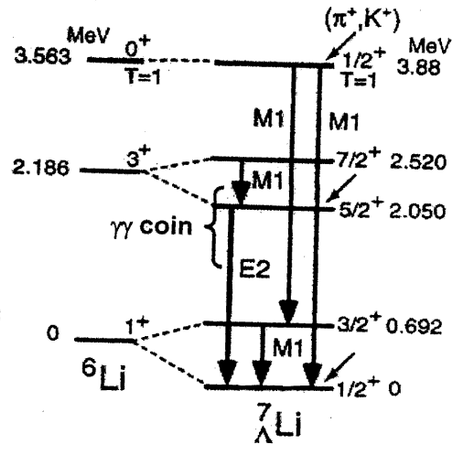

γ γ coincidence after loose event selection

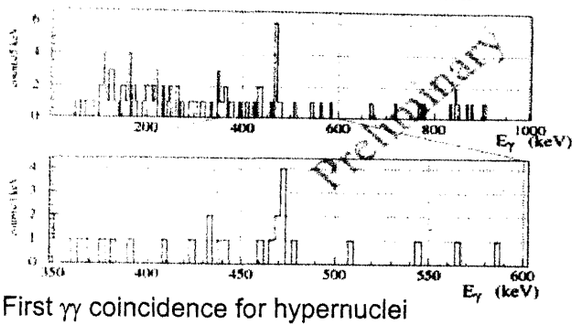

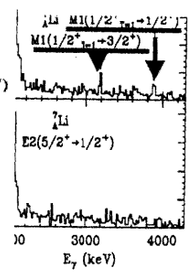

First γγ coincidence for hypernuclei

$^{7}_{\Lambda}$Li
Best-studied Hypernucleus

: E419: ^{7}Li (π$^+$,K$^+$) $^7_\Lambda$Li

E930-2: ^{10}B (K$^-$,π$^-$)$^{10}_{\Lambda}$B* -> $^7_\Lambda$Li*

KEK E419

^{7}Li (π$^+$,K$^+$γ) $^7_\Lambda$Li

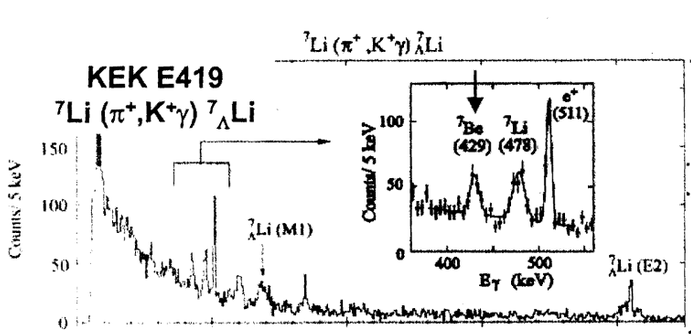

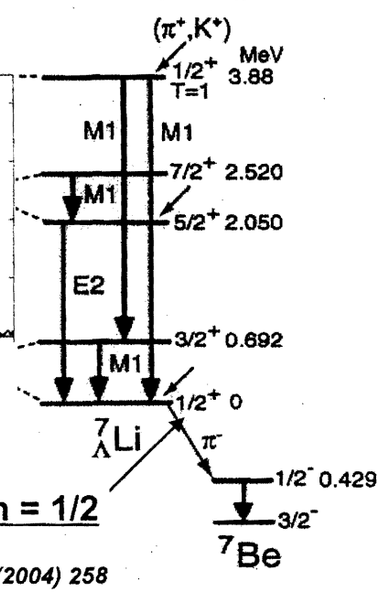

Non-spin-flip in weak decay Λ ->N π

$^7_\Lambda$Li (1/2$^+$) -> $^7_\Lambda$Be*(1/2$^-$) + π$^-$

$^7_\Lambda$Li (3/2$^+$) -> $^7_\Lambda$Be*(3/2$^-$) + π$^-$

g.s.spin = 1/2

Sasao et al., PLB 579 (2004) 258

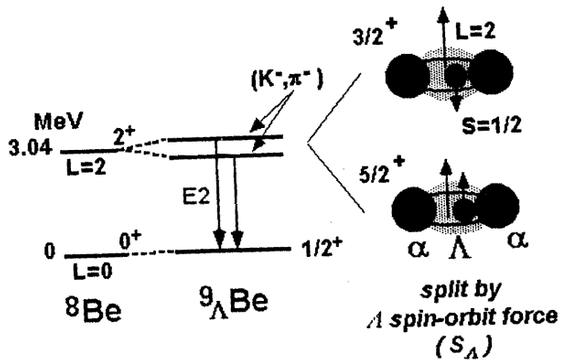

$^{9}_{\Lambda}$Be
ΛN spin-orbit force

BNL E930('98)

- Hiyama et al: *PRL 85 (2000) 270*
  $E(3/2^+)-E(5/2^+)$
  Meson exch. 0.08 - 0.20 MeV
  ~quark model 0.035 - 0.040 MeV
  -> Favors quark models

- Millener:
  $E(3/2^+)-E(5/2^+)$
  $= -0.035\,\Delta - 2.465 S_\Lambda + 0.936T$
  S_Λ= -0.01 MeV

Consistent with very small LS splitting in $^{13}_{\Lambda}$C

^{9}Be (K^-, $\pi^-\gamma$) $^{9}_{\Lambda}$Be 43±5 keV

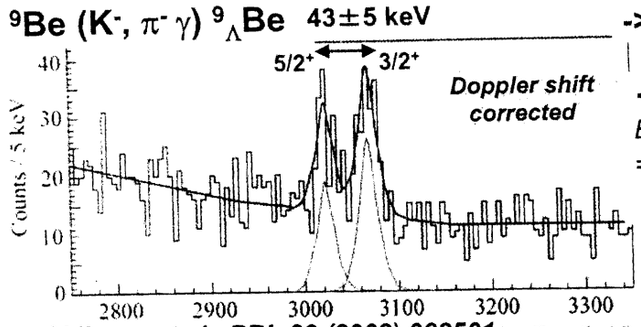

Akikawa et al., PRL 88 (2002) 082501;
Tamura et al., HYP03

Hypernuclear Fine Structure

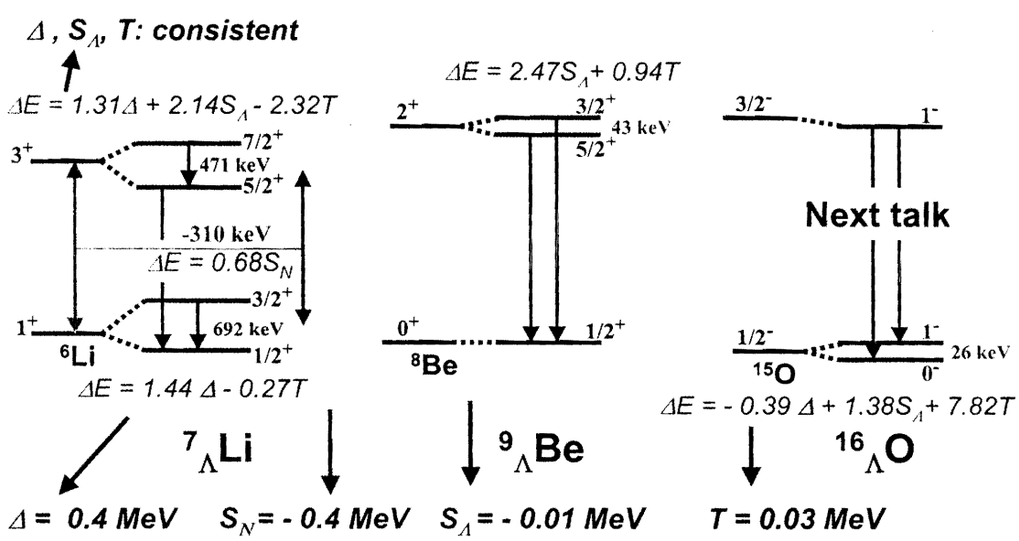

Δ = 0.4 MeV ***S_N= - 0.4 MeV*** ***S_Λ= - 0.01 MeV*** ***T = 0.03 MeV***

All the spin-dependent force parameters determined.

J-PARC (Japan Proton Accelerator Research Complex)

By KEK+JEARI, completed in 2008 at Tokai, Japan

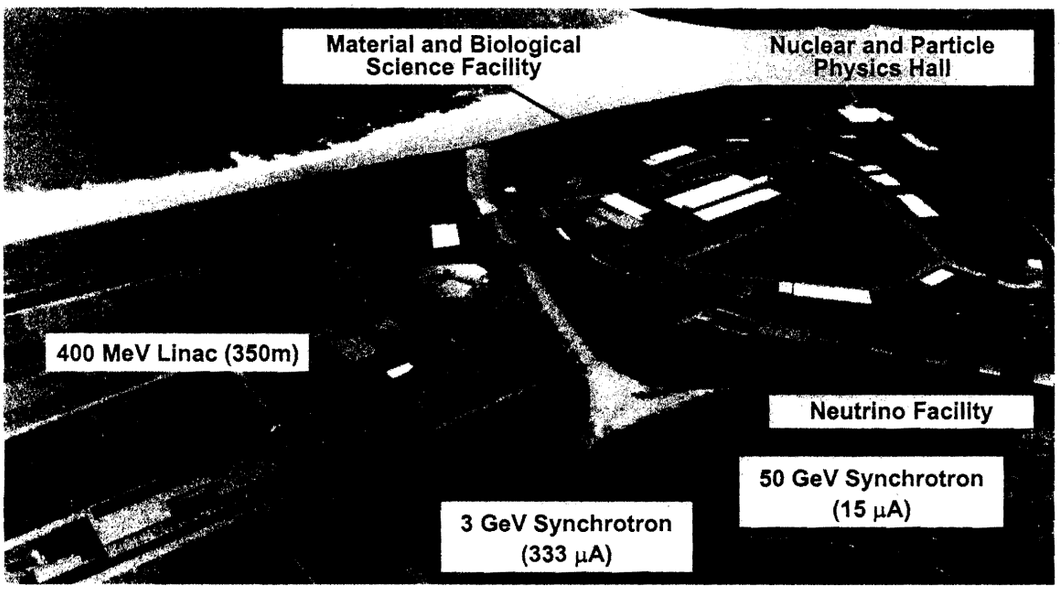

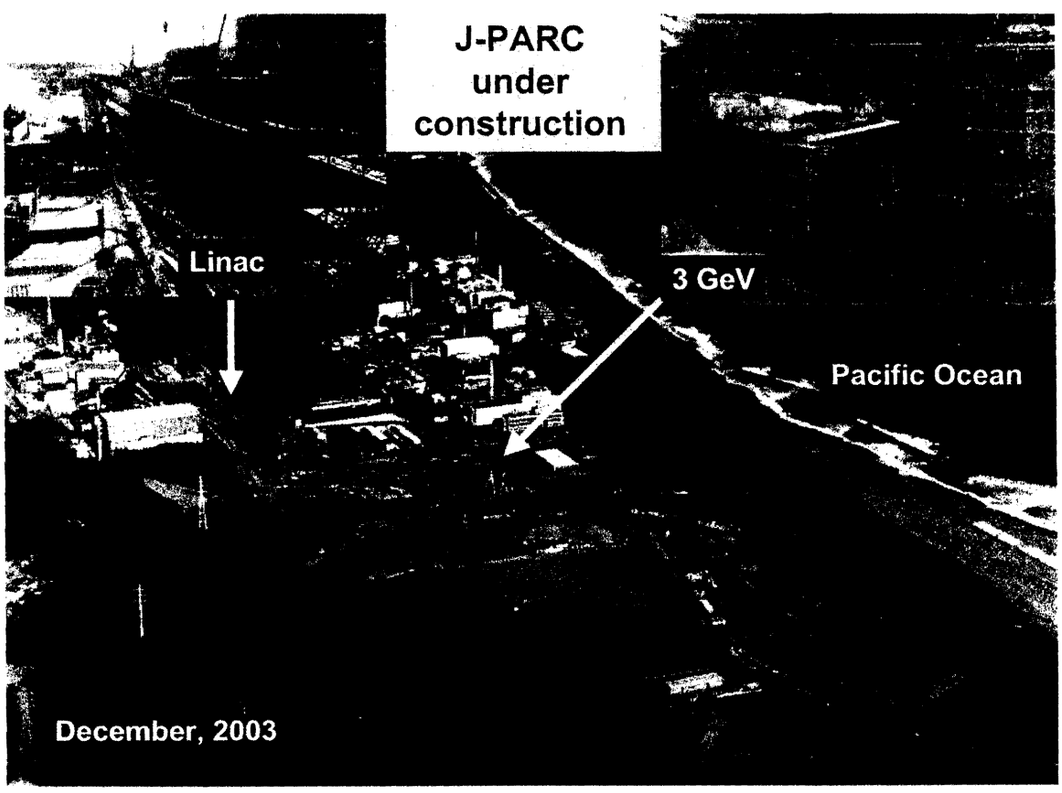

New Hyperball for J-PARC

Hyperball-J

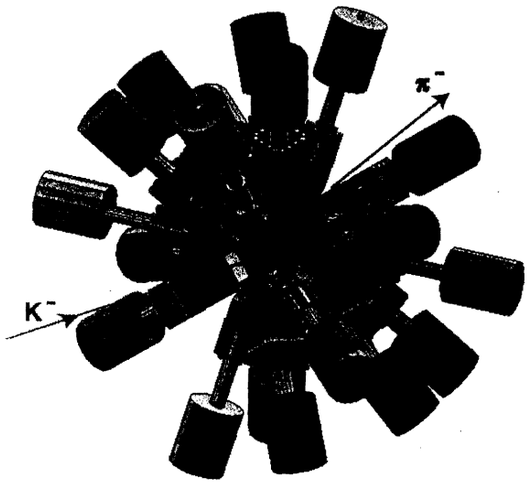

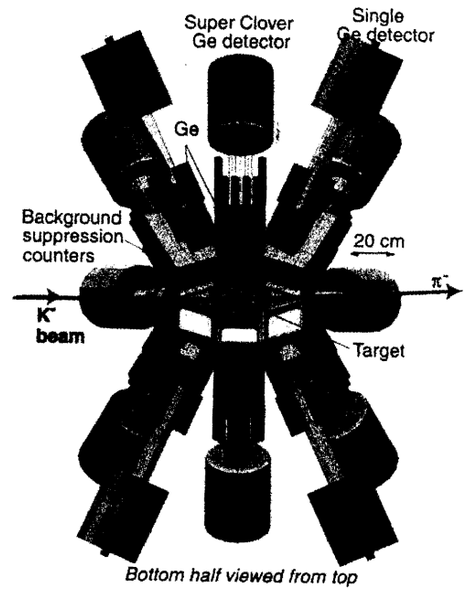

- ε > 10% at 1 MeV (x4 of Hyperball)
- Rate limit ~2x10^7 particles /s (x5)
- Yield: x20 for single γ
  x80 for γγ

Plans of γ spectroscopy at J-PARC

(1) Complete study of light (A<30) hypernuclei

(2) Systematic study of medium and heavy hypernuclei

(K^-,π^- γ) *spin-flip/ no-flip productions* — **ΛN force (ΛN–ΣN, p-wave,..)**
B(E2)-> shrinkage, New symmetries

(3) n-rich/ p-rich/ morrir hypernuclei

(K^-, γ γ) *in-beam method* — **Charge sym. break in ΛN force**
(K^-, π^0 γ) *mirror hypernuclei* — **Shrinkage of n-halo**

(4) Spin-flip *B(M1)*

(K^-,π^- γ), (π^+,K^+ γ) *Doppler shift atten.* — **μ_Λ in nuclei (ρ-dependence)**
(K^-,π^- γ *p*) *γ-weak coincidence*

(5) Double strangenss (Ξ⁻ atom X rays and ΛΛ-hypernuclei)

(K^-, K^+ γ) — **ΞN, ΛΛ interactions**

Λ-Spin-flip B(M1)

μ_Λ in nucleus -> medium effect of baryons

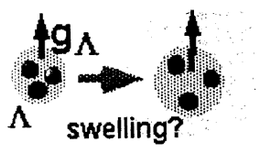

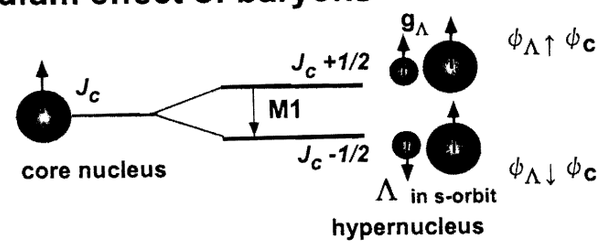

$\frac{e\hbar}{2mc}$?

$$B(M1) \propto |\langle\Phi_f|\mu^z|\Phi_i\rangle|^2$$
$$= |\langle\phi_{\Lambda\uparrow}\,\phi_c|\; g_c J_c^z + g_\Lambda J_\Lambda^z \;|\phi_{\Lambda\downarrow}\,\phi_c\rangle|^2$$
$$\propto (g_c - g_\Lambda)^2$$

- **Doppler shift attenuation method** *[established method for B(E2)]*
  for light hypernuclei
- **γ-weak coincidence method** (K^-, $\pi^-p\gamma$) *[new, used when τ(weak) ~ τ(M1)]*
  for heavy hypernuclei

Accuracy Δg_Λ < 5% achievable at J-PARC -> ρ dependence of g_Λ

Summary

- Hypernuclear γ spectroscopy with Hyperball in progress
  -> ΛN interaction, shrinking effect from B(E2)
- $^7_\Lambda$Li, $^9_\Lambda$Be, $^{16}_\Lambda$O : Hypernuclear fine structure
  -> All the ΛN spin-dependent force parameters
  (Δ, S_Λ, S_N, T) determined.
  -> origin of "nuclear force"
  LS force (S_Λ, S_N) *quark picture favored*
  Tensor force (T) *meson exchange OK*
- First success of γγ coincidence
- J-PARC high-intensity K beam + Hyperball-J
  -> "Table of Hyper-isotopes" incl. heavy, n-rich, ...
  g_Λ in nucleus

Λ-N interaction studied from hypernuclear gamma spectroscopy

Mifuyu Ukai Dept. of Phys. Tohoku Univ.
for the E930('01) collaboration

The excitation energies of low-lying p-shell hypernuclear levels are described with four parameters of the spin-dependent ΛN effective interactions. They are the spin-spin force (Δ), the Λ-spin-dependent spin-orbit force (S_Λ), the N-spin-dependent spin-orbit force (S_N) and the tensor force (T). Our purpose is the study of the spin-dependent ΛN interactions through precise measurement of hypernuclear structure. The past experiments using Hyperball succeded in determination of Δ, S_Λ and S_N from the ^{7}Li $(\pi^+, K^+)^7_\Lambda$Li[1] and the ^{9}Be (K^-, π^-) $^9_\Lambda$Be[2] reactions. The present experiment aims at determination of the tensor force strength, T and consistency check of all the spin-dependent interactions by measurement of various p-shelll hypernuclear levels.

In 2001, we performed γ-ray spectroscopy experiment of p-shell hypernuclei ($^{16}_\Lambda$O, $^{15}_\Lambda$N, $^{10}_\Lambda$B, $^9_\Lambda$Be and $^7_\Lambda$Li) using Hyperball, E930('01) at the AGS D6 beam line of Brookhaven National Laboratory (BNL). Bound states of $^{16}_\Lambda$O and $^{15}_\Lambda$N were produced by the ^{16}O (K^-, π^-) reaction and those of $^{10}_\Lambda$B, $^9_\Lambda$Be and $^7_\Lambda$Li were produced by the ^{10}B (K^-, π^-) reaction directly or via particle emissions.

I will present the results on E930('01), in particular, on $^{16}_\Lambda$O and $^7_\Lambda$Li data. We observed two γ rays of $^{16}_\Lambda$O and we found very small level structure of $^{16}_\Lambda$O which is the smallest structure by far ever measured in a hypernucleus. The small structure provided a small strength of the ΛN tensor force. This is the first experimental data on the ΛN tensor force. Then all the ΛN interactions are experimentally determined. And we observed a new γ-ray peak by taking $\gamma\gamma$ coincidence with another known γ-ray peak of $^7_\Lambda$Li. It is the first success of $\gamma\gamma$ coincidence. It is worthy of specially mention, the $^7_\Lambda$Li data was taken only 48 hour beam time while most of hypernuclear γ-ray spectroscopy experiments take one month or more beam time.

References

[1] H. Tamura *et al.*, Phys. Rev. Lett. **84** (2000) 5936.

[2] H. Akikawa *et al.*, Phys. Rev. Lett. **88** (2002) 082501, and
H. Tamura Proc. HYP03 Nucl. Phys. A to be published.

Λ-N interaction studied from hypernuclear gamma spectroscopy

Mifuyu Ukai

Dept. of Phys., Tohoku Univ.

Introduction

Experiment

Analysis

Result

Summary

Experimental purposes

BNL E930 ('01)

Gamma-ray spectroscopy of *p*-shell hypernuclei
with Hyperball in the (K^-,π^-) reaction at BNL AGS D6 line

- $^{16}O(K^-,\pi^-\gamma)$ levels $^{16}_{\Lambda}O$ $^{15}_{\Lambda}N$

  Determination of the ΛN tensor force strength, T

- $^{10}B(K^-,\pi^-\gamma)$ levels $^{10}_{\Lambda}B$ $^{9}_{\Lambda}Be$ $^{7}_{\Lambda}Li$

Consistency check of all the ΛN spin-dependent interactions

BNL-E930('01) collaboration

Tohoku Univ.	**H. Tamura, Y. Miura, K. Mizunuma, M. Ukai O. Hashimoto, S. N. Nakamura, Y. Okayasu, T. Miyoshi**
Riken	**K. Tanida**
Kyoto Univ.	**H. Akikawa, K. Imai, H. Takahashi**
Osaka Univ	**S. Ajimura, T. Hayakawa, K. Kishimoto, S. Minami**
KEK	**T. Nagae, Y. Sato**
Gifu Univ.	**K. Nakazawa**
BNL	**H. Hotchi, D. E. Alburger, R. E. Chrien M. May, P. Pile, A. Rusek**
CMU	**G. B. Franklin, B. P. Quinn**
GSI	**A. Banu**
Hampton Univ	**L. Tang, L. Yuan**
Univ. Freiburg	**J. Franz**

ΛN spin-dependent parameters

for the p-shell hypernuclei with Λ in 0s-orbit

	Δ spin-spin	S_Λ spin-orbit	S_N spin-orbit	T tensor
typical levels with large contribution	${}^{7}_{\Lambda}$Li($\frac{3}{2}^+,\frac{1}{2}^+$)	${}^{9}_{\Lambda}$Be($\frac{5}{2}^+,\frac{3}{2}^+$)	${}^{7}_{\Lambda}$Li($\overline{\frac{7}{2}^+,\frac{5}{2}^+}$)-($\overline{\frac{3}{2}^+,\frac{1}{2}^+}$)	${}^{16}_{\Lambda}$O ($1^-,0^-$)
	${}^{10}_{\Lambda}$B($2^-,1^-$)			${}^{15}_{\Lambda}$N ($\frac{3}{2}^+,\frac{1}{2}^+$)
Experimentally determined by previous experiments with Hyperball				**No data**

Tensor force of ΛN interaction

one pion exchange
(origin of large NN tensor force)

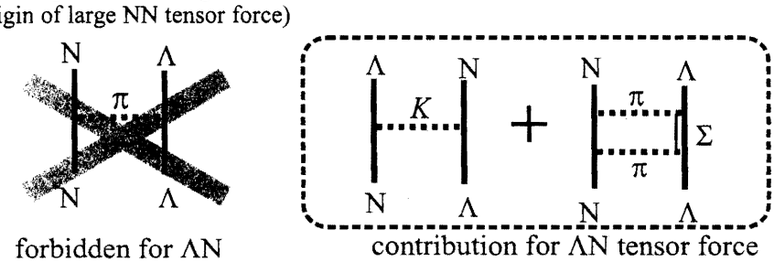

forbidden for ΛN — contribution for ΛN tensor force

predicted strength T

T :20 keV ~ 60 keV (meson exchange models)

	ND	NF	NSC89	NSC97f
[MeV]	0.018	0.033	0.036	0.054

$^{16}_{\Lambda}$O as a probe of the tensor force

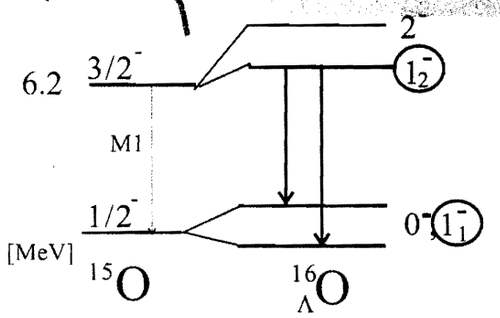

populated by (K^-,π^-)

↓ expected γ transition

$\Delta E_{doublet}$ ($^{16}_{\Lambda}$O$_{g.s.}$) is sensitive to the tensor force

$E(1_1^-)-E(0^-)=$
$-0.38\Delta+1.38S_\Lambda-0.005S_N+7.8T+\Lambda\Sigma$
$= -0.05 \sim +0.15$ [MeV]

D.J. Millener

$\Delta=0.47\sim0.37$, $S_\Lambda=-0.01$, $S_N=-0.44$, $(\Lambda\Sigma=0.031)$
(from experiments)
$T=+0.02\sim0.06$ [MeV]
(from meson exchange models)

Other shell model calculation
$E(1_1^-)-E(0^-)=+0.1\sim0.6$ [MeV]

S. Fujii

Experimental setup

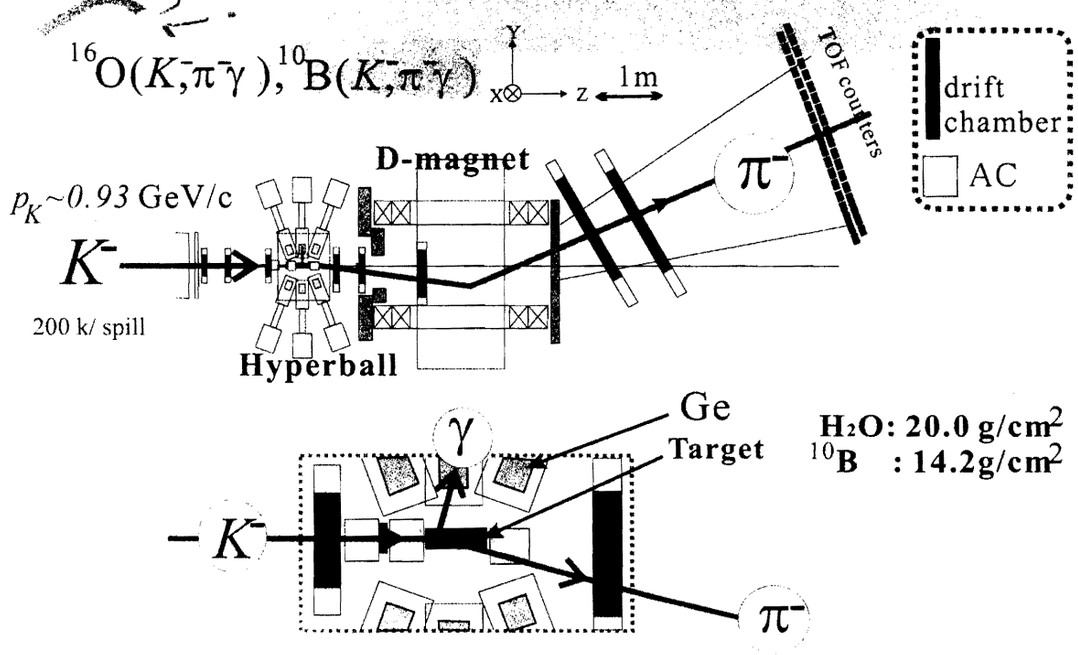

Doppler shift correction

$^{16}_{\Lambda}O^{*}(1^{-})$ life time << stopping time
(< fs) (1 ps)

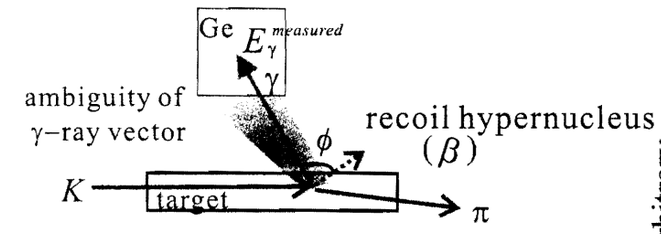

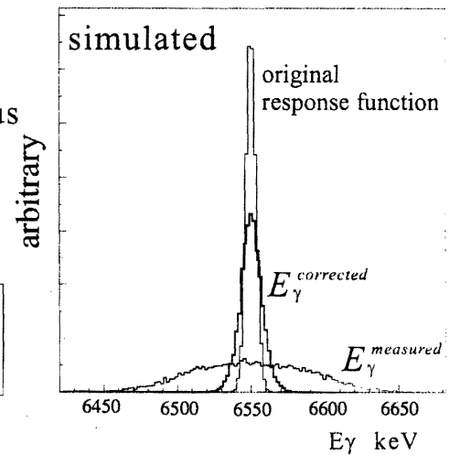

$$E_{\gamma}^{corrected} = \frac{1}{\sqrt{1-\beta^2}}\cdot(1-\beta\cos\phi)\cdot E_{\gamma}^{measured}$$

Doppler shift correction formula

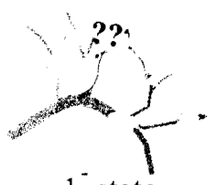

γ−ray and mass spectra in the $^{16}O(K^{-},\pi^{-})$ reaction

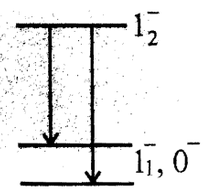

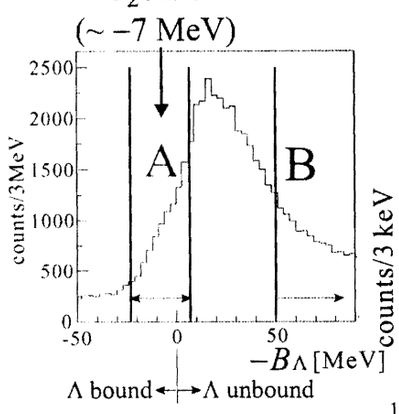

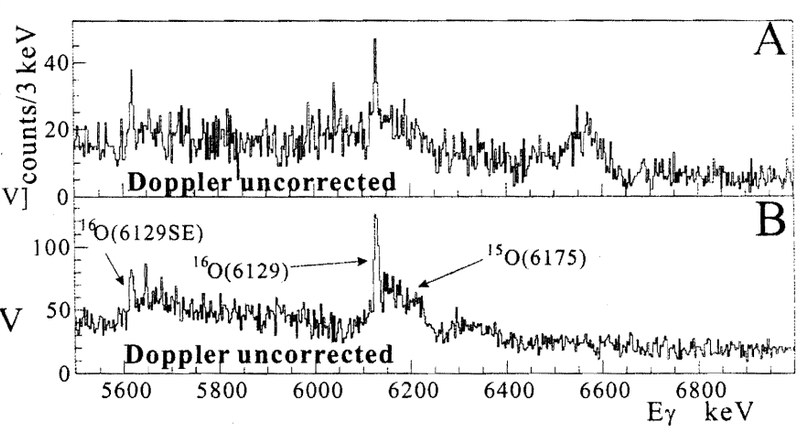

A:−22 < −BΛ < 8 MeV
B: −BΛ> 50 MeV

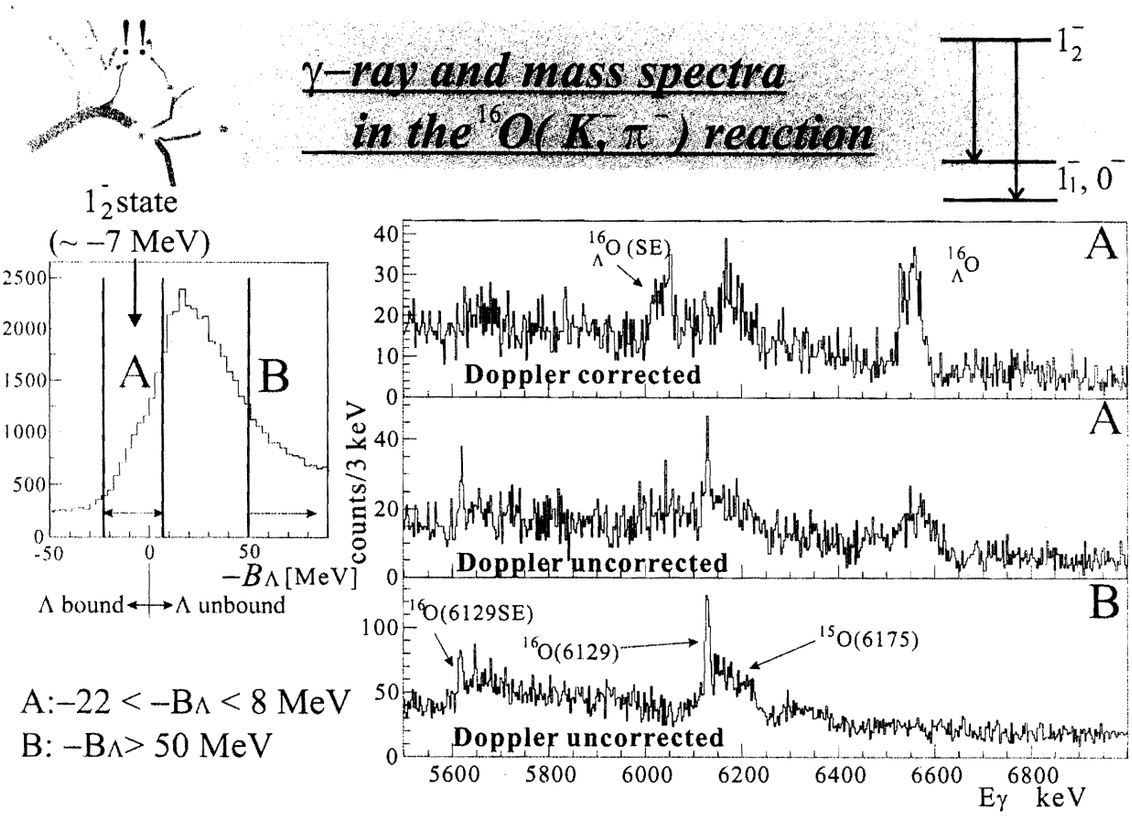

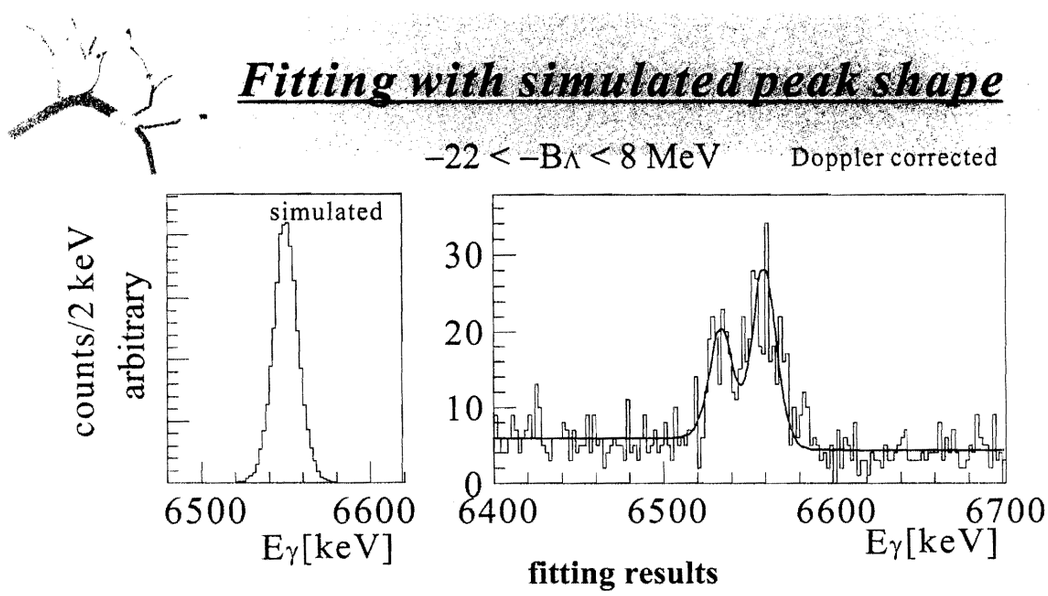

fitting results

peak energy	6534.1 ± 1.5± 1.7	6560.2 ± 1.3 ± 1.7	keV
energy spacing	26.1 ± 2.0 ± 0.2		keV
yield	137 ± 18 ±5	210 ± 30 ± 5	counts
yield ratio	0.64 ± 0.12		

level assignment

Branching ratio

$I\gamma(1^- \to 1^-)/I\gamma(1^- \to 0^-)$ = 0.5 weak coupling

0.41 level mixing (Millener)

effective efficiency from $\pi\gamma$ angular correlation

$\varepsilon(1^- \to 1^-)/\varepsilon(1^- \to 0^-)$ = 0.80 +0.02 (sys.) simulated

$Y(1^- \to 1^-)/Y(1^- \to 0^-) = 0.42, 0.34$

$Y(1^- \to 0^-)/Y(1^- \to 1^-) = 2.38, 2.94$

exp. $N(6534)/N(6560) = 0.64 \pm 0.12$

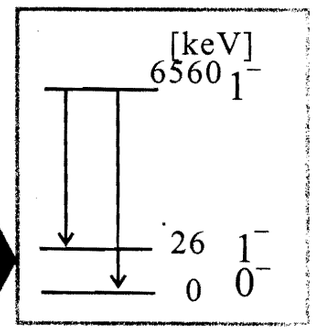

Strength of the tensor force

$^{16}_{\Lambda}O$ g.s. doublet — 1^- — 0^- $\Delta E_{g.s\ doublet} = 26.1 \pm 2.0$ keV

$E(1^-) - E(0^-)$

$= -0.38\Delta + 1.38 S_\Lambda - 0.005 S_N + \mathbf{7.8}\boldsymbol{T} + \Lambda\Sigma$

$= +26$ [keV]

$\Delta = 0.48 \sim 0.37$, $S_\Lambda = -0.012$, $S_N = -0.48$, $\Lambda\Sigma = 0.031$ [MeV]

$T = +26 \sim 32$ keV

meson exchange model prediction $+20 \sim 60$ keV

agree with our result

First result on the ΛN tensor force

Summary

γ-ray spectroscopy of p-shell hypernuclei

Hyperball + (K^-, π^-) reaction

${}^{16}_{\Lambda}$O g.s levels determined -- First result on the ΛN tensor force.

The tensor force T = 0.03 MeV

Meson-exchange models OK

We determined **all** the strengths of the spin-dependent interactions (present and previous experiments with **Hyperball**)

Consistency check of all the spin-dependent interactions

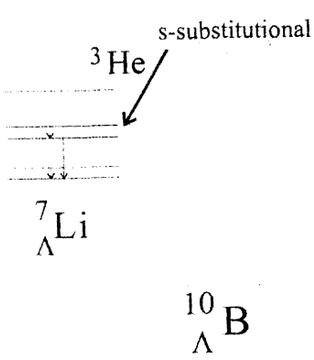

γ rays of ${}^{7}_{\Lambda}$Li
in the ^{10}B(K^-, π^-)${}^{10}_{\Lambda}$B reaction
via ^{3}He emission

Consistency check by $^{7}_{\Lambda}$Li

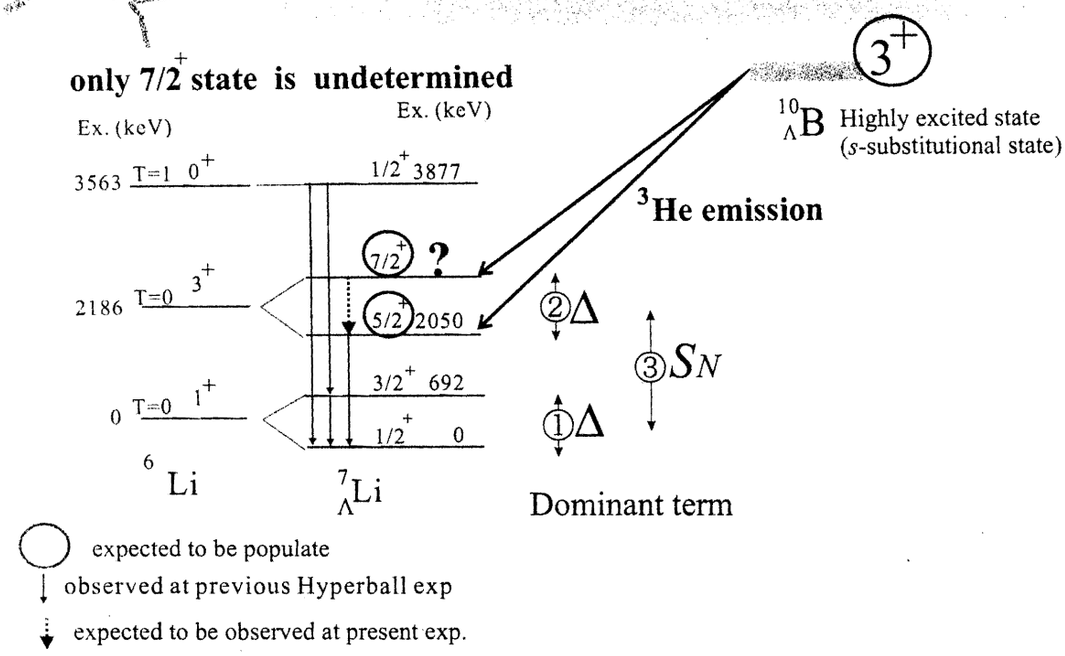

γ–ray and mass spectra in the $^{10}B(K^-, \pi^-)$ reaction

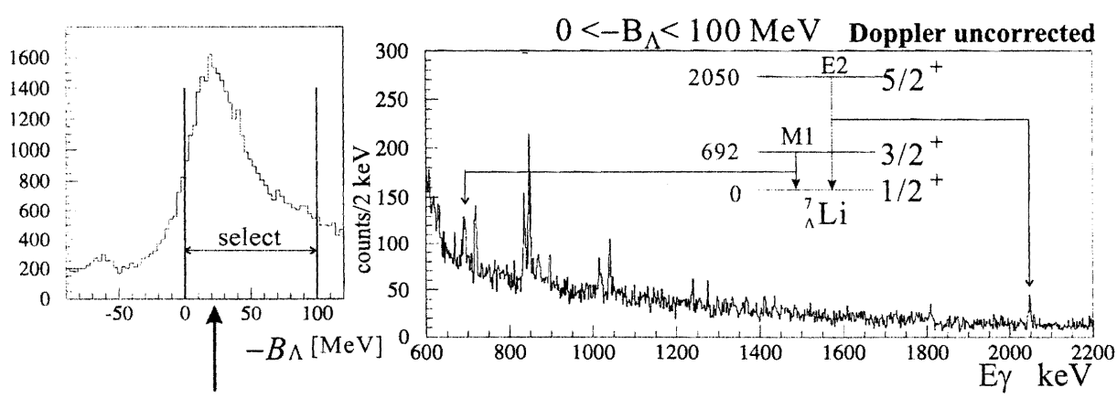

s-substitutional state
(~ 20 MeV)

Observed M1 and E2 γ rays of $^{7}_{\Lambda}$Li
via baryonic decay

also observed in the previous experiment
via ^{7}Li(π^+,K^+)

γ–γ coincidence with E2 transition

single γ spectrum
$0 < -B_\Lambda < 100$ MeV

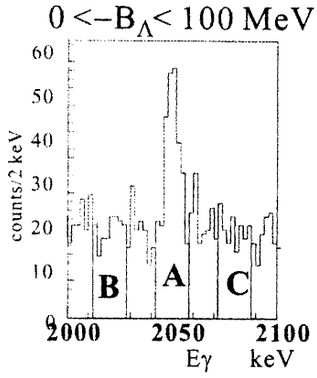

E2 γ-ray single count
132 ± 18

coincidence γ spectra
$0 < -B_\Lambda < 100$ MeV

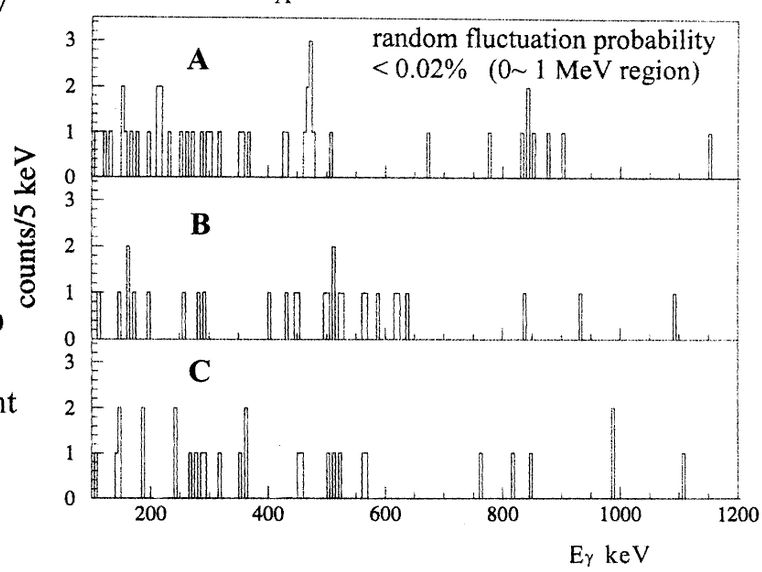

Search for M1 transition of upper doublet

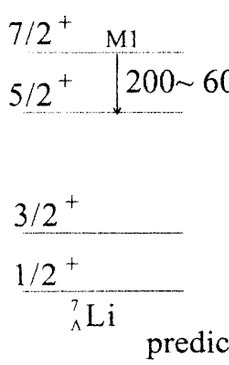

$0 < -B_\Lambda < 40$ MeV (Best S/N for M1(692) peak)

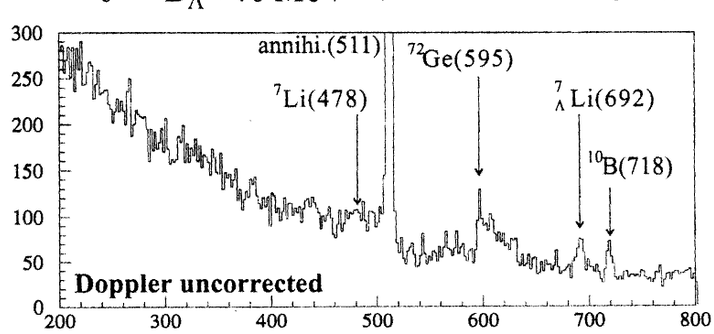

No prominent peak

S/N ratio bad ?
------ hopefully find with other way

γ–γ coincidence with E2 transition

single γ spectrum
$0 < -B_\Lambda < 100$ MeV

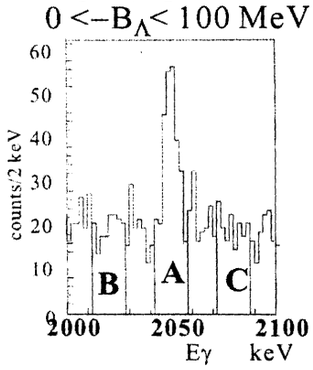

E2 γ-ray single count
132 ± 18

coincidence γ spectra
$0 < -B_\Lambda < 100$ MeV

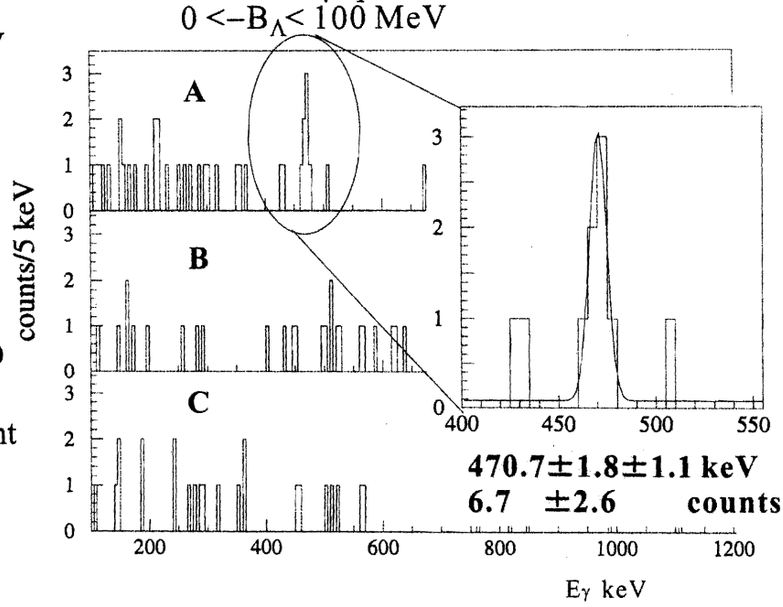

470.7±1.8±1.1 keV
6.7 ±2.6 counts

471 keV peak interpretation

coincidence γ ray with the E2

✕ **^{7}Li γ ray after weak decay**
expected yield of ^{7}Li(478)
~ 0.2 counts

$^7_\Lambda$Li M1 transition($7/2^+ \rightarrow 5/2^+$)

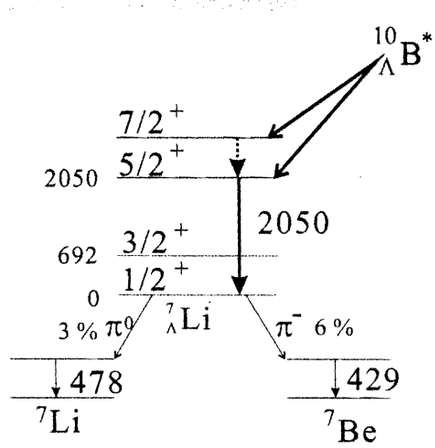

first success in γ–γ coincidence for hypernuclei

Strength of Δ and S_N

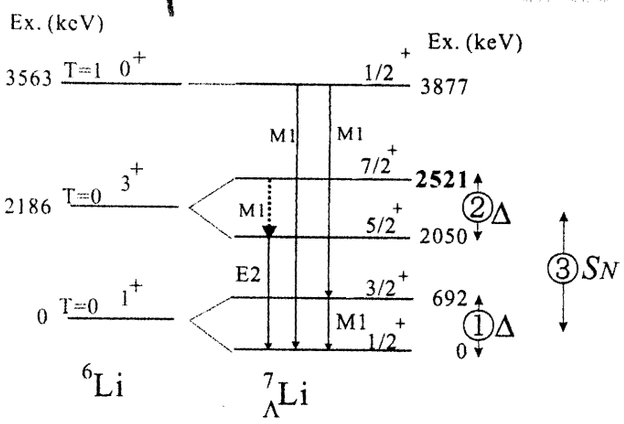

① $E(3/2)-E(1/2)=$
$1.44\Delta+0.05S_\Lambda+0.02S_N+0.27T+\Lambda\Sigma_1$
$=692$ keV

$\Delta = 440$ keV

② $E(7/2)-E(5/2)=$
$1.31\Delta+2.14S_\Lambda+0.02S_N-2.32T+\Lambda\Sigma_2$
$=471$ keV

$\Delta = 378$ keV

③ $\overline{E}(7/2,5/2)-\overline{E}(3/2,1/2)-E(3,{}^{+6}\mathrm{Li})=$
$-0.06\Delta+0.08S_\Lambda+0.68S_N+0.05T$
$=-368$ keV

$S_N = -444$ keV

Value of Δ seems consistent ~ 0.4 MeV

Reliable value of S_N is derived

The ΛN spin-orbit force

(S_Λ, S_N) (–0.01,–0.45) **experiment**

level study of Be -- E930('98) and E930('01)
Li -- E930('01)

(–0.15,–0.25) meson-exchange models

(0.0 ,–0.40) quark model

strength MeV

ΛN spin-orbit force is explained well by **quark model**

NN spin-orbit force -- both quark model and meson-exchange model

Summary

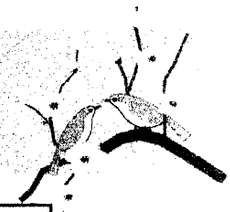

$^{16}_{\Lambda}$O g.s levels determined -- First result on the ΛN tensor force.

The tensor force T = 0.03 MeV

All $^{7}_{\Lambda}$Li levels determined from γ γ coincidence for the first time

The spin-spin force, Δ ~ 0.4 MeV

The N-spin dependent spin-orbit force, S_N ~ 0.44 MeV

<u>The ΛN ensor force</u> Experimental result ⟷ Meson-exchange models

<u>The ΛN spin-orbit force</u> Experimental result ⟷ Quark model

We determined **all** the strengths of the spin-dependent interactions (present and previous experiments with **Hyperball**)

Pairing effect on the giant dipole resonance width at low temperature

Nguyen Dinh Dang [1] and Akito Arima [2]
1 - RIKEN, 2-1 Hirosawa, Wako, 351-0198 Saitama, Japan
2 - House of Councilors, 2-1-1 Nagata-cho, Chiyoda-ku, Tokyo 100-8962, Japan

Intensive experimental studies of γ decays of highly-excited nuclei during the last two decades have shown that the width of the giant dipole resonance (GDR) increases sharply with increasing the temperature T from $T > 1$ MeV up to $\simeq 3$ MeV. At higher T a width saturation has been reported. The increase of the GDR width with T is described reasonably well within the phonon damping model (PDM) [1], which considers the coupling of the GDR to particle-particle and hole-hole configurations at $T \neq 0$ as the mechanism of the width increase and saturation. In general, pairing was neglected in the calculations for hot GDR as it was believed that the gap vanishes at $T = T_c < 1$. In reality, however, thermal fluctuations in finite systems smear out the superfluid-normal phase transition so that the pairing gap survives up to $T \gg 1$ MeV [2, 3].

Very recently the γ decays were measured in coincidence with ^{17}O particles scattered inelastically from ^{120}Sn [4]. A GDR width of around 4 MeV has been extracted at $T = 1$ MeV. This result and the existing systematic for the GDR width in ^{120}Sn up to $T \simeq 2$ MeV are significantly lower than the prediction by the thermal shape-fluctuation model [5]. Based on this, Ref. [4] concluded that the narrow width observed in ^{120}Sn at low T is not understood. In the present work we included the thermal pairing gap obtained from the modified-BCS theory [3] in the PDM [1], and carried out the calculations for the GDR width in ^{120}Sn at $T \leq 5$ MeV. In difference with the gap given within the conventional BCS theory, the modified-BCS gap never vanishes, but monotonously decreases with increasing T up to $T \simeq 5$ MeV. The results obtained show that thermal pairing plays an important role in lowering the width at $T \leq 2$ MeV as compared to the value obtained without pairing. This improves significantly the overall agreement between theory and experiment, including the width at $T = 1$ MeV extracted in the latest experiment [4] (See Fig. 1).

[1] N.D. Dang and A. Arima, Phys. Rev. Lett. **80**, 4145 (1998).
[2] L.G. Moretto, Phys. Lett. B **40**, 1 (1972).
[3] N. Dinh Dang and A. Arima, Phys. Rec. C **68**, 014318 (2003).
[4] P. Heckman *et al.*, Phys. Lett. B **555**, 43 (2003).
[5] W.E. Ormand, P.F. Bortignon, and R.A. Broglia, Phys. Rev. Lett. **77**, 607 (1996); D. Kusnezov, Y. Alhassid, and K.A. Snover, Phys. Rev. Lett. **81**, 542 (1998).

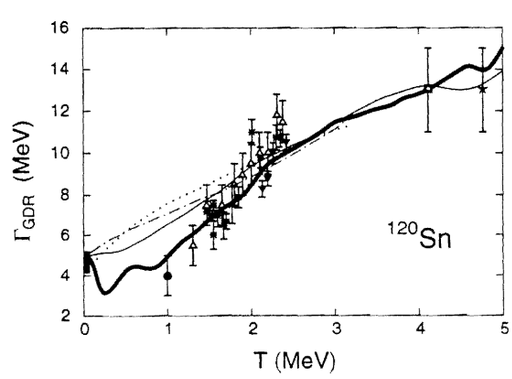

FIG. 1: GDR width Γ_{GDR} as functions of T for ^{120}Sn. The thin and thick solid lines show the PDM results obtained without and including the thermal pairing gap, respectively. Solid circles are the low-T data from Ref. [4]. The predictions by two versions of the thermal shape-fluctuation model [5] are shown as the dash-dotted and thin dotted lines.

Pairing effect on the GDR width at low temperature

Nguyen Dinh Dang
RIKEN

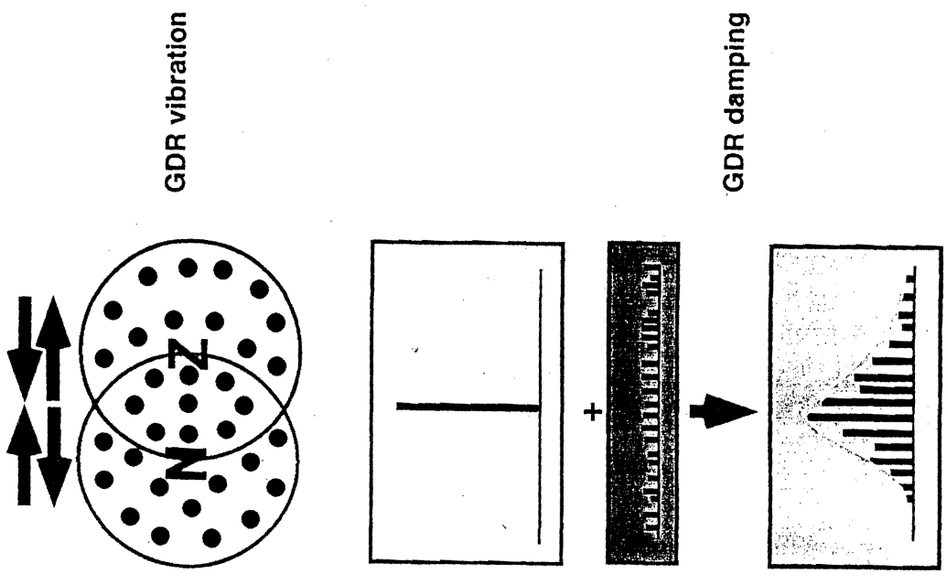

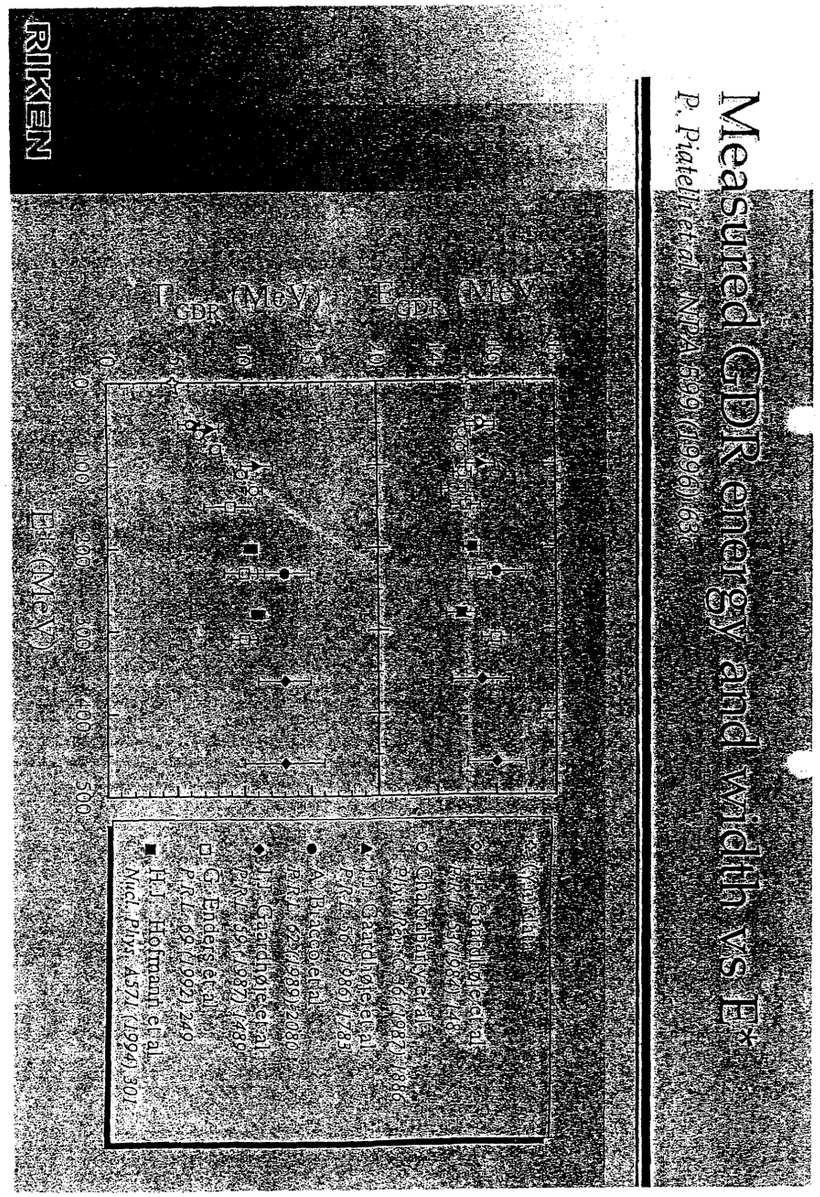

The GDR's parameters

1) Energy E_{GDR} $(80/A^{1/3})$

2) FWHM Γ (~ 4 - 5 MeV)

3) EWSR (~ 60 NZ/A MeV.mb)

Microscopic description

RPA

$Q^{+}|0) = \Sigma(X_{ph}a^{+}_{p}a_{h}+Y_{ph}a^{+}_{h}a_{p})|0)$

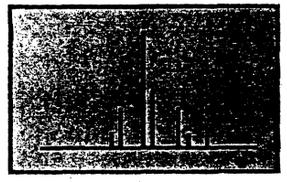

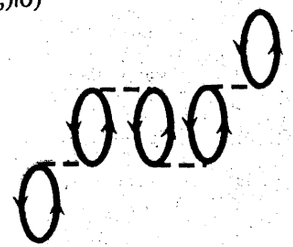

Beyond RPA

$\Omega^{+}|0) = \{ \mathbf{RQ^{+}} + \mathbf{P[Q^{+}\cdot Q^{+}]} \}|0)$

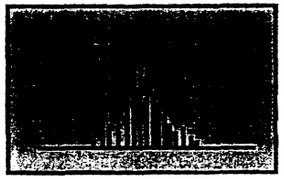

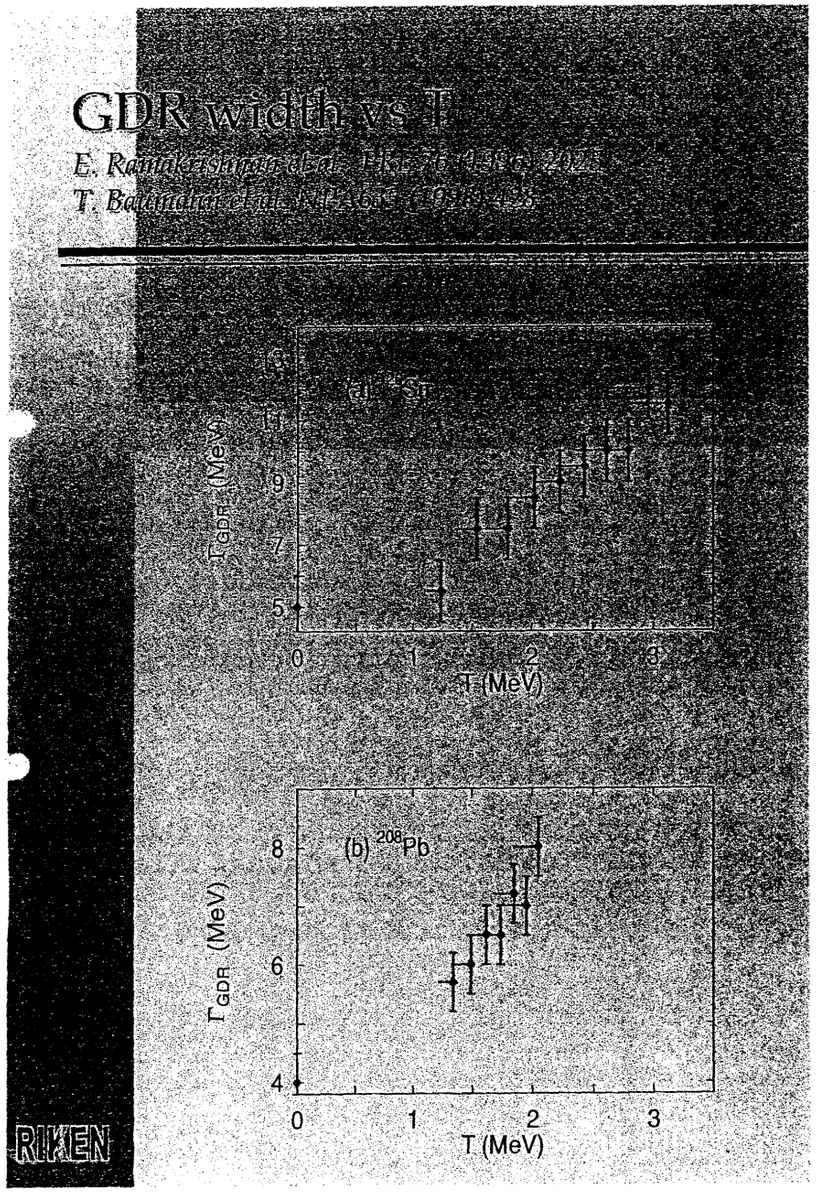

At finite temperatures the poles of the *ph* excitations remains essentially in their original location (stability of the HF energies); their residues, however,decrease according to $(f_h\text{-}f_p)$. Simultaneously, a large number of additional poles appears at energies $(E_h\text{-}E_{h'})$ and $(E_p\text{-}E_{p'})$. As the temperature increases, the corresponding residues will first increase due to the factor $(f_h\text{-}f_{h'})$ and $(f_p\text{-}f_{p'})$. Only at very high temperatures all occupation numbers will be equal, causing all residues to approach zero.

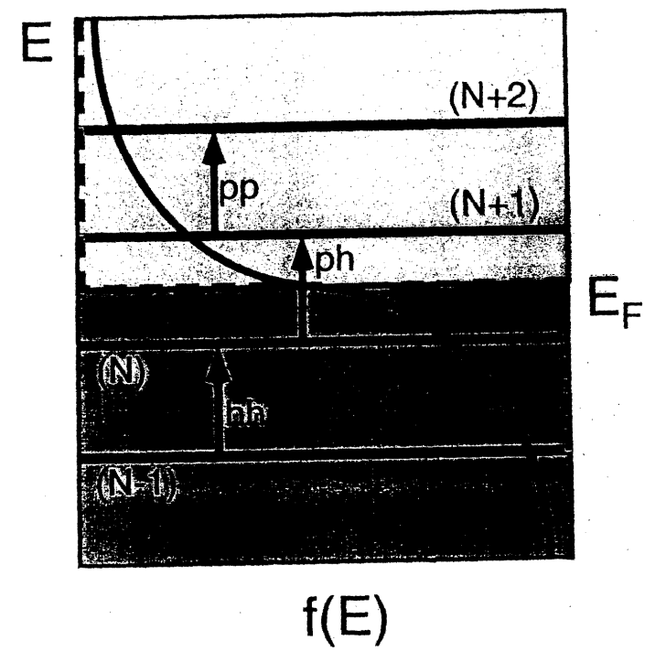

Hot GDR width

NDD [illegible] *PRL* [illegible]

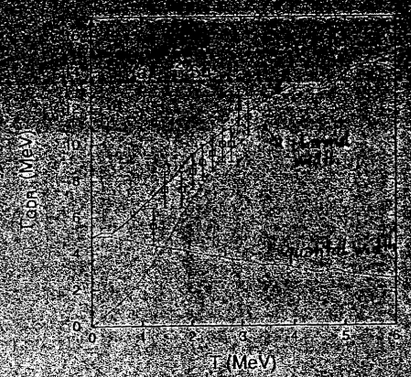

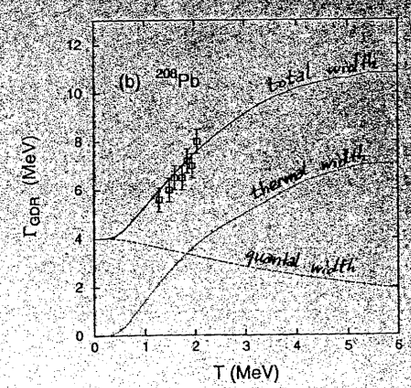

RIKEN

Comparison with other models

GDR width

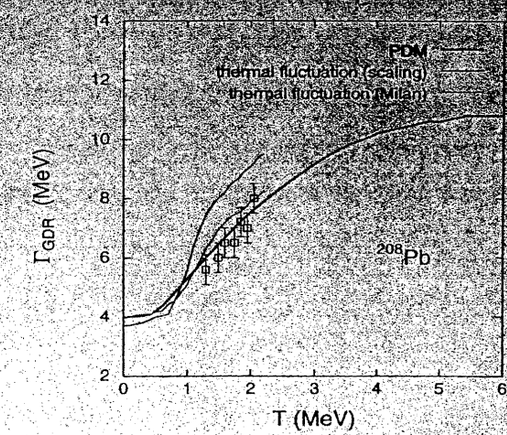

RIKEN

Hot GDR's shapes (CASCADE)

NDD, K. Eisenman, J. Seitz, M. Thoennessen, PRC 61 (2000) 027302

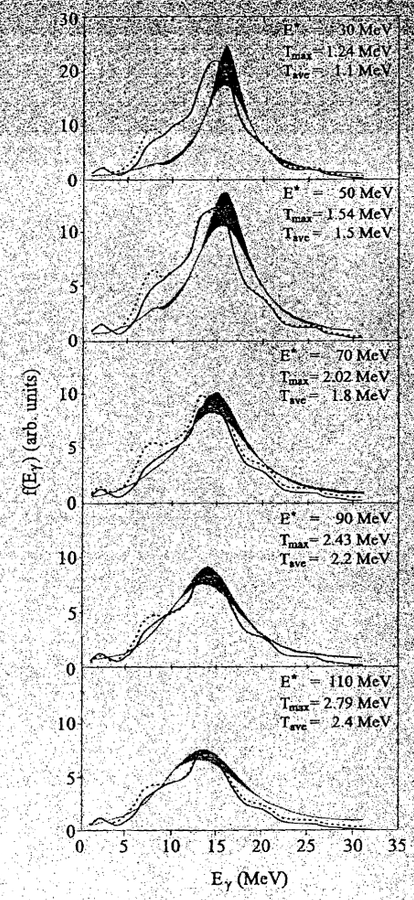

RIKEN

Comparison with other models
GDR width

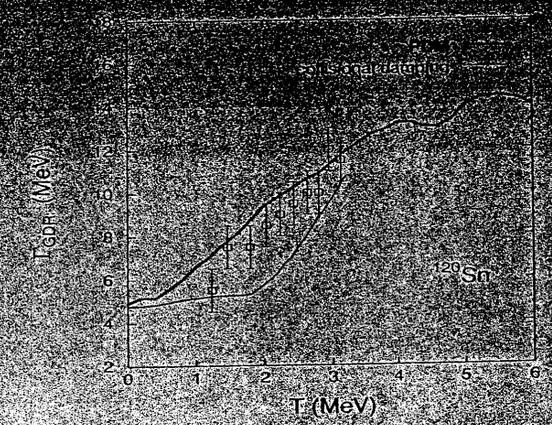

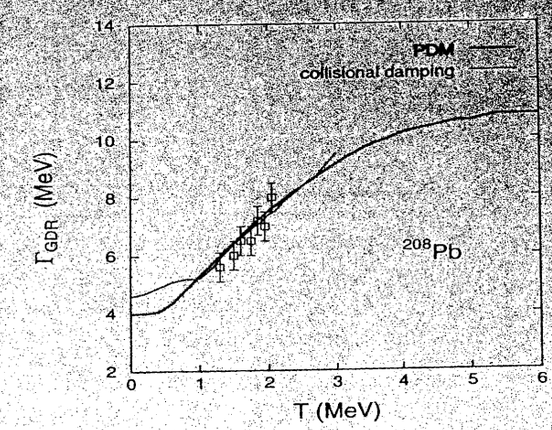

RIKEN

■ Pairing at finite temperature

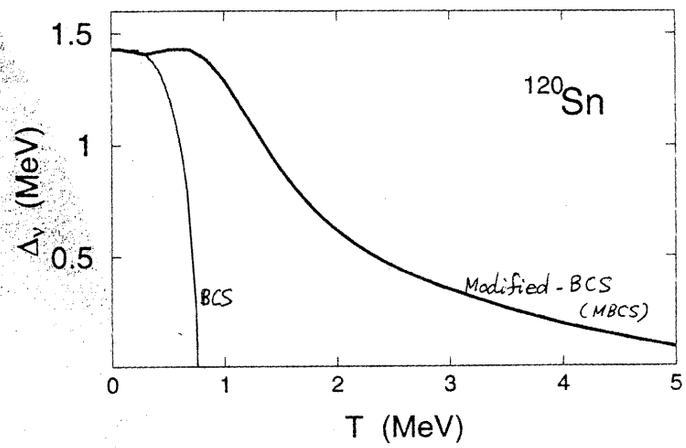

Heat capacity, level-density parameter, and level density

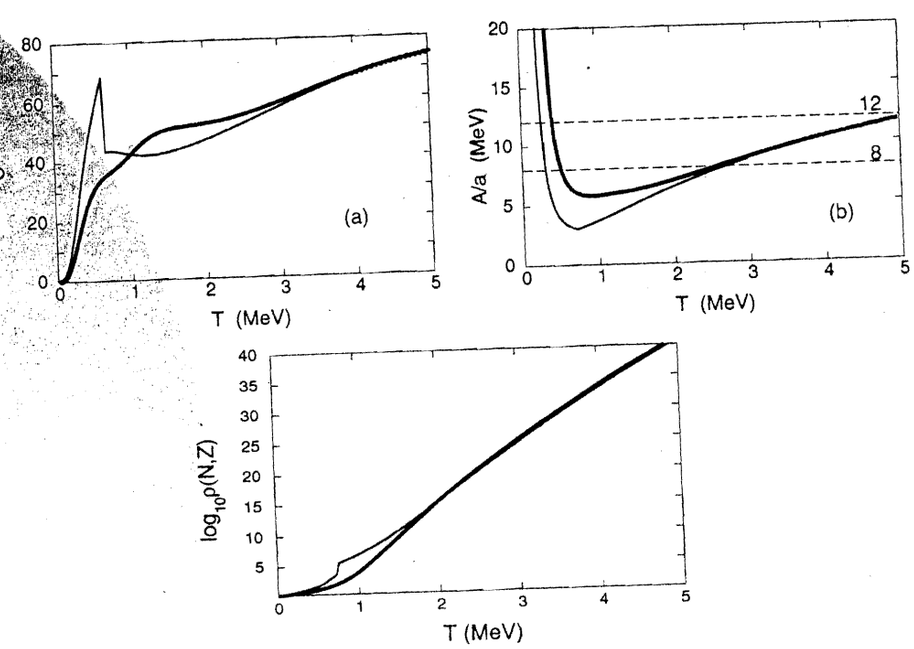

▪ Pairing effect on GDR width at low T

The GDR width is calculated within the phonon damping model (PDM) as [NDD & Arima, PRL 80, 4145 (1998), NDD *et al.*, PRC 63, 044302 (2001)]

$$\Gamma_{\mathrm{GDR}} = \Gamma_{\mathrm{Q}} + \Gamma_{\mathrm{T}} \ ,$$

$$\Gamma_{\mathrm{Q}} = 2\gamma_{\mathrm{Q}}(E_{\mathrm{GDR}}) = 2\pi F_1^2 \sum_{ph} \left[u_{ph}^{(+)}\right]^2 (1 - n_p - n_h)\delta(E_{\mathrm{GDR}} - E_p - E_h) \ ,$$

$$\Gamma_{\mathrm{T}} = 2\gamma_{\mathrm{T}}(E_{\mathrm{GDR}}) = 2\pi F_2^2 \sum_{\substack{ss' = pp', \\ hh'}} \left[v_{ss'}^{(-)}\right]^2 (n_{s'} - n_s)\delta(E_{\mathrm{GDR}} - E_s + E_{s'}) \ ,$$

$$n_s = \frac{1}{\pi}\int_{-\infty}^{\infty} \frac{n_{\mathrm{F}}(E)\gamma_j(E)}{\left[E - E_j - M_j(E)\right]^2 + \gamma_j^2(E)} dE \ , \qquad E_{\mathrm{GDR}} - \omega_q - P_q(E_{\mathrm{GDR}}) = 0 \ .$$

$$S_{\mathrm{GDR}}(\omega) = \frac{1}{\pi} \frac{\gamma(\omega)}{(\omega - E_{\mathrm{GDR}})^2 + \gamma^2(\omega)}$$

PDM prediction vs experimental data

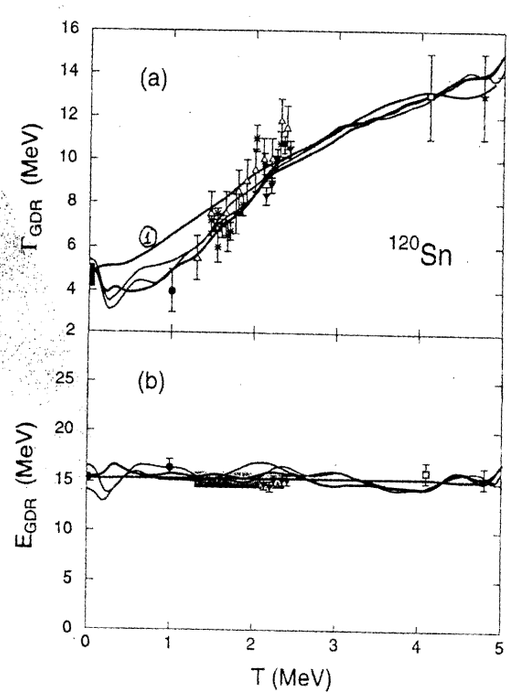

Data point at T=1: Heckman *et al.* **PLB 555 (2003) 43** (of gamma-decays in coincidence with ^{17}O scattered inelastically from ^{120}Sn)

GDR line shape at low T

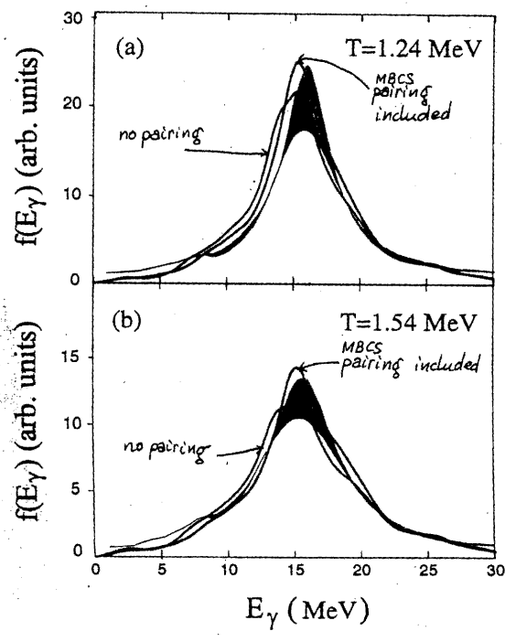

Conclusions

- Thermal pairing gap determined within the modified BCS theory was included in the phonon damping model to calculate the GDR width in ^{120}Sn at temperatures up to T = 5 MeV.

- In difference with the gap given by the conventional BCS theory, the modified-BCS gap decreases monotonously with increasing T and remains finite even at T as high as 5 MeV.

- Because of this effect the GDR width at T< 2 MeV becomes smaller than the value obtained when pairing was neglected. This improves significantly the overall agreement between theory and experiment, including the most recent data point at T=1 MeV.

High-Spin Isomer in ^{93}Mo

T. Fukuchi, Y. Gono[a], A. Odahara[b], H. Watanabe[c], S. Tanaka[a], M. Inoue[a], Y. Wakabayashi[a], T. Sasaki[a], M. Kibe[a], N. Hokoiwa[a], T. Shinozuka[c], M. Fujita[c], A. Yamazaki[c], T. Sonoda[c], C.S. Lee[d], Y.K. Kwon[d], J.H. Lee[d]

Center for Nuclear Study (CNS), University of Tokyo, Wako, Saitama 351-0198, Japan
[a]*Department of Physics, Kyushu University, Hakozaki, Fukuoka 812-8581, Japan*
[b]*Nishinippon Institute of Technology, Kanda-machi, Fukuoka-ken 812-8581, Japan*
[c]*Cyclotron and Radioisotopes Center (CYRIC), Tohoku University, Aoba, Sendai 980-8578, Japan*
[d]*Department of Physics, Chung-Ang University, Seoul 156-756, Korea*

The high-spin states of ^{93}Mo were studied up to 9.7 MeV excitation using the ^{82}Se(^{16}O,5n)^{93}Mo fusion evaporation reaction. The ^{16}O beam of 100 MeV was supplied by AVF cyclotron at Cyclotron and Radioisotopes Center (CYRIC), Tohoku University. A new γ-ray detection system with clover type high-purity Germanium detectors have been developed.

Two high-spin isomers were discovered as a $27/2^-$ state at 4.4 MeV and a $(39/2^-)$ state at 9.7 MeV excitation energy in this experiment. Eleven γ-rays and 11 levels were newly found using the γ-γ coincidence data. Spins and parities of states were assigned for 5 levels based on angular distribution and linear polarization measurements. The life-times of high-spin isomers at $27/2^-$ and $(39/2^-)$ states were determined to be 0.8(1) nsec and 1.1(4) μsec from beam-delayed and delayed γ-γ coincidence measurements.

High-spin isomer were systematically studied in N=83 isotones, and these isomer are consider to be caused by the sudden shape changes from near spherical to an oblate shape. Based on the analogy of configuration of high-spin isomers in N=83 and 51 isotones, a configuration of the high-spin isomer in ^{93}Mo at $(39/2^-)$ state was deduced to be $[\nu(d_{5/2}g_{7/2}h_{11/2})\otimes\pi(g_{9/2}{}^2)]_{39/2^-}$. A population of the high-spin isomer of $(39/2^-)$ was extracted to be 1.8(4)%. The excitation energy of this high-spin isomer is 1 - 2 MeV higher comparing with that of the yrast line. This may explain the small population of the high-spin isomeric states. A non-yrast high-spin isomer was not reported previously except for the K-isomers.

The high-spin states and the isomers of ^{92}Mo which is a member of Molybdenum isotopes were also studied in this experiments using the ^{82}Se(^{16}O,6n)^{92}Mo fusion evaporation reaction as a by-product of ^{93}. The shape of near yrast lines in excitation energies vs spin plots of ^{92}Mo and ^{93}Mo were compared. As a results, the near yrast states in ^{93}Mo were well described using the weak coupling picture of a $d_{5/2}$ neutron to a neutron magic core nucleus ^{92}Mo.

High-spin Isomer in ^{93}Mo

T. Fukuchi, Y. Gono[a], A. Odahara[b], H. Watanabe[c], S. Tanaka[a], M. Inoue[a], Y. Wakabayashi[a], T. Sasaki[a], M. Kibe[a], N. Hokoiwa[a], T. Shinozuka[d], M. Fujita[d], A. Yamazaki[d], T. Sonoda[d], C.S. Lee[e], Y.K. Kwon[e], J.H. Lee[e]

Center for Nuclear Study (CNS), University of Tokyo, Japan
[a]Department of Physics, Kyushu University, Japan
[b]Nishinippon Institute of Technology, Japan
[c]RIKEN, Japan
[d]Cyclotron and Radioisotopes Center (CYRIC), Tohoku University, Japan
[e]Department of Physics, Chung-Ang University, Korea

18 March 2004 GAMMA04

High-spin Isomers in N=83 Isotones

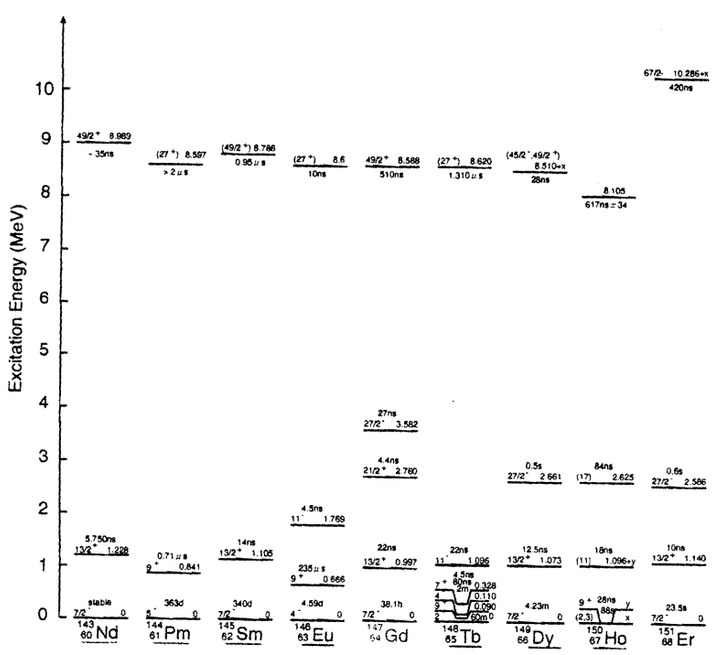

High-spin Isomers

Excitation energies
: 8-9 MeV
Spin & Parity
: $49/2^+$ (Odd)
27^+ (Odd-Odd)

References

T. Murakami et al., Z.Phys. A345, 123 (1993)
A. Odahara et al., NPA620, 363 (1997)
E. Ideguchi et al., Z. Phys. A352, 363 (1995)
R. Broda et al., Z. Phys. A305, 281 (1982)
I.A. Szucs et al., NDS46, 1 (1985)
X.H. Zhou et al., PRC61 014303 (1999)
M. Gupta et al., PRC54, 1610 (1996)
S. Andre et al., Z. Phys. A337, 349 (1990)

High-spin Isomer in ^{147}Gd

The experimental and calculated deformation parameter β in ^{147}Gd

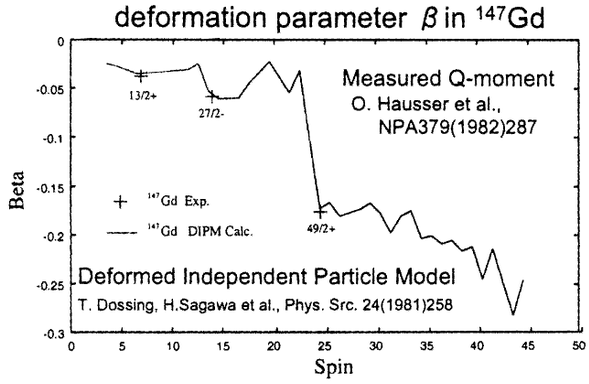

The DIPM calculation reproduces the experimentally determined deformation parameter well.

The nuclear shapes suddenly change at the high-spin isomeric state.

→ Shape Isomer

The configuration of the high-spin isomer

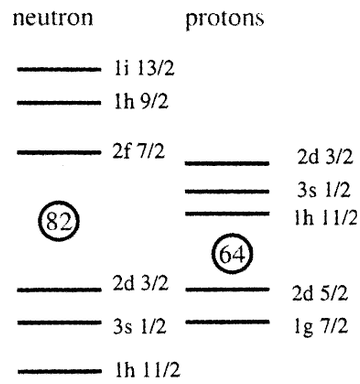

$[\nu(f_{7/2}h_{9/2}i_{13/2})\ \pi(h_{11/2}{}^2)]_{49/2^+}$

Measured g-factor was consistent with this configuration
O. Hausser et al., PRL42(1979)1451

N=51 Isotones

$[\nu(f_{7/2}h_{9/2}i_{13/2})\ \pi(h_{11/2}{}^2)]_{49/2^+}$ odd

$[\nu(f_{7/2}h_{9/2}i_{13/2})\ \pi(d_{5/2}{}^{-1}h_{11/2}{}^2)]_{27^+}$ odd-odd

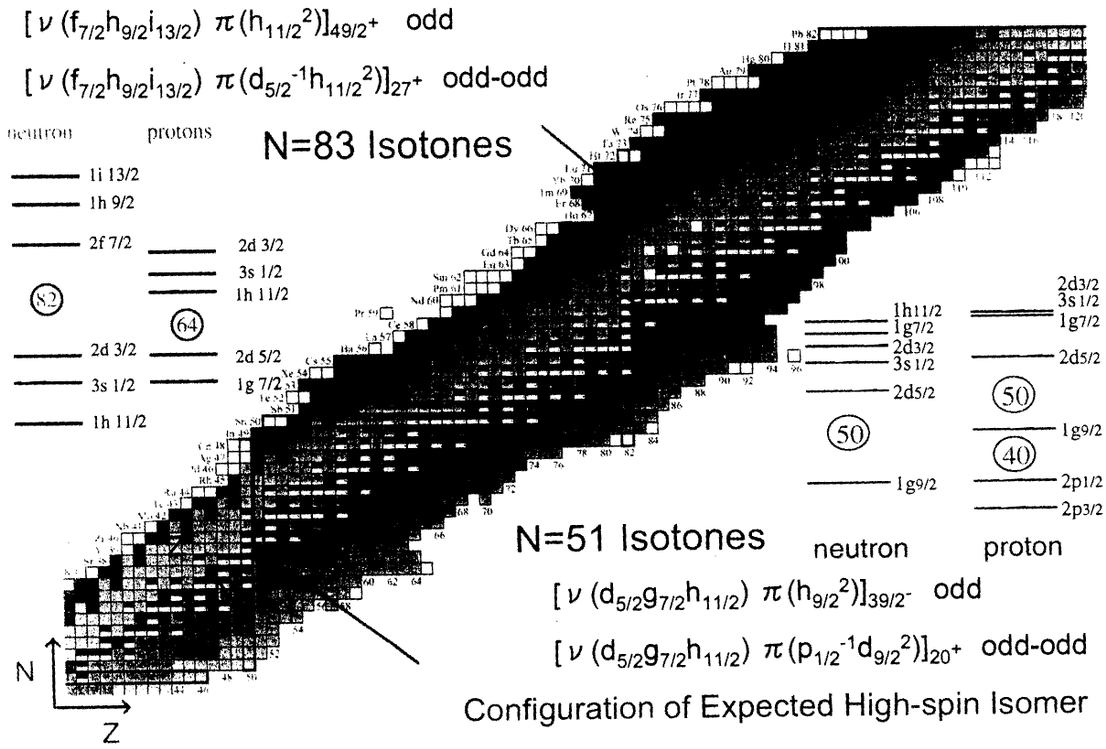

N=51 Isotones neutron proton

$[\nu(d_{5/2}g_{7/2}h_{11/2})\ \pi(h_{9/2}{}^2)]_{39/2^-}$ odd

$[\nu(d_{5/2}g_{7/2}h_{11/2})\ \pi(p_{1/2}{}^{-1}d_{9/2}{}^2)]_{20^+}$ odd-odd

Configuration of Expected High-spin Isomer

Experimental systematics of isomers in N=51 isotones

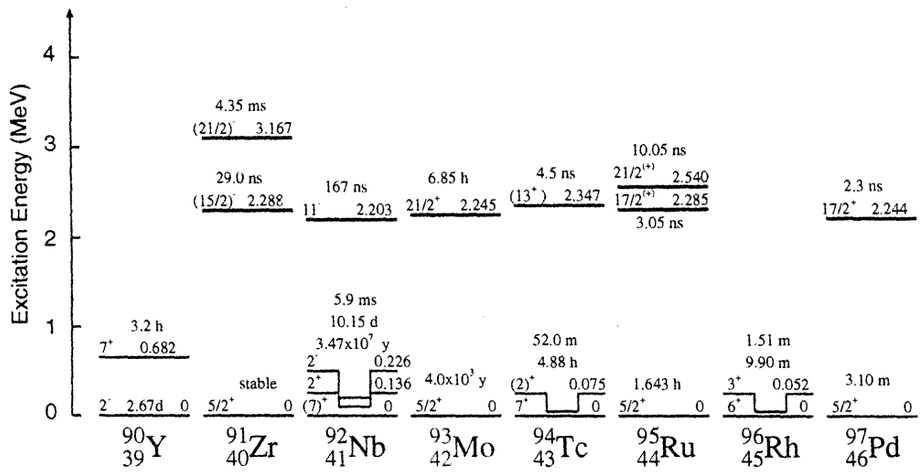

No high-spin data.
At first, we chose ^{93}Mo for the study.
(stable beam & target)

Experiment at CYRIC Tohoku University (Cyclotron and Radioisotope Center)

Beam : ^{16}O 100 MeV
Target : ^{82}Se 5.0 mg/cm^2
(90% enriched)
Reaction :
^{82}Se (^{16}O,5n) ^{93}Mo*

Detectors :
3 clover type Ge detectors
with BGO ACS
2 co-axial type Ge detectors
1 LEPS type Ge detector

Total efficiency :
0.94 % @1.3 MeV (Add-Back)

Data amount : ~ 1.2 x 10^9
coincidence events in 5 days

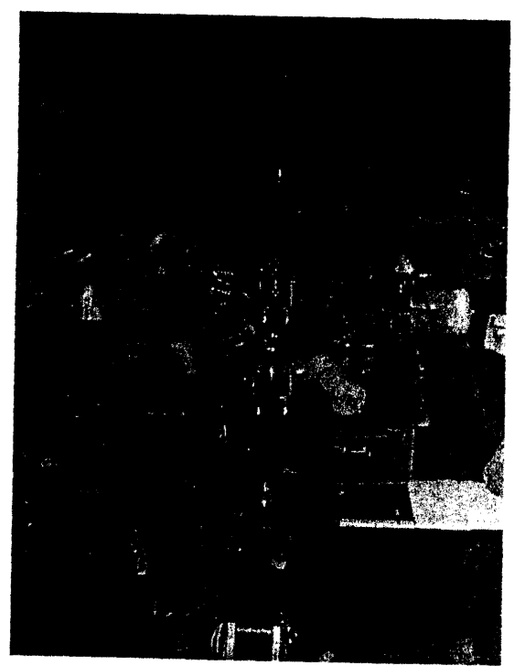

Schematic figure of detection system

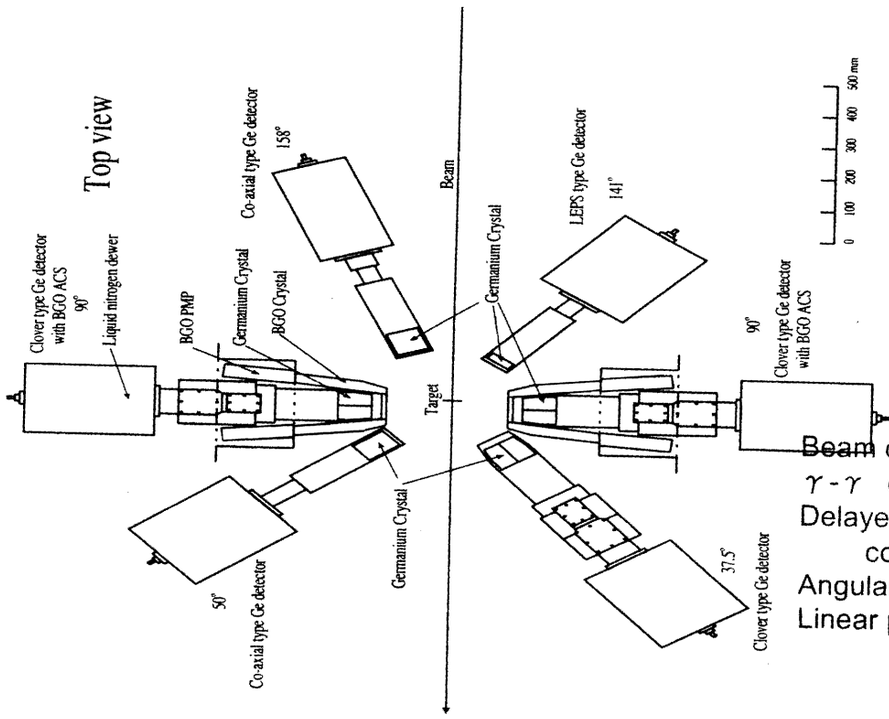

Beam delayed-γ
γ-γ coincidence
Delayed γ-γ coincidence
Angular distribution
Linear polarization

Prompt γ-γ coincidences

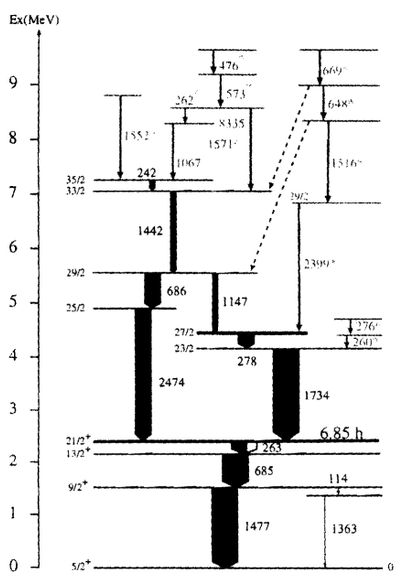

Level scheme for ^{93}Mo

Gamma-ray spectra obtained by gating on ^{93}Mo new γ-rays

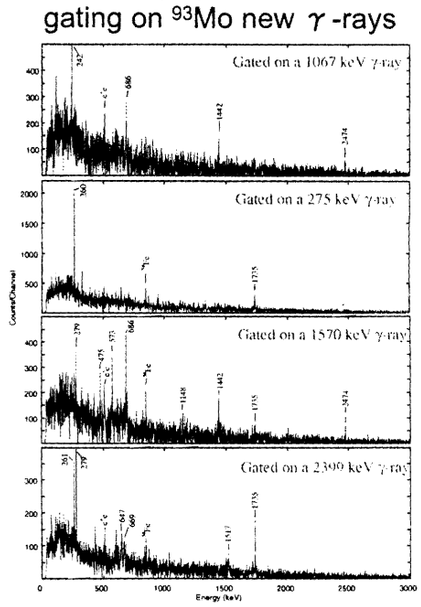

In the past, up to the 35/2 state at 7.3 MeV. (A.E. Zobov et al., NDS 80(1997)1)

In the this work, extended to the 9.6 MeV.

Linear polarizations

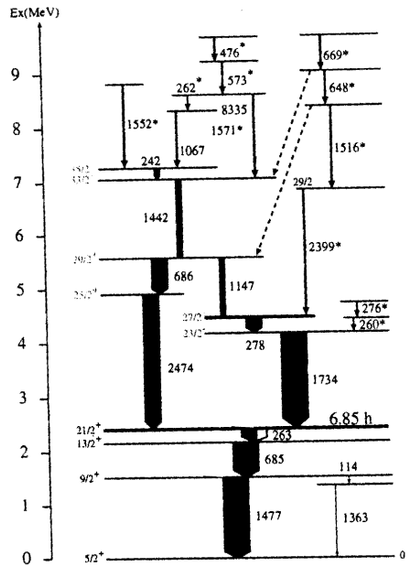

Difference spectrum between Computon scattered events in parallel and in perpendicular with respect to the reaction plane.

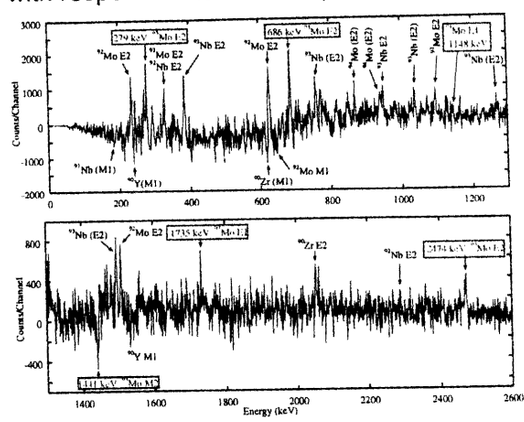

Electric and magnetic transition were distinguished in positive and negative peak respectively.

With the angular distribution information, spins and parities were determined.

Delayed γ-γ coincidences

New high-spin Isomer
Ex = 9.7 MeV

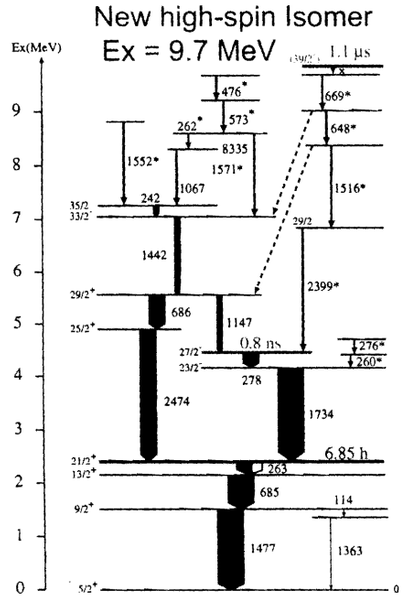

Difference spectrum between post-prompt and pre-prompt. The delayed time conditions were in range of 1 to 3 μsec.

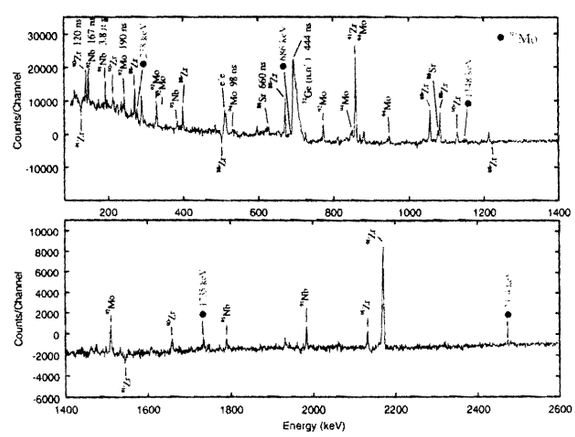

From the time distribution of γ-rays, the half life of the high-spin isomer was determined to be $T_{1/2}$=1.1(4) μsec.

A population of this high-spin isomer is extracted to be 1.8(4)%.

The level scheme for ^{92}Mo and ^{93}Mo

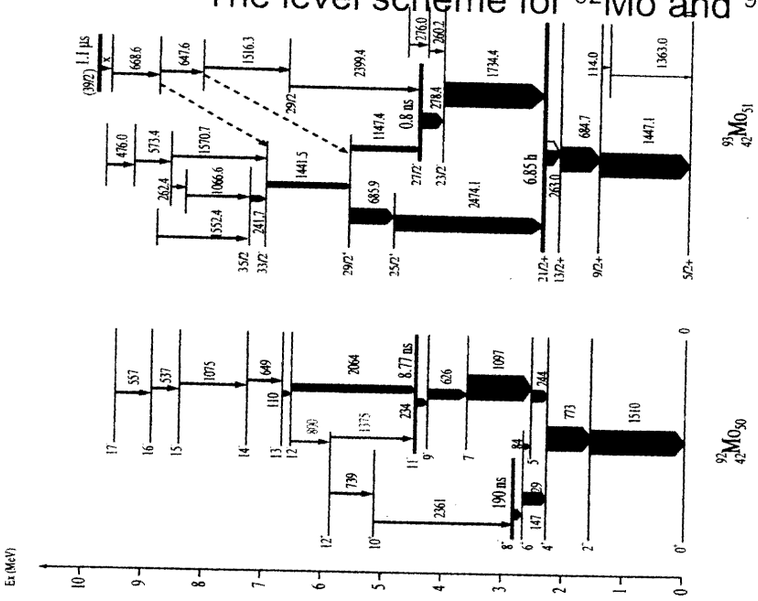

^{93}Mo were well understood using the weak coupling picture of a d5/2 neutron to a neutron magic core nucleus ^{92}Mo.

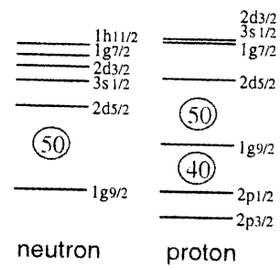

Level scheme of ^{92}Mo was also constructed in this work.

But we could not found the high-spin isomer.

The yrast lines of ^{92}Mo and ^{93}Mo

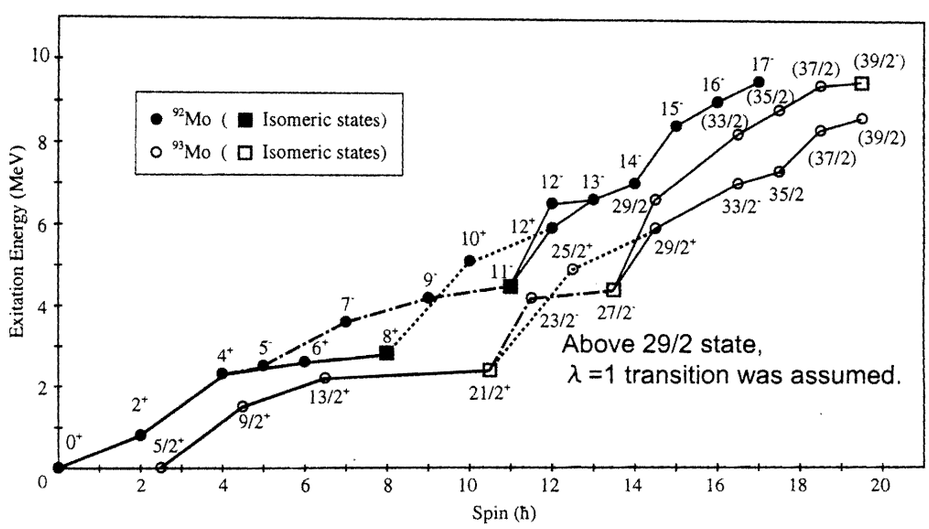

The high-spin isomer in ^{93}Mo was excited 1-2 MeV from the yrast line.
This non-yrast character may explain the small population of the high-spin isomer.

In the high-spin, two yrast line was different,
One valence neutron play an important role (same as N=83 isotones).

Summary

The high-spin states of ^{93}Mo have been studied.

The level scheme was extended to 9.7 MeV.

The high-spin isomer was discovered as a $(39/2^-)$ state at about 9.7 MeV.

Future

Experiments for other nuclei in N=51 isotones.

DIPM calculations in N=51 isotones.
(Now not fix the parameter)

Shell Model Description of High Spin Isomers in Ba Isotopes

N. Yoshinaga

Department of Physics, Saitama University

Xe, Ba and Ce isotopes around mass $A=130$ show the γ instability in low-lying states, which is characterized by the energy staggering in quasi-γ bands and some forbidden transition rates. During the past 20 years, these nuclei in this mass region were extensively investigated in terms of various models. One of the successful models to explain these features was the interacting boson model (IBM). Its application to the Xe and Ba isotopes indicated that the O(6) dynamical symmetry provides a successful description of the energy spectra and electromagnetic transitions in this mass region [1].

There exists another prominent feature in the even-even nuclei with mass $A\sim130$ region. Sudden decreases of level spacing and $B(E2)$ value around the states of spin 10 were experimentally observed in many of these nuclei. These high-spin anomalies are called backbending phenomena. They are attributed to band crossing between the ground-state band and s band originating from the alignment of two neutrons in the $0h_{11/2}$ orbital. There are very few microscopic calculations of backbending phenomena in this region. The backbending phenomena as well as the low-lying states were extensively investigated in terms of a pair-truncated shell model [2]. A full-fledged shell model calculation was also performed for Xe isotopes $^{130-136}$Xe under the assumption of $N=Z=64$ subshell closure [3].

Recently, we have studied the Xe and Ba isotopes in the $A\sim130$ mass region by means of the full-fledged shell model. This calculation uses the single particle orbitals $0g_{7/2}$, $1d_{5/2}$ and $0h_{11/2}$ ($1d_{3/2}$, $0h_{11/2}$ and $2s_{1/2}$) for neutrons (protons), and the phenomenological multipole interactions are employed. The energy levels for quasi-γ band as well as ground band and $E2$ transition rates are well reproduced in each nucleus. The results of this calculation will be presented and discussed.

[1] R. F. Casten and P. von Brentano, Phys. Lett. **152B**, 22 (1985).

[2] K. Higashiyama, N. Yoshinaga, and K. Tanabe, Phys. Rev. C **67**, 044305 (2003).

[3] K. Higashiyama, N. Yoshinaga, and K. Tanabe, Phys. Rev. C **65**, 054317 (2002).

Shell Model Description of High Spin Isomers in Ba Isotopes

N. Yoshinaga

Saitama University

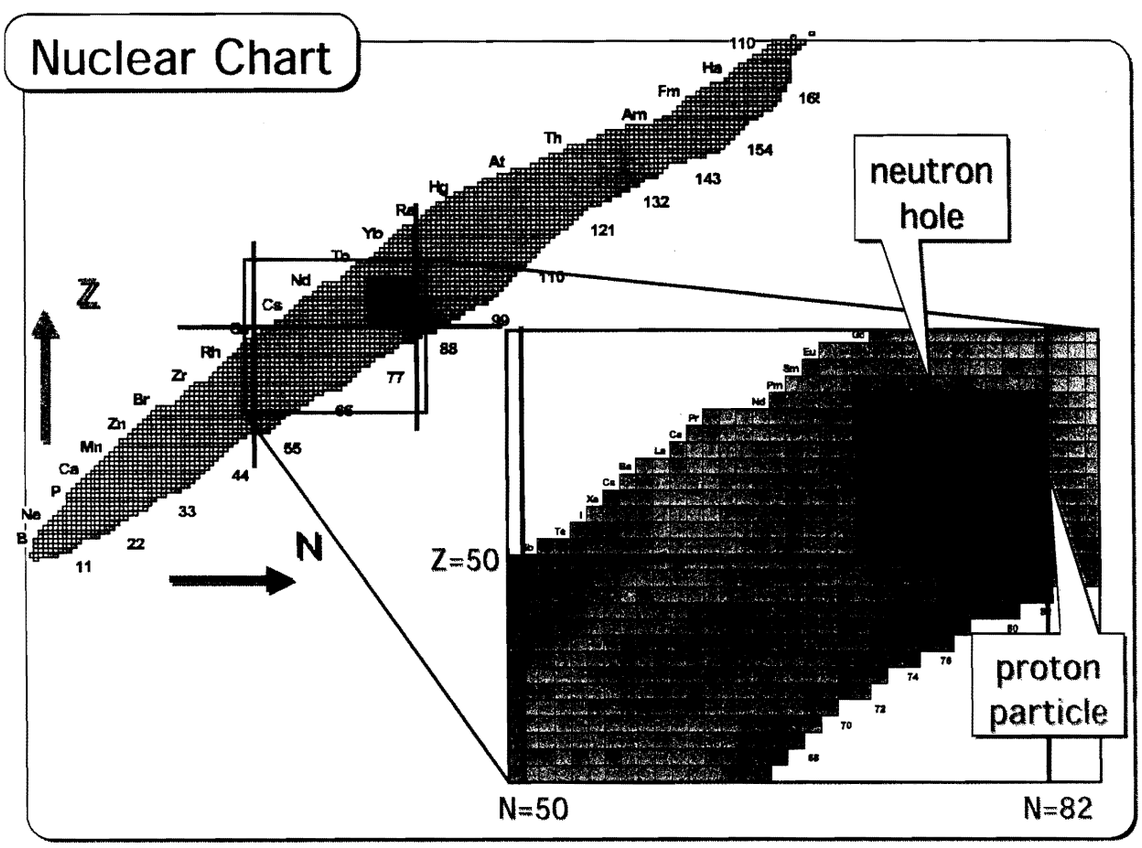

Triaxial deformation

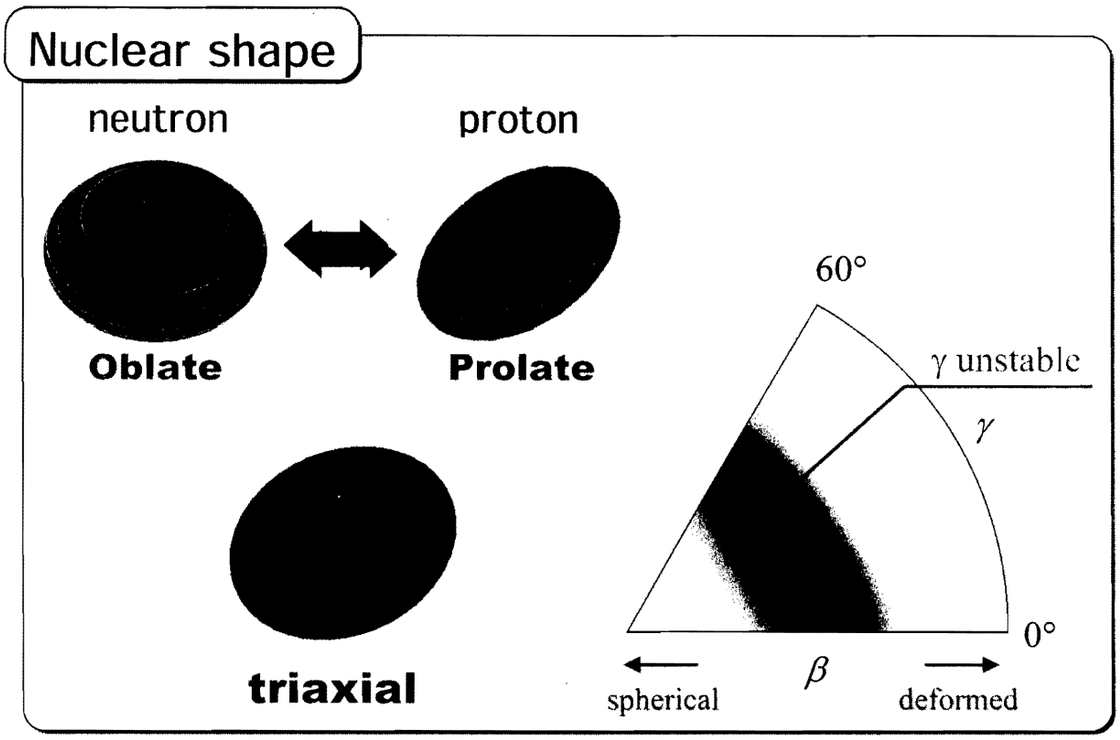

Backbending phenomena

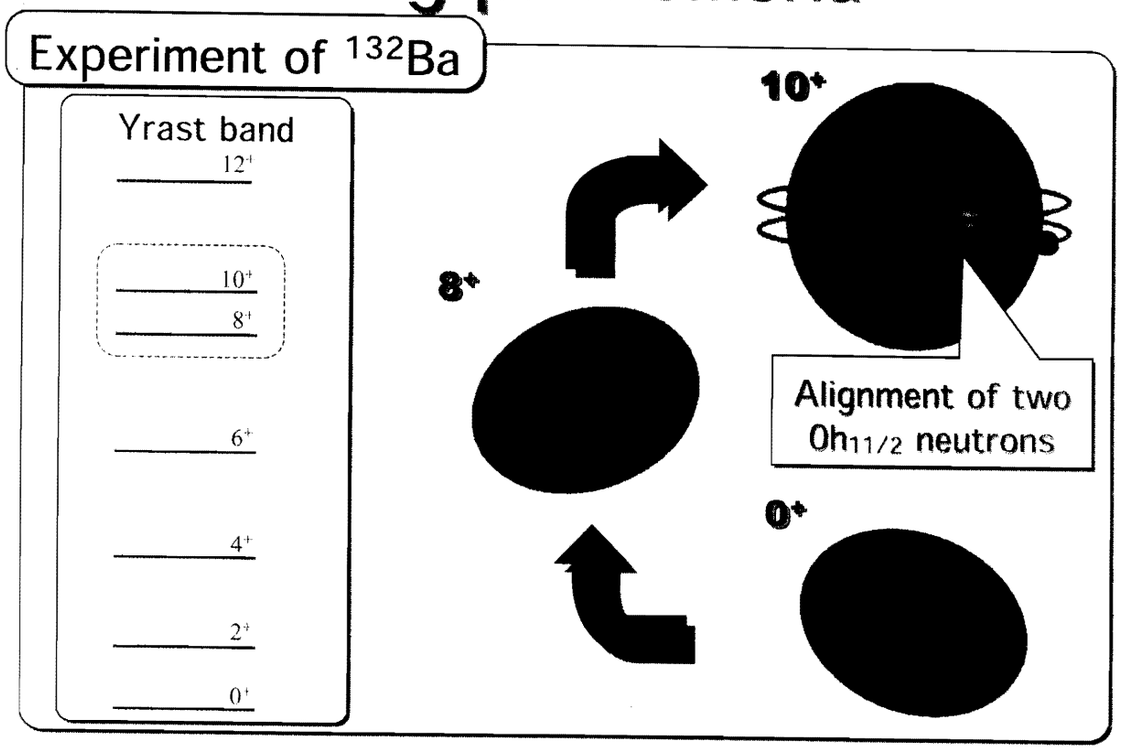

Experiment of N=80 isotones

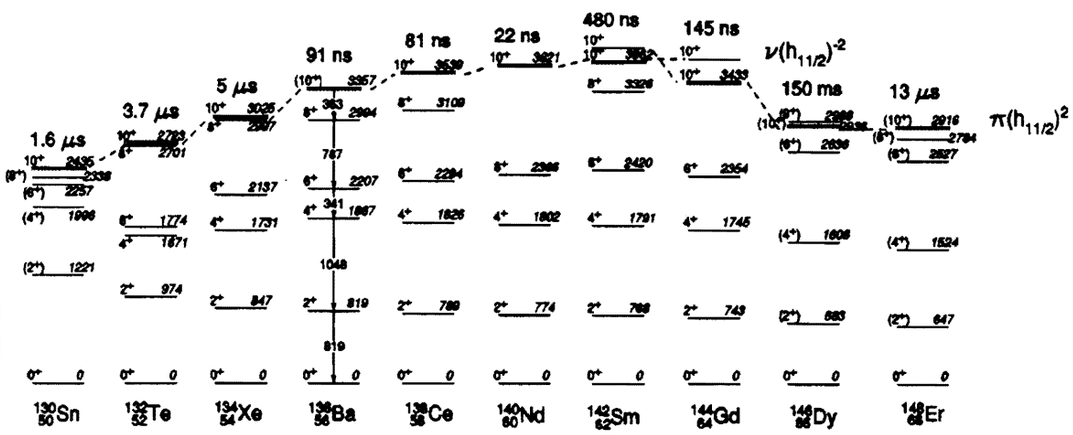

Pair truncated shell model (PTSM)

SD-pair states

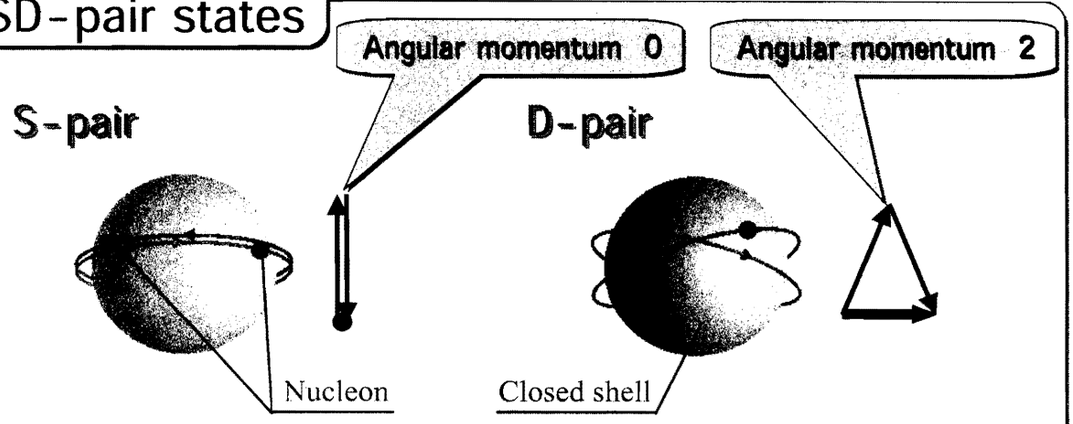

nuclear states

$$|\Phi(J)\rangle = \left[\left|S_\nu^{n_{s\nu}} D_\nu^{n_{d\nu}} J_\nu\right\rangle \otimes \left|S_\pi^{n_{s\pi}} D_\pi^{n_{d\pi}} J_\pi\right\rangle\right]^{(J)}$$

Single particle orbitals

The single particle (hole) energies for proton (neutron)

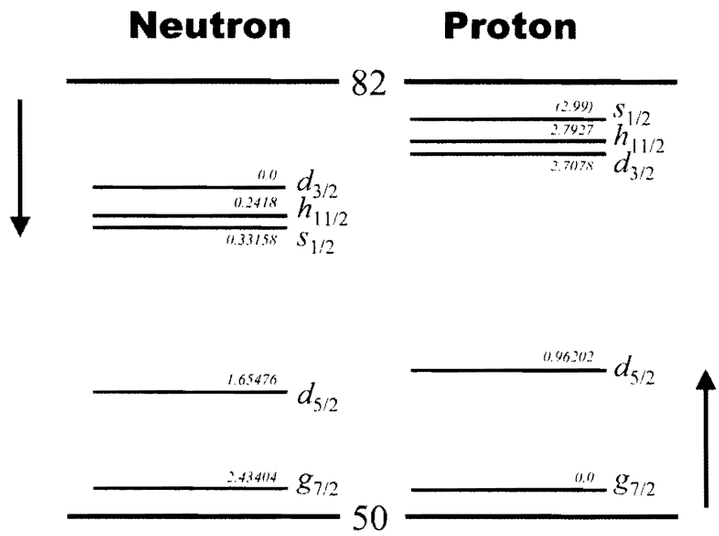

Full 5 levels (50<N(Z)<82) for both protons and neutrons.

Hamiltonian

Pairing+quadrupole interaction

$$H = \sum_{jm\tau=\nu,\pi} \varepsilon_{j\tau} c^{\dagger}_{jm\tau} c_{jm\tau}$$
$$- \sum_{\tau=\nu,\pi} \left[G_{0\tau} P^{\dagger(0)}_{\tau} P^{(0)}_{\tau} + G_{2\tau} P^{\dagger(2)}_{\tau} \cdot \tilde{P}^{(2)}_{\tau} + \kappa_{\tau} :Q_{\tau} \cdot Q_{\tau}: \right] - \kappa_{\nu\pi} Q_{\nu} \cdot Q_{\pi}$$

Strengths of two-body interactions

$$G_{0\nu} = 0.160 - 0.010\,\bar{N}_{\nu} \qquad G_{0\pi} = 0.200 - 0.010\,\bar{N}_{\nu} - 0.005\,N_{\pi}$$
$$G_{2\nu} = 0.017 + 0.0005\,N_{\pi} \qquad G_{2\pi} = 0.010 + 0.001\,N_{\pi}$$
$$\kappa_{\nu} = 0.075 - 0.0015\,N_{\pi} \qquad \kappa_{\pi} = 0.014 + 0.006\,N_{\pi}$$
$$\kappa_{\nu\pi} = -0.044 - 0.002\,\bar{N}_{\nu}$$

$\bar{N}_{\nu}$ number of neutron holes

N_{π} number of proton particles

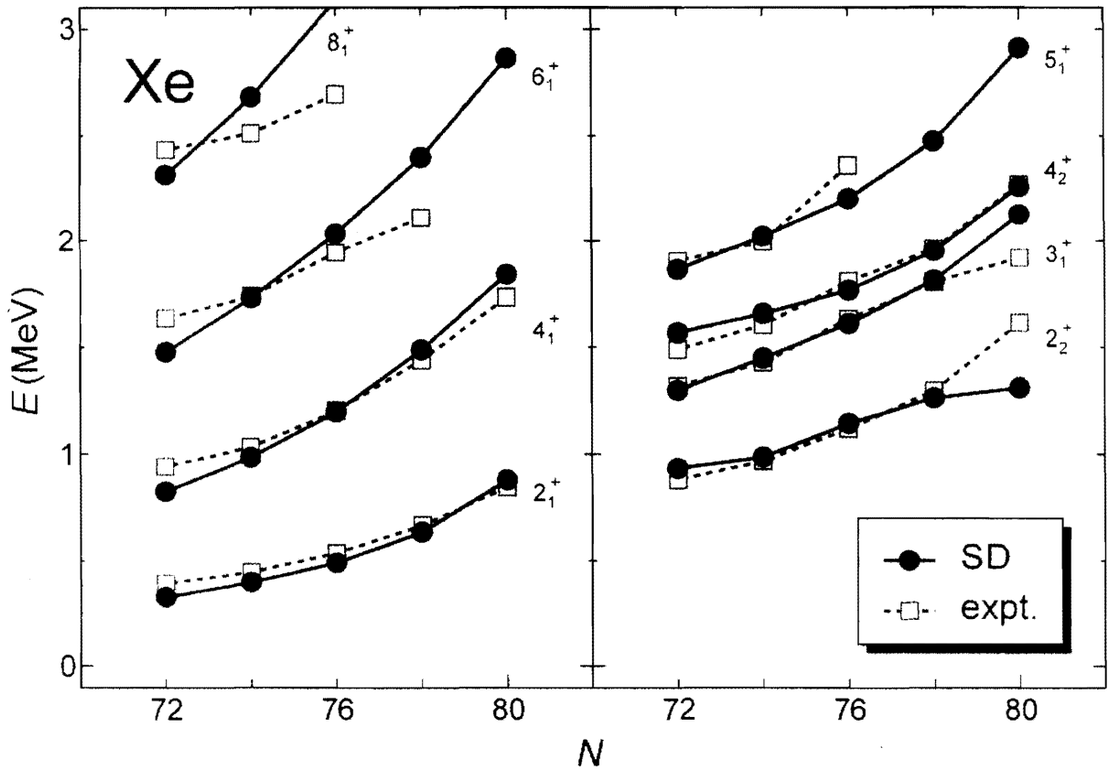
Xe
E (MeV)
N
SD
expt.
8_1^+
6_1^+
4_1^+
2_1^+
5_1^+
4_2^+
3_1^+
2_2^+

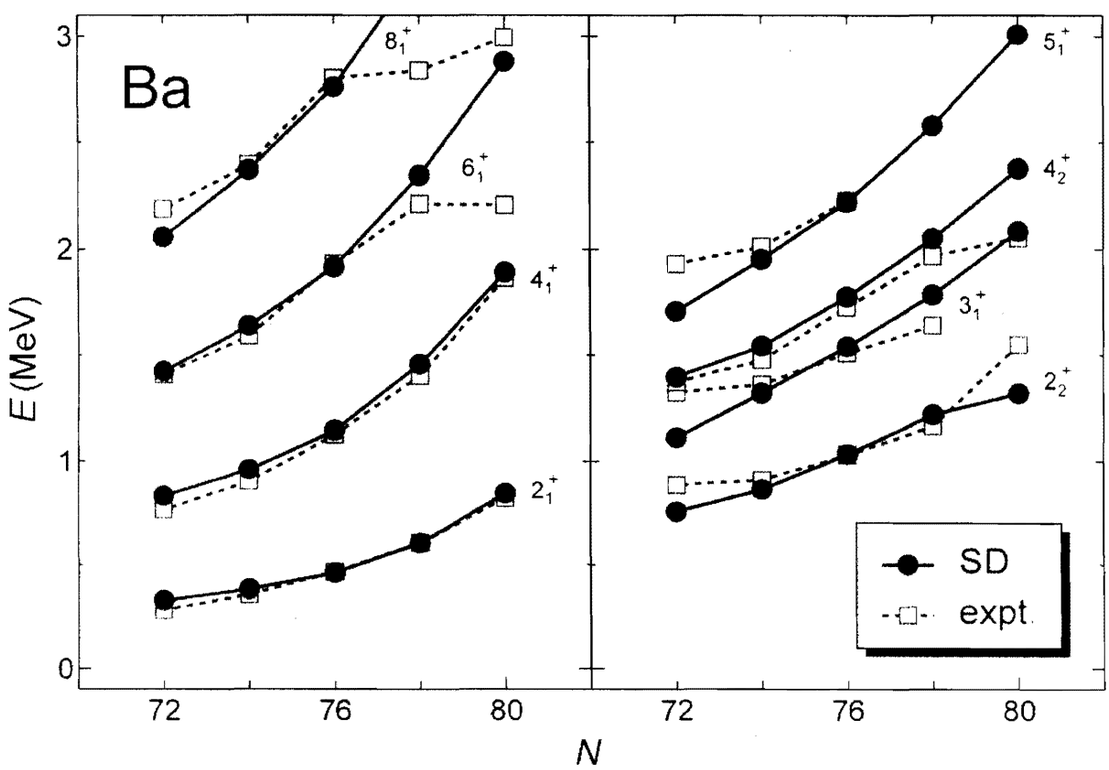
Ba
E (MeV)
N
SD
expt.
8_1^+
6_1^+
4_1^+
2_1^+
5_1^+
4_2^+
3_1^+
2_2^+

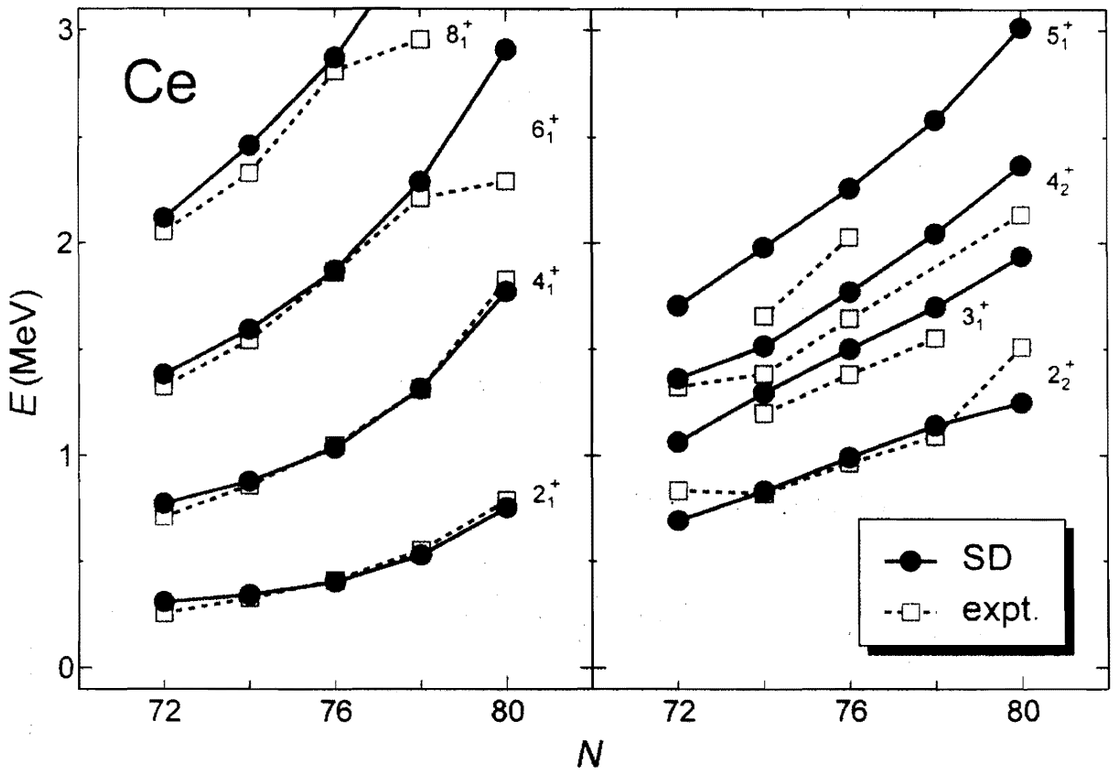
Ce
8_1^+
6_1^+
4_1^+
2_1^+
5_1^+
4_2^+
3_1^+
2_2^+
SD
expt.
E (MeV)
N
0
1
2
3
72
76
80

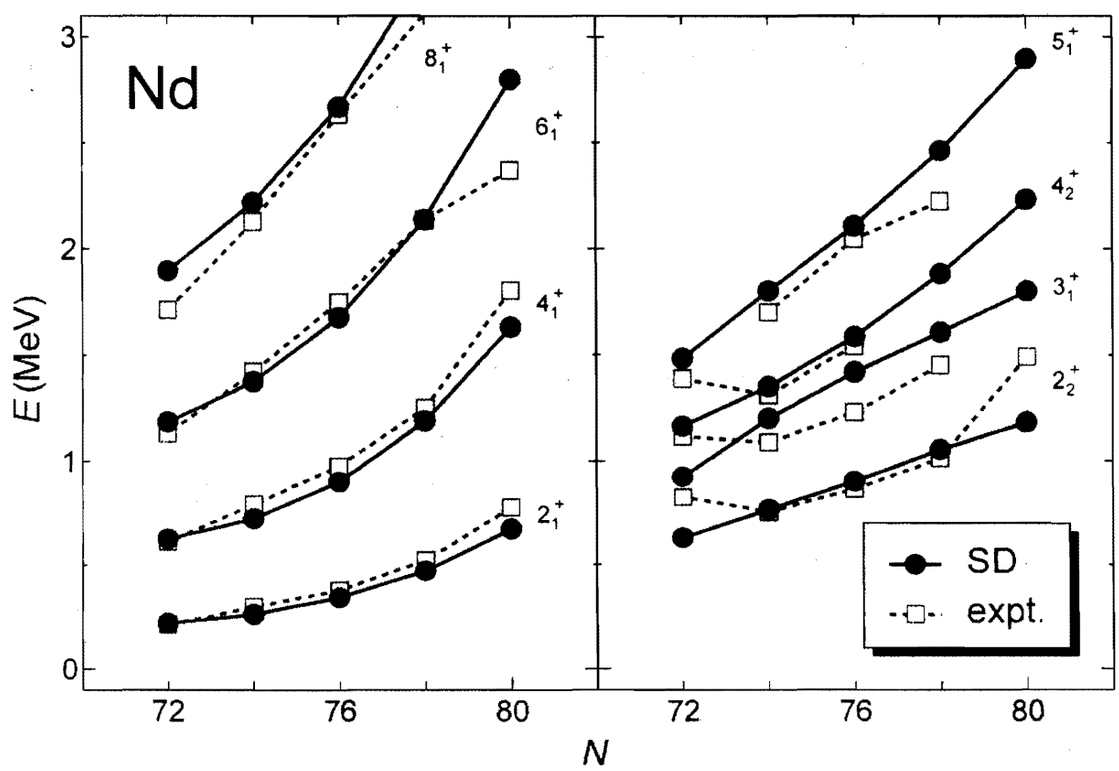
Nd
8_1^+
6_1^+
4_1^+
2_1^+
5_1^+
4_2^+
3_1^+
2_2^+
SD
expt.
E (MeV)
N
0
1
2
3
72
76
80

SD+H-pair states

H-pair operator

$$\mathrm{H} = (h_{11/2})^2$$

$$\mathrm{H} = (h^{\dagger}_{11/2})^2 = [c^{\dagger}_{11/2}\ c^{\dagger}_{11/2}]^{(J)} \quad ; \quad J = 10$$

Unique structure

SD+H-pair system

$$(S^{\dagger})^{n_s}(D^{\dagger})^{n_d}(H^{\dagger})^{n_h}\,|-\rangle = \left|S^{n_s}D^{n_d}H^{n_h}\ J\right\rangle$$

even-even nuclear states

$$|\Phi(J)\rangle = \begin{bmatrix} \left|S_{\nu}^{n_{s\nu}}D_{\nu}^{n_{d\nu}}H_{\nu}J_{\nu}\right\rangle \otimes \left|S_{\pi}^{n_{s\pi}}D_{\pi}^{n_{d\pi}}H_{\pi}J_{\pi}\right\rangle \\ \left|S_{\nu}^{n_{s\nu}}D_{\nu}^{n_{d\nu}}J_{\nu}\right\rangle \qquad \left|S_{\pi}^{n_{s\pi}}D_{\pi}^{n_{d\pi}}J_{\pi}\right\rangle \end{bmatrix}^{(J)}$$

Hamiltonian

Pairing+quadrupole interaction

$$H = \sum_{jm\tau=\nu,\pi} \varepsilon_{j\tau} c^{\dagger}_{jm\tau} c_{jm\tau}$$
$$- \sum_{\tau=\nu,\pi} \left[\, G_{0\tau} P^{\dagger(0)}_{\tau} P^{(0)}_{\tau} + G_{2\tau} P^{\dagger(2)}_{\tau} \cdot \tilde{P}^{(2)}_{\tau} + \kappa_{\tau} {:}Q_{\tau} \cdot Q_{\tau}{:} \,\right] - \kappa_{\nu\pi} Q_{\nu} \cdot Q_{\pi}$$

Strengths of two-body interactions

Mass	^{134}Ba			^{132}Ba			^{130}Ba		
	G_0	G_2	κ	G_0	G_2	κ	G_0	G_2	κ
neutron	0.110	0.034	0.150	0.110	0.042	0.150	0.110	0.048	0.150
proton	0.130	0.014	0.040	0.130	0.020	0.040	0.130	0.030	0.030
n-p int.			0.070			0.070			0.070

(in MeV)

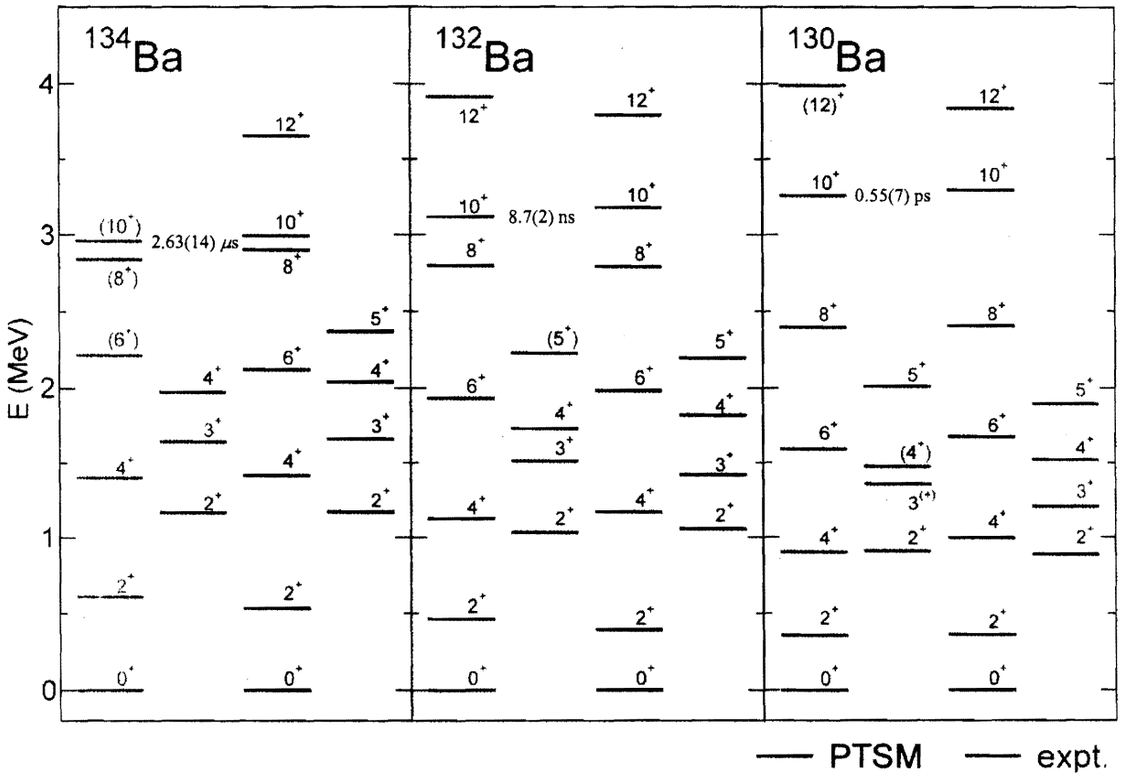
134Ba
132Ba
130Ba
E (MeV)
2.63(14) μs
8.7(2) ns
0.55(7) ps
PTSM
expt.

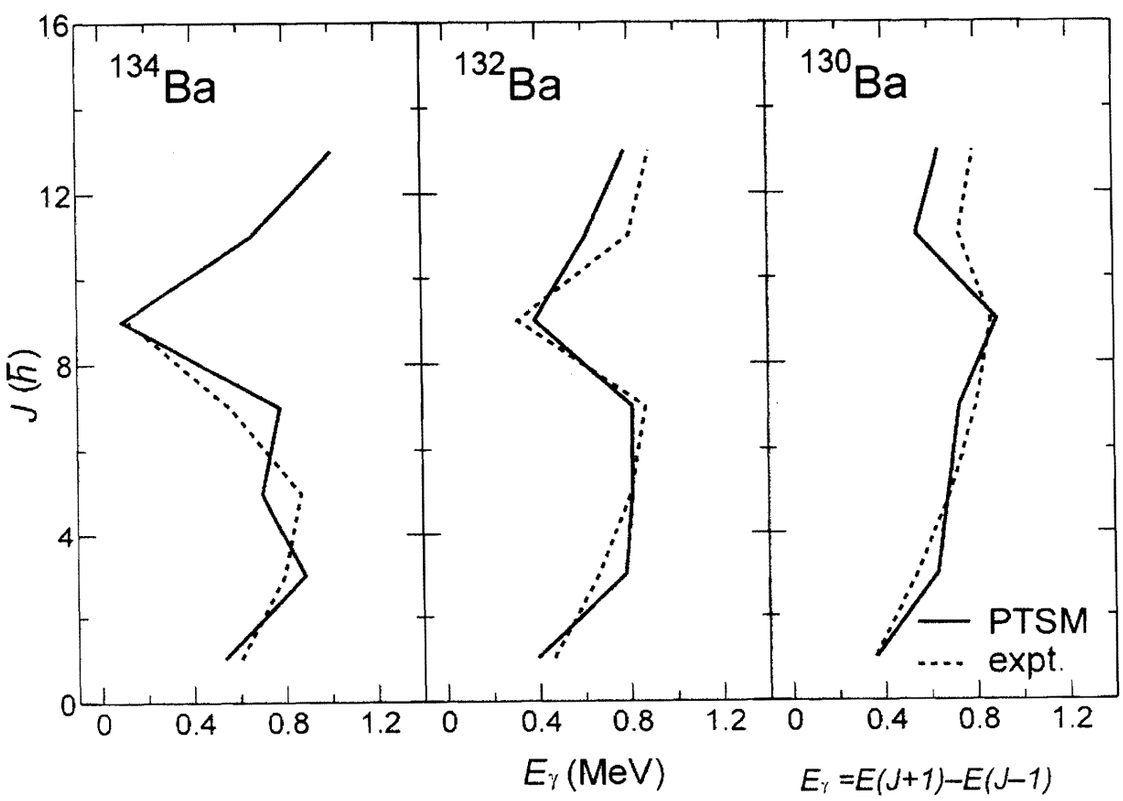
134Ba
132Ba
130Ba
J (ħ)
Eγ (MeV)
Eγ =E(J+1)−E(J−1)
PTSM
expt.

Transition

E2 transition

$$T(E2;\mu) = e_\nu Q_{\nu\mu} + e_\pi Q_{\pi\mu}$$

effective charges

$$e_\nu = -1.2e \qquad e_\pi = 2.2e$$

The neutron effective charge is negative, because we adopt the hole picture for neutrons.

M1 transition

$$T(M1;\mu) = \mu_N \sqrt{\frac{3}{4\pi}} \sum_{\tau=\nu,\pi} \left[g_{\ell\tau} \boldsymbol{j}_\tau + (g_{s\tau} - g_{\ell\tau}) \boldsymbol{s}_\tau \right]_\mu$$

gyromagnetic ratios

$$g_{\ell\nu} = 0.05 \qquad g_{\ell\pi} = 1.05 \qquad g_{s\nu} = -2.68 \qquad g_{s\pi} = 3.91$$

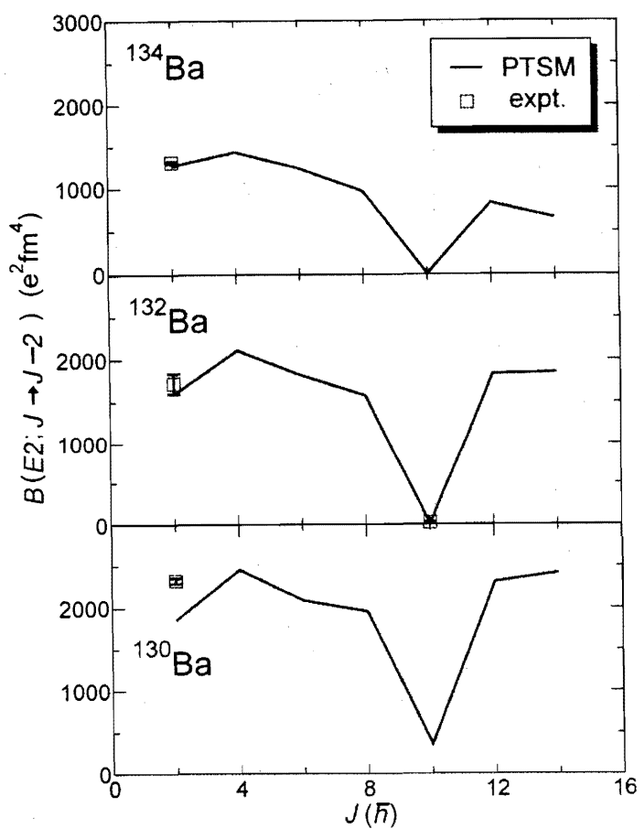

Relative B(E2) values

	^{134}Ba		^{132}Ba		^{130}Ba		
$J_i^+ \to J_f^+$	PTSM	expt.	PTSM	expt.	PTSM	expt.	O(6)
$2_2^+ \to 2_1^+$	100	100	100	100	100	100	100
$\to 0_1^+$	9.8	0.9(2)	19	2.7(4)	6.7	6.2(7)	
$3_1^+ \to 2_2^+$	100	100	100	100	100	100	100
$\to 4_1^+$	36	≧2.6	39	38(6)	38	22(3)	40
$\to 2_1^+$	12	1.1	15	2.6(4)	6.4	4.5(6)	0
$4_2^+ \to 2_2^+$	100	100	100	100	100	100	100
$\to 3_1^+$	17		30	≦50(11)	38		0
$\to 4_1^+$	31	73	51	73(10)	57	54(10)	91
$\to 2_1^+$	30	2.4	6.0	1.8(3)	16	2.3(4)	0
$5_1^+ \to 3_1^+$	100	100	100	100	100	100	100
$\to 4_2^+$	82		49	≦45(7)	60		46
$\to 6_1^+$	32		42		47		45
$\to 4_1^+$	0.036		2.4	≦2.2(3)	0.17		0

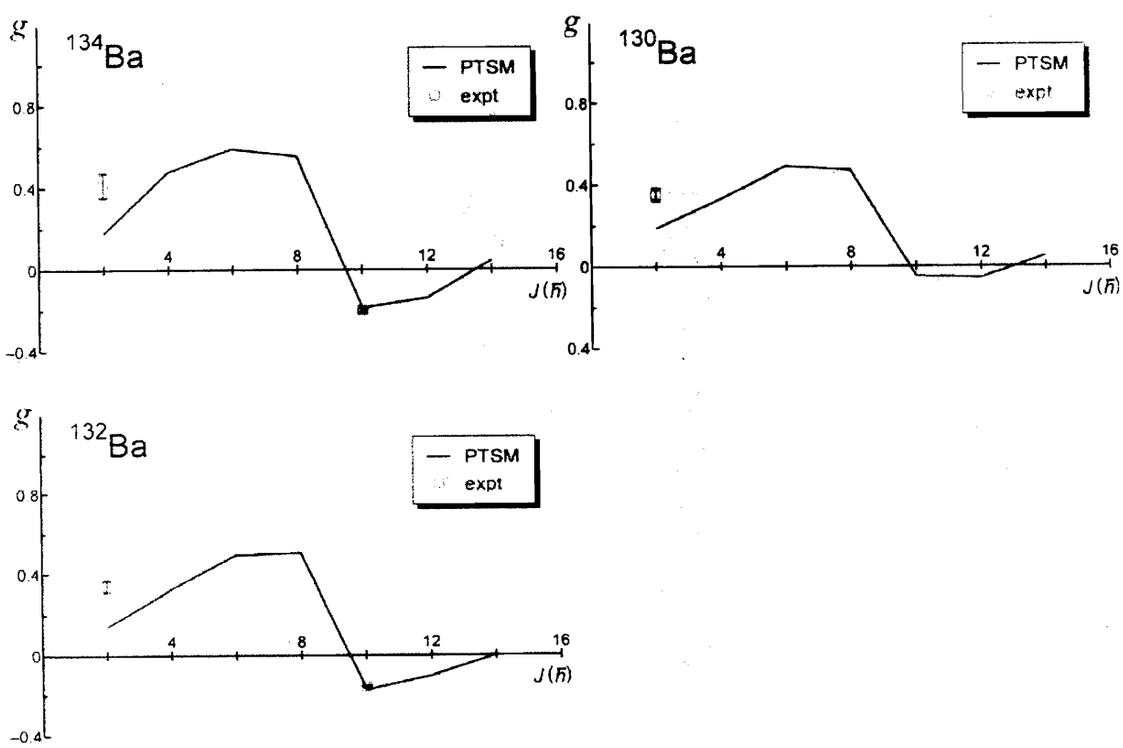

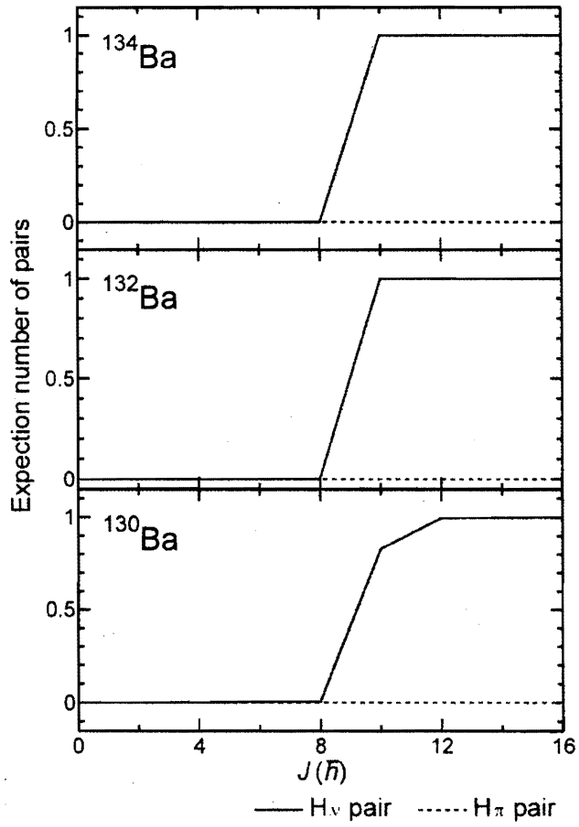

Experiment of ^{136}Ba

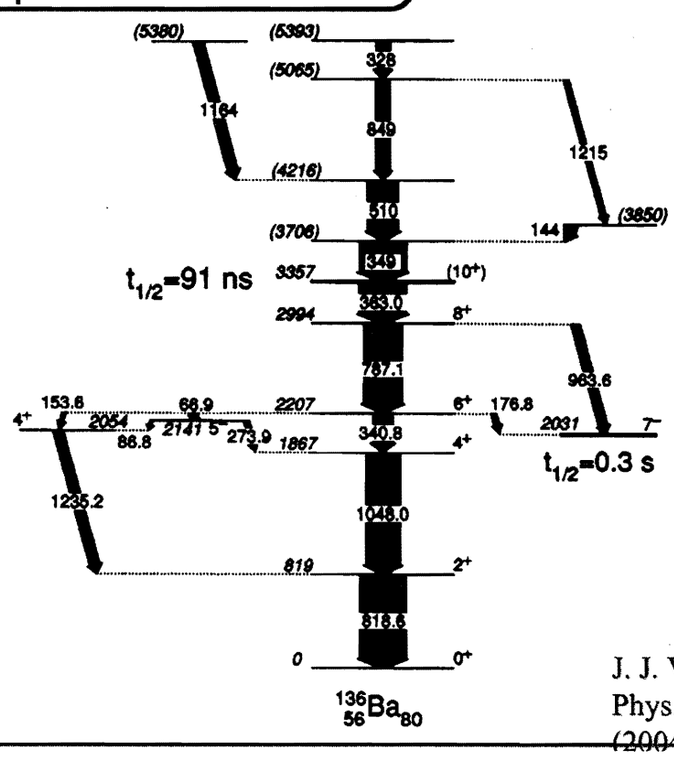

J. J. Valiente-Dobón *et al*, Phys. Rev. C **69**, 024316 (2004).

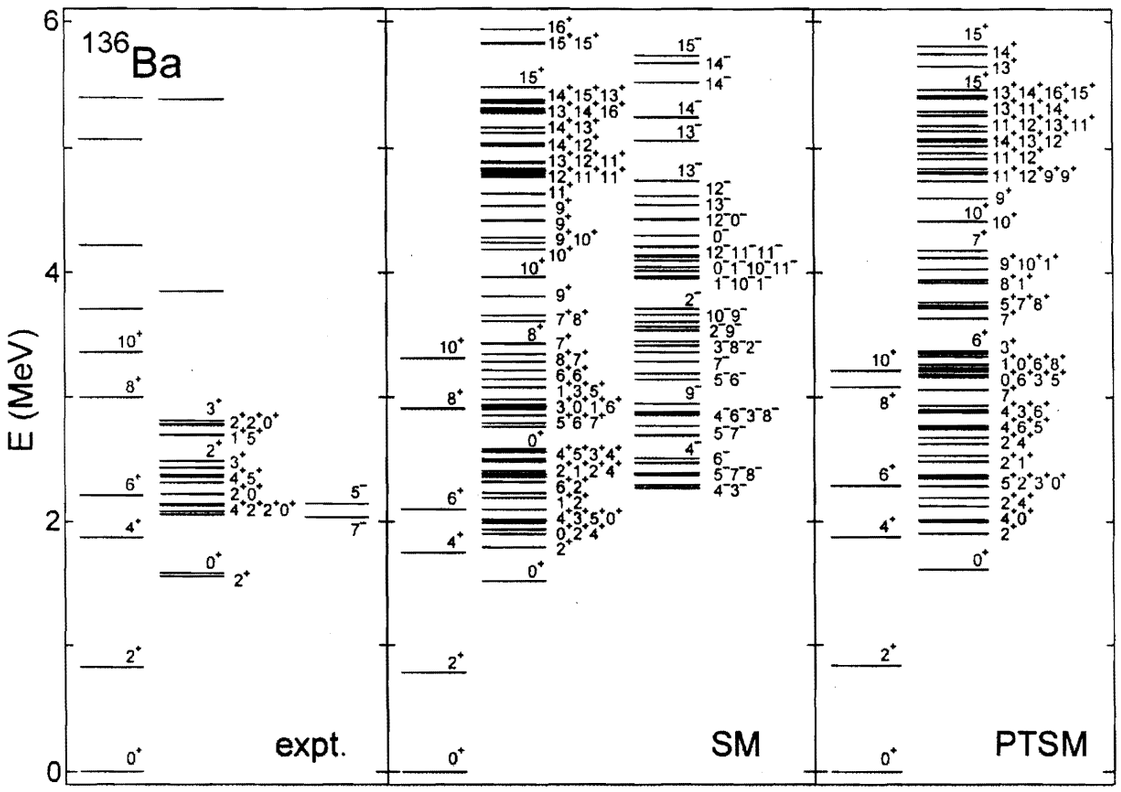
136Ba
E (MeV)
expt.
SM
PTSM

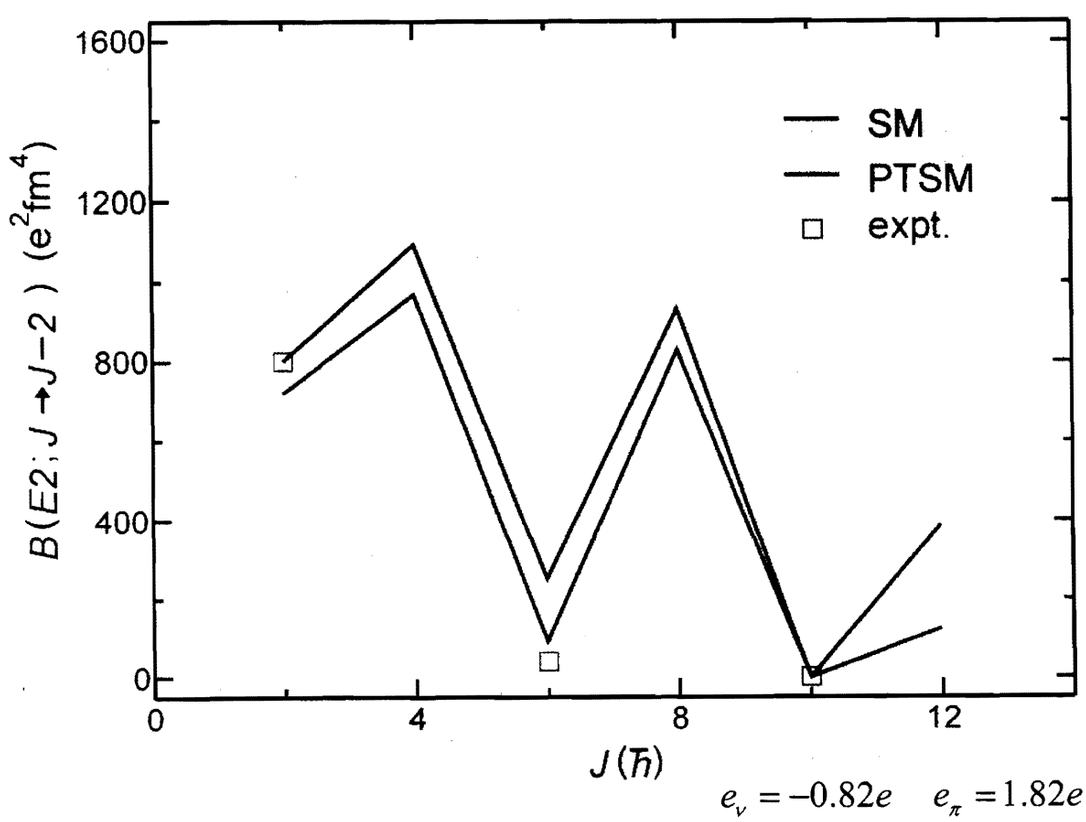
SM
PTSM
expt.
B(E2; J → J−2) (e²fm⁴)
J (ħ)
$e_\nu = -0.82e \quad e_\pi = 1.82e$

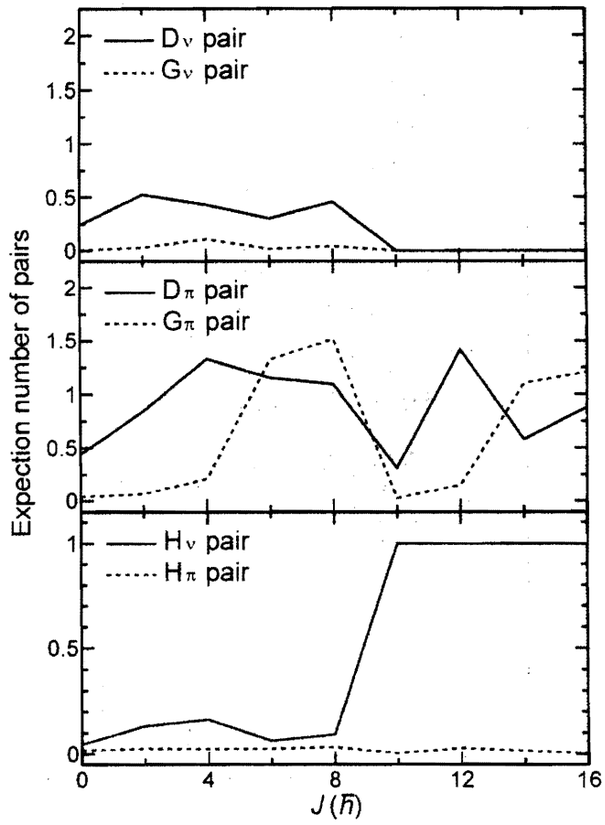

Summary

- Using the pair-truncated shell model, we have successfully reproduced energy spectra of Ba isotopes in addition to the $E2$ transition rates and g-factors near closed shell of N=82.

- Our analysis shows that the 10^+ isomeric states of Ba isotopes are understood as the rapid structural change by the alignment of neutron pairs in $h_{11/2}$ orbital.

The RISING project at GSI and its first results

Takehiko R. Saitoh*
for the RISING collaboration
* *Gesellschaft für Schwerionenforschung (GSI), Planckstrasse 1, D-64291 Darmstadt, Germany*

The RISING project (Rare ISotope INvestigations at GSI) combines the EUROBALL Cluster Ge-detectors, MINIBALL Ge-detectors in a second phase, HECTOR BaF_2-detectors and the fragment separator (FRS) at GSI for high-resolution γ-ray spectroscopy measurements after in-flight isotope separation. The SIS/FRS facility at GSI provides secondary beams of unstable rare isotopes produced via fragmentation reactions or fission of relativistic heavy ions. These unique radioactive beams have sufficient intensity to perform γ-ray spectroscopy measurements. We are currently performing γ-ray spectroscopy with the FRS-RISING fast beam setup and an in-beam technique by using Coulomb excitation and secondary fragmentation reactions at relativistic energies. We also plan to perform experiments with a stopped-beam technique for decay studies and with slowed-down beam technique for performing experiments with multiple Coulomb excitation, a few nucleon transfer reaction and a fusion evaporation reaction. We would like to investigate various important subjects for nuclear physics with RISING, and they are
- shell structure of unstable doubly magic nuclei and nuclei in their vicinity,
- isospin symmetry along the N=Z line and mixed symmetry states,
- deformed shapes and shape coexistence,
- collective modes of nuclear excitation and E1 strength distribution.

The RISING project started in summer, 2003, with the fast beam setup for in-beam γ-ray spectroscopy at relativistic energies. We will perform experiments with the same setup in 2004, but with the MINIBALL array in addition in December. In 2005, we plan to perform experiments both with fast and stopped beams. The Feasibility study of slowed-down beam experiments will be performed in 2006. The overview of the RISING project will be presented in the lecture.

Four experiments have been successfully performed with the FRS-RISING fast beam setup. In the first experiment, a primary beam of ^{84}Kr was impinging on a gold target mounted at the center of the RISING Ge and HECTOR BaF_2 arrays in the final focal plane of FRS, in order to investigate feasibility of Coulomb excitation measurements under excellent beam condition by measuring the $2^+ \rightarrow 0^+$ transition of ^{84}Kr and to study the particle-γ-ray angular correlation at relativistic energies. Two relativistic Coulomb excitation experiments with secondary beams were also performed to measure B(E2) values of transitions depopulating the first 2^+ state in neutron rich ^{56}Cr and neutron deficient ^{108}Sn. A two-step fragmentation method was applied to observe excited states in ^{53}Ni. The goal of the measurement was to study the mirror symmetry between ^{53}Ni and ^{53}Mn. A secondary beam of ^{55}Ni was produced in fragmentation of ^{58}Ni primary beam on a beryllium target and was bombarded on a secondary beryllium target mounted in the final focal plane of FRS in order to produce secondary fragments. Experimental detail and the first results of these experiments will be presented.

The RISING project at GSI and its first results

Take R. Saitoh
for the RISING collaboration
GSI

What is RISING?

FRagment Separator + Euroball cluster Ge detectors

Detail study for nuclei far from stability!!!

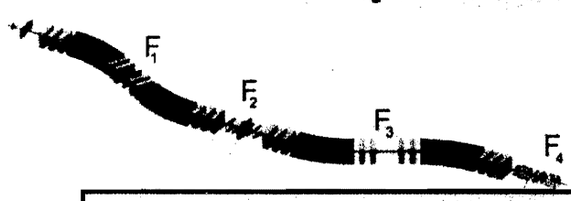

Exploring the whole nuclear landscape
- ➢ Shell structure.
- ➢ Nuclear shape and softness.
- Giant dipole resonance.
- Symmetries.

• Exc
and Z :

Rare ISotope INvestigation at GSI

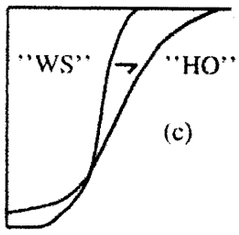

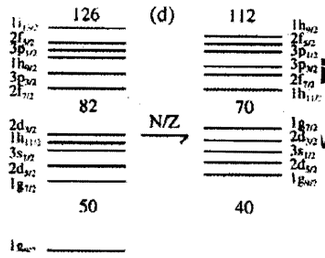

studied

ward ^{56}Ni and ^{100}Sn (N=Z).

Single particle shell structure.

Effective n-charge and core polarization.

- p-n interaction and correlation.

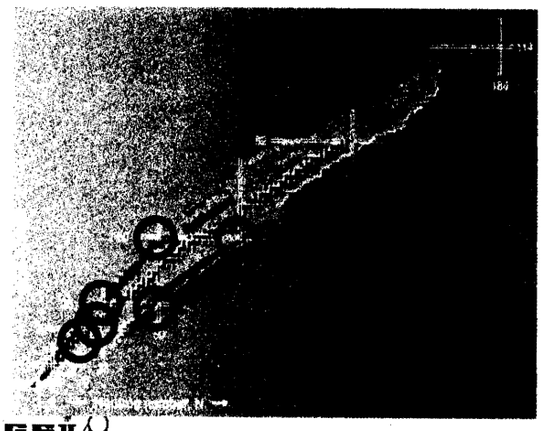

- N>>Z nuclei.
  - Different N/Z ratio.
  - Melting of Woods-Saxon shell gaps and enforcement of harmonic oscillator shell.
  - Isovector part of the interaction.
  - ^{54}Ca, ^{78}Ni and ^{132}Sn.

Physics to be studied

- **Nuclear Shell structure.**
- **Nuclear shapes.**

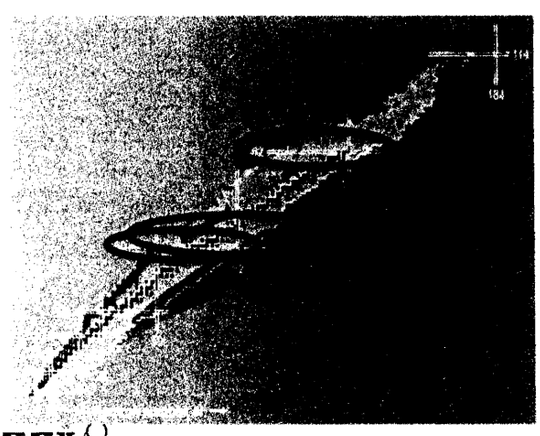

- Shape coexistence.
  - Near Z=50 and Z=82.
- Shapes and softness.
  - Octupole deformation.
  - Triaxial shape and nuclear chirality.
- High-K isomers and multi quasiparticle configurations.
  - Doubly K-magic nuclei with Z,N=72 and 116.

Physics to be studied

- **Nuclear Shell structure.**
- **Nuclear shapes.**
- **Nuclear symmetries.**

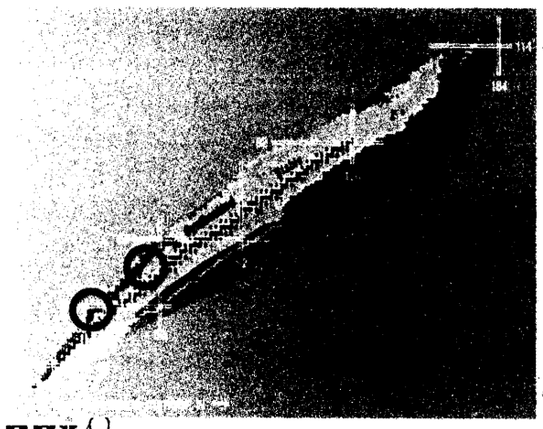

- Nuclear mirror symmetry.
  - Coulomb energy difference.
  - Far from the N=Z line.
- A full mapping of the limiting symmetries.
  - U(5) : vibrator.
  - O(6) : triaxial.
  - SU(3) : axial symmetric.
  - X(5) : transitional.

Physics to be studied

- **Nuclear Shell structure.**
- **Nuclear shapes.**
- **Nuclear symmetries.**
- **Collective modes.**

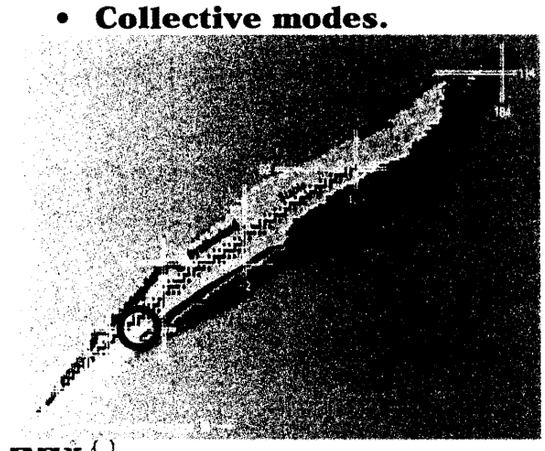

- At N>>Z.
  - A new low-lying E1 GDR mode : Pygmy resonance.
  - Effective in-medium NN interaction.

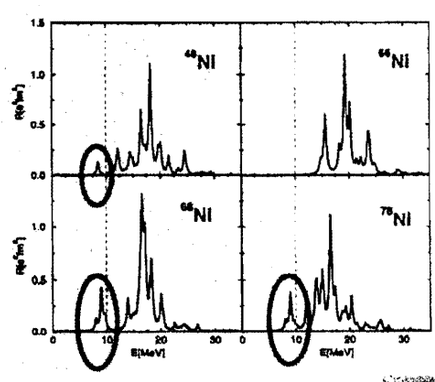

The Rising experiments at relativistic energies

RISING

18.03.2004 *Gamma04, RIKEN* **Take R. Saitoh**

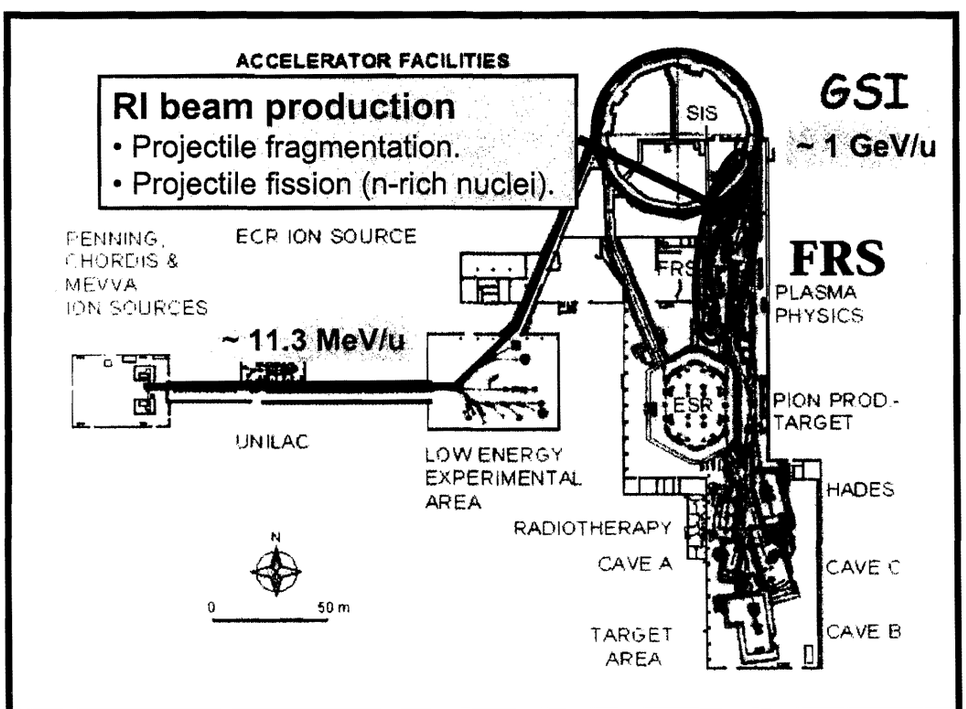

18.03.2004 *Gamma04, RIKEN* **Take R. Saitoh**

FRagment Separator

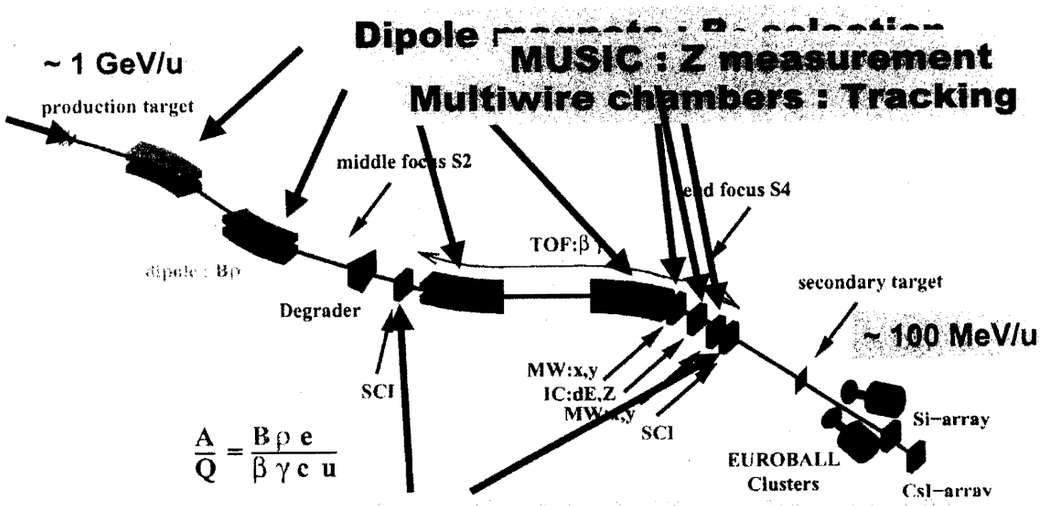

Fast plastic scintillator : Time-Of-Flight (TOF)

Two types of experiments

- Secondary fragmentation.
  - With a Be target.
  - Suppression of the inelastic excitation of the projectile.
  - Broad angular momentum distribution to high spins.
- Coulomb excitation.
  - With a Au target.
  - One step excitation.
  - High energy.

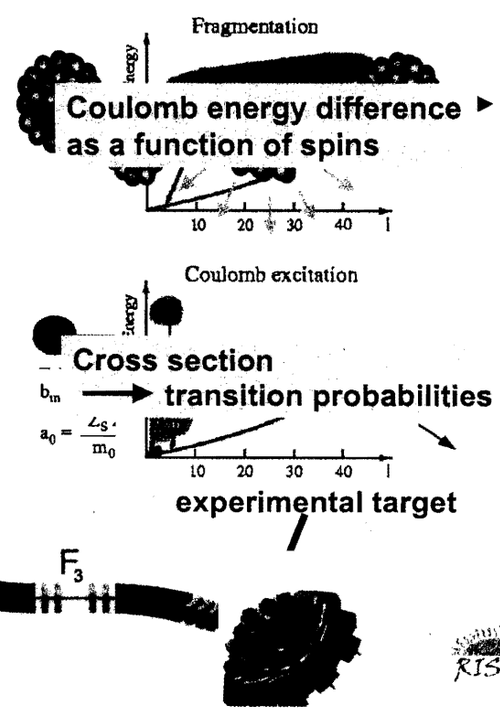

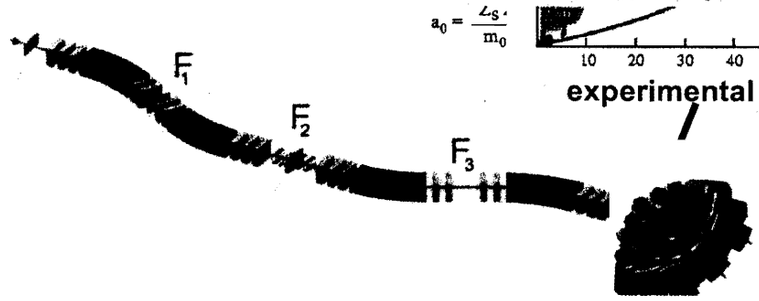

RISING detectors

RISING Ge-array

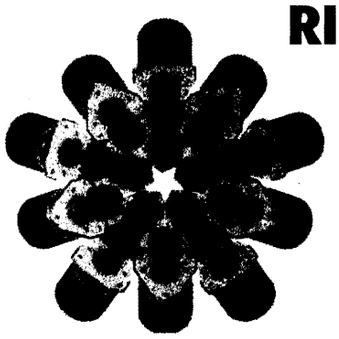

15 EUROBALL cluster detectors.

- 7 crystals each.
- A total of 105 crystals.

8 MINIBALL detectors (en

Wall-like array at forward angle.

- **Large Lorentz boost (β~0.4).**
- Op
- Mi

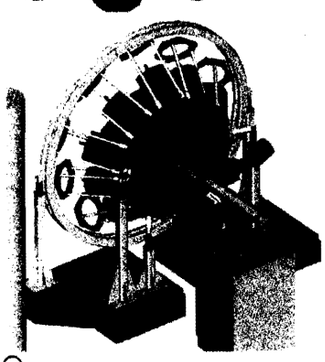

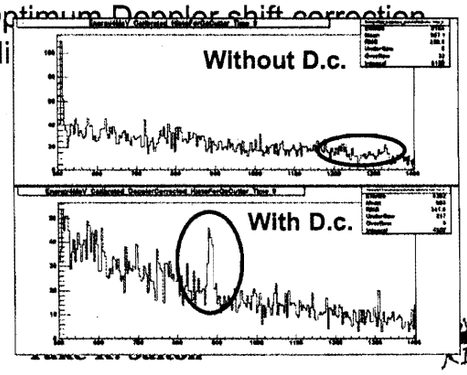

RISING Ge-array

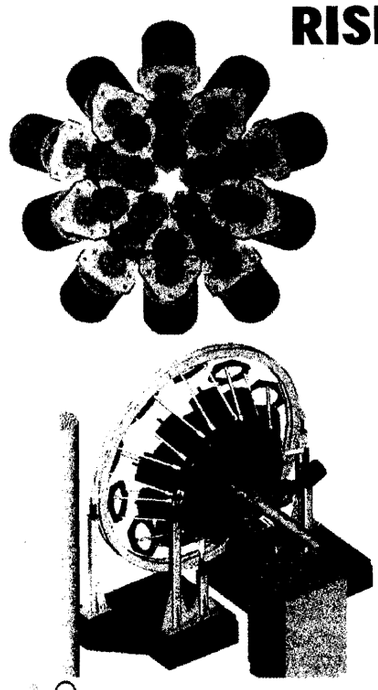

- **15 EUROBALL cluster detectors.**
  - 7 crystals each.
  - A total of 105 crystals.
- **8 MINIBALL detectors (end of 2004).**
- **Wall-like array at forward angle.**
  - **Large Lorentz boost (β~0.4).**
  - Optimum Doppler shift correction.
  - Minimizing Doppler broadening.
- **Energy resolution (FWHM) : ~1.2 %.**
- **Total efficiency : ~3 % at 1.3 MeV.**
- **Scattering experiment at 1000 p/s beam intensity feasible!!**

RISING detectors

RISING detectors

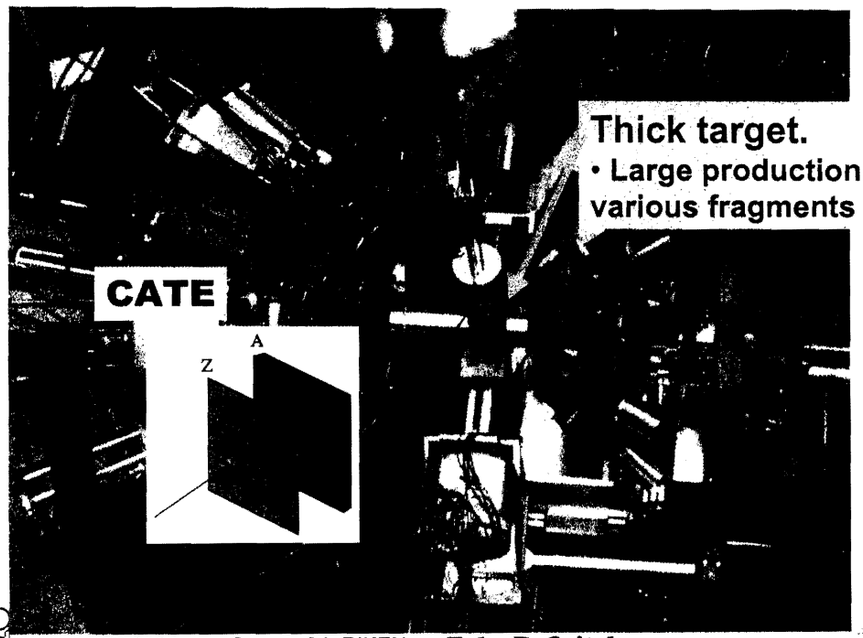

Thick target.
- Large production of various fragments

CAlorimeter TElescope array

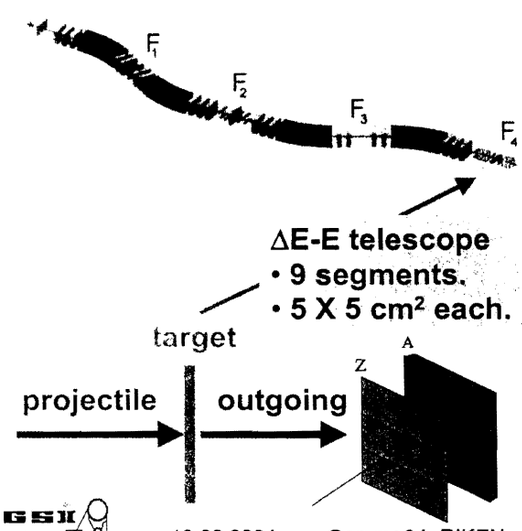

- Fragmentation

Outgoing ≠ Incoming

- Inelastic scattering

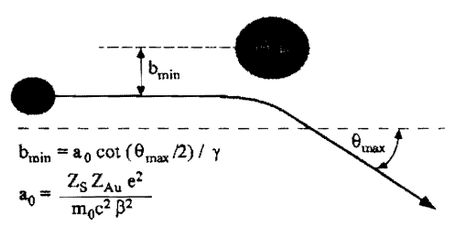

$b_{min} = a_0 \cot(\theta_{max}/2) / \gamma$

$a_0 = \frac{Z_S Z_{Au} e^2}{m_0 c^2 \beta^2}$

Outgoing = Incoming

CAlorimeter TElescope array

ΔE
- 0.3 mm thick Si detectors.
- For Z identification.
- Position sensitive.

Position resolution ~5 mm.

E
- CsI detectors.
- For mass identification.

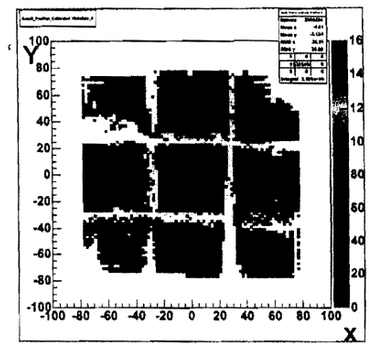

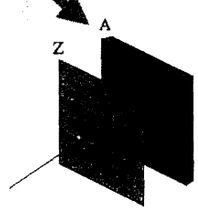

CAlorimeter TElescope array

ΔE
- 0.3 mm thick Si detectors.
- For Z identification.
- Position sensitive.

Position resolution ~5 mm.

E
- CsI detectors.
- For mass identification.

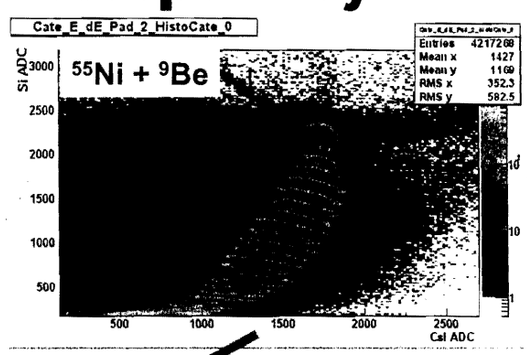

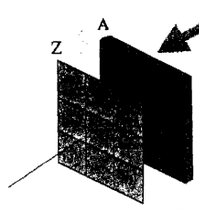

- Excellent Z resolution.
- Mass analyses in progress.

CAlorimeter TElescope array

ΔE
- 0.3 mm thick Si detectors.
- For Z identification.
- Position sensitive.

Position resolution ~5 mm.

E
- CsI detectors.
- For mass identification.

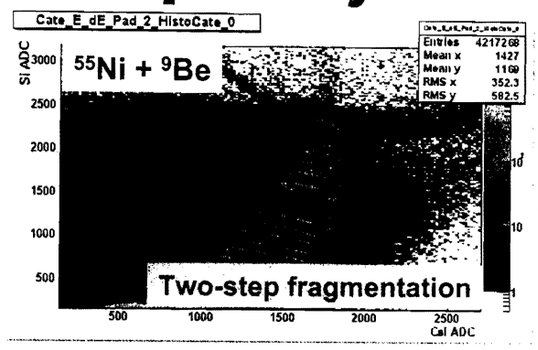

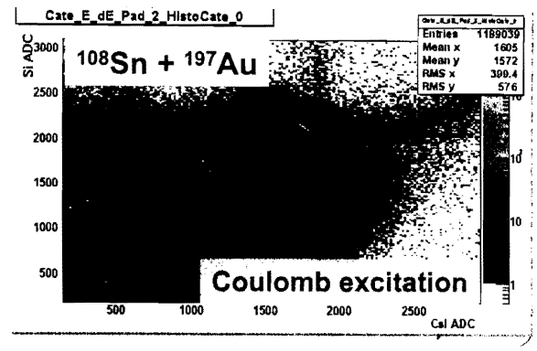

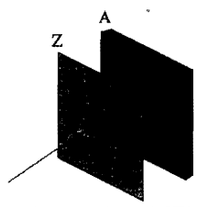

First Accepted proposals

No.	Nuclei of Interest	Primary Beam	Spokespersons	Experiment Type	Accepted Request (days)
1 (S244)	$^{34/36}$Mg	^{48}Ca	P. Mayet	2 step fragmentation lifetime	6
2	^{45}Cr, ^{53}Ni, ^{45}Sc, ^{53}Mn	^{58}Ni	M. Bentley	2 step fragmentation	7
3	[redacted]				
4	^{54}Ca, ^{78}Ni	^{86}Kr	H. Grawe, H. Hübel, P.Reiter	Coulex	13
5	^{88}Kr, ^{90}Sr, ^{86}Se	^{238}U	D. Tonev	Coulex	10
6	$^{102-110}$Sn, $^{94-98}$Ru	^{124}Xe	C. Fahlander, M. Górska	Coulex	6
7	^{132}Sn	^{238}U	G. de Angelis	Knock-out	5
8	^{138}Xe	[redacted]	[redacted]	[redacted]	[redacted]
9	^{134}Te	^{136}Xe	K.-H. Speidel	Coulex, g-factor	7
10	^{185,186,187}Pb	^{238}U	J. Gerl, A. Andreyev, G.D. Dracoulis	2 step fragmentation lifetime	8
	^{84}Kr	[redacted]	[redacted]	[redacted]	~7

Relativistic Coulomb excitation with primary beams

- Goals:
  - Study the feasibility of the Coulomb excitation.
  - Particle-γ angular correlation.
- ^{84}Kr primary beam at ~100 MeV/u.
  - Energy well defined.
- 400 mg/cm^2 Au target.

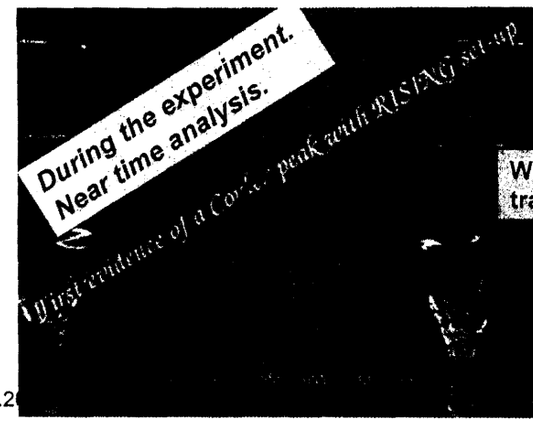

GSI 18.03.2 RISING

Determination of the impact parameters

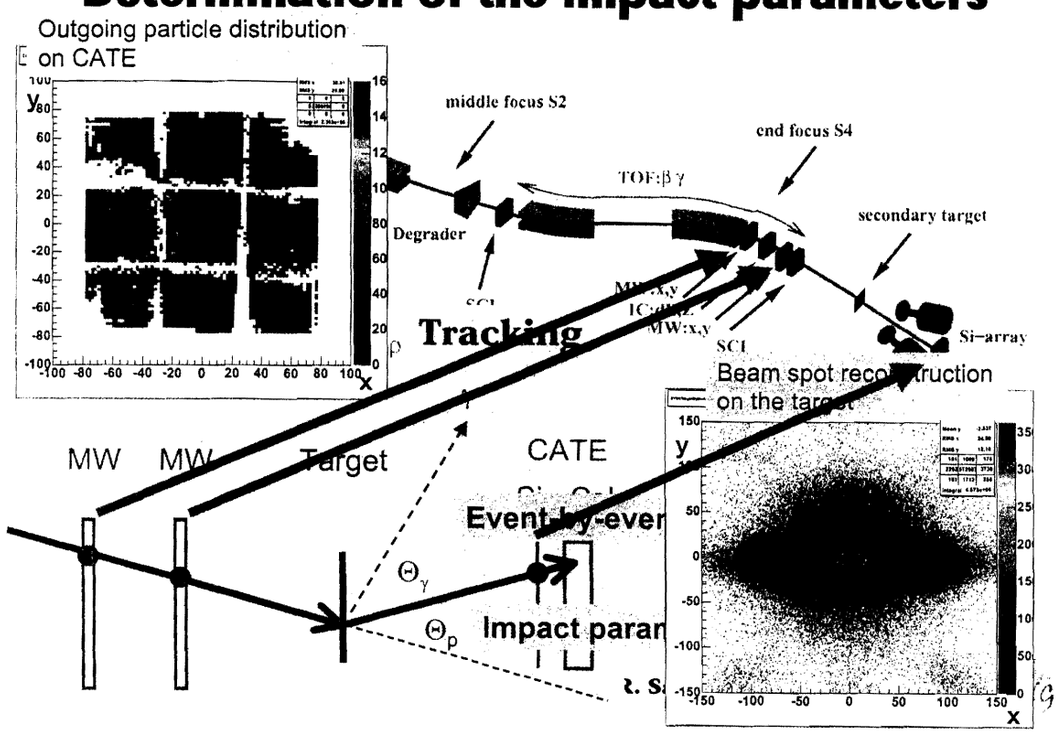

Relativistic Coulomb excitation with the ^{84}Kr primary beam

Scattering angle dependence

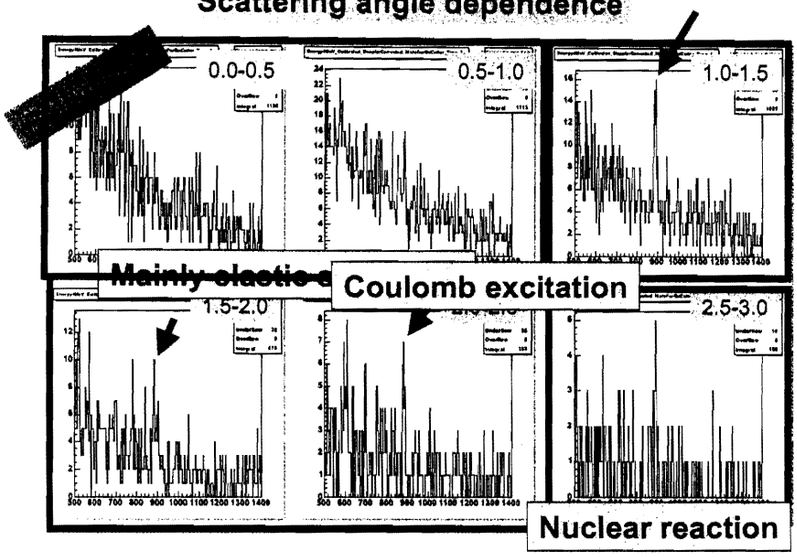

Relativistic Coulomb excitation with the ^{84}Kr primary beam : Off-line analyses

- Event-by-event tracking.
- Scattering angle selection : 0.5 ~ 2.5 degrees.
- $\langle M_\gamma \rangle = 1$: Selectivity of Coulomb excitation.

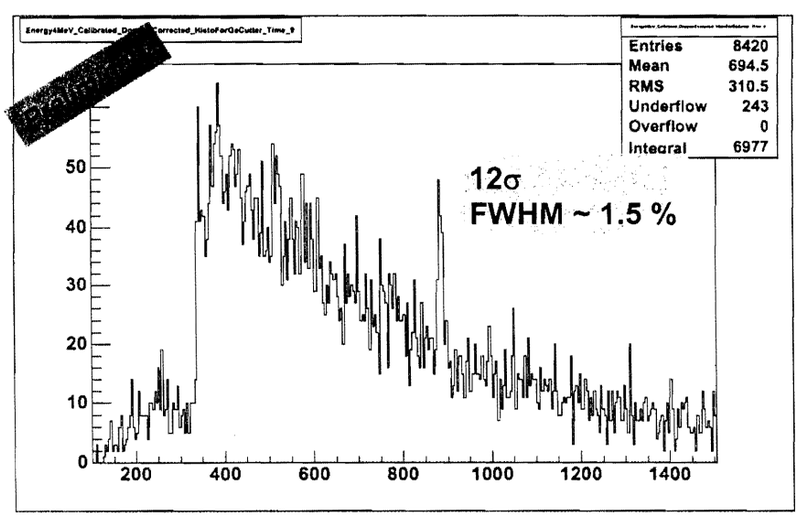

Relativistic Coulomb excitation of the fragment beam

New shell structure at N>>Z
Relativistic Coulex in N=28-34 and N=40-50 nuclei

- Secondary beam : ^{56}Cr ~ 100 MeV/u.
  - Large beam spot on the target.
  - Large momentum dispersion of the secondary beam.
- Coulomb excitation target : ^{197}Au, 1 g/cm^2.

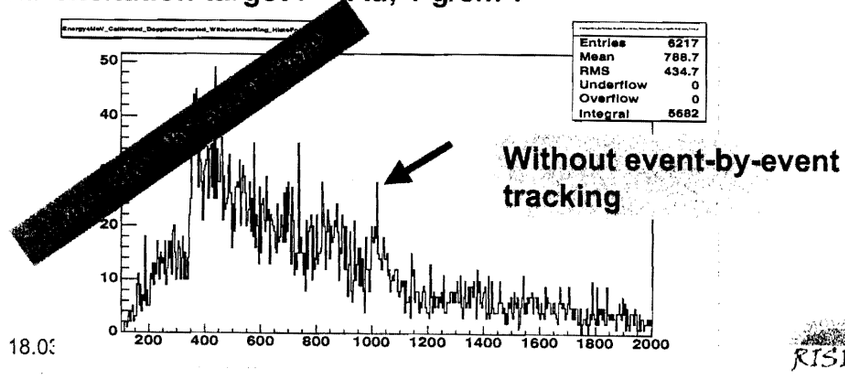

Relativistic Coulomb excitation of ^{56}Cr Offline analyses

- Event–by-event tracking.
- Scattering angle selection : 0.5 ~ 3.5 degrees.
- Event-by-event v/c measurement by TOF.

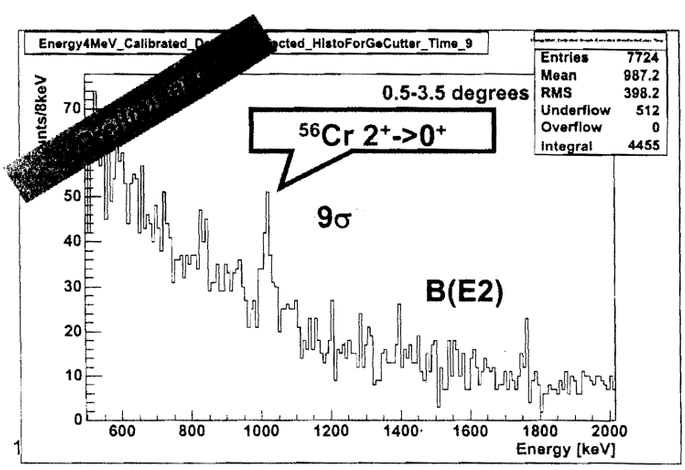

Two step fragmentation experiment

Isospin Symmetry and Coulomb Effects Towards the Proton Drip-Line

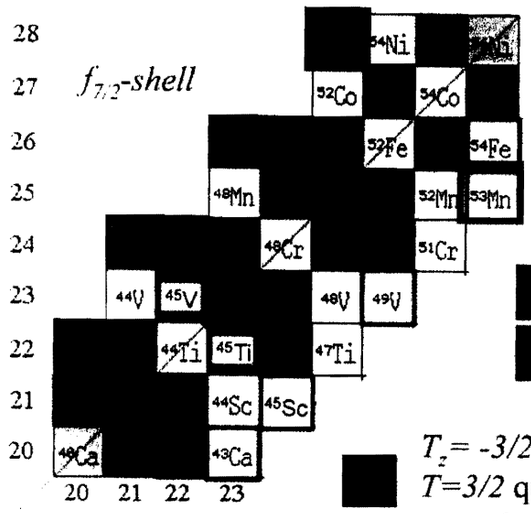

Complete isobaric multiplets in $f_{7/2}$-shell…

$T = 1/2$ mirror-pairs

$T = 1$ isobaric triplets

$T_z = -3/2$ ($N=Z-3$) members of the $T=3/2$ quadruplet - no excited states known…

Two step fragmentation experiment

Isospin Symmetry and Coulomb Effects Towards the Proton Drip-Line

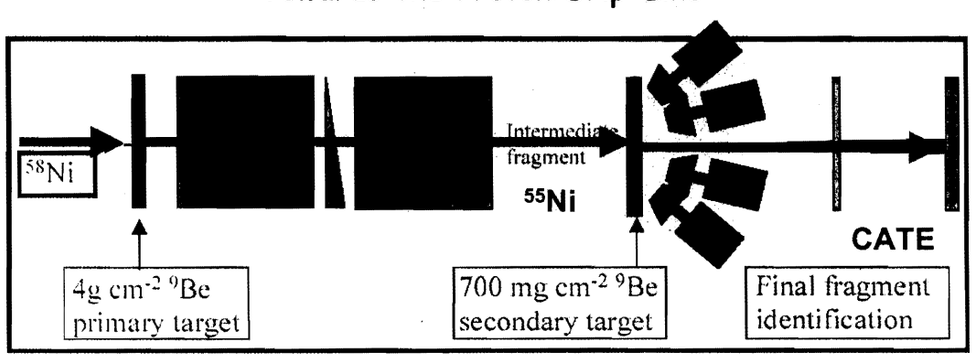

- **Primary beam : ^{58}Ni, 600 MeV/u.**
- **Secondary beam : ^{55}Ni, 171 MeV/u.**
- **Secondary fragment target : ^{9}Be, 700 mg/cm2**
- **All outgoing fragments from the target were identified by CATE.**
  Series of studies on different nuclei with one experiment.
- **^{53}Ni and ^{53}Mn for studying the mirror symmetry. C.E.D.**

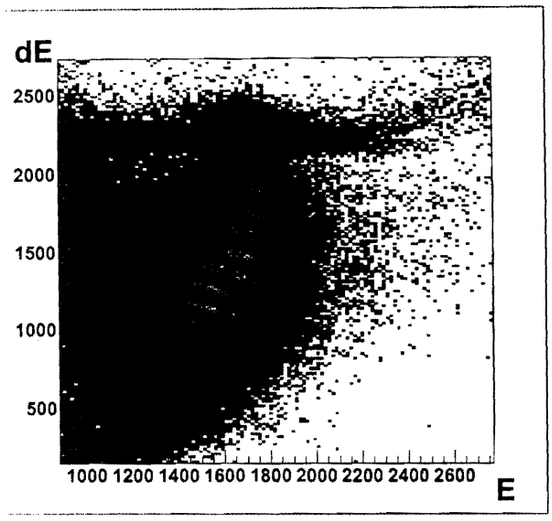
dE
2500
2000
1500
1000
500
1000 1200 1400 1600 1800 2000 2200 2400 2600
E

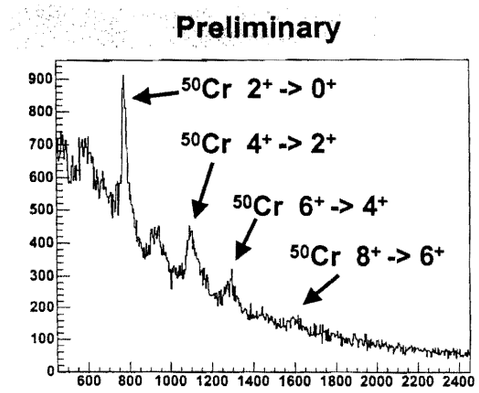
Preliminary
^{50}Cr 2$^+$ -> 0$^+$
^{50}Cr 4$^+$ -> 2$^+$
^{50}Cr 6$^+$ -> 4$^+$
^{50}Cr 8$^+$ -> 6$^+$
900
800
700
600
500
400
300
200
100
0
600 800 1000 1200 1400 1600 1800 2000 2200 2400

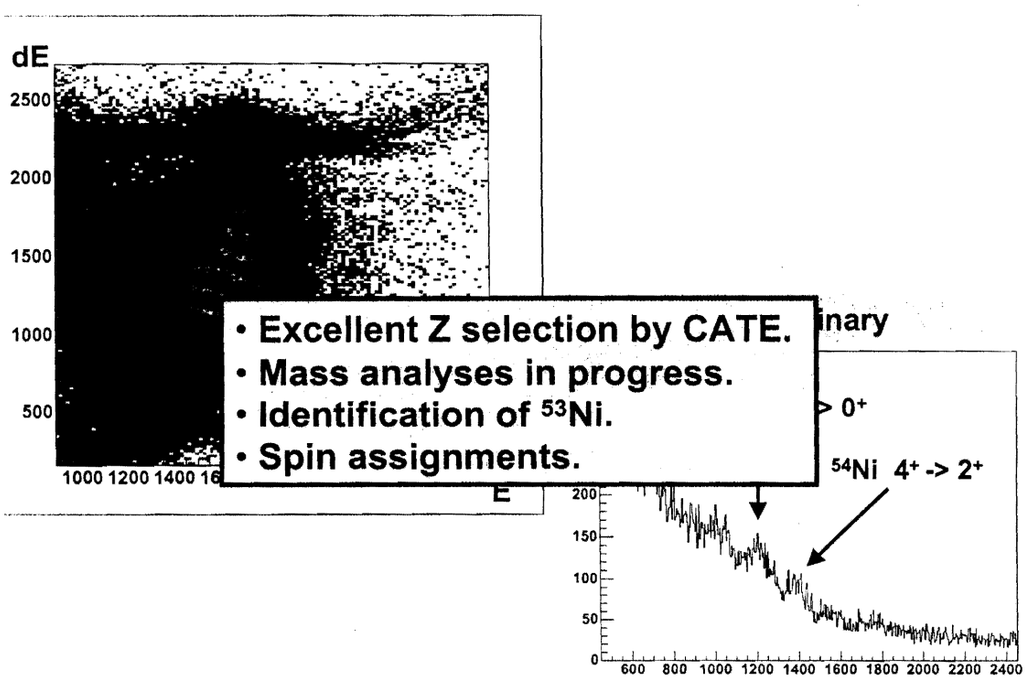
dE
2500
2000
1500
1000
500
1000 1200 1400 16
E
• Excellent Z selection by CATE.
• Mass analyses in progress.
• Identification of ^{53}Ni.
• Spin assignments.
inary
> 0$^+$
^{54}Ni 4$^+$ -> 2$^+$
200
150
100
50
0
600 800 1000 1200 1400 1600 1800 2000 2200 2400

γ-ray (crystal) multiplicity

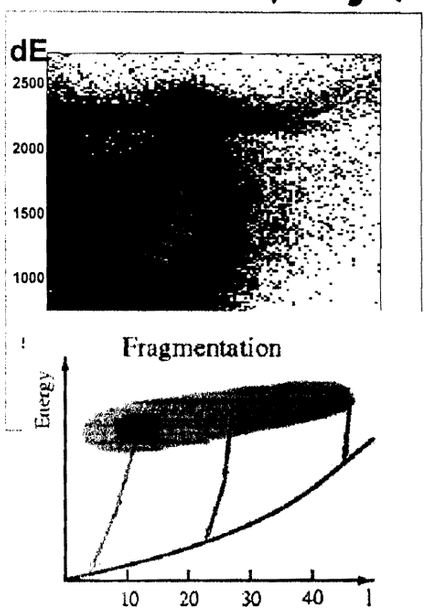

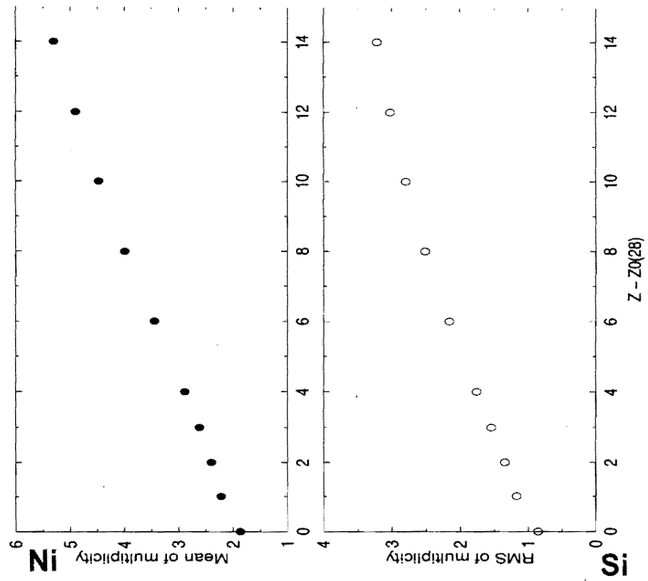

^{50}Cr

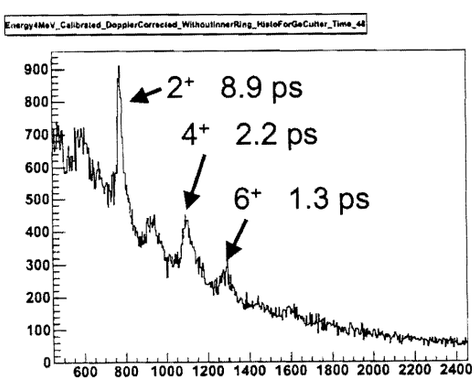

Changing the velocity

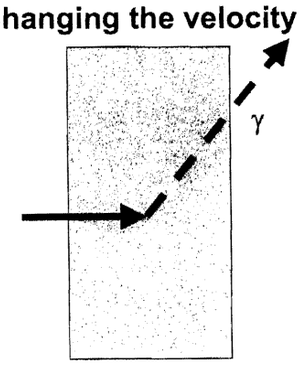

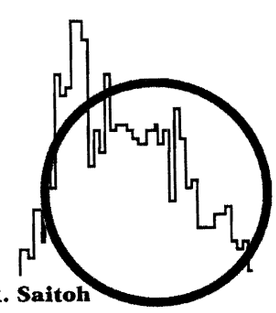

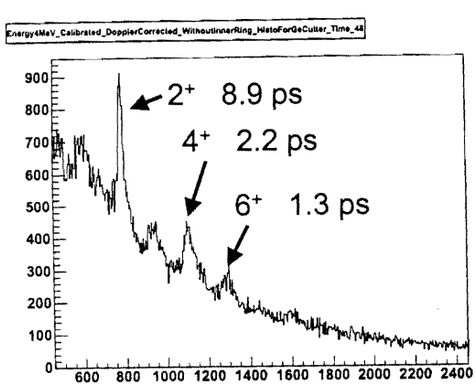

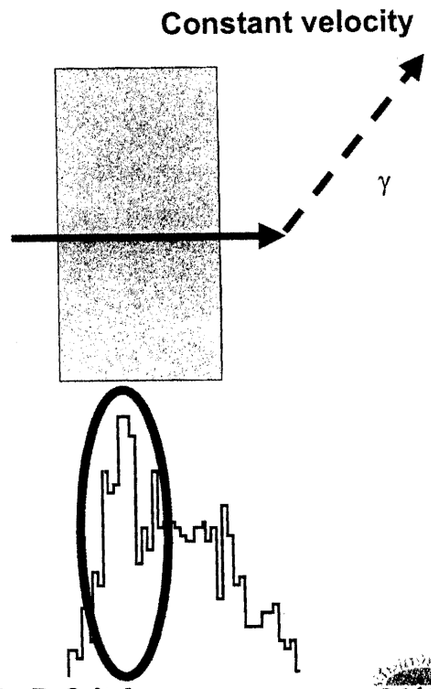

GSI 18.03.2004 *Gamma04, RIKEN* **Take R. Saitoh** RISING

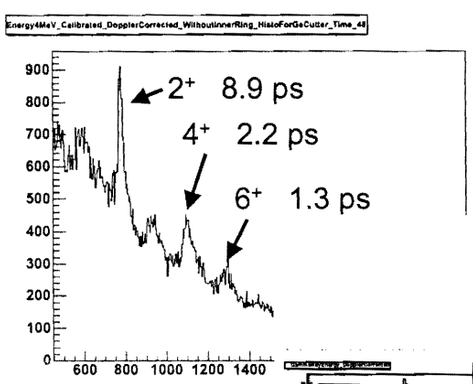

GEANT4 simulation

132Xe
Target : 197Au 300 mg/cm2
Energy : 600 keV
Energy at S4 : 100 MeV

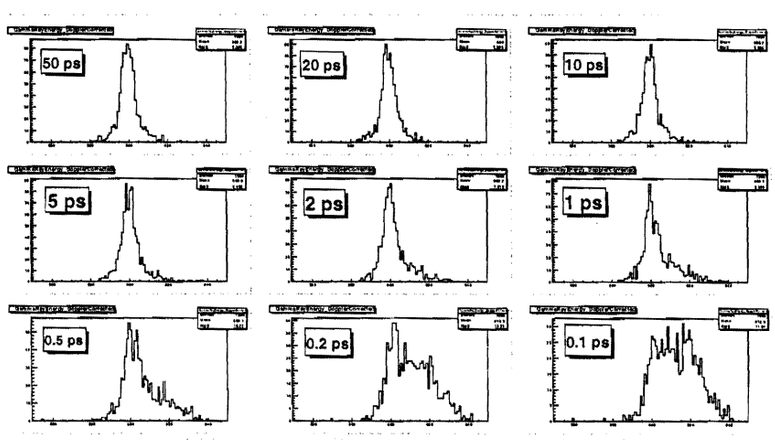

Lifetime, B(E2)
Excitation

GSI 18.03.2004

γ-ray angular distribution

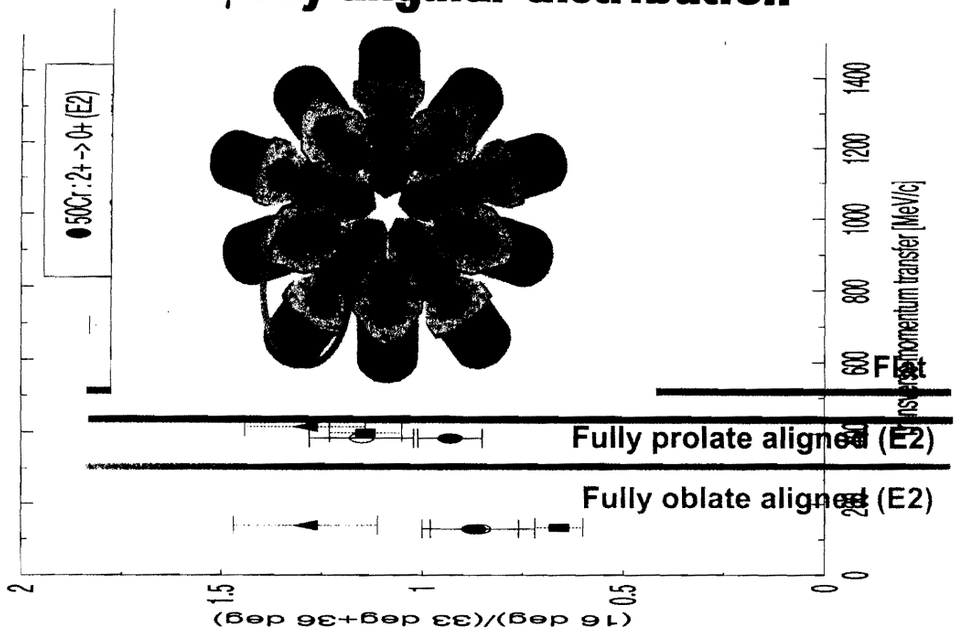

RISING with stopped beams

What is the stopped beam experiment?

- Fragment beam production at relativistic energies.
- De-accelerate the fragments with
- Stop the fragment at the catcher.
- Decay study with the EUROBALL

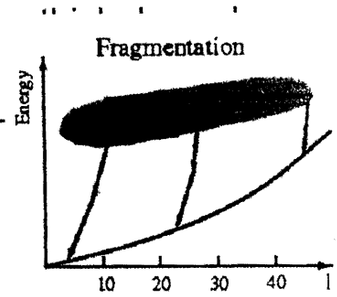

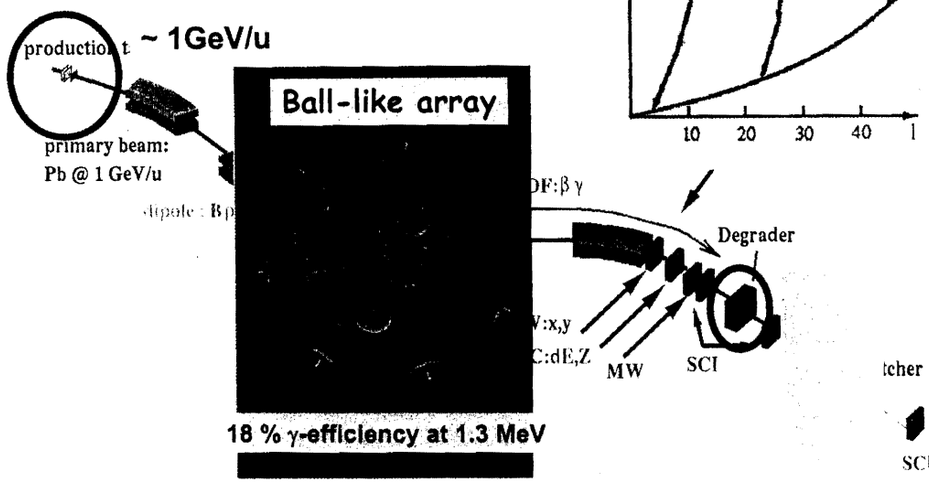

What is studied with stopped beams?

- **To study the nuclear structure at extreme.**
- Decay study.
  - Low background.
- **Feasible with very low fragment intensity ~ 1 p/s.**
  c.f. 1000 p/s needed for experiments at relativistic energies.
  - Example : ^{190}W experiment in 2000. ~ 1p/s.

- **γ-isome**
- **α- and**
- **Electro** **easurements**
in ps~ns

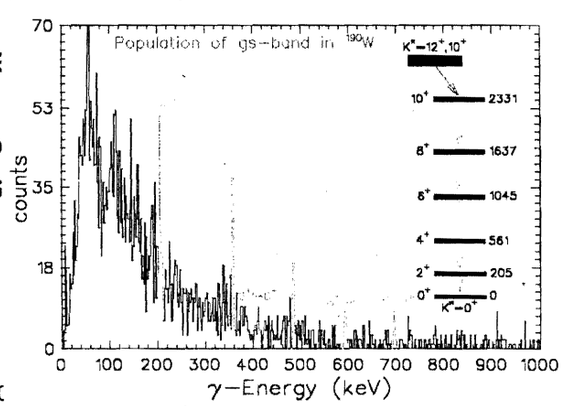

Coming up

- 2004
  - ➢ May : Experiments at relativistic energies with HECTOR, for GDR and N>>Z nuclei.
  - ➢ December : Experiments at relativistic energies with MINIBALL.
    - Seven proposals being already approved.
    - Five new proposals submitted and four approved.

γ-efficiency : 4-10 %

Coming up

- 2004
  - ➢ May : Experiments at relativistic energies with HECTOR, for GDR and N>>Z nuclei.
  - ➢ December : Experiments at relativistic energies with MINIBALL.
    - Seven proposals being already approved.
    - Five new proposals submitted and four approved.
- 2005
  - ➢ Winter : Experiments at relativistic energies with MINIBALL.
  - ➢ Summer : Experiments with stopped beams.
    - γ-isomer decay.
    - α- and β-decay.
    - Life time measurements in ps~ns with electrical timing methods.
- 2006
  - ➢ Experiments with relativistic beams and wit[redacted]s.
  - ➢ Feasibility studies for experiments with slow[redacted]s.
    - Multiple Coulomb excitation.
    - One- and two-particle transfer reactions.
    - Fusion and deep inelastic reactions.

18 % γ-efficiency at 1.3 MeV

Institu[redacted]NG

GANIL, Caen, France CSNCM Orsay, France IPN Orsay, France CEA Saclay, France	Univ. Demokritos, Greece
CLRC Daresbury, UK Univ. Keele, UK. Univ. Liverpool, UK Univ. Manchester, UK Univ. Paisley, UK Univ. Surrey, UK Univ. York, UK	Univ. Firenze, Italy INFN Genova, Italy INFN Legnaro, Italy INFN/Univ. Napoli, Italy INFN/Univ. Padova, Italy Univ. Milano, Italy Univ. Camerino, Italy
HMI Berlin, Germany Univ. Bonn, Germany GSI Darmstadt, Germany TU Darmstadt, Germany MPI Heidelberg, Germany FZ Jueliich, Germany Univ. Koeln, Germany LMU Muenchen, Germany TU Muenchen, Germany FZ Rossendorf, Germany	Univ. Lund, Sweden KTH Stockholm, Sweden Univ. Uppsala, Sweden NBI Copenhagen, Denmark
Univ. Leuven, Belgium	IFJ Cracow, Poland Univ. Cracow, Poland IPJ Swierk, Poland Univ. Warsaw, Poland

The local RISING team

Study of high-spin states by using secondary fusion reaction

Eiji Ideguchi
Center for Nuclear Study (CNS), University of Tokyo

Studies of high-spin states in atomic nuclei by in-beam gamma-ray spectroscopy have provided detailed information on the nuclear structure. In such studies, high-spin states are achieved mostly through a fusion reaction using a combination of a stable-isotope beam and a stable-isotope target, since large angular momentum can be brought to the nucleus of interest in the reaction. However, nuclei produced in the fusion reaction are limited, in many cases, to the proton-rich side relative to the β-stability line. By utilizing a neutron-rich beam in the fusion reaction, nuclei will be produced in the neutron-rich side and the region available for high-spin studies will be largely expanded.

In order to actualize this method, an experiment to produce a low-energy secondary beam (~6MeV/nucleon), which is indispensable for inducing the fusion reaction, was performed at the RIKEN accelerator research facility. In the first experiment, a secondary ^{37}P beam was produced at the RIPS Facility [1] in RIKEN by the fragmentation reaction of an ^{40}Ar beam (63 MeV/nucleon) impinging on a ^{9}Be target with 1.5 mm thick. The energy of the ^{37}P beam was lowered by using a wedge degrader at first momentum dispersive focal plane (F1) and a rotatable degrader placed at the second focal plane (F2). The ^{37}P beam was transported to the final focal plane (F3) and irradiated on the secondary ^{9}Be target 10 μm thick in order to induce the secondary fusion reaction, ^{9}Be(^{37}P, xn)$^{46-x}$K. The intensity of the ^{37}P beam at F3 was about 1.0×10^{5} counts per second. Gamma rays from the secondary reaction were measured by using the CNS Ge array [2].

In the second experiment, neutron-rich ^{45}Cl, ^{46}Ar beams are employed to induce secondary fusion reactions with thin ^{9}Be target, and high-spin states in ^{49}Sc and ^{50}Ti are investigated. In the symposium the results obtained in these experiments will be presented.

References

[1] T. Kubo et al.: Nucl. Instrum. and Methods. **B 461**, 309 (1992).
[2] S. Shimoura et al.: CNS Annual Report, p. 5 (2001).

Study of high-spin states by using secondary fusion reactions

CNS, University of Tokyo
Eiji Ideguchi

Collaborators

CNS: S. Shimoura, H. Iwasaki, T. Fukuchi,
S. Michimasa, M. Tamaki, M. Niikura
RIKEN: T. Suda, K. Yoshida, K. Morimoto,
T. Oonishi, M. Kurokawa, T. Kubo, I.Tanihata
Tsukuba: A. Ozawa, T. Komatsubara, K. Miyakawa
Rikkyo: H. Baba
Kyoto: S. Ota
Kyushu: Y. Wakabayashi, N. Hokoiwa
KTH: C. Ishida, B. Cederwall
SUNY Stonybrook: T. Koike

Secondary fusion reaction for high-spin study

- High-spin study established

  Fusion reaction:
  Stable isotope beam + Stable isotope target

- High-spin study induced by RI beam

  Fusion reaction:
  RI beam + Stable isotope target

  → High-spin states in Stable | Neutron rich nuclei

High-spin studies done

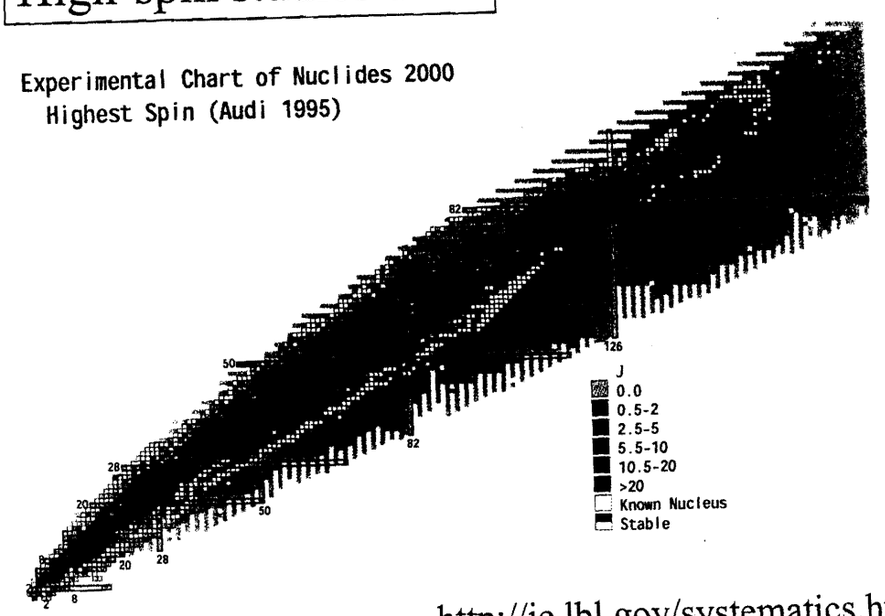

http://ie.lbl.gov/systematics.html

Study in Ca region

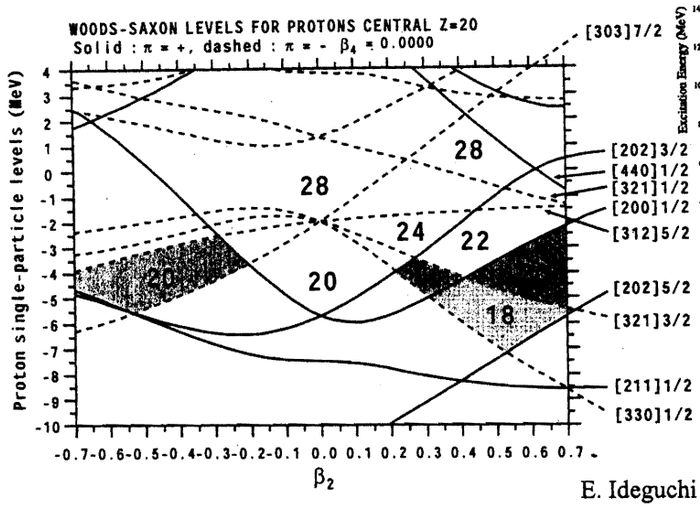

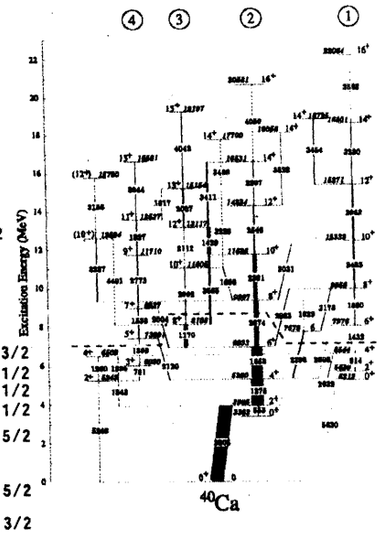

E. Ideguchi *et al.*, PRL87, 222501 (2001)
C. J. Chiara *et al.*, *PRC67*, 041303(R) (2003)

Developmental item

• Production of low-energy secondary beam

$^{40}Ar + {}^{9}Be \rightarrow {}^{37}P \rightarrow {}^{9}Be(^{37}P, xn)^{46-x}K$

$^{48}Ca + {}^{9}Be \rightarrow {}^{44}S \rightarrow {}^{9}Be(^{44}S, xn)\ ^{53-x}Ca$

$^{45}Cl \rightarrow {}^{9}Be(^{45}Cl, xn)\ ^{54-x}Sc$

$^{46}Ar \rightarrow {}^{9}Be(^{46}Ar, xn)\ ^{55-x}Ti$

Fragment separator (RIPS) + Energy degrader

• Gamma-ray detector

CNS Ge Array : GRAPE (Gamma-Ray detector Array with Position and Energy sensitivity)

Production of Low-energy 2ndary beam using RIPS

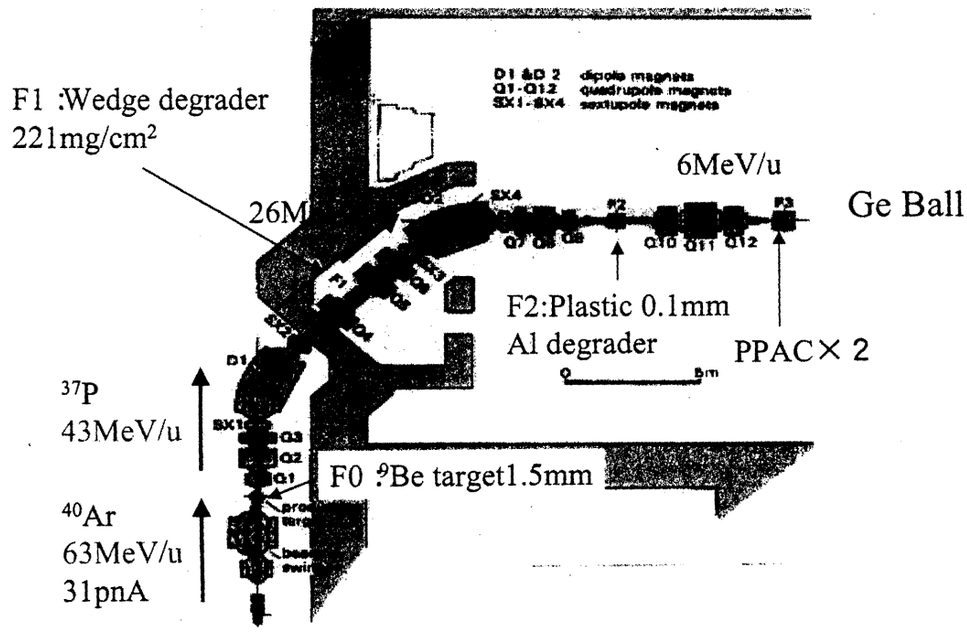

Low energy ^{37}P beam at F3

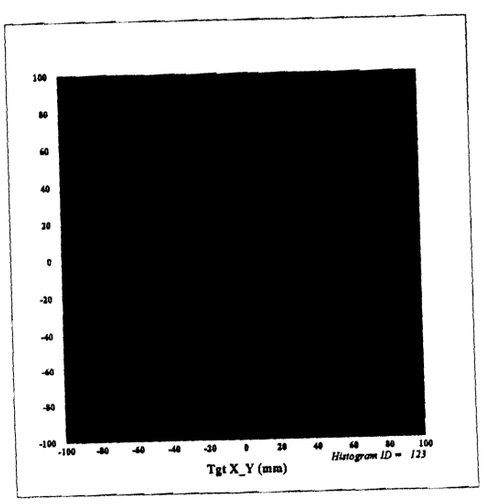

X-Y at Target (mm)

X: ±18mm, Y: ±7.5mm

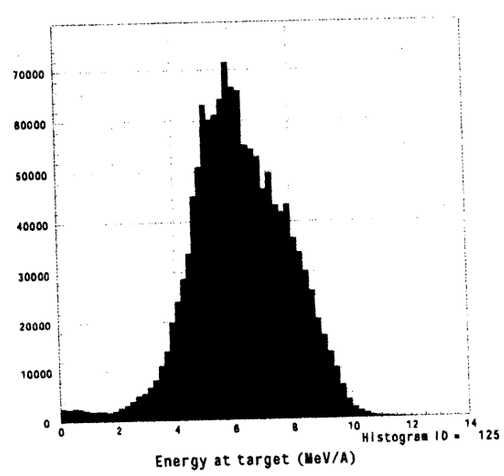

Energy at Target

E = 6±2 MeV/A

^{37}P beam on 2ndary target

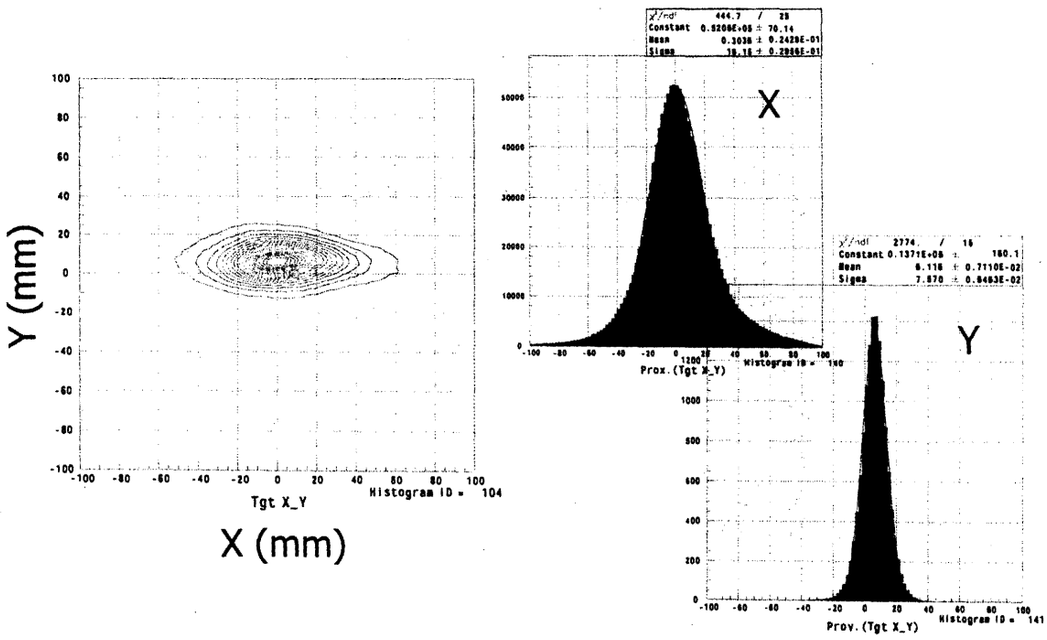

Experimental setup

(Schematic)

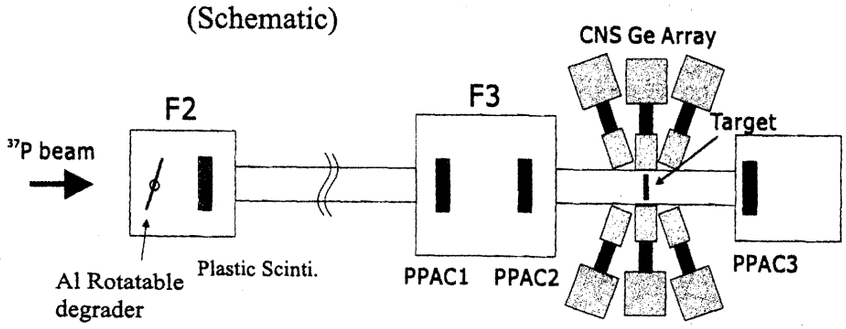

- Secondary target ^{9}Be 10 μm (1.8mg/cm^2) thick、10cm ϕ
- 2 PPAC's before 2ndary target
  → Beam Image, incident angle on target → Doppler correction
- F2 Plastic－F3PPAC TOF
  → Beam Energy
- CNS Ge Array (about 5% for 1MeV γ ray)

GRAPE

CNS Gamma-Ray detector Array with Position and Energy sensitivity

18 segmented planar Ge's

S. Shimoura et al.:
CNS Annual Report, p. 5 (2001).

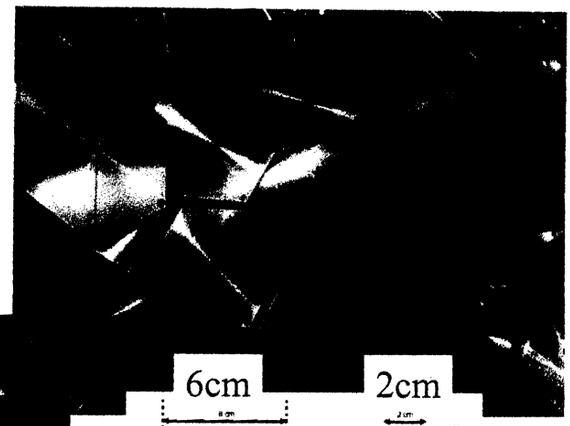

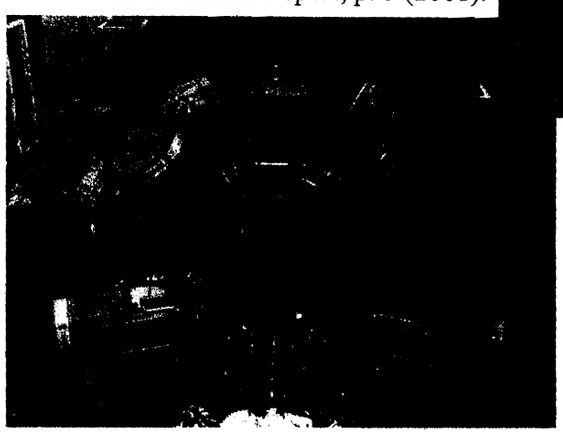

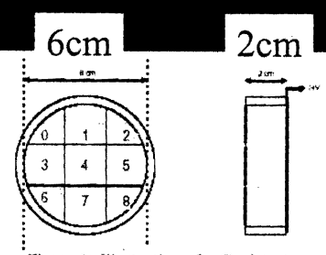

Figure 1: Illustration of a Ge detector.

type	d	ρ (cm^{-3})
p^+ (segmented)	0.2 μm	10^{11}
p	2.0 cm	0.8 - 10^{10}
n^+ (high voltaged)	300 μm	10^{11}

Block diagram

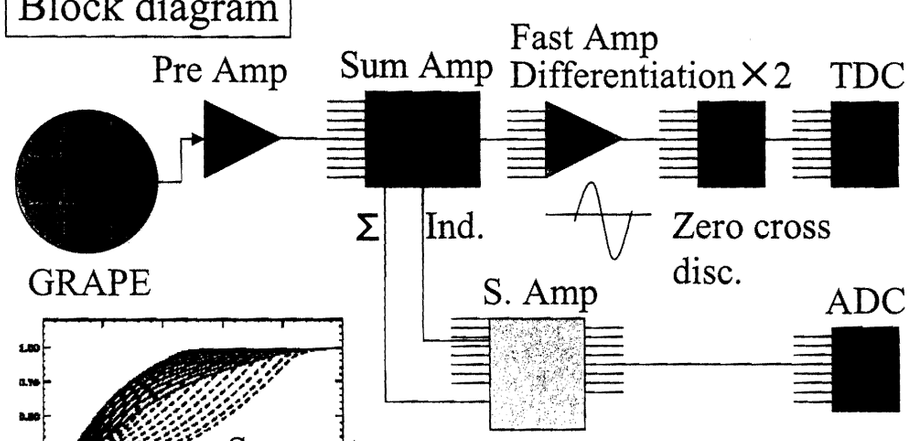

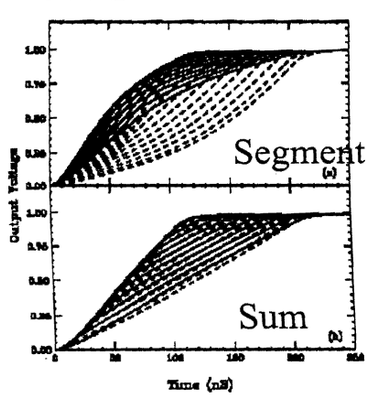

M. Kurokawa et al., IEEE Trans. Nucl. Sci. , 50(2003)1309

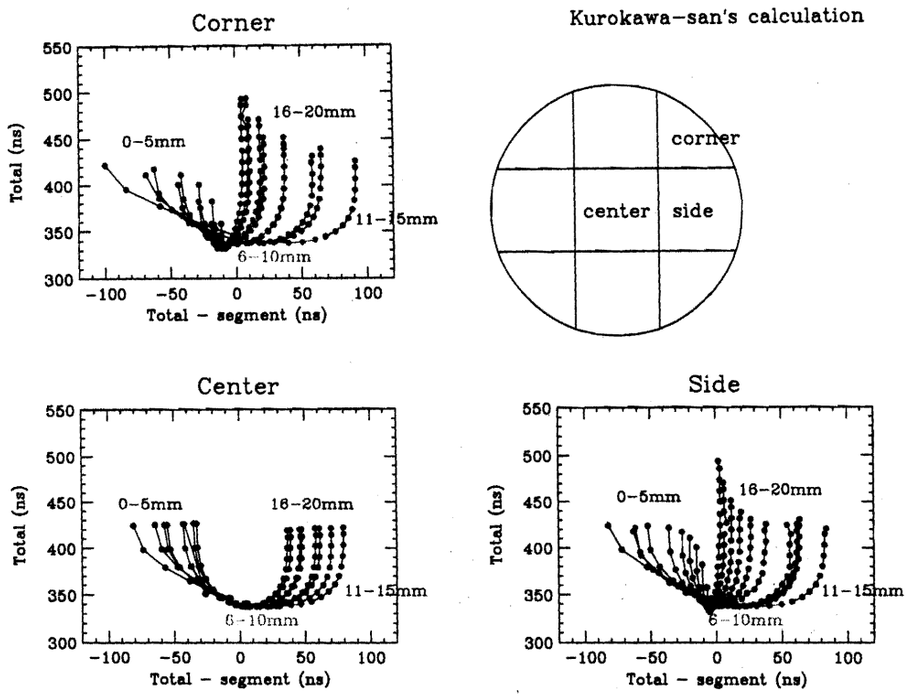
Corner
Kurokawa-san's calculation
Total (ns)
Total − segment (ns)
0−5mm
16−20mm
11−15mm
6−10mm
corner
center
side
Center
Side

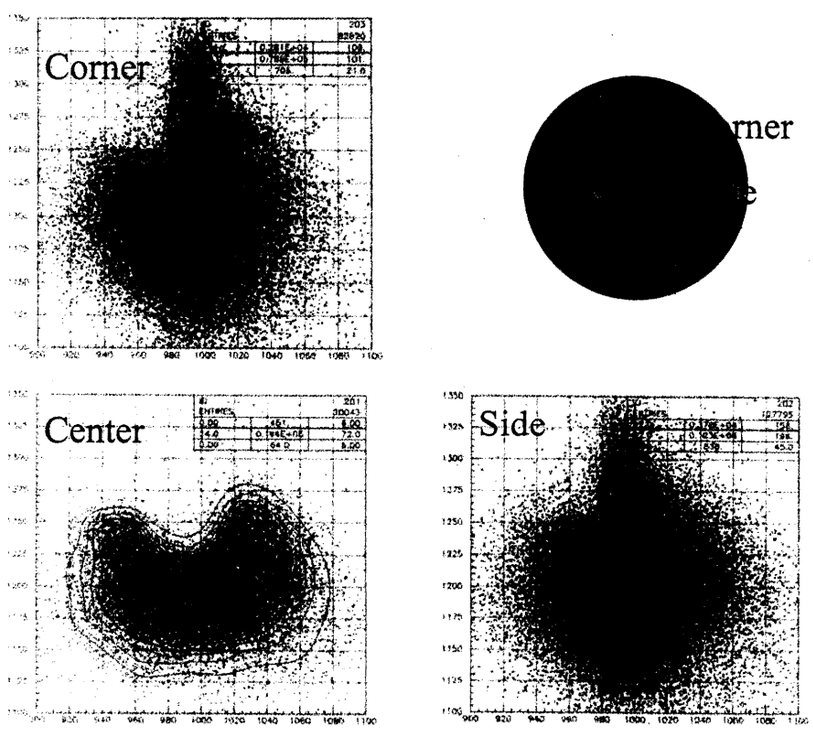
Corner
Center
Side

Secondary reactions

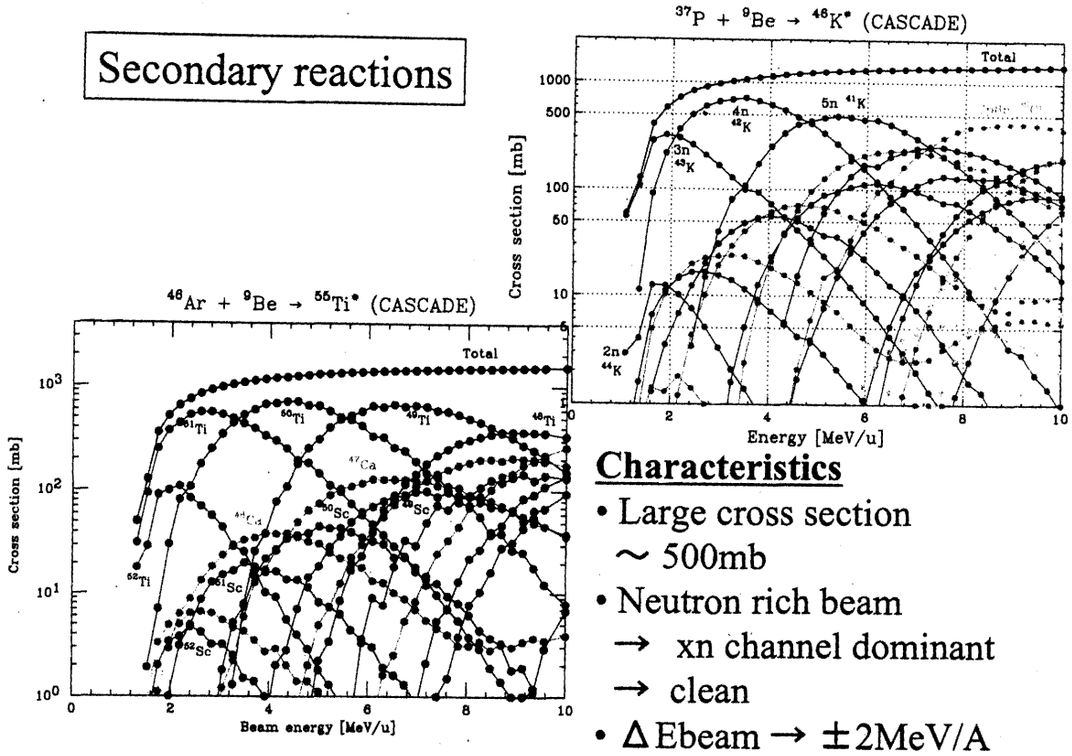

Characteristics

- Large cross section
  ~ 500mb
- Neutron rich beam
  → xn channel dominant
  → clean
- ΔEbeam → ±2MeV/A

Ge Time-Energy spectrum

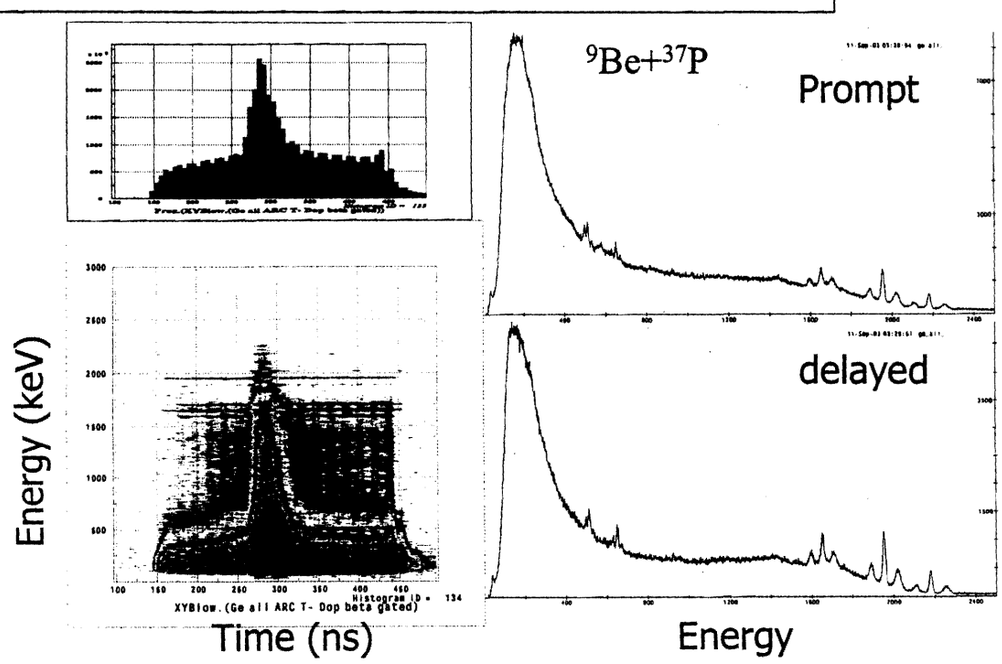

Gamma-ray spectrum (Preliminary)

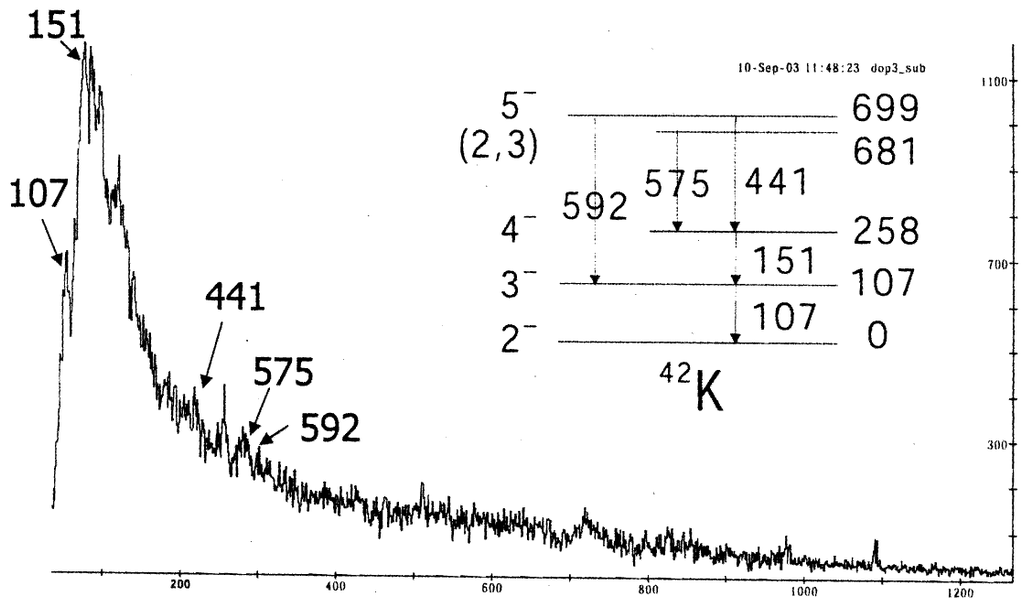

$^{9}Be + ^{48}Ca \rightarrow ^{45}Cl$

$\rightarrow ^{46}Ar$

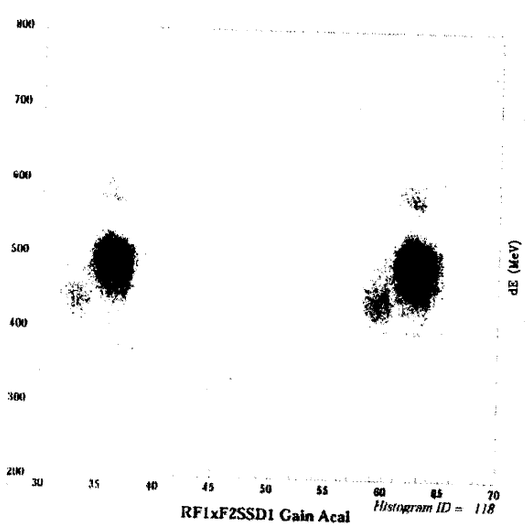

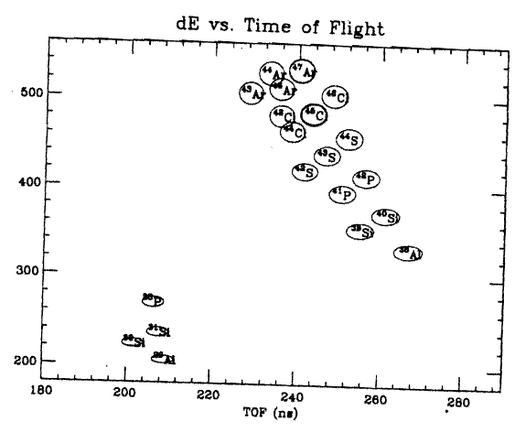

3.2×10^{5}cps on 2ndary target

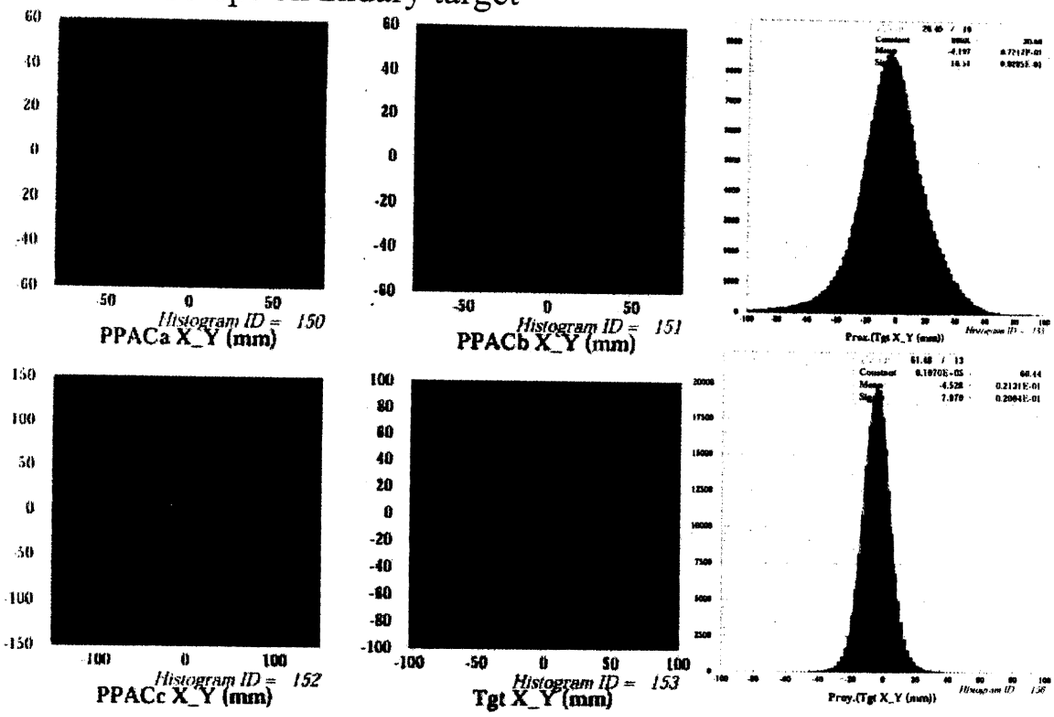

Energy of 2ndary beam deduced by TOF

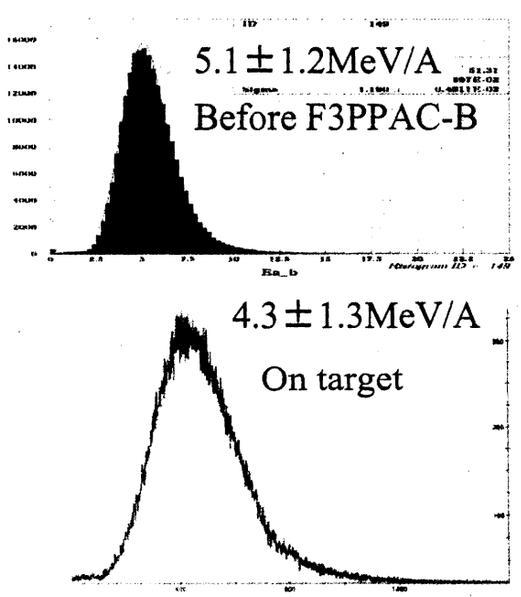

Gamma timing relative to F3PPACb

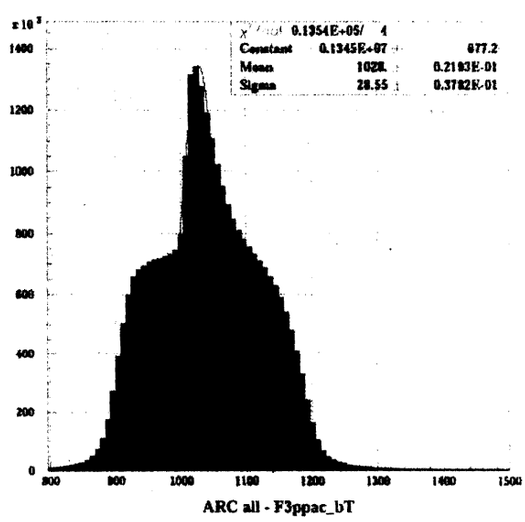

E_γ spectrum bofore Doppler correction

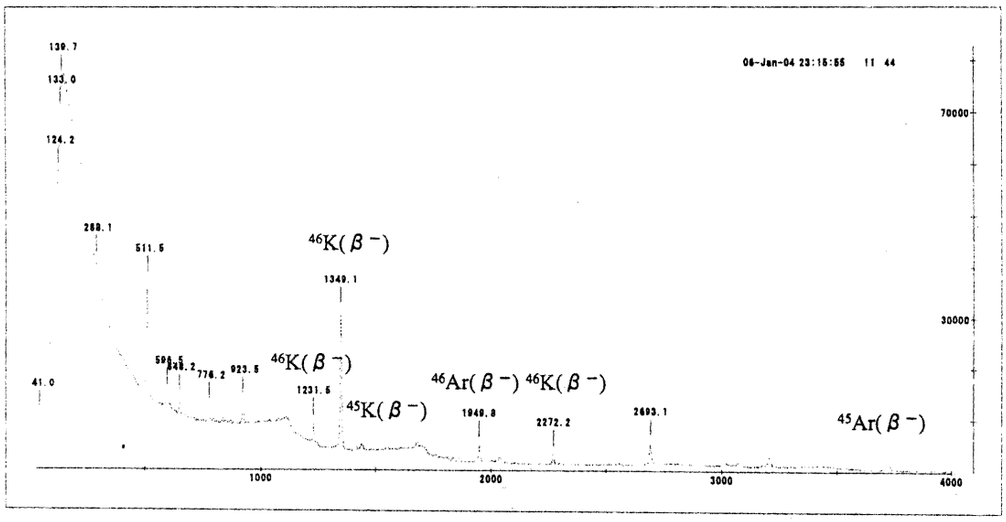

E_γ (keV)

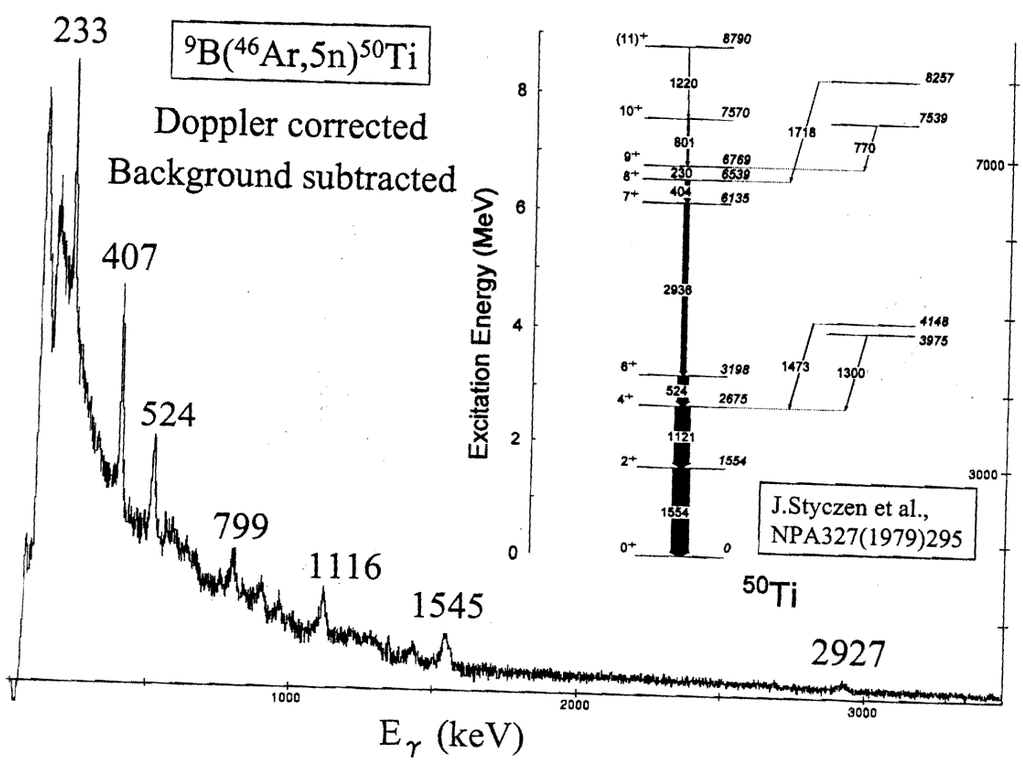

E_γ (keV)

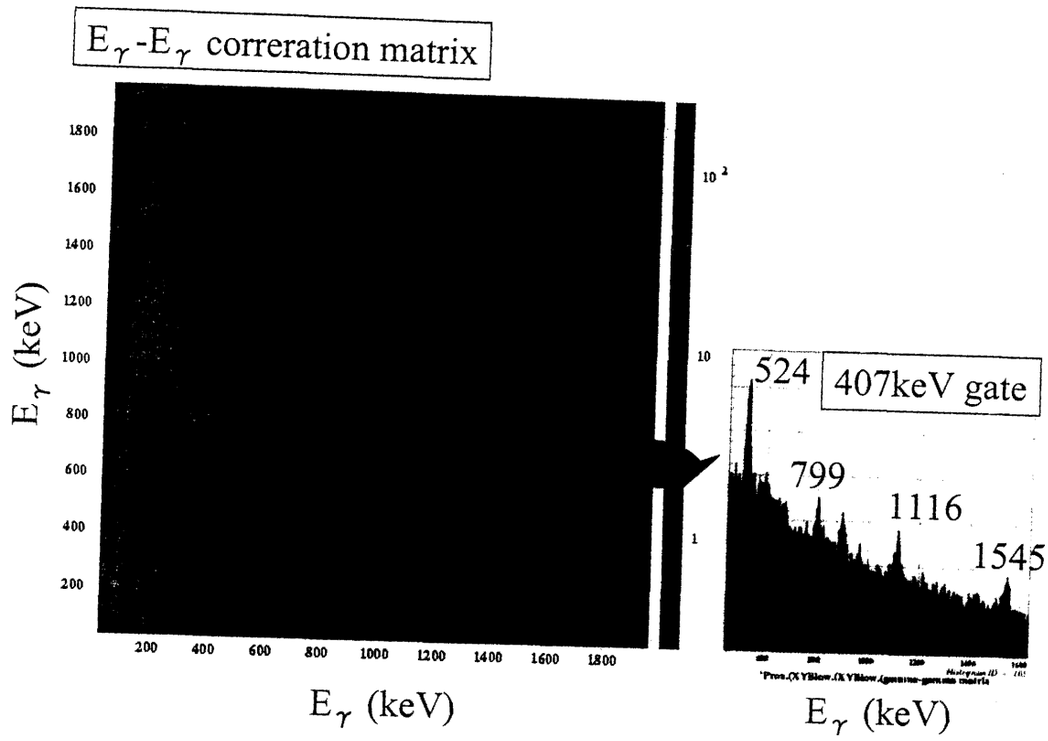
E_γ-E_γ correration matrix
E_γ (keV)
E_γ (keV)
524
407keV gate
799
1116
1545
E_γ (keV)

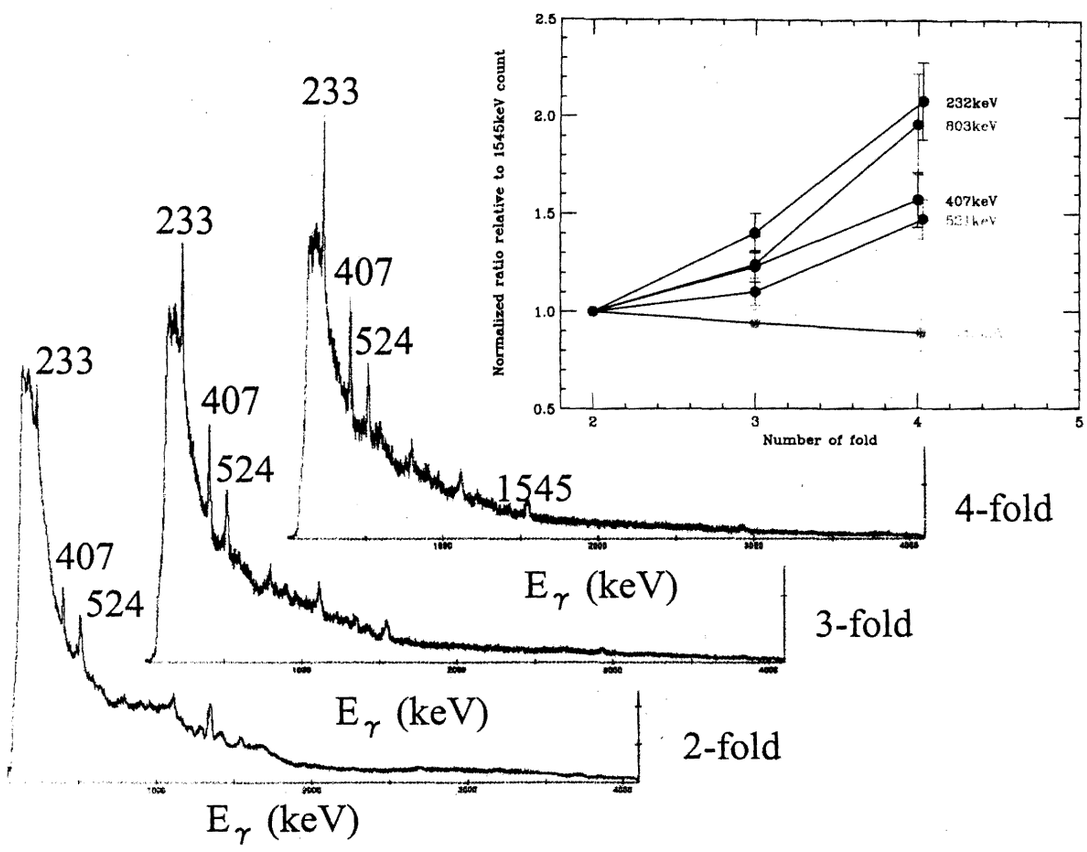
233
407
524
1545
4-fold
E_γ (keV)
233
407
524
3-fold
E_γ (keV)
233
407
524
2-fold
E_γ (keV)
Normalized ratio relative to 1545keV count
Number of fold
232keV
803keV
407keV
523keV

Summary

- Development of low-energy 2ndary beam

  ^{37}P beam: Intensity = 1×10^5cps at F3

  Purity = almost 100%

  Energy = 6 ± 2MeV/A

  ^{45}Cl, ^{46}Ar beam: Intensity = 3.2×10^5cps at F3

  Purity = ^{46}Ar 50%, ^{45}Cl 50%

  Energy = 4.3 ± 1.3MeV/A

- Gamma-rays due to 2ndary reactions

  ^{42}K, ^{50}Ti

γ-ray spectroscopy on unstable nuclei at RIBF

H. Sakurai

Department of Physics, University of Tokyo,
7-3-1 Hongo, Bunkyo-ku, Tokyo 113-0033, Japan

Radioactive isotope (RI) beams, bringing out a high isospin degree of freedom, have given great opportunities to reveal out new and exotic phenomena in extreme conditions of isospin asymmetry. Such potentials of the RI beams have been demonstrated by the in-beam γ spectroscopy with fast RI beams delivered at RIKEN. To enforce the great advantages of RI beams, the RI Beam Factory (RIBF) is being constructed [1].

Since the intermediate energy CEX was applied for ^{32}Mg [2], several methods have been developed and applied for the light mass region available at the present facility; the proton inelastic scattering for finding collective natures [3] and for determining energies of low lying excited states [4], the RI beam fragmentation method for observing higher excited states [5], the transfer reaction for single particle states [6], and very recently the recoil shadow method for life-time measurements [7]. In addition, technical efforts have been made in developing cryostat targets for hydrogen and helium as well as a NaI crystal ball [8], a segmented Ge detector system [9], and a combination of stripped and coaxial Ge crystals [10].

Such unique and powerful methods and techniques have proceeded into heavier and more neutron-rich region at RIBF, where the newly constructed accelerator complex and fragment separator lead to high performances in RI beam production. One of experimental setups following the separator is the zero-degree forward spectrometer (ZFS) [11], to identify ejectiles scattered from secondary targets with a high resolving power, and to realize high signal-to-background ratios. These features are necessary for RI beams with low intensities in the medium and heavy mass region.

The γ-ray spectroscopy on unstable nuclei with fast RI beams at the RIBF, is illustrated through the overview of the RIBF facility as well as the present R&D activities.

References

[1] T. Kubo, Nucl. Instrum. Meth. B 204 (2003) 97.
[2] T. Motobayashi et al., Phys. Lett. B 346 (1995) 9.
[3] H. Iwasaki et al., Phys. Lett. B 481 (2000) 7.
[4] Y. Yanagisawa et al., Phys. Lett. B 566 (2003) 84.
[5] K. Yoneda et al., Phys. Lett. B 499 (2001) 233.
[6] S. Ota et al., CNS-Rep. 59 (2003) 14.
[7] N. Imai et al., Phys. Rev. Lett. 92 (2004) 062501.
[8] S. Takeuchi et al., contribution of this symposium.
[9] M. Kurokawa et al., IEEE Nucl. Sci. 50 (2003) 1309.
[10] M.K. Suzuki, Master thesis, Dept. of Phys., Univ. of Tokyo (2004).
[11] H. Sakurai et al., proposal submitted to the INPAC for RIBF, 2001

Gamma-ray Spectroscopy on unstable nuclei at RIBF

H.Sakurai
Univ. of Tokyo

Layout of the RI Beam Factory (RIBF)

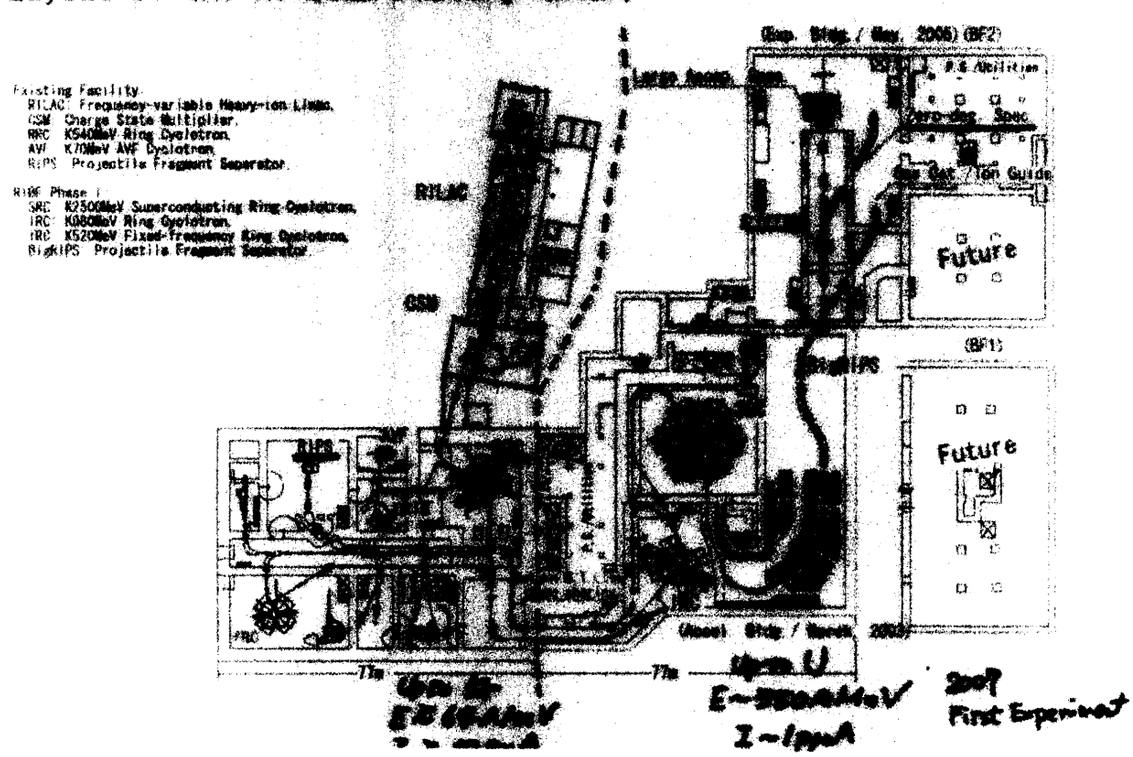

Progress of Research Opportunities with RI Beams

Construction of a dedicated facility for RI beam production via the projectile fragmentation

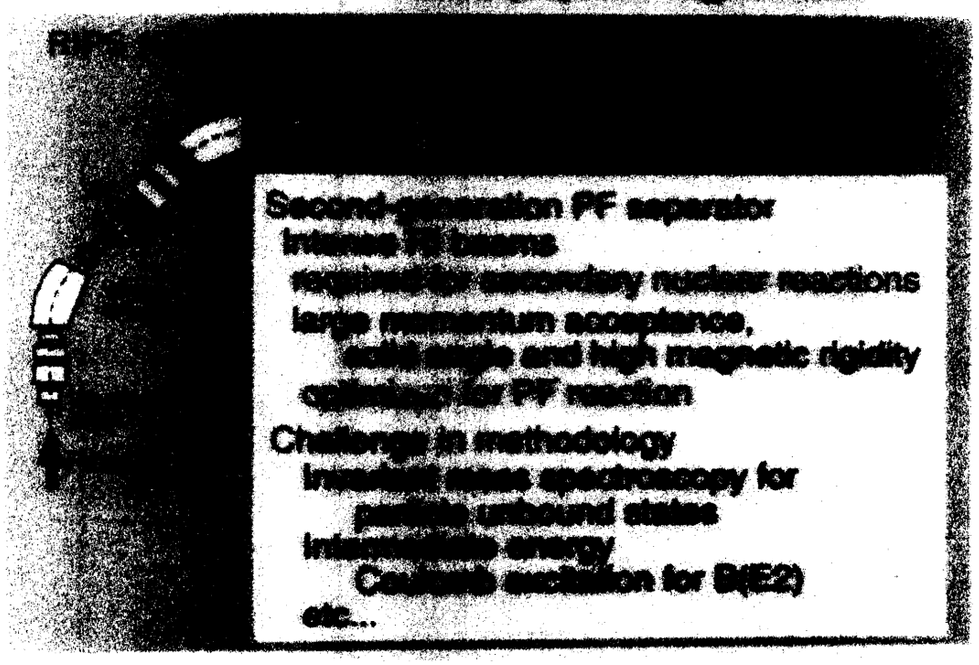

Present facility

RI beam
A < 40
E ~ 50A MeV

RIBF

RI beam
A < 200
E ~ 250A MeV

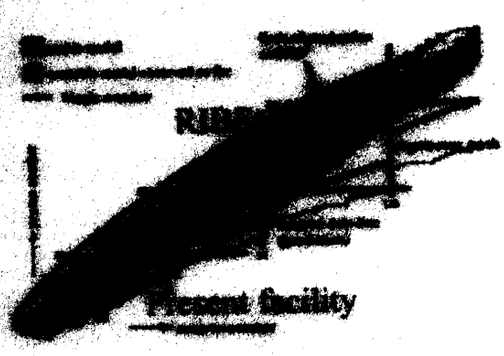

In-beam gamma spectroscopy with fast RI beams

1. Present activities
2. Future plan

Large deformation of ^{32}Mg

T.Motobayashi, et al., PLB 346, 9 (1995)

In-beam gamma spectroscopy
via intermediate energy Coulomb excitation

E2 excitation: Coulomb dominant if Z_p>10
high energy beam -> thick target
kinematical focusing -> high efficiency
weak interaction -> single step excitation

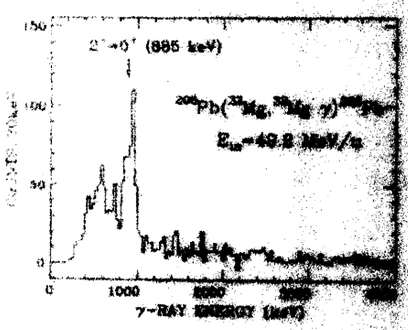

NaI detectors

B(E2) for N=20 isotones

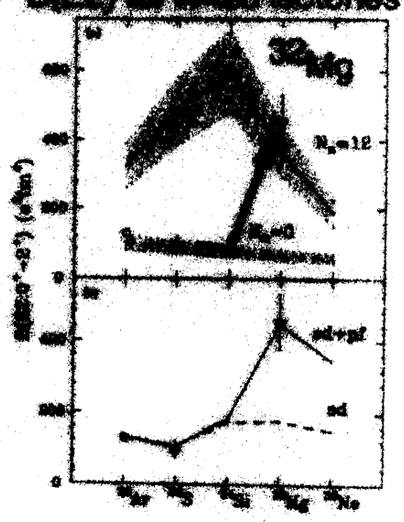

The dawn of in-beam gamma spectroscopy with intermediate energy

- B(E2) measurement for ^{32}Mg -

Reaction intermediate energy CEX

Target Pb

Detector NaI array (DALI)

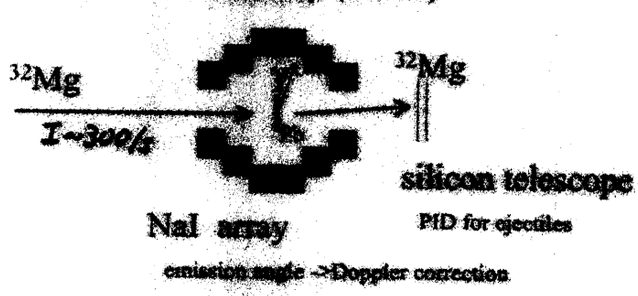

Expansion of activities with fast RI beams to observe exotic phenomena

Reaction more information

CEX	B(E2)
(p,p')	E(2⁺), β_N
fragmentation with RI beams	E(2⁺), E(4⁺) ...
transfer reaction (d,p)	single particle states → Michimasa

Target more luminosity and larger variety

cryogenic targets liquid H_2(D_2), liquid He

Detector more efficient and more accurate

highly segmented NaI array (DALI-II) -> Takeuchi

segmented Ge array (CNS-Ge) -> Ideguchi

strip Ge telescope (SSD)

New method recoil shadow method

mean-life measurements of excited states for Z<10 -> Imai

^{14}C B(E2; $2^+ \to 0^+$) ~ 0.3 W.u.

Development of liquid hydrogen target at RIKEN

Akiyoshi et al., RIKEN Accel. Prog. Rep. 32 (1998) 167

target size

25 mmΦ

target thickness

180 mg/cm^2

target temperature

16K

window foil

6 μm Harvar foil

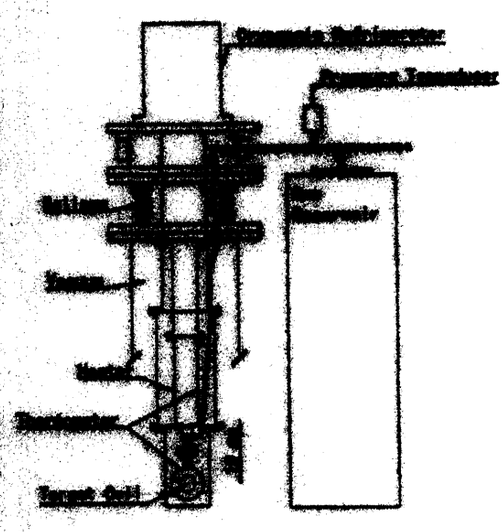

E(2$^+$) [illegible] (2003)

(p,p') liquid hydrogen target [illegible]

Number of target nuclei [illegible] x Nt Hydrogen A = 1 Pb target A = 208

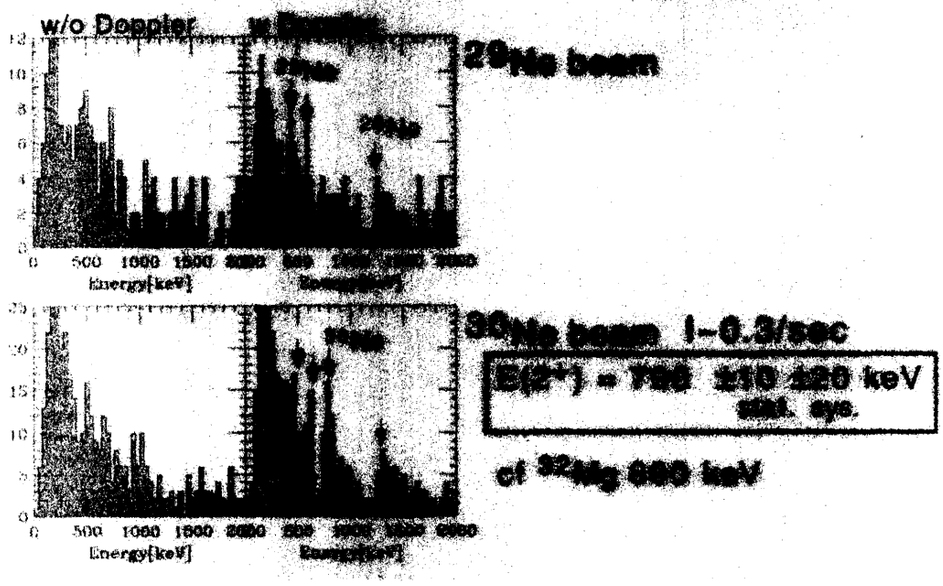

Ex(2$^+$) and [illegible]

Collective properties of nuclei in the Island-of-Inversion region

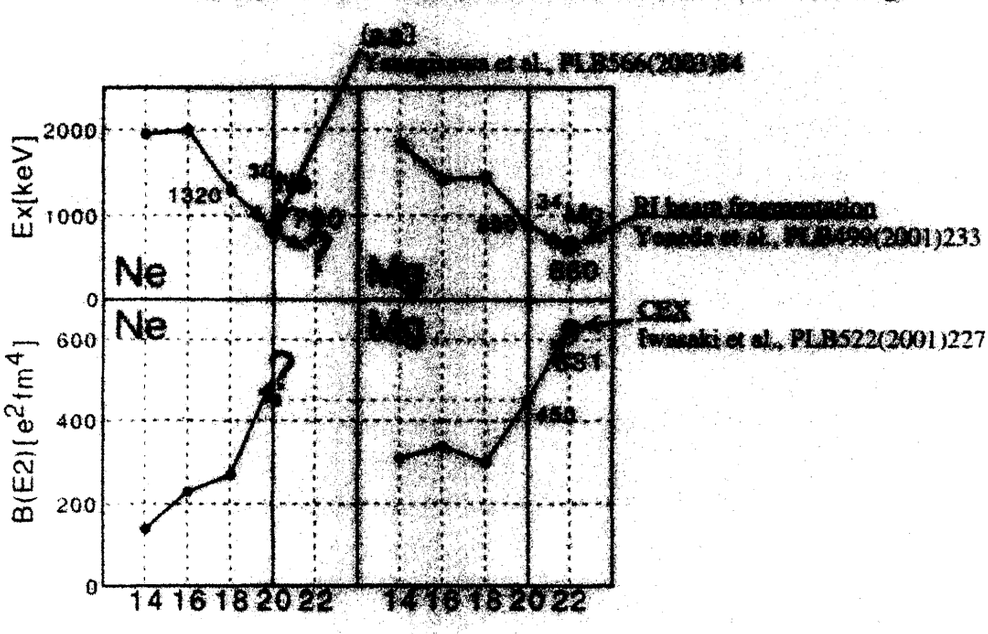

Strip Ge Telescope

M.K. Suzuki et al., in preparation.

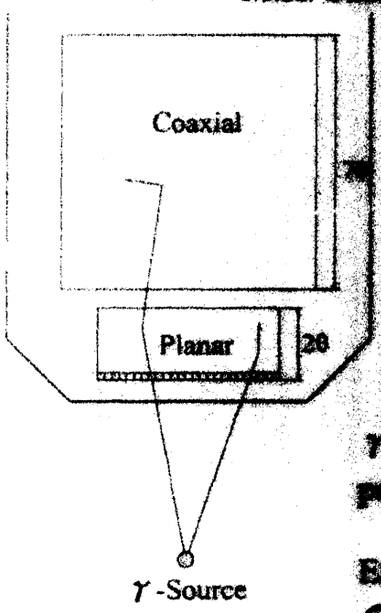

1) Planar Ge crystal 50x50x20 mm^3
Anode 2mm Strip → position sensitivity
Cathode → Energy information E_P
2) Coaxial Ge crystal 70ϕx70 mm^3
Energy information E_C
1)+2) Relative Efficiency = 55%

γ-ray energy $E_\gamma = E_C + E_P$
position information hit pattern of strips
position resolution = 2 mm (FWHM)
Efficiency for position determination = 25 %
Simple analysis

Doppler Corrected Energy Spectrum of ^{18}O

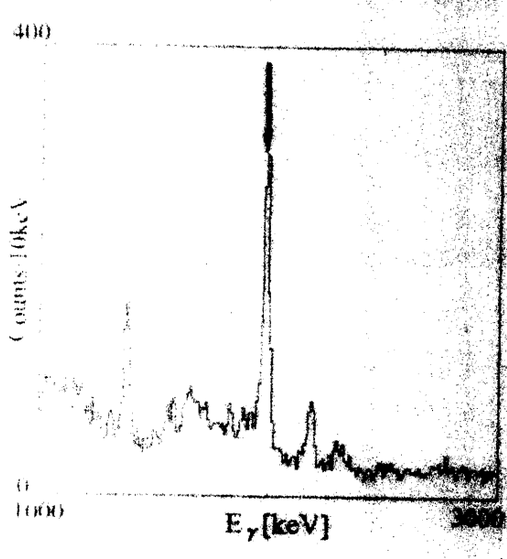

^{18}O beam (β = 0.4)
^{9}Be target (0.5 mm thick)

$2^+ \rightarrow 0^+$ 1982keV
δE = 25keV (1.3%, FWHM)
distance between the target and the SGT= 6.3cm
w/ anti-compton shield (NaI)
at $\theta \sim 90°$

Spectroscopy on Medium and Heavy Neutron-rich Nuclei at RIBF

RIPS -> RIBF

A<40 A<230

E~100 A MeV E~350 A MeV

Magicity Loss

N=8,20,28,50,82, ...?

New Magicity

N=16,34, ...?

In-beam gamma-spectroscopy at RIBF

At present facility

RI beams

A<~40

β ~ 0.3

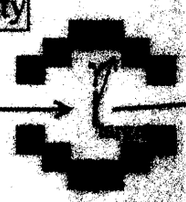

charged particle detectors

PID for ejectiles

gamma-ray detectors

At RIBF

higher segmentation e.g. DALI-II

RI beams

A~ 200

β ~ 0.6

Zero-degree forward spectrometer

To determine final channels

To achieve good S/N ratios

for low-intensity RI beams

⟶ Nice quality of data

Zero-degree Forward Spectrometer at RIKEN

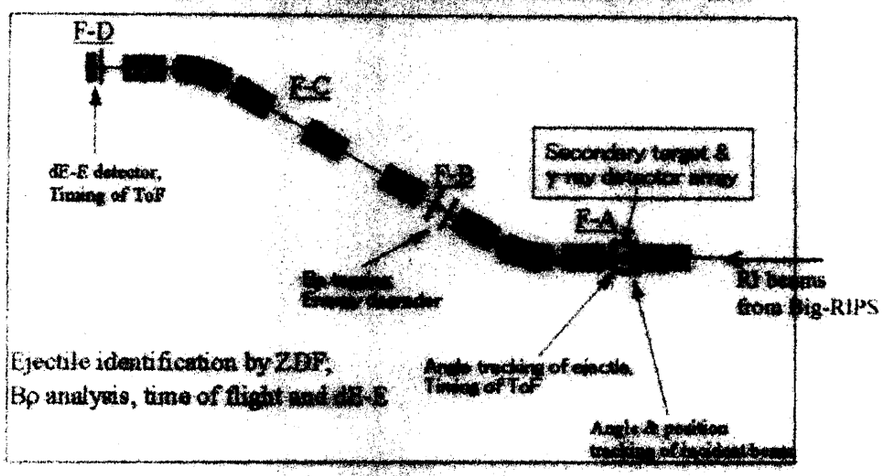

1. Achromatic large acceptance mode
2. Achromatic high resolution mode
   (x,p)/(x,x) ~ 2100
3. Dispersive spectrometer mode
   (x,p)/(x,x) ~ 4500

[illegible] ~36m
[illegible] dθ ~+/- 45mrad, dφ~+/- 30mrad
at 250A MeV neutron-rich RI beams
grazing angle ~ 20 mrad for Pb targets
momentum acceptance Δp/p ~+/- 3%
momentum resolution (x,p)/(x,x) ~ 1200
maximum magnetic rigidity 7.3 Tm
3 isotopes separation in A at A~200

A Flag-ship Region on the Nuclear Chart
- ^{78}Ni and vicinity -

^{78}Ni >0.1 particles/sec [illegible] 350A MeV ^{238}U >10pnA

challenges to observe exotic phenomena beyond N=50

β-spectroscopy	$T_{1/2}$, excited states, mass, ...
transmission	radii
in-beam γ spectroscopy	$E(2_1^+)$, $E(4_1^+)$, $B(E2)$, β_N, ...

Gamma-ray Spectroscopy in the Digital Era

A.J. Boston, University of Liverpool, Liverpool, UK

ajb@ns.ph.liv.ac.uk

Experimental nuclear physics research is underpinned by the development of state-of-the-art instrumentation based on semiconductor technology. Over the last 30 years nuclear structure research, utilising the technique of gamma-ray spectroscopy, has relied on the excellent energy resolution associated with high purity germanium detector technology in order to resolve the complex decay schemes associated with excited nuclei. Large arrays of escape suppressed germanium detectors, such as Euroball and Gammasphere, were built with the aim of probing nuclei at high spin and high excitation energy.

With the advent of radioactive ion-beam facilities such as SPIRAL, at GANIL France and ISAC II at TRIUMF Canada, the extremes of isospin will be probed for the first time. These new facilities deliver beams with intensities several orders of magnitude below that of existing stable beam facilities and therefore have presented a challenge for the experimentalist wishing to use these facilities.

A new generation of gamma-ray arrays offering a much higher efficiency, while maintaining the quality of the collected spectra are being assembled. These new arrays have required advances in detector fabrication techniques and utilise digital signal processing. The advent of digital gamma-ray spectroscopy allows not only the energy and time of an event to be derived but also provides the mechanism to identify the interaction position of the incident photon. Such work requires precise calibration of the detector response, in order to allow Pulse Shape Analysis (PSA) algorithms to be developed. This detector characterisation work will be presented in the context of existing detector arrays such as EXOGAM and future spectrometers such at the Advanced GAmma Tracking Array (AGATA).

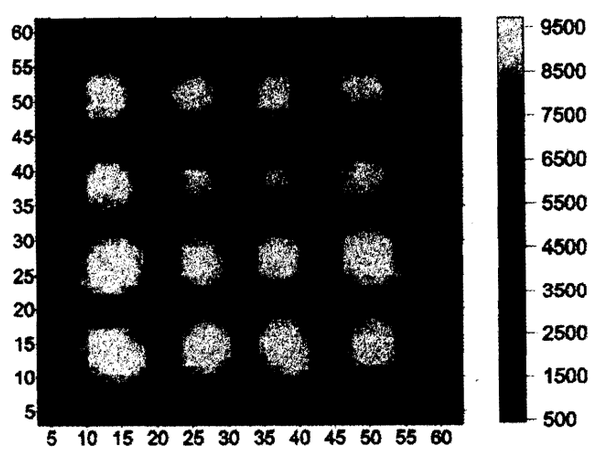

Figure 1: The characterised intensity map of an EXOGAM Clover detector

Gamma-ray spectroscopy in the Digital Era

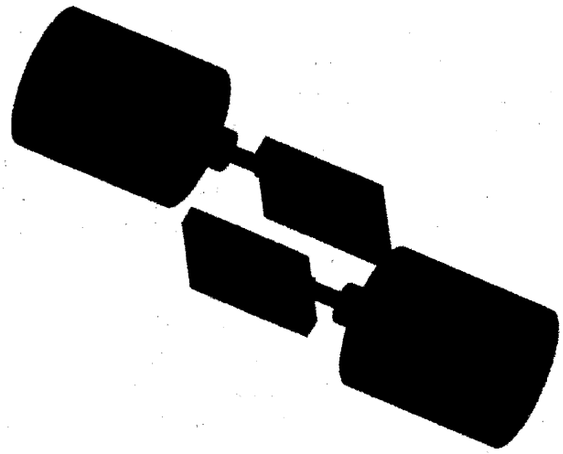

Dr Andy Boston
ajboston@liv.ac.uk

THE UNIVERSITY of LIVERPOOL

Frontiers of gamma-ray spectroscopy and its applications

Digital Gamma-ray Spectroscopy

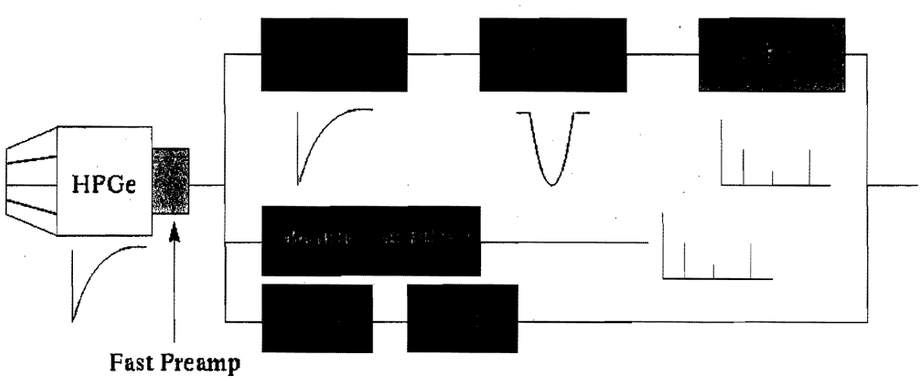

- Digital sampling of detector signal provides powerful alternative to conventional analogue electronics.
  - High rate capability
  - Improved gain stability
  - Ability to extract more than energy and time from signal.

Highly segmented Ge Detectors

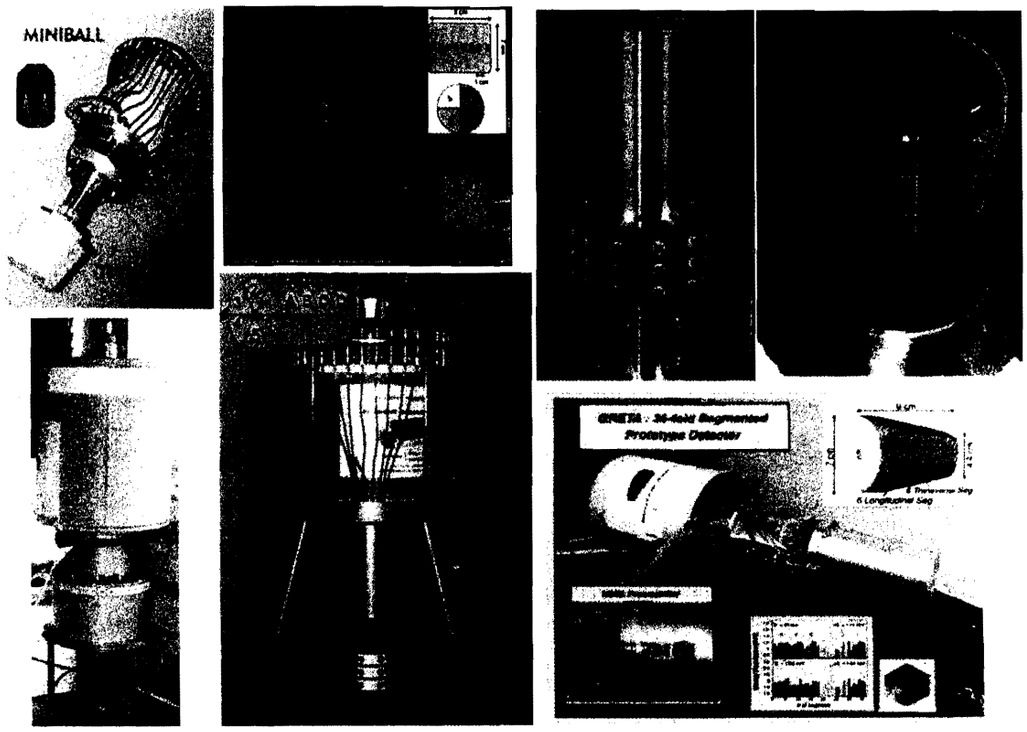

Frontiers of gamma-ray spectroscopy and its applications

Detector Characterisation

What is characterisation?

- Provides a full description of the detector response
- Calculation of reference pulse shapes
  - Calculation of E-fields
  - Simulation of interaction points
- Full characterisation of germanium crystals
  - Detailed source scans
- Define how to characterise detectors
  - Define reference points
- Standardise scanning set-ups

Automated Scanning Tables

Liverpool System

- Parker linear positioning table
- Pacific scientific stepper motors
- 0.3mCi ^{137}Cs/0.2mCi ^{57}Co
- 1-2mm collimator
- Singles/coincidence system

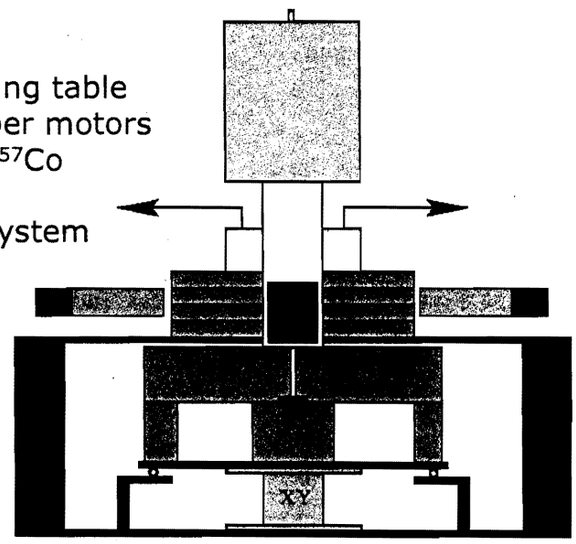

Precise position calibration

GSI / CSNSM Orsay

Frontiers of gamma-ray spectroscopy and its applications

Liverpool Detector Scanning System

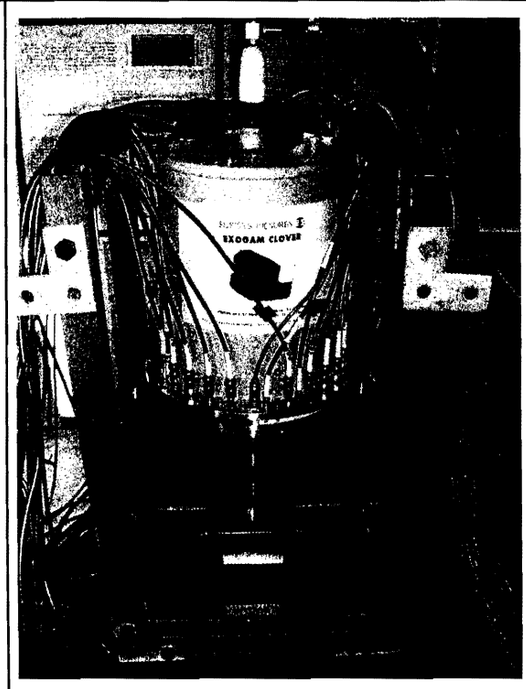

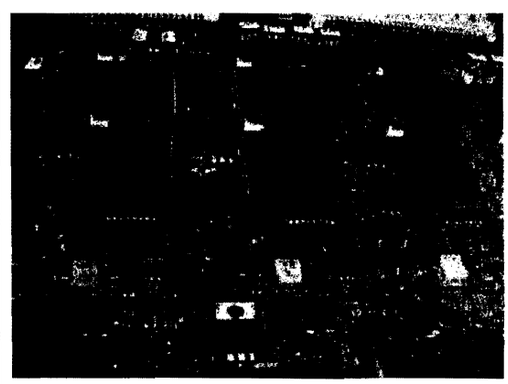

Data recorded using 14 bit 80Mhz digital electronics to disk.

Pulse shape analysis of detector response as a function of position.

Detector scan results

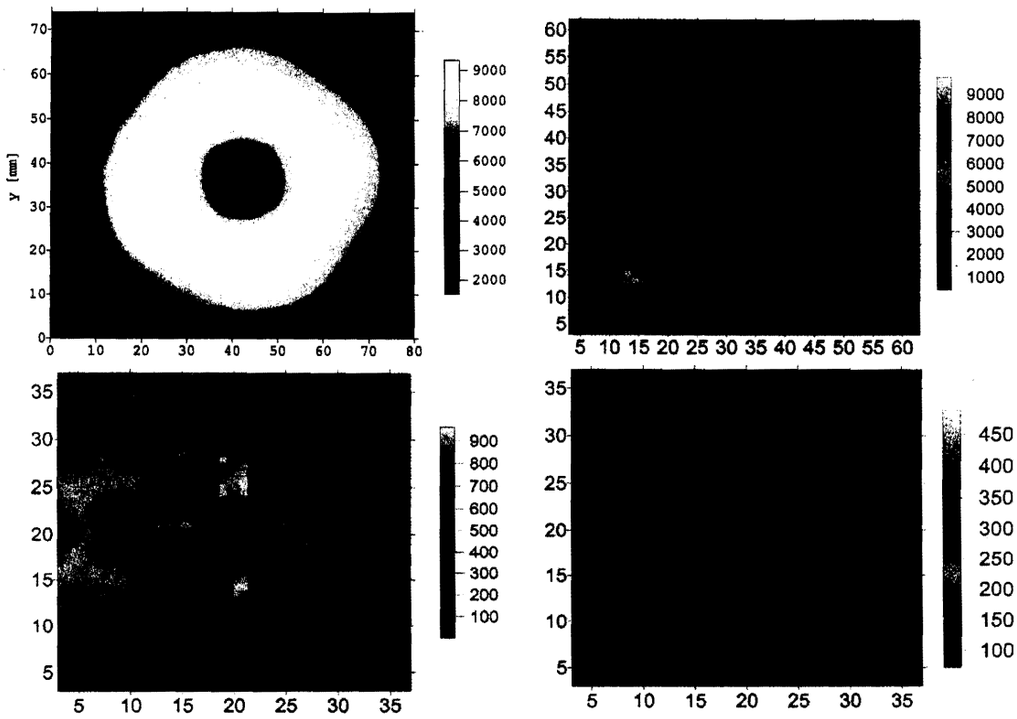

Frontiers of gamma-ray spectroscopy and its applications

Charge pulse response

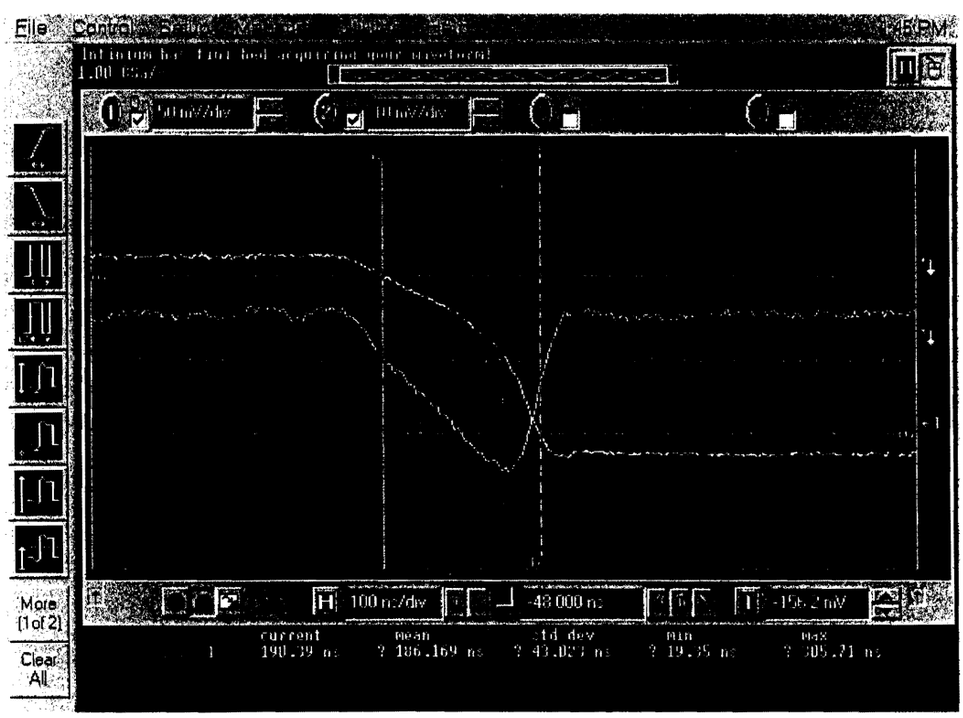

Analysis of the pulse shapes

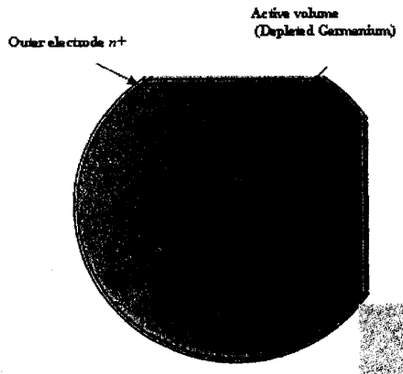

- T30, T60 T90 variation gives the position between anode and cathode:
  - **Radial position** of interaction in Coaxial (Clover)

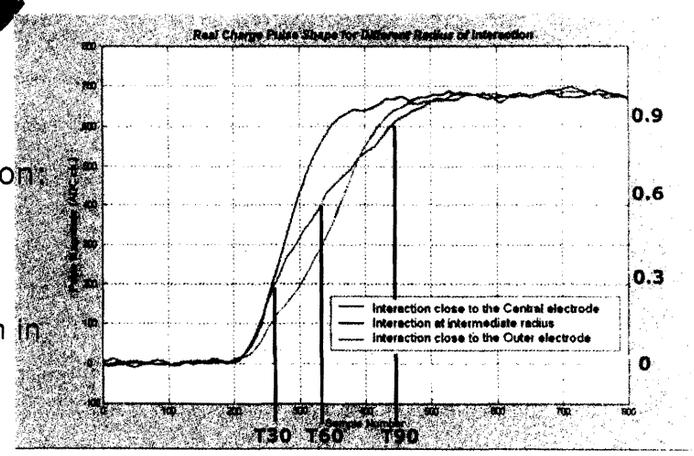

- Energy determination:
  - Moving Window Deconvolution
- Image charges:
  - Azimuthal position in Clover

Frontiers of gamma-ray spectroscopy and its applications

6x6 Risetime Analysis

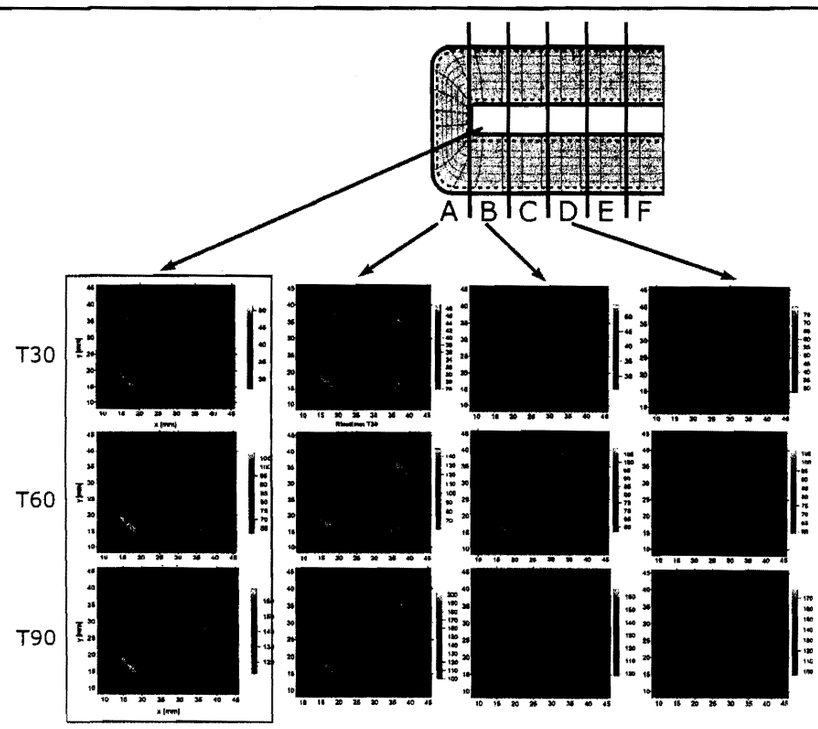

Risetime: Linear fits for radius

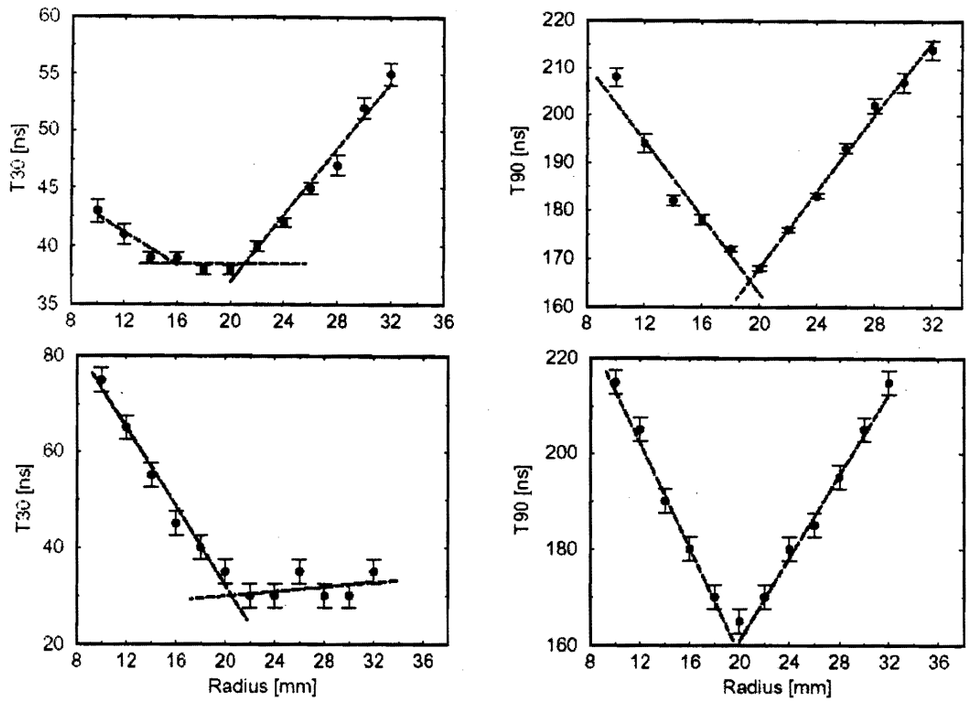

Frontiers of gamma-ray spectroscopy and its applications

Risetime vs Azimuthal position

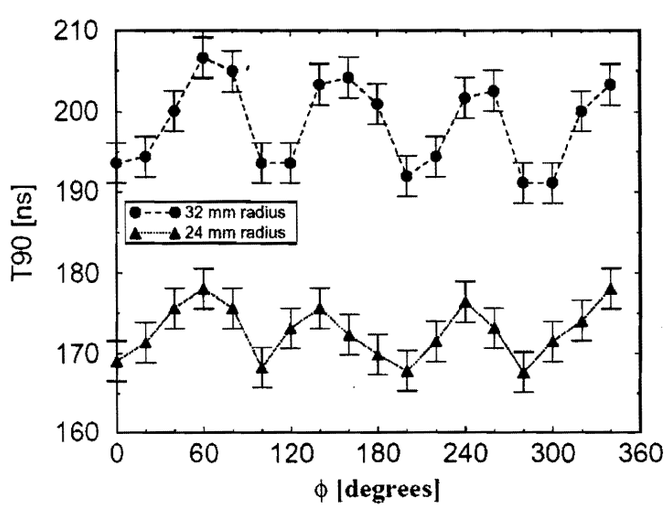

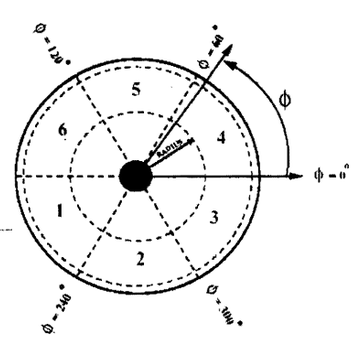

Mirror Charge Asymmetry Analysis

$$A = \frac{Q_l - Q_r}{Q_l + Q_r}$$

- Q_l and Q_r are magnitudes of mirror charge signal in the left and right neighbour.
- The asymmetry cancels out the radial contribution and yields information regarding the azimuthal position of the main interaction.

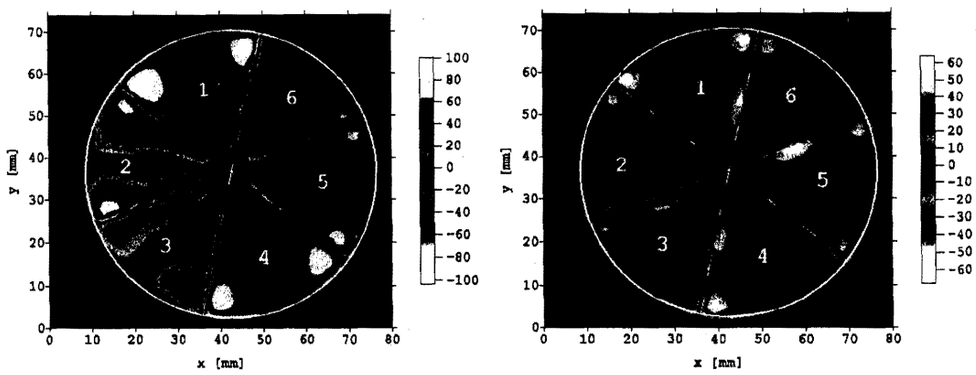

Frontiers of gamma-ray spectroscopy and its applications

Image charge asymmetry results

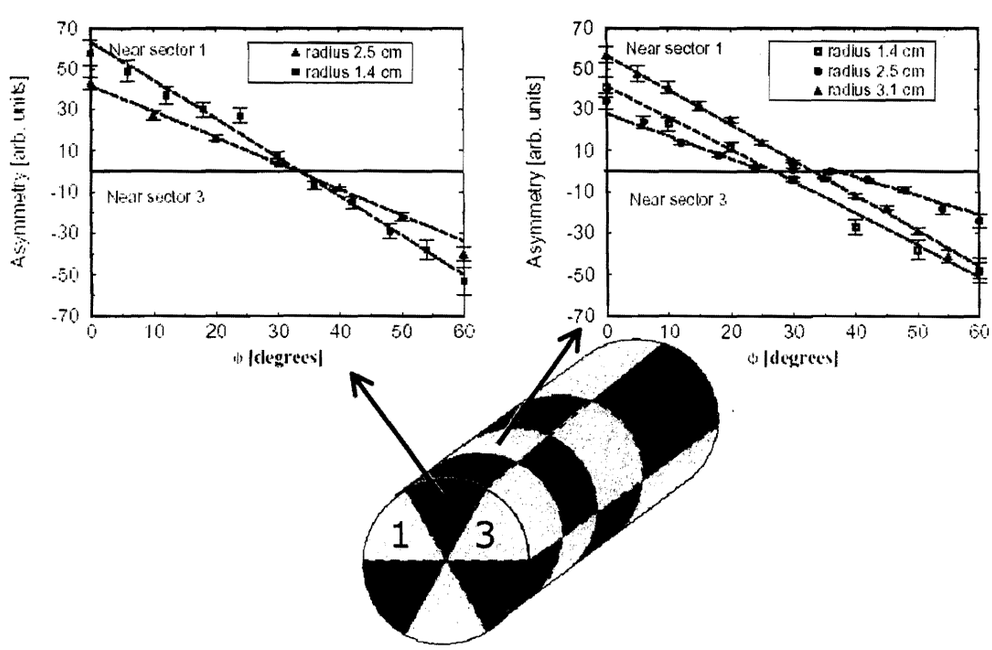

AGATA prototype triple cluster

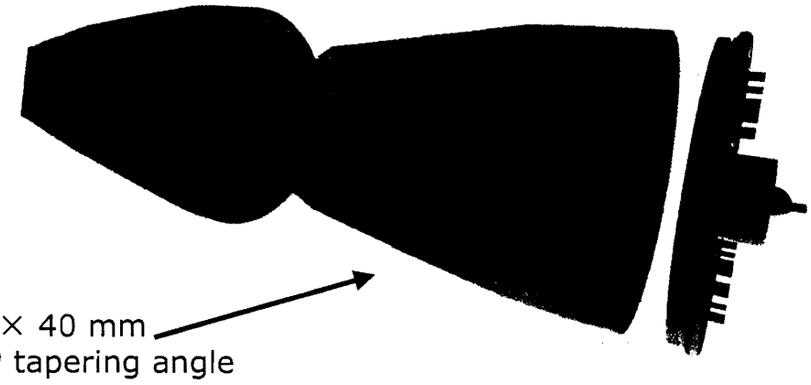

90 × 40 mm
10° tapering angle

- Prototype symmetric triple cluster
- Ordered from EM
- Requirement to define segmentation scheme of detector
- Database of calculated pulse shapes constructed for consideration.

Frontiers of gamma-ray spectroscopy and its applications

Calculation of pulse shapes

- Calculation of the signals induced on the contacts using the **weighting field method**

FEM-model of detector

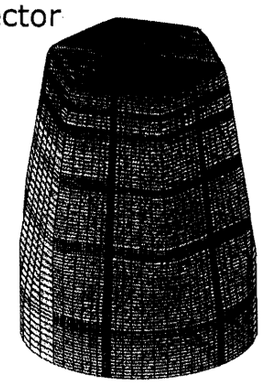

Calculate weighting fields →

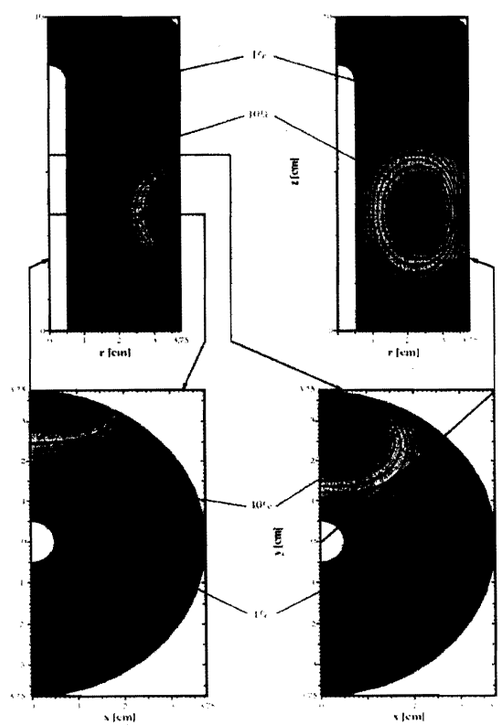

Calculation of pulse shapes

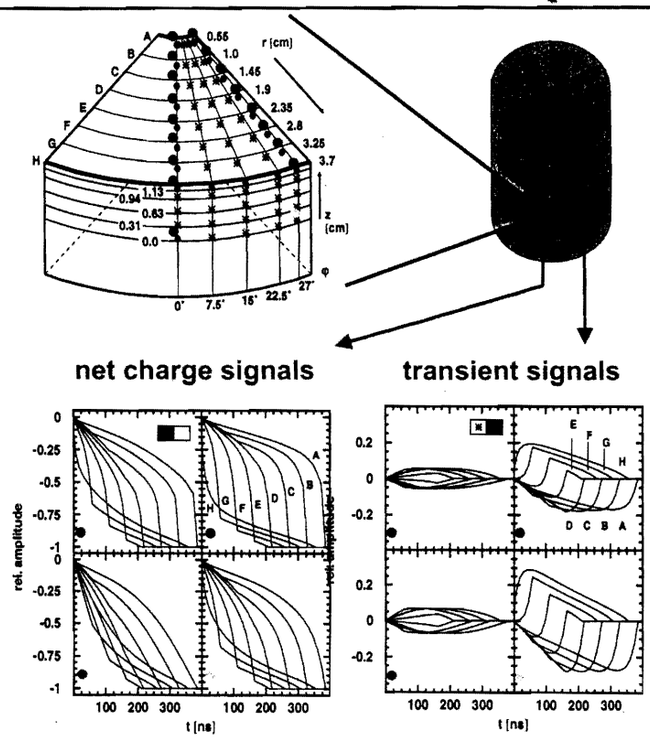

Frontiers of gamma-ray spectroscopy and its applications

Pulse shape database

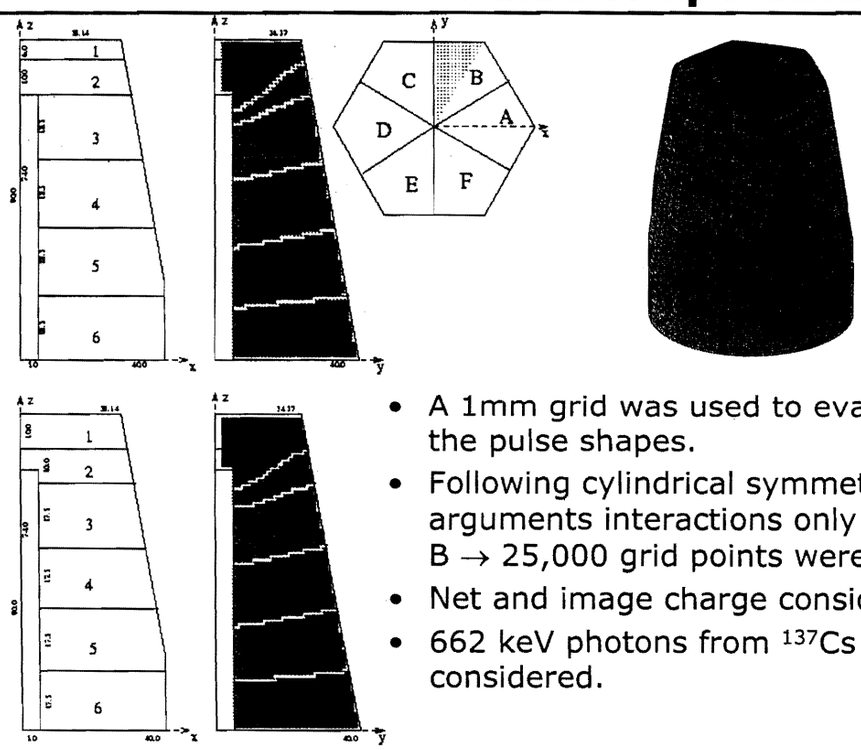

- A 1mm grid was used to evaluate the pulse shapes.
- Following cylindrical symmetry arguments interactions only in seg. B → 25,000 grid points were used.
- Net and image charge considered.
- 662 keV photons from ^{137}Cs considered.

Design of detector

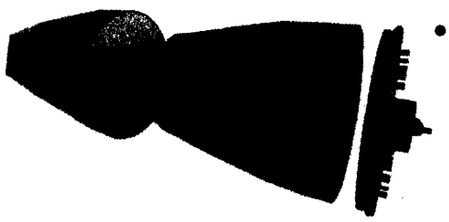

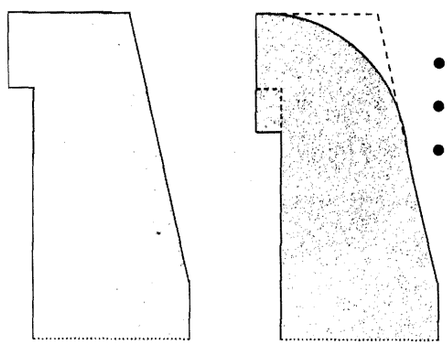

- Layout of segments:
  - Enhance amplitudes of transient signals
  - Counting rates per segment
  - Capacitance of segments
  - Equalise mean charge collection times
- Shape of front part of detector
- Length of inner hole
- We would prefer a more semi-spherical shape of the front part of the crystal!

(Liverpool/Milano/CSMSM Orsay)

Frontiers of gamma-ray spectroscopy and its applications

EXOGAM Detector Scans – Intensities

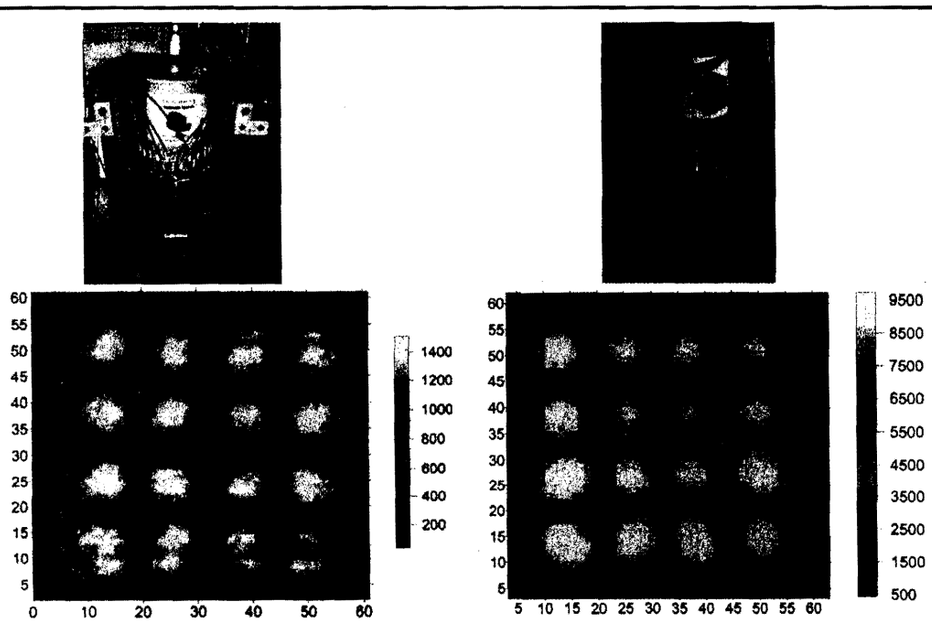

Different manufacturers have different manufacturing philosophies

Small Animal Imaging with Semiconductor Detectors

Dr Andy Boston
University of Liverpool
ajboston@liv.ac.uk

smartPET

THE UNIVERSITY of LIVERPOOL

Daresbury Laboratory CCLRC

Project funded by the Medical Research Council

smartPET : Prototype detector

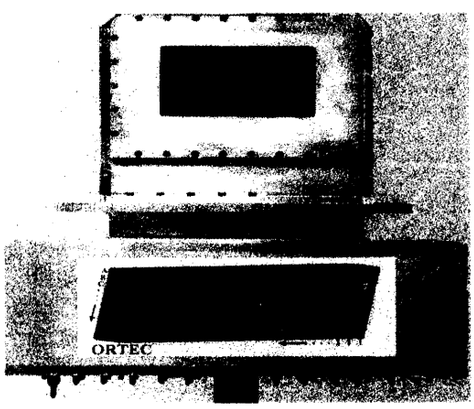

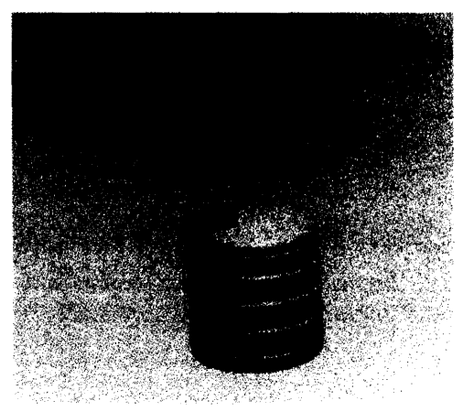

- The prototype detector for the imaging project was the GREAT planar detector
- On loan from the GREAT collaboration.
- The detector is a 24 x 12 germanium orthogonal strip detector.
- The crystal is fully depleted at +600V and operating voltage is +800 V.

The GREAT Planar Detector

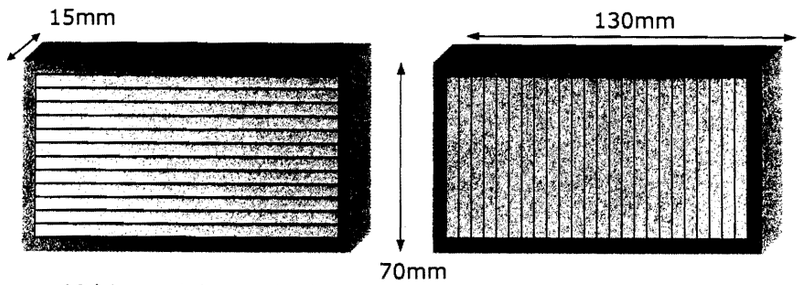

Lithium-strip contact
Anode

Boron-strip contact
Cathode

Anode configuration
Lithium diffusion: 0.7mm deep
12 horizontal strips
Strip width: 5mm
Inter strip distance: 0.7mm

Cathode configuration
Boron ion implanted: 0.3μm deep
24 vertical strips
Strip width: 5mm
Inter strip distance: ~0.1mm

Frontiers of gamma-ray spectroscopy and its applications

The GREAT Planar Detector – A Top View

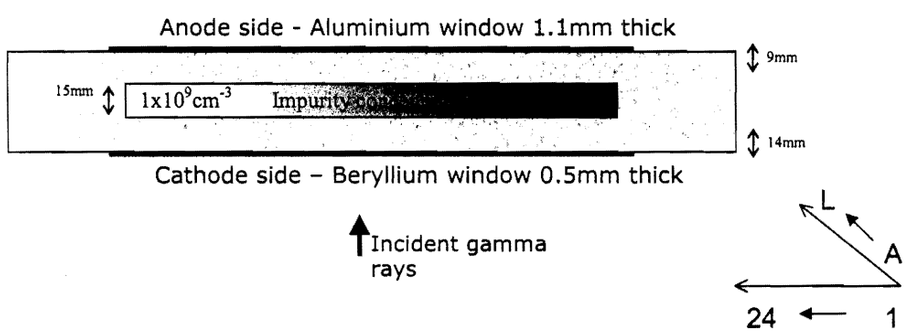

- The detector casing is aluminium
- 0.5mm beryllium window in front of the boron implanted side (cathode)
- 1.1mm aluminium window on the lithium diffused side (anode).

Scan Intensity Plots – Cathode strips 1-24

- Intensity/position
- Co-57 source
- 1mm steps
- 1mm collimator
- @ 5min/position
- Gated on 122keV

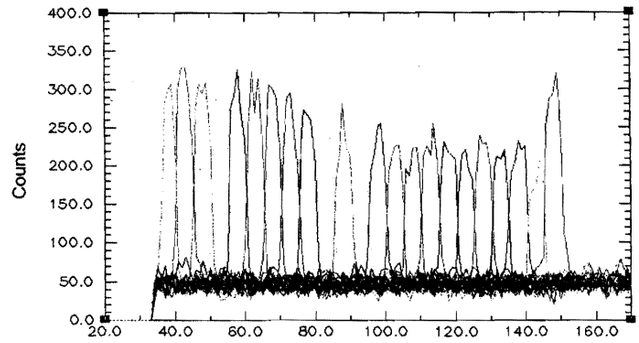

- Intensity/position 2d surface
- Co-57 source
- 2mm steps
- 2mm collimator
- @ 3min/position
- Gated on 122keV

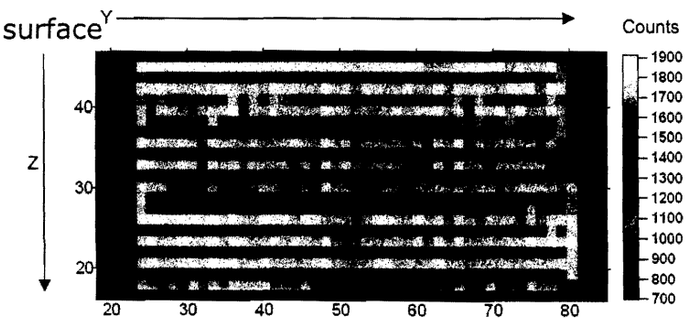

Frontiers of gamma-ray spectroscopy and its applications

Pulse Shape Analysis – Interaction Depth

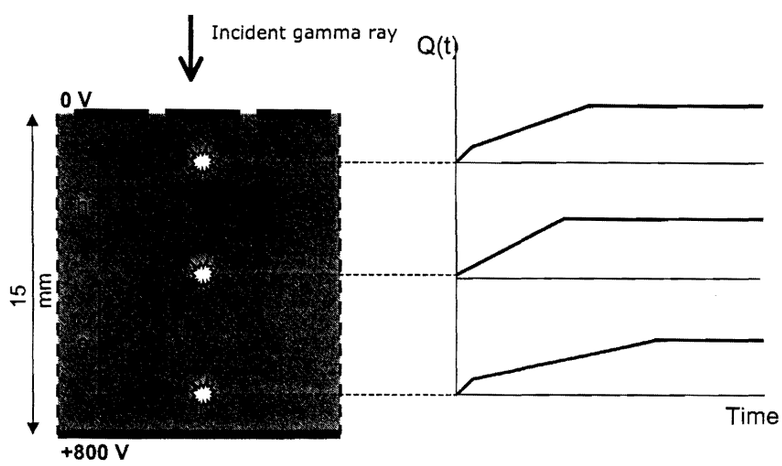

- The shape of the charge pulse is position dependent:
- Rise times at T30, T60 and T90 used to find interaction depth
- Time difference method – time to collect electrons vs. holes

smartPET : Image charges

Drift of charge carriers induces a signal on adjacent electrodes:

- Magnitude depends on the position of interaction relative to the electrode
- Image Charge Asymmetry parameter
- Vertical and horizontal position

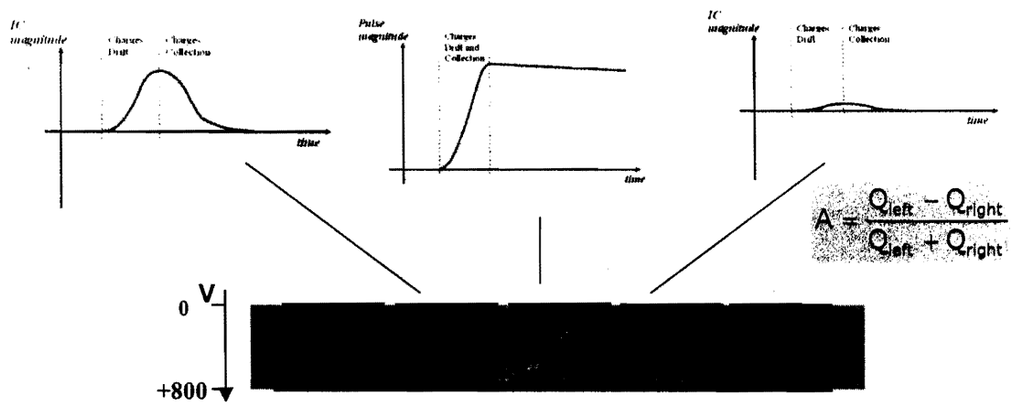

smartPET : Pulse Shape Response

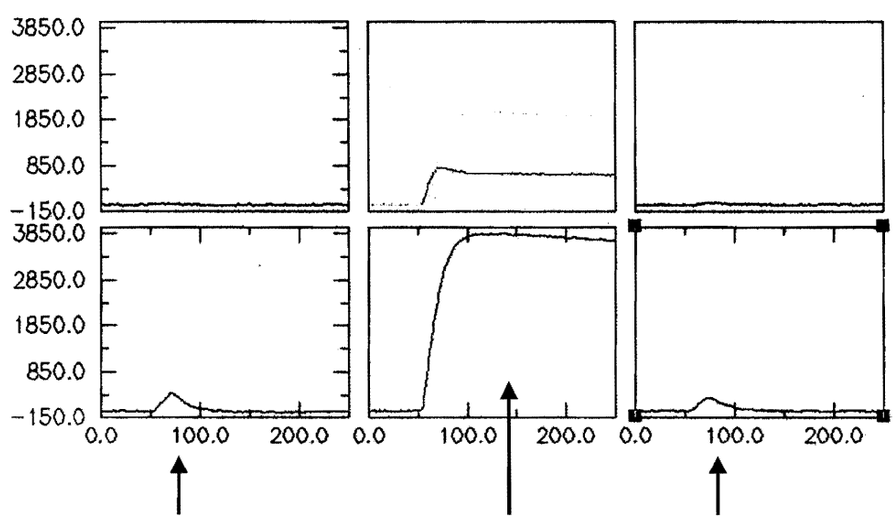

Transient charge Charge collection Transient charge

Compton Camera Characterisation

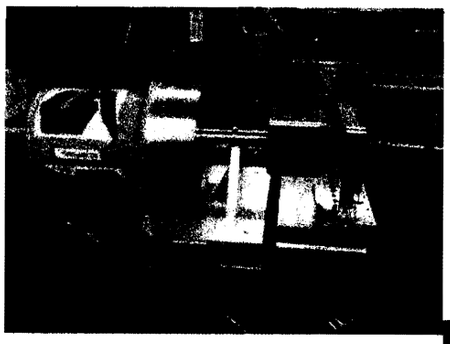

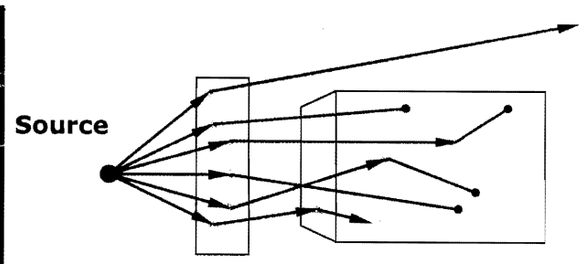

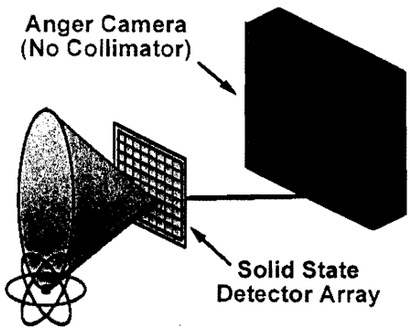

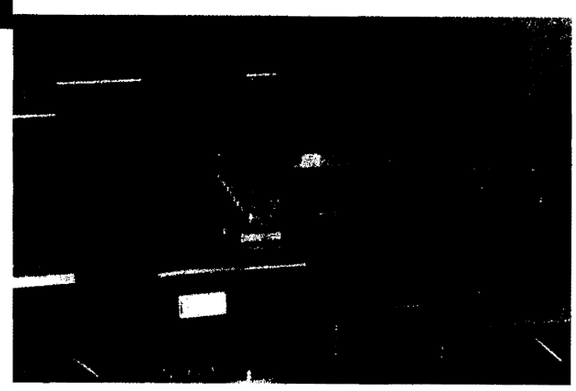

Frontiers of gamma-ray spectroscopy and its applications

Gamma-ray spectroscopy in the Digital Era

Frontiers of gamma-ray spectroscopy

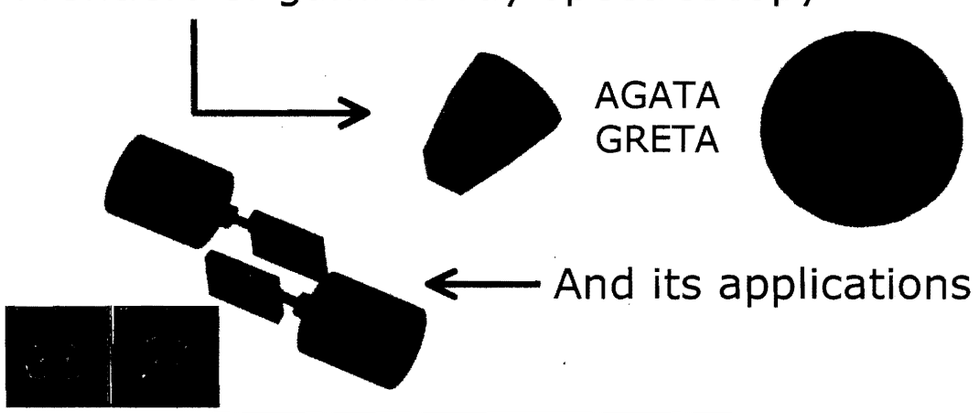

Dr Andy Boston
ajboston@liv.ac.uk

THE UNIVERSITY of LIVERPOOL

Perspectives of AGATA and lifetime measurements for dipole bands in the ^{142}Gd region with EUROBALL

R.M. Lieder
Institut für Kernphysik, Forschungszentrum Jülich, D-52425 Jülich, Germany

The investigation of new phenomena in atomic nuclei requires the study of their structure under extreme conditions at the boundary of stability, where the excitation energy, the spin or isospin take extreme values. The most powerful means for such studies is the high-precision γ-ray spectroscopy with highly efficient and highly granulated γ-detector arrays. The array should for a maximum coverage of the total solid angle consist only of Ge detectors. Such a detector system is the Advanced Gamma-Tracking Array AGATA, designed by a European collaboration. A new type of Ge detector has been developed for this array which allows to follow the tracks of the γ-rays in the Ge shell. These γ-ray tracking detectors consist of high-fold segmented Ge detectors and front-end electronics, based on digital signal processing techniques, which allows to extract energy, timing and spatial information for a γ-ray by pulse shape analysis of the Ge detector signals. Utilizing the information on the positions of the interaction points and the energies released at each point the tracks of the γ-rays in a Ge shell can be reconstructed in three dimensions on the basis of the Compton scattering formula. For AGATA a geometry consisting of 192 tracking detectors is considered. The total number of segments in the array is 6780 and, with the conservative assumption of a position resolution of 5 mm, the calculated photopeak efficiency is 40% and 25% at γ-ray multiplicities of 1 and 30, respectively. This gives a sensitivity of AGATA for high-spin spectroscopy which is about two orders of magnitude larger than that of present-day γ-detector arrays.

In the nuclei ^{141}Eu and ^{142}Gd, lying close to the magic nucleus ^{146}Gd, dipole bands have been found which are considered as magnetic rotational bands [1,2]. To prove this interpretation lifetimes have been measured with EUROBALL IV using DSAM to determine the $B(M1)$ and $B(E2)$ values. They were compared with $B(M1)$ and $B(E2)$ values calculated in the framework of the TAC model [3] and the semi-classical SPAC model [1] in which the shears mechanism is combined with principal axis cranking. To the dipole bands DB1 and DB3 in ^{142}Gd, $\nu h_{11/2}^{-2}\pi h_{11/2}^{2}$ and $\nu h_{11/2}^{-2}\pi h_{11/2}^{1}g_{7/2}^{-1}$ configurations have been assigned. The dipole bands DB2 and DB4 may originate from those due to the breakup of a second $h_{11/2}$ neutron-hole pair. The dipole bands DB1 and DB2 in ^{141}Eu have similar features as the dipole bands DB1 and DB2 in ^{142}Gd and their configurations may result from the subtraction of an $h_{11/2}$ proton. Calculations in the framework of the TAC model have been carried out considering these configurations and deformations ranging from $\varepsilon_2 = -0.05$ to -0.15. The SPAC model calculations have been carried out for an "inverse" initial alignment in which the angular momentum vectors of the involved particles and holes $\vec{j}_1$ and $\vec{j}_2$ are initially oriented in such a way that the angles with respect to the rotation axis are $\theta_1 = 90°$ and $\theta_2 = 180°$, respectively. The angle θ_2 decreases much more rapidly with increasing spin than θ_1 so that a crossing occurs at a certain spin value with the result that then the $B(M1)$ values become small. Such small values have been found for the $17^+ \rightarrow 16^+$ transition in DB1 and the $12^- \rightarrow 11^-$ transition in DB3 of ^{142}Gd. The dipole bands in ^{141}Eu and ^{142}Gd can generally quite well be described in the framework of the TAC and SPAC models, indicating that they can indeed be considered as magnetic rotational bands.

This work was partly supported by the IB of BMBF at DLR, Germany under the WTZ contract RUS 99/191 and by the EU under the contracts no. ERBFMRXCT970123 and HPRI-CT-1999-00078EU.

[1] E. Podsvirova et al., Eur. Phys. J. A, to be published
[2] R.M. Lieder et al., Eur. Phys. J. A13 (2002) 297
[3] S. Frauendorf, Rev. Mod. Phys. 73 (2001) 463

GAMMA 04

CNS-RIKEN Joint Symposium

Frontier of Gamma-Ray Spectroscopy in Nuclear Structure Research

RIKEN, March 2-4, 2004

Lifetime measurements for [illegible] with EUROBALL

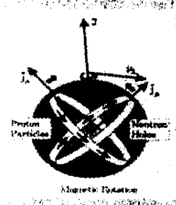

Outline

1. Features of magnetic rotational bands
2. Observation of dipole bands [illegible] arrays interpretation as magnetic rotation
3. DSAM experiment to determine [illegible] lifetime the dipole bands in ^{141}Eu and [illegible]
4. Interpretation of the dipole bands in [illegible] tracking arrays in the framework of the TAC and SPAC [illegible]
5. Conclusions

RIKEN

GAMMA 04

GAMMA 04

Magnetic rotational and Shear [illegible]

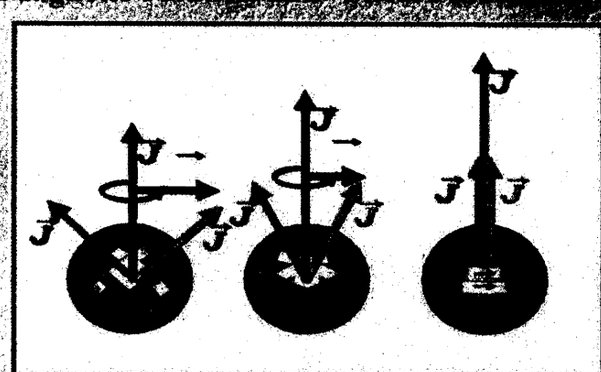

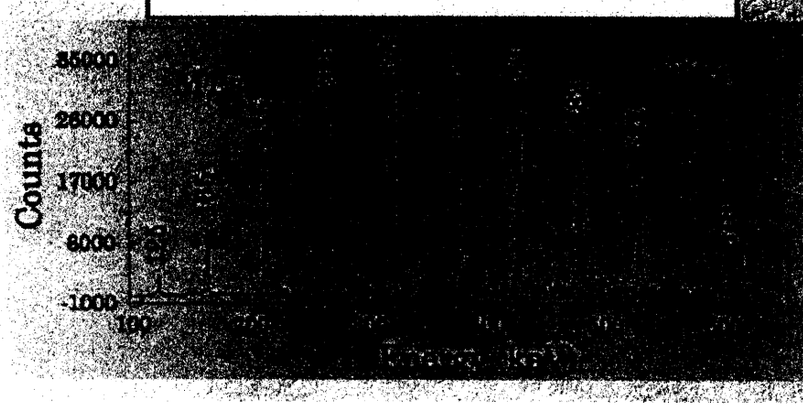

RIKEN

GAMMA 04

Dipole bands in ^{167}Lu and ^{197}Pb

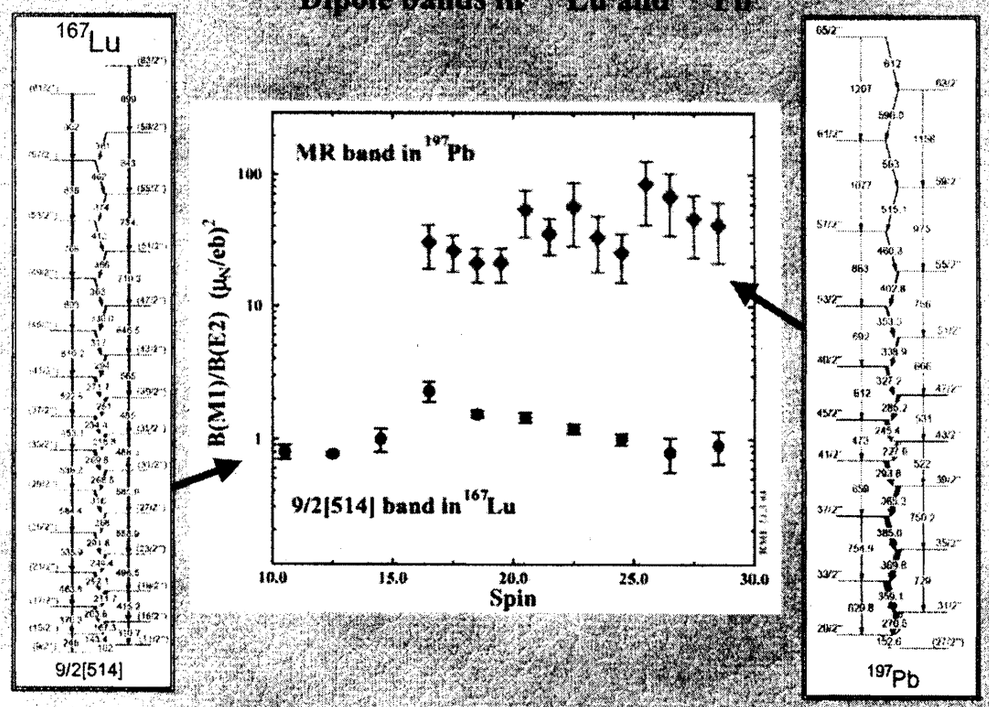

Level scheme of ^{142}Gd

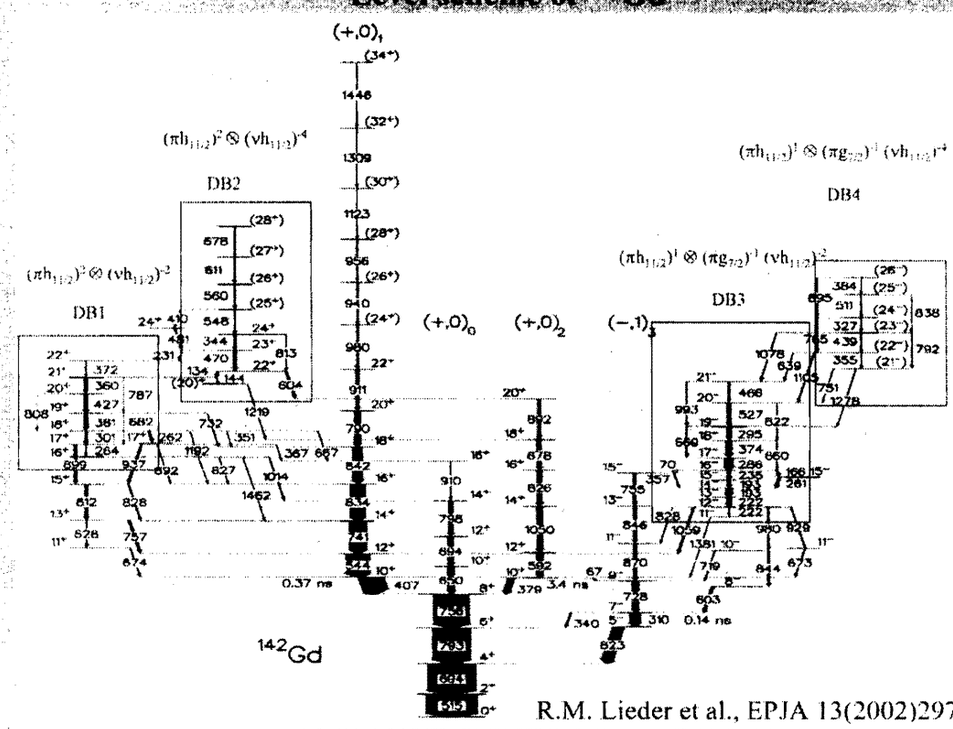

R.M. Lieder et al., EPJA 13(2002)297

Level scheme of ^{141}Eu

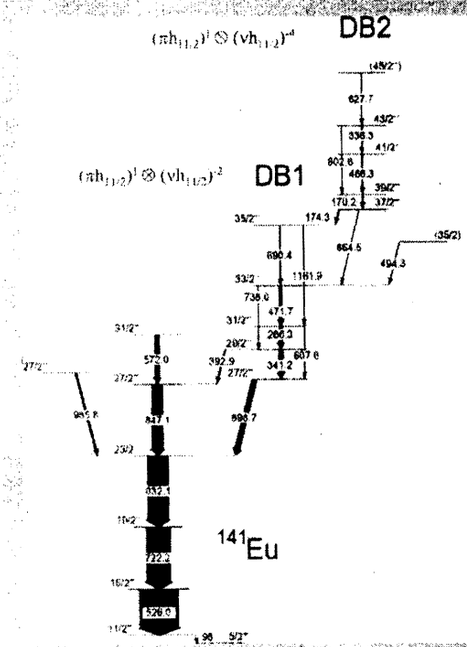

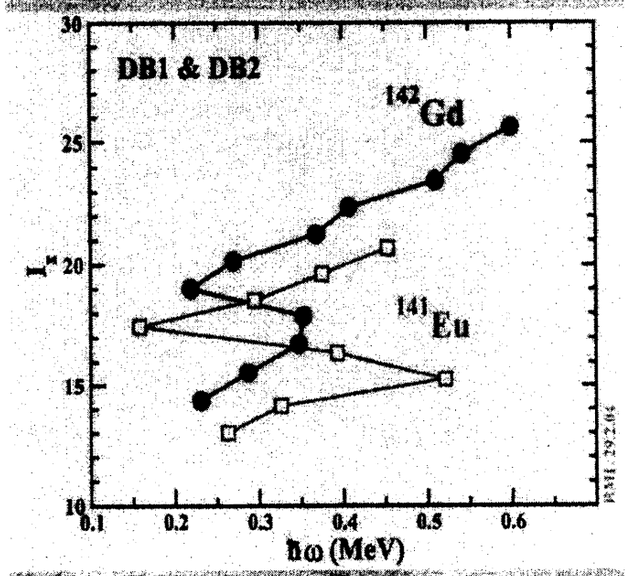

Lifetime measurements for ^{141}Eu and ^{142}Gd with EUROBALL IV using DSAM

Reaction: ^{114}Sn(^{32}S,γpxn)

Beam Energy: 160 MeV

Target: 8 mg/cm^2

Initial recoil velocity: v/c = 2.2%

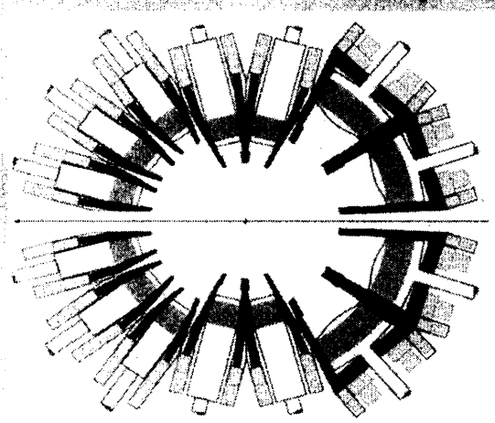

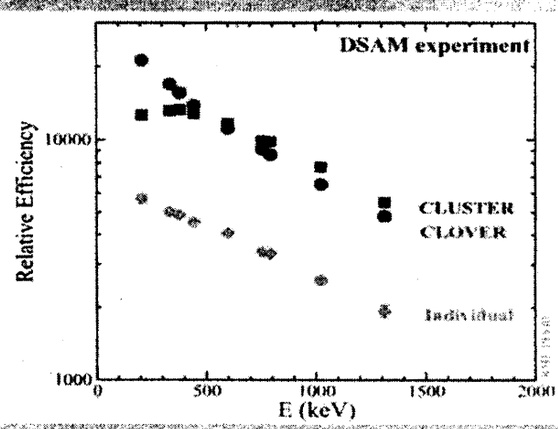

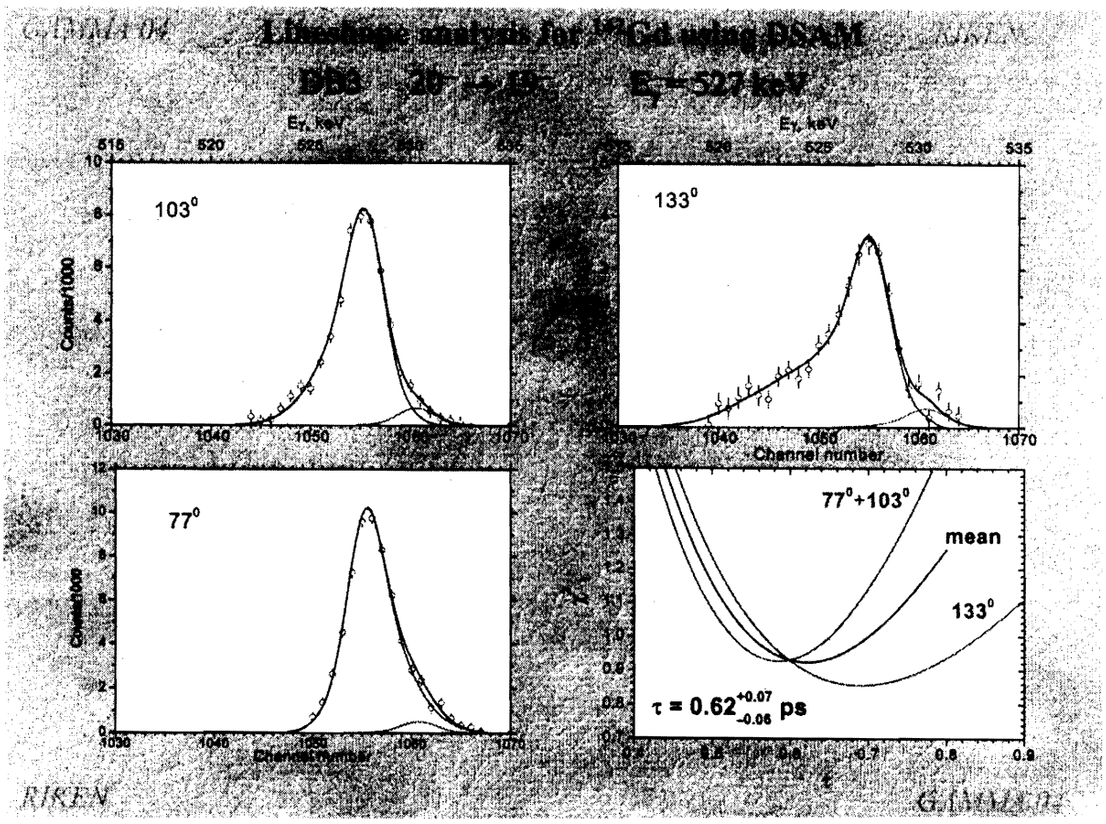
Lineshape analysis for ^{142}Gd using DSAM
DB3 20⁻ → 18⁻ E_γ = 527 keV
103°
133°
77°
77°+103°
mean
133°
$\tau = 0.62^{+0.07}_{-0.06}$ ps
Channel number
Counts/1000
RIKEN

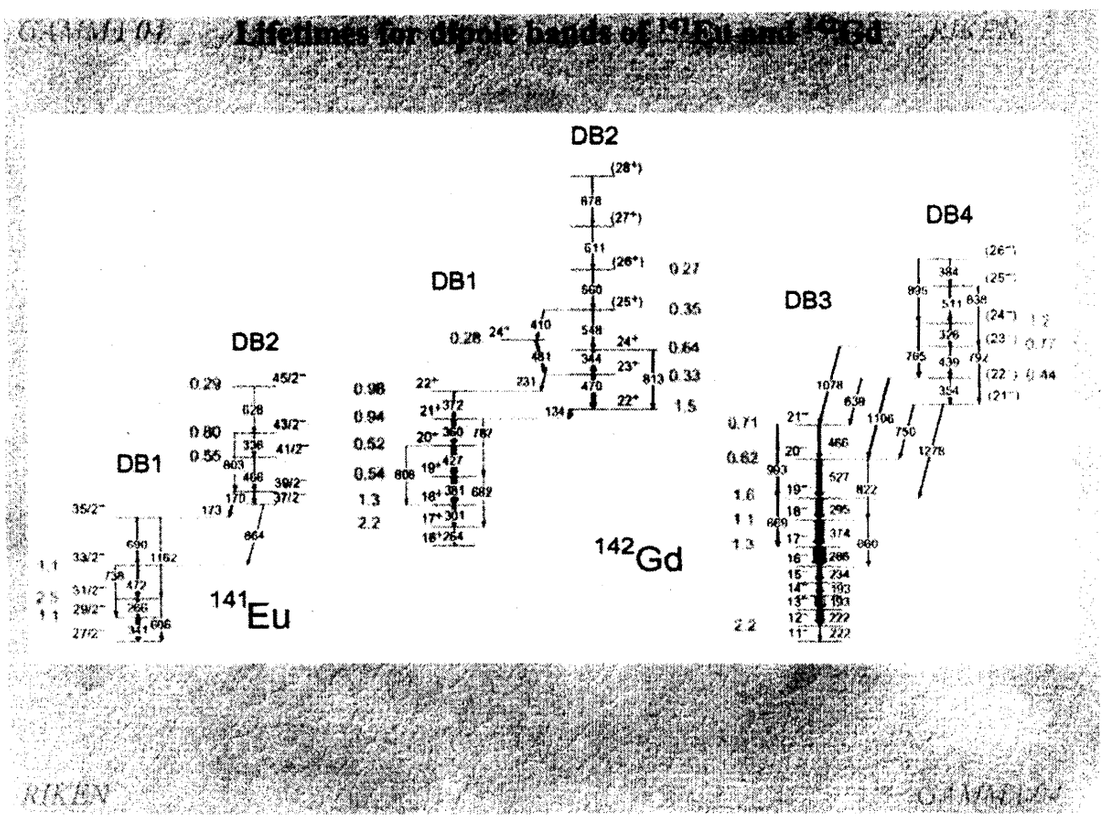
Lifetimes for dipole bands of ^{141}Eu and ^{142}Gd
DB1
DB2
DB3
DB4
^{141}Eu
^{142}Gd
RIKEN

Shears mechanism with PAC (SPAC)

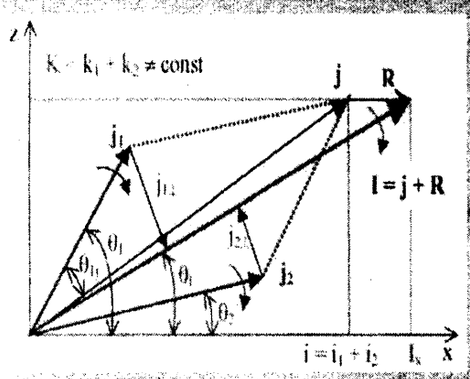

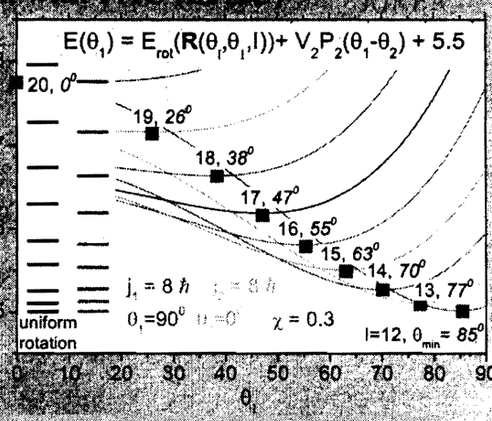

$$E(I,\theta_1,\theta_2) = \frac{1}{2J(I)}R^2(I,\theta_1,\theta_2) + V_2\,\frac{3\cos^2(\theta_2-\theta_1)-1}{2} + \text{const}$$

$$\mathbf{R} = \mathbf{I}-\mathbf{j};\ R(I,\theta_1,\theta_2) = \sqrt{I^2-(j_1\sin\theta_1+j_2\sin\theta_2)^2} - j_1\cos\theta_1 - j_2\cos\theta_2$$

$$B(M1;\ I\to I-1) = \frac{3}{8\pi}\mu_\perp^2;\ \mu_\perp = \mu_{1\perp}+\mu_{2\perp} = g_1^*\,j_1\cos(\theta_1-\theta_I) - g_2^*\,j_2\sin(\theta_I-\theta_2)$$

$$g_1^* = g_1 - g_R;\ g_2^* = g_2 - g_R;\ g_R = \frac{Z}{A}$$

$$B(E2;\ I\to I-2) = \frac{15}{128\pi}\left[(eQ)_{eff}\sin^2\theta_{12} + Q_{coll}\cos^2\theta_I\right]^2$$

"Normal" and "inverse" initial orientations in SPAC

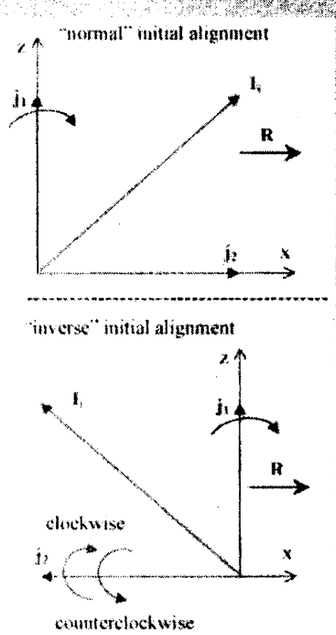

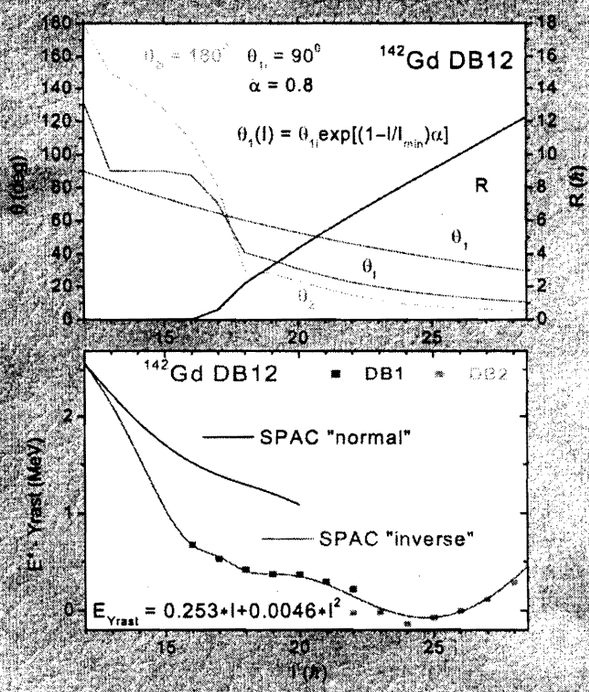

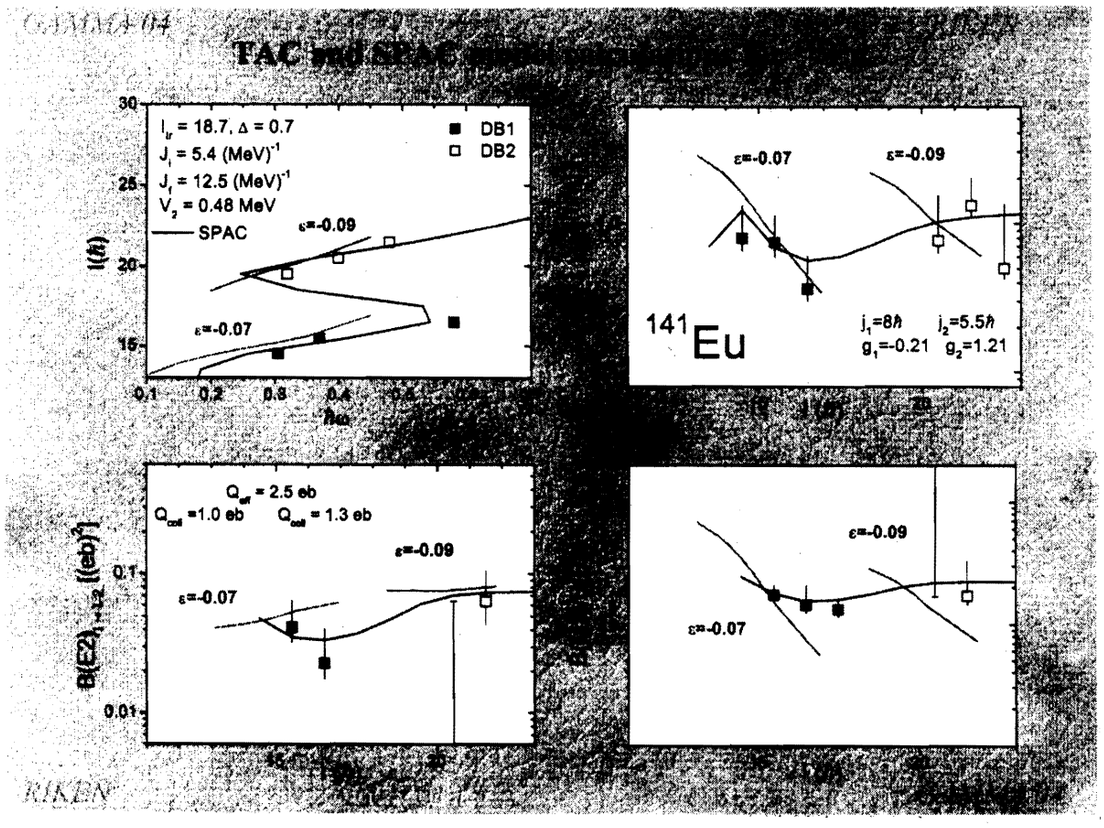
GAMMA-04
TAC and SPAC
I_{tr} = 18.7, Δ = 0.7
J_l = 5.4 (MeV)$^{-1}$
J_t = 12.5 (MeV)$^{-1}$
V_2 = 0.48 MeV
SPAC
DB1
DB2
ε=-0.09
ε=-0.07
I(ħ)
ħω
^{141}Eu
j_1=8ħ j_2=5.5ħ
g_1=-0.21 g_2=1.21
Q_{eff} = 2.5 eb
Q_{coll} =1.0 eb Q_{coll} = 1.3 eb
B(E2)$_{I\to I-2}$ [(eb)^2]
RIKEN

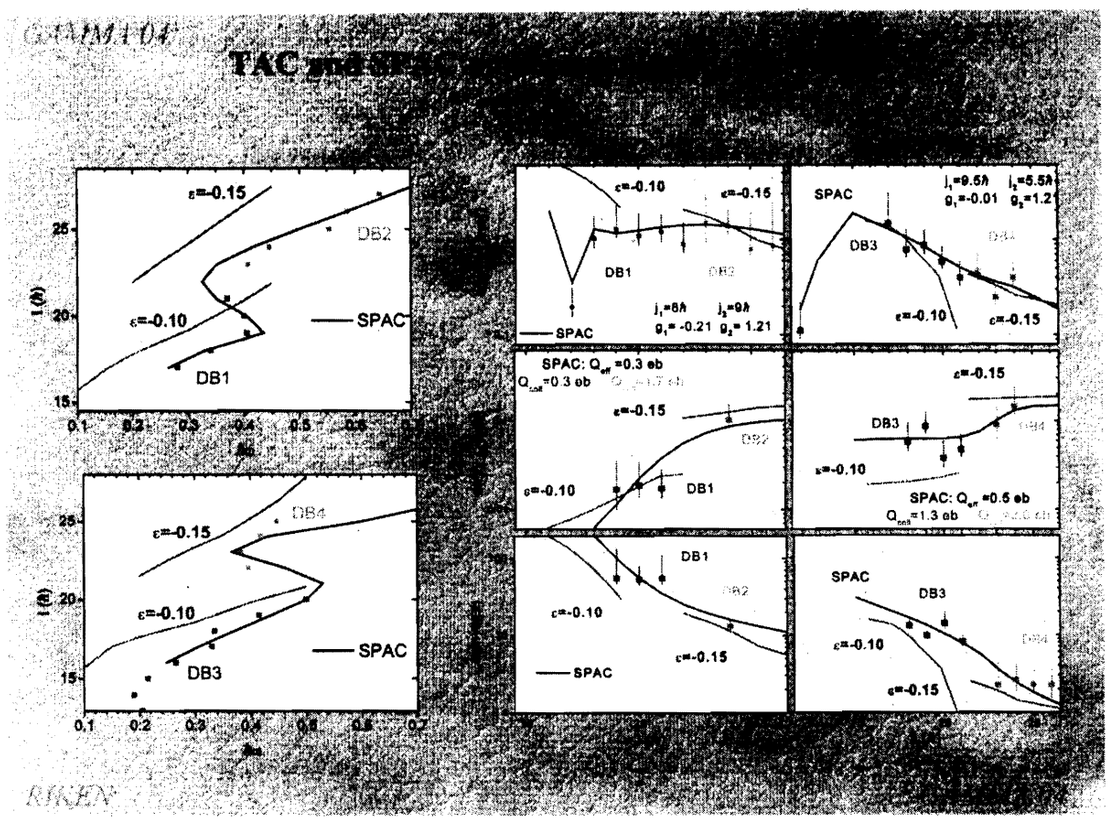
GAMMA-04
TAC and SPAC
ε=-0.15
ε=-0.10
DB1
DB2
DB3
DB4
SPAC
I(ħ)
ħω
j_1=6ħ j_2=9ħ
g_1= -0.21 g_2= 1.21
j_1=9.5ħ j_2=5.5ħ
g_1=-0.01 g_2=1.21
SPAC: Q_{eff} =0.3 eb
Q_{coll}=0.3 eb
SPAC: Q_{eff} =0.6 eb
Q_{coll}=1.3 eb
RIKEN

List of collaborators

E. Podsvirova[1], A. Pasternak[1], R.M. Lieder, W. Gast, H.M. Jäger, L. Mihailescu

Institut für Kernphysik, FZ Jülich, Germany

[1] *A.F. Ioffe Physical Technical Institute, St. Petersburg, Russia*

S. Chmel

Institut für Strahlen- und Kernphysik, University of Bonn, Germany

A. Dewald

Institut für Kernphysik, University of Cologne, Germany

D. Bazzacco, E. Farnea, S. Lunardi, R. Menegazzo, C. Rossi Alvarez

Dipartimento di Fisica dell'Università and INFN, Sezione di Padova, Italy

G. de Angelis, D.R. Napoli, A. Gadea

INFN, Laboratori Nazionali di Legnaro, Italy

Ts. Venkova

Institute of Nuclear Research and Nuclear Energy, Bulgarian Academy of Sciences, BG-1784 Sofia, Bulgaria

W. Urban, T. Rzaça-Urban, T. Morek

Institute of Experimental Physics, University of Warsaw, Poland

G. Duchêne

Institut de Recherches Subatomique IReS, Strasbourg, France

R. Wyss

Royal Institute of Technology, Physics Department Frescati, S-10405 Stockholm, Sweden

Large γ-rays arrays

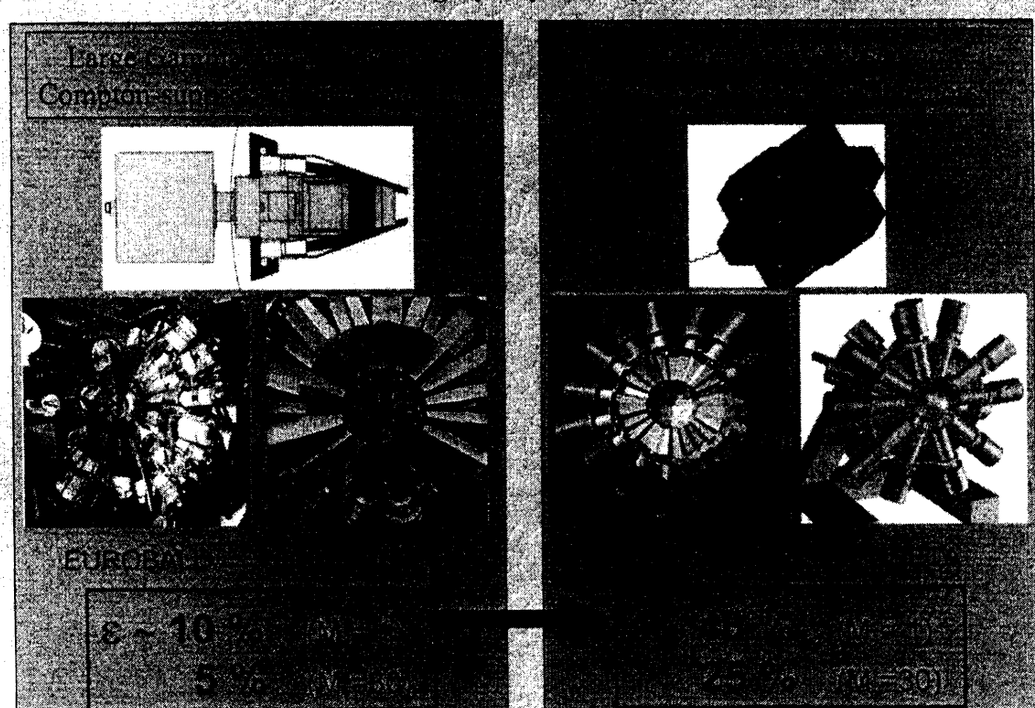

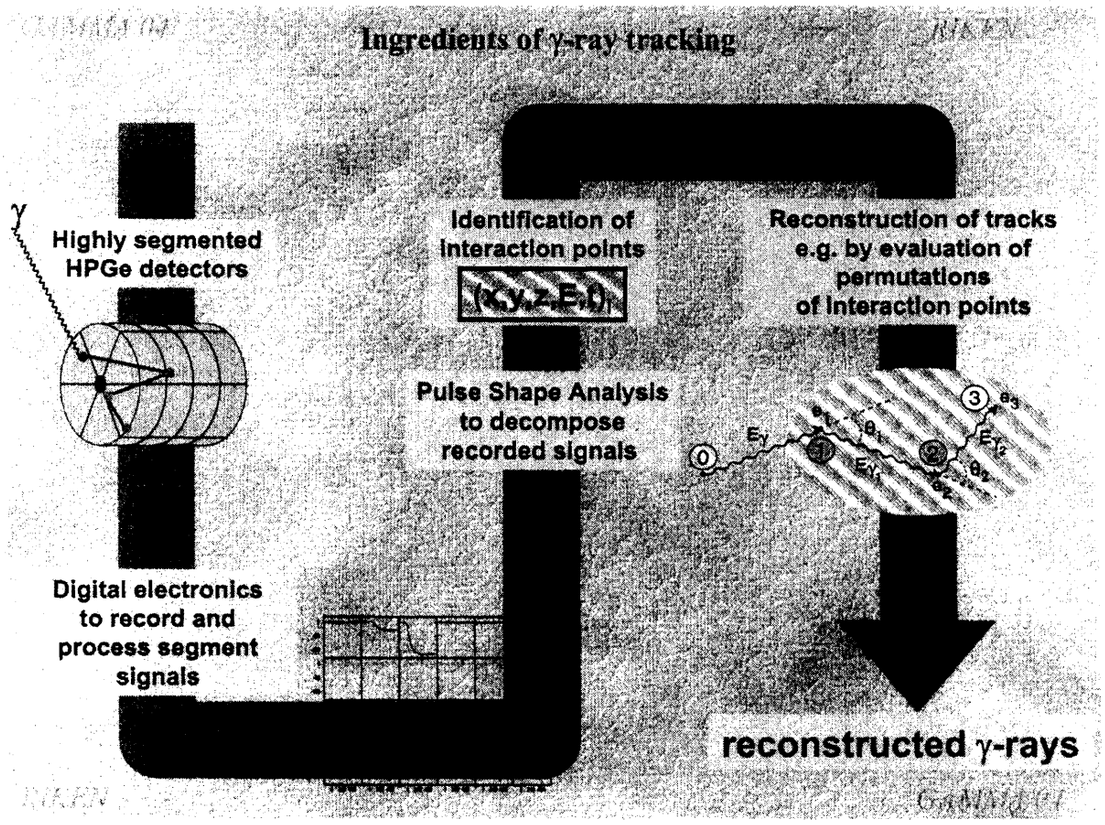
Ingredients of γ-ray tracking
γ
Highly segmented HPGe detectors
Identification of interaction points
(x,y,z,E,t)i
Reconstruction of tracks e.g. by evaluation of permutations of interaction points
Pulse Shape Analysis to decompose recorded signals
Digital electronics to record and process segment signals
reconstructed γ-rays

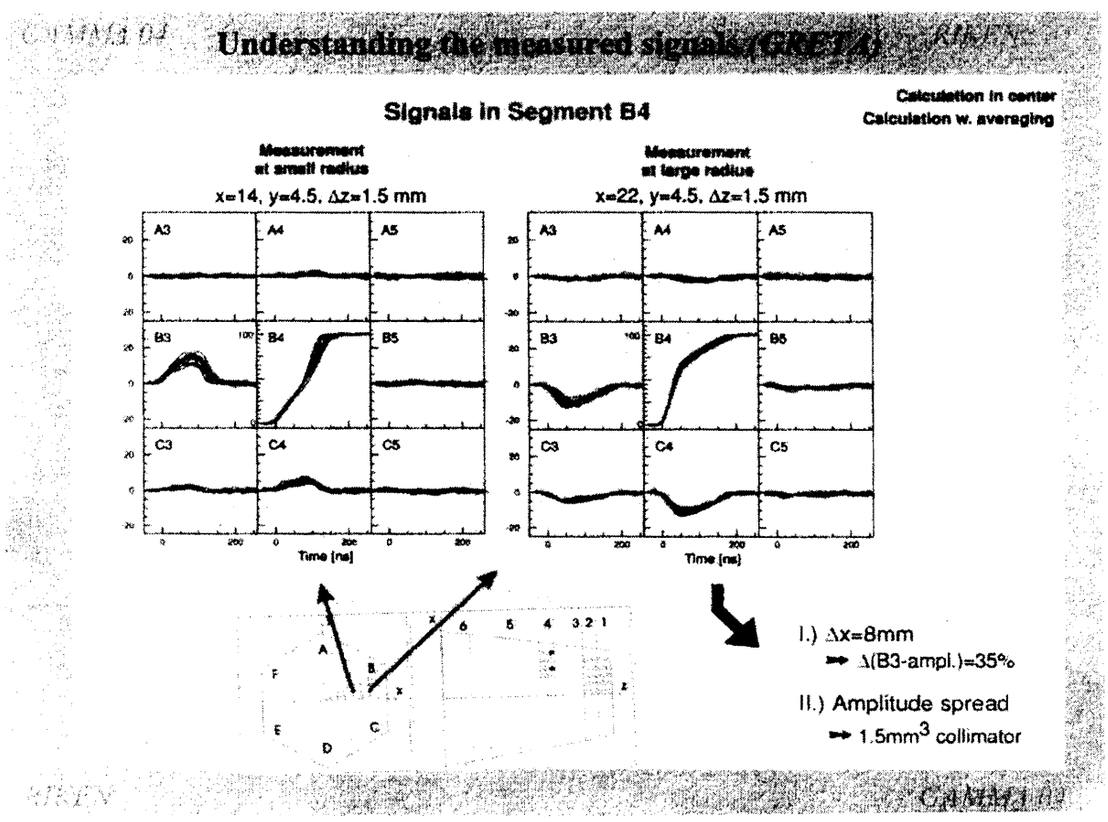
Understanding the measured signals (GRETA)
Signals in Segment B4
Calculation in center
Calculation w. averaging
Measurement at small radius
x=14, y=4.5, Δz=1.5 mm
Measurement at large radius
x=22, y=4.5, Δz=1.5 mm
A3
A4
A5
B3
B4
B5
C3
C4
C5
Time [ns]
I.) Δx=8mm
➡ Δ(B3-ampl.)=35%
II.) Amplitude spread
➡ 1.5mm³ collimator

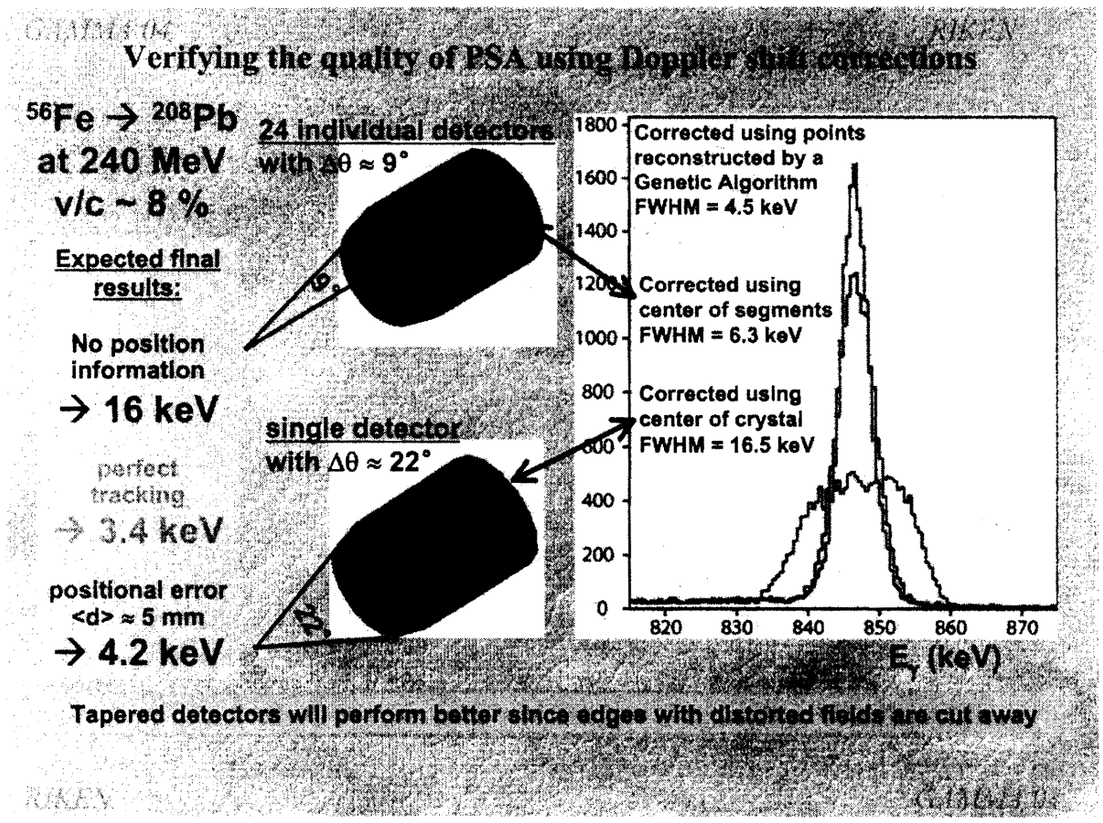
Verifying the quality of PSA using Doppler shift corrections
$^{56}Fe \rightarrow {}^{208}Pb$
at 240 MeV
v/c ~ 8 %
Expected final results:
No position information
→ 16 keV
perfect tracking
→ 3.4 keV
positional error
<d> ≈ 5 mm
→ 4.2 keV
24 individual detectors with Δθ ≈ 9°
single detector with Δθ ≈ 22°
Corrected using points reconstructed by a Genetic Algorithm
FWHM = 4.5 keV
Corrected using center of segments
FWHM = 6.3 keV
Corrected using center of crystal
FWHM = 16.5 keV
E_γ (keV)
Tapered detectors will perform better since edges with distorted fields are cut away

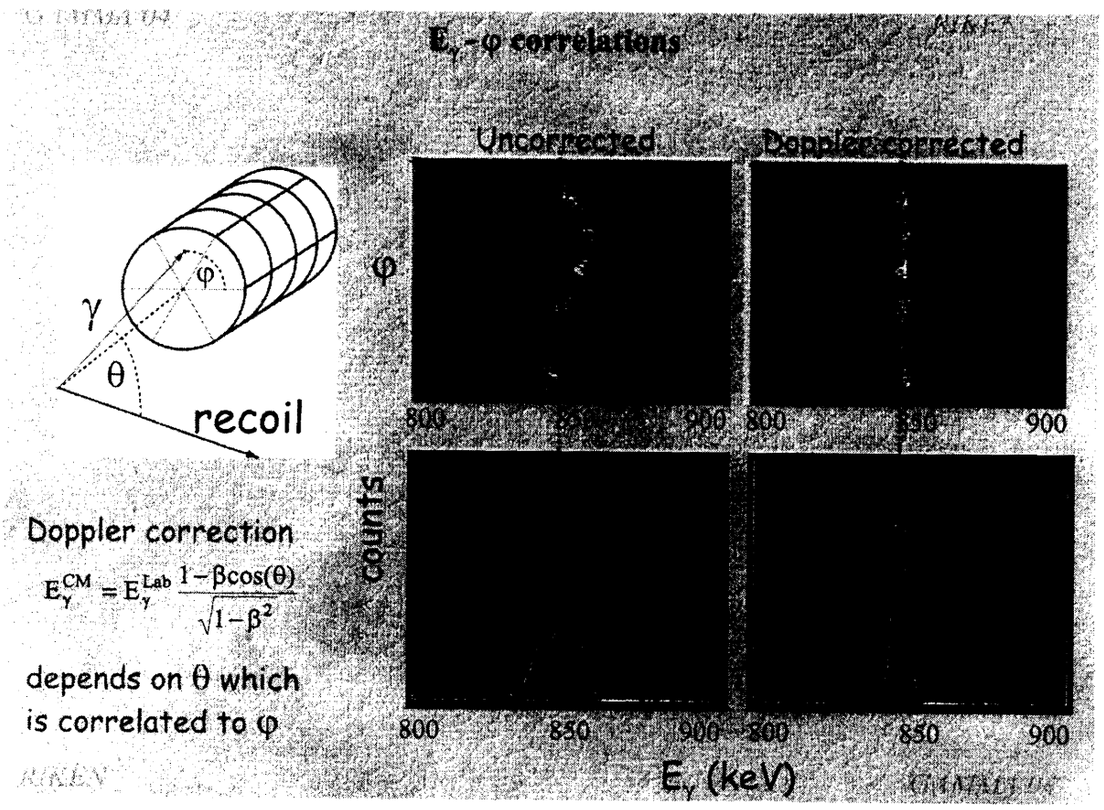
E_γ-φ correlations
Uncorrected
Doppler corrected
φ
γ
θ
recoil
counts
Doppler correction
$E_\gamma^{CM} = E_\gamma^{Lab} \frac{1-\beta\cos(\theta)}{\sqrt{1-\beta^2}}$
depends on θ which is correlated to φ
E_γ (keV)

GAMMA 04

The Symmetry [illegible]

Idealized configuration to [illegible] the maximum attainable [illegible]

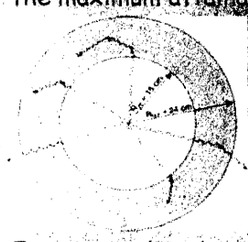

R_i = [illegible]
R_o = 24 cm
230 kg of Ge

Events simulated using GEANT4
Response of shell at 1.33 MeV [illegible]

ε_{ph} = 70% P/T = 77%

Reconstruction by Cluster-[illegible]
Packing Distance: 5 mm
Position Resolution: 5 [illegible]

1.33 MeV	$M_\gamma = 1$	$M_\gamma = 30$
ε_{ph} (%)	65	36
P/T(%)	85	60

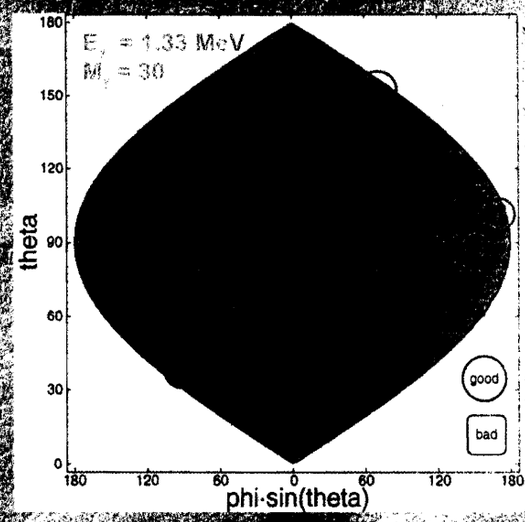

[illegible] photopeak

GAMMA 04

AGATA

(Advanced [illegible])

4π γ-array for Nuclear Physics [illegible] at European [illegible] providing radioactive and high-intensity stable beams

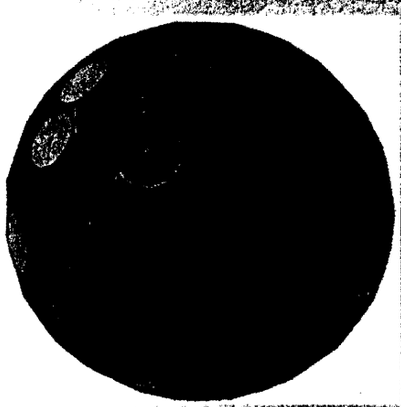

Main features of AGATA

Efficiency: 40% (M_γ=1) 26% (M_γ=30)
today's arrays ~10% (gain ~4) 8% (gain ~1000)

Peak/Total: 65% (M_γ=1) 50% (M_γ=30)
today ~55% 40%

Angular Resolution: ~1° →
FWHM (1 MeV, v/c=50%) ~6 keV !!!
today ~40 keV

Rates: 3 MHz (M_γ=1) 300 kHz (M_γ=30)
today 1 MHz 20 kHz

- 180 large volume [illegible] Ge crystals [illegible] detectors
- Digital electronics and [illegible] Pulse Shape [illegible] low operation of Ge detectors in a position sensitive mode [illegible]
- Demonstrator ready by 2007. Construction of full array [illegible]
- Installation sites: GSI, GANIL, at the RIB facilities, ...

GAMMA 04

AGATA Detectors

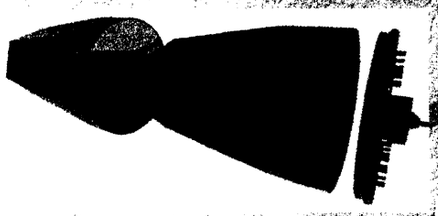

Hexaconical Ge crystals
90 mm long
80 mm max diameter
36 segments
Al encapsulation
0.5 mm spacing
0.7 mm thickness
37 vacuum feed-throughs

Distance between faces of crystals
in same cluster ~3 mm
between adjacent clusters ~9 mm

The First Step

The AGATA Demonstrator

Objective of the Demonstrator Phase 2001-2003

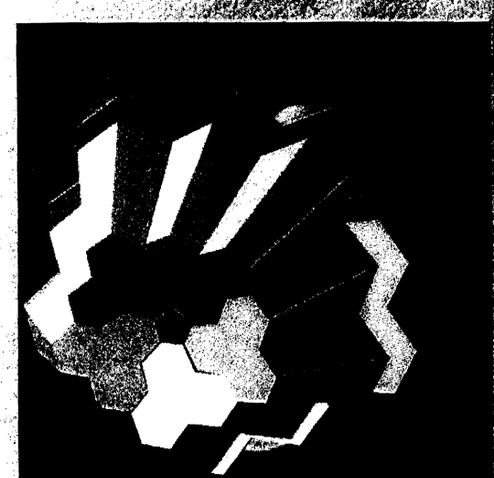

1 symmetric triple-cluster
5 asymmetric triple-clusters
36-fold segmented crystals
[illegible] segments
[illegible] digital channels
[illegible] 8 - 8 % @ M = 1
[illegible] 4 - 7 % @ M = 30
Full DAQ
with online PSA and γ-ray tracking
Test Sites:
GANIL, GSI, [illegible]via, Köln, LNL
Cost ~ 7 M[illegible]

The AGATA Collaboration

Bulgaria:	Univ. Sofia
Denmark:	NBI Copenhagen
Finland:	Univ. Jyväskylä
France:	GANIL Caen, IPN Lyon, CSNSM Orsay, IPN Orsay, CEA-DSM-DAPNIA Saclay, IReS Strasbourg
Germany:	HMI Berlin, Univ. Bonn, GSI Darmstadt, TU Darmstadt, FZ Jülich, Univ. Köln, LMU München, TU München
Italy:	INFN/Univ. Padova, Milano, Legnaro, Firenze, Camerino, Napoli, Genova
Poland:	NINP & IFJ Krakow, SINS Swierk, HIL & IEP Warsaw
Romania:	NIPNE & PU Bucharest
Sweden:	Univ. Lund, KTU Stockholm, Univ. Uppsala
UK:	CLRC Daresbury, Univ. Brighton, Keele, Liverpool, Manchester, Paisley, Surrey, York

SUMMARY

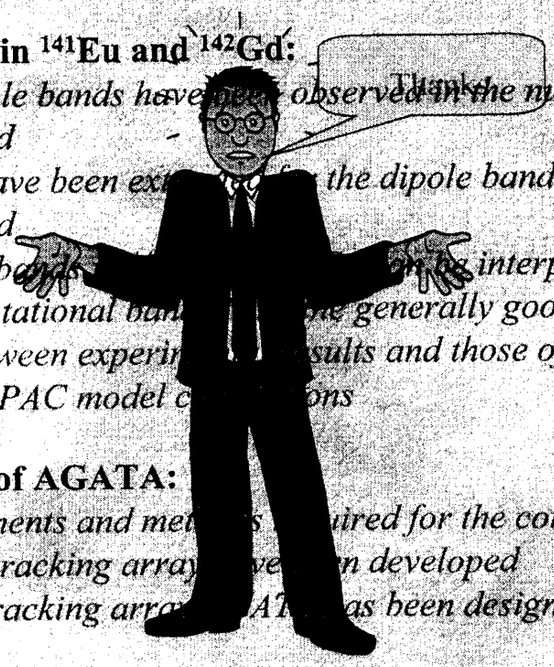

Dipole bands in ^{141}Eu and ^{142}Gd:

- *Several dipole bands have been observed in the nuclei ^{141}Eu and ^{142}Gd*
- *Lifetimes have been ex[illegible] the dipole bands in ^{141}Eu and ^{142}Gd*
- *The dipole b[illegible] interpreted as magnetic rotational ban[illegible] generally good agreement between experi[illegible]sults and those of the TAC and SPAC model c[illegible]ons*

Perspectives of AGATA:

- *The components and me[illegible]s [illegible]ired for the construction of a 4π γ-ray tracking arra[illegible]n developed*
- *The γ-ray tracking arr[illegible]AT[illegible]as been designed*

Gamma-ray Compton imaging by strip Ge telescope

Shinji Motomura, Hiroshige Takeichi, Shuichi Enomoto, Michiya Kibe,* Yasuyuki Gono,* and Yasushige Yano

The Institute of Physical and Chemical Research (RIKEN), Saitama 351-0198, Japan
* Graduate School of Science, Kyushu University, Fukuoka 812-8581, Japan

We have constructed a prototype of the Compton camera for the γ-ray emission imaging[1,2] (GREI) system. The GREI system enables us to visualize distributions of mixed radioisotopes (RIs) simultaneously and nondestructively. This system is expected to establish new methodologies in biology, nuclear medicine, and so forth[3].

The Compton camera consists of two sets of double-sided orthogonal-strip germanium detectors which are arranged in parallel. The dimensions are 39 mm × 39 mm × 10 mm and 39 mm × 39 mm × 20 mm for the front and rear detectors, respectively. The strip pitch is 3mm for both detectors. The transverse position of a γ-ray interaction in the detector can be determined by a combination of the anode and cathode strips with the accuracy given by the width of the strip. It is also possible to determine the depth of the interaction point by the time difference between the signals from the anode and cathode strips[4,5].

In order to prove the feasibility of the Compton camera by examples, we have performed experiments to visualize the RIs distributed in soybean samples. A soybean sample was administered with the three RIs of ^{137}Cs, ^{59}Fe and ^{65}Zn. The sample was fixed on a plane 15mm apart from the center of the front detector.

The sections of the cones defined for each detected event were accumulated on the plane where the sample was fixed, in order to obtain a two-dimensional image called a simple back-projection (SBP). The SBP image was separately obtained for each RI and then deconvoluted using a point-spread function. It was successfully visualized that each RI has a different distribution in the sample (Fig. 1).

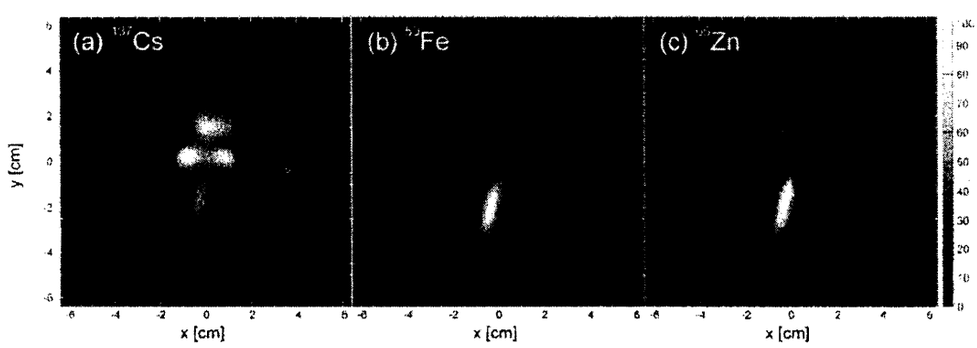

Fig. 1. Distribution of each RI in the soybean sample visualized by the Compton camera.

References
[1] S. Motomura and S. Enomoto: J. Clin. Exper. Med. **205**, 884 (2003).
[2] Y. F. Yang et al.: IEEE Trans. Nucl. Sci. **48**, 656 (2000).
[3] S. Enomoto: RADIOISOTOPES **52**, 631 (2003).
[4] M. Momayezi et al.: SPIE **3768**, 530 (1999).
[5] S. Motomura et al.: RIKEN Accel. Prog. Rep. **36**, 154 (2003).

Gamma-ray Compton imaging by strip germanium telescope

Shinji Motomura, Hiroshige Takeichi, Shuichi Enomoto, Michiya Kibe,*
Yasuyuki Gono,* and Yasushige Yano

RIKEN (The Institute of Physical and Chemical Research)
*Graduate School or Science, Kyushu University

CNS–RIKEN Joint Symposium
Frontier of gamma-ray spectroscopy and its application

March 18–19, 2004

Topics

- Introduction of the multitracer method
  - Production of multitracer at RIKEN
  - Gamma rays of multitracer
- Present status of the Compton camera
  - Principle of γ-ray Compton imaging
  - Strip Ge telescope
  - Implementation with DOI measurment
  - Image reconstruction method
- Examples of γ-ray imageing
  - Imaging of a single tracer
  - Imaging of multitracer
  - Example of 3D imaging

Introduction of Multitracer method

- Production of Multitracer at RIKEN

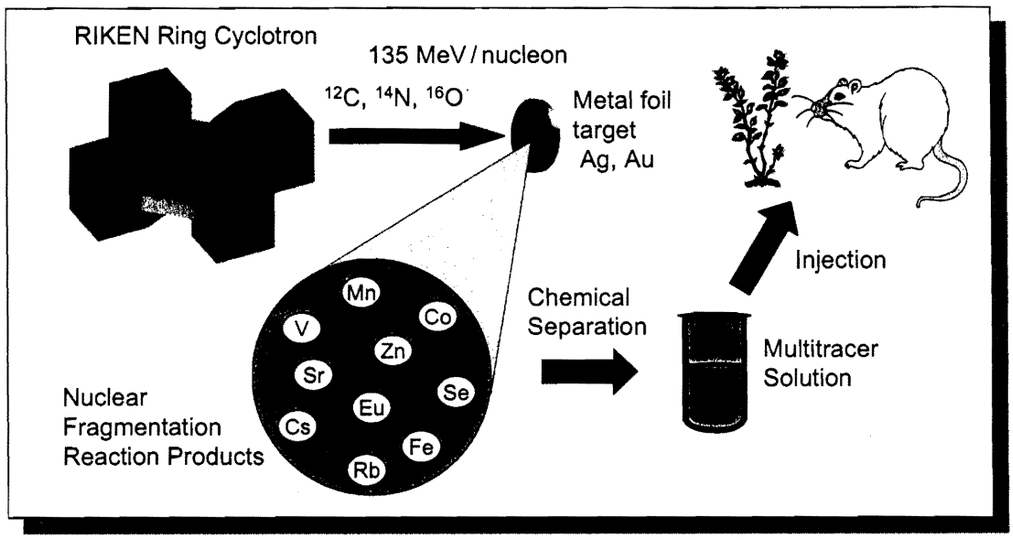

Introduction of multitracer method

- Gamma rays of multitracer

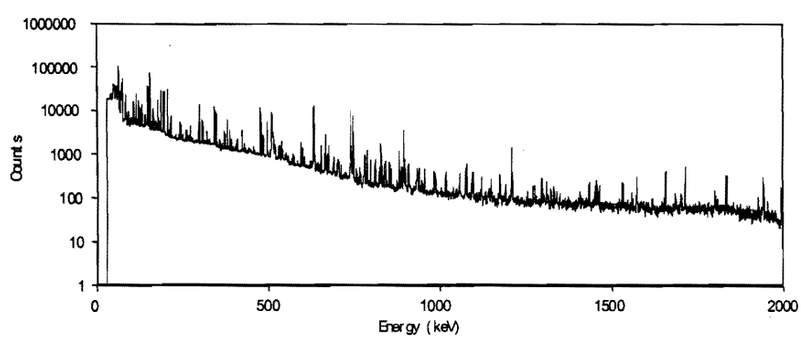

- There are more than 100 peaks of γ rays between 100 keV and 2 MeV—using Ge detectors is almost the only solution for separating these peaks.
- With conventional γ-ray imager equipped with collimators, the spatial resolution gets worse when the γ-ray energy is higher than ~300 keV.

⬇

A Compton camera consisting of segmented Ge detectors was proposed for an imager of multitracer γ rays.

Present status of the Compton camera

- Principle of γ-ray Compton imaging

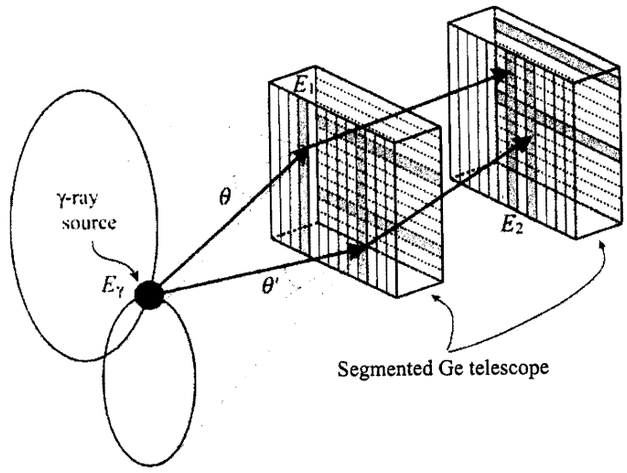

$$E_\gamma = E_1 + E_2$$

$$\cos\theta = 1 + m_e c^2 \left(\frac{1}{E_\gamma} - \frac{1}{E_\gamma - E_1} \right)$$

Present status of the Compton camera

- Strip Ge telescope—two crystals are enclosed in the common cryostat.

  - Dimensions
    Front: 39mm x 39mm x 10mm
    Rear: 39mm x 39mm x 20mm
  - Strip pitch: 3 mm for both detectors
    (13 strips on each side)
  - Distance between the detectors: 60 mm

Present status of the Compton camera

- Implementation with depth-of-interaction (DOI) measurment

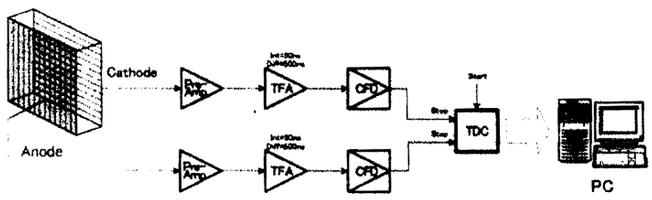

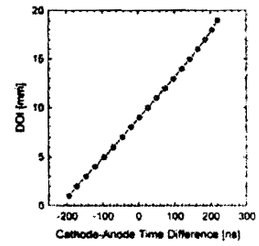

- DOI resolution of ~1 mm is achieved by using the current modules

Present status of the Compton camera

- Image reconstruction method

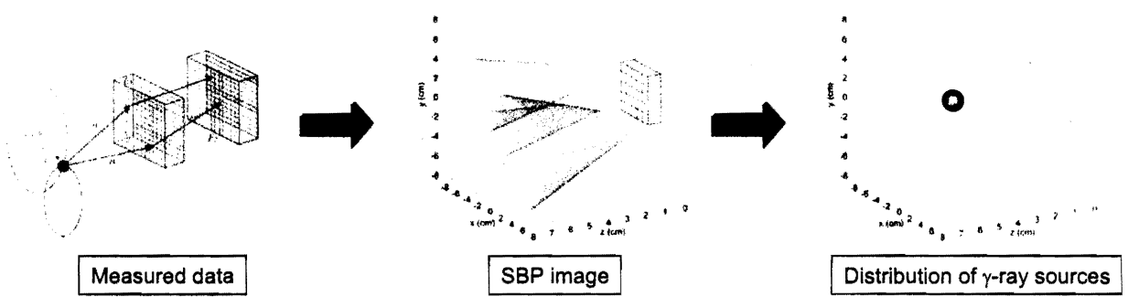

- Measured data → Simple back-projection (SBP) image
  - The cone determined for each event is simply accumulated—but there are counts even where there are no sources in the SBP image.
- SBP image → Distribution of γ-ray sources
  - We have tried deconvolution with a point-spread function
- We call this two-step reconstruction "deconvolution after back-projection (DABP)."

Examples of γ-ray imaging

- Imaging of a single tracer (^{65}Zn)

Soybean sample administered with ^{65}Zn

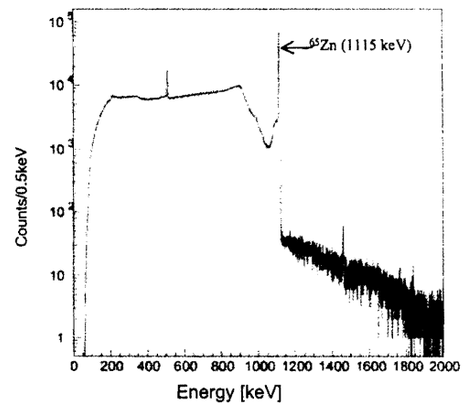

Gamma-ray energy spectrum measured by the Compton camera

Examples of γ-ray imaging

- Imaging of a single tracer (^{65}Zn)

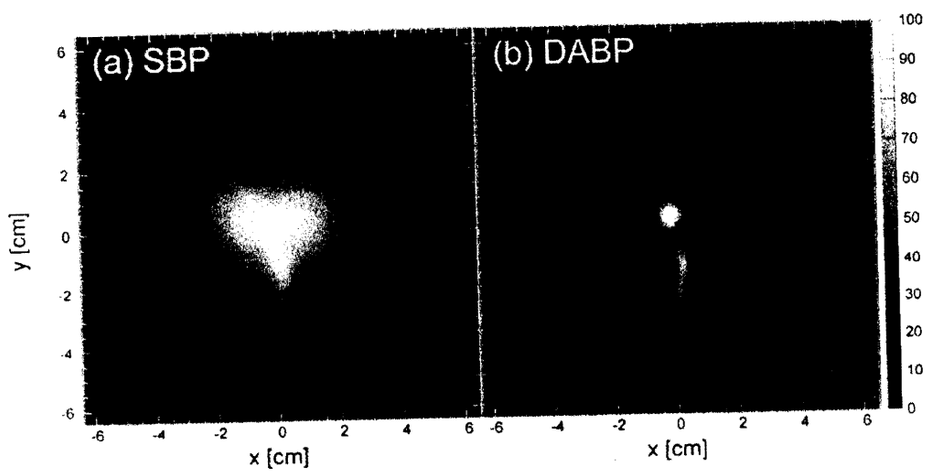

Reconstructed images of ^{65}Zn

Examples of γ-ray imaging

- Imaging of multitracer (^{137}Cs, ^{59}Fe and ^{65}Zn)

Soybean sample administered with ^{137}Cs, ^{59}Fe and ^{65}Zn

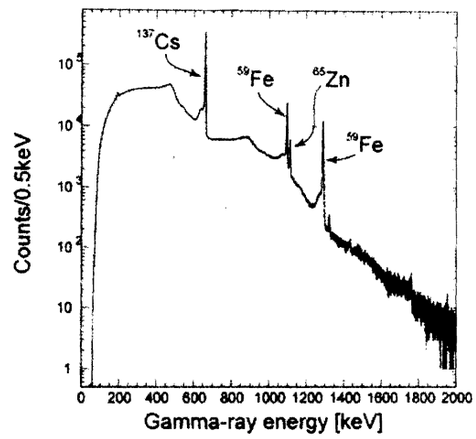

Gamma-ray energy spectrum measured by the Compton camera

Examples of γ-ray imaging

- Imaging of multitracer (^{137}Cs, ^{59}Fe and ^{65}Zn)

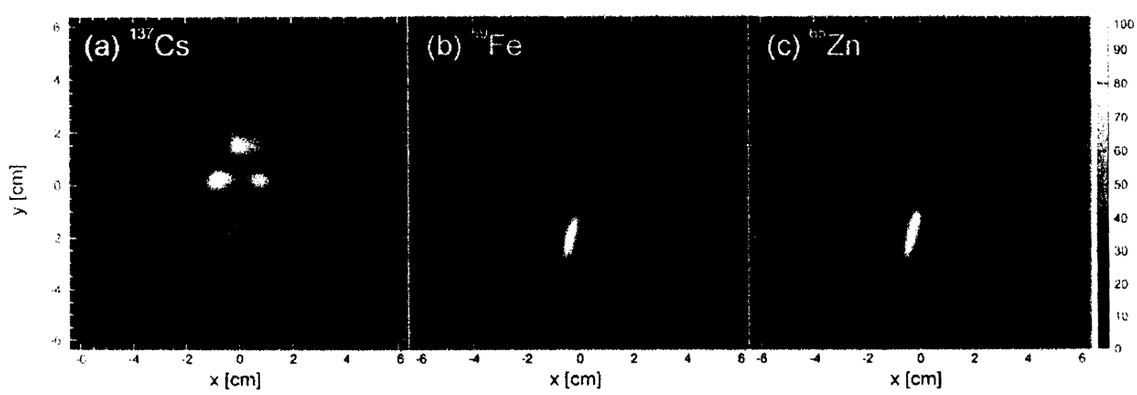

DABP image of each tracer

Examples of γ-ray imaging

- Example of 3D imaging—3D image can be obtained by measuring from only one direction

Soybean sample administered with ^{137}Cs, ^{59}Fe and ^{65}Zn

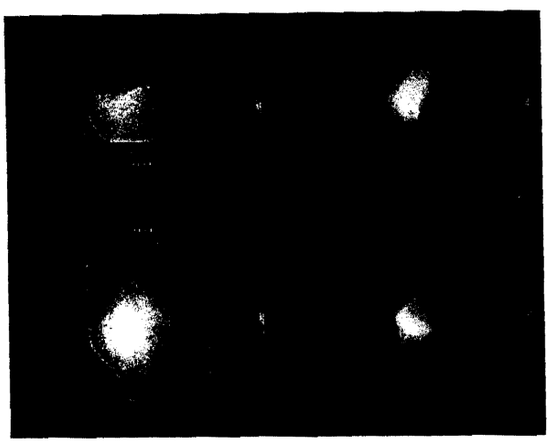

3D SBP (^{137}Cs)

3D DABP (^{137}Cs)

Summary

- We have constructed a prototype of the Compton camera suitable for multitracer imaging and its feasibility was demonstrated by examples.
- Both 2D and 3D images were successfully obtained by DABP reconstruction method.

Detector Array for Low Intensity radiation

S. Takeuchi[a,*], T. Motobayashi[a], H. Murakami[b], K. Demichi[b], H. Hasegawa[b] and Y. Togano[b]

[a] *The Institute of Physical and Chemical Research (RIKEN), Wako, Saitama 351-0198, Japan*
[b] *Department of Physics, Rikkyo University, Toshima, Tokyo 171-8501, Japan*

A new array of NaI(Tl) detectors has been developed to be used in studying structures of unstable nuclei by in-beam γ-ray spectroscopy at the RIKEN Accelerator Research Facility (RARF) and the RI beam factory (RIBF)[1]. In those facilities, unstable nuclei are provided as fast secondary beams, and γ rays to be detected are emitted from fast-moving residual nuclei of secondary reactions with appropriate targets. Since the γ-ray energy is Doppler-shifted depending on the emission angle with respect to the direction of the residual nuclei, a high angular resolution of the detection system is necessary for a high energy resolution after Doppler-corrections. The present development is aimed at improving the detection efficiency and energy resolution, which are crucial for detailed spectroscopy of very unstable nuclei with a very-low-intensity beam, such as that with γ-γ coincidence.

A detection array consists of 160 NaI(Tl) scintillators surrounding the target. A typical intrinsic resolution is around 8-9% at 662 keV (^{137}Cs). Sixteen layers, each of which consists of 8-14 scintillators, are arranged coaxially with respect to the beam axis, and are closely packed to cover the angular range of 22-162°. The angular resolution of γ-ray detection is 7-9°, which is much better than that of about 20° for the previous NaI(Tl) array.

The improvement of the energy resolution was demonstrated in two independent experiments, which conditions are almost the same, (secondary beams of ^{12}Be with $\beta \simeq 0.3$ on a liquid helium target), except for the γ-ray detectors. The width of full energy peak for the new array is 30% better than that of the previous array for γ rays of $E_\gamma = 2.1$ MeV corresponding to $2^+ \rightarrow 0^+$ transition in ^{12}Be.

The efficiency was estimated by means of the GEANT code[2] to be 24% at $E_\gamma = 1$ MeV with $\beta = v/c = 0.36$. This condition of E_γ and β corresponds to typical inelastic scattering experiments in RARF. In the case of RIBF, secondary beams are faster than the present facility, and the efficiency is estimated to be 18% at $E_\gamma = 1$ MeV with $\beta \sim 0.6$.

References

[1] S. Takeuchi et al., RIKEN Accel. Prog. Rep. 36 (2003) 148.
[2] GEANT3: *Detector Description and Simulation Tool* (CERN, Geneva, 1993).

E-mail address: takesato@rarfaxp.riken.jp

Detector Array for Low Intensity radiation

DALI and DALI2

S.Takeuchi, T.Motobayashi

Heavy Ion Nuclear Physics Laboratory, RIKEN

H.Murakami, K.Demichi, H.Hasegawa, Y.Togano

Department of Physics, Rikkyo University

2004/03/19 CNS-RIKEN Joint Symposium on Frontier of gamma-ray spectroscopy and its application

γ-RAY SPECTROSCOPY WITH UNSTABLE NUCELI

RIPS

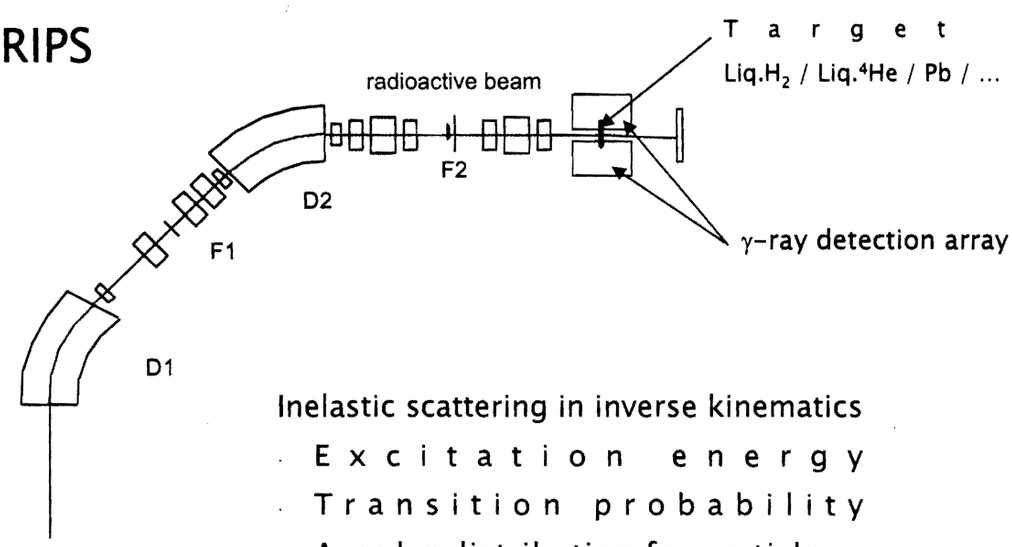

Inelastic scattering in inverse kinematics

- Excitation energy
- Transition probability
- Angular distribution for particle-γ

2004/03/19 CNS-RIKEN Joint Symposium on Frontier of gamma-ray spectroscopy and its application

- Unstable nuclei
  - Low Beam intensity
    → High detection efficiency
- Fast secondary beams
  - RARF (β ~ 0.3) and RIBF (β ~ 0.6)
    → Doppler Shift
    Depending on the emission angle
    → High angular resolution for High energy resolution

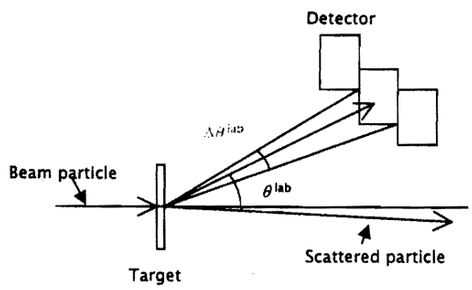

DALI

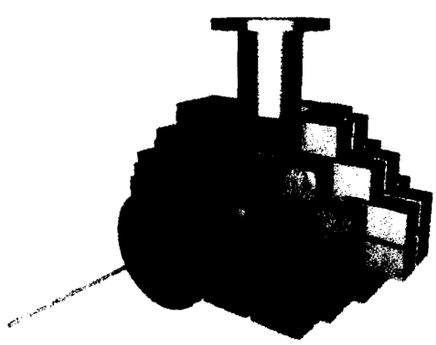

Previous system (typical spec.)
up to 68 NaI(Tl) detectors
angular resolution : ~15 degree
efficiency : about 15% for 1MeV

^{32}Mg(p,p') β~0.3

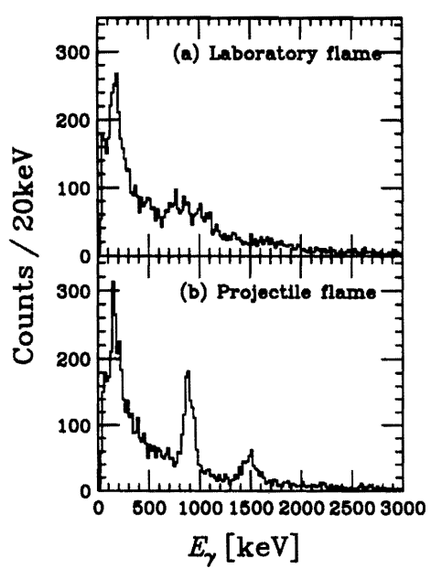

H.Hasegawa, Master's thesis, Rikkyo Univ., 2003

DEVELOPMENT of A NEW ARRAY

M O T I V A T I O N :

- For More neutron-rich nuclei : Low Intensity
- For using at RIBF : Fast beam

REQUIREMENTS:

- Higher Efficiency
- Higher Angular Resolution

↔ • High Energy Resolution

• Angular Distribution measurements

↓

160 NaI(Tl) Detectors

Large Volume and Many Segments

Half of DALI2

OVERVIEW - DALI2 -

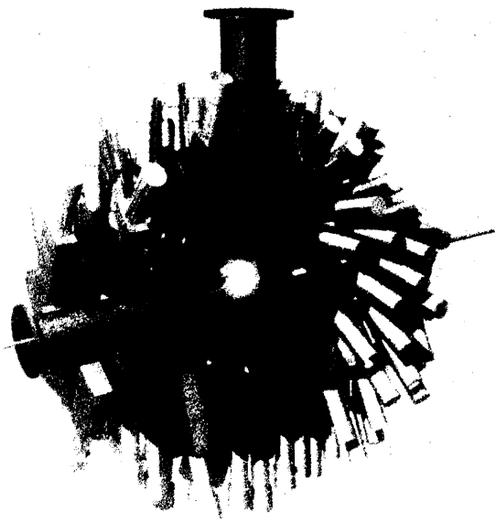

160 NaI(Tl) detectors

Each detector
- 4.5 x 8 x 16 (cm^3)
- $\Delta E/E \sim 9\%$ @ 662keV

Array
- 16 layers
- 6~14 detectors in each layer

DALI [redacted] and DALI2

	DALI	DALI2
Arrangement	Brick wall like	Hedgehog like
Size	6 x 6 x 12 (cm^3)	4.5 x 8 x 16 (cm^3)
# of Detectors	68	160
Volume	~ 30 liter	~ 90 liter
# of Layers	6 - 8	16
Angular resolution	~ 15 degree	~ 8 degree
Energy resolution (β~0.3)	12% @ 1MeV	9% @ 1MeV
Efficiency (β~0.3)	15% @1MeV	24% @1MeV

IMPROVEMENT of ENERGY RESOLUTION

$^{12}Be(\alpha,\alpha')^{12}Be^*$

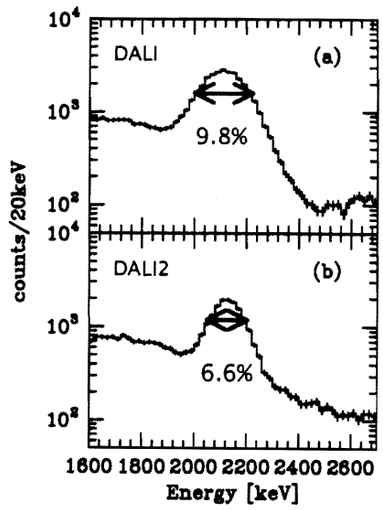

$E\gamma$ = 2100 keV, $\beta \sim 0.3$

(a) : DALI ($\Delta\theta \sim 15°$)
$\Delta E/E$ = 9.8% (FWHM)

(b) : DALI2 ($\Delta\theta \sim 8°$)
$\Delta E/E$ = 6.6% (FWHM)

IMPROVEMENT of ANGULAR DISTRIBUTION

DALI $^{36}Si(Be,Be')^{36}Si^*$
E(2+) = 1399 keV

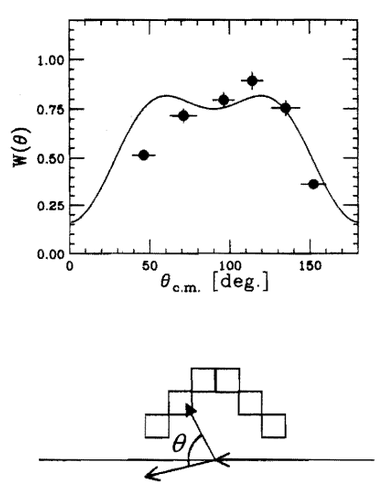

DALI2 $^{16}C(p,p')^{16}C^*$
E(2+) = 1766 keV

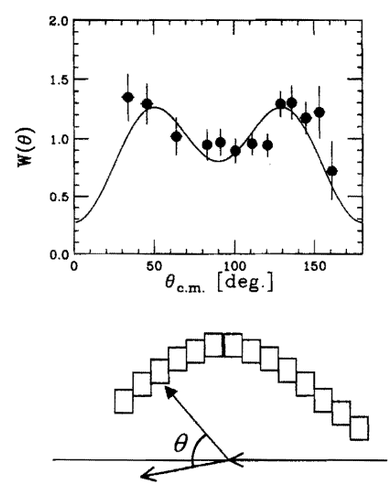

PAST EXPERIMENTS with DALI2

- $^{12}Be(\alpha,\alpha')^{12}Be^*$, $^{12}Be(\alpha,t)^{13}B^*$ (CNS, Rikkyo, RIKEN)
- ^{54}Ni, ^{50}Fe, ^{46}Cr Coulex (Rikkyo, RIKEN)
- $^{27}F(p,p')^{27}F^*$, $^{16}C(p,p')^{16}C^*$ (ATOMKI, Tokyo, RIKEN)
- $^{4}He(^{22}O,^{23}F^*)$ (CNS, RIKEN)
- $^{26}Ne(Pb,Pb)^{26}Ne^*$ (Orsay, TIT, RIKEN)
- $^{78-82}Ge$ Coulex (Tokyo, RIKEN)
- $^{19}C(p,p')^{19}C^*$ (ATOMKI, RIKEN)

EXAMPLES

^{48}Cr Coulex (K. Yamada et al.)

$\beta \sim 0.3$, $E\gamma = 752$ keV

$\Delta E/E = 10.8\%$ (FWHM)

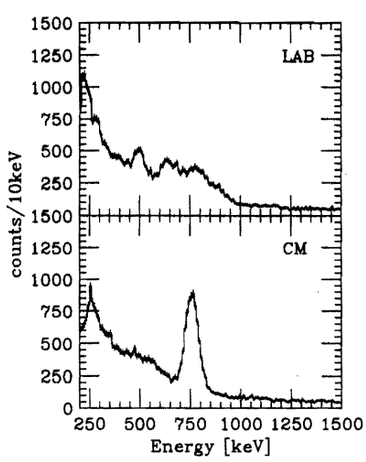

γ-γ coincidence

→ Efficiency ~ $\varepsilon_1 \times \varepsilon_2$

DALI : DALI2 = 1 : 3

COMING EXPERIMENTS with DALI2

- γ-γ coincidence of ^{32}Mg and ^{34}Si
- Inelastic scattering of ^{64}Cr
- Inelastic scattering of ^{42}Si

  With Liquid hydrogen and/or helium targets

FUTURE EXPERIMENTS in RIBF

Efficiency and Energy resolution : 18% and 12% for 1MeV (β~0.6)
Target : More neutron-rich nuclei (ex. ^{78}Ni >0.1 cps)

Possible array for higher efficiency and energy resolution is the combination of DALI and DALI2. ? '1+2=3' DALI3?

SUMMARY

- We have developed DALI2 for in-beam γ-ray spectroscopy with fast unstable nuclei (@RIBF).
- The performance is improved compared with DALI.
  - Energy Resolution $\Delta E/E \sim 9\%$@1MeV
  - Detection Efficiency $\varepsilon \sim 24\%$@1MeV
- Several experiments have already done with DALI2 and we are planning experiments with low intensity beam and/or measuring γ-γ coincidence.

DOPPLER SHIFT and BROADENING

$$E_\gamma^{\mathrm{proj}} = \gamma\left(1-\beta\cos\theta^{\mathrm{lab}}\right)E_\gamma^{\mathrm{lab}}$$

$$\left(\frac{\Delta E_\gamma^{\mathrm{proj}}}{E_\gamma^{\mathrm{proj}}}\right)^2 = \boxed{\left(\frac{\beta\sin\theta^{\mathrm{lab}}}{1-\beta\cos\theta^{\mathrm{lab}}}\right)^2\left(\Delta\theta^{\mathrm{lab}}\right)^2} + \boxed{\left(\frac{\beta\gamma^2\left(\beta-\cos\theta^{\mathrm{lab}}\right)}{1-\beta\cos\theta^{\mathrm{lab}}}\right)^2\left(\frac{\Delta\beta}{\beta}\right)^2} + \boxed{\left(\frac{\Delta E_\gamma^{\mathrm{lab}}}{E_\gamma^{\mathrm{lab}}}\right)^2}$$

Detector arrangement | Beam velocity or Target thickness | Intrinsic resolution

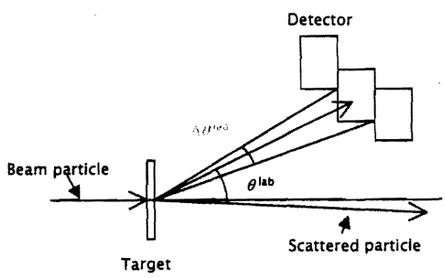

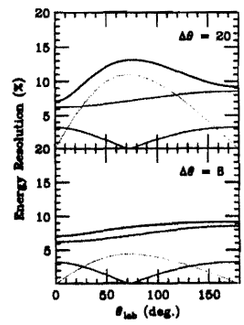

2004/03/19 CNS-RIKEN Joint Symposium on Frontier of gamma-ray spectroscopy and its application

STRUCTURE OF ^{11}Be STUDIED IN β-DELAYED NEUTRON- AND γ-DECAY FROM POLARIZED ^{11}Li

Y. Hirayama[a], T. Shimoda[a], H. Izumi[a], H. Yano[a], M. Yagi[a],
A. Hatakeyama[b], C.D.P. Levy[c], K.P. Jackson[c], and H. Miyatake[d]

[a] *Department of Physics, Osaka University, Osaka 560-0043, Japan*
[b] *Institute of Physics, Graduate School of Arts and Sciences, University of Tokyo, Tokyo 153-8902, Japan*
[c] *TRIUMF, 4004 Wesbrook Mall, Vancouver, BC V6T2A3, Canada*
[d] *IPNS KEK, Tsukuba, Ibaraki 305-0801, Japan*

The structures of the ground and the first excited states of a light neutron-rich nucleus ^{11}Be has been discussed related with the single-particle level inversion, the halo structure and so on. However, the structures of the higher excited states have not been investigated experimentally. We have applied the new method of β-delayed decay spectroscopy [1] for a spin-polarized ^{11}Li in order to establish the level scheme, in particular firm spin-parity assignments, and the decay scheme of ^{11}Be, successfully. This method takes advantage of the discrete nature of the β-decay asymmetry depending on the spin values of the daughter states.

The ^{11}Li beam with polarization as high as 50% was obtained at TRIUMF ISAC. The β-decay asymmetries from ^{11}Li were measured in coincidence with the delayed neutrons and/or γ-rays. The line shapes of the γ-rays emitted from ^{10}B showed the broader width than Ge detector resolution due to the preceding neutron emissions. From the Doppler-broaden line shape analysis, the lifetime of the ^{10}B state and the neutron decay path were determined successfully. The neutron TOF spectrum was unfolded into individual peaks with the help of not only the coincidence relation but also the β-decay asymmetry. The detailed decay scheme of ^{11}Li $\rightarrow$ ^{11}Be $\rightarrow$ ^{10}Be was established, clarifying the previous contradictory delayed neutron measurements [2, 3]. From the β-decay asymmetry the spins and parities of 8 states in ^{11}Be were assigned unambiguously. The $\log ft$-values of the ^{11}Li decay and the neutron spectroscopic factors of the ^{11}Be states were determined.

The present results were compared with the predictions by the Anti-symmetrized Molecular Dynamics (AMD) theory which predicts various types of cluster structures both in ^{11}Be [4] and ^{10}Be [5]. Some of the levels in ^{11}Be show good accord with the AMD predictions.

References

[1] H. Miyatake, *et al.*, Phys. Rev. C **67** (2003) 014306.

[2] N. Aoi *et al.*, Nucl. Phys. **A616** (1997) 181c.

[3] D.J. Morrissey *et al.*, Nucl. Phys. **A627** (1997) 222.

[4] Y. Kanada-En'yo *et al.*, Phys. Rev. C **66** (2002) 024305.

[5] Y. Kanada-En'yo *et al.*, Phys. Rev. C **60** (1999) 064304.

Structure of ^{11}Be studied in β-delayed neutron- and γ- decay from polarized ^{11}Li

Y. Hirayama[a], T. Shimoda[a], H. Izumi[a] H. Yano[a], M. Yagi[a],
A. Hatakeyama[b], C.D.P. Levy[c], K.P. Jackson[c], and H. Miyatake[d]

[a]*Department of Physics, Osaka University*

[b]*Institute of Physics, Graduate School of Arts and Sciences, University of Tokyo*

[c]*TRIUMF*

[d]*IPNS KEK*

Aim of the present work

Bench mark nucleus to test nuclear models for neutron-rich nuclei

only a few spin-parity assignments

prevents comparison
between experiment and theory
level by level

⬇

Establish
level scheme of ^{11}Be
in particular firm spin-parity assignments

decay scheme of ^{11}Be

⬇

structure of ^{11}Be excited states

Latest compilation of energy levels in ^{11}Be

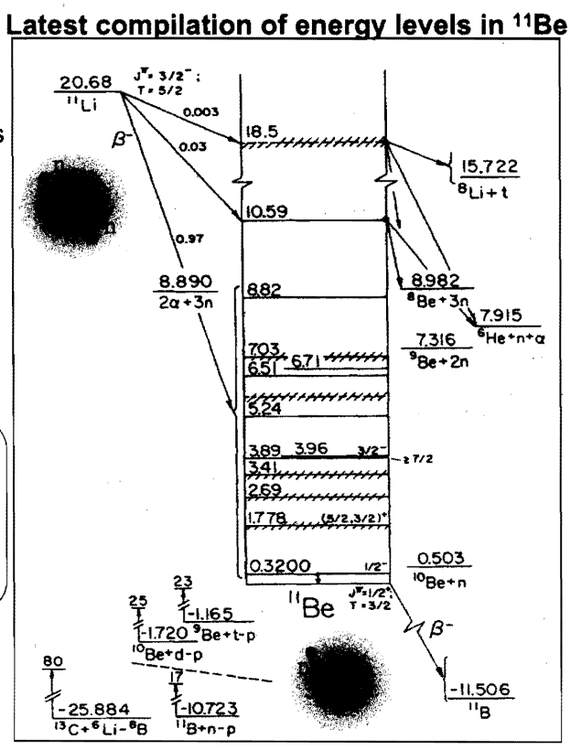

F. Ajzenberg-Selove, Nucl. Phys. A506 (1990) 1.

a new method of β-delayed decay spectroscopy from a polarized nucleus

β -delayed decay spectroscopy

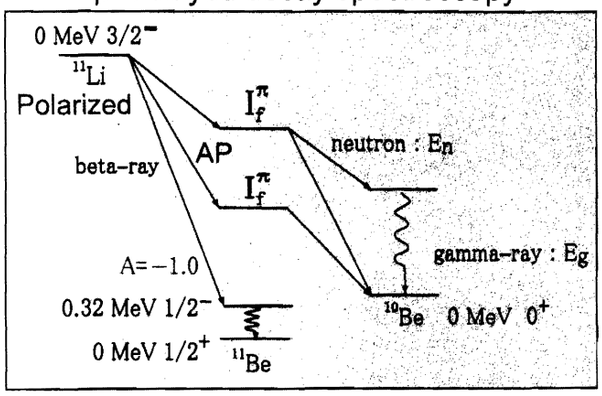

Establish
level scheme of ^{11}Be
decay scheme of ^{11}Be

Assign a spin-parity firmly and simultaneously

β - decay from a spin polarized nucleus

β -ray angular distribution :

$$W(\theta)=1+v/c\ AP\cos\theta$$

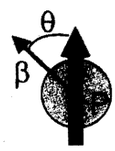

A : asymmetry parameter
P : Polarization

^{11}Li	^{11}Be	
I_i	I_f	A
3/2⁻	5/2⁻	+0.6
	3/2⁻	−0.4
	1/2⁻	−1.0

$$AP = \frac{\sqrt{R}-1}{\sqrt{R}+1} \qquad R=\frac{(W(0)\ /\ W(\pi))_+}{(W(0)\ /\ W(\pi))_-}$$

TRIUMF - ISAC

- Production of ^{11}Li nuclei
  spallation reaction
  Ta target with 500 MeV – 40 μA
  proton beam

- Collinear optical pumping method

ISAC at TRIUMF

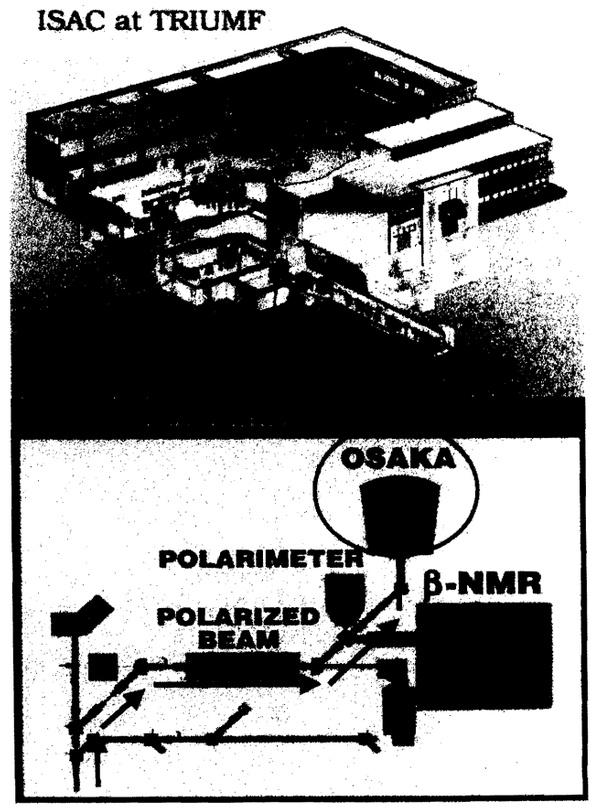

Detector Setup

β(asymmetry) - n, β(asymmetry) - γ, β(asymmetry) - n-γ coincidence

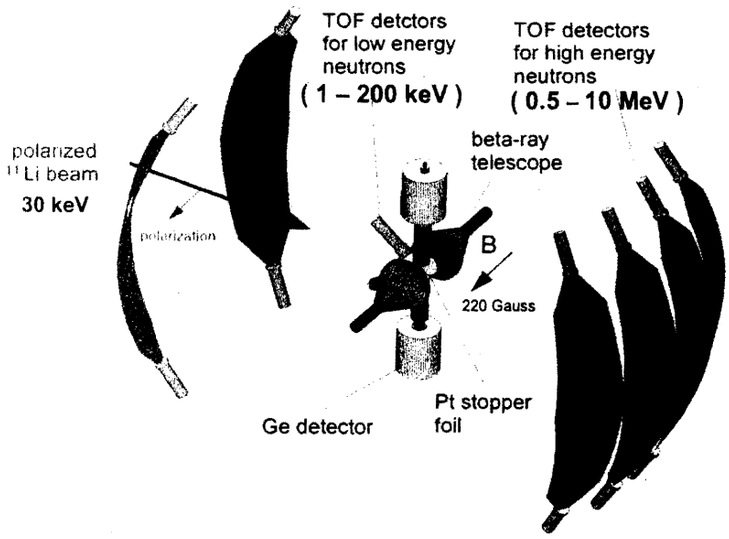

β-ray telescope: $\Delta\Omega_\beta$ = 14.7% x 2,
ε_β = 90%

Ge detector: HPGe, 50 and 60 %,
$\Delta\Omega_\gamma\,\varepsilon_\gamma = 3.2\times10^{-3}$ @3 MeV

plastic scintillator: $\Delta\Omega_n$ = 1.8% x 6,
ε_n = 19%@2 MeV,
En ≳500 keV
Flight Length: 1.5 m

^{6}Li-glass scintillator: $\Delta\Omega_n$ = 0.92% x 2,
^{6}Li+n ▶ α+t+4.8MeV ε_n =2.1%@15 keV,
ε_n = 1.3%@80 keV
En ≳1 keV
Flight Length: 130 mm

γ-ray spectra & analysis

β-γ coincidence

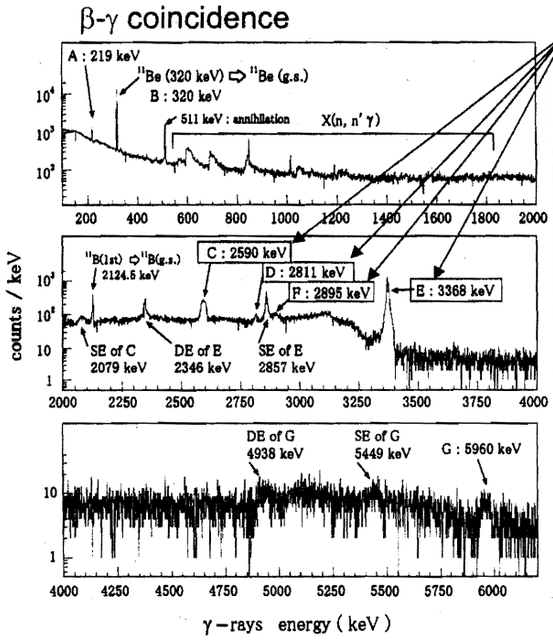

Doppler broadened line-shape
due to preceding neutron emission

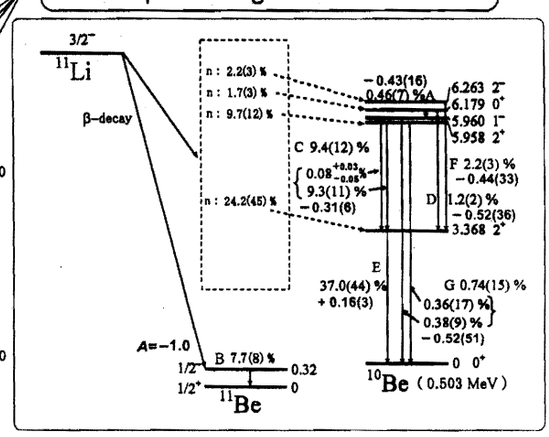

$A\, f_1\, f_2\, P = -0.38(1)$
f_1(solid angle) =0.80
f_2(spin relaxation) =0.98
$P = +0.48(2)$

normalized to average value between Aoi et al. and Morrissey et al.

N. Aoi et al. Nucl. Phys. A616 (1997) 181c

D.J. Morrissey et al, Nucl. Phys. A627 (1997) 222.

Analysis of Doppler broadened line-shape due to preceding neutron emission

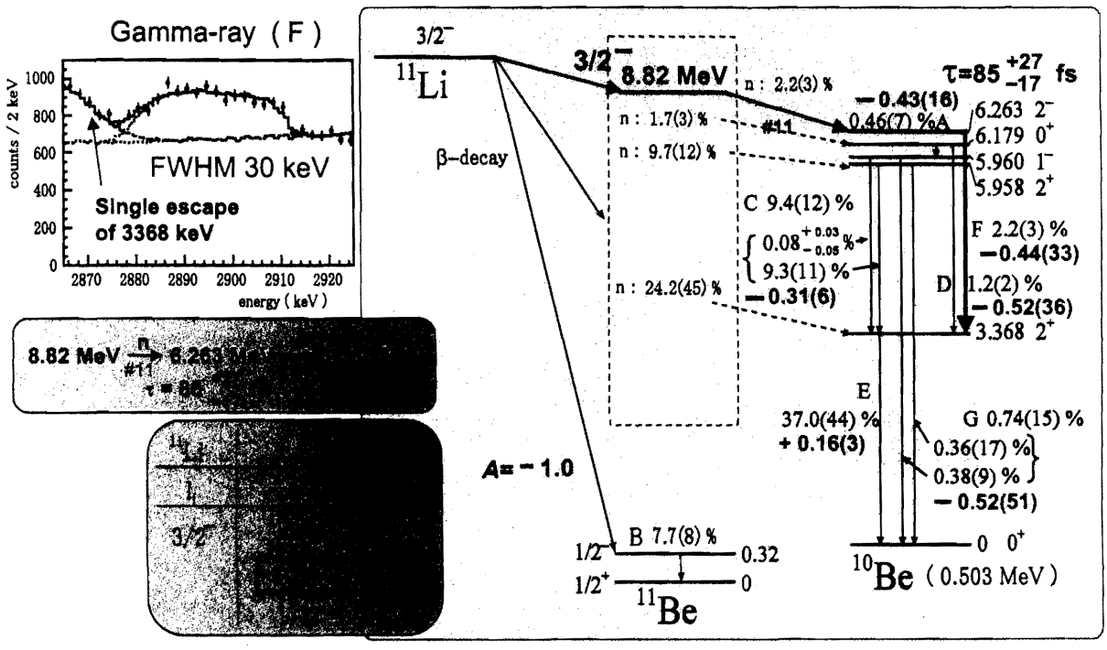

Neutron TOF and asymmetry spectra

(0.5 – 10 MeV)

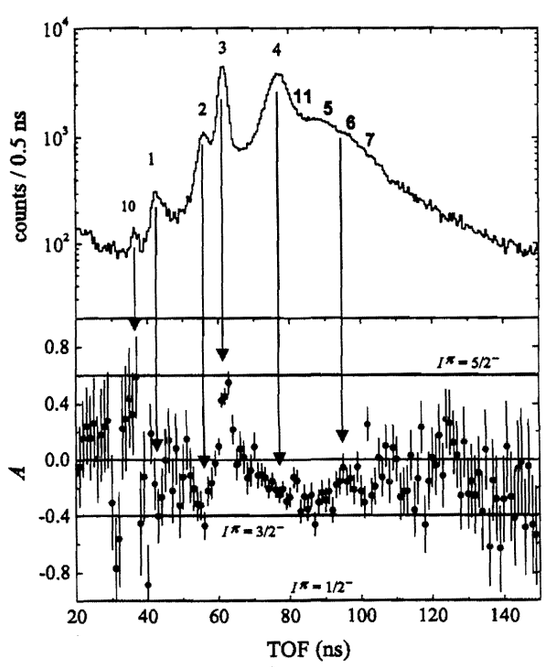

- Determine spin-parity of each neutron emitting state in ^{11}Be from beta-asymmetry
- Establish level and decay scheme of ^{11}Be from β-n-γ triple coincidence measurements

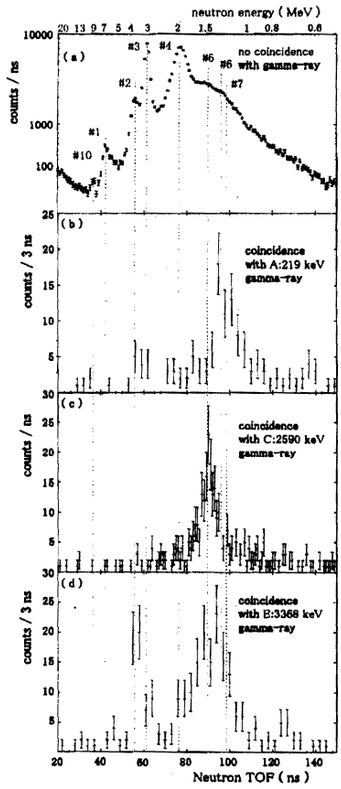

Neutron transition and spin-parity assignments

γ-ray intensities, coincidence relations and beta-asymmetries

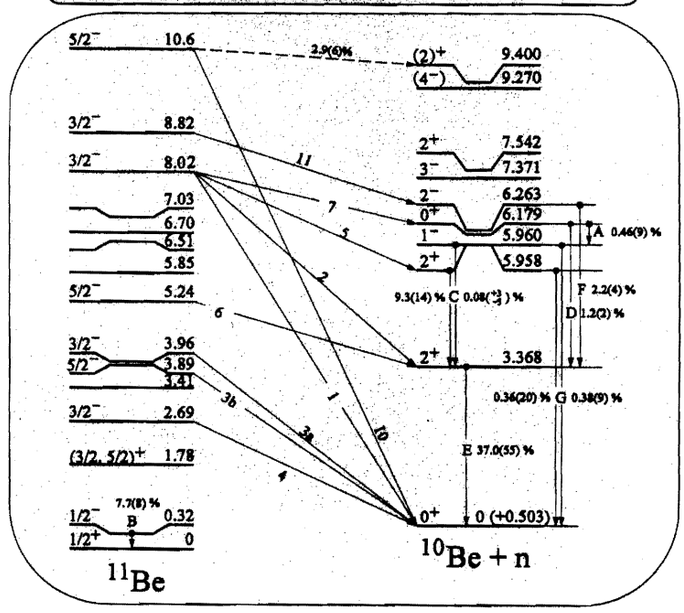

8.02 MeV state : existence previously claimed by Aoi et al.

Reproduction of spectra based on observed decays and assigned spin-parities

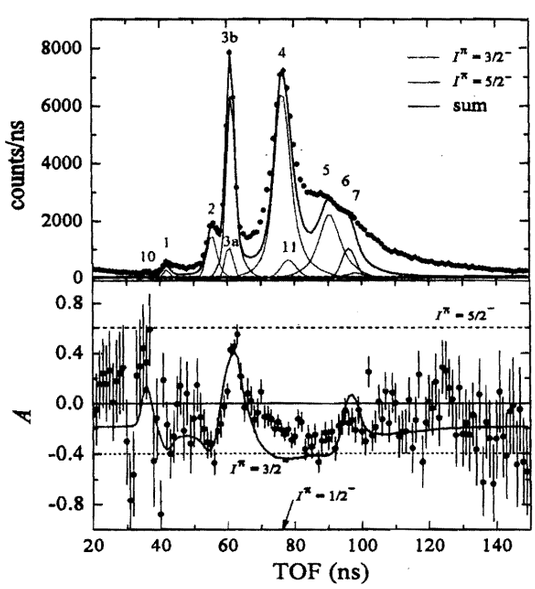

TOF line-shape

- neutron energy
- level width
- **detector response**
- spin-parity

β-n-γ triple coincidence spectra

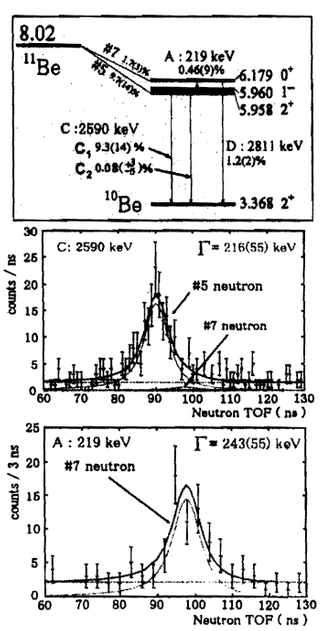

Disagreement points exist ⟹ Hidden peaks exist

Reproduction of spectra by including unknown neutron decays from known levels and assumed levels

further included neutron decays

from known levels

from assumed levels

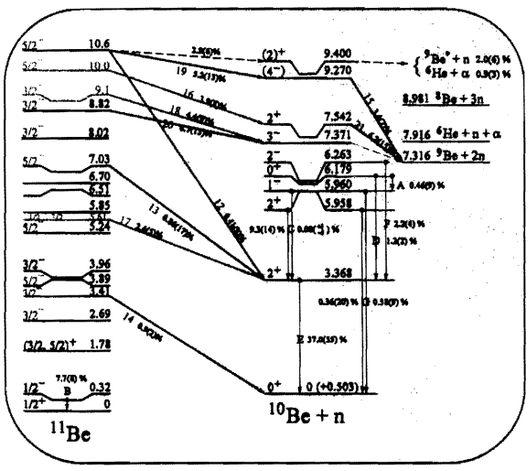

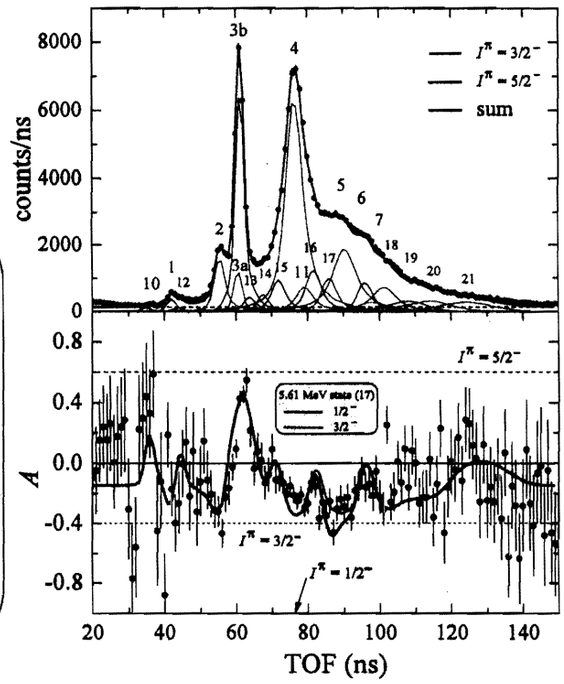

New Level and Decay Schemes of ^{11}Be

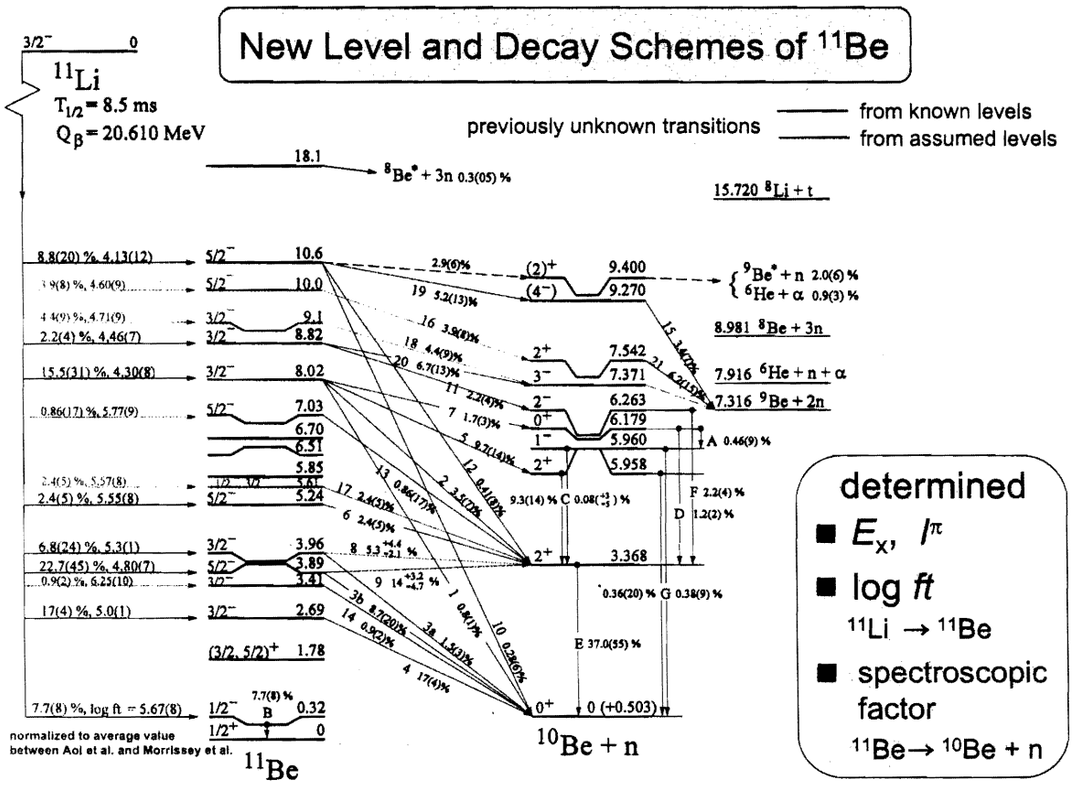

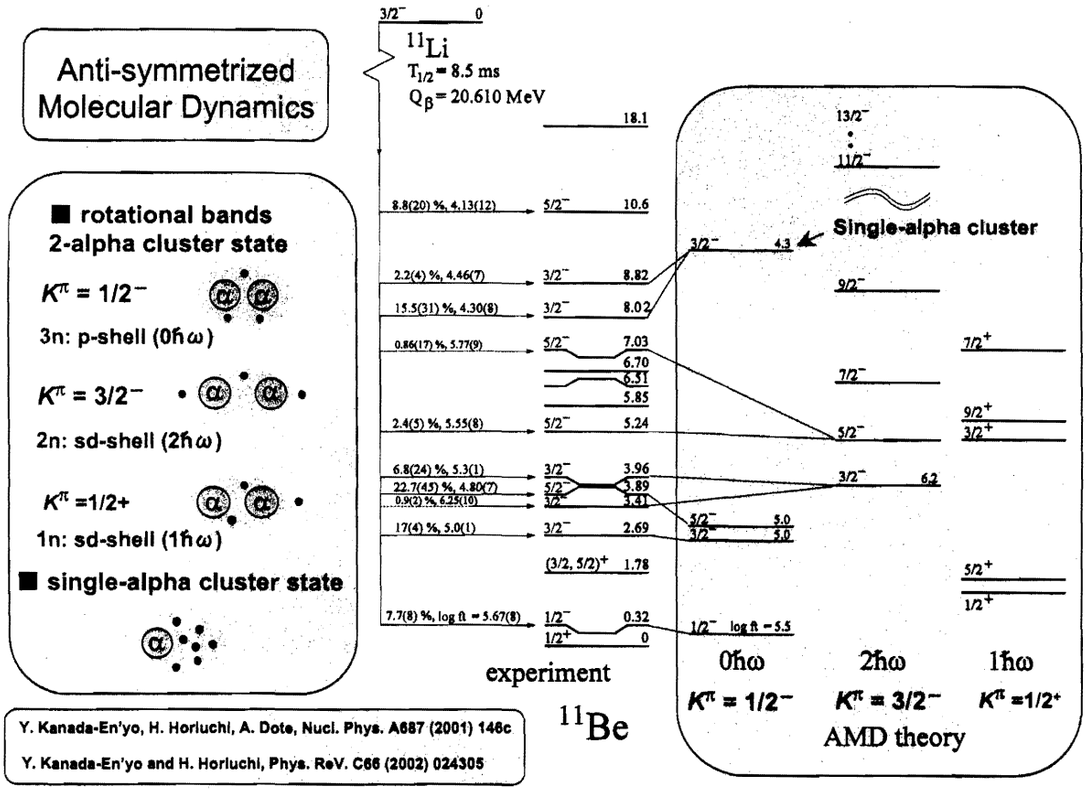
Anti-symmetrized Molecular Dynamics
■ rotational bands
2-alpha cluster state
Kπ = 1/2−
3n: p-shell (0ħω)
Kπ = 3/2−
2n: sd-shell (2ħω)
Kπ =1/2+
1n: sd-shell (1ħω)
■ single-alpha cluster state
11Li
T1/2 = 8.5 ms
Qβ = 20.610 MeV
experiment
11Be
Single-alpha cluster
0ħω
2ħω
1ħω
Kπ = 1/2−
Kπ = 3/2−
Kπ =1/2+
AMD theory
Y. Kanada-En'yo, H. Horiuchi, A. Dote, Nucl. Phys. A687 (2001) 146c
Y. Kanada-En'yo and H. Horiuchi, Phys. ReV. C66 (2002) 024305

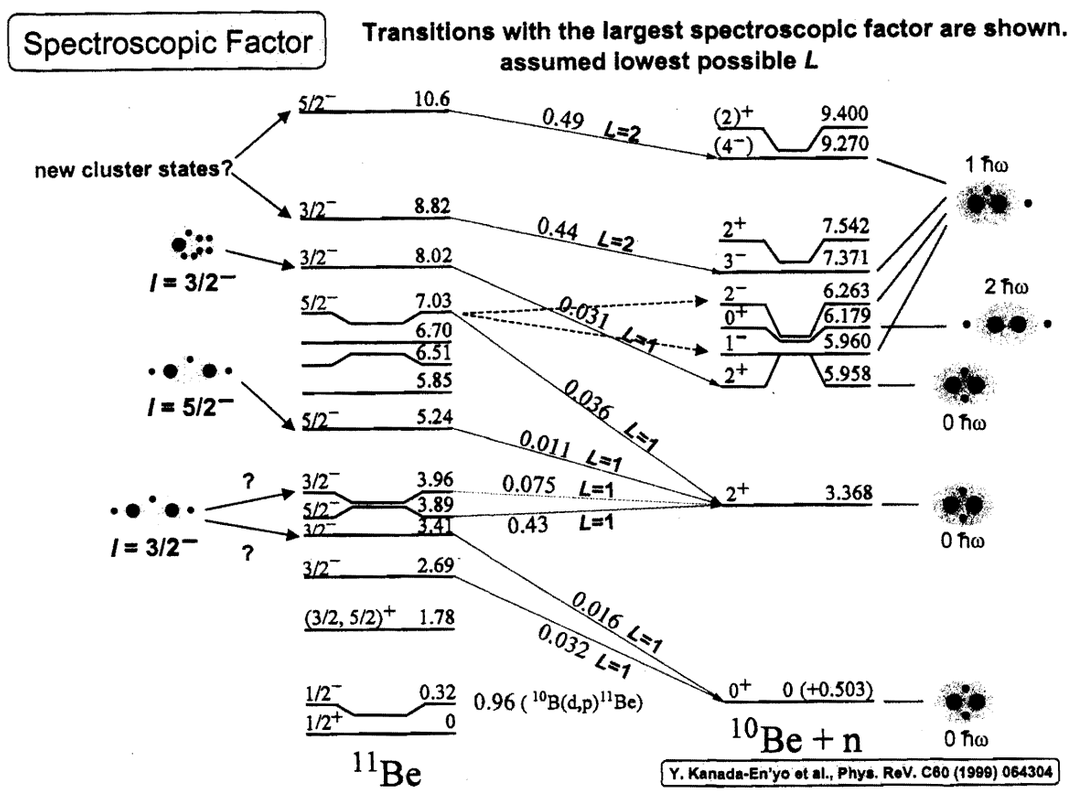
Spectroscopic Factor
Transitions with the largest spectroscopic factor are shown.
assumed lowest possible L
new cluster states?
I = 3/2−
I = 5/2−
I = 3/2−
0.49 L=2
0.44 L=2
0.031 L=1
0.036 L=1
0.011 L=1
0.075 L=1
0.43 L=1
0.016 L=1
0.032 L=1
0.96 (10B(d,p)11Be)
1 ħω
2 ħω
0 ħω
0 ħω
0 ħω
11Be
10Be + n
Y. Kanada-En'yo et al., Phys. ReV. C60 (1999) 064304

Summary of ^{11}Li experiment

- We applied a new method of β-delayed decay spectroscopy for a spin polarized ^{11}Li.
  The β-decay asymmetry was measured in coincidence with the delayed neutrons and γ-rays.
- We established the level scheme and decay scheme of ^{11}Be.
  Spins and parities have been assigned for 8 states.
  From the analysis of the Doppler broadened line shape, we determined the neutron decay path and the lifetime of ^{10}Be excited state.
  β-decay intensities (log-ft) from ^{11}Li have been determined.
  The neutron decay paths and their intensities have been determined, and the neutron spectroscopic factors have been estimated.
  Three new levels are suggested to account for the observed spectra.
- The present results are in accord with the theoretical prediction by the Anti-symmetrized Molecular Dynamics.
  Various types of cluster states exist in ^{11}Be.
- The polarized radioactive nuclear beams are very effective to study structure of unstable nucleus.

Gamow-Teller beta decay of ^{46}Cr

T. K. Onishi[1], A. Gelberg[2], H. Sakurai[1], K. Yoneda[3], N. Aoi[3], N. Imai[3], H. Baba[4], P. von Brentano[2], N. Fukuda[3], Y. Ichikawa[1], M. Ishihara[3], H. Iwasaki[1], D. Kameda[5], T. Kishida[3], A. F. Lisetskiy[6], H. J. Ong[1], M. Osada[1], T. Otsuka[1], M. K. Suzuki[1], K. Ue[1], Y. Utsuno[7], and H. Watanabe[3]

1. Department of Physics, University of Tokyo,
2. Institut für Kernphysik der Universität zu Köln, 3. RIKEN,
4. Rikkyo University, 5. Tokyo Institute of Technology,
6. Michigan State University, 7. Japan Atomic Energy Research Institute

The Gamow-Teller (GT) strength B(GT) in the β decay of ^{46}Cr was measured. It is suggested that the strengths of the GT transition of the even-even nuclei with $|N - Z| = 2$ ($T = 1$) and $A = 4n + 2$ (n: integer) can be a good test for the Wigner SU(4) symmetry. For the medium mass nuclei such as ^{58}Zn, such GT transitions were observed. But, for ^{46}Cr, no GT transition was found yet [1]. Only the 1^+ state at 993 keV was known in the daughter nucleus ^{46}V [2]. In the present work we observed the GT transition to this 1^+ state and determined the strength B(GT) for the first time.

The experiment was carried out at RIPS in RIKEN. A ^{46}Cr beam was produced by the fragmentation of a 80 MeV/nucleon ^{50}Cr beam on a 139 mg/cm^2 Be target. The ^{46}Cr ions were implanted into a 5-mm-thick plastic scintillator. The beam was pulsed to observe the decay of the implanted ^{46}Cr. To detect β-rays from ^{46}Cr, we used two sets of ΔE-ΔE-E plastic scintillators of 2 mm, 2 mm and 130 mm thick, respectively. For γ-rays, we used 4 Clover type Ge detectors and measured γ single and β-γ coincidence spectrum. The branching ratio of the GT decay was deduced from the ratio of the observed γ-rays to the number of implanted ^{46}Cr, which was extracted from the measured purity of ^{46}Cr and the total number of ions implanted into the stopper.

A γ line at 993 keV was observed in both γ single and β-γ coincidence spectrum. This line corresponds to the known 1^+ state in ^{46}V [2]. The branching ratio of this GT decay was determined to be 0.216 ± 0.050 and the half-life of ^{46}Cr was determined to be 240 ± 140 ms, which is consistent with the previous value, 260 ± 60 ms [1]. Thus, we obtained the log ft value of $3.78^{+0.10}_{-0.13}$ for this GT decay, using a weighted average of the ^{46}Cr half-life (257 ± 55 ms). This corresponds to the B(GT) value of 0.64 ± 0.20. The result is compared with other experimental data in the vicinity of ^{46}Cr and shell model calculations in the full pf shell space in this talk.

References

[1] J. Zioni et al., Nucl. Phys. **A181**, 465 (1972)

[2] C. Friessner et al., Phys. Rev. **C60**, 011304 (1999)

Gamow-Teller beta decay of ^{46}Cr

T. K. Onishi [1], A. Gelberg [2], H. Sakurai [1],
K. Yoneda [3], N. Aoi [3], N. Imai [3], H. Baba [4],
P. von Brentano [2], N. Fukuda [3], Y. Ichikawa [1],
M. Ishihara [3], H. Iwasaki [1], D. Kameda [5], T. Kishida [3],
A. Lisetskiy [7], H. J. Ong [1], M. Osada [1], T. Otsuka [1],
M. K. Suzuki[1], K. Ue[1], Y. Utsuno [6], and H. Watanabe [3]

1. Department of Physics, University of Tokyo,
2. Institut fuer Kernphysik der Universitaet zu Koeln,
3. RIKEN, 4. Rikkyo University, 5. Tokyo Institute of Technology,
6. Japan Atomic Energy Research Institute,
7. NSCL, Michigan State University

Introduction

- ^{46}Cr is a nucleus of A=4n+2(n:integer),N=Z-2.
- These nuclei decay with strong GT transitions.← Wigner's SU(4) symmetry

  (cf. GT transitions of the nuclei of A=4n,N=Z-2 are forbidden.)
- The gap of the B(GT) values between ^{42}Ti and ^{50}Fe is large.

  →What about ^{46}Cr?

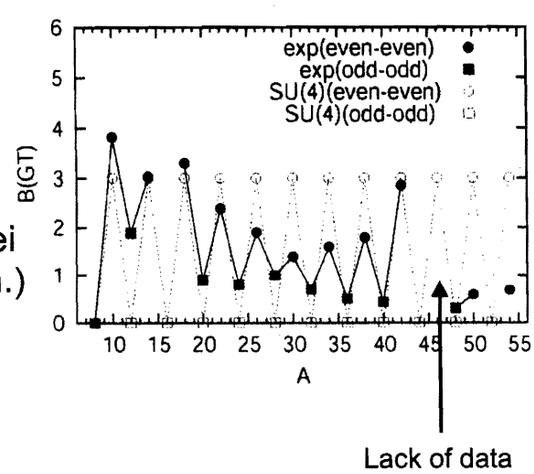

Purpose of this experiment

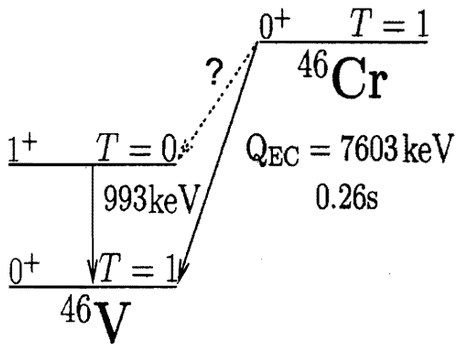

✓ ^{46}Cr

(J. Zioni et al., Nucl. Phys. A 181(1972) 465)

- half-life: 260±60ms
- Only Fermi decay was observed
  (^{46}Cr $0^+ \rightarrow {}^{46}$V 0^+)

✓ ^{46}V

(C. Frissner et al., Phys. Rev. C 60,011304(1999))

- Recently, 1^+ state at 993 keV has been found with in-beam γ spectroscopy.

^{46}Cr can decay with GT transition to this 1^+ state of ^{46}V

→observation of the 993 keV β-delayed γ-ray
→determination of B(GT) (branching ratio, half-life)

Experimental setup
～beam line～

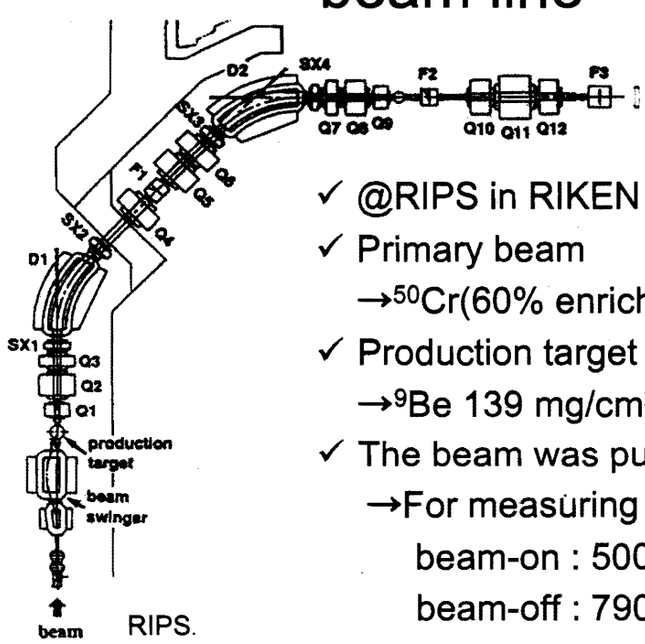

✓ @RIPS in RIKEN

✓ Primary beam
→^{50}Cr(60% enriched),80AMeV,5pnA

✓ Production target
→^{9}Be 139 mg/cm^2

✓ The beam was pulsed
→For measuring the half-life of ^{46}Cr
beam-on : 500ms
beam-off : 790ms

Particle identification

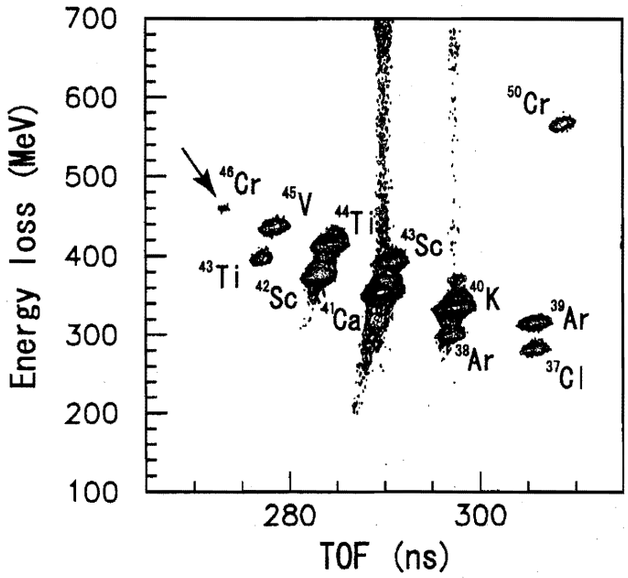

Purity of ^{46}Cr
→0.1%
Intensity of ^{46}Cr
→20cps

Experimental setup
～detectors～

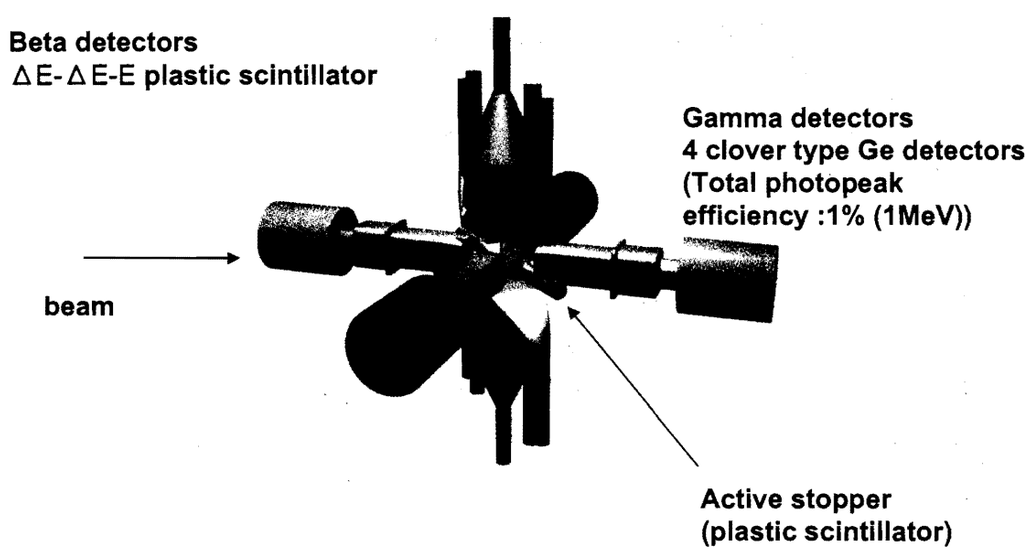

Observation of the β-delayed-γ-ray of ^{46}Cr

Without β coincidence

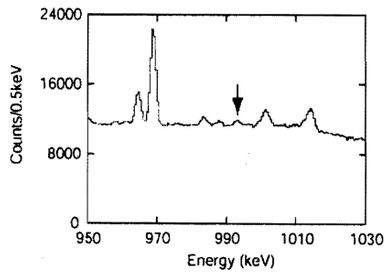

With β coincidence

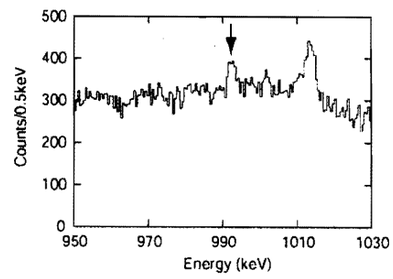

- In both spectra, there is a gamma line at 993 keV
  →The 993 keV γ-ray is a β-delayed γ-ray.
- 993 keV is the energy of 1^+ state of ^{46}V.

Half-life

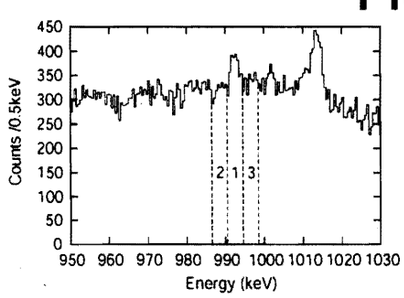

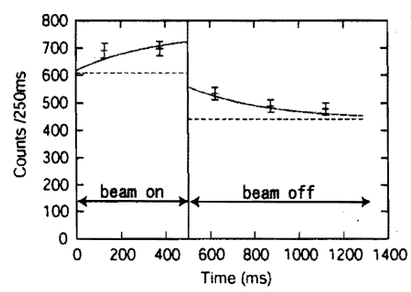

- The photopeak→1
- The backgrounds→2,3
- The dead time correction (by random trigger)
  Half-life: 240±140 ms cf. the previous value 260±60 ms

A GT transition of ^{46}Cr has been observed for the first time.

GT branching ratio

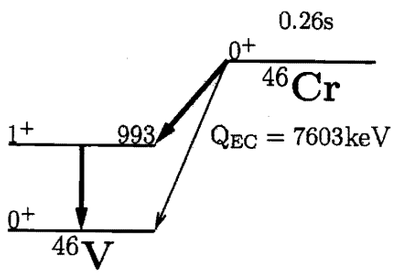

Fig.8 decay scheme of ^{46}Cr (this work)

$$b_\beta = \frac{\dfrac{N_{count}}{\varepsilon_\gamma \times d_c}}{N_{46Cr}}$$

b_β: branching ratio of GT transition to the 1^+ state in ^{46}V
N_γ: number of counts in the 993 keV peak
e_γ: total photopeak efficincy
N_{46Cr}: Total number of implanted ^{46}Cr fragments

RESULT

b_β=0.216±0.050

log *ft*,*B*(GT)

- Half-life (weighted average) :0.257±0.055 s
- Partial half-life :1.19±0.37 s
- *f*-value :4980
- *ft*=5926±1842 s

log *ft*=3.78 (+0.11,-0.17)

$$B(GT) = \frac{K}{(g_A / g_V)^2 ft}$$

$K = 6145\,\mathrm{sec}$

$g_A / g_V = -1.267$

B(GT)=0.64±0.20

cf. B(F;^{46}Cr,$0^+ \rightarrow {}^{46}$V,0^+)=1.75±0.37

Discussion1

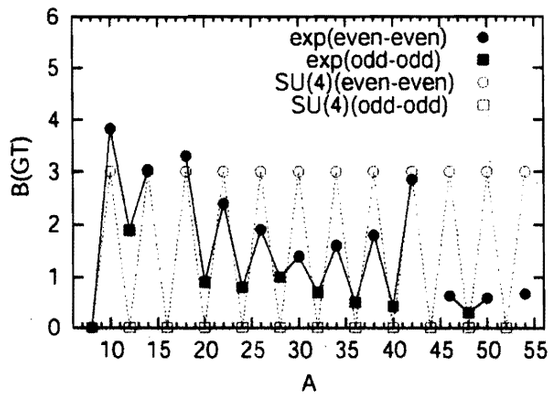

- The B(GT) value of ^{46}Cr is smaller than lighter nuclei and near to the value of ^{50}Fe.
- An effect of deformation?

(^{46}V is a deformed nucleus.)

Discussion2

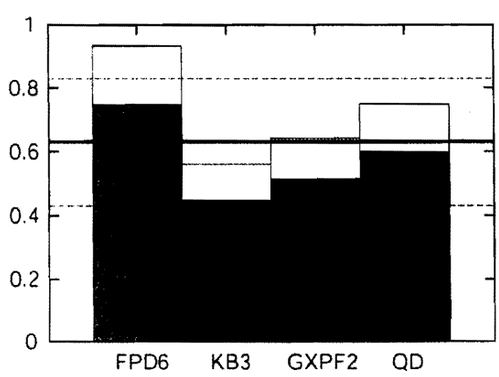

Theoretical calculations and exp data
(open box: unquenched
filled box: quenched(0.8)
redline: experimental data)

- Theoretical calculations
  shell model
  FPD6,KB3,GXPF2
  quasideuteron model
- Theoretical calculations reproduce the experimental data.

Summary

- The GT transition of ^{46}Cr to the 1^+ state in ^{46}V has been observed for the first time.
- The branching ratio of this GT transition was determined. Its value is 0.216 ± 0.050.
- The GT strength was deduced, $B(GT)=0.64 \pm 0.20$.
- The B(GT) value is smaller than lighter nuclei and near to the value of ^{50}Fe.
- Theoretical calculations reproduce the experimental data.

g-Factor measurements of high-spin isomers and condensed matter studies with γ-TDPAD method

H. Watanabe, H. Ueno, A. Yoshimi, Y. Kobayashi, T. Haseyama, T. Kishida
RIKEN (The Institute of Physical and Chemical Research), 2-1 Hirosawa, Wako, Saitama 351-0198, Japan

K. Asahi, D. Kameda, H. Miyoshi, K. Shimada, S. Emori, G. Kato
Department of Physics, Tokyo Institute of Technology, 2-12-1 Oh-okayama, Meguro, Tokyo 152-8551, Japan

Y. Gono
Department of Physics, Kyushu University, Fukuoka 812-8581, Japan

A. Odahara
Nishinippon Institute of Technology, Kanda, Fukuoka 800-03, Japan

A large number of isomeric states with various lifetimes and spins have been discovered so far. In general, an isomeric state produced by a heavy-ion fusion reaction is highly oriented due to the large orbital angular momentum brought in perpendicularly to the direction of projectile. It is well known that the angular distribution of the γ ray from the oriented state is anisotropic for a nuclear spin $I \geq 1$. Suppose such an aligned isomer is subjected to an extranuclear field B_{eff}, the angular distribution rotates around the magnetic field axis with the Larmor frequency $\omega_L = g\mu_N B_{eff}/\hbar$, where μ_N is the nuclear magneton. A nuclear g-factor can be derived from the measured ω_L if the magnitude of B_{eff} is precisely known. On the other hand, information about the hyperfine field can be obtained with a known g-factor. Thus, aligned isomeric states formed in nuclear reactions become excellent probes for studies of nuclear moments and/or condensed matter physics.

High-spin isomers have been systematically observed for $N = 83$ isotones with $60 \leq Z \leq 66$. By means of conventional γ-ray spectroscopic studies, it has turned out that the excitation energies of these high-spin isomers are nearly constant. Among these isomers, however, both the magnetic dipole and electric quadrupole moment have been measured only in ^{147}Gd so far; the configuration and the deformation parameter were determined to be $[\pi(h^2_{11/2}(d^{-2}_{5/2})_0) \otimes \nu(f_{7/2}h_{9/2}i_{13/2}(d^{-2}_{3/2})_0)]_{49/2^+}$ and $\beta = -0.19$, respectively. It is worth extending this kind of study to other $N = 83$ isotones to investigate the mechanism producing the yrast traps at very high spin. We have measured the g-factors of the high-spin isomers in ^{143}Nd ($T_{1/2} = 35$ ns) and ^{149}Dy ($T_{1/2} = 28$ ns) by combining the recoil-shadow and the γ-ray time-differential perturbed angular distribution (TDPAD) techniques with the pulsed beam method. The experimental results indicate that the g-factors of these high-spin isomers slightly increase as the atomic numbers Z decrease.

Furthermore, we plan to develop spin-aligned isomers as secondary beams and to apply them to condensed matter studies. A series of intermetallic Ce compounds reveal very interesting physical phenomena caused by the competition between the RKKY interaction and the Kondo effect. The $I^\pi = 10^+$ isomer in ^{134}Ce ($T_{1/2} = 308$ ns) is appropriate to the investigation of the hyperfine fields at Ce site. In this symposium, we also introduce the application of this isomeric beam to the microscopic study of the ferromagnet $CeRh_3B_2$ compound which has an anomalously high Curie temperature $T_C = 115$ K.

g-Factor measurements of high-spin isomers and condensed matter studies with γ-TDPAD method

Hiroshi Watanabe

Applied Nuclear Physics Laboratory,
The Institute of Physical and Chemical Research

Outline

- Introduction
- g-Factor measurements of the high-spin isomers in ^{149}Dy and ^{143}Nd
- Condensed matter studies with the spin-aligned ^{134}Ce isomeric beam

Spin-oriented isomers as probes for studies of nuclear moment and solid-state physics

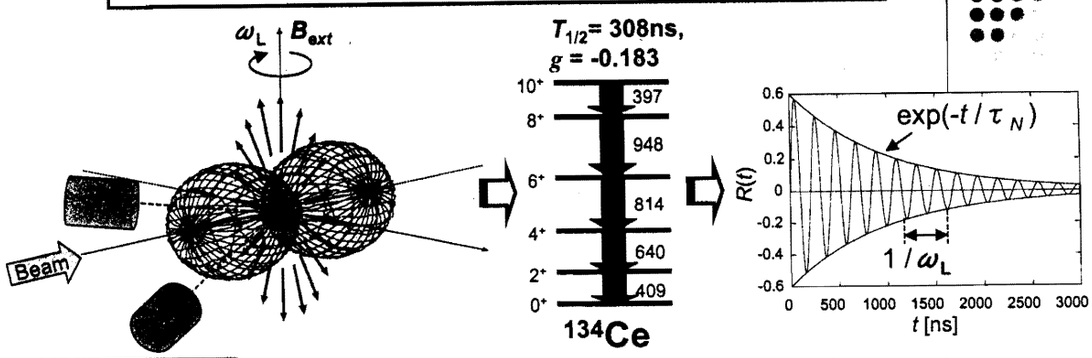

Larmor frequency

$$\omega_L = \frac{g_N \mu_N B_{ext} \beta(T)}{\hbar}$$

β **known** → **Isomeric g-factor** → Nuclear structure: **• Configuration of the isomer** (Core-excitation, -polarization effect, etc.)

g **known** → **Local susceptibility**

$$\chi_{loc} = \beta(T) - 1 = \frac{g_J (J+1) \mu_B B(0)}{3 k_B T}$$

→ Material science: **• Local moment**

Nuclear relaxation time

$$\tau_N^{-1} = \frac{2(J+1)\{g_N \mu_N B(0) \hbar\}^2}{J} \tau_J$$

→ **4f electron spin fluctuation**

$$\tau_J^{-1} = \frac{4\pi}{\hbar} \{D_c(\varepsilon_F) J_{cf}(T)\}^2 k_B T$$

→ Material science: **• Exchange interaction**

Systematics of the high-spin isomers in N=83 isotones

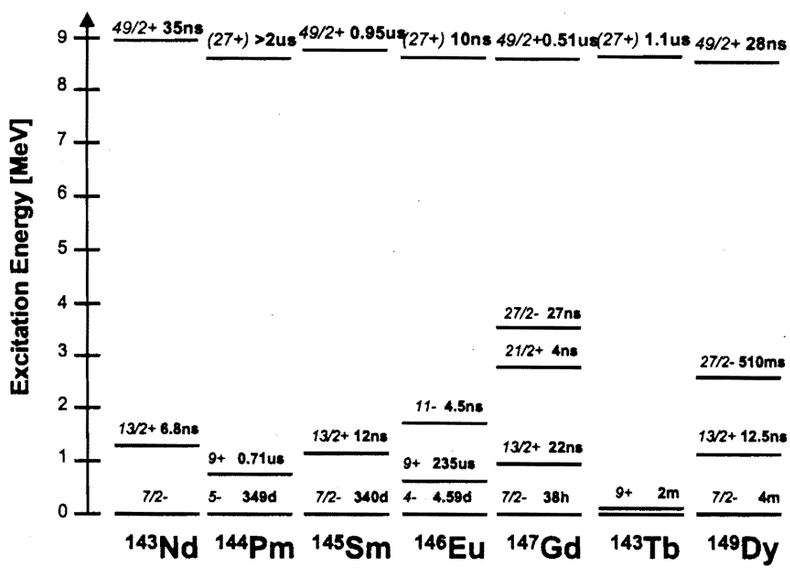

g-Factor measurements of the high-spin isomers in ^{149}Dy and ^{143}Nd

- **High-spin isomer in ^{149}Dy (Z = 66)**

  E_{ex}= 8.52 MeV, $T_{1/2}$ = 28 ns
  I = (47/2, 49/2) not determined

  Y. Gono *et al.*, Eur. Phys. J. **A13** (2002) 5-8

- **High-spin isomer in ^{143}Nd (Z = 60)**

  E_{ex}= 8.98 MeV, $T_{1/2}$ = 35 ns,
  I^p = 49/2$^+$ ⟵ Angular distribution + Linear polarization

  X. H. Zhou *et al.*, Phys. Rev. **C61** (1999) 014303

[redacted]

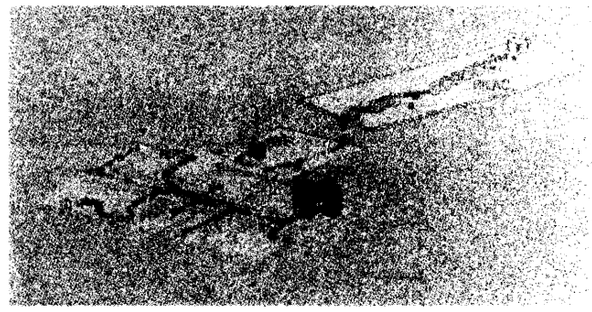

RIKEN Accelerator Research Facility (RARF)

Injector : RIKEN Heavy-ion Linac (RILAC)
Main accelerator : K540 RIKEN Ring Cyclotron (RRC)

Production of the high-spin isomer in ^{149}Dy
- ✧ Projectile : ^{132}Xe 7.0 MeV/u, $T = 1\,\mu s$
- ✧ Target : natural Mg of 6.0 mg/cm^2 thickness

Production of the high-spin isomer in ^{143}Nd
- ✧ Projectile : ^{136}Xe 7.6 MeV/u → 6.5 MeV/u, $T = 1\,\mu s$
- ✧ Target : ^{12}C of 1.7 mg/cm^2 thickness

Experimental setup for the measurement of g-factors

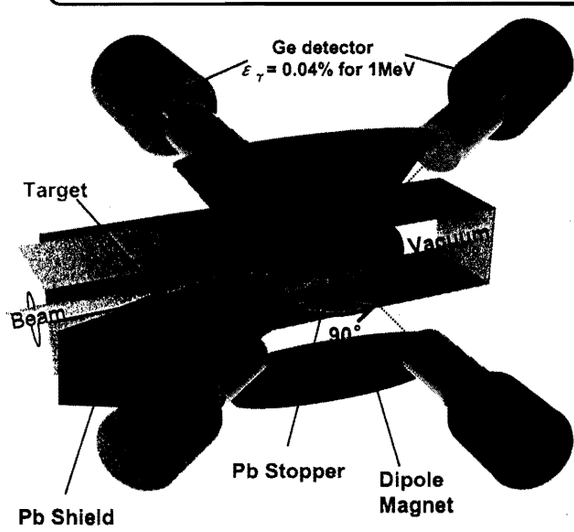

① **Inverse reaction & Recoil shadow method**
➡ Only γ rays emitted through isomeric states can be detected
② Spin relaxation control
(Ⅰ) **Recoil into Gas** ➡ Suppress the nuclear spin relaxation during flight
(Ⅱ) **Stopper heating system** ➡ Make the relaxation time long after stopping

[redacted]

γ-ray Time-Differential Perturbed Angular Distribution (TDPAD) technique

Intensity of γ ray : $N(t,\theta_r,B_{eff}) = N_0 \exp\left(-\frac{\ln 2}{T_{1/2}}\cdot t\right) W(t,\theta_r,B_{eff})$

Angular distribution : $W(t,\theta_r,B_{eff}) = \sum_{k,even} B_k(I) A_k(\gamma) P_k[\cos(\theta_r - \omega_L \cdot t)]$

$$R(t,\theta_r,B_{eff}) = \frac{N(t,\theta_r,B_{eff}) - N(t,\theta_r+\pi/2,B_{eff})}{N(t,\theta_r,B_{eff}) + N(t,\theta_r+\pi/2,B_{eff})}$$

$$\cong \frac{3A_{22}}{4+A_{22}}\cos[2(\theta_r - \omega_L \cdot t)] \quad \text{for } k \le 2$$

ω_L : Larmor frequency

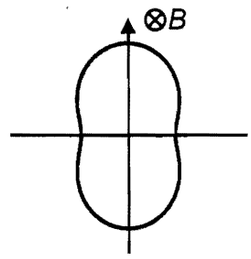

g factor : $g = \frac{\hbar\omega_L}{\mu_N B_{eff}}$

$B_{eff} = B_{ext} + B_{int} = \beta(T) B_{int}$

$\beta(T)$: Paramagnetic Correction Factor $\quad \beta(T) = 1 + \frac{g_J(J+1)\mu_B B(0)}{3k_B T}$

Calibration of the paramagnetic field

For Dy^{3+} ion : J = 15/2, g_J = 4/3

calibrated with the known g-factor of the isomeric state in ^{152}Dy (produced concurrently with the ^{149m}Dy)

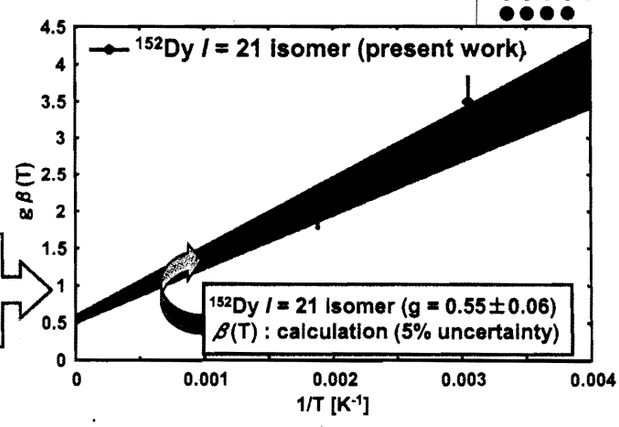

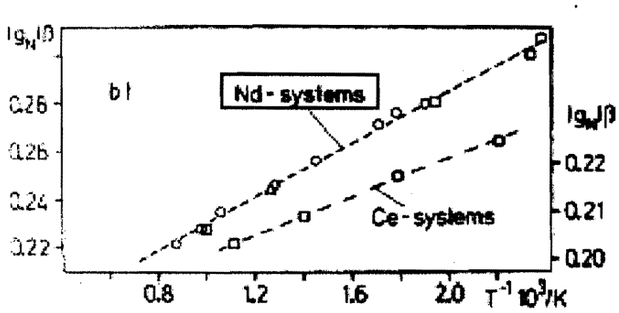

For Nd^{3+} ion : J = 9/2, g_J = 8/11

calibrated with
$B(0)$ = 3.51(10) MG
for Nd^{3+} ion given by D.Riegel *et al.*

Result for the high-spin isomer in ^{149}Dy

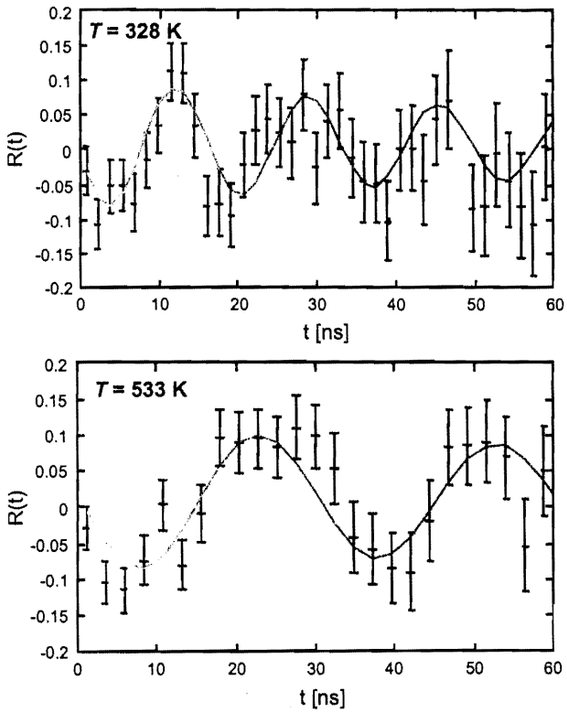

T [K]	ω_L [rad/ns]	β	[redacted]
328	0.19(2)	6.4(9)	[redacted]
533	0.11(2)	3.6(5)	[redacted]

g_{exp} = 0.41(6)

Nucl. Phys. **A 728** (2003) 365

Result for the high-spin isomer in ^{149}Nd

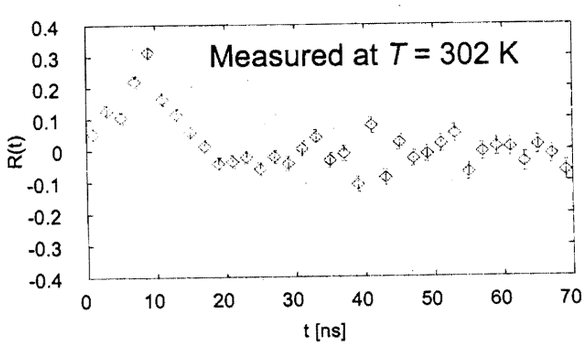

ω_L = 0.082(6) rad/ns, τ_N = 11(3) ns

g_N = 0.56(4)

consistent

Estimation of τ_N for Nd in Pb

$$\tau_N = \frac{J \cdot \hbar^2}{2(J+1)\{g_N \mu_N B(0)\}^2} \cdot \frac{1}{\tau_J}$$

$$\frac{1}{\tau_J} = \frac{4\pi}{\hbar}(NJ_c)^2 k_B T\left[1 + 2(2J+1)NJ_c \cdot \ln\left(\frac{k_B T}{D'}\right)\right]$$

$NJ_c = -0.04$

$D' = 104 meV$

$B(0) = 3.51 MG$ for Nd^{3+} ion in Sn and Pb given by D.Riegel *et al.*

$J = 9/2$

g_N = 0.56

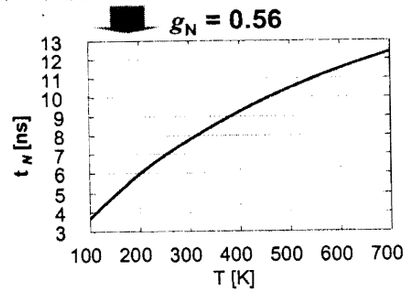

τ_N = 8 ns @T = 302 K

Overview of the experimental g-factors of the high-spin isomers in N = 83 isotones

^{143m}Nd : g_{exp} = 0.56(4)
^{147m}Gd : g_{exp} = 0.446(8)
^{149m}Dy : g_{exp} = 0.41(6)

Main configuration

$[\pi(h^2_{11/2}) / \nu(f_{7/2}\, h_{9/2}\, i_{13/2})]_{49/2+}$
g_{cal} = 0.46

* $g_l(\pi)$ = 1.1, $g_l(\nu)$ = -0.03, g_s = 0.6g_s(free)

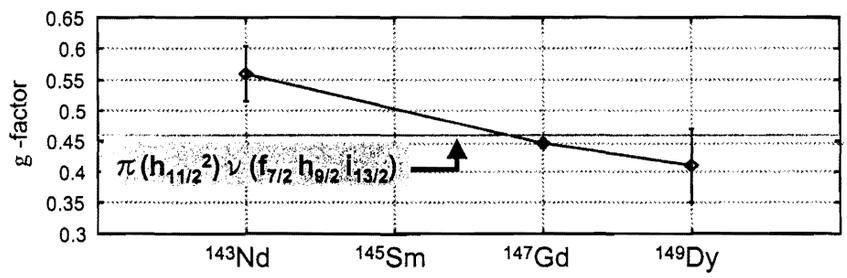

The observed g-factors gradually increase as the proton number decreases !

The investigation is now in progress .....

Condensed matter studies with the spin-aligned ^{134}Ce isomeric beam

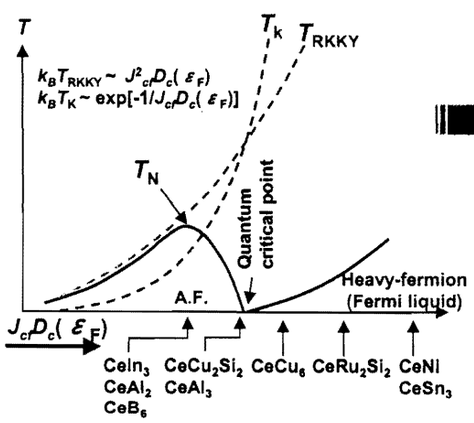

Many interesting physical phenomena can take place in Ce-based compounds and alloys.

Why Ce beam ?

Information on both static and dynamic hyperfine fields at Ce sites can be obtained.

Anomalous ferromagnetism in **$CeRh_3B_2$** → **T_c = 115 K**

the highest Curie temperature among known Ce-based compounds with nonmagnetic constituents

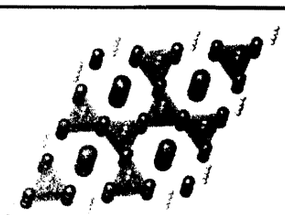

- **Ce local moment**
- **4f spin fluctuation**

→ Mechanism producing the anomalous ferromagnetism can be unveiled.

Production of the spin-aligned [illegible]

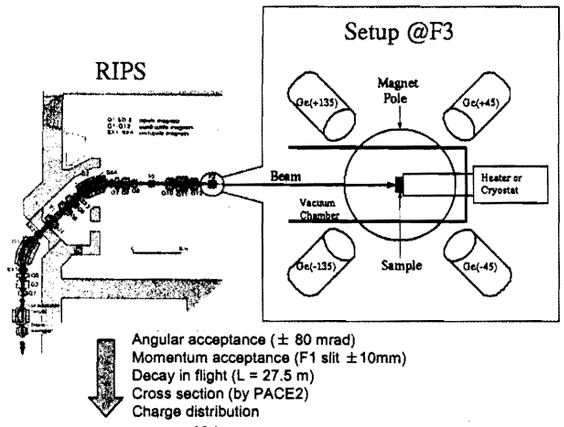

Angular acceptance (± 80 mrad)
Momentum acceptance (F1 slit ±10mm)
Decay in flight (L = 27.5 m)
Cross section (by PACE2)
Charge distribution

Yields of ^{134m}Ce (Q = 48+) @F3

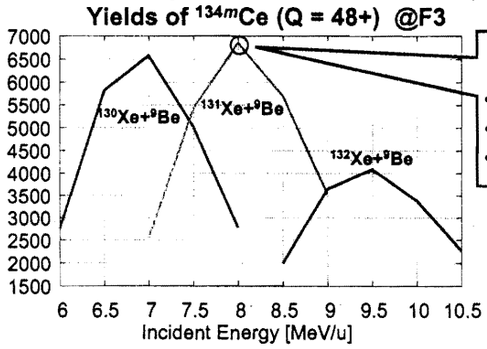

Fusion reaction with inverse-kinematics
- Low energy beam
- Charge state distribution

Very strong hyperfine fields are produced by the atomic electrons

Keep the initial nuclear alignment by transporting only Ce ion which has the Ne-like atomic shell ($^1S_0$)

Optimal condition for the production of $^{134m}Ce^{48+}$
- Projectile : ^{131}Xe, E = 8 MeV/u, I = 5 pnA (T = 3 μs)
- Target : ^{9}Be, 7.5 μm
- Reaction : ^{9}Be(^{131}Xe, 6n) ^{134m}Ce (Isomer ratio = 17 %)

^{134m}Ce intensity @F3 ... 6.9×10^3 /s

Summary

Spin-aligned isomers become excellent probes for studies of nuclear moments and condensed matter studies.

g-Factor measurements of high-spin isomers

g(^{149m}Dy) = 0.41 ± 0.06

g(^{143m}Nd) = 0.56 ± 0.04

Main configuration of the high-spin isomers in N = 83 isotones

$$[\pi\ (h_{11/2}{}^2) \otimes \nu\ (f_{7/2}h_{9/2}i_{13/2})]$$

The g-factors of these isomers gradually increase as the proton number decreases.

Condensed matter studies with spin-aligned isomeric beams

^{134}Ce isomeric beam will be developed.

$CeRh_3B_2$ (T_c = 115 K) will be studied in near future.

Acknowledgements

- *RIKEN*
  H. Ueno, W. Sato, A. Yoshimi, Y. Kobayashi, T. Haseyama, T. Kishida
- *Tokyo Institute of Technology*
  K. Asahi, D. Kameda, H. Miyoshi, K. Shimada, S. Emori, G. Kato
- *Kyushu University*
  Y. Gono
- *Nishinippon Institute of Technology*
  A. Odahara

γ-ray spectroscopy with 6 Clover detectors at Tohoku ISOL

M.Fujita, T.Endo, T.Miyake, A.Yamazaki, T.Sonoda*, T.Suzuki*, A.Goto*, Y.Miyashita*, N.Sato*, E.Tanaka, H.Tamura* and T.Shinozuka

Cyclotron and Radioisotope Center, Tohoku University, Sendai, Japan
*Department of Physics, Tohoku University, Sendai, Japan

The new detectors for precise $\beta - \gamma$ and $\gamma - \gamma$ spectroscopy measurements have been installed in combination with the ion-guide technique at Tohoku ISOL facility. The ion-guide is a kind of ion source for the ISOL and has a great advantage of widely applicable to any elements. Recently, a new type of the ion-guide system called "RF ion-guide" have been developed to obtain higher efficiency. The new RF ion-guide system provides us more neutron-rich unstable nuclei produced by proton-induced fission reactions.

A high resolution and large solid angle γ-ray detection system has been developed with six clover-type HPGe detectors and BGO Compton suppressors. The clover detector consists of four coaxial n-type Germanium crystals of 50 mm diameter and 70 mm length mounted in a common cryostat. The average photopeak efficiency of the individual crystals at 1.33 MeV is 2.58×10^{-4} at 25 cm from the ^{60}Co source, whereas the total photopeak efficiency in add-back mode is 16.1×10^{-4}, which corresponds to 122 % of the relative efficiency. A new goniometer for 6 clover detectors has been constructed and placed at 2 m higher place than the ISOL beam line. The permanent magnet for the measurement of the perturbed angular correlation has been located at the center of the goniometer. The mass-separated unstable nuclei are transferred to the magnet position from ISOL beam line by the tape transport system.

By combination of the RF ion-guide and the newly developed γ-ray detection system, several experiments are planned. For example, a search for ^{78}Ni and a precise $\beta - \gamma$ spectroscopy around this region in addition to the nuclear g-factor measurement for the low lying isomeric states of short-lived isotopes are planned.

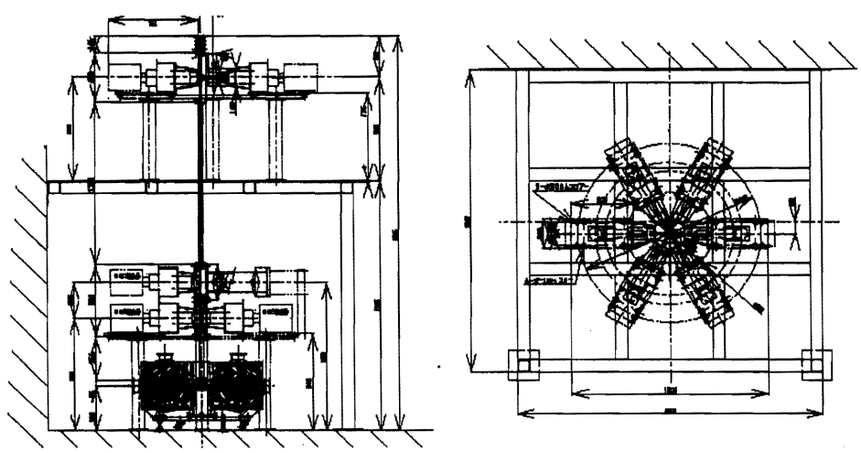

Figure 1: 6 clover detectors and PAC system for mass-separated neutron-rich unstable nuclei

γ - ray spectroscopy with 6 clover detectors at Tohoku ISOL

M.Fujita , T.Sonoda*,T.Endo, T.Miyake, A.Yamazaki, T.Suzuki*, A.Goto*,
Y.Miyashita*, N.Sato*, E.Tanaka, T.Otsuki*, H.Tamura* and T.Shinozuka

Cyclotron and Radioisotope Center , Tohoku University
* Department of Physics, Tohoku University

- clover -type HPGe Detectors
- RF-IGISOL method
- Application of Clovers + RF-IGISOL
  (PAC system for the g-factor measurement)
- Future Experiments

Clover Detectors at CYRIC

6 clover-type HPGe detectors have been installed in 2001.

In April 2004, all 6 detectors will be able to use simultaneously.

Each detector consists of four coaxial N-type Ge detectors, arranged like a four leaf clover.

dimension : 51 mm ϕ × 71 mm (for each crystal)

active volume : 470 cm^3 (89% of the original crystal volume)

Ge-Ge distance : ~ 0.5 mm

the distance from the surface to end cap : 20 mm

the end-cap : Be (2 mm thick)

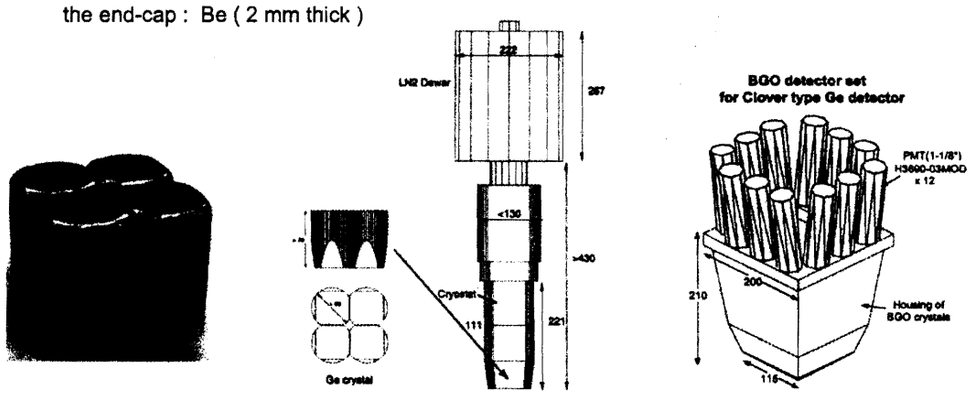

BGO Compton Suppression Shields

The Compton-suppressors consist of 12 crystals of BGO ($Bi_4Ge_3O_{12}$)

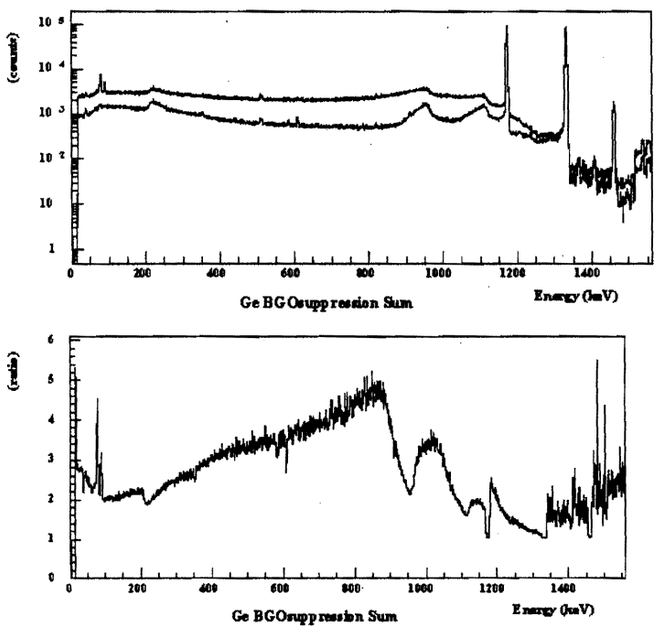

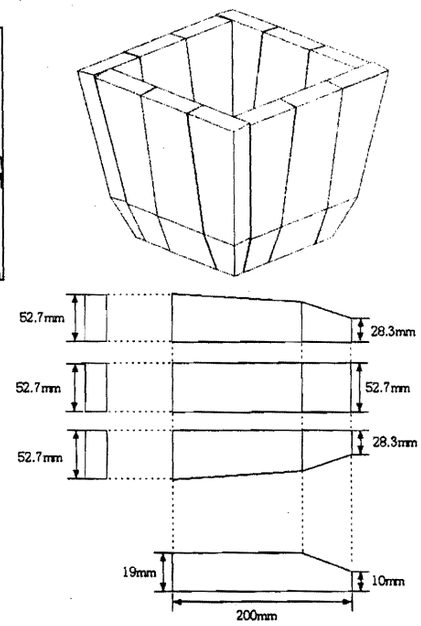

specifications for the clover detectors

PULCLO #1

	03 April 2003			
	#1	#2	#3	#4
Resolution in keV at 1.33 MeV	1.93	2.07	1.87	2.01
Resolution in keV at 122 keV	1.01	1.17	1.08	1.02
Resolution in keV at 14 keV	1.01	1.17	1.08	1.02
Relative efficiency in %	19.4 %	19.5 %	19.5 %	20.5 %
Peak to Compton ratio	47.0	43.6	48.8	44.7
FWTM / FWHM	1.80	1.89	1.85	1.87
FWFM / FWHM	2.42	2.60	2.45	2.51

122 % in add-back mode

Improvement of the clover detector

The electronic flashes broke the FET in many times

- **Stop electronic flashes**
  - Electronic components
  - High voltage-ground proximity
  - Different materials

  (at the end, the mounted detector has been measured at 5000 V without electronic flashes)
- **Reinforce Eurifet and improve it to reduce restore time without any resolution degradation.**

  The inner Eurifet restore was restored by an external restore transistor

  The restore time is currently almost 3 μs for a saw signal amplitude of 12 V

Ion-Guided Isotope Separator On-Line (IGISOL)

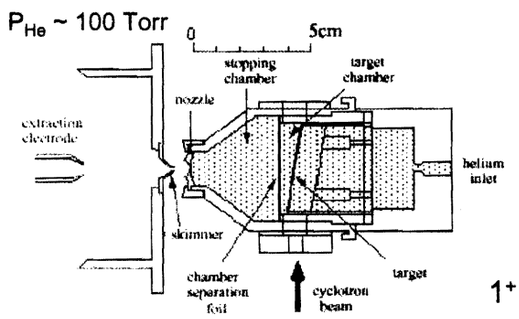

reaction products or fission products are stopped in the He gas atmosphere

↓

most ions **remain in 1^+ state**

(He 1st ionization energy : 24.6 eV)

↓

1^+ ions are transferrd by He gas flow

Advantages of the IGISOL method
• Applicable to any elements (no limitation)
• Stable operation

Low efficiency (< 0.1 %) ⟶ RF-IGISOL method

- Low stopping power in He gas
- ions are collected by gas flow only

- Use Large Volume Gas Cell
- gas flow + DC&RF electric field

RF-IGISOL(2)

The volume of the gas cell is 1000 times larger than the original one

- ions are transferred by DC field
- 100 ring electrodes (RF-carpet) make the barrier

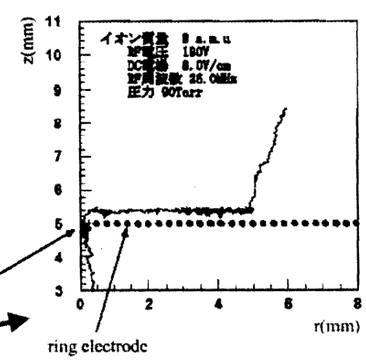

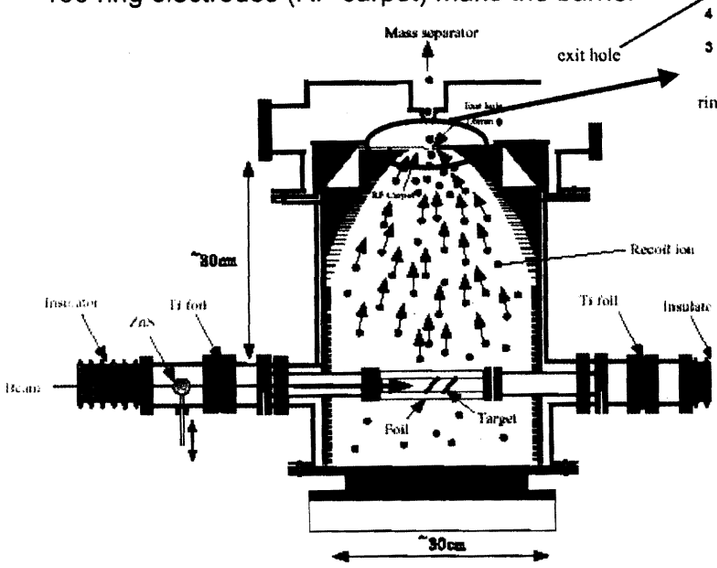

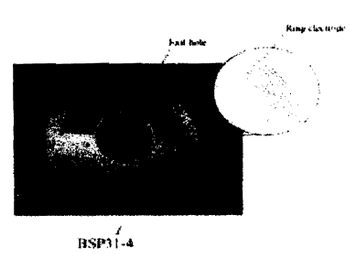

^{238}U (p,f) E_p = 50 MeV, I_p = 10 nA - 3μA

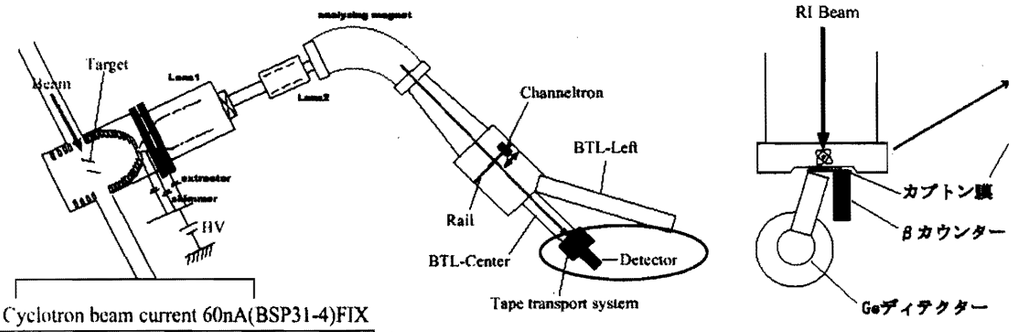

Cyclotron beam current 60nA(BSP31-4)FIX

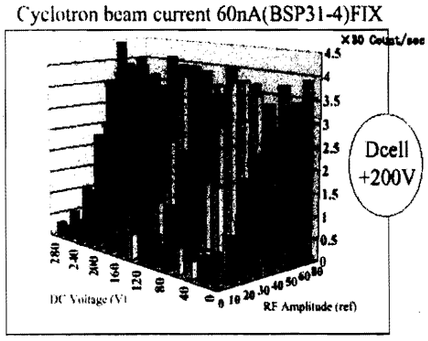

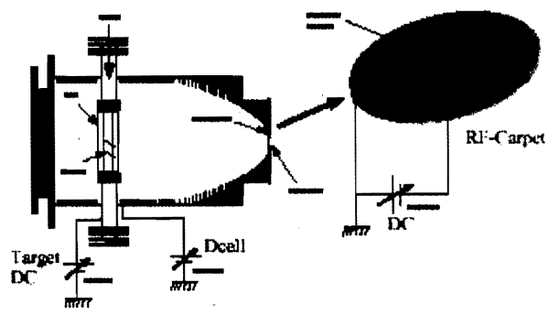

Mass = 100 β-ray counts

a slit at the focal plane was removed

Mass 100 region

Yields **^{99}Y 5.2 ± 1.0 ions/μC,mb**

^{100}Y 10 ± 0.6 ions/μC,mb

A=100領域で質量分離されたRIと収量

ガンマ線で確認できた核

cf. ^{97}Y 1.8 ions/μC,mb by old IGISOL

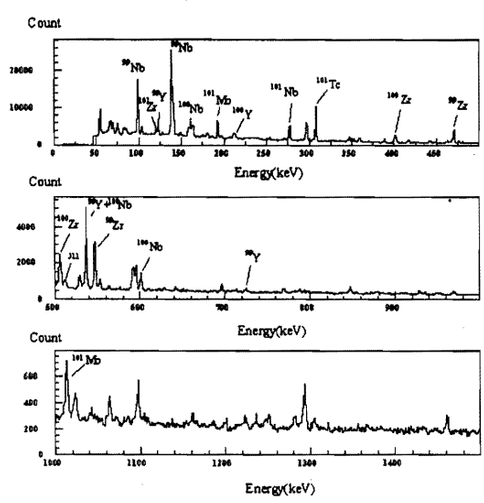

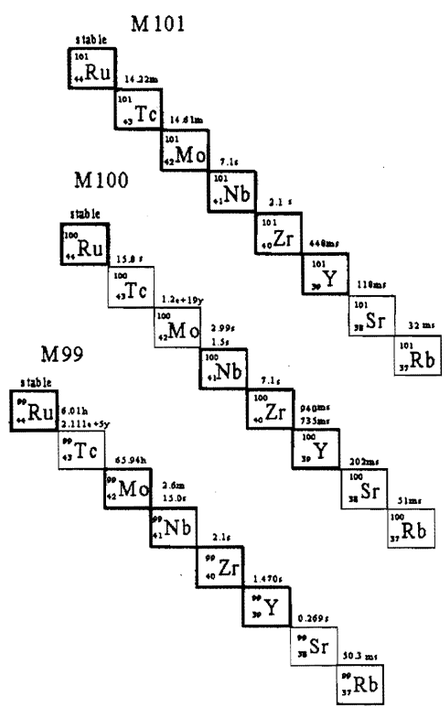

PAC Measurement system

applications of "RF-IGISOL" + " 6 clovers"

- g-factor measurement of the low-lying isomer states of the N-rich RIs

Perturbed Angular Correlation method for nano-second isomer

6 Clover-type HPGe Detectors + goniometer + 1.2 T permanent magnet

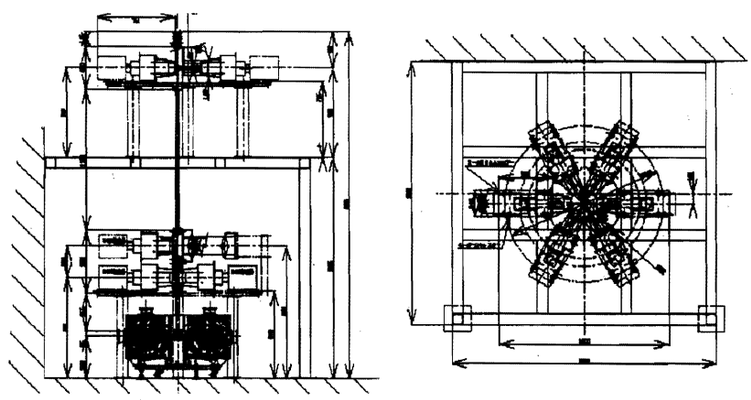

Future Experiment 1
g-factor measurement of ^{134}I (79.5 keV, $T_{1/2}$=1.62 ns) state

^{238}U (p,f) reaction at E_p = 50 MeV

σ (^{134}Te) = 16.3 mb $\quad Y_{RF\text{-}IGISOL}$ ~ 240 [ions / s]

N_{coin} ~ 500 events / day

configuration of the first 3$^+$ state is expected to
$(\pi d_{5/2})\,(\nu s_{1/2})^{-1}$ or $(\pi d_{5/2})\,(\nu d_{3/2})^{-1}$

g ~ +1.02 $\qquad$ g ~ +1.24

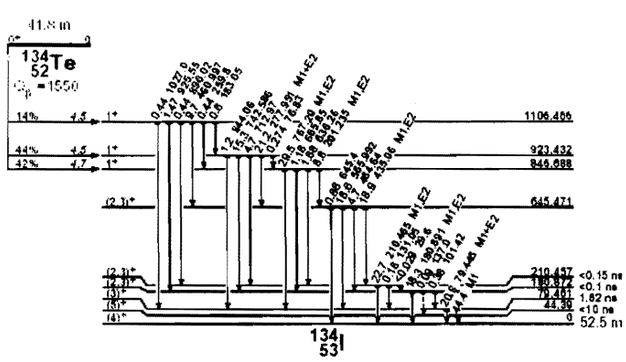

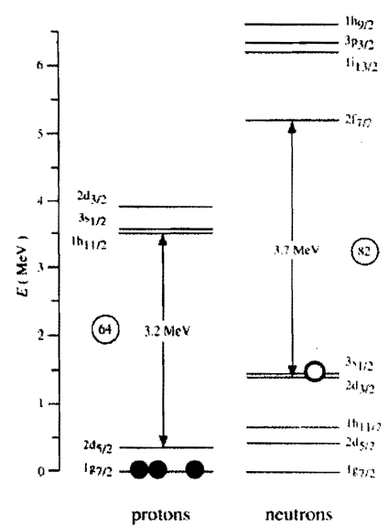

Future Experiment 2
Magnetic field measurement of ^{99}Tc in C_{60}

^{100}Mo(γ,n)^{99}Mo @ LNS in Tohoku Univ.

g (5/2$^+$) = +3.62(5) I.Alfter et.al. ZP A347 1(93)

$$g = -\frac{\hbar\omega_L}{\mu_N B_{eff}}.$$

known g-factor → deduce the magnetic field in materials

How much does the magnetic field change in Fullerenes ??

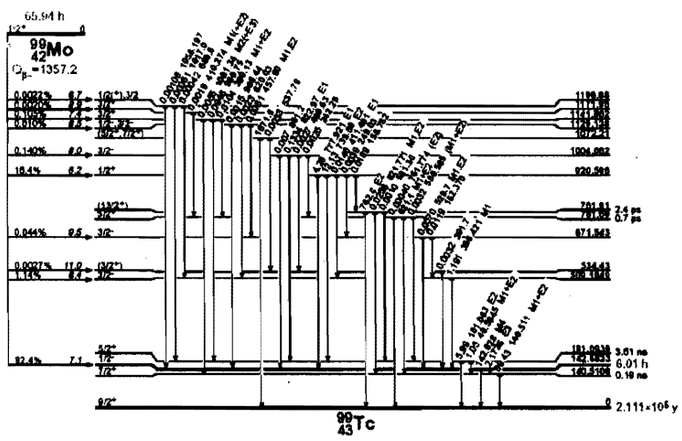

Summary

- 6 clover-type HPGe detectors with BGO Compton suppressors have been installed in CYRIC
- In April 2004, all clover-detectors will be abailable.
- The RF-IGISOL method has been developed in CYRIC. (JPS : 28pZB-1 T.Sonoda)
- The PAC measurement system which consist of 6 clovers, a goniometer and a permanent magnet has been constructed.
- g-factor measurements (^{134}I 79.5keV state & ^{99}Tc in C_{60}) are planned.

Results of the Offline/Online experiments

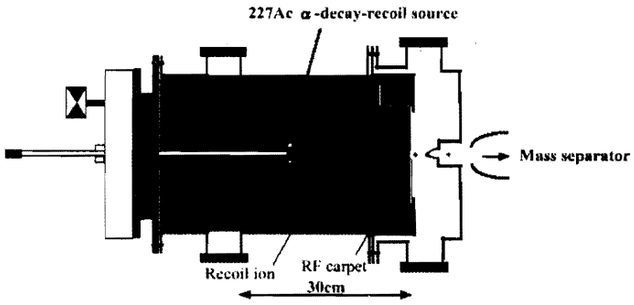

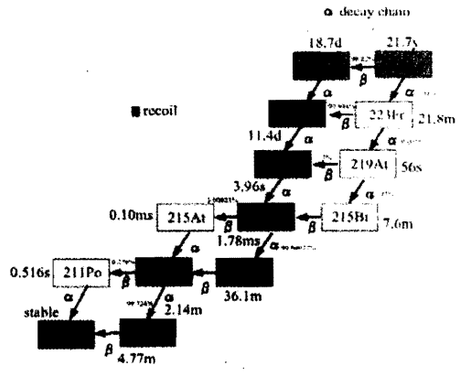

α-decay-recoil nuclei are emitted into the gas cell

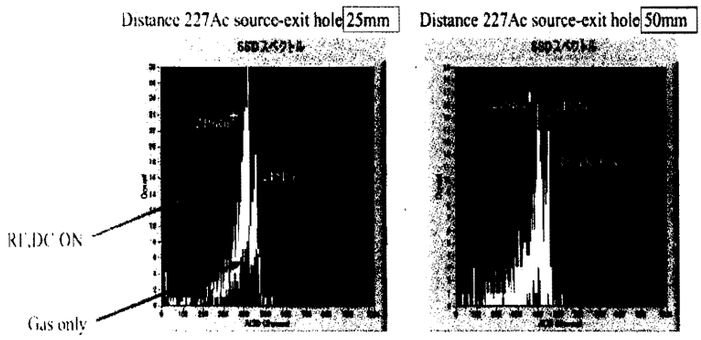

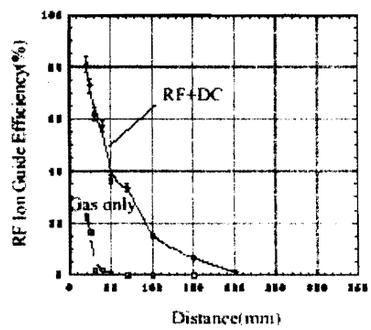

A new experimental technique for B(E2) measurement of ^{16}C

N. Imai[A], H.J. Ong[B], N. Aoi[A], H. Sakurai[B], K. Demichi[C], H. Kawasaki[C], H. Baba[C], Zs. Dombrádi[D], Z. Elekes[A1], N. Fukuda[A], Zs. Fülöp[D], A. Gelberg[E], T. Gomi[C], H. Hasegawa[C], K. Ishikawa[F], H. Iwasaki[B], E. Kaneko[C], S. Kanno[C], T. Kishida[A], Y. Kondo[F], T. Kubo[A], K. Kurita[C], S. Michimasa[G], T. Minemura[A], M. Miura[F], T. Motobayashi[A], T. Nakamura[F], M. Notani[G], T.K. Onishi[B], A. Saito[C], S. Shimoura[G], T. Sugimoto[F], M.K. Suzuki,[B], E. Takeshita[C], S. Takeuchi[A], M. Tamaki[G], K. Yamada[C], K. Yoneda[A2], H. Watanabe[A], and M. Ishihara[A]

RIKEN[A], Univ. of Tokyo[B], Rikkyo Univ.[C], ATOMKI[D], Universität zu Köln[E], Tokyo Inst. of Tech.[F], CNS, Univ. of Tokyo[G]

In the present work, the mean lifetime τ of the 2_1^+ state in an unstable nucleus ^{16}C has been directly measured by a new experimental technique. The τ is inversely proportional to the reduced transition probability, $B(\mathrm{E2};2_1^+ \rightarrow 0_1^+)$. The technique essentially follows the recoil shadow method (RSM) [1], which has been applied to the charged-particle decays with velocities of $\beta \simeq 0.01$. Instead, we applied the concept of the RSM to deexcitation γ rays from inelastically excited ^{16}C with a velocity of $\beta \simeq 0.3$.

If the τ is 50 ps and $\beta = 0.3$, the mean decay length, $\beta\gamma c\tau$, has a macroscopic distance of 4.7 mm. In the case, when one puts a lead plate surround the target and places γ-ray detectors to make their detection efficiencies sensitive to the position of deexcitation by using a shadowing effect of the lead plate, the τ can be determined by measurement of the γ-ray yields.

The experiment was performed at the RIKEN accelerator research facility. A radioactive beam of ^{16}C was produced by the projectile fragmentation reaction of a 100 MeV/nucleon ^{18}O beam. The ^{16}C beam was separated by the RIPS beam line and bombarded on a Be target of 370 mg/cm^2-thickness to excite the beam. The ^{16}C beam had a typical intensity of 2×10^5 particles per second. The average energy in the target was 34.6 MeV/nucleon. The target was surrounded by a 5 cm-thick lead plate. The de-excitation γ rays from the inelastically excited ^{16}C nuclei were detected by two rings of NaI(Tl) scintillation detectors composed of rectangular crystals with volume of $6 \times 6 \times 12$ cm^3. The centers of rings were set at polar angles of 121° and 102°, respectively, from the target position with respect to the beam direction.

The τ has been determined to be 77 ± 14(sta)±19(sys) ps. The central value of τ corresponds to B(E2) of 0.26 Weisskopf units [4], which is smallest among all the known B(E2) values of the other even-even nuclei. The new experimental method will be reported and the B(E2) obtained will be discussed through comparison with the global systematics between the excitation energies and B(E2) values [5], and theoretical works [6, 7].

References

[1] H. Backe, *et al.*, Phys. Lett. **B285**, 159 (1978).
[2] T. Motobayashi, *et al.*, Phys. Lett. **B346**, 9 (1995).
[3] H. Scheit, *et al.*, Phys. Rev. Lett. **77**, 3967 (1996).
[4] N. Imai, et al., Phys. Rev. Lett. **92**, 062501 (2004).
[5] S. Raman, C.W. Nestor, Jr., and K.H. Bhatt, Phys. Rev. C **37**, 805 (1988).
[6] Y. Kanada-En'yo and H. Horiuchi, Phys. Rev. C **55**, 2860 (1997).
[7] R. Fujimoto, Ph.D. thesis, Univ. of Tokyo (2003).

[1] On leave from ATOMKI, Debrecen, Hungary.
[2] Present address: NSCL, Michigan State University, USA.

A new experimental technique for B(E2) measurement of ^{16}C

Nobuaki IMAI
RIKEN

Known B(E2;2^+->0^+)

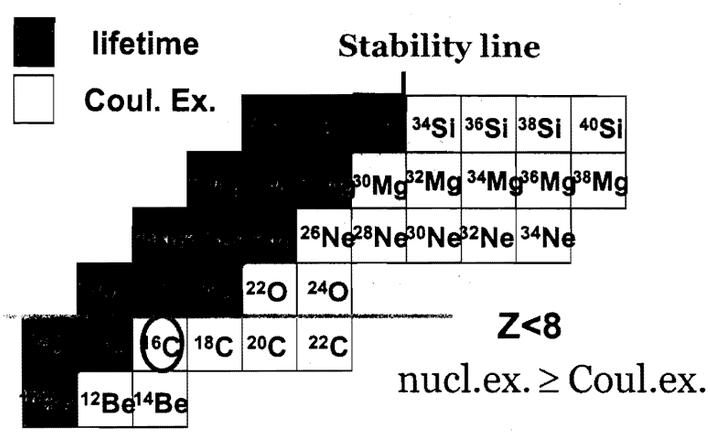

nucl.ex. ≥ Coul.ex.

New method for B(E2) measurement of ^{16}C is needed

Mean lifetime measurement

- **Inelastic Scattering of RI beams**
- **High velocity** (β=0.3)
  - ⇨ $\lambda = \beta\gamma\tau c$
    $\approx 1.0\text{cm}(\tau = 100\text{ps}, \beta = 0.3)$
- **Thick lead shield**
  - ⇨ γ-ray path is different
  - ⇨ effective efficiency is different
    $\mathcal{E} = \exp(-\mu\, l)$ μ: attenuation coeff. l: path length in lead

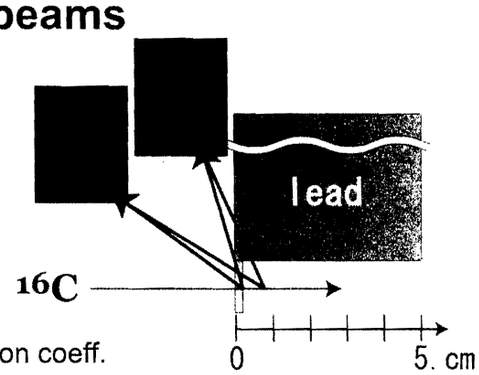

R1/R2 ratio ⇨ Mean life τ

Experimental setup

RIPS beam line in RIKEN

target: 370 mg/cm^2 ^{9}Be
beam: ^{16}C of 34.6 AMeV, 200kcps
lead: 5-cm thickness
γ-ray detector: 32 NaI(Tl)
R1: 14xNaI(Tl) 121 deg.
R2: 18xNaI(Tl) 102 deg.

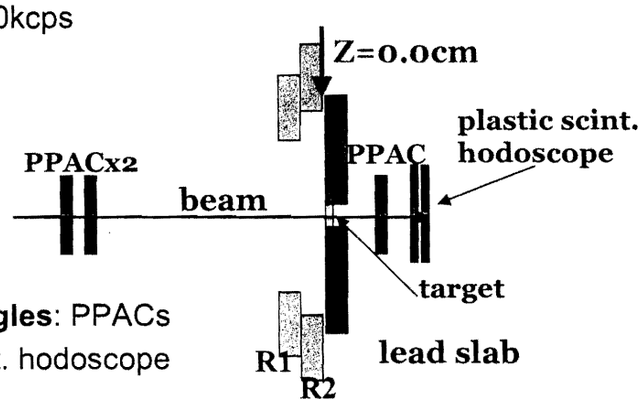

incoming and outgoing angles: PPACs
PID of ejectiles: plastic scint. hodoscope

Energy spectrum of γ ray

Doppler uncorrected Spectrum of R1

Shape: GEANT simulation

Background: Exponential

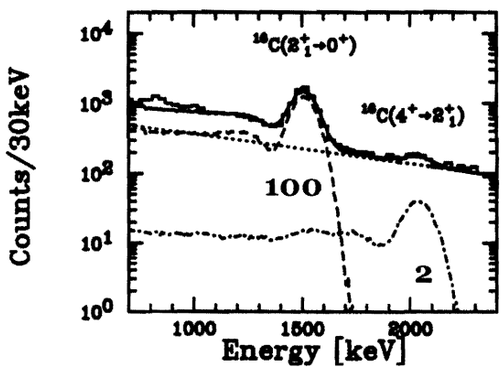

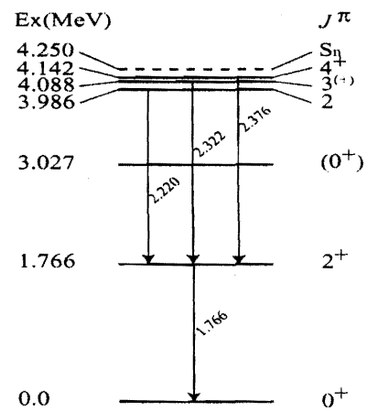

Level scheme of ^{16}C

Monte Carlo Simulation

GEANT 3 code

Geometry

energy dependence (^{137}Cs, ^{22}Na, ^{60}Co)

position dependence (^{22}Na z=0.0-2.0cm)

Beam profile

experimentally obtained parameters for emittance and scattering angles

Angular distribution of γ rays

ECIS79 with optical potential sets for $^{12}C+^{12}C$ @35AMeV and $^{16}O+^{12}C$@38AMeV

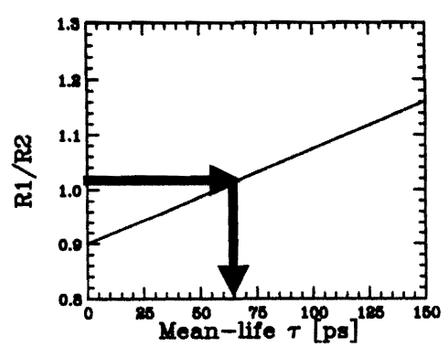

Mean lifetime of $^{16}C(2^+)$

Cross check (Target: Z=0.0 and 1.0 cm)

	R1/R2	τ [ps]
Z=1.0	1.70 ± 0.06	63 ± 17
Z=0.0	1.06 ± 0.03	92 ± 22

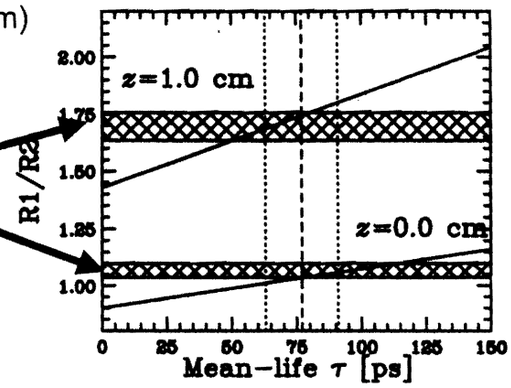

Hatched zone: measured R1/R2 ratio

Solid line: Monte Carlo simulation

Weighted average= 77 ±14 [ps]

Systematic error: 25%

target position (20%) + optical pot. (5%)

$$\tau = 77 \pm 14(\text{stat}) \pm 19(\text{syst})\ [\text{ps}]$$

N. Imai et al, PRL92,062501('04)

2004/19/March gamma04

Comparison with systematics

^{16}C: $B(E2\downarrow)$ = 0.63 e^2fm^4
= 0.26 [W.u.]

$$B(E2)_{sys} = 6.47 \times E^{-1.0} Z^2 A^{-0.69}$$

S. Raman et.al.,PRC37, 805 ('88).

^{16}C: $B(E2)/B(E2)_{sys}$ = 0.032

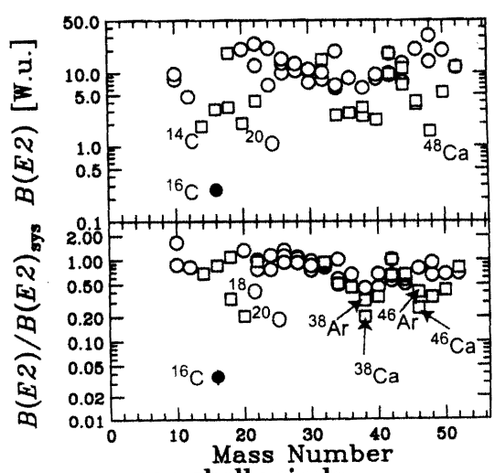

open-shell : circle
closed-shell : square

Anomalously hindered $B(E2)$

2004/19/March gamma04

Theoretical Calculations

- **AMD Calc.**

  proton/neutron ↔ oblate/prolate (?)

  e.g.) Y. Kanada-Enyo, PRC 55, 2860 (1997)

  B(E2) = 1.3 e^2fm^4

  (Y. Kanada-E'nyo private com.)

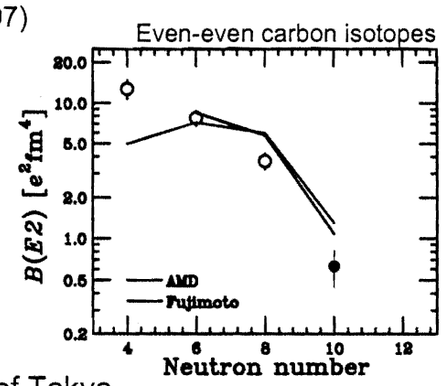

- **Shell model Calc.**

  small effective charge of n (?)

  e.g.) Q-moment of ^{15,17}B

  H.Izumi et al, PLB366, 51('96)

  H. Ogawa et al, PRC67, 64308('03)

  large proton shell gap (?)

  e.g.) R. Fujimoto PhD. Thesis Univ. of Tokyo

Fujimoto int.+ Sagawa-Asahi effective charges (e_p~1.15e e_n~*0.1e*)

B(E2) = 1.1 e^2fm^4

Other experiments of ^{16}C

- **Inelastic scattering on Pb**

Interference between nucl. and Coul. Excitation

Angular distribution of $d\sigma/d\Omega$

⇨ δ_M/δ_C=3.1+/-0.5

Absolute value of $d\sigma/d\Omega$

⇨ δ_C = 0.42 +/- 0.05 fm

(B(E2↓)=0.28(6)e^{2}fm^4)

Z. Elekes et al., PLB in press

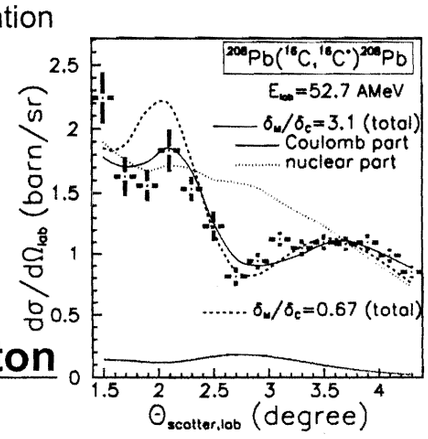

- **Inelastic scattering on proton**

H.J. Ong et al., to be submitted to PLB

Summary

- New experimental technique to directly measure lifetime of the excited state
- The mean-life of $^{16}C(2^+)$ is determined to be
  $\tau = 77 \pm 14(\mathrm{stat}) \pm 19(\mathrm{syst})$ [ps]
- The corresponding B(E2) is anomalously small.
- The same B(E2) value is obtained from the inelastic scattering on Pb.

Collaborators

N. Imai[1], H.J. Ong[2], N. Aoi[1], H. Sakurai[2], K.Demichi[3], H.Kawasaki[3], H.Baba[3],Zs. Dombradi[4], Z. Elekes[1], N. Fukuda[1], Zs. Fulop[4], A.Gelberg[5], T. Gomi[3], H. Hasegawa[3], K. Ishikawa[6], H. Iwasaki[2], E. Kaneko[3], S. Kanno[3], T. Kishida[1], Y. Kondo[6], T. Kubo[1], K. Kurita[3], S. Michimasa[7], T. Minemura[1], M. Miura[6], T. Motobayashi[1], T. Nakamura[6], M. Notani[7], T.K. Ohnishi[2], A. Saito[3], S. Shimoura[7], T. Sugimoto[6], M.K. Suzuki[2], E. Takeshita[3],S. Takeuchi[1], M. Tamaki[7], K. Yoneda[1], H. Watanabe[1], and M. Ishihara[1]

[1] RIKEN, Japan, [2]Univ. of Tokyo, Japan, [3]RIkkyo Univ. Japan, [4]ATOMKI, Hungary, [5]Univ. of Koln, Germany, [6]Tokyo Int. Tech. Japan, [7]CNS, Univ. of Tokyo, Japan

In-beam Gamma-ray Spectroscopy of Neutron-rich Nucleus ^{23}F

S. Michimasa[A], S. Shimoura[A], H. Iwasaki[B], M. Tamaki[A], N. Aoi[C], H. Baba[D], N. Iwasa[E], S. Kanno[D], S. Kubono[A], K. Kurita[D], M. Kurokawa[C], T. Minemura[C], T. Motobayashi[C], M. Notani[A], H.J. Ong[B], S. Ota[F], A. Saito[D], H. Sakurai[B], S. Takeuchi[C], E. Takeshita[D], Y. Yanagisawa[C], A. Yoshida[C]

[A] *Center for Nuclear Study, University of Tokyo*
[B] *Department of Physics, University of Tokyo*
[C] *RIKEN*
[D] *Department of Physics, Rikkyo University*
[E] *Department of Physics, Tohoku University*
[F] *Department of Physics, Kyoto University*

Neutron-rich fluorine isotopes are interesting in their features. The stability of neutron-rich isotopes remarkably changes between oxygen and fluorine isotopes. The fluorine isotopes are extended up to ^{31}F with $N = 22$ beyond the magic number of $N = 20$ while the heaviest oxygen isotope is ^{24}O with $N = 16$. For understanding this feature, it is essential to investigate proton/neutron shell structures in the nuclei.

The present study aims at searching single proton states in neutron-rich fluorine isotope ^{23}F. We have, hence, measured de-excitation γ rays from the excited states in ^{23}F via the proton transfer reaction, ^{4}He(^{22}O,^{23}F). The experiment was performed at the RIPS beam line in RIKEN. The secondary beam of ^{22}O was produced by a projectile fragmentation reaction of 63-MeV/nucleon ^{40}Ar beam with a ^{9}Be target, and bombarded a liquid helium target[1] of 100 mg/cm^2. The mean energy of ^{22}O was 35 MeV/nucleon, and its intensity was 2×10^3 particles/s on average. The ^{22}O ions and contaminating beam particles were identified event-by-event using ΔE and TOF. Reaction products were identified from TOF, ΔE, and E, which were measured by a telescope consisting of 9 SSDs and 36 NaI(Tl) scintillators[2]. Furthermore, de-excited γ rays from the reaction products were detected by 150 NaI(Tl) scintillators[3] surrounding the secondary target.

In the talk, I introduce the details of this experiment and reported its preliminary results.

References

[1] H. Akiyoshi et al.: RIKEN Accel. Prog. Rep. **34**, 193 (2001).
[2] M. Tamaki et al.: CNS-REP-59, 76 (2003).
[3] S. Takeuchi et al.: RIKEN Accel. Prog. Rep. **36**, 148 (2003).

In-Beam Gamma-ray Spectroscopy of Neutron-rich Nucleus ^{23}F

S.Michimasa, S.Shimoura, H.Iwasaki[1], M.Tamaki, N.Aoi[2], H.Baba[3] N.Iwasa[4], S.Kanno[3], S.Kubono, K.Kurita[3], M.Kurokawa[2], T.Minemura[2], T.Motobayashi[2], M.Notani, H.J.Ong[1], S.Ota[5], A.Saito[3], H.Sakurai[1], E.Takeshita[3], S.Takeuchi[2], Y.Yangisawa[2], A.Yoshida[2]

Center for Nuclear Study, University of Tokyo.
[1]Department of Physics, University of Tokyo.
[2]RIKEN(The Institute of Physical and Chemical Research).
[3]Department of Physics, Rikkyo University.
[4]Department of Physics, Tohoku University.
[5]Department of Physics, Kyoto University.

Contents

- Motivation
- Experiment and Its Setup
- Analyses
  - a) Secondary Beams
  - b) Outgoing Particles
  - c) Gamma-rays
- Results and Discussions
- Summary

Motivation

Neutron Drip lines of Z~8

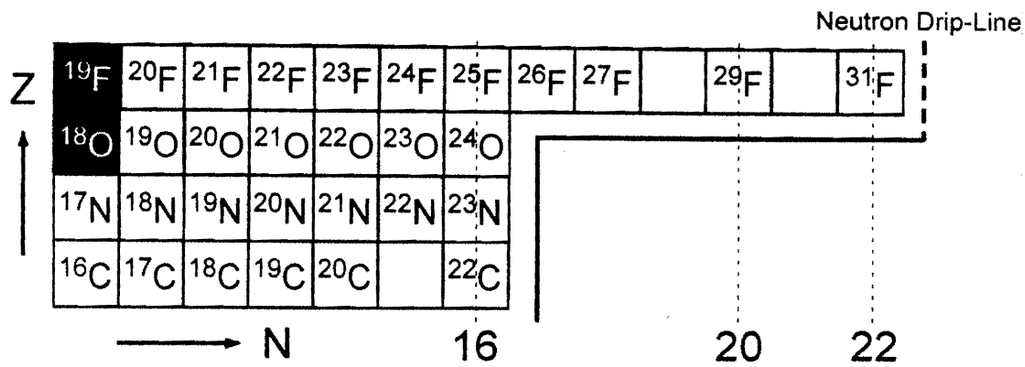

Z=8 to Z=9 : Neutron Shell Changes Attractively!

As the Function of Neutron Numbers,
Proton Shell Changes??

Motivation

○ To Investigate on the Proton Shell in Fluorine Isotopes.

⇒Search for **Single Particle States**.

Approaching by **Proton Transfer Reaction**

Experimental Target : ^{23}F

- 6 Known Excited States (Resolution: ~50keV)
- No J^{π} information on ^{23}F.
- Transfer Reaction onto Unstable Nucleus ^{22}O with Inverse Kinematics.
- Excitation Energy Determined by De-excited γ-rays.

Experiment

Measurement :

Three Different Reaction Approaching $^{23}F^{*}$

- $^{4}He(^{22}O,^{23}F\gamma)$: Proton Pickup Reaction
- $^{4}He(^{23}F,^{23}F\gamma)$: Inelastic Scattering
- $^{4}He(^{24}F,^{23}F\gamma)$: Fragmentation

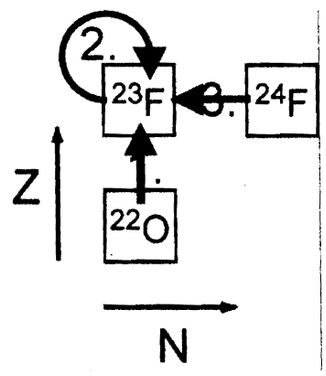

Experimental Setup

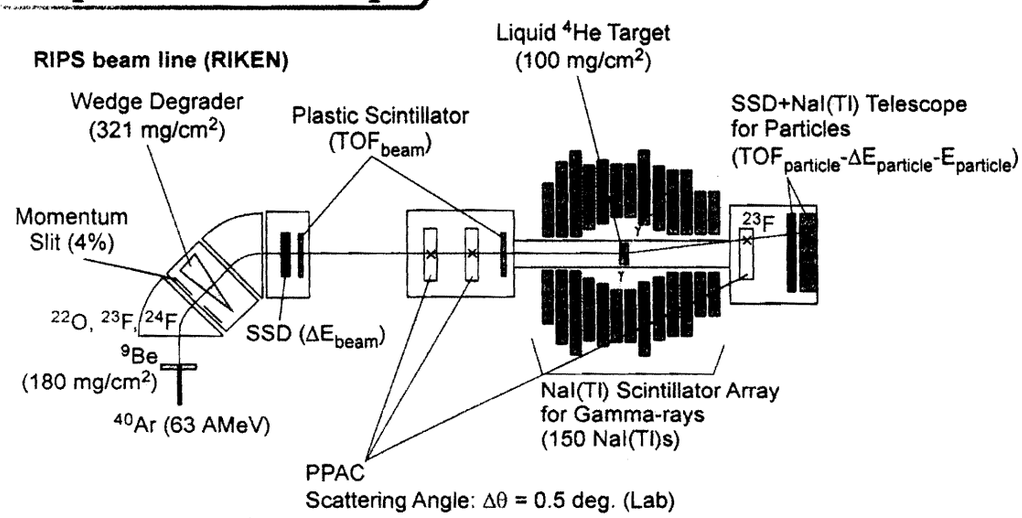

Beam Particle Identification: TOF_{beam}-ΔE_{beam}
Outgoing Particle Identification: $TOF_{particle}$-$\Delta E_{particle}$-$E_{particle}$

Analysis: Secondary Beams

Property of Secondary Beams

Produced by Fragmentation Reaction of $^{40}Ar + ^{9}Be$

Secondary Beam	^{22}O	^{23}F	^{24}F
Beam Energy	35*A* MeV	41.5*A* MeV	36*A* MeV
Momentum Spread	4 %	4 %	4 %
Purity	42.0 %	12.8 %	6.9 %
Intensity [counts/sec]	2×10^3	6×10^2	3×10^2
Measurement Period	3 days		

Analysis: Outgoing Particles

SSD-NaI(Tl) Telescope for Outgoing Particles

• Schematic View

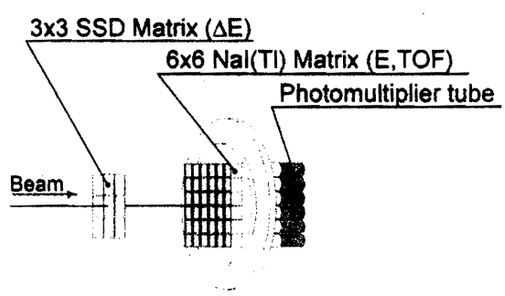

Acceptance:
θ_{scat} = 0-6 deg. (Lab. flame)

• Particle Identification for F isotopes

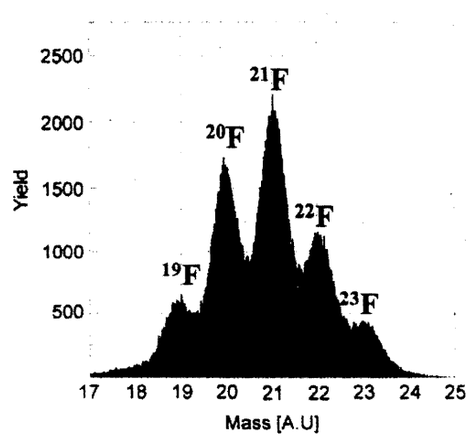

Mass Resolution : σ_{mass} = **0.34**

Analysis: Gamma-rays

NaI(Tl) Scintillator Array for γ-rays

Specifications

- **150** NaI(Tl) Crystals
- Surrounding a secondary target:
  θ_{lab} = **20-160** degrees.
- Efficiency for γ-rays:
  17.6% for 1.33-MeV γ-ray (^{60}Co)
- Energy Resolution for Moving Particles:
  8.2%(σ) for 3.2-MeV γ-rays
  from $^{22}O(2_1^+ \rightarrow 0_1^+)$ at β = 0.27.

Photograph taken at the position of the secondary target.

Result & Discussion I: Gamma-ray Spectra

- **Comparison with γ-ray Spectra**

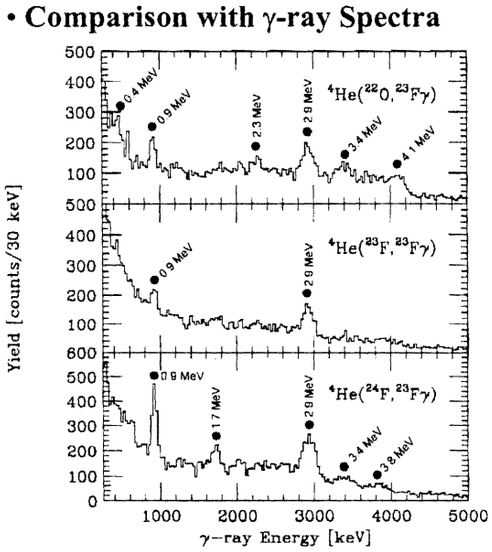

4.1-MeVγ is a candidate of de-excited γ from a single particle state!

- **γ-γ Coincidence Events**

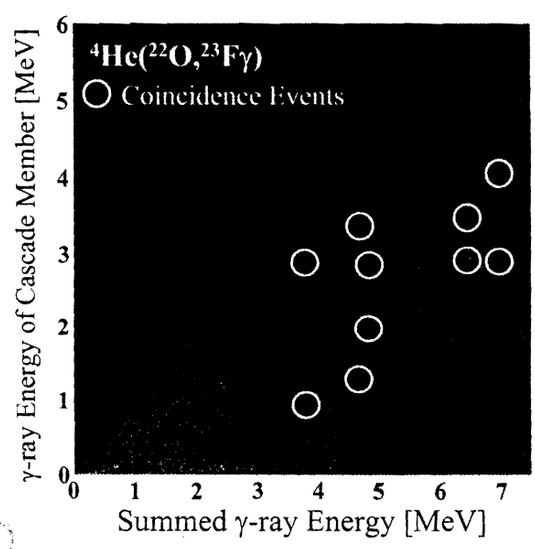

Result & Discussion II: Level Scheme of ^{23}F

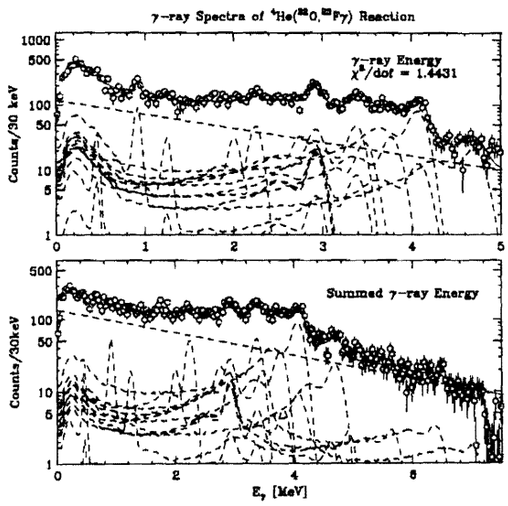

Reconstruction of Gamma-Energy Spectra
by Simulated Response Functions

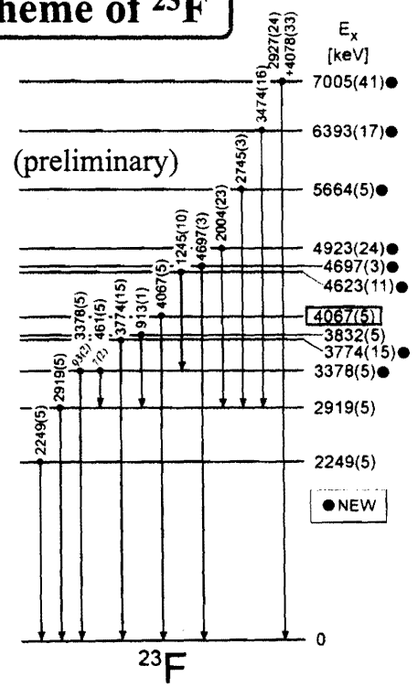

Next Step in Analysis

Angular distribution for the 4.1-MeV state

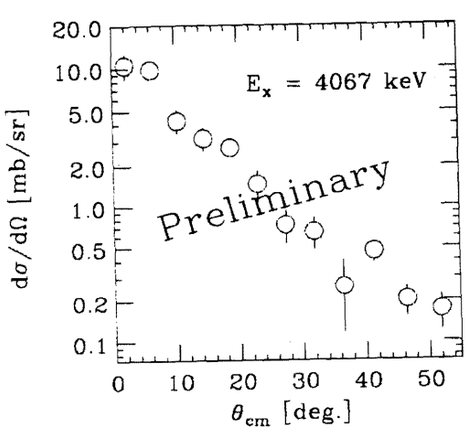

To deduce J^{π} of excited states by DWBA analysis.

Search for adequate optical potentials
e.g. Global potentials modified
by inelastic scattering on ^{22}O.

Summary

- Measurement of De-excited γ-rays in ^{23}F by Proton Transfer Reaction onto ^{22}O.
  [additionally (^{23}F,$^{23}F\gamma$) and (^{24}F,$^{23}F\gamma$)]
- Candidate of Single Particle State at 4.067 MeV.
- Level Scheme of ^{23}F Constructed by γ-γ Events.
- Comparison of Angular Distributions with DWBA for J^{π} Assignments and S-factors.

Liquid Helium Target

Specification of Liquid Helium Target

- Thickness : 100 mg/cm^2
- Size : 30 mm diameter
- Window : 6-mm Havor
- Cryostat : Keeping at 4K
  [Melting Point of ^{4}He is at 4.2K @ 1atm]
- Developed in CNS/RIKEN[1)]

[1)] H.Akiyoshi *et. al.*: RIKEN Accel. Prog. Rep. 34, 193 (2001).

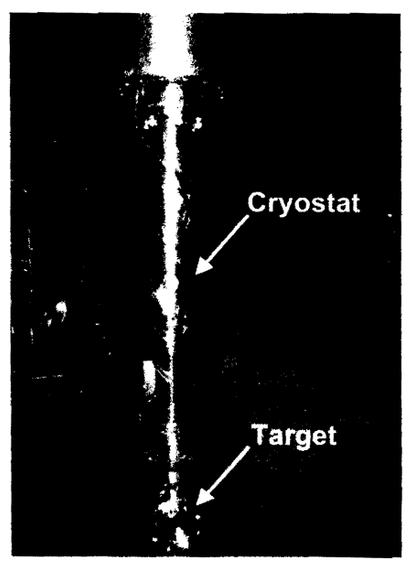

New effective interaction for pf-shell nuclei and its implications for the stability of the N=Z=28 closed core

[a]M. Honma, [b,c]T. Otsuka, [d]B. A. Brown and [e]T. Mizusaki

[a] *Center for Mathematical Sciences, University of Aizu, Tsuruga, Ikki-machi, Aizu-Wakamatsu, Fukushima 965-8580, Japan*
[b] *Department of Physics and Center for Nuclear Study, University of Tokyo, Hongo, Tokyo 113-0033, Japan*
[c] *RIKEN, Hirosawa, Wako-shi, Saitama 351-0198, Japan*
[d] *National Superconducting Cyclotron Laboratory and Department of Physics and Astronomy, Michigan State University, East Lansing, MI 48824-1321, USA*
[e] *Institute of Natural Sciences, Senshu University, Higashimita, Tama, Kawasaki, Kanagawa 214-8580, Japan*

The nuclear shell model has been one of the most powerful tools for the study of nuclear structure. Owing to recent developments in computational facilities and numerical calculation techniques, most of the pf-shell nuclei are now in the scope of exact $0\hbar\omega$ calculations. The current frontier of such direct calculations corresponds to the middle of the pf-shell ($A \sim 60$), where the maximum M-scheme dimension reaches to two billion.

The γ-ray data provide us with crucial information of the effective interaction for shell-model calculations. The microscopic theory for deriving the effective interaction from the nucleon-nucleon potential is not necessarily successful especially for cases of many valence nucleons. For a practical use, we have derived a new effective interaction GXPF1 [1] for full pf-shell calculations, by modifying such a microscopic interaction empirically, including the knowledges from many-body data.

One important problem in this mass region is the softness of ^{56}Ni core. The recent γ-ray spectroscopy has revealed the amount of the core excitation in low-lying states. For example, the measurements of electromagnetic transitions in ^{58}Cu [2] suggest the enhancement/hindrance of low-lying electormagnetic transitions in comparison with the prediction with an inert ^{56}Ni, which can reasonably be explained by taking into account the core excitation explicitly. Another interesting topic is the shell evolution as a function of the valence nucleon number, especially in neutron rich nuclei. The systematic experiments [3, 4] for neutron rich Ti isotopes suggest the appearance of $N = 34$ shell gap for $Z \sim 20$, which has been predicted by our shell-model calculations.

References

[1] M. Honma et al., Phys. Rev. C **65**, 061301 (2002).
[2] A. F. Lisetski et al., Phys. Rev. C **68**, 034316 (2003).
[3] R. V. F. Janssens et al., Phys. Lett. B **546**, 55 (2002).
[4] S. N. Liddick et al., Phys. Rev. Lett. **92**, 072502 (2004).

New effective interaction for *pf*-shell nuclei and its implications for the stability of N=Z=28 closed core

2004. 3. 18-19 CNS-RIKEN joint symposium "gamma04"

M. Honma (Univ. of Aizu)
T. Otsuka (Univ. of Tokyo/RIKEN)
B. A. Brown (MSU)
T. Mizusaki (Senshu Univ.)

Contents

- Introduction
- Effective interaction GXPF1
- Softness of the ^{56}Ni closed core
- Summary

Shell model

- Powerful tool for the study of nuclear structure
  - Data analysis and prediction
- pf-shell
  - Current frontier of shell model calculation
    $M = 0$ dim. $\sim 2\times 10^9$ for ^{60}Zn
  - "soft" ^{56}Ni core ⇒ active 2-shell problem
- Conventional Lanczos diagonalization
  - Feasible up to $\sim 10^8$ … code MSHELL by T. Mizusaki
  - Truncation of model space: $(f_{7/2})^{n_1-t}(p_{3/2}\ f_{5/2}\ p_{1/2})^{n_2+t}$
  - $t \sim 5$ calculation is possible for most pf-shell nuclei
- Monte-Carlo shell model

Effective interaction

- Microscopic (realistic)
  - Derived from NN-interaction (renormalized G-matrix)
    - KB … T.T.S.Kuo and G.E.Brown Nucl. Phys. A114 (1968) 241
      - Hamada-Johnston potential,
      - Renormalization due to core-polarization
    - Problems for many valence nucleons
- Microscopic + monopole correction
  - Modify monopole part of KB interaction empirically
    - KB3G … A. Poves et al., NPA694 (2001) 157
    - Excellent for A≦52, but Fails for ^{56}Ni, ^{57}Ni, ^{55}Co, …
    - Problems in cross-shell excitation over N, Z=28 shell gap

GXPF1 interaction

M. Honma et al., PRC65 (2002) 061301(R)

- Modify realistic G interaction

  M. Hjorth-Jensen, et al., Phys. Repts. 261 (1995) 125
  - Bonn-C potential
  - 3rd order Q-box + folded diagram
- Fit to 699 experimental energy data of 87 nuclei
- Vary 70 well-determined LC's of 195 TBME and 4 SPE
- Mass dependence $V(A) = V(A=42) \times \left(\frac{A}{42}\right)^{-0.3}$
- Data selection to avoid intruder: $47 \le A, \quad Z \le 32$
- Energy evaluation by FDA* ⟶ 168keV rms error

G vs. GXPF1

$V(abcd\,;JT)$

⬇

$abcd\,;JT$

$7=f_{7/2},\ 3=p_{3/2},\ 5=f_{5/2},\ 1=p_{1/2}$

- T=0 … attractive
- T=1 … repulsive
- Large modifications in
  - $V(abab\,;J0)$ with large J
  - $V(aabb\,;J1)$ pairing

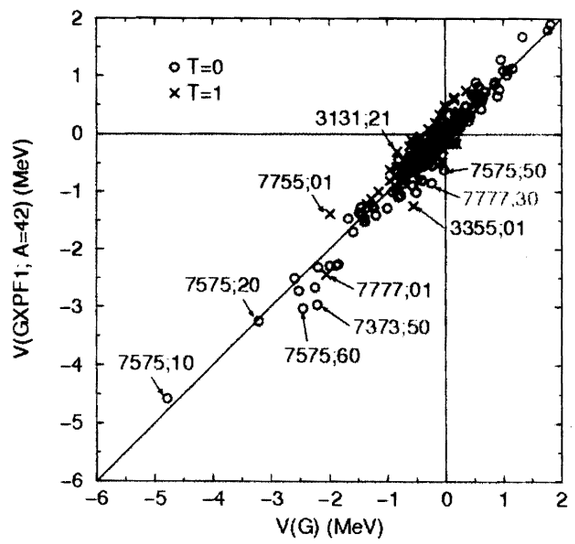

Monopole part

- Monopole part H_m
  - Average energy of a given configuration
    ⇒ B.E., shell gap

$$V^T_{ab} = \frac{\sum_J (2J+1) V^{JT}_{abab}}{\sum_J (2J+1)}$$

- Effective single-particle energy (ESPE)
  - Assume the lowest filling configuration
  - Energy difference by H_m due to removing (adding) one nucleon

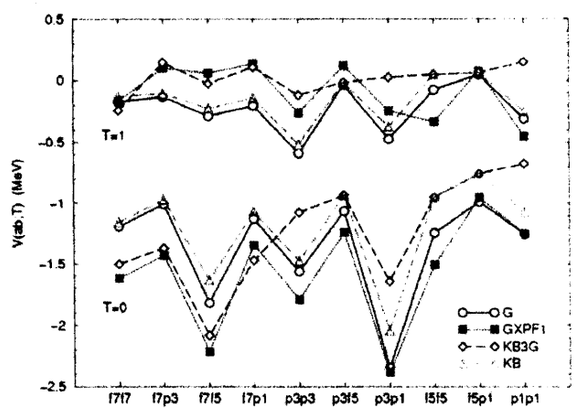

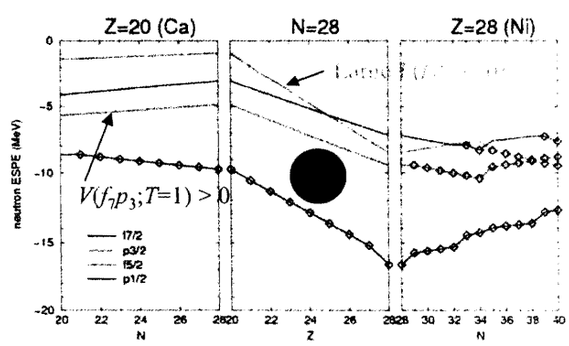

Collective strength

M. Dufour et al., PRC54 (1996) 1641

- Multipole part H_M $(=H-H_m)$
  - Particle-particle

$$H_M \Rightarrow \sum_{JT\alpha} E_\alpha^{JT} P^\dagger_{JT\alpha} P_{JT\alpha} \qquad P_{JT}{}^\dagger = \sum_{ij} U_{ij}^{JT} c_i^\dagger c_j^\dagger$$

  - Particle-hole

$$H_M \Rightarrow \sum_{\lambda\tau k} e_k^{\lambda\tau} Q_{\lambda\tau k} \cdot Q_{\lambda\tau k} \qquad Q_{\lambda\tau k} = \sum_{ij} u_{ij}^{\lambda\tau k} c_i^\dagger c_j$$

- Empirical fit reduces collective T=0 strength (E^{10} and e^{20})
- Pairing strength : T=0 > T=1 in G and GXPF1

	T=1 pairing	T=0 pairing	r^2Y_2	r^4Y_4	$\sigma\tau$
Interaction	E^{01}	E^{10}	e^{20}	e^{40}	e^{11}
G	–4.20	–5.61	–3.33	–1.30	+2.70
GXPF1	–4.18	–5.07	–2.92	–1.39	+2.67
KB3G	–4.75	–4.46	–2.79	–1.39	+2.47

Binding energies

Empirical Coulomb energy

$$E_C = V_{\pi\pi}\frac{\pi(\pi-1)}{2} - V_{\pi\nu} + e_\pi \pi \qquad \pi, \nu \cdots \text{valence nucleon \#}$$

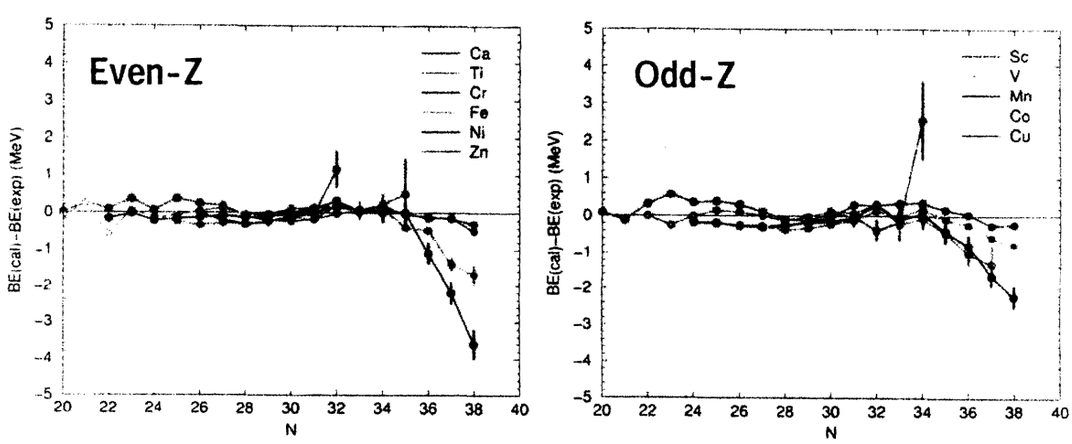

Systematics of 2^+_1

- Shell gap
  N=28
  N=32 for Ca, Ti, Cr
  N=34 for Ca ??
- Deviations in E_x
  Cr at N≧36
  Fe at N≧38
- Deviations in B(E2)
  Ca, Ti for N≦26
  Cr for N≦24
    ^{40}Ca core excitations
  Zn, Ge
    $g_{9/2}$ is needed

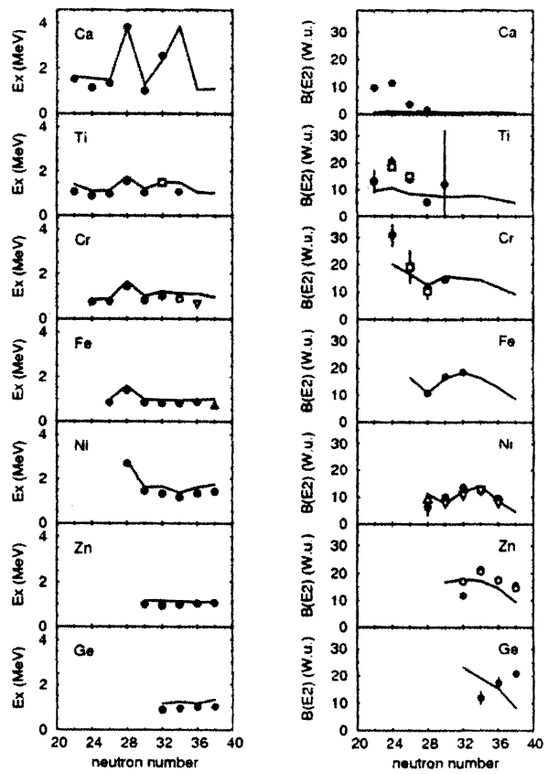

^{56}Ni closed core probability

Probability of closed-core configurations ($f_{7/2}$ orbit is maximally occupied) in the calculated ground-state wave functions
⇒ Measure of core-breaking

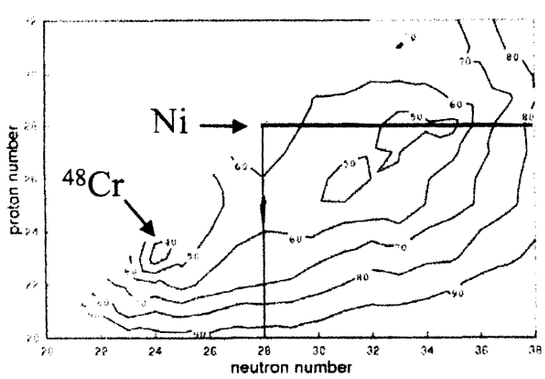

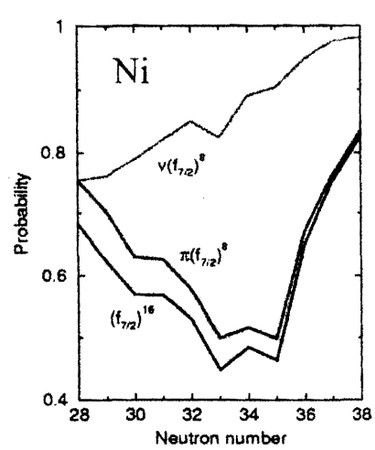

Semi-magic nuclei

- Good test of effective interaction
  - Yrast states … lowest configuration is dominant
    ⇒ test of ESPE (monopole properties)
  - Core-excited configurations can appear at low-energy
    ⇒ test of multipole properties
  - Relatively small low-lying level density
  - Shape coexistence

    ex. ^{56}Ni 4p-4h deformed band

    D. Rudolph, et al., PRL82 (1999) 3763
- Examples:
  - ^{54}Fe … ^{56}Ni + two proton-holes in $f_{7/2}$
  - ^{58}Ni … ^{56}Ni + two neutron-particles in $p_{3/2}$

^{54}Fe yrast

- 0p-2h configuration
  $0^+, 2^+, 4^+, 6^+ \ldots \pi(f_{7/2})^{-2}$
  more than 40% prob.
- 1p-3h … 1st gap
  One-proton excitation
  $3^+, 5^+$
  $7^+ \sim 11^+$
- 2p-4h … 2nd gap
  Two-protons excitation
  $12^+ \sim$

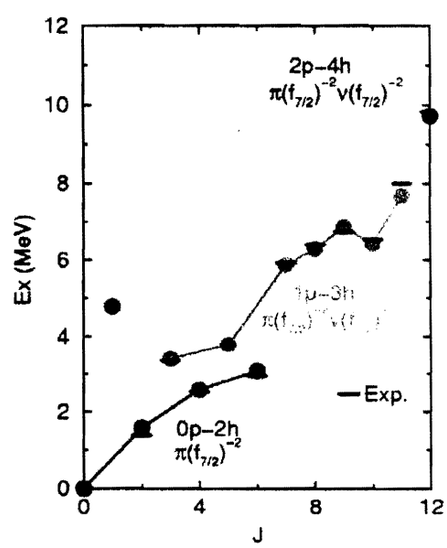

^{54}Fe 2p-4h band

- Band head $Ex \sim 2.5$MeV
- $0^+_2, 2^+_3, 4^+_5 \ldots \nu(f_{7/2})^{-2} \sim 30\%$
- $Q(2^+_3) = -0.09$ eb (mixing with 2^+_2)
- $B(E2; 2^+_3 \downarrow) = 11$ W.u.

B(E2) & B(M1) (W.u.)

J^π_i	J^π_f	type	Exp.	Cal.
0^+_2	2^+_1	E2	<16	3.8
2^+_3	2^+_1	M1	0.0035(21)	0.0013
	2^+_1	E2	1.0(13)	1.7
	0^+_1	E2	0.74(19)	0.8

$e_p = 1.5$, $e_n = 0.5$
$g_{lp} = 1.1$, $g_{ln} = -0.1$, $g_s^{\rm eff} = 0.9 g_s^{\rm free}$

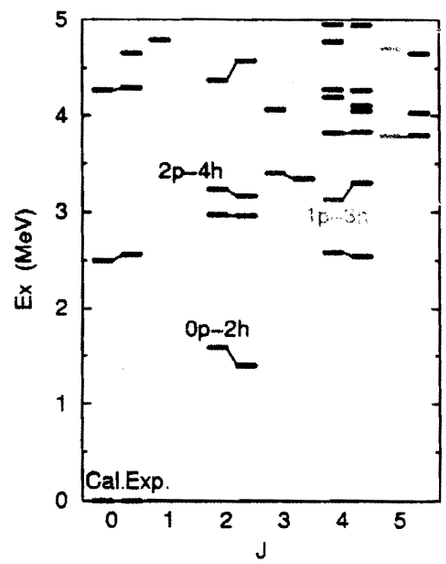

^{58}Ni yrast

- 2p-0h configuration
  $0^+, 2^+ \ldots \nu(p_{3/2})^2$
  $1^+, 3^+, 4^+ \ldots \nu(p_{3/2})^1(f_{5/2})^1$
  more than 40% prob.
- 3p-1h … 1st gap
  One-proton excitation
  $5^+ \sim 8^+$
- 4p-2h … 2nd gap
  One-proton &
  one-neutron excitation
  $10^+ \sim 12^+$

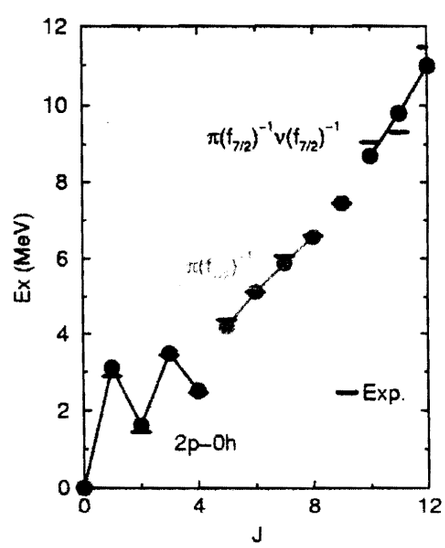

^{58}Ni 4p-2h band

- Band head Ex ~3.5MeV
- 0^+_3, 2^+_6 … $\pi(f_{7/2})^{-2}$ ~ 40%
- $Q(2^+_6)$ = –0.30 eb
- B(E2; ↓)= 18 W.u.

B(E2) & B(M1) (W.u.)

J^π_i	J^π_f	type	Exp.	Cal.
0^+_3	2^+_1	E2	5.5	3.5
2^-_6	2^+_2	M1	0.0051(20)	0.0089
	2^+_1	M1	0.0032(8)	0.0003
	2^+_1	E2	0.30(10)	0.29
	0^+_1	E2	0.15(4)	0.08

e_p= 1.5, e_n= 0.5
g_{lp}=1.1, g_{ln}= –0.1, $g_s^{\rm eff}$= 0.9$g_s^{\rm free}$

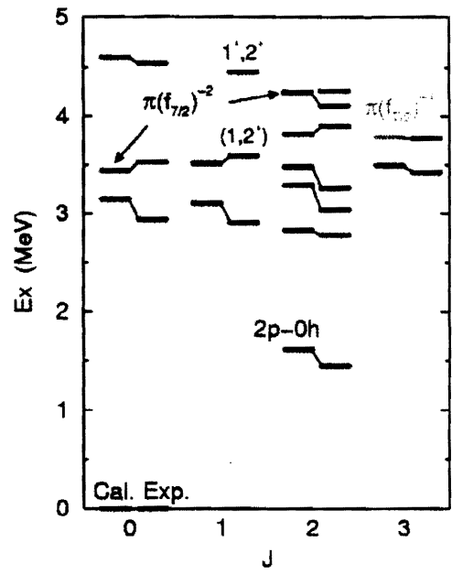

N=Z odd-odd nuclei

- Good test of isospin properties
- T=0 and T=1 states are almost degenerate near the g.s.
- Large isovector M1 transition between T=0 and T=1 states for a proton-neutron pair in j=l+1/2 orbit

  Quasideuteron configuration (QDC)

  A. F. Lisetskiy, et al., PRC60 (1999) 064310

  Core-excitations ⇒ breaking of a simple picture ?
- Examples:
  - ^{54}Co … $f_{7/2}$
  - ^{58}Cu … $p_{3/2}$

^{54}Co energy levels

- T=1
  $0^+_{1,2}$, $2^+_{1,3}$, $4^+_{3,4}$, 6^+_2
  IAS …^{54}Fe
- B(M1; $1^+_{T=0} \rightarrow 0^+_{T=1}$) (W.u.)
  - No experimental data
  - Single-j, g_s^{free} 3.4
    $0.7*g_s$ 2.3
  - $f_{7/2}+p_{3/2}$
    with one p and n
    $0.7*g_s$ 2.1
  - Full-pf, g_s^{free} 1.9
    g^{eff} 1.7

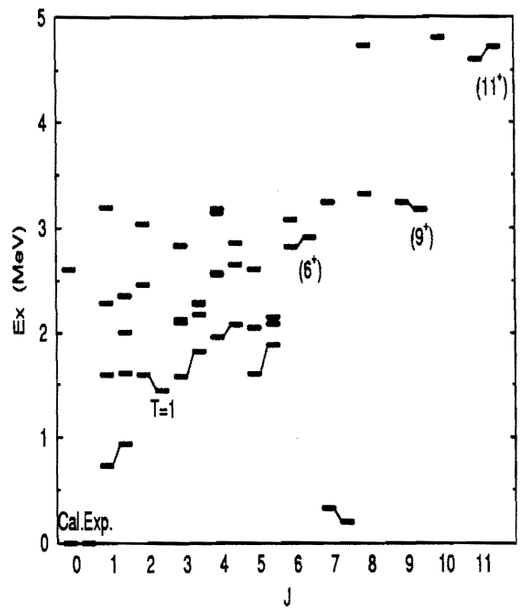

^{58}Cu energy levels

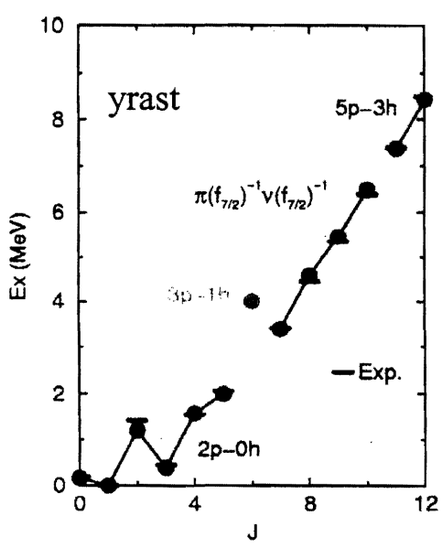

- Core excitation for J≧6
- T=1 … $0^+_{1,2}$, 2^+_2, 4^+_3

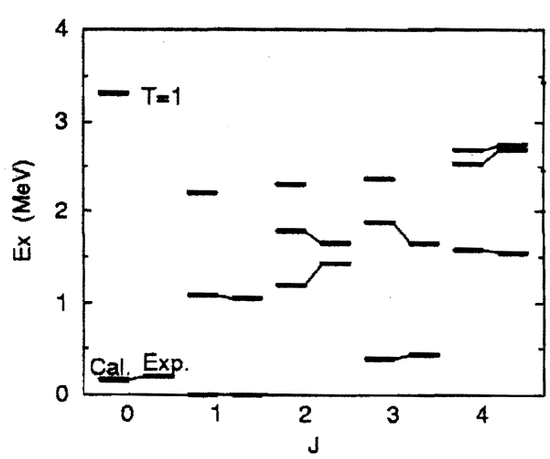

Isovector M1

- QDC (single-j) … $\pi(p_{3/2})^1\ \nu(p_{3/2})^1$
- pf5 (inert ^{56}Ni) … $p_{3/2}f_{5/2}p_{1/2}$ space, SDI int.
- Full pf-shell … $f_{7/2}p_{3/2}f_{5/2}p_{1/2}$ space, GXPF1 int.
- Free g-factors

^{58}Cu B(M1)

* A. F. Lisetskiy et al., PRC68 (2003) 034316

$J^\pi;T$ (*ini.*)	$J^\pi;T$ (*fin.*)	[redacted]	pf5	QDC
$0^-_1;1$	$1^+_1;0$	[redacted]	8.8	13
$1^+_2;0$	$0^+_1;1$	[redacted]	2.94	
$2^+_2;1$	$1^+_1;0$	[redacted]	0.23	
	$3^+_1;0$	[redacted]	4.32	
	$1^+_2;0$	[redacted]	1.53	

Summary

- Microscopic interaction can be modified for a practical use
  - T=0 … more attractive
  - T=1 … more repulsive
  - Monople corrections
  - Pairing, QQ
- ^{56}Ni core excitation is important
  - Proton excitations enhance in Ni isotopes
  - Semi-magic nuclei …high-spin states & low-lying collective bands
  - N=Z odd-odd nuclei …deviation of isovector M1 from a simple picture

Gamma-Ray Spectroscopy by Secondary Fusion Reactions using CRIB

A. Odahara[a], Y. Gono[b], Y. Wakabayashi[b], T. Fukuchi[c], N. Hokoiwa[b], M. Kibe[b], T. Teranishi[c], S. Kubono[c], M. Notani[c], Y. Yanagisawa[d], S. Michimasa[c], J.J. He[c], H. Iwasaki[e], S. Shimoura[c], H. Watanabe[d], T. Kishida[d], E. Ideguchi[c], H. Baba[f], S. Nishimura[d], M. Nishimura[d], J.Y. Moon[g] S. Kato[h] and H. Sagawa[i]

[a] *Nishinippon Institute of Technology, Kanda-tyo, Fukuoka-ken, 800-0394, Japan*
[b] *Department of Physics, Kyushu University, Hakozaki, Fukuoka, 812-8581, Japan*
[c] *Center for Nuclear Study(CNS), University of Tokyo, Wako, Saitama 351-0198, Japan*
[d] *RIKEN, Wako, Saitama 351-0198, Japan*
[e] *Department of Physics, University of Tokyo, Hongo, Tokyo 113-0033, Japan*
[f] *Department of Physics, Rikkyo University, Nishi-Ikebukuro, Tokyo, 171-8501, Japan*
[g] *Chung-Ang University, HukSuk-Dong, DongJak-Ku, Seoul, 156-756, Korea*
[h] *Yamagata University, Kojirakawa-machi, Yamagata, 990-8560, Japan*
[i] *Center for Mathematical Sciences, University of Aizu, Aizu-Wakamatsu, Fukushima, 965-8580, Japan*

Search for high-spin isomers in N=51 isotones with Z<40 has been started by means of the γ-ray spectroscopy method using secondary fusion reaction. Since these isotones are close to the stability line, it is difficult to produce high-spin states using reactions by combinations of stable beams and targets. Therefore, it is very effective to use the radioisotope beam. High-spin isomers in the N=51 isotones can be searched for, using the ^{82}Se+^{17}N reaction. An unstable nuclear beam of ^{17}N was developed using the low energy radioisotope beam separator(CRIB)[1] of the Center for Nuclear Study(CNS), University of Tokyo.

High-spin isomers of N=51 isotones are expected to be shape isomers stemmed from a sudden shape change from near spherical to an oblate shape. They may also be expected to have stretch coupled configurations resulting from the breaking of a neutron magic 50 core, as a similar type of isomerism observed in N=83 isotones[2]. The configurations of these isomers in N=51 isotones are considered to be $[\nu(d_{5/2}g_{7/2}h_{11/2})\pi g_{9/2}{}^2]_{39/2}{}^-$ for odd nuclei and $[\nu(d_{5/2}g_{7/2}h_{11/2})\pi(p_{1/2}g_{9/2}{}^2)]_{20}{}^+$ for odd-odd nuclei.

The CRIB consists of two dipole, three quadrupole and small correction magnets. The ^{17}N beam was produced by the transfer reaction of ^{9}Be(^{18}O,^{17}N)^{10}B. An ^{18}O primary beam of 126.4MeV was accelerated by the AVF cyclotron in RIKEN with 0.4pμA intensity. This primary beam was stopped by slit at a dispersive focal plane(F1). The mixed RI beam of the ^{17}N(73%) and ^{17}O(27%) was obtained at the secondary target position, since both particles with the same $B\rho$ values could not be separated. The beam energy and intensity of ^{17}N was 104$\pm$2MeV and 1.1×10^5particles/s, respectively.

Seven γ-rays coming from the secondary fusion reaction were observed by the measurement for 2.4 days using two clover Ge detectors, although the background level originating from the thermal neutron capture γ-rays was 200 times higher than the counts of these peaks. These seven γ-rays were assigned to be transitions belonging to ^{92}Nb and ^{93}Nb produced by 7n and 6n channels of the ^{82}Se+^{17}N reaction, respectively.

References

1 S. Kubono et al., Eur. Phys. J. **A 13** (2002) 217.
2 Y. Gono et al., Eur. Phys. J. **A 13** (2002) 5.

Gamma-Ray Spectroscopy by Secondary Fusion Reactions using CRIB

CRIB
low-energy radioisotope beam separator
CNS, University of Tokyo
(CRIB is installed in RIKEN.)

- Odahara[a], Y. Gono[b], Y. Wakabayashi[b], T. Fukuchi[c], N. Hokoiwa[b], M. Kibe[b], T. Teranishi[c], S. Kubono[c], M. Notani[c], Y. Yanagisawa[d], S. Michimasa[c], J.J. He[c], H. Iwasaki[e], S. Shimoura[c], H. Watanabe[d], T. Kishida[d], E. Ideguchi[c], H. Baba[f], S. Nishimura[d], M. Nishimura[d], J.Y. Moon[g], S. Kato[h] and H. Sagawa[i]

[a] Nishinippon Institute of Technology
[b] Kyushu University
[c] CNS, University of Tokyo
[d] RIKEN
[e] Dep. of Phys., University of Tokyo
[f] Rikkyo University
[g] Chung-Ang University, Korea
[h] Yamagata University
[i] University of Aizu

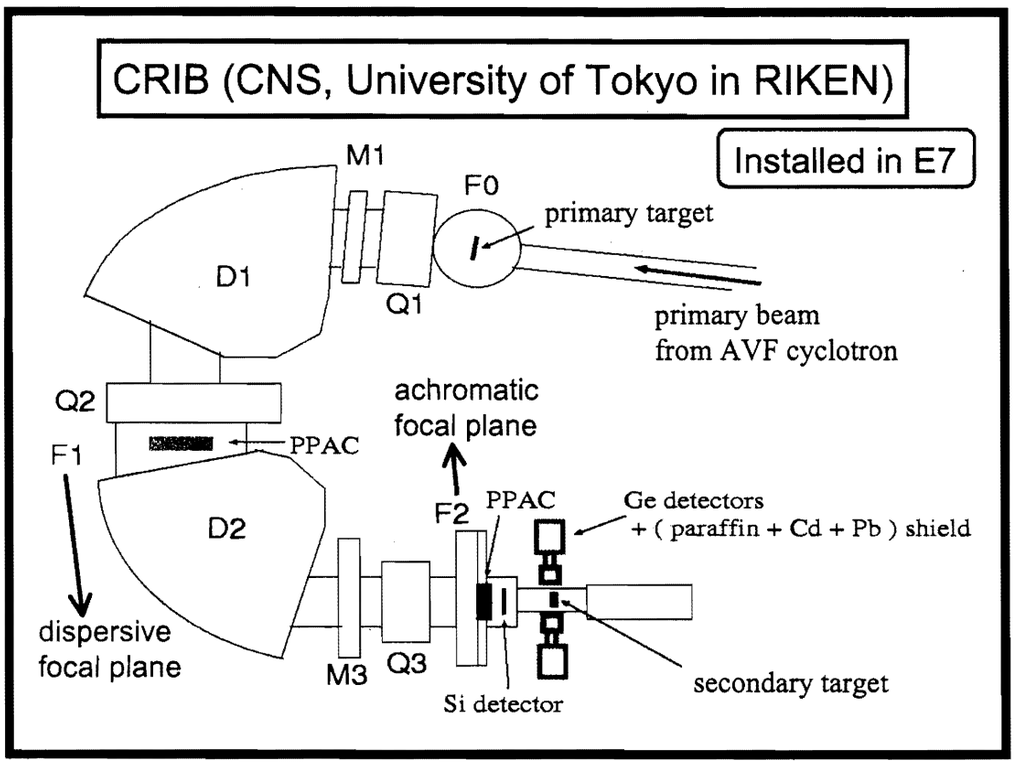

Search for High-Spin Isomers in N=51 isotones

1. Development of ^{17}N Secondary Beam using CRIB

2. Gamma Spectroscopy Method

   Search for High-Spin Isomers

   in N=51 Isotones with Z<40

1. <u>High-Spin Shape Isomers</u>

(1) N=83 Isotones

(2) N=51 Isotones

2. <u>CRIB experiment</u>

(1) Development of ^{17}N RI beam

(2) Preliminary γ-ray Spectrum
from the Experiment
using Secondary Fusion Reaction
^{82}Se+^{17}N

High-Spin Shape Isomer

oblate
$\beta \sim -0.19$

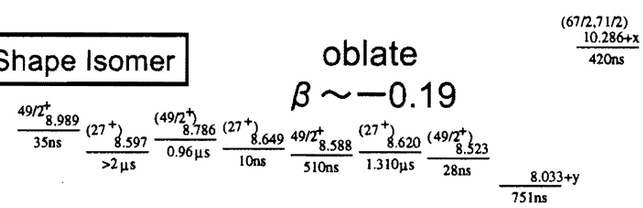

Systematics
of High-Spin Isomers
in N=83 Isotones

odd nuclei
$[\nu(f_{7/2}h_{9/2}i_{13/2})\pi h_{11/2}{}^2]_{49/2}+$

odd-odd nuclei
$[\nu(f_{7/2}h_{9/2}i_{13/2})\pi(h_{11/2}{}^2d_{5/2})]_{27}+$

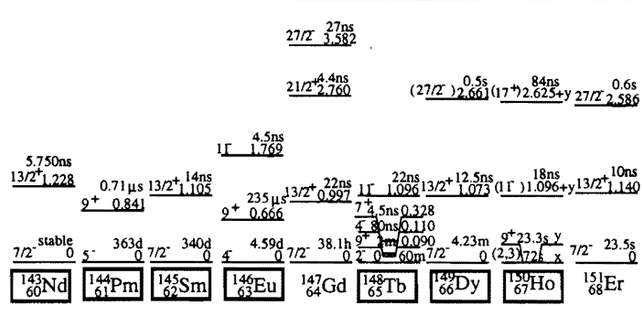

Systematical Study of High-Spin Isomers in *N*=83 Isotones

- High-Spin Shape Isomers
- *Z*=64 sub-shell gap

etc....

N=83 Isotones
Systematics
of High-Spin Isomers

[DIPM calculation]

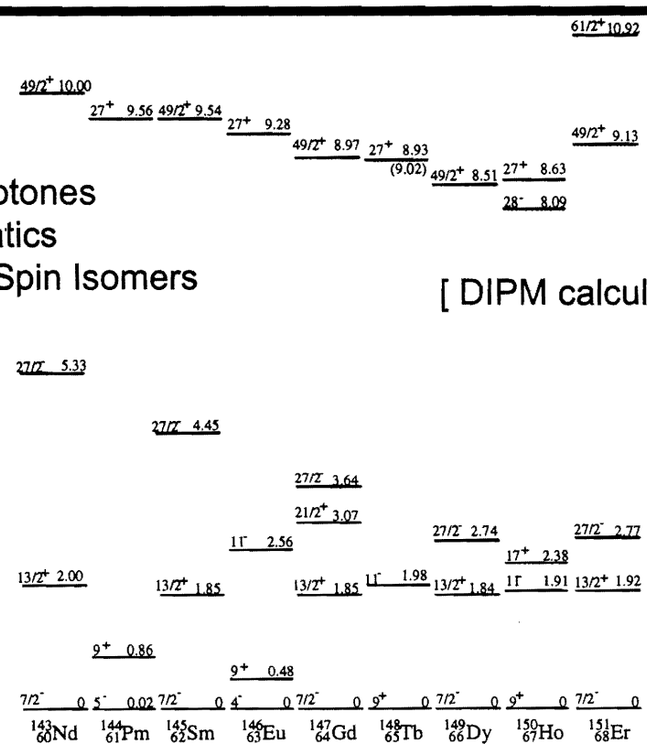

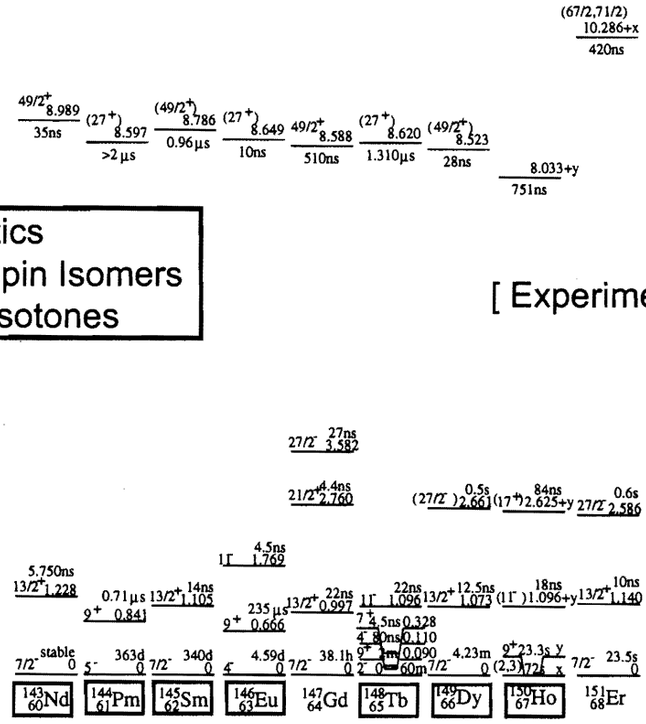
Systematics
of High-Spin Isomers
in N=83 Isotones
[Experiment]
143 60 Nd
144 61 Pm
145 62 Sm
146 63 Eu
147 64 Gd
148 65 Tb
149 66 Dy
150 67 Ho
151 68 Er

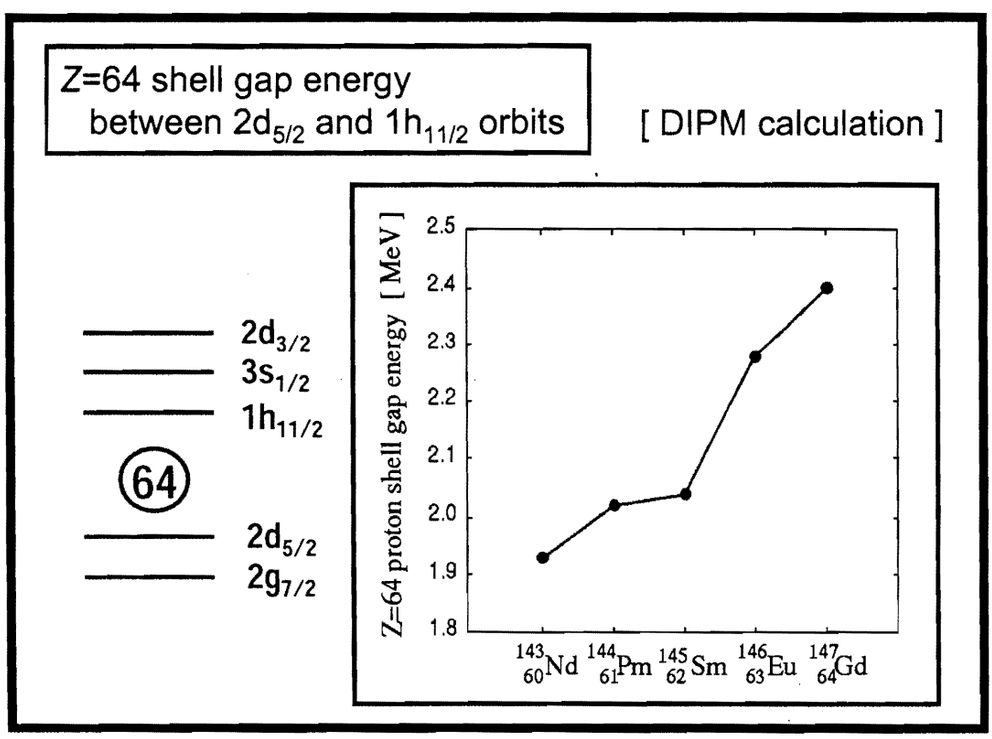
Z=64 shell gap energy
between 2d5/2 and 1h11/2 orbits
[DIPM calculation]
2d3/2
3s1/2
1h11/2
64
2d5/2
2g7/2
Z=64 proton shell gap energy [MeV]
2.5
2.4
2.3
2.2
2.1
2.0
1.9
1.8
143 60 Nd
144 61 Pm
145 62 Sm
146 63 Eu
147 64 Gd

Search for high-spin shape isomers
with the same isomerism
as those of N=83 isotones
in other mass region
stretch coupled configuration
oblate shape

We selected N=51 isotones.

Why did we select N=51 isotones?

N=83 isotones
high-spin shape isomers
odd nuclei
$[\nu(f_{7/2}h_{9/2}i_{13/2})\pi h_{11/2}^2]_{49/2+}$
odd-odd nuclei
$[\nu(f_{7/2}h_{9/2}i_{13/2})\pi(h_{11/2}^2 d_{5/2})]_{27+}$

N=51 isotones
expected high-spin shape isomers
odd nuclei
$[\nu(d_{5/2}g_{7/2}h_{11/2})\pi g_{9/2}^2]_{39/2-}$ $^{89}_{38}Sr$
odd-odd nuclei
$[\nu(d_{5/2}g_{7/2}h_{11/2})\pi(g_{9/2}^2 p_{1/2})]_{20+}$ $^{90}_{39}Y$, $^{88}_{37}Rb$

semi-double closed
shell nucleus

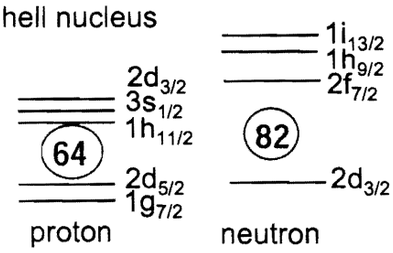

$^{146}_{64}Gd_{82}$

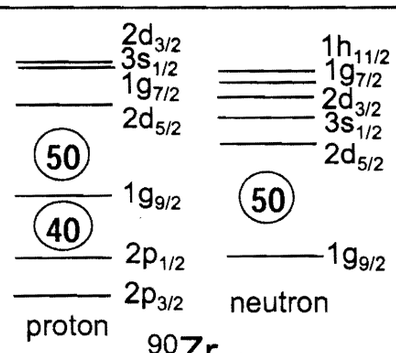

$^{90}_{40}Zr_{50}$

Search for High-Spin Isomers in N=51 Isotones with Z>=40

stable beam ^{16}O and ^{18}O

reaction $^{82}Se+^{16}O$, $^{82}Se+^{18}O$

Cyclotron RI center (CYRIC)

Tohoku University

N=51 Isotones
Systematics of Isomers

^{93}Mo high-spin isomer
T. Fukuchi et al.,
Phys. Rev. C,
to be submitted
$^{82}Se(^{16}O,5n)^{93}Mo$
110 MeV

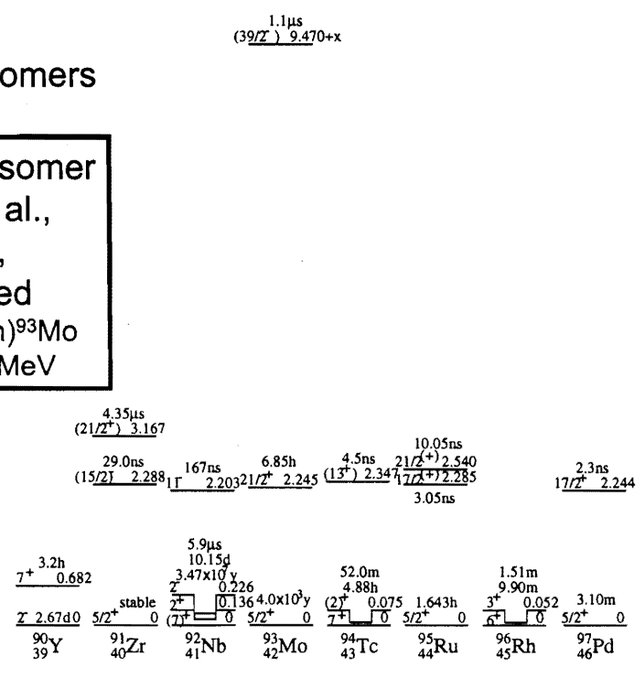

Systematic Study of High-Spin Isomer in N=51 Isotones

	N=83 isotones	N=51 isotones
1.	yrast isomer	non-yrast isomer

- Change of proton sub-shell gap energy

Z<64 Z<40

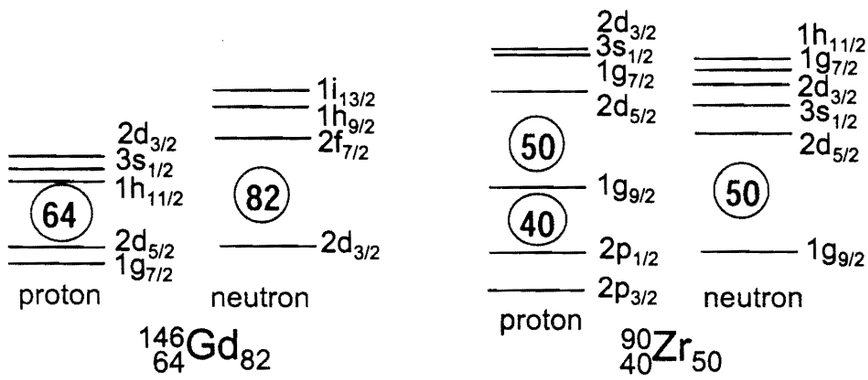

Search for High-Spin Isomers N=51 Isotones with Z<40

unstable nuclear beam ^{17}N

It is difficult to populate high-spin states of N=51 isotones with Z<40 ($^{90}_{39}$Y, $^{89}_{38}$Sr, $^{88}_{37}$Rb), because these nuclei are close to stability line.

primary reaction ^{9}Be(^{18}O,^{17}N)^{10}B

CRIB low-energy radioisotope beam separator
CNS, University of Tokyo
(CRIB is installed in RIKEN.)

secondary reaction ^{82}Se(^{17}N, α5n)^{90}Y
^{82}Se(^{17}N, αp5n)^{89}Sr
^{82}Se(^{17}N, 2α3n)^{88}Rb

Set up using CRIB (CNS, University of Tokyo)

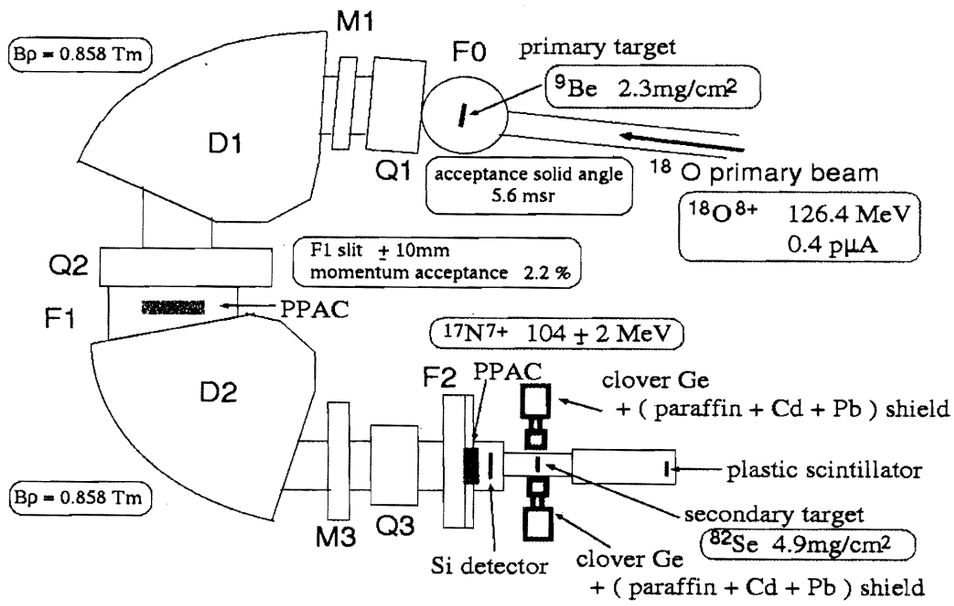

Particle Identification

Primary beam ^{18}O 126 MeV, 0.4pμA
Primary target ^{9}Be 2.3 mg/cm^2

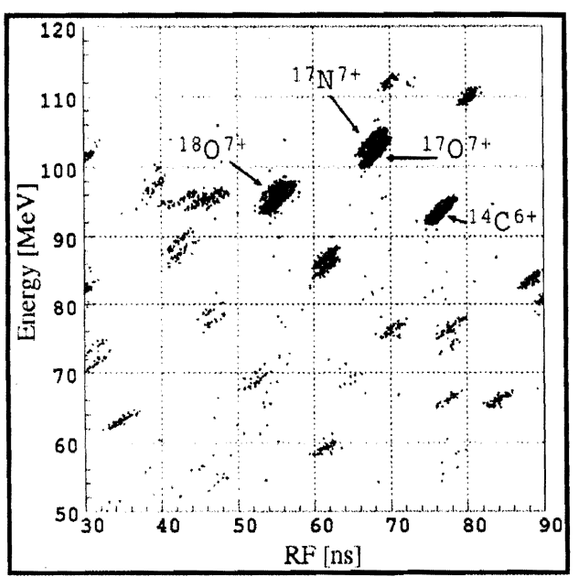

secondary beam

	energy [MeV]	intensity [pps]
^{17}N^{7+}	104	1.1×10^5 (24%)
^{17}O^{7+}	103	0.4×10^5 (9%)
^{18}O^{7+}	94	1.5×10^5 (31%)
^{14}O^{6+}	93	0.9×10^5 (20%)

projection spectrum
of $\gamma\gamma$ coincidence
using secondary
fusion reaction

for 2.4 days

$^{82}Se(^{17}N,7n)^{92}_{41}Nb$
$^{82}Se(^{17}N,6n)^{93}_{41}Nb$

after subtraction
of background
γ-rays

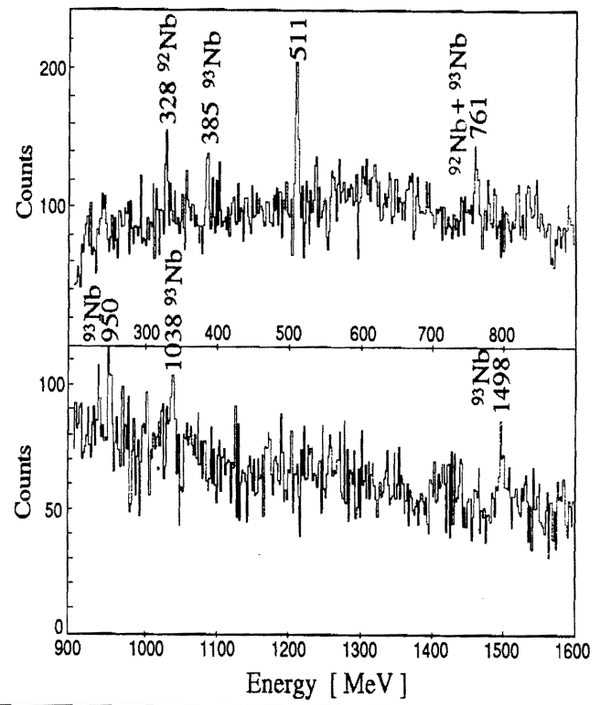

Conclusion

1. Search for high-spin isomers in N=51 isotones
with the same isomerism as N=83 isotones.
1.1μs high-spin isomer in ^{93}Mo
using stable beam ^{16}O [CYRIC, Tohoku Univ.]

2. Search for high-spin isomers for systematic study
<u>N=51 isotones with Z<40 using CRIB (Univ. Tokyo)</u>
(1) Development of ^{17}N RI beam
(2) We succeeded to observe γ-rays of nuclei
produced by secondary fusion reaction
$^{82}Se(^{17}N,7n)^{92}Nb$, $^{82}Se(^{17}N,6n)^{93}Nb$
(3) After shield test of thermal neutron,
we will start to search for high-spin isomers
$^{82}Se(^{17}N, \alpha 5n)^{90}Y$, $^{82}Se(^{17}N, \alpha p5n)^{89}Sr$, $^{82}Se(^{17}N, 2\alpha 3n)^{88}Rb$

GAMMA04

High-spin shape isomer and Ge-telescope

Yasuyuki Gono

Department of Physics, Kyushu University

We performed high spin isomer search experiments at RIKEN Accelerator Research Facility. A gas-filled isotope separator system was used to separate reaction products from primary beams. The recoil catcher technique was applied using the fusion reactions in the inverse kinematics.

Filled gases, ^{14}N, ^{16}O and ^{20}Ne, worked as targets unexpectedly and high spin isomers in ^{144}Pm, ^{145}Sm and ^{147}Gd isotopes were produced. These high spin isomers were further studied and showed characteristics of oblate shape isomers [1].

Furthermore it turned out that the recoiling isomers have enough kinetic energies to induce secondary fusion reactions. Then the development of a high spin isomer secondary beam was started. It was relatively difficult to develop a stable secondary high spin isomer beam. A Coulomb excitation of ^{174m}Hf beam was only successful example of the use of this kind of secondary beam [2].

To develop the high spin isomer beams, a new type of windowless gas target was developed [3]. Also segmented germanium detectors were prepared for the correction of Doppler shifts of gamma rays. They were used combining with clover detectors forming germanium telescopes.

Two segmented Ge's were later combined together to form a Compton camera. The development of the Compton camera is now under progress.

References

[1] Y.Gono et al., Eur. Phys. J. A13, (2002) 5..
[2] T.Morikawa et al., Phys.Lett. B350 (1995).169.
[3] T.Kishida et al., NIM A438 (1999) 70..

High-spin shape isomer and Ge-telescope

GAMMA04

CNS/RIKEN Joint Symposium

Yasuyuki Gono

Kyushu University

March 16, 2004

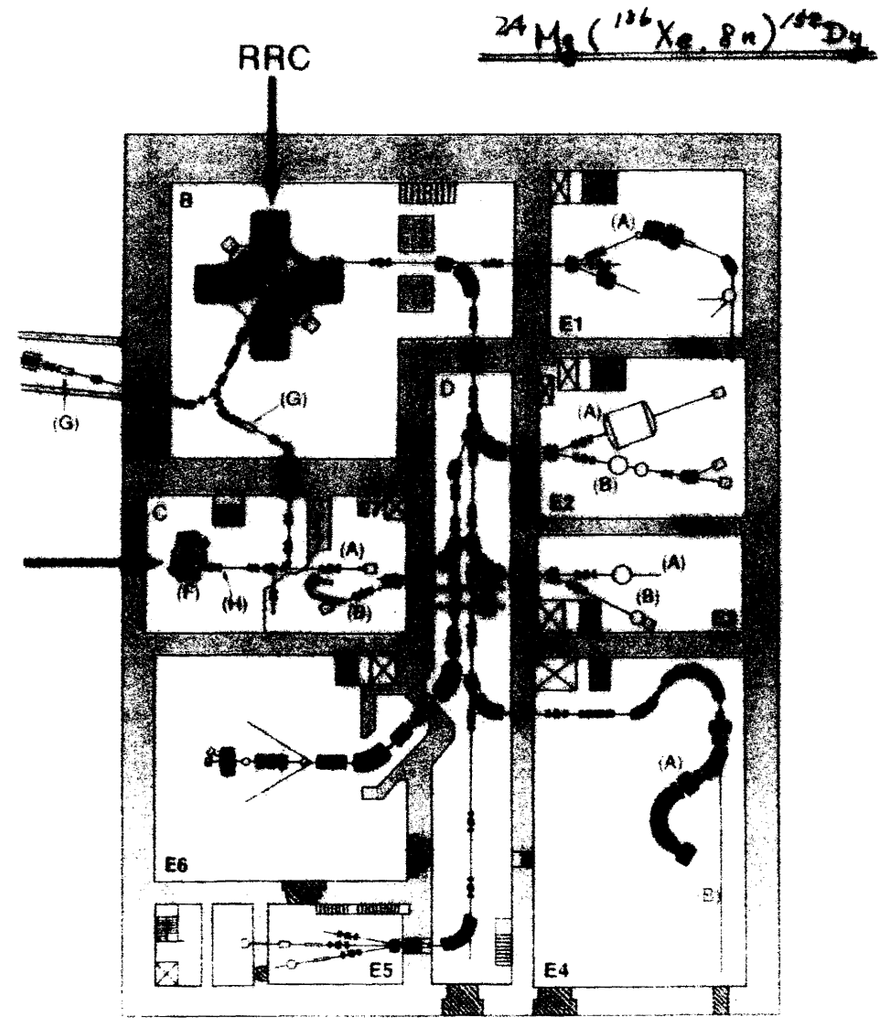

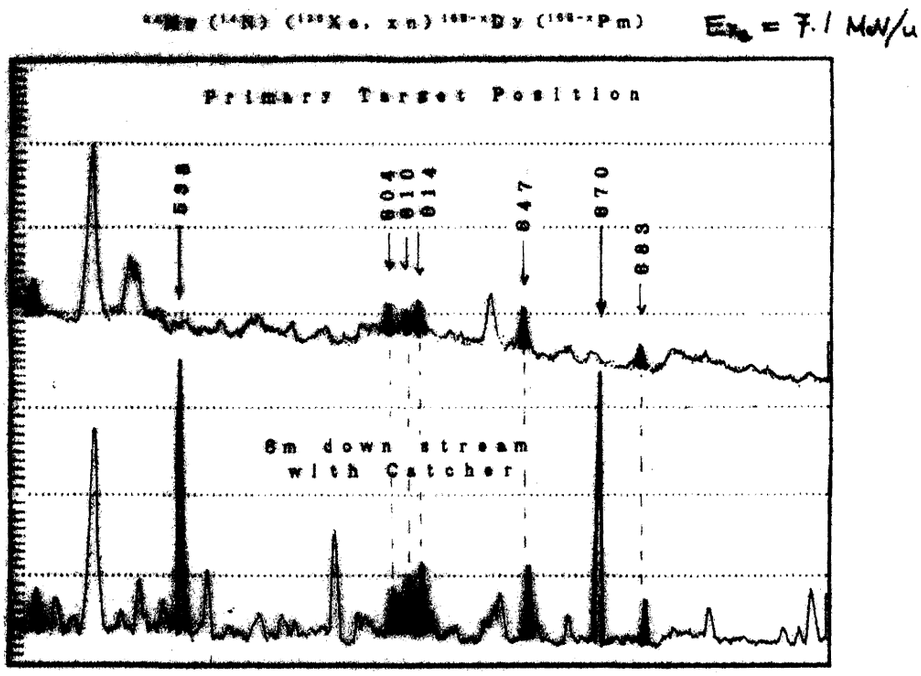
Primary Target Position
598
804
810
814
847
870
883
8m down stream
with Catcher

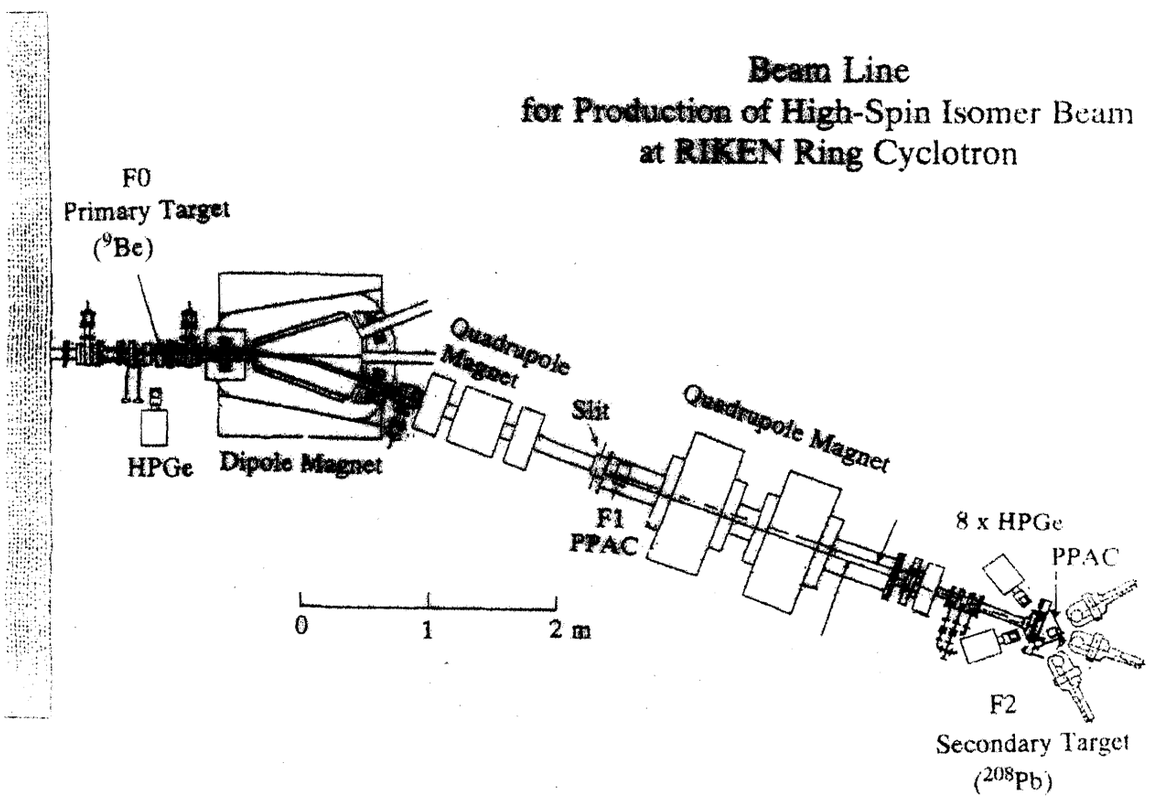
Beam Line
for Production of High-Spin Isomer Beam
at RIKEN Ring Cyclotron
F0
Primary Target
(^{9}Be)
HPGe
Dipole Magnet
Quadrupole Magnet
Slit
F1
PPAC
Quadrupole Magnet
8 x HPGe
PPAC
F2
Secondary Target
(^{208}Pb)
0
1
2 m

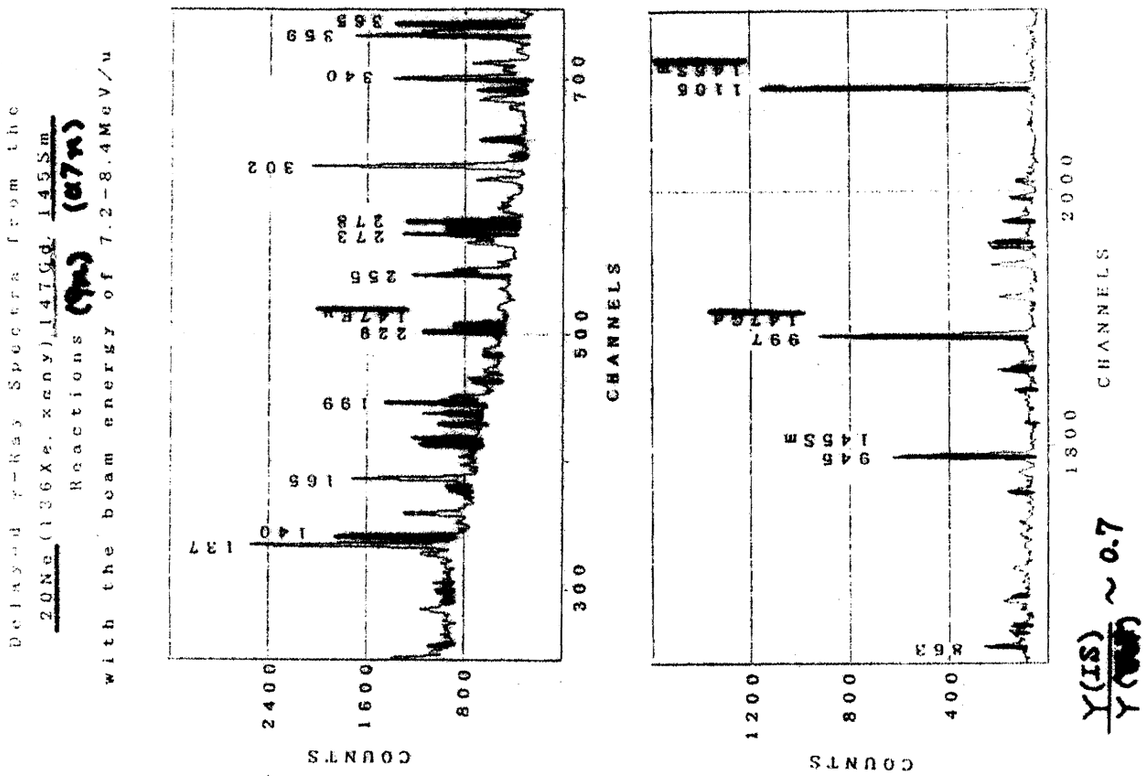
Delayed γ-Ray Spectra from the
20Ne(136Xe, xnγ)147Gd, 145Sm
Reactions
with the beam energy of 7.2-8.4MeV/u
COUNTS
CHANNELS
137
140
165
199
229
255
273
302
340
359
365
945
997
1105

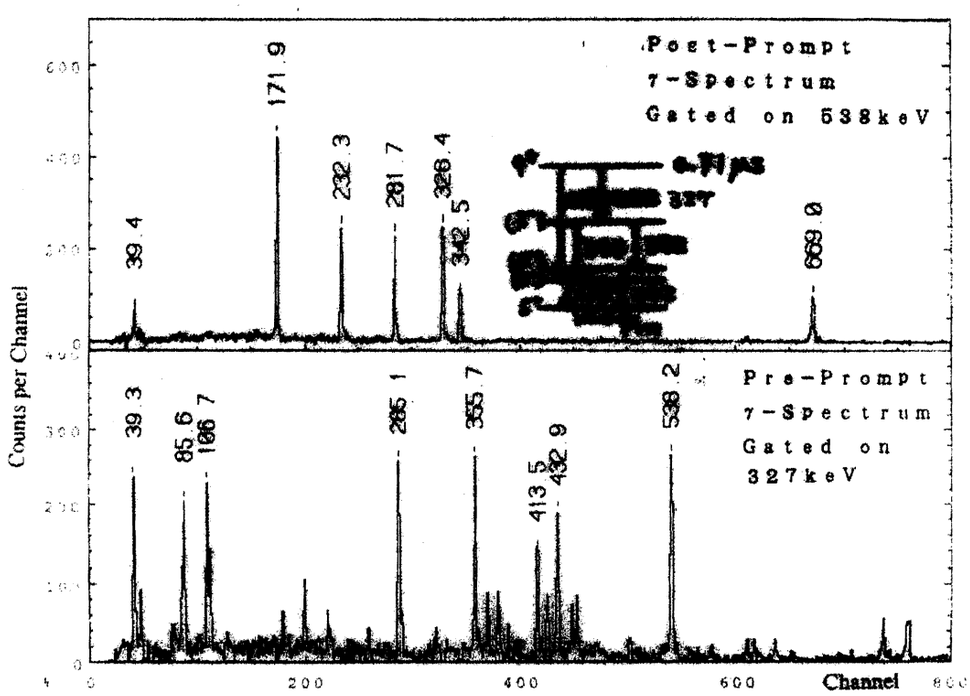
Post-Prompt
γ-Spectrum
Gated on 538keV
Pre-Prompt
γ-Spectrum
Gated on
327keV
Counts per Channel
Channel
39.4
171.9
232.3
281.7
326.4
342.5
669.0
39.3
85.6
166.7
265.1
355.7
413.5
432.9
538.2

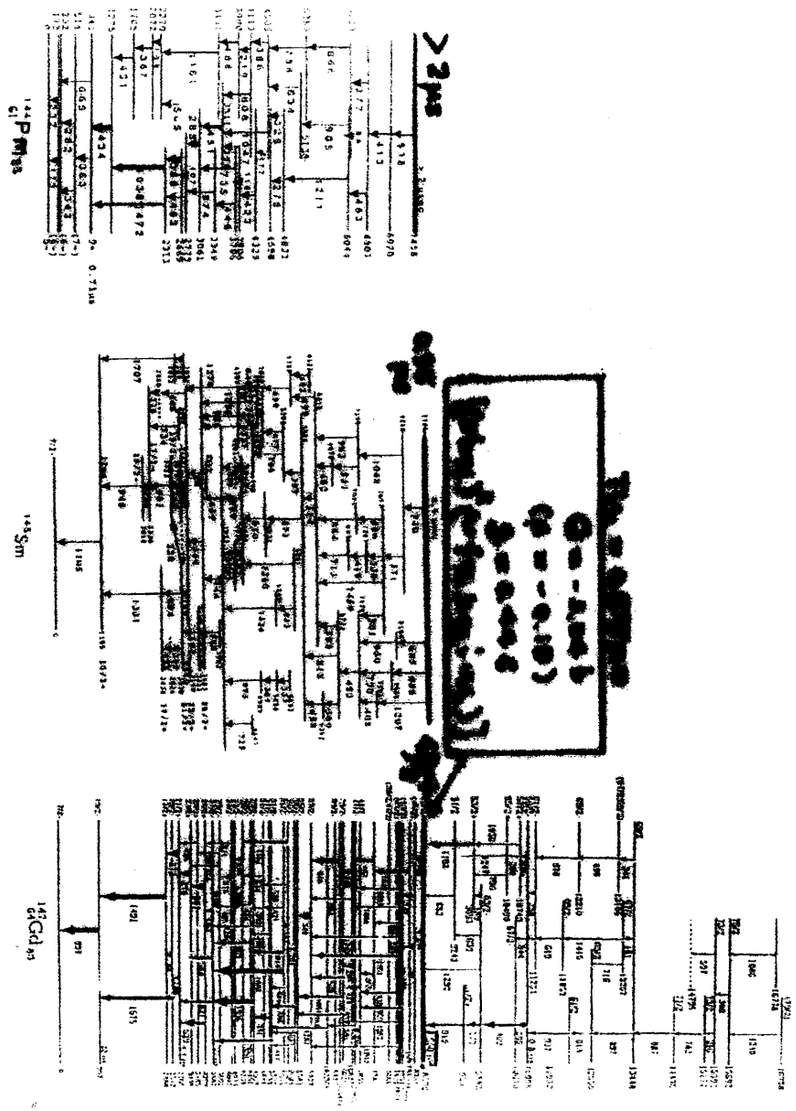

Reactions used to study isomers in N=83 isotones

$^{143}_{60}$Nd : ^{130}Te(^{18}O , 5n) ^{143}Nd (Kyushu U. KEK-T, CNS-U.Tokyo)
X.H.Zhou et al., Phys.Rev. C61, 014303 (2000)

$^{144}_{61}$Pm : ^{14}N (^{136}Xe, 6n) ^{144}Pm (RIKEN)
~~^{138}Ba(^{10}B , 4n) ^{144}Pm~~ (Tsukuba)
Y.H.Zhang et al., High Ene. Phys. and Nucl.Phys. 21, 110 (1997)

$^{145}_{62}$Sm : ^{16}O (^{136}Xe, 7n) ^{145}Sm (RIKEN)
~~^{138}Ba (^{13}C , 6n) ^{145}Sm~~ (JAERI)
^{139}La (^{10}B , 4n) ^{145}Sm (Kyushu U.)
A.Odahara et al., Z.Phys. A350, 185 (1994)
Nucl.Phys. A620, 363 (1997)

$^{146}_{63}$Eu : ^{139}La (^{13}C , 6n) ^{146}Eu (JAERI)
E.Ideguchi et al., European Phys.J. A6, 387 (1999)

$^{147}_{64}$Gd : ^{20}Ne (^{136}Xe, 9n) ^{147}Gd (RIKEN)

$^{148}_{65}$Tb : ^{141}Pr (^{13}C , 6n) ^{148}Tb (JAERI)
E.Ideguchi et al. Z.Phys. A352, 363 (1995)

$^{149}_{66}$Dy : ^{141}Pr (^{16}O , p7n) ^{149}Dy (CNS U.Tokyo)
T.Fukuchi, Master Thesis of Kyushu U. (2000)

↓

Cyric (Tohoku-U.)

N=83 isotones
Systematics of high-spin isomers

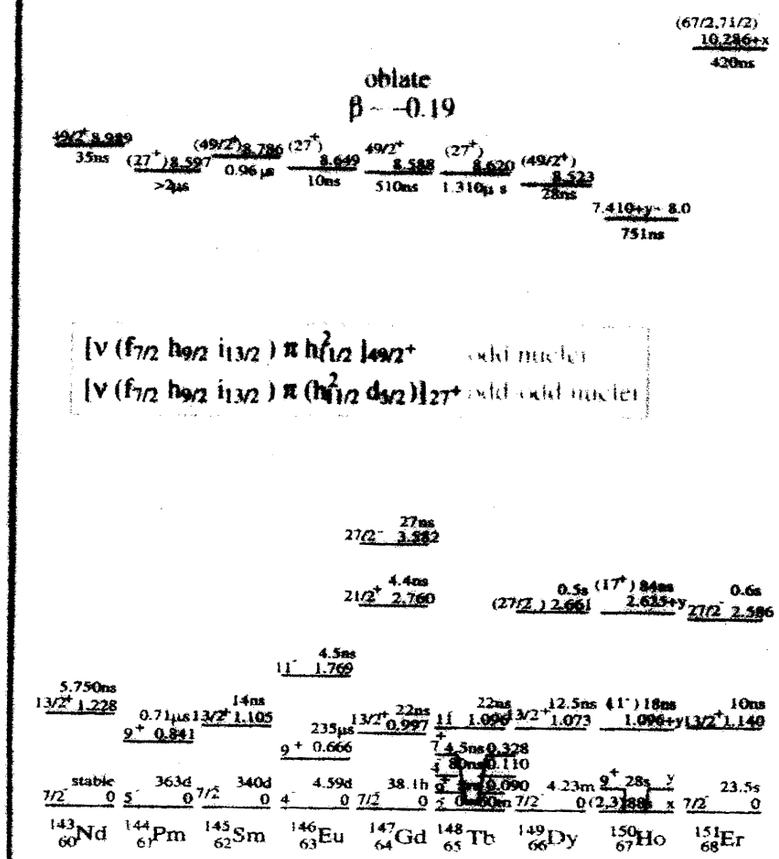

[^{146}Gd semi-double closed shell nucleus]

Shape isomer

deformation parameter β of yrast states

[DHFM calculation]

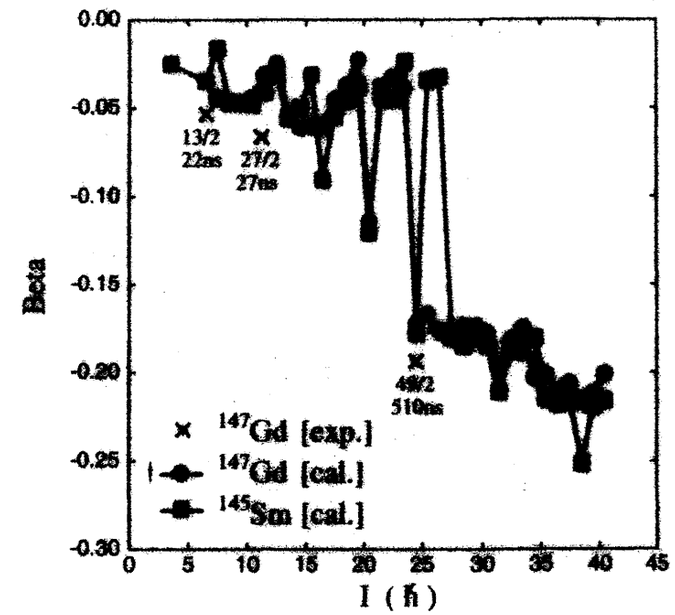

Measurements of quadrupole moment of isomers in ^{147}Gd
O. Häusser et al.,
Nucl. Phys. A379(1982)289
E. Dafni et al.
Nucl. Phys. A443(1985)135

Possibility of Phase Transition

^{147}Gd Ex − I(I+1)
[experimental yrast states]

average moment of inertia

I < 49/2 81

I ≥ 49/2 127

rigid body value

(β = -0.2) 128

Reduced transition probability

$^{147}_{64}Gd_{83}$

O. Bakander et al., Nucl. Phys. A389(1982)93

E_γ [keV]	$m\lambda$	$B(m\lambda)/B_{W.u.}(m\lambda)$
255	E2	1.9×10^{-2}
594	E3	2.1
764	M1	5.4×10^{-9}

$^{143}_{60}Nd_{83}$

X.H. Zhou, et al., Phys. Rev. C61(2000)014303

E_γ [keV]	$m\lambda$	$B(m\lambda)/B_{W.u.}(m\lambda)$
339	E1	1.7×10^{-7}

H. Sagawa (Aizu-u.)

$^{147}_{64}Gd_{83}$ E2 transition

[DIPM calculation]

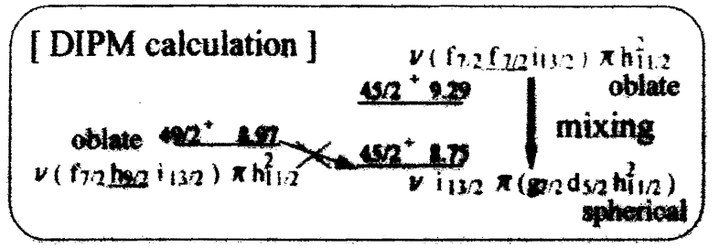

It is necessary for the $45/2^+$ yrast state with spherical shape to have admixture of the state with oblate shape

$$\langle h_{9/2} | E2 | f_{7/2} \rangle_{exp} \sim 1.9 \times 10^{-2}$$

$$|49/2^+\rangle = |\text{oblate};49/2^+\rangle$$

$$|45/2^+\rangle = |\text{spherical};45/2^+\rangle + \alpha\ |\text{oblate};45/2^+\rangle$$

$$\langle 49/2^+ | E2 | 45/2^+ \rangle \quad \curvearrowright 0$$

$$= \underline{\langle \text{oblate};49/2^+ | E2 | \text{spherical};45/2^+ \rangle} + \alpha \langle \text{oblate};49/2^+ | E2 | \text{oblate};45/2^+ \rangle$$

$$= \alpha \langle \text{oblate};49/2^+ | E2 | \text{oblate};45/2^+ \rangle$$

$$\alpha^2 = 1.9 \times 10^{-2}$$

$$\Downarrow$$

mixing amplitude of oblate shape α 0.1

High spin shape isomer

K-isomer

K selection rule log Fw = 2 (ΔK-1)

Fw : hindrance factor

If N=83 high spin isomer is K-isomer,

ΔK = 49/2 - 7/2 = 21

log Fw = 40

Fw = 10^{40} !

It may be stable nuclei.

N=83 high-spin isomers could be considered to be shape isomer.

Ge - Telescope

for Position Sensitive γ-Ray Detection

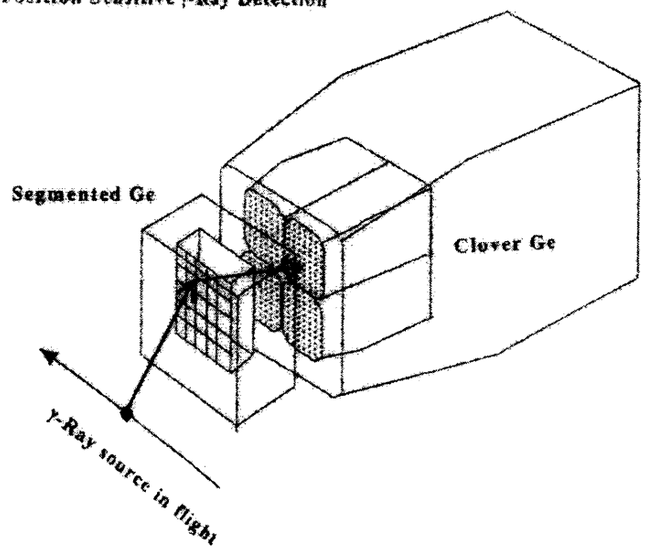

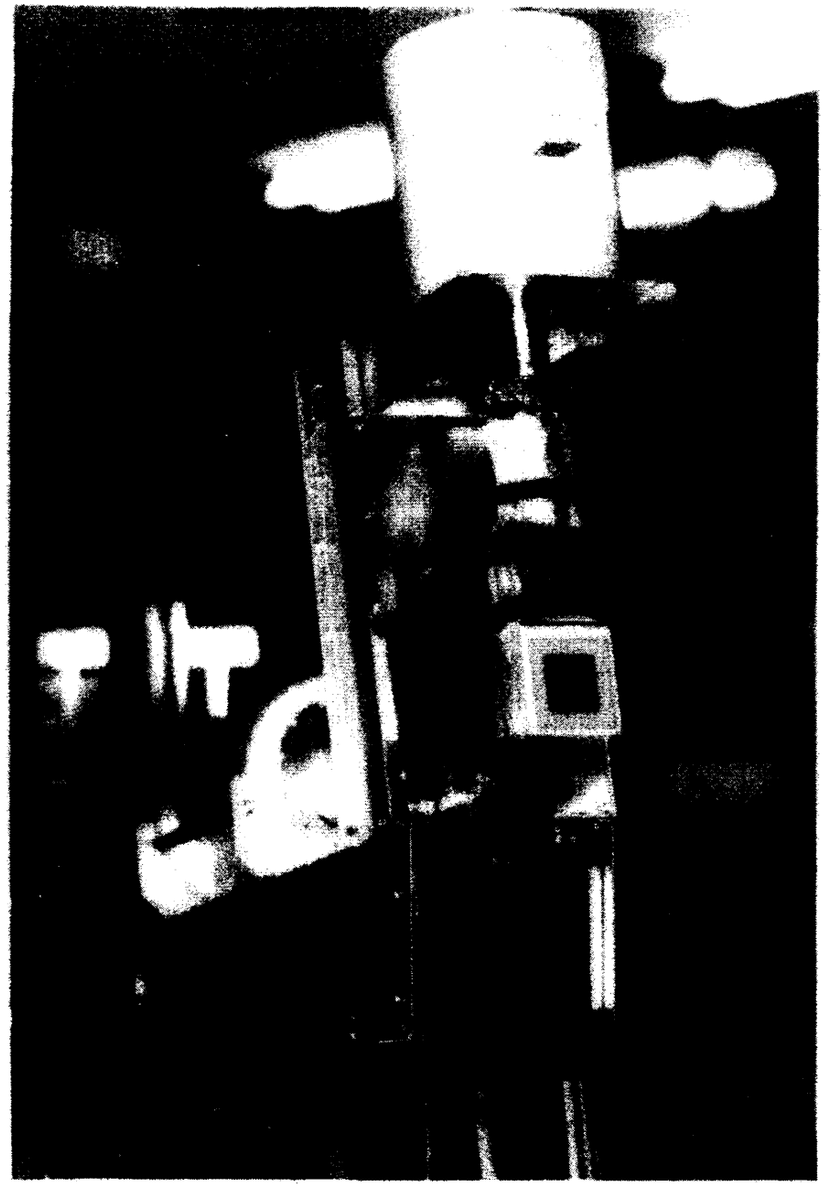

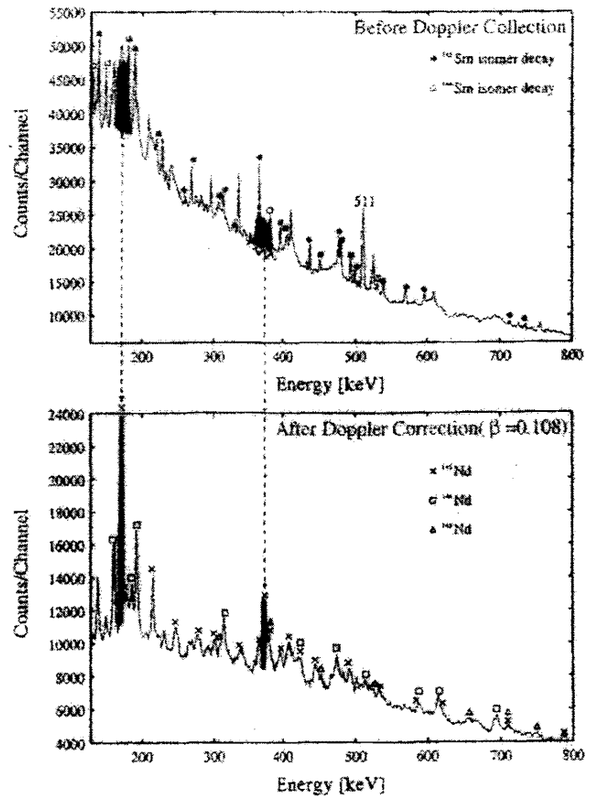

Figure 32: γ-ray spectra measured by the telescope Ge counter. The upper figure is a spectrum before the Doppler correction, and the lower is after the Doppler correction with $\beta_R = 0.108$. Meaning of marks in this figure is same with those in Figure 31.

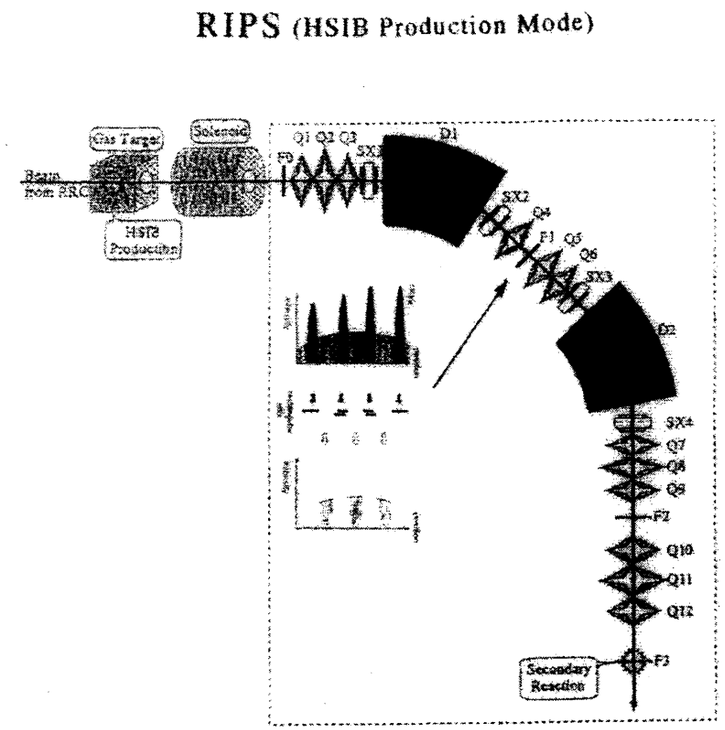

Production of the HSIB ($T_{1/2}$ = 0.95 μs, I = 49/2 ħ)

Primary beam : ^{136}Xe of E = 7.6 MeV/u with 50 - 100 pnA

Production target : CO_2 gas of 1.3mg/cm² thickness

(corresponds to ^{12}C of 0.95mg/cm²)

Production reaction : ^{12}C(^{136}Xe, 7n)^{145m}Sm

↳inverse-kinematic fusion reaction

Properties of the ^{145m}Sm HSIB

- **Energy** :
- **Intensity** :
- **Purity** : (Plastic-RF)
  - [Components in the secondary beam]
    - ^{136}Xe charge state component
    - ^{136}Xe scattered component
    - Other reaction products

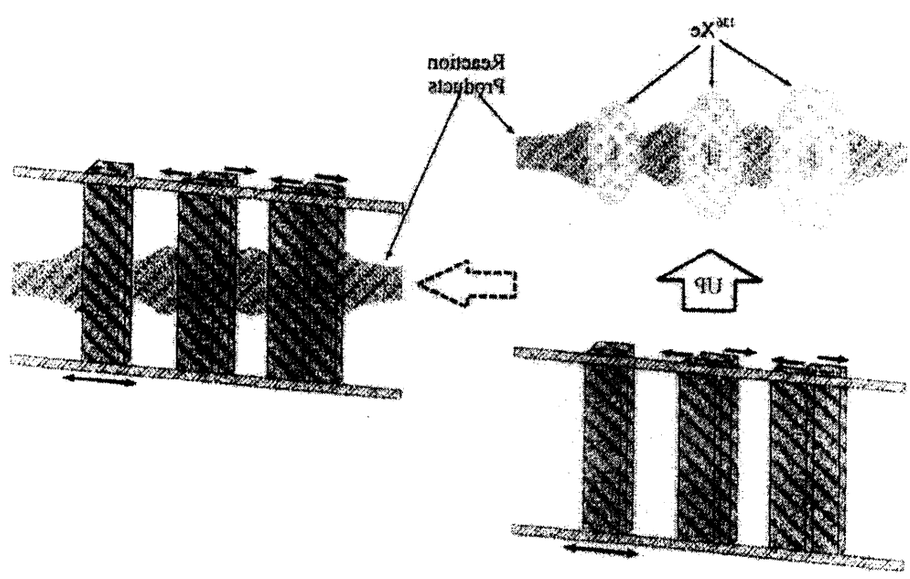

Figure 2.12: Image of the beam spot and the rectangular slit at F1

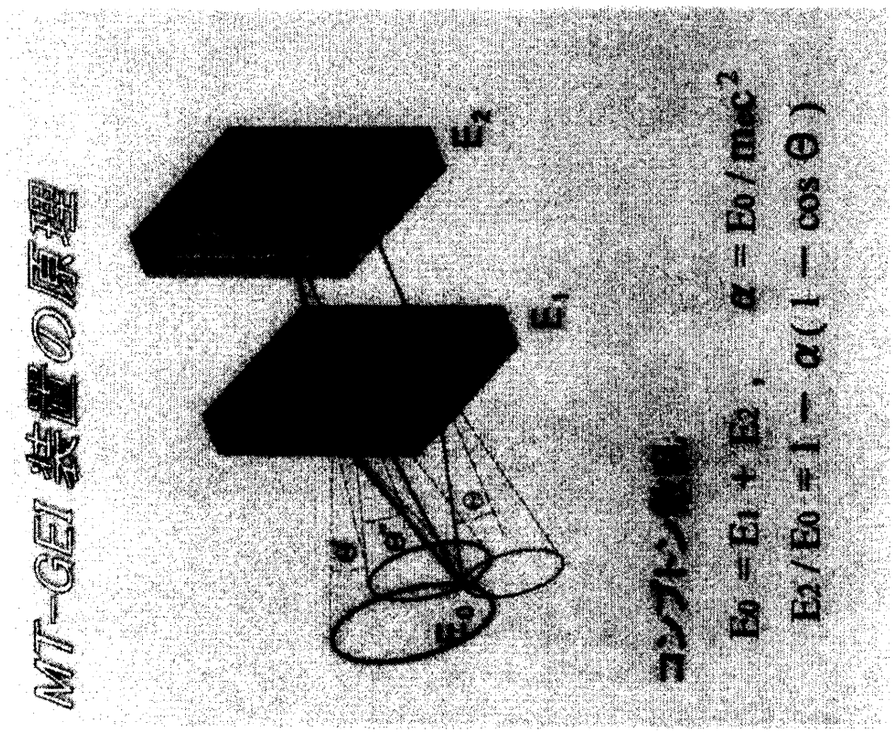
MT-GEI 装置の原理
E2
E1
E0
コンプトン散乱
E0 = E1 + E2 , α = E0 / mec2
E2 / E0 = 1 − α(1 − cos θ)

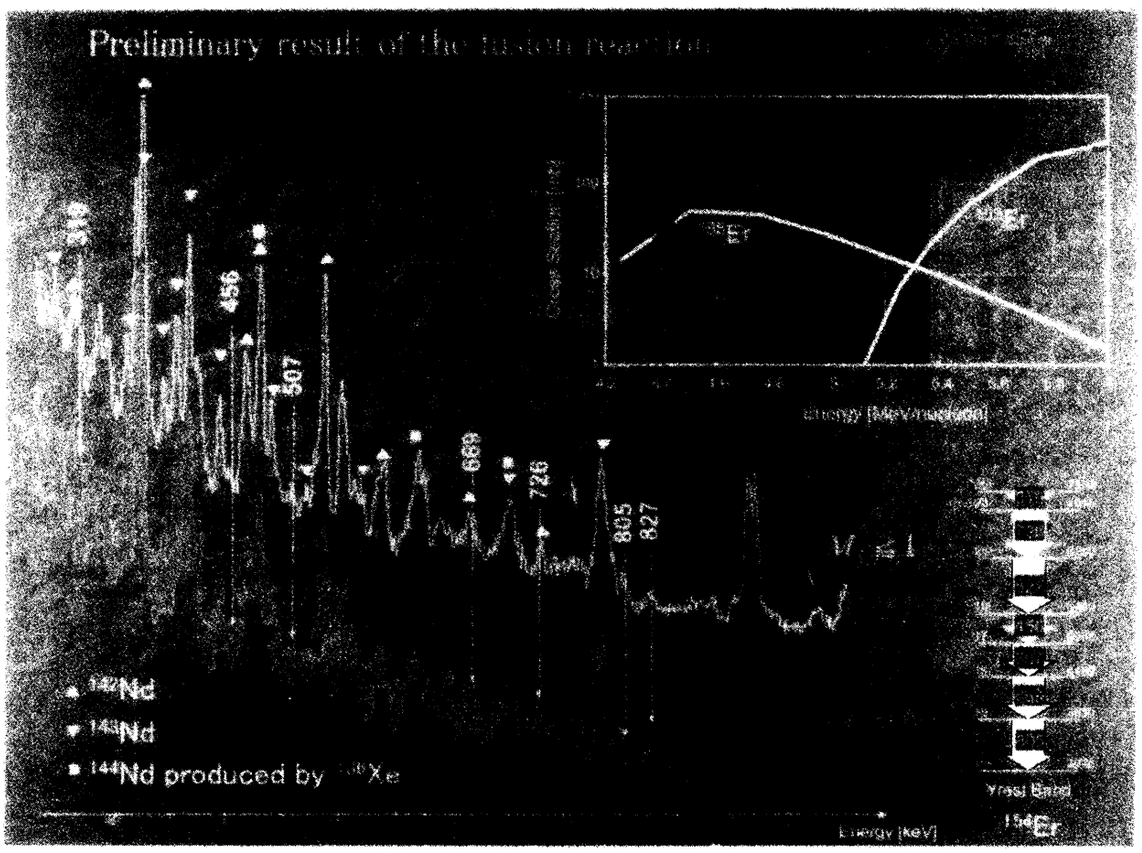
Preliminary result of the fusion reaction
310
456
507
669
726
805
827
142Nd
143Nd
144Nd produced by 136Xe
Energy [keV]
Cross Section [mb]
Energy [MeV/nucleon]
136Xe
144Xe
Xrasi Band
154Er

E1+E2 のスペクトル

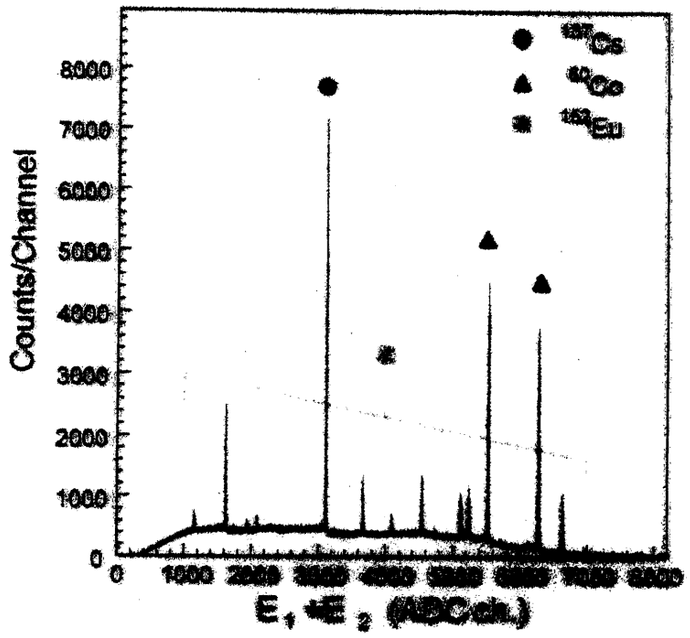
Counts/Channel
8000
7000
6000
5000
4000
3000
2000
1000
0
0
1000
^{137}Cs
^{60}Co
^{152}Eu
E_1+E_2 (ADC ch.)

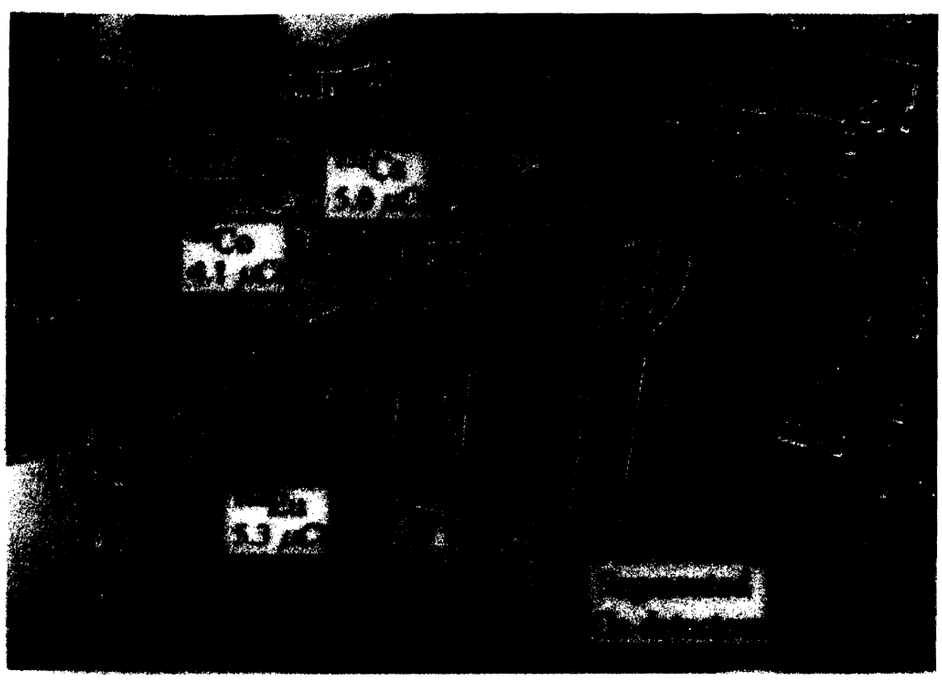

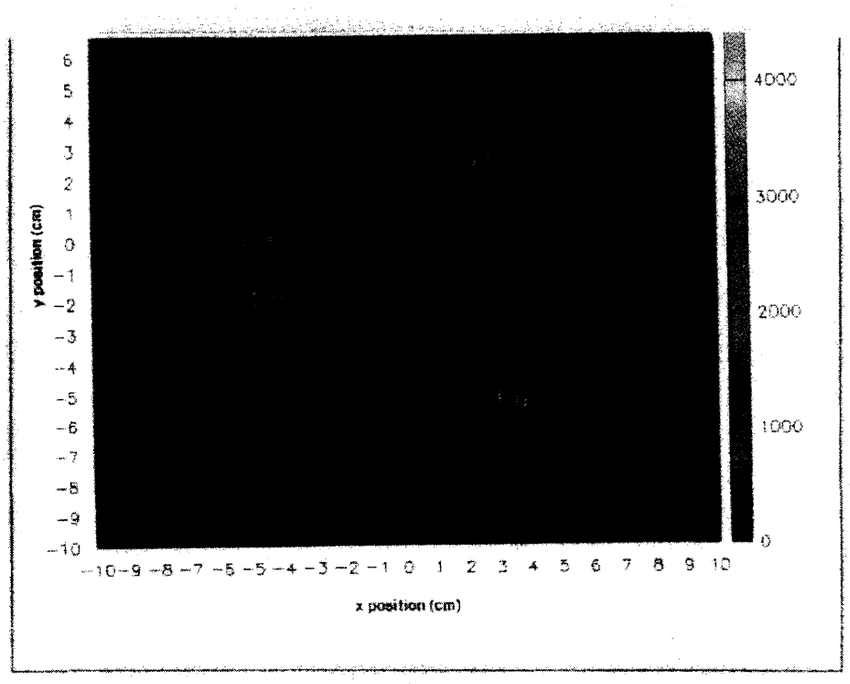

Threshold = 95%